

# ORAL ELECTROSPUN MULTI-COMPONENT MEMBRANOUS DRUG DELIVERY SYSTEMS

---

**RUBINA PERVEEN SHAIKH**



A dissertation submitted to the Faculty of Health Sciences, University of the Witwatersrand, in fulfilment of the requirements for the degree of Master of Pharmacy

**Supervisor:**

Professor Viness Pillay

Department of Pharmacy and Pharmacology, University of the Witwatersrand,  
South Africa

**Co-Supervisors:**

Professor Yahya E. Choonara and Ms Lisa C. du Toit

Department of Pharmacy and Pharmacology, University of the Witwatersrand,  
South Africa

Johannesburg, 2012

## DECLARATION

---

I, Rubina Perveen Shaikh, declare that this dissertation is my own work. It has been submitted for the degree of Master of Pharmacy in the Faculty of Health Sciences at the University of the Witwatersrand, Parktown, Johannesburg, South Africa. It has not been submitted before for any other degree or examination at this or any other University.

.....

This 23<sup>rd</sup> day of August 2012

## RESEARCH OUTPUTS

---

### Conference Proceedings

#### Poster Presentations

Rubina P Shaikh, Tasneem Kader, Viness Pillay, Yahya E Choonara and Lisa C du Toit. *In vitro Assessment of an Impetuous Film-casted Membranous Drug Delivery System*. Poster presented at 29th Annual Conference of the Academy of Pharmaceutical Sciences, 22-26 September 2008, Rustenburg (Abstract in Appendix A1).

Rubina P Shaikh, Viness Pillay, Yahya E Choonara and Lisa C du Toit. *Evaluation of Electrospun Polymeric Membranes for Potential Rate-Modulated Drug Delivery*. Poster presented the 2009 5th ICPPS conference, 23-26 September 2009, Potchefstroom (Abstract in Appendix A2).

Rubina Shaikh, Viness Pillay, Yahya E. Choonara and Lisa C. du Toit, Valence M.K. Ndesendo and Pradeep Kumar. *A pH-responsive Mucoadhesive Membrane for Prolonged Oral Drug Delivery*. Poster presented at the International Symposium on Stimuli-Responsive Materials at the University of Southern Mississippi, Hattiesburg, MS, USA 2010 (Abstract in Appendix A3).

#### Podium Presentations

Rubina P. Shaikh, Viness Pillay, Yahya E. Choonara and Lisa C. du Toit. *Synthesis of Multilayered Mucoadhesive Membranes for Prolonged and Site-Specific Oral Drug Delivery*. Podium Presentation for the Young Scientist Competition: 6<sup>th</sup> International Conference on Pharmaceutical and Pharmacological Sciences, 25-28 September 2011, Durban (Abstract in Appendix A4).

## Research Publications

### Review Article

Rubina P Shaikh, Viness Pillay, Yahya Choonara, Lisa C du Toit, Valence MK Ndesendo, Priya Bawa, Shivaan Cooppan. A Review of Multi-Responsive Membranous Systems for Rate-Modulated Drug Delivery. *AAPS PharmSciTech Journal*, **11(1)** (2010) (Abstract in Appendix B1).

### Research Papers

Rubina P. Shaikh, Viness Pillay, Yahya E. Choonara, Lisa C. Du Toit, Valence M.K. Ndesendo, Pradeep Kumar and Riaz A. Khan. The application of a crosslinked pectin-based wafer matrix for gradual buccal drug delivery. *Journal of Biomedical Materials Research Part B* 2012 (Abstract in Appendix B2).

Rubina P Shaikh, Pradeep Kumar, Yahya E Choonara, Lisa C du Toit and Viness Pillay. Crosslinked electrospun PVA nanofibrous membranes: elucidation of their physicochemical, physicomechanical and molecular disposition. *Biofabrication* **4**, 2012; 025002 (Abstract in Appendix B3).

## PATENTS

---

- *Development of a Membranous Oral Pharmaceutical Dosage Form*, Rubina P. Shaikh, Viness Pillay, Yahya E. Choonara and Lisa C. du Toit, SA *Patent Application No: 2010/03740*, 12 October 2010.
- *A Pharmaceutical Dosage Form*, P. Shaikh, Viness Pillay, Yahya E. Choonara and Lisa C. du Toit, *Patent Application No: PCT/IB2011/055331*.

## ANIMAL ETHICS DECLARATION

---

I hereby confirm that the following study entitled “*An in vivo assessment of novel biocompatible polymeric drug delivery systems in pigs*” had received the approval from the Animal Ethics Committee of the University of the Witwatersrand with ethics clearance number 2009/01/05 (Appendix C1).

## SUMMARY

---

Oral drug delivery is perceived by many as the ideal method of drug delivery due to its versatility, ease and convenience. However, the bioavailability of drugs delivered via the oral route remains questionable. Typically, conventional marketed drug delivery systems release drugs in variable and erratic fashions, causing sub-therapeutic or even toxic doses. As a result, patient compliance is threatened, ultimately affecting the success of the therapeutic intervention. Furthermore, the harsh gastric environment further compromises oral bioavailability due to the presence of a highly acidic environment and proteolytic enzymes.

A multi-component, membranous drug delivery system (MMDDS) was thus designed, formulated and evaluated for the site-specific delivery of two (or more) drugs in a prolonged release manner, ultimately easing complicated treatment regimens, and improving patient compliance. The MMDDS essentially comprises of a gastric-targeted and an intestinal-targeted component, each containing a protective coat, a drug-loaded layer incorporating the respective drugs, and a pH-responsive mucoadhesive layer for site-specific mucoadhesion. The MMDDS employs a combination of controlled and targeted drug release mechanisms, in addition to gastro-retentive or intestinal retentive mechanisms. Furthermore, the system physically protects the drug delivery system from acidic or proteolytic degradation within the human gastro-intestinal tract. The present study employed the use of pH-dependant mucoadhesion for site-specific, segregated and gastroretentive drug delivery while crosslinking was employed for rate-modulated drug delivery. Rifampicin and isoniazid were selected as the model drugs in this study as they are known for interacting when administered simultaneously (detrimentally affecting the bioavailability of rifampicin). Notwithstanding this interaction, rifampicin and isoniazid must be taken concurrently for successful TB therapy. Therefore these drugs would benefit from the site-specific drug delivery offered by the MMDDS.

The primary aim of the pH-responsive mucoadhesive layer was to ensure prolonged adhesion of the MMDDS at a specific site within the human gastro-intestinal tract. The pH-responsive mucoadhesive layer was the fundamental aspect that promoted site-specific and segregated drug delivery. Preliminary *in vitro* investigations led to the identification of a combination of polymers best suited to develop the respective pH-responsive mucoadhesive layers. A central composite design was employed to determine the optimal ratios of the polymers selected which would impart the largest degree of mucoadhesion within the respective pH ranges. Each mucoadhesive layer was thereafter optimized and subject to various *in vitro* investigations to determine the effects of the GIT on the properties of the mucoadhesive layer, as well as determine the behaviour of the mucoadhesive layer when subject to simulated gastrointestinal conditions.

Electrospinning, a versatile technique employed in the fabrication of fibres in the nanometre size range, was employed to develop the drug loaded layer. Poly(vinyl alcohol) (PVA) nanofibres were thereafter crosslinked employing glutaraldehyde vapours to ensure controlled release of the incorporated drugs. The drug-loaded layer demonstrated good versatility in incorporating vastly different drugs, with only minor adjustments to the fabrication procedure. Furthermore, PVA demonstrated good loading of rifampicin and isoniazid, and near zero-order drug release was achieved after the crosslinking procedure. Prolongation of drug release fundamentally decreases the numbers of doses required to be taken daily, and as such, patient compliance is improved.

Furthermore, *in vitro* analysis revealed that the developed MMDDS behaved superiorly in terms of controlling drug delivery in a site-specific and prolonged fashion in comparison to a marketed gold standard formulation, Rifinah<sup>®</sup>. These findings were further substantiated by *in vivo* analysis, which was conducted in a swine model. Results indicated that minimal release of isoniazid was observed in the stomach, based on the plasma concentrations of the drug. Release of isoniazid was initiated only when the intestinal-targeted component entered the intestine of the pig, corresponding to higher plasma concentrations of isoniazid. In this manner, the delivery of isoniazid and rifampicin was segregated, thus improving the oral bioavailability of rifampicin.

To summarize, the MMDDS was able to overcome the many challenges associated with oral drug delivery, by easing complicated treatment regimens, and improving the bioavailability of drugs delivered orally. The benefits associated with oral drug delivery have clearly been exploited by the present study, producing a versatile drug delivery "tool" which can successfully be adapted to incorporate any number of drugs (including an entire treatment regimen in one dosage form!) for targeted delivery within the human gastro-intestinal tract in a prolonged manner.

## ACKNOWLEDGEMENTS

---

In completion of this work, the author would like to convey her sincerest gratitude and appreciation to various individuals that have assisted and guided her towards this goal.

Firstly, to The Almighty, The All-Knowing, without Whom, none of this would have been possible.

To my Supervisor and Professor, Viness Pillay, for the invaluable role played in the successful completion of this dissertation. You not only served as my supervisor, but encouraged and challenged me throughout my academic programme, never accepting less than my best efforts. By always expecting perfection, hard work, and commitment, you have instilled in me qualities which would allow me to excel in life and I thank you for this. Your passion and dedication to the field of Pharmaceuticals and hunger for knowledge is inspirational! I will always be grateful to for the opportunity you have provided me in participating in cutting edge research.

To my co-supervisors, the newly (and well deserved) awarded Professor, Yahya Choonara, and Ms Lisa du Toit, you were always willing to provide the necessary direction and assistance when needed. The time and effort you invested has only made the completion of this dissertation so much easier. Your valuable feedback and suggestions helped me improve both my lab experiments and my thesis in many ways. I wish you both all the success in your future endeavours.

To my parents, Abdul Samad and Bilqis Shaikh, you are my inspiration, I have strived to be what I am today by following your example. It is through your unconditional love, support, guidance, encouragement and, not forgetting, your unfaltering confidence in me that I have (finally) completed my masters successfully. Had you not pushed me to reach my full potential in all aspects of life, I would never have had the ability or means to have come this far in life. In the most difficult times, your unconditional love was my pillar of strength that helped me move forward in life. You always believed in me. I am honoured and blessed to have you as my parents and I only hope that I make you proud.

To my husband and best friend, Ebrahim Patel, words cannot express my gratitude. For always believing in me and with your unwavering support, encouragement, patience and



understanding, you provided with the strength to perform better than I expected. You always went out of your way to ensure that I was successful in this endeavour, and endured the moods, tantrums and “hissy fits” I had to get through it. I will eternally be grateful that you always understood the demanding nature of this study. You never questioned my ability to complete this dissertation successfully, even if I did. You were my shoulder to cry on during the tough times and always lifted my spirits when I needed it most. I will always be grateful for all your advice, guidance and unconditional love. I could never have done this without you.

To my siblings, Shahina Suliman, Iqbal Shaikh, Naheeda Shaikh, Nazeha Shaikh, Zaid Suliman and (not forgetting) the new additions, Tanya Knowles and Ayaz Alam Arab, thank you for your constant motivation and advice, it made all the difference. I finally did it guys! I could always count on you for your well-reasoned opinions (and the countless hours of teasing). Your encouragement and moral support was vital! To my new family in Lenasia, my parents- (Naeem and Razia Patel) and siblings-in-law, (Naadiera, Muneer Muhammed Riyaaz and Saadiya), I would like to sincerely thank you for all your support and for always believing in me. I will always be grateful to you for making the completion of this dissertation so much easier.

To my fellow eighth floor researchers, my friends, Yusuf Dawood, Ameena Wadee, and Kovanya Moodley, the long, tiring yet enlightening and fulfilling journey since first year (many moons ago!) as undergrads is now nearing an end. I will miss our times together. To my office mates, Priya Bawa and Shivaan Cooppan you were always willing to provide me with much needed guidance and solutions to my many problems. To my friends and fellow colleagues, Yasien Docrat, Zaheeda Khan, Caragh Murphy, Clare Dott, Deshika Reddy, Valence Ndesendo, Derusha Frank, Tasneem Rajan, Tong-sheng Tsai, Thiresen Govender, Ndidi Ngwuluka, Pius Fasinu, Oluwatoyin Kolawole, Steven Mufamad, Deshnee Naidoo, Sajida Suliman, and the rest on the eighth floor, all the fun and laughter made the lab work more bearable. A special thank you to Pradeep Kumar, I firmly believe that you really are a genius, and will do great things to come! Thank you all for the advice, direction and providing me with the necessary (and needless to say-brilliant) molecular modelling. To my elective students, Tasneem Kader and Tshepo Ramotshela, I will always be thankful to you for easing the burden of lab work.

To the Wits staff, Mr David Bayever, Ms Shirona Naidoo, Mrs Deanne Johnston, Ms Nompumelelo Damane, Professor Sandy Van Vuuren, Ms Neelaveni Padayachee,

Professor Paul Danckwerts and Ms Neha Singh thank you for all the advice, assistance and much needed motivation.

To the technical staff, who ensured the labs were always neat and tidy, the late Elizabeth, Mama Florence, Kleinbooie (KB), Bafana, Sello, and Tebogo, you always went out of your way to ensure that I got what I needed and I will always be grateful to you.

To Dr. Leith Meyer and Sister Mary-Ann Costello and their team at the Central Animal Services (CAS) at the University of the Witwatersrand, I thank you for all your advice and assistance when undertaking animal studies. By being very accommodating and helpful, you have made the very arduous *in vivo* portion of this study so much easier.

To the Mintek Group, for the use of your facilities that added so much to my research, and to RGC Engineering, for designing and constructing our very own electrospinner which was paramount in completing this research.

And finally, to my funders, without whom this research would not have been possible, I would like to extend my heartfelt gratitude to the National Research Foundation of South Africa, TATA Africa and The Department of Education. The scholarships and funding have lightened my financial burden beyond measure.

To summarize, over the last few years I ventured far away from home, I experienced, I made mistakes, I learned, I matured...The excitement does not stop here of course, for I still have a lot to learn...

*“The real voyage of discovery consists not in seeking new landscapes, but in having new eyes.”*

- Marcel Proust (French novelist: 1871 - 1922)

## DEDICATION

---

This work is dedicated to the three most important people in my life, my parents, Abdul Samad and Bilqis Shaikh; for all that I am today, and to my loving husband, Ebrahim Patel, for being with me every step of the way.

# TABLE OF CONTENTS

---

## CHAPTER 1

### INTRODUCTION AND MOTIVATION FOR STUDY

|       |  |    |
|-------|--|----|
| 1.1   | Background to the Study.....   | 1  |
| 1.2   | Rationale and Motivation for the Study .....   | 8  |
| 1.3   | Consideration of the Gastrointestinal Physiology in the Development of a Smart Drug Delivery System Intended to Enhance Oral Bioavailability ..... | 12 |
| 1.3.1 | The GIT physiology and its ramifications on drug delivery .....  | 12 |
| 1.3.2 | pH as a stimulus employed for targeting in oral drug delivery .....  | 17 |
| 1.3.3 | Architectural strategy employed to exploit and overcome the GIT physiology .....   | 17 |
| 1.4   | Novelty of the Study.....  | 18 |
| 1.5   | Aim and Objectives of the Study: Description of the Oral Multi-component Membranous Drug Delivery System.....                                      | 19 |
| 1.6   | Synopsis of the Dissertation .....   | 21 |
| 1.7   | Concluding Remarks .....   | 22 |

## CHAPTER 2

### A REVIEW ENCOMPASSING STIMULI-RESPONSIVE POLYMERS WITH SPECIFIC APPLICATION IN MEMBRANOUS SYSTEMS AND THE FORMULATION THEREOF

|         |   |    |
|---------|---|----|
| 2.1     | Introduction.....   | 23 |
| 2.2     | Membrane Applications in Drug Delivery .....  | 24 |
| 2.3     | Methods Employed in the Fabrication of Polymeric Membranes .....                            | 25 |
| 2.3.1   | Phase separation .....  | 25 |
| 2.3.1.1 | Vapour-induced phase separation .....   | 26 |
| 2.3.1.2 | Thermal-induced phase separation .....  | 26 |
| 2.3.1.3 | Immersion precipitation .....   | 26 |
| 2.3.1.4 | Film/dry-casting technique.....   | 27 |
| 2.3.2   | Electrospinning.....  | 28 |
| 2.3.3   | Foaming .....   | 29 |
| 2.3.4   | Particle leaching.....  | 29 |
| 2.3.5   | Emulsion freeze-drying.....   | 30 |
| 2.3.6   | Sintering.....  | 30 |
| 2.4     | Stimuli-responsive Polymers and their Application in Drug Delivery Systems .....            | 31 |
| 2.4.1   | Thermo-responsive polymers and their applications in membranous drug delivery systems.....  | 38 |
| 2.4.2   | pH-responsive polymers and their applications in membranous drug delivery systems.....      | 41 |
| 2.4.3   | Glucose-responsive polymers and their applications in membranous drug delivery systems..... | 42 |
| 2.4.4   | Dual-responsive systems .....   | 45 |
| 2.5     | Concluding Remarks .....  | 47 |

## CHAPTER 3

### PRELIMINARY DESIGN OF THE STIMULI-RESPONSIVE MUCOADHESIVE LAYERS OF THE MULTI-COMPONENT MEMBRANOUS DRUG DELIVERY SYSTEM

|         |   |    |
|---------|---|----|
| 3.1     | Introduction.....   | 48 |
| 3.1.1   | Theories of mucoadhesion .....  | 49 |
| 3.1.1.1 | The electronic theory .....   | 49 |
| 3.1.1.2 | The adsorption theory.....  | 49 |
| 3.1.1.3 | The wetting theory.....   | 50 |
| 3.1.1.4 | The diffusion theory .....  | 50 |
| 3.1.1.5 | The fracture theory .....   | 50 |
| 3.1.1.6 | The mechanical theory .....   | 50 |
| 3.1.2   | Classification and properties of mucoadhesive polymers.....   | 51 |
| 3.1.3   | Factors affecting mucoadhesion.....   | 55 |
| 3.1.4   | Preliminary formulation design .....  | 55 |
| 3.2     | Materials and Methods.....  | 56 |
| 3.2.1   | Materials .....   | 56 |
| 3.2.2   | Formulation and evaluation of various mucoadhesive polymers for their pH-responsive properties.....                                     | 56 |
| 3.2.3   | The effect of employing a combination of mucoadhesive polymers in the development of the pH-responsive mucoadhesive layer .....         | 57 |
| 3.2.4   | The influence of PVA addition to develop a durable mucoadhesive layer able to withstand the conditions of the GIT .....                 | 58 |
| 3.2.5   | The influence of PAA substitution with PVP for the further improvement of mucoadhesive properties over a prolonged period of time ..... | 59 |
| 3.2.6   | Determining the upper and lower variables of the formulation required for input into the Central Composite Design .....                 | 60 |
| 3.2.7   | Determination of mucoadhesive properties through textural analysis .....  | 60 |

|       |  |    |
|-------|--|----|
| 3.2.8 | Evaluation of variations in mucoadhesive properties as a function of time .....  | 62 |
| 3.3   | Results and Discussion.....  | 62 |
| 3.3.1 | Most appropriate mucoadhesive polymer demonstrating pH-responsive properties for the respective mucoadhesive layers .....      | 62 |
| 3.3.2 | Identification of the most effective polymer combination in the respective pH-responsive mucoadhesive layers .....             | 66 |
| 3.3.3 | Effect of PVA incorporation in the respective pH-responsive mucoadhesive layers.....   | 68 |
| 3.3.4 | Effect of PAA substitution with PVP in the pH-responsive mucoadhesive layer .....  | 71 |
| 3.3.5 | Determining the upper and lower limits of the formulation variables required for input into the Central Composite Design ..... | 74 |
| 3.4   | Concluding Remarks .....   | 75 |

## CHAPTER 4

### FABRICATION AND STATISTICAL OPTIMIZATION OF THE STIMULI-RESPONSIVE MUCOADHESIVE LAYERS OF THE MULTI-COMPONENT MEMBRANOUS DRUG DELIVERY SYSTEM EMPLOYING A DESIGN STRATEGY

|   |   |    |
|---|---|----|
| 4.1   | Introduction.....   | 76 |
| 4.1.1   | Selection of independent variables for input into a Central Composite Design.....   | 77 |
| Part I – Fabrication and statistical optimization of gastric-targeted mucoadhesive layer of the MMDDS ..... |   | 79 |
| 4.2   | Material and Methods .....  | 79 |
| 4.2.1   | Materials .....   | 79 |
| 4.2.2   | Construction of a randomized Central Composite Design for the optimization of the gastric-targeted component .....                  | 79 |
| 4.2.3   | Fabrication of the gastric-targeted mucoadhesive layer.....   | 80 |
| 4.2.4   | Mucoadhesive analysis through textural profiling.....   | 81 |
| 4.2.5   | Variations in mucoadhesive characteristics of the gastric-targeted experimental formulations as a function of time.....             | 81 |
| 4.2.6   | Constrained statistical optimization of the gastric-targeted mucoadhesive layer of the MMDDS .....                                  | 81 |
| 4.3   | Results and Discussion.....   | 82 |
| 4.3.1   | Central Composite Experimental Design for optimization of the gastric-targeted mucoadhesive layer of the MMDDS.....                 | 82 |
| 4.3.1.1   | Measured responses for experimental optimization .....  | 82 |
| 4.3.1.2   | Correlation of the experimental and fitted response values.....   | 83 |
| 4.3.1.3   | Analysis of the central composite surface design .....  | 84 |
| 4.3.1.4   | Residual Analysis of the Central Composite Experimental Design for the optimization of the gastric-targeted mucoadhesive layer..... | 86 |
| 4.3.1.5   | Constrained optimization of the gastric-targeted mucoadhesive layer.....  | 88 |



|  |    |
|--|----|
| Part II – Fabrication and statistical optimization of the intestinal-targeted mucoadhesive layer of the MMDDS.....                             | 89 |
| 4.4 Materials and Methods.....   | 89 |
| 4.4.1 Materials .....  | 89 |
| 4.4.2 Construction of a randomized central composite design for the optimization of the intestinal-targeted component.....                     | 90 |
| 4.4.3 Fabrication of the intestinal-targeted mucoadhesive layer .....  | 90 |
| 4.4.4 Mucoadhesive analysis through textural profiling.....  | 91 |
| 4.4.5 Variations in the mucoadhesive characteristics of the intestinal-targeted experimental formulations as a function of time .....          | 91 |
| 4.4.6 Constrained statistical optimization of the intestinal-targeted mucoadhesive layer of the MMDDS .....                                    | 91 |
| 4.5 Results and Discussion.....  | 92 |
| 4.5.1 Central Composite Experimental Design for optimization of the gastric-targeted mucoadhesive layer of the MMDDS.....                      | 92 |
| 4.5.1.1 Measured responses for experimental optimization .....   | 92 |
| 4.5.1.2 Correlation of the experimental and fitted response values.....  | 93 |
| 4.5.1.3 Analysis of the central composite surface design .....   | 94 |
| 4.5.1.4 Residual Analysis of the Central Composite Experimental Design for the optimization of the intestinal-targeted mucoadhesive layer..... | 95 |
| 4.5.1.5 Constrained optimization of the intestinal-targeted mucoadhesive layer of the MMDDS .....  | 97 |
| Part III: Physicochemical and physicomechanical characterization of the optimized gastric- and intestinal-targeted mucoadhesive layers.....    | 99 |
| 4.6 Materials and Methods.....   | 99 |
| 4.6.1 Materials .....  | 99 |
| 4.6.2 Fabrication of the optimized mucoadhesive layers .....   | 99 |
| 4.6.3 Physical characterization of the optimized mucoadhesive layers: Evaluation of membrane uniformity .....                                  | 99 |

|       |  |     |
|-------|--|-----|
| 4.6.4 | Determination of the tensile properties and Young's Modulus of the optimized gastric-targeted mucoadhesive layer .....   | 99  |
| 4.6.5 | Simultaneous qualitative and quantitative analysis of the mucoadhesive layer surface morphology and porosity .....   | 100 |
| 4.6.6 | Evaluation of the polymeric structural and vibrational frequency variations of the mucoadhesive layer relative to its exposure to simulated GIT conditions ..... | 101 |
| 4.6.7 | Evaluation of the degree of swelling and polymeric erosion on the mucoadhesive characteristics of the optimized formulation relative to GIT exposure.....        | 102 |
| 4.6.8 | Evaluation of the surface morphology variations of the optimized mucoadhesive layers relative to exposure to simulated gastro-intestinal conditions .....        | 103 |
| 4.6.9 | Magnetic Resonance Imaging (MRI) of the swelling behaviour of the optimized formulations.....  | 103 |
| 4.7   | Results and Discussion.....  | 104 |
| 4.7.1 | Physical characterization of the optimized mucoadhesive layers: Characterization of membrane uniformity .....  | 104 |
| 4.7.2 | Determination of the tensile properties and Young's Modulus of the optimized mucoadhesive layers.....  | 105 |
| 4.7.3 | Simultaneous qualitative and quantitative analysis of the mucoadhesive layer surface morphology and porosity .....   | 108 |
| 4.7.4 | Evaluation of the polymeric structural and vibrational frequency variations of the mucoadhesive layer relative to its exposure to simulated GIT conditions ..... | 109 |
| 4.7.5 | The influence of exposure to simulated gastro-intestinal conditions on the degree of swelling and polymeric erosion .....  | 113 |
| 4.7.6 | Analysis of the surface morphology variations of the optimized mucoadhesive layers relative to exposure to simulated gastro-intestinal conditions .....          | 115 |
| 4.7.7 | Magnetic Resonance Image analysis of the swelling behaviour of the optimized formulations.....   | 117 |
| 4.8   | Concluding Remarks .....   | 119 |

## CHAPTER 5

### PRELIMINARY DESIGN OF THE DRUG-LOADED NANOFIBROUS MATRICES OF THE MULTI-COMPONENT MEMBRANOUS DRUG DELIVERY SYSTEM

|  |  |     |
|--|--|-----|
| 5.1  | Introduction.....  | 120 |
| 5.1.1  | The electrospinning procedure .....  | 122 |
| 5.1.2  | Parameters affecting the electrospinning procedure.....                              | 123 |
| 5.1.3  | Methods of drug incorporation .....  | 126 |
| 5.1.4  | Preliminary formulation design .....   | 128 |
| PART I: Identification of a suitable polymer for electrospinning followed by determination of the optimal electrospinning parameters ..... |  | 128 |
| 5.2  | Materials and Methods.....   | 128 |
| 5.2.1  | Materials .....  | 128 |
| 5.2.2  | Preparation of nanofibrous matrices by electrospinning.....                          | 129 |
| 5.2.3  | Analysis of nanofibre morphology employing scanning electron microscopy.....         | 129 |
| 5.2.4  | Construction of a calibration curve for UV spectroscopic determination of DPH.....   | 130 |
| 5.2.5  | Drug entrapment efficiency.....  | 130 |
| 5.3  | Results and Discussion.....  | 131 |
| 5.3.1  | Analysis of the degree of success of polymers investigated for electrospinning ..... | 131 |
| 5.3.1.1  | Carboxymethyl cellulose.....   | 131 |
| 5.3.1.2  | Poly(ethylene glycol) 4000.....  | 132 |
| 5.3.1.3  | Poly(ethylene glycol) 6000.....  | 133 |
| 5.3.1.4  | Chitosan .....   | 133 |
| 5.3.1.5  | Hydroxypropyl cellulose.....   | 134 |
| 5.3.1.6  | Cellulose acetate.....   | 134 |
| 5.3.1.7  | Cellulose acetate phthalate .....  | 135 |

|          |   |     |
|----------|---|-----|
| 5.3.1.8  | Eudragit® RS 100 .....  | 137 |
| 5.3.1.9  | Poly(vinyl alcohol) .....   | 137 |
| 5.3.1.10 | Poly(ethylene oxide) .....  | 138 |
| 5.3.2    | Calibration curves for UV spectrophotometric determination of DPH.....  | 139 |
| 5.3.3    | Drug entrapment efficiency of electrospun nanofibres .....  | 140 |
| Part II: | Improving the electrospinnability of poly(vinyl alcohol) solutions with the<br>incorporation of excipients .....          | 141 |
| 5.4      | Materials and Methods.....  | 141 |
| 5.4.1    | Materials .....   | 141 |
| 5.4.2    | Preparation of PVA nanofibrous matrices by electrospinning.....   | 142 |
| 5.4.3    | Influence of sodium chloride addition on the electrospinnability PVA.....   | 142 |
| 5.4.4    | Influence of Tween® 80 addition on the electrospinnability of PVA .....   | 142 |
| 5.4.5    | Influence of Span® 80 addition on the electrospinnability of PVA.....   | 142 |
| 5.4.6    | Influence of silicone addition on the electrospinnability of PVA.....   | 143 |
| 5.4.7    | Influence of glycerol addition on the electrospinnability of PVA .....  | 143 |
| 5.4.8    | Influence of drug incorporation on the electrospinnability of PVA .....   | 143 |
| 5.4.9    | Elucidation of pertinent rheological properties of the polymer<br>solutions employed in electrospinning .....             | 143 |
| 5.4.10   | Determination of the electrical conductivity of the polymer solutions<br>employed in electrospinning .....                | 144 |
| 5.5      | Results and Discussion.....   | 144 |
| 5.5.1    | Determination of the optimal PVA concentration for the<br>electrospinning of three-dimensional nanofibrous matrices ..... | 144 |
| 5.5.2    | Effect of excipient addition on the electrospinnability of PVA.....   | 146 |
| 5.5.3    | Effect of drug incorporation on the electrospinnability of PVA<br>solutions.....  | 149 |
| 5.6      | Concluding Remarks .....  | 151 |

## CHAPTER 6

### FABRICATION, MODIFICATION AND CHARACTERIZATION OF THE DRUG-LOADED NANOFIBROUS MATRICES OF THE MULTI-COMPONENT MEMBRANOUS DRUG DELIVERY SYSTEM

|        |   |     |
|--------|---|-----|
| 6.1    | Introduction.....   | 152 |
| 6.2    | Materials and Methods.....  | 154 |
| 6.2.1  | Materials .....   | 154 |
| 6.2.2  | Electrospinning of drug-loaded nanofibres .....   | 154 |
| 6.2.3  | Modification of the drug-loaded nanofibrous matrices through crosslinking .....   | 155 |
| 6.2.4  | Construction of calibration curves for the UV spectroscopic determination of RIF and INH.....                               | 156 |
| 6.2.5  | Determination of the Drug Entrapment Efficiency of PVA nanofibres.....  | 156 |
| 6.2.6  | In vitro drug release studies .....   | 157 |
| 6.2.7  | Influence of drug-loading and crosslinking on the surface morphology and network density of the nanofibrous membranes ..... | 157 |
| 6.2.8  | Image processing using Mathematica™ 8.0 .....   | 157 |
| 6.2.9  | Determination of PVA:GA structural interactions as a result of nanofibre crosslinking with GA .....                         | 158 |
| 6.2.10 | Elucidation of pertinent rheological properties of the polymer solutions employed in electrospinning .....                  | 158 |
| 6.2.11 | Determination of the tensile properties and Young's Modulus of crosslinked and non-crosslinked nanofibrous membranes.....   | 158 |
| 6.2.12 | Static lattice atomistic simulations .....  | 159 |
| 6.3    | Results and Discussion.....   | 160 |
| 6.3.1  | Calibration curves for UV spectrophotometric determination of RIF and INH.....  | 160 |
| 6.3.2  | Drug Entrapment Efficiency (DEE) of PVA nanofibres.....   | 161 |
| 6.3.3  | In vitro drug release from crosslinked nanofibrous matrices .....   | 161 |

|         |  |     |
|---------|--|-----|
| 6.3.4   | Surface Morphology and network density of the nanofibrous membranous system .....  | 163 |
| 6.3.5   | Image processing algorithm for electrospun nanofibres.....   | 166 |
| 6.3.6   | PVA:GA structural interactions as a result of nanofibre crosslinking .....   | 170 |
| 6.3.7   | Rheological characteristics of the non-drug loaded and drug loaded polymeric solutions employed in electrospinning ..... | 174 |
| 6.3.8   | Tensile properties and Young's Modulus of crosslinked and non-crosslinked nanofibrous membranes .....                    | 175 |
| 6.3.9   | Molecular Mechanics Assisted Model Building and Energy Refinements .....   | 178 |
| 6.3.9.1 | MMER analysis .....  | 178 |
| 6.3.9.2 | Formulation of drug-loaded PVA fibres.....   | 179 |
| 6.3.9.3 | Tensile analysis of drug-loaded PVA nano fibres.....   | 180 |
| 6.3.9.4 | Performance of crosslinked PVA electrospun fibres .....  | 183 |
| 6.4     | Concluding Remarks .....   | 186 |

## CHAPTER 7

### ***IN VITRO* AND *IN VIVO* ANALYSIS OF THE MULTI-COMPONENT MEMBRANOUS DRUG DELIVERY SYSTEM IN RELATION TO A MARKETED GOLD STANDARD FORMULATION**

|           |  |     |
|-----------|--|-----|
| 7.1       | Introduction.....  | 187 |
| 7.1.1     | Overview of MMDDS formulation components .....   | 187 |
| 7.1.2     | Selection of an appropriate animal model for <i>in vivo</i> analysis .....   | 188 |
| 7.2       | Materials and Methods.....   | 189 |
| 7.2.1     | Materials .....  | 189 |
| 7.2.2     | Fabrication of the MMDDS .....   | 190 |
| 7.2.2.1   | Mucoadhesive layer.....  | 190 |
| 7.2.2.2   | Drug-loaded layer.....   | 191 |
| 7.2.2.3   | Assembling the MMDDS .....   | 191 |
| 7.2.3     | Comparative analysis of the <i>in vitro</i> drug release behaviour of the MMDDS in relation to a marketed gold standard formulation .....                        | 192 |
| 7.2.3.1   | <i>In vitro</i> dissolution.....   | 192 |
| 7.2.3.2   | UPLC analysis of <i>in vitro</i> dissolution samples.....  | 193 |
| 7.2.3.2.1 | Priming solvents employed in the washing protocol  | 194 |
| 7.2.3.2.2 | Mobile phases employed for sample analysis   | 194 |
| 7.2.3.2.3 | UPLC-PDA analysis for drug content quantification  | 194 |
| 7.2.3.3   | Construction of calibration curves employing a known series of analytical standards .....  | 195 |
| 7.2.4     | Comparative analysis of the <i>in vivo</i> drug release behaviour of the MMDDS in relation to a marketed gold standard formulation employing a swine model ..... | 196 |
| 7.2.4.1   | Surgical implantation of the jugular vein catheter.....  | 196 |
| 7.2.4.2   | Administration of the MMDDS or marketed gold standard formulation .....  | 198 |

|         |  |     |
|---------|--|-----|
| 7.2.4.3 | Blood sampling protocol .....  | 199 |
| 7.2.4.4 | Plasma extraction of drug .....  | 199 |
| 7.2.4.5 | Determination of plasma extraction efficiency.....   | 201 |
| 7.2.4.6 | UPLC-PDA analysis for drug content quantification .....                                    | 201 |
| 7.2.4.7 | Preparation of analytical standards for the construction of<br>the calibration curves..... | 201 |
| 7.3     | Results and Discussion.....  | 202 |
| 7.3.1   | In vitro comparison of marketed formulations .....   | 202 |
| 7.3.1.1 | Chromatograms obtained through UPLC analysis .....   | 202 |
| 7.3.1.2 | Calibration Curves .....   | 203 |
| 7.3.1.3 | <i>In vitro</i> drug release.....  | 204 |
| 7.3.2   | In vivo analysis.....  | 206 |
| 7.3.2.1 | Chromatograms obtained through UPLC analysis .....   | 206 |
| 7.3.2.2 | Recovery efficiency .....  | 207 |
| 7.3.2.3 | Calibration curves.....  | 208 |
| 7.3.2.4 | Comparative <i>in vivo</i> plasma concentration profiles .....                             | 209 |
| 7.4     | Concluding Remarks .....   | 210 |



**CHAPTER 8**  
**CONCLUSIONS AND RECOMMENDATIONS**

|                        |                      |            |
|------------------------|----------------------|------------|
| 8.1                    | Conclusions .....    | 212        |
| 8.2                    | Recommendations..... | 214        |
| <b>REFERENCES.....</b> |                      | <b>215</b> |

**APPENDICES**

|   |     |
|---|-----|
| APPENDIX A .....                        | 261 |
| Abstracts of Conference Proceedings     |     |
| APPENDIX B .....                        | 266 |
| Abstracts of Papers Published/Submitted |     |
| APPENDIX C.....                         | 270 |
| Animal Ethics Clearance                 |     |

## LIST OF FIGURES

---

|             |   |    |
|-------------|---|----|
| Figure 1.1: | Schematic illustration of the GIT, including the limitations to oral drug delivery. ....  | 2  |
| Figure 1.2: | Various studies which have aimed to overcome the limitations of oral drug delivery. ....  | 4  |
| Figure 1.3: | Componential configuration of multilayered mucoadhesive archetype, where a) represents the protective coating; b) represents the electrospun drug loaded layer, containing the respective drugs; and c) represents the stimuli-responsive mucoadhesive layer, specific to the gastric or intestinal targeted component. Both components are then rolled and inserted into a capsule. ....   | 8  |
| Figure 1.4: | Technology applied in the development of the MMDDS thereby improving oral drug bioavailability. ....  | 9  |
| Figure 1.5: | Decomposition mechanism of rifampicin in the presence of isoniazid within the acidic conditions of the stomach. ....  | 10 |
| Figure 1.6: | Prospective applications of the MMDDS. ....   | 11 |
| Figure 1.7: | Simplified illustration of the proposed mode of drug delivery of the MMDDS with a depiction of the architectural strategy employed to overcome and exploit the human GIT physiology. ....   | 18 |
| Figure 1.8: | Schematic illustration depicting differential release, representing a) the gastric targeted component for the delivery of RIF to the stomach, containing a gastric targeted pH-responsive mucoadhesive layer, a RIF-loaded nanofibrous matrix and a protective coat; b) the intestinal targeted component for the delivery of INH to the intestine containing an intestinal targeted pH-responsive mucoadhesive layer, an INH-loaded electrospun matrix and a protective coat; and c) proposed strategy employed to ensure site-specific, segregated and prolonged delivery of both drugs. .... | 20 |

|             |  |    |
|-------------|--|----|
| Figure 2.1: | Schematic illustration of the mass transfer of solvent and non-solvent occurring during immersion precipitation (Adapted from Pereira <i>et al.</i> , 2000).....   | 27 |
| Figure 2.2: | A schematic illustration of the electrospinning process, where $d$ = distance between capillary tip and collecting surface and $\theta$ = Capillary angle. ....  | 28 |
| Figure 2.3: | Common uses of stimuli-responsive polymers in terms of drug delivery (Adapted from Tomlinson, 1987).....   | 32 |
| Figure 2.4: | Factors that can transform unswollen polymer into swollen polymer (Adapted from Dispenza, 2009).....   | 33 |
| Figure 2.5: | Schematic illustration of a) the 'on-off' valve mechanism of polymeric brushes grafted onto porous support, and b) the permeability changes occurring as a result of temperature changes of surface grafted polymeric chains (Adapted from Lue <i>et al.</i> , 2008).....                          | 39 |
| Figure 2.6: | A glucose-responsive insulin releasing system based on PVA/poly(NVP-co-PBA) (Adapted from Kitano <i>et al.</i> , 1992). ....   | 43 |
| Figure 2.7: | Schematic representation of a typical glucose-responsive microcapsule. The pores contain surface immobilised enzyme GOD with grafted pH-responsive PAA hains which, upon exposure to glucose, causes the pore opening and consequent insulin release (Adapted from Chu <i>et al.</i> , 2004b)..... | 44 |
| Figure 2.8: | A simplified schematic illustrating the permeation of solutes through a nanoparticulate thermo- and pH-responsive membrane (Adapted from: Zhang and Wu, 2004). ....  | 46 |
| Figure 3.1: | Mechanisms of which mucoadhesion improves oral bioavailability of drugs.....   | 48 |
| Figure 3.2: | Schematic demonstration of the mucoadhesive process (divided into the contact and consolidation phases) (Adapted from Khutoryanskiy, 2010). ....   | 51 |

|              |  |    |
|--------------|--|----|
| Figure 3.3:  | Mucoadhesive polymers, their respective concentrations and solvents employed in the preliminary design of the pH-responsive mucoadhesive layer. ....   | 57 |
| Figure 3.4:  | Schematic illustration of the textural analysis method employed to generate force: distance profiles for mucoadhesive analysis, where a) is lowering of the probe onto the mucoadhesive layer, and b) is the contact between the SGM and mucoadhesive layer. ....  | 61 |
| Figure 3.5:  | Typical textural profiles elucidating the MDF (N) and WA ( $AUC_{FD}$ ) (mJ). ....   | 63 |
| Figure 3.6:  | A comparison of a) the Maximum Detachment Force (MDF) (N) and b) Work of Adhesion ( $AUC_{FD}$ ) (mJ) of the preliminary mucoadhesive layers in acidic and alkaline pH ranges (n=3; SD < 0.028 in all cases). ....   | 64 |
| Figure 3.7:  | Variations in the ionisation state of the CHT molecules as a function of changes in the pH range (Adapted from Luo <i>et al.</i> , 2010).....  | 65 |
| Figure 3.8:  | Variations in the ionisation state of the PEC molecules as a function of changes in the pH range.....  | 66 |
| Figure 3.9:  | A comparison of a) the Maximum Detachment Force (MDF) (N) and b) Work of Adhesion ( $AUC_{FD}$ ) (mJ) of the experimental CHT-based formulations; and c) the Maximum Detachment Force (MDF) (N) and d) Work of Adhesion ( $AUC_{FD}$ ) (mJ) of the experimental PEC-based formulations (n=3; SD < 0.037 in all cases). ....                                    | 68 |
| Figure 3.10: | A comparison of the effect of PVA incorporation on a) the Maximum Detachment Force (MDF) (N) and b) Work of Adhesion ( $AUC_{FD}$ ) (mJ) of the experimental CHT-based formulations; and c) the Maximum Detachment Force (MDF) (N) and d) Work of Adhesion ( $AUC_{FD}$ ) (mJ) of the experimental PEC-based formulations (n=3; SD < 0.075 in all cases). .... | 69 |

|              |   |    |
|--------------|---|----|
| Figure 3.11: | Variations in a) the Maximum Detachment Force (MDF) (N), and b) Work of Adhesion ( $AUC_{FD}$ ) (mJ) (mJ) of experimental Formulation GT12 as a function of time (n=3; SD < 0.034 in all cases).....  | 71 |
| Figure 3.12: | A comparison of the effect of PAA substitution with PVP on a) the Maximum Detachment Force (MDF) (N) and b) Work of Adhesion ( $AUC_{FD}$ ) (mJ) of the experimental CHT-based formulations; and c) the Maximum Detachment Force (MDF) (N) and d) Work of Adhesion ( $AUC_{FD}$ ) (mJ) of the experimental PEC-based formulations (n=3; SD < 0.023 in all cases)..... | 72 |
| Figure 3.13: | Variations in a) the MDF (N), and b) the $AUC_{FD}$ (mJ) of experimental Formulation GT15 and c) the MDF (N), and d) the $AUC_{FD}$ (mJ) of experimental Formulation IT15 as a function of time (n=3; SD < 0.088 in all cases).....   | 73 |
| Figure 4.1:  | Variations in $AUC_{FD}$ of the Experimental Formulations a) 1-3; b) 4-6; c) 7-9; and d) 10-13 as a function of time (n=3; SD < 0.072 in all cases).....  | 82 |
| Figure 4.2:  | Regression plots of Area Under the Curve of the Work of Adhesion (mJ) vs. Time (hours) profile for the determination of the correlation between the experimental vs. the fitted response values.....  | 84 |
| Figure 4.3:  | Illustration of the relationship between independent variables and the response of mucoadhesive properties through a) 3-D surface plots and b) contour plots for the gastric-targeted mucoadhesive layer.....   | 85 |
| Figure 4.4:  | Residual plots of AUC of the Work of Adhesion (mJ) vs. Time (hours) profile for the gastric-targeted mucoadhesive layer of the MMDDS.....   | 87 |
| Figure 4.5:  | Optimization plots displaying factor levels and desirability values for the optimized gastric-targeted mucoadhesive layer of the MMDDS.....   | 88 |

|              |   |     |
|--------------|---|-----|
| Figure 4.6:  | Variations in $AUC_{FD}$ of the optimized gastric-targeted mucoadhesive layer as a function of time (n=3; SD < 0.071 in all cases). .....   | 89  |
| Figure 4.7:  | Variations in $AUC_{FD}$ of the Experimental Formulations a) 1-3; b) 4-6; c) 7-9; and d) 10-13 as a function of time (n=3; SD < 0.067 in all cases). .....  | 92  |
| Figure 4.8:  | Regression plots of Area Under the Curve of the Work of Adhesion (mJ) vs. Time (hours) profile for the determination of the correlation between the experimental vs. the fitted response values. ....             | 94  |
| Figure 4.9:  | Illustration of the relationship between independent variables and the response of mucoadhesive properties through a) 3-D surface plots and b) contour plots for the intestinal-targeted mucoadhesive layer. .... | 95  |
| Figure 4.10: | Residual plots of AUC of the Work of Adhesion (mJ) vs. Time (hours) profile for the intestinal-targeted mucoadhesive layer of the MMDDS. ....   | 96  |
| Figure 4.11: | Optimization plots displaying factor levels and desirability values for the optimized gastric-targeted mucoadhesive layer of the MMDDS. ....  | 97  |
| Figure 4.12: | Variations in $AUC_{FD}$ of the optimized intestinal-targeted mucoadhesive layer as a function of time (n=3; SD < 0.094 in all cases). .....  | 98  |
| Figure 4.13: | Sample preparation procedure for analysis on a Hysitron nanoTensile <sup>®</sup> analyzer. ....   | 100 |
| Figure 4.14: | Digital images of a) the optimized gastric-targeted formulation and b) the optimized intestinal-targeted formulation i) upon removal from the mould, and ii) when cut into predetermined dimensions. ....         | 105 |
| Figure 4.15: | Typical stress-strain nanotensile profile of a) the optimized gastric-targeted component with inset i) digital image illustrating insertion   |     |

|              |   |     |
|--------------|---|-----|
|              | into a capsule, and b) the optimized intestinal-targeted component, with inset ii) digital image illustrating insertion into a capsule. ....  | 107 |
| Figure 4.16: | Isotherm plots and scanning electron micrographs depicting the surface morphology of a) the optimized gastric-targeted formulation and b) the optimized intestinal-targeted formulations. ....  | 109 |
| Figure 4.17: | FTIR spectra of the native polymers a) CHT; b) PVA; and c) PVP employed in the fabrication of d) the optimized gastric-targeted component. ....   | 110 |
| Figure 4.18: | FTIR spectra of the native polymers a) PEC; b) PVA; and c) PVP employed in the fabrication of d) the optimized intestinal-targeted formulation. ....  | 111 |
| Figure 4.19: | FTIR spectra demonstrating the changes in band intensities of the formulation in relation to exposure to simulated gastro-intestinal conditions of a) the optimized gastric-targeted formulation and b) the optimized intestinal-targeted formulation with the characteristic C-O peak of PVP highlighted in red. ....                                      | 112 |
| Figure 4.20: | Schematic illustration of the proposed processes causing the fluctuations observed in the swelling and hence mucoadhesive characteristics of the formulations. ....   | 113 |
| Figure 4.21: | Graphic illustration of the variations in a) the $AUC_{FD}$ (n=3; SD < 0.094 in all cases); b) the degree of swelling (n=3; SD < 11.5% in all cases) and c) degree of erosion (n=3; SD < 7.25% in all cases) of optimized gastric-(highlighted in red) and intestinal-targeted (highlighted in green) mucoadhesive formulations as a function of time. .... | 114 |
| Figure 4.22: | Scanning electron micrographs of a) the optimized gastric-targeted formulation in simulated gastric conditions and b) the optimized intestinal-targeted formulation at various time points and magnifications in simulated intestinal conditions. ....  | 116 |
| Figure 4.23: | Magnetic resonance images of the hydration state and accompanying weight changes of the a) optimized gastric-targeted formulation and b) the optimized intestinal formulation when  |     |

|             |  |     |
|-------------|--|-----|
|             | exposed to simulated gastro-intestinal conditions at different time points. ....   | 118 |
| Figure 5.1: | Common nanofibre applications (Sourced from Huang <i>et al.</i> , 2003; Venugopal <i>et al.</i> , 2004; Lu and Ding, 2008; Sill and Von Recum, 2008).....  | 120 |
| Figure 5.2: | Schematic illustration of the horizontal electrospinning process, where $d$ = distance between capillary tip and collecting surface and $\theta$ = Capillary angle. ....   | 123 |
| Figure 5.3: | Methods of nanofibre drug incorporation and resultant fibre morphology, where the red particles indicate the drug molecules and the green indicates the nanofibre. ....  | 127 |
| Figure 5.4: | Microscopic analysis of CMC electrospun at a concentration of 3.5% <sup>w/v</sup> CMC.....   | 132 |
| Figure 5.5: | a) Microscopic and b) Scanning electron micrographic analysis at a magnification of 2400x depicting the surface morphology of PEG 4000 electrospun at a concentration of 60% <sup>w/v</sup> .....                          | 132 |
| Figure 5.6: | a) Microscopic analysis and b) Scanning electron micrographic analysis at a magnification of 8600x depicting the surface morphology of PEG 6000 electrospun at a concentration of 80% <sup>w/v</sup> .....                 | 133 |
| Figure 5.7: | a) Microscopic analysis and b) Scanning electron micrographic analysis at a magnification of 8600x depicting the surface morphology of HPC electrospun at a concentration of 15% <sup>w/v</sup> .....                      | 134 |
| Figure 5.8: | a) Microscopic; and scanning electron micrographic analysis at magnifications of b) 445x and c) 2400x depicting the surface morphology of CA electrospun at a concentration of 5% <sup>w/v</sup> . ....                    | 135 |
| Figure 5.9: | Scanning electron micrographic analysis depicting the surface morphology of the 5% <sup>w/v</sup> CAP at magnifications of a) 495x and b) 2400x; and 10% <sup>w/v</sup> CAP at magnifications of c) 480x and d) 2400x..... | 136 |



|              |  |     |
|--------------|--|-----|
| Figure 5.10: | a) Microscopic analysis and b) scanning electron micrograph at a magnification of 440x depicting the surface morphology of electrospun Eudragit <sup>®</sup> RS 100 at a 30% <sup>w/v</sup> solution.....  | 137 |
| Figure 5.11: | Scanning electron micrographs at magnifications of a) 455x and b) 2420x depicting the surface morphology of PVA electrospun at a 10% <sup>w/v</sup> concentration.....   | 138 |
| Figure 5.12: | Scanning electron micrographs depicting the surface morphology of PEO electrospun at concentrations of a) 3% <sup>w/v</sup> at a magnification of 2040x; b) 4% <sup>w/v</sup> at a magnification of 2080x and c) 5% <sup>w/v</sup> at a magnification of 2060x.....  | 139 |
| Figure 5.14: | Comparison of Diphenhydramine HCl entrapment efficiency within PVA and PEO nanofibres.....   | 140 |
| Figure 5.13: | Diphenhydramine HCl calibration curves in PBS (pH 1.2 at 37°C). .....  | 140 |
| Figure 5.15: | Scanning electron micrographs illustrating the surface morphology of PVA electrospun at concentrations of a) 6% <sup>w/v</sup> ; b) 7.5% <sup>w/v</sup> ; c) 8% <sup>w/v</sup> ; d) 10% <sup>w/v</sup> and e) 12% <sup>w/v</sup> at magnifications of 2020x, 2080x, 2420x, 2380x, 2000x respectively. ....   | 145 |
| Figure 5.16: | Scanning electron micrographs depicting the changes in surface morphology of PVA nanofibres with the addition of a) sodium chloride at 2400x; b) Tween 80 at 2380x; c) Span <sup>®</sup> 80 at 2400x, d) silicone at 2480x and e) glycerol at 2480x.....   | 146 |
| Figure 5.17: | Scanning electron micrographs depicting the surface morphology of a) an 8% <sup>w/v</sup> PVA solution; b) an 8% <sup>w/v</sup> PVA solution containing 2% <sup>w/v</sup> RIF; c) an 8% <sup>w/v</sup> PVA solution containing 2% <sup>w/v</sup> RIF and 5% <sup>w/v</sup> Tween 80; d) 10% <sup>w/v</sup> PVA solution; e) a 10% <sup>w/v</sup> PVA solution containing 2% <sup>w/v</sup> INH, and f) a 10% <sup>w/v</sup> PVA solution containing 2% <sup>w/v</sup> INH and 0.1% <sup>w/v</sup> silicone at magnifications of 2420x, 2400x, 2480x, 2380x, 2400x, and 1200x respectively..... | 150 |
| Figure 6.1:  | Crosslinking reaction occurring between PVA and Glutaraldehyde in the presence of HCl.....   | 153 |

|              |  |     |
|--------------|--|-----|
| Figure 6.2:  | Schematic illustration of the crosslinking procedure of PVA nanofibre membranes. ....  | 156 |
| Figure 6.3:  | Constructed calibration curves of a) RIF in PBS (pH 1.2; 37°C) at a wavelength of 237nm and b) INH in PBS at a wavelength of 263nm (pH 6.8; 37°C). ....  | 160 |
| Figure 6.4:  | Graphical representation of the Drug Entrapment Efficiency of RIF- and INH-loaded nanofibres. ....   | 161 |
| Figure 6.5:  | <i>In vitro</i> fractional drug release of a) Formulations 3-5 in PBS (pH 1.2) at 37°C and b) Formulations 8-10 in PBS (pH 6.8) at 37°C. ....  | 163 |
| Figure 6.6:  | Scanning electron micrographs of a) Formulation 1; b) Formulation 2; c) Formulation 3; and d) Formulation 4. ....  | 165 |
| Figure 6.7:  | Scanning electron micrographs of a) Formulation 6; b) Formulation 7; c) Formulation 8; and d) Formulation 9. ....  | 166 |
| Figure 6.8:  | Image processing of PVA nanofibre micrographs representing a) Formulation 6; b) Formulation 7; c) Formulation 3; and d) Formulation 4 in Mathematica™ 8.0 format. ....   | 168 |
| Figure 6.9:  | ImageHistograms of scanning electron micrographs representing a) Formulation 6-original, b) Formulation 7-original, c) Formulation 3-original, d) Formulation 4-original; e) Formulation 6-processed, f) Formulation 7-processed, g) Formulation 3-processed and h) Formulation 4-processed. Note that each channel is only capable of highlighting most of the pores and fibres. ....   | 170 |
| Figure 6.10: | FTIR spectra of a) Pure PVA and b) an electrospun PVA nanofibrous matrix. ....   | 171 |
| Figure 6.11: | FTIR spectra of a) INH, b) INH-loaded nanofibres (Formulation 2) and c) crosslinked INH-loaded nanofibres (Formulation 4). The red arrow indicates transmittance bands at 1380cm <sup>-1</sup> and 1030cm <sup>-1</sup> associating with C–OH stretching of PVA; the green arrow indicates transmittance band at 3348cm <sup>-1</sup> associating with O–H bonding in PVA, the blue arrow indicates transmittance band 1150cm <sup>-1</sup> associating with C–O–C groups formed through |     |

crosslinking. The areas highlighted in purple demonstrate minimal change, before and after crosslinking, to the  $-NH_2$  related transmittance bands of INH..... 172

Figure 6.12: FTIR spectra of a) RIF, b) RIF-loaded nanofibres (Formulation 7) and c) crosslinked RIF-loaded nanofibres (Formulation 9). The red arrow indicates transmittance bands at  $1347cm^{-1}$  and  $1023cm^{-1}$  associating with C–OH stretching of PVA; the blue arrow indicates transmittance band  $1150cm^{-1}$  associating with C–O–C groups formed through crosslinking. The green arrow indicates the transmittance bands at  $3348cm^{-1}$ , associated with the –OH bonding of PVA. The areas highlighted in purple demonstrate minimal change, before and after crosslinking, to the –OH related transmittance bands of RIF. .... 173

Figure 6.13: FTIR spectra of a) RIF-loaded nanofibres (Formulation 7); b) Formulation 8 (crosslinking for 6 hours); c) Formulation 9 (crosslinked for 12 hours) and d) Formulation 10 (crosslinked for 24 hours). The red arrow indicates transmittance bands at  $1023cm^{-1}$  associating with C–OH stretching of PVA; the blue arrow indicates transmittance band  $1150cm^{-1}$  associating with C–O–C groups formed through crosslinking. The green arrow indicates the transmittance bands at  $3348cm^{-1}$ , associated with the –OH bonding of PVA. The areas highlighted in purple demonstrate minimal change, before and after crosslinking, to the –OH related transmittance bands of RIF. .... 174

Figure 6.14: Typical stress-strain nanotensile profile where a) is the linear portion of the slope from which Young’s Modulus is determined; and b) depicts the fracture point of the sample..... 176

Figure 6.15: Vertical bar chart each outlining variations between the 10 formulations of a) Young’s Modulus ( $E$ ; MPa); b) Yield Stress ( $\sigma_y$  : MPa); c) Ultimate Strength ( $\sigma_u$  : MPa); d) Ultimate Strain ( $\epsilon_u$ ); e) Toughness ( $u_f$  :  $J/cm^{-3}$ ) of Formulations 1-10. .... 177

Figure 6.16: Visualization of energy minimized geometrical preferences of two PVA molecules in conjugation with a) an isoniazid molecule; and

|              |   |     |
|--------------|---|-----|
|              | b) a rifampicin molecule showcasing the intra- and inter- molecular interactions after molecular simulations in vacuum. Color codes for elements: C (cyan), O (red), N (blue) and H (white). .....  | 181 |
| Figure 6.17: | Visualization of energy minimized geometrical preferences of a) PVA-glutaraldehyde showing the double linking; b) PVA in conjugation with two glutaraldehyde molecules showcasing the intra- and inter- molecular interactions; and c) Two PVA molecules in conjugation with three glutaraldehyde molecules showcasing the intra- and inter- molecular interactions after molecular simulations in vacuum. Color codes for elements: C (cyan), O (red) and H (white). ..... | 184 |
| Figure 7.1:  | Schematic overview of the componential architecture of the MMDDS. ....  | 188 |
| Figure 7.2:  | Schematic illustration of the fabrication of the MMDDS in its entirety. The gastric- and intestinal-targeted components differed with regard to the polymer type and quantity, and crosslinking procedure.....  | 192 |
| Figure 7.3:  | Sequential digital images depicting the surgical procedure for the implantation of the chronic jugular vein catheter.....   | 197 |
| Figure 7.4:  | Sequential digital images depicting the process of dosage administration.....   | 198 |
| Figure 7.5:  | Schematic depicting the simultaneous plasma extraction method of RIF and INH.....   | 200 |
| Figure 7.6:  | A typical a) two-dimensional chromatogram and b) three-dimensional chromatogram obtained from the UPLC analysis of <i>in vitro</i> dissolution samples at a wavelength of 263nm depicting the distinct separation of INH ( $R_t=0.621$ ), RIF ( $R_t=1.903$ ) and MP ( $R_t=2.064$ ). .....   | 203 |
| Figure 7.7:  | Constructed calibration curves of a) RIF in PBS (pH1.2; 37°C) at a wavelength of 263nm and b) INH in PBS at a wavelength of 263nm (pH 6.8; 37°C). .....   | 204 |

|              |  |     |
|--------------|--|-----|
| Figure 7.8:  | Comparative <i>in vitro</i> dissolution profiles of a) rifampicin and b) isoniazid from the Rifinah <sup>®</sup> (with the digital image highlighted in red) and MMDDS (with the digital image highlighted in green) (SD < 0.0336 for all MMDDS cases; and SD < 0.155 for all Rifinah <sup>®</sup> cases). ..... | 206 |
| Figure 7.9:  | A typical a) two-dimensional chromatogram and b) three-dimensional chromatogram obtained from UPLC analysis, depicting the distinct separation of INH ( $R_t=0.674$ ), RIF ( $R_t=1.962$ ) and FUR ( $R_t=2.134$ ) at 272nm obtained from porcine plasma samples. ....   | 207 |
| Figure 7.10: | Constructed calibration curves of a) RIF and b) INH when extracted from plasma at a wavelength of 272nm. ....  | 208 |
| Figure 7.11: | Comparative plasma concentration profiles of a) RIF and b) INH with corresponding digital images of the MMDDS and Rifinah <sup>®</sup> formulations which were orally administered to a swine model (SD < 0.0473 for all MMDDS cases; SD < 0.389 for all Rifinah <sup>®</sup> cases). .....                      | 210 |

## LIST OF TABLES

---

|            |   |    |
|------------|---|----|
| Table 1.1: | The physiological effects of the GIT on an orally delivered DDS, and technologies exploiting said parameters for targeted drug delivery. ....   | 14 |
| Table 2.1: | Stimuli-responsive polymers and their drug delivery and other medical applications.....   | 35 |
| Table 2.2: | Application of thermo-responsive polymer p(NIPAAm) in ‘on-off’ valve mechanisms.....  | 40 |
| Table 2.3: | Variations in pH values in different tissue and cellular compartments (Adapted from Schmaljohann, 2006; Mania-Pramanik <i>et al.</i> , 2008).....                                       | 42 |
| Table 3.1: | Classification of various mucoadhesive polymers (Adapted from Salamat-Miller <i>et al.</i> , 2005). ....  | 53 |
| Table 3.2: | Experimental formulations evaluated for the identification of the optimal combination of mucoadhesive polymers for application in the respective pH-responsive mucoadhesive layers..... | 58 |
| Table 3.3: | Experimental formulations evaluated for the optimal PVA quantity required to impart enduring mucoadhesive properties.....   | 59 |
| Table 3.4: | Experimental formulations investigating the effects of substitution with PVP on mucoadhesive characteristics. ....  | 60 |
| Table 3.5: | Textural analysis settings for mucoadhesive test sequence. ....   | 61 |
| Table 3.6: | Periods of which the experimental formulations were able to withstand the GIT conditions. ....  | 70 |
| Table 3.7: | The identified variables and their corresponding upper and lower limits for input into the Central Composite Design. ....   | 74 |
| Table 4.1: | Design points employed in the generation of the 2 factor, face-centred central composite design.....  | 80 |

|             |   |     |
|-------------|---|-----|
| Table 4.2:  | Central composite design template of the 13 statistically derived formulations for the fabrication of the gastric-responsive mucoadhesive layer of the MMDDS. ....    | 80  |
| Table 4.3:  | Measured responses of the experimental runs for the optimization of the gastric-targeted mucoadhesive layer of the MMDDS. ....  | 83  |
| Table 4.4:  | Estimated p-values for the response: AUC of the WA: Time profile. ....  | 87  |
| Table 4.5:  | Comparison of the fitted and experimental values of the response parameter. ....  | 88  |
| Table 4.6:  | Central composite design template of the 13 statistically derived formulations for the fabrication of the intestinal-responsive mucoadhesive layer of the MMDDS. .... | 90  |
| Table 4.7:  | Measured responses of the experimental runs for the optimization of the gastric-targeted mucoadhesive layer of the MMDDS. ....  | 93  |
| Table 4.8:  | Estimated p-values for the response: AUC of the WA: Time profile. ....  | 97  |
| Table 4.9:  | Comparison of the fitted and experimental values of the response parameter. ....  | 98  |
| Table 4.10: | Parameters and settings employed during degassing and analysis of the optimized mucoadhesive layers. ....   | 101 |
| Table 4.11: | Image acquisition parameters applied during magnetic resonance imaging using MARAN-ip. ....   | 104 |
| Table 4.12: | Experimental values obtained from nanotensile analysis of the optimized gastric-targeted mucoadhesive layer. ....   | 106 |
| Table 4.13: | Quantitative properties of the optimized formulations' surface structure. ....  | 108 |
| Table 5.1:  | Polymers electrospun drug for delivery applications (Adapted from Sill and Von Recum, 2008). ....   | 121 |
| Table 5.2:  | Effects of electrospinning parameters on fibre morphology. ....   | 124 |

|            |  |     |
|------------|--|-----|
| Table 5.3: | Polymers and their respective parameters investigated for the development of a nanofibrous matrix. ....            | 129 |
| Table 5.4: | Effects of excipient addition on the viscosity of PVA solutions.....   | 147 |
| Table 6.1: | Polymers crosslinked with GA vapours and their intended application.....   | 153 |
| Table 6.2: | Electrospinning parameters of INH- and RIF-loaded nanofibres.....  | 155 |
| Table 6.3: | Crosslinking variables of non-drug and drug-loaded PVA nanofibres. ....  | 155 |
| Table 6.4: | Parameters employed to determine DEE of drug-loaded PVA nanofibres. ....   | 156 |
| Table 6.5: | Effect of drug and/or excipient addition on the viscosity of PVA solutions employed during electrospinning.....    | 175 |
| Table 6.6: | Experimental values obtained from nanotensile analysis of the crosslinked and non-crosslinked fibres.....          | 176 |
| Table 6.7: | Calculated energy parameters (kcal/mol) of polymer-crosslinker and drug loaded crosslinked-polymer assemblies..... | 181 |
| Table 7.1: | UPLC Gradient method parameters for the simultaneous quantification of isoniazid and rifampicin. ....              | 195 |



## LIST OF EQUATIONS

---

|                |  |     |
|----------------|--|-----|
| Equation 3.1:  | Mathematical relationship describing the Work of Adhesion between two interfaces.....                              | 61  |
| Equation 4.1:  | Regression equation generated for the optimization of the gastric-targeted mucoadhesive layer of the MMDDS .....   | 87  |
| Equation 4.2:  | Regression equation generated for the optimization of the intestinal-targeted mucoadhesive layer of the MMDDS..... | 97  |
| Equation 4.3:  | Determination of PBS uptake.....   | 102 |
| Equation 4.4:  | Determination of Degree of Erosion.....  | 103 |
| Equation 5.1:  | Determination of Drug Entrapment Efficiency .....  | 130 |
| Equation 6.1:  | MMER model for the potential energy factor determination in molecular complexes.....                               | 178 |
| Equation 6.2:  | Global energy relationship for PVA.....  | 179 |
| Equation 6.3:  | Global energy relationship for PVA-PVA.....  | 179 |
| Equation 6.4:  | Global energy relationship for INH.....  | 179 |
| Equation 6.5:  | Global energy relationship for PVA2-INH.....   | 179 |
| Equation 6.6:  | Global energy relationship for RIF .....   | 179 |
| Equation 6.7:  | Global energy relationship for PVA2-RIF .....  | 179 |
| Equation 6.8:  | Global energy relationship for GA.....   | 179 |
| Equation 6.9:  | Global energy relationship for PVA2-GA3.....   | 179 |
| Equation 6.10: | Young's Modulus Equation 1 .....   | 180 |
| Equation 6.11: | Young's Modulus Equation 2 .....   | 180 |
| Equation 6.12: | Relationship between Young's Modulus and molar volume .....  | 180 |
| Equation 6.13: | Relationship between cohesive energy density and molar volume.....   | 180 |
| Equation 6.14: | Sprigg's Equation .....  | 182 |
| Equation 6.15: | Young's Modulus in relation to the quantity of crosslinks .....  | 185 |

## LIST OF ABBREVIATIONS

---

|                   |   |
|-------------------|---|
| 3-FR:             | 3-formyl rifamycin                                      |
| ACN:              | acetonitrile  |
| AMBER:            | Assisted Model Building and Energy Refinements          |
| ANOVA:            | Analysis of Variance                                    |
| ARVs:             | Antiretroviral drugs                                    |
| ATR-FTIR:         | Attenuated Total Reflectance Fourier-Transform Infrared |
| AUC:              | Area under the Curve                                    |
| BET:              | Brunauer-Emmett-Teller                                  |
| BJH:              | Barrett-Joiner-Halenda                                  |
| CA:               | cellulose acetate                                       |
| CAP:              | cellulose acetate phthalate                             |
| CED:              | Cohesive energy density                                 |
| CHT:              | chitosan  |
| $C_{max}$ :       | maximum plasma concentration                            |
| CMC:              | carboxymethylcellulose                                  |
| CO <sub>2</sub> : | carbon dioxide  |
| CYP3A4:           | Cytochrome P450 (CYP) enzyme type 3A4                   |
| DDS:              | drug delivery system                                    |
| DEE:              | drug entrapment efficiency                              |
| DNA:              | deoxyribonucleic acid                                   |
| DoE:              | Design of Experiments                                   |
| DPH:              | diphenhydramine HCl                                     |
| FCCCD:            | face-centered central composite design                  |
| FTIR:             | Fourier-Transform Infrared                              |
| FUR:              | furosemide  |
| FW:               | formic water  |
| GA:               | glutaraldehyde  |
| GBI:              | Global Business Intelligence                            |
| GIT:              | gastro-intestinal tract                                 |
| GORD:             | gastro-oesophageal reflux disease                       |
| GR:               | gastro-retentive  |
| G-CSF:            | recombinant human granulocyte-stimulating factor        |
| HCL:              | hydrochloric acid                                       |
| HIV:              | human immunodeficiency virus                            |

|            |   |
|------------|---|
| HPC:       | hydroxypropyl cellulose                         |
| IBS:       | irritable bowel syndrome                        |
| IHZ:       | isonicotinyl hydrazone                          |
| INH:       | isoniazid                                       |
| IPN:       | interpenetrating polymeric network              |
| LCST:      | lower critical solution temperature             |
| MDDSs:     | mucoadhesive drug delivery systems              |
| MDF:       | maximum displacement force                      |
| MMDDS:     | multi-component membranous drug delivery system |
| MMER:      | molecular mechanics energy relationship         |
| MP:        | methylparaben                                   |
| MRI:       | Magnetic Resonance Imaging                      |
| $M_w$ :    | molecular weight                                |
| n:         | sample size                                     |
| NAW:       | narrow absorption window                        |
| $N_2$ :    | nitrogen  |
| NT:        | nanotensile                                     |
| OROS:      | osmotic-controlled release oral delivery system |
| OVAT:      | one-variable-at-a-time                          |
| PAA:       | poly(acrylic acid)                              |
| PBS:       | phosphate buffered saline                       |
| PDA:       | photodiode array                                |
| PEC:       | pectin  |
| PEG:       | poly(ethylene glycol)                           |
| PEO:       | poly(ethylene oxide)                            |
| P(EVAL):   | poly(ethylene-co-vinyl alcohol)                 |
| P(NIPAAm): | poly(N-isopropylacrylamide)                     |
| PVA:       | poly(vinyl alcohol)                             |
| PVDF:      | Polyvinylidene fluoride                         |
| PVP:       | polyvinylpyrrolidone                            |
| $R^2$ :    | correlation coefficient                         |
| RIF:       | rifampicin                                      |
| RSM:       | response surface methodology                    |
| SD:        | standard deviation                              |
| SEM:       | scanning electron microscope                    |
| SGM:       | simulated gastric membrane                      |
| SIM:       | simulated intestinal membrane                   |

|                  |   |
|------------------|---|
| SPE:             | solid phase extraction                  |
| T <sub>g</sub> : | glass transition temperature            |
| TB:              | tuberculosis                            |
| TIPS:            | thermal-induced phase separation        |
| TMC:             | trimethylated chitosan chloride         |
| UPLC:            | ultra performance liquid chromatography |
| VIPS:            | vapour-induced phase separation         |
| WA:              | work of adhesion                        |
| WAC:             | water absorption capacity               |

# CHAPTER 1

## INTRODUCTION AND MOTIVATION FOR STUDY

---

*“To raise new questions, new possibilities, to regard old problems from a new angle, requires creative imagination and marks real advance in science.”*

- *Albert Einstein (1879-1955)*

### 1.1 Background to the Study

With new discoveries and further improvement each year, drug delivery is a quickly progressing and rapidly advancing pharmaceutical industry. Innovation in the pharmaceutical industry has led to the development of numerous technologies in drug delivery, leading to new and improved methods of drug delivery such as implantable systems, inhalation therapy, and transdermal, intranasal, ocular, oral, buccal and sublingual delivery systems (Leung and Ko, 2011). Global Business Intelligence (GBI) Research has reported that oral drug delivery controlled 52% (R49 billion) of the global drug delivery market share in 2009 and is expected to increase to R92 billion by 2016 (GBI Research Report, November, 2010). This rapid increase can be attributed to the fact that the oral route of drug administration is one of the most favoured and extensively employed methods of drug delivery in the pharmaceutical industry by both the patients and pharmaceutical manufacturers alike (Grabovac *et al.*, 2008).

Factors promoting oral drug delivery includes the convenient and natural mode of administration; versatility in application; the avoidance of pain, discomfort and risk of infection as associated with injections; all contributing to higher patient compliance, and ultimately, lower costs (Sastry *et al.*, 2000; Yamagata *et al.*, 2006; Grabovac *et al.*, 2008). Furthermore, the relatively large fluid volume available, the increased mucosal area available for absorption and the profuse blood supply to the gastric mucosa aids the absorption of many drugs (Helliwell, 1993).

Although oral drug delivery is an easy and convenient means of administering drugs and bioactives to the body, there are limitations on which drugs can be delivered through this route due to the physiological makeup of the gastro-intestinal tract (GIT), as illustrated in Figure 1.1. In addition, the bioavailability of drugs or bioactives delivered through the oral route remains questionable. Apart from having a relatively poor bioavailability in

comparison to intravenous and inhaled dosage forms, drug bioavailability of oral formulations differs in the presence or absence of food and other drugs within the GIT; between patients such as geriatrics or paediatrics; and can be drastically affected by the presence of disease states such as constipation, diarrhoea or renal disease. Such differences in bioavailability can lead to serious side effects, toxicity or treatment failure (Thomas, 1995; González Canga *et al.*, 2010; Mason; 2010; Zvonar *et al.*, 2010).

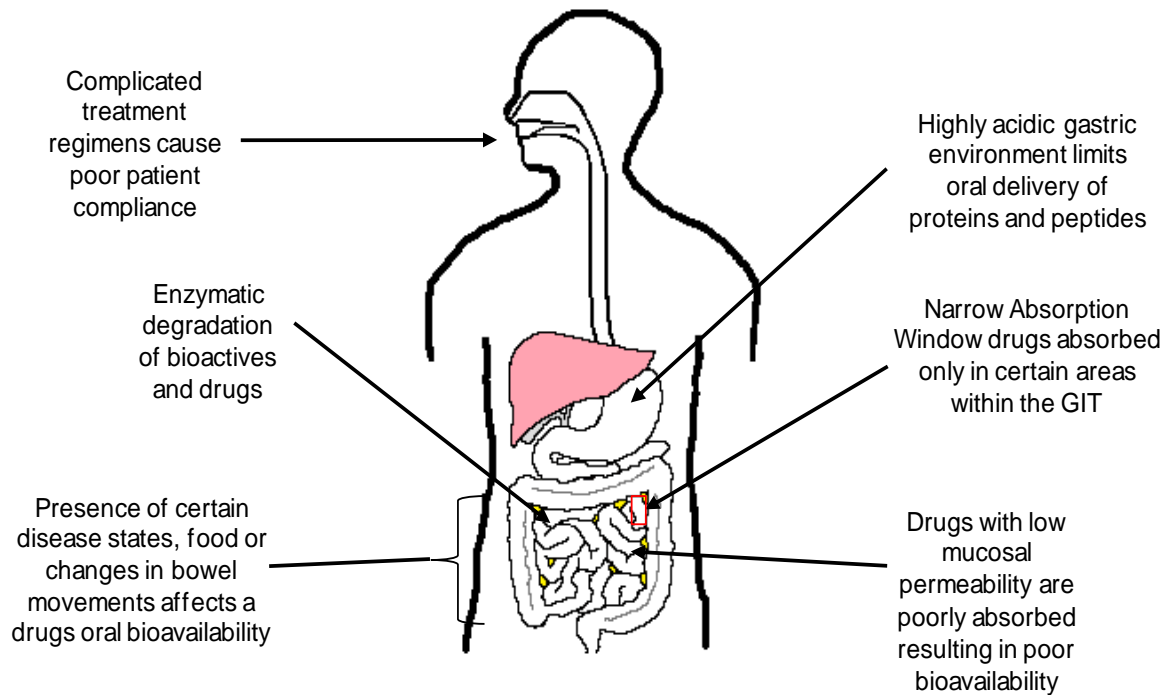


**Figure 1.1:** Schematic illustration of the GIT, including the limitations to oral drug delivery.

In a highly competitive environment, there is an ongoing race for pharmaceutical industries to develop new drugs boasting improved bioavailabilities with a reduced side effect profile. However, “pharmagenesis” or the discovery of a new drug is a costly and time consuming process. The cost, the bulk of which originates from extensive research and development, contributes to the escalating prices of drug products so pharmaceutical companies can recover their expenses. With international governments pressurising pharmaceutical industries to regulate these prices, there is no incentive for pharmaceutical industries to spend large amounts of money producing drugs without salvaging their costs. Furthermore, despite extensive testing and regulation, the possibility of detecting unpredicted side effects is present even after years of use, while the risk and uncertainty associated with marketing a new drug product hinders new drug development (Barrett, 1999; Sekel, 1999).

It is therefore not surprising that many pharmaceutical technology researchers have shifted from new drug discovery and development, to “re-inventing” established drugs by redesigning dosage forms to provide safer, more effective or convenient alternatives, hence the term “new drugs from old”. Crowley and Martini (2004) highlighted the reformulation strategies that are currently employed to enhance the efficacy of existing drugs, which include improving absorption or prolonging the effects of drugs, enhancing patient convenience or designing novel ways to administer a drug (Speers, 1999; Crowley and Martini, 2004; Mythri *et al.*, 2011). In this manner, drug delivery systems can be engineered to realise the full potential of existing (old) drugs without incurring hefty costs.

The bioavailability of orally administered drugs is principally dependant on the transit of a drug delivery system (DDS) through the GIT. Conventional oral DDS are transported through the GIT, releasing drug into non-specific regions within the GIT (Helliwell, 1993). If the drug is not released in sufficient quantities at the site of absorption, the drug will not reach effective plasma concentrations to achieve the desired therapeutic effect (Davis, 2005). Oral bioavailability is further compromised in Narrow Absorption Window Drugs (NAW), where these drugs are absorbed at only specific sites within the GIT. Thus many drugs are poorly absorbed (NAW drugs) or are sensitive to gastric juices and enzymes (proteins and peptides), and therefore conventional oral drug delivery systems need to be modified or novel drug delivery systems need to be developed in order to effectively administer these drugs (Shen *et al.*, 2002). In a bid to improve oral bioavailability, Figure 1.2 depicts how researchers have aimed at developing oral DDS based on mechanical protection of gastric sensitive agents from the harsh gastric environment with the use of microparticles (Shen *et al.*, 2002), polymers acting as protective carriers (Dupeyrón *et al.*, 2005), liposomes, biochemical protection with the aid of enzyme inhibitors (Youn *et al.*, 2006; Grabovac *et al.*, 2008) or by increasing gastric residence time of the DDS (Davis, 2005).

Apart from the physiological setbacks to oral drug delivery, poor patient compliance across multiple indications, has drastically affected therapeutic outcomes. Poor patient compliance due to various factors including the ease of drug administration, complex dosing regimens and severity of side-effects, has severe consequences such as bacterial and viral resistance in infectious diseases i.e. TB and HIV treatment (Kruk *et al.*, 2006). Studies conducted by Dankwerts and co-authors, and Prakabaran and co-authors have investigated simple dosing, where a single dosage form has the ability to deliver multiple drugs for an extended period of time, thus decreasing dosage frequency and quantity (Dankwerts *et al.*, 2003; Prakabaran *et al.*; 2004).

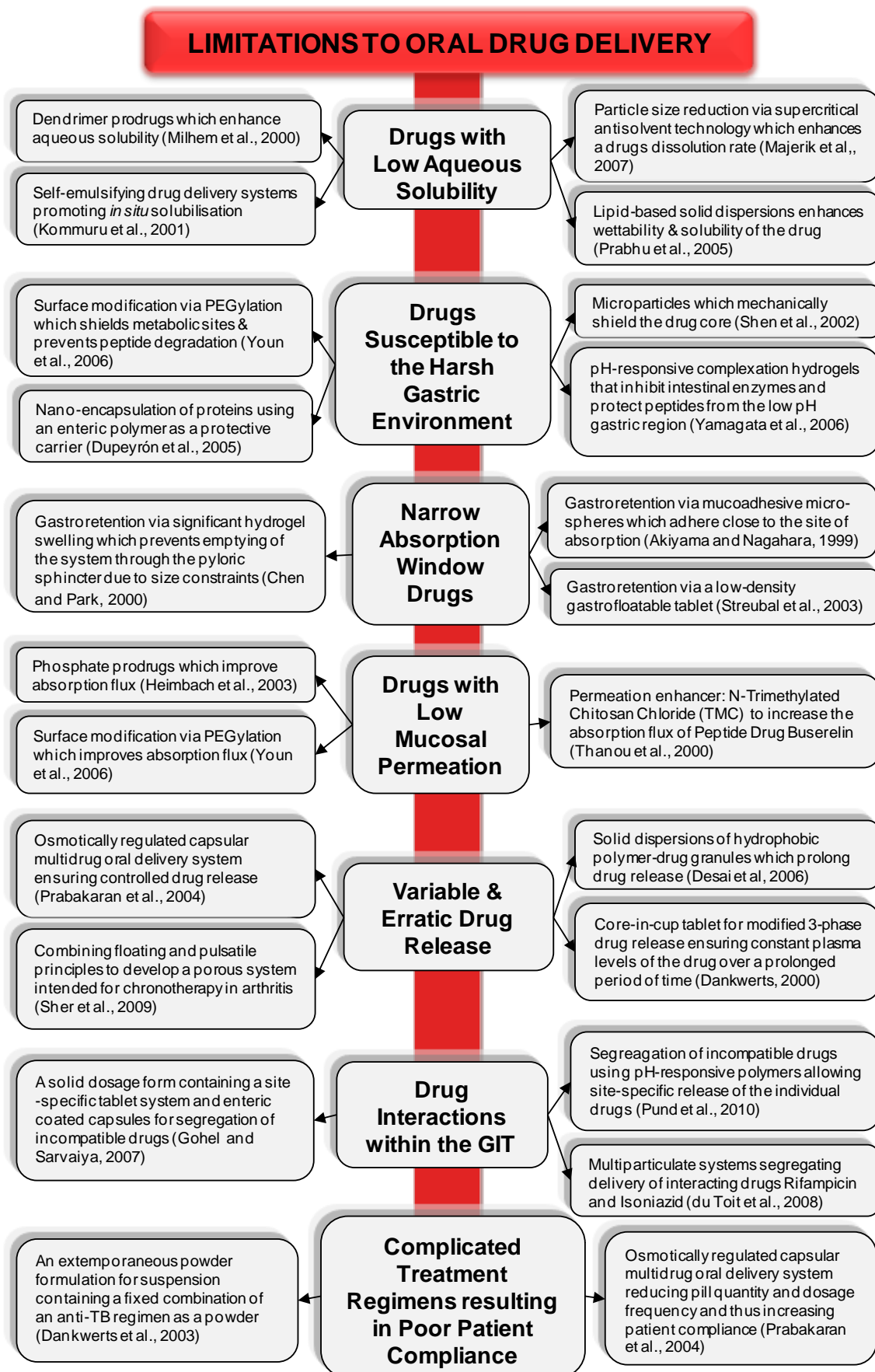


**Figure 1.2:** Various studies which have aimed to overcome the limitations of oral drug delivery.



Prolonged release systems would result in the extended release of drug into the systemic circulation over an extended duration of time, thus achieving sustained and therapeutically effective concentrations of the drug, which can be easily achieved through crosslinking (Tanaka *et al.*, 2006). During crosslinking, a covalent bond is formed between the crosslinking agent and polymeric chains. When polymeric chains are crosslinked, there is a decrease in the solubility of the polymer network due to slower chain relaxation within the polymeric network upon hydration, hence retarding drug release (Hennink *et al.*, 2002; Rastogi *et al.*, 2007). However, oral prolonged release formulations may provide lower bioavailability as compared to immediate release formulations, as drug release from the prolonged release formulations is not completed during transit of the delivery system through the GIT (Nakamura *et al.*, 2006). Manipulating the prolonged drug delivery system to be gastroretentive can overcome this challenge by increasing the GIT transit time of the system, thus allowing for complete release of drug or bioactives from the DDS.

As reported by Davis (2005), there are currently two methods based on the concept of increasing gastric residence time that have been proposed to improve the oral bioavailability of drugs,

- i) By slowing down gastric transit through the GIT with the aid of mucoadhesive systems, and/or
- ii) Attempting to retain the drug formulation above the absorption window through gastro-retention (Davis, 2005).

These orally delivered mucoadhesive systems are able adhere to the mucosa within the GIT, ensuring that there is a constant concentration of drug at the site of absorption thus maintaining therapeutically effective plasma concentrations of the drug. Bioavailability is improved as the time available for absorption is increased (Grabovac *et al.*, 2008; Surana and Kotecha, 2010).

Mucoadhesive drug delivery systems include multiparticulate mucoadhesive microspheres (Patel *et al.*, 2007), mucoadhesive tablets (Guggi *et al.*, 2003) and mucoadhesive membranes (Eaimtrakarn, 2002). In multiparticulate mucoadhesive systems, the entire particle surface is exposed to the surrounding gastric and intestinal fluid and therefore there is a loss of drug into the surrounding luminal fluid and certain enzyme sensitive agents may not obtain sufficient protection from proteolytic degradation (Shen *et al.*, 2002). Mucoadhesive tablets have shown to have difficulty adhering to the stomach wall (Davis, 2005), and thus drug does not enter the systemic circulation and will

not achieve the desired therapeutic effect. A membranous DDS as opposed to other mucoadhesive systems has the advantage of being layered with the incorporation of various excipients into different layers, where the layers of the system can perform different functions, including mucoadhesion, drug encapsulation, and protection of the drug delivery system from enzymes and biodegradation in the GIT (Shen *et al.*, 2002), and therefore the DDS proposed in this dissertation will consist of a multi-layered membranous system. Several studies have of late successfully improved the oral bioavailability of insulin (Grabovac *et al.*, 2008), low molecular mass heparins (Schmitz *et al.*, 2005), recombinant human granulocyte-stimulating factor (G-CSF) (Eaimtrakarn *et al.*, 2002) with the use of multi-layered membranous DDS. These studies have shown promising results in further improving a drug's oral bioavailability.

A recent advance in drug delivery technology is the application of 'smart', 'active' or stimuli-responsive polymeric materials, which are capable of responding in any desirable manner to a change in temperature, pH, electric and/or magnetic fields (Lue *et al.*, 2008; Kumar, 2009). These polymers that offer altered physicochemical properties under differing environmental conditions can be utilised in drug delivery systems such as surgical implants, scaffolds for tissue engineering, supports for *in vitro* cell culture and biotechnological screening, as well as in drug delivery systems (Anseth *et al.*, 2002; Tang *et al.*, 2003; Packhaeuser *et al.*, 2004; Furth *et al.*, 2007; Nagahama *et al.*, 2008; Stamatialis *et al.*, 2008). In drug delivery, stimuli-responsive polymers may be used to target drugs to specific sites (site affected by disease or site of absorption) in the body or as a 'smart' surface which can be switched from an adhesive to a non-adhesive state or from a hydrophilic to a hydrophobic state and thus can swell or shrink, thereby controlling properties such as drug release. The changes are reversible which implies that the polymer is capable of returning to its initial state as soon as the trigger is removed (Stayton *et al.*, 2005; Schmaljohann, 2006).

Targeting of the DDS to specific regions within the GIT can potentially improve the bioavailability of NAW drugs or drugs and bioactives which are absorbed principally in the stomach (i.e. basic drugs) or intestine (i.e. acidic drugs), and can provide segregated drug delivery in the case where multiple drugs are delivered in one system (Nakamura *et al.*, 2006). Due to the physiological pH changes occurring along the GIT, pH is commonly identified as a stimulus to target drug delivery with the use of pH-responsive polymers in oral drug delivery. Polymer swelling and changes in mucoadhesive characteristics in response to pH changes have been employed to induce the controlled and targeted release of drugs and bioactives at specific sites within the GIT (Schmaljohann, 2006).

Several studies have exploited the use of targeted or site-specific drug delivery to prevent any deleterious drug-drug interactions that occur amongst certain bioactives within a given treatment regimen thus providing segregated drug delivery within the GIT and consequently, improved oral bioavailability. Segregation is achieved because drugs can be targeted with the aid of pH-responsive polymers, to differing pH ranges within the GIT, thereby isolating the release of the individual drugs and thus preventing any drug interactions (Gohel and Sarvaiya, 2007; du Toit *et al.*, 2008; Pund *et al.*, 2010). pH-responsive polymers were employed in this study to ensure that the differing components of the membranous system are targeted to specific regions of the GIT, i.e. the gastric or intestinal region, and thus segregating and prolonging drug delivery by adhering to the mucosal surface within that region only.

Membranes intended for drug delivery can be formulated by a range of methods including phase separation (Sun *et al.*, 2007a; Kao *et al.*, 2008), electrospinning (Kim *et al.*, 2007, Sill and Von Recum, 2008), foaming (Krause *et al.*, 2002; Matsuyama *et al.*, 2002; Sun *et al.*, 2007a), particle leaching (Sanguanruksa *et al.*, 2004; RoyChowdhury and Kumar, 2005), emulsion freeze-drying (Ho *et al.*, 2004; Cheng *et al.*, 2008) and sintering (Rezwan *et al.*, 2006; Stamatialis *et al.*, 2008), the methods which are further discussed in *Chapter 2* of the present dissertation. The type of the polymer and method employed, as well as the conditions during formulation determines the final morphology of the membranes (Witte *et al.*, 1996; Altinkaya *et al.*, 2005). Several studies have examined the possibility of utilizing electrospun membranous matrices as a controlled release system for the delivery of various drugs including antibiotics, anti-cancer drugs and vitamins in addition to tissue engineering applications for the delivery of proteins and DNA (Luu *et al.*, 2003; Kim *et al.*, 2004; Casper *et al.*, 2005; Chew *et al.*, 2005; Zeng *et al.*, 2005a; Taepaiboon *et al.*, 2007; Sill and Von Recum, 2008). Electrospun fibrous matrices possess a three dimensional porous structure ideal for controlling drug delivery due to its relatively large surface area. Controlling parameters during electrospinning influences drug release patterns, and hence, electrospun membranous matrices can be customized to achieve desired drug release patterns (Kim *et al.*, 2007; Sill and Von Recum 2008).

To overcome many of the challenges associated with oral drug delivery, the drug delivery system proposed in the present dissertation is designed to deliver multiple drugs of differing solubility, targeted to differing regions within the GIT for a prolonged period of time in a prolonged release manner. The proposed Multi-component Membranous Drug Delivery System (MMDDS) consists of a pH-responsive mucoadhesive layer allowing for site-specific drug delivery, a crosslinked electrospun layer encapsulating drug, and a

water insoluble backing layer offering mechanical protection. In order to orally deliver the MMDDS, it will be encapsulated within a capsule shell.

## 1.2 Rationale and Motivation for the Study

An ideal drug delivery system aims to deliver drug to a specific site, for a particular period of time with a specific drug release pattern. Conventional drug delivery systems often deliver drug in a peak-to-trough pattern, with the peaks usually being above the required dose, followed by ineffective plasma concentrations. A successful therapeutic outcome is dependent on patient compliance, and where adverse effects due to high plasma drug concentrations are experienced by patients, patient compliance is threatened, causing potential setbacks to successful treatment (Stamatialis, 2008). Formulating a membranous DDS, as shown in Figure 1.3, is beneficial as the challenges associated with conventional drug delivery systems can be overcome by formulating a crosslinked, pH-responsive, mucoadhesive membranous DDS.

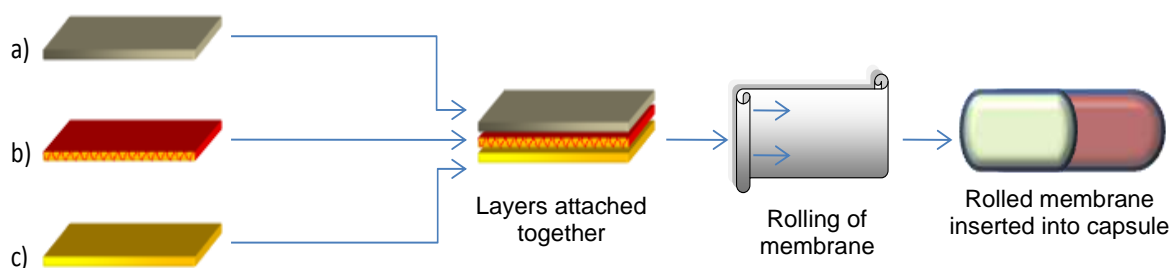


**Figure 1.3:** Componential configuration of multilayered mucoadhesive archetype, where a) represents the protective coating; b) represents the electrospun drug-loaded layer, containing the respective drugs; and c) represents the stimuli-responsive mucoadhesive layer, specific to the gastric or intestinal targeted component. Both components are then rolled and inserted into a capsule.

Figure 1.3 represents a) a water insoluble protective coat protecting the MMDDS from the harsh gastric environment, b) a crosslinked, electrospun drug containing layer containing drug encapsulated within nanofibres, c) a pH-responsive mucoadhesive layer providing site-specific mucoadhesion. pH-responsive polymers incorporated within this layer targets the system to a specific area of the GIT. In an attempt to improve oral drug bioavailability, the postulated MMDDS employed the use of the technology outlined in Figure 1.4 to develop a single dosage form for multiple and segregated drug delivery.

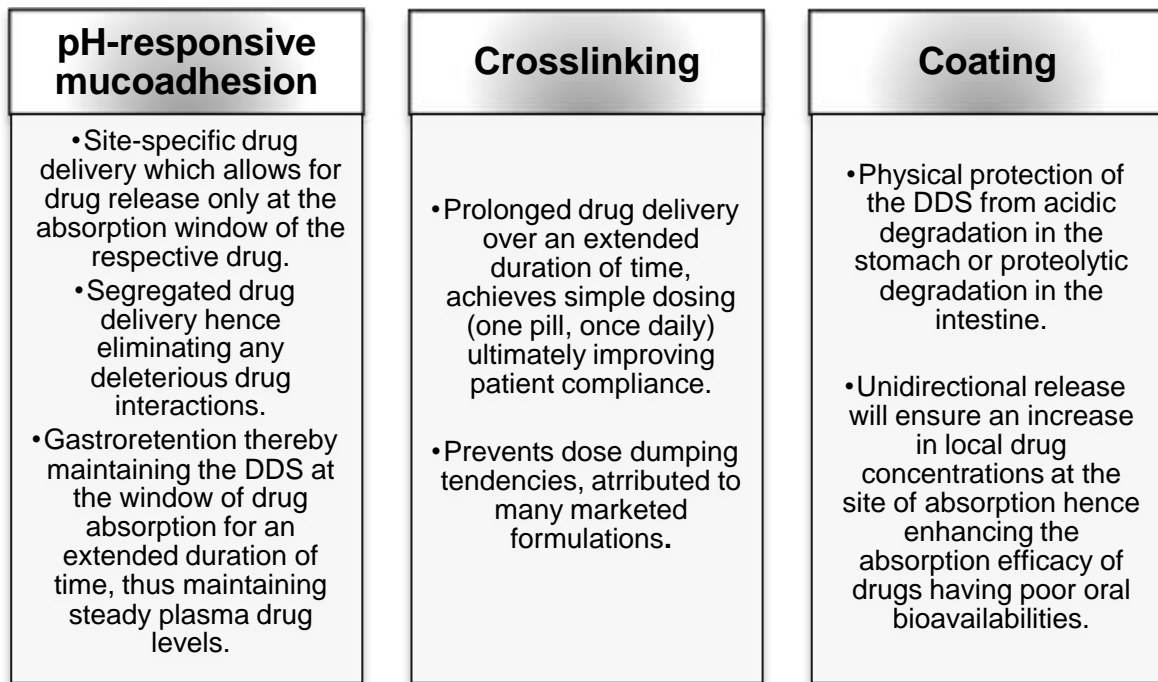


**Figure 1.4:** Technology applied in the development of the MMDDS thereby improving oral drug bioavailability.

The use of site-specific drug delivery to prevent deleterious drug interactions within the GIT has been outlined previously. Even within prescribed treatment regimens, deleterious drug interactions occur which ultimately affects the oral bioavailability of one or more drugs. These drugs are often administered a few hours apart to ensure complete absorption of the one drug before the other is administered. Subsequently, complex dosing regimens are developed and patient compliance is threatened (Shishoo *et al.*, 2001; Gohel and Sarvaiya, 2007; du Toit *et al.*, 2008; Tanno *et al.*, 2008; Pund *et al.*, 2010; Pund *et al.*, 2011).

One such example includes anti-tuberculosis (TB) therapy, where standard treatment warrants the use of isoniazid (INH) and rifampicin (RIF) concurrently. However, in acidic conditions, RIF is hydrolysed in the upper gastric region of the GIT into a poorly absorbable form, 3-formyl rifamycin (3-FR) (via a pseudo second order reaction), which INH interacts with, forming isonicotinyl hydrazone (IHZ). IHZ, being unstable is then reverted back to INH and 3-FR following a pseudo first order reaction as illustrated in Figure 1.5. RIF bioavailability is compromised because all the reactions in the illustrated sequence favours the formation of 3-FR (faster initial degradation of RIF into 3-FR combined with a faster first order reaction of the IHZ to INH and 3-FR than the second order reaction where INH forms the IHZ), and there is thus further increase in the formation of the 3-FR, ultimately threatening RIF bioavailability (Singh *et al.*, 2000a; Singh

*et al.*, 2000b; Singh *et al.*, 2001; Shishoo *et al.*, 2001; Mohan *et al.*, 2003; Mariappan *et al.*, 2004). This compromised RIF bioavailability has the potential to lead to multi-drug resistant strains of TB, a serious setback in global eradication of the disease (Singh *et al.*, 2001; Mariappan and Singh, 2003).

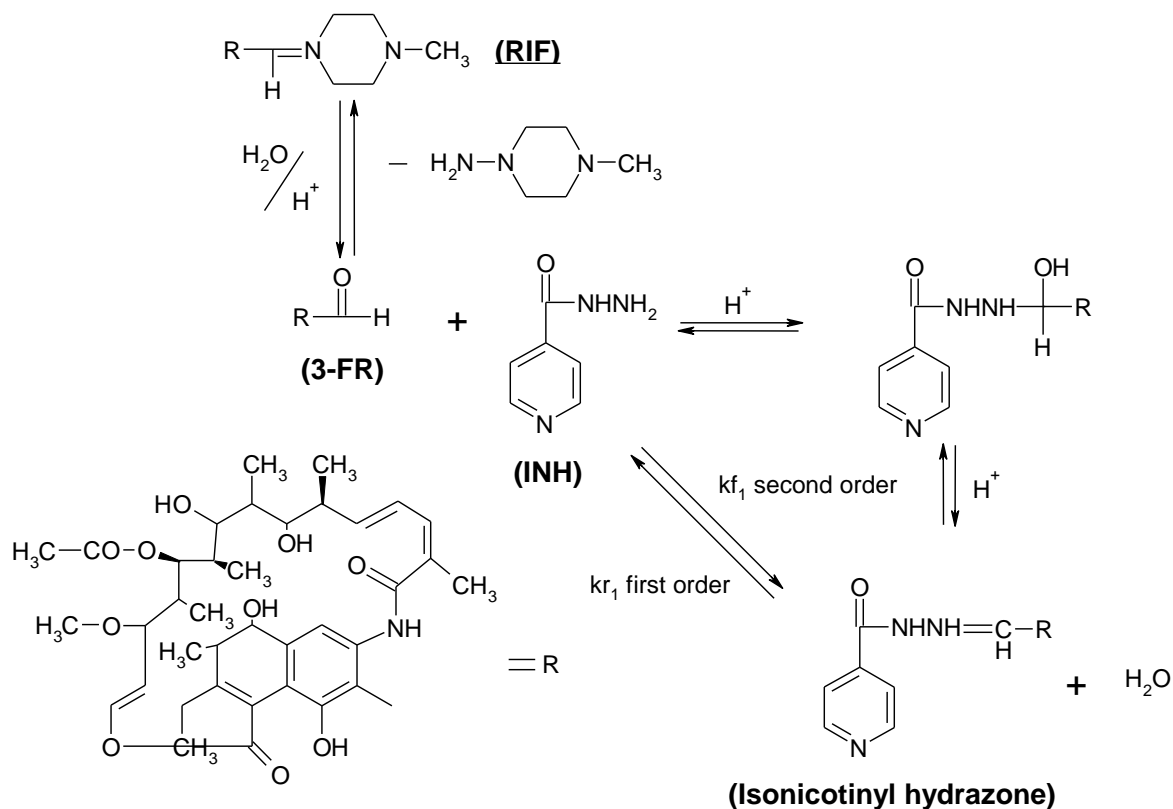


**Figure 1.5:** Decomposition mechanism of rifampicin in the presence of isoniazid within the acidic conditions of the stomach.

Mariappan and Singh (2003) investigated the variations in absorption of RIF and INH along the GIT and their findings revealed that RIF is well absorbed from the stomach because of its high solubility between pH 1 and 2, while INH being relatively poorly absorbed from the stomach, is well absorbed from all 3 segments of the intestine (Mariappan and Singh; 2003). Site-specific drug delivery would negate the above, and other interactions, from occurring, even though both drugs are administered in a single dosage form (Gohel and Sarvaiya, 2007; du Toit *et al.*, 2008; Pund *et al.*, 2010). These drugs would therefore benefit from such site-specific drug delivery, by targeting the drug to its respective absorption window. The proposed MMDDS can successfully achieve such segregated drug delivery, whereby the system releases RIF in the stomach, while, to ensure the intestinal delivery of INH, the system retards INH release in the stomach. Furthermore, the MMDDS has potential in wide range of other drug delivery applications, illustrated in Figure 1.6.

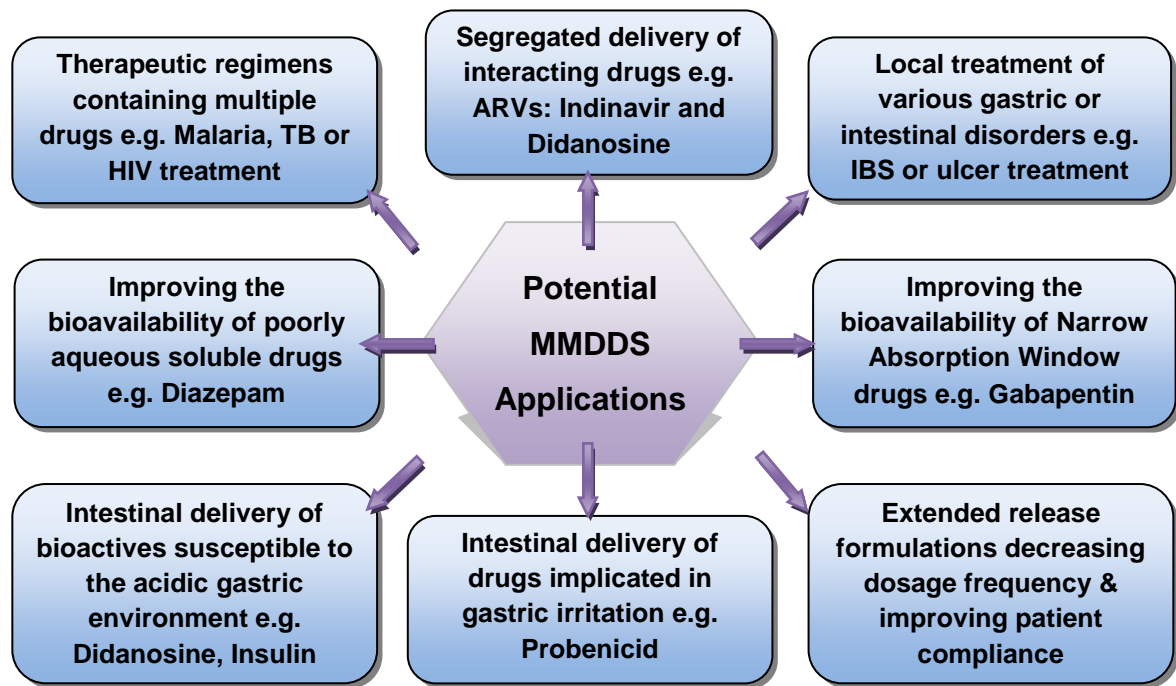


**Figure 1.6:** Prospective applications of the MMDDS.

In terms of local ulcer treatment, the advantages of employing the MMDDS to deliver the indicated drugs are two-fold. Duodenal ulcers can be treated with a combination of drugs including a proton pump inhibitor (omeprazole) or a Histamine<sub>2</sub> receptor antagonist (ranitidine) which require delivery to the stomach lining (to decrease acid secretion) in combination with a locally acting agent such as bismuth subcitrate or sucralfate which require release at the site of the ulcer to promote healing of the ulcer wound. Therefore the MMDDS would achieve site-specific drug delivery of both drugs, as well as improve patient compliance by offering a simple dosage form that contains both drugs. A didanosine/ketoconazole combination can also be delivered using the MMDDS in order to avoid the drug interaction occurring between these drugs. Didanosine, employed in antiretroviral (ARV) therapy, is highly susceptible to the acidic environment of the upper GIT region, and is thus prepared as a buffered formulation containing an antacid which improves the oral bioavailability of didanosine. Due to their suppressed immune systems, HIV-positive patients are commonly afflicted with infections, for which antifungals like ketoconazole are often prescribed. Ketoconazole absorption is limited by the presence of the antacids present in didanosine formulations, and hence requires segregation of administration by at least two hours (Gibbon, 2005). By incorporating ketoconazole into the gastric-targeted component of the MMDDS, ketoconazole absorption would be improved in the upper gastric region of the GIT, while by being incorporated in the intestinal component of the MMDDS; didanosine delivery will be limited to the intestine, thus protecting it from the harsh gastric environment.

### **1.3 Consideration of the Gastrointestinal Physiology in the Development of a Smart Drug Delivery System Intended to Enhance Oral Bioavailability**

As of late, the GIT physiology is being considered as a key parameter which affects the release and absorption, and hence bioavailability, of orally delivered drugs. Previously, the GIT physiology did not denote how drug delivery systems were designed to ensure optimal bioavailability of orally delivered drugs. It should be noted that dosage forms fabricated or modelled without comprehending and understanding the complexity of the GIT physiology and its ramifications on oral drug delivery systems, will not be functional and/or behave in a consistent manner in terms of the oral bioavailability of drugs. Conventional drug delivery systems have of late been reformed with the advent of newer scientific data and technologies. Such novel DDS are able to enhance oral bioavailability by exploiting the conditions of the GIT, consequently improving the therapeutic efficacy of many existing drugs. Not only will comprehension of the GIT environment allow for better dosage form design, it will also augment the predictability of dosage forms by improving *in vitro* and pre-clinical *in vivo* testing thus allowing for better *in vitro-in vivo* correlations. Furthermore, novel areas and opportunities in oral drug delivery can be brought to light, making oral drug delivery safer, easier and more effective (McConnel *et al.*, 2008).

#### **1.3.1 The GIT physiology and its ramifications on drug delivery**

In simple terms, the GIT or gut is essentially a tube, nine metres in length, that runs through the middle of the body from the mouth to the anus, and includes the throat (pharynx), oesophagus, stomach, small intestine (duodenum, jejunum and ileum) and large intestine (cecum, appendix, colon and rectum). The mucosal wall of the GIT is typically similar in structure throughout most of its length from the oesophagus to the anus, with some local variations for each region (Chanda *et al.*, 2010). Each distinct section within the GIT has its individual physiological function and is varied in terms of pH, composition and nature of the luminal contents, surface area and length, and the presence of drug transporter systems (e.g. P-glycoprotein) and drug metabolising enzymes (e.g. CYP3A4) (Mouly and Paine, 2003; Yuen 2010). It is widely accepted that oral bioavailability of drugs is affected by physiological factors such as gastric emptying, intestinal transit, local pH, and nutritional status, intestinal efflux and carrier-mediated transport, first-pass metabolism in the gut, and subsequent first-pass hepatic extraction, as well as pharmaceutical factors such as rate of dissolution from the DDS, a drug's inherent permeability and particle sizes of the dosage form (Agoram *et al.*, 2001).



The volume of fluid in the GIT is paramount for disintegration, dispersion, dissolution and absorption of a drug delivered through the oral route, while differences in the pH range throughout the GIT affects the ionisable state of a drug. A drug, in its ionised form, has a higher solubility and hence a faster dissolution rate out of the DDS, while in its unionised form, a drug is readily absorbed through the GIT mucosa (Kararli, 1995). Transit within the GIT differs and is largely dependent of gut motility and flow, which depends and varies on the type and timings of meal ingestion and the nature of the formulation, rather than the size of a formulation. However, the transit of a dosage form through the gut is not continuous and retro-propulsion may occur (Weitschies *et al.*, 2005; Goodman *et al.*, 2010; Varum *et al.*, 2010). Furthermore, gastrointestinal fluid is not always consistent in quantity, and therefore DDSs may be subjected to periods without gastric fluid contact as it moves through the gut, detrimentally altering drug release characteristics (Schiller *et al.*, 2005). To summarise, Varum and co-workers (2010) adequately concluded that *“Gastrointestinal transit for a modified-release dosage form could be thought of as a starting and stopping process, sometimes moving quickly, sometimes slowly, sometimes passing through fluid of varying composition, and being subject to peristaltic pressures and forces”*.

The inherent characteristics of the GIT physiology include significant variations in environment (pH ranges, gastrointestinal transit time, surface area, enzymatic activity and colonic microflora) which influence drug release and absorption from a DDS. The modality of site-specific drug delivery using the oral route is based on exploiting these variations along the GIT, achieving controlled and modified drug delivery. In this manner, drugs can therefore be delivered to a specific site or region within the GIT, by preventing premature drug release (before it reaches its absorption site/window). Furthermore, the dosage form can be maintained at the site of absorption for a prolonged period of time with the aid of gastroretentive technologies (Rouge *et al.*, 1996). When a dosage form is administered via the peroral route, it is subject to the differing GIT conditions in the order illustrated in Table 1.1. This table also describes the various technologies and methods used for bioavailability enhancing and drug targeting to the various regions within the GIT.

**Table 1.1:** The physiological effects of the GIT on an orally delivered DDS, and technologies exploiting said parameters for targeted drug delivery.

| Anatomical unit and parameter  | Parameters (normal conditions)  | Effects of human physiology on the DDS, or incorporated drugs   | Design of drug delivery systems which consider and exploit the GIT physiology for enhanced bioavailability  | Conclusions  | References  |
|--|---|---|---|--|---|
| <b>Mouth Cavity</b> <ul style="list-style-type: none"> <li>• Length</li> <li>• Surface area</li> <li>• pH</li> <li>• Secretions</li> <br/> <li>• Transit Time</li> </ul> | <ul style="list-style-type: none"> <li>• 15-20cm</li> <li>• <math>\pm 0.07\text{m}^2</math></li> <li>• 5.5-7.0</li> <li>• Saliva, Mucus, Amylase</li> <li>• 10-20sec</li> </ul> | <p>With the transit of a DDS through mouth cavity being so quick, they are generally not affected by this region.</p> <p>However, if the DDS is subject to mastication, it may lead to premature disintegration of the DDS, thus adversely affecting drug release profiles.</p> <p>Furthermore, drugs delivered locally are exposed to saliva of which the composition may contribute to some drugs undergoing chemical modification.</p> | <p>Chewing dosage forms are commonly used to topical drug delivery of drugs (e.g. antimycotics) to the oral cavity. For drugs with higher solubility's, release is generally quick from system, while the rate of release of a drug with lower solubility is dependent on chewing time.</p> <p>DDSs, such as single or multi-layered films, tablets or gels, adhering to the buccal mucosa provide prolonged drug delivery to the oral cavity. These DDSs often contain cellulosic polymers or Carbopol® for prolonged adhesion to the buccal cavity.</p> <p>Fast dissolving systems are prepared for immediate and acute relief of symptoms especially in asthma and myocardial infarction for absorption sublingually. Films are commonly prepared via phase separation and include superdisintegrants.</p> <p>Fast disintegrating dosage forms are effectively employed for geriatrics or paediatrics, which have difficulty swallowing tablets and capsules. The dosage form rapidly disintegrates in the mouth upon contact with saliva releases microparticles or solubilised drug that is easily swallowed and enters the stomach or intestine for absorption. Lyophilisation, superdisintegrants and effervescency are technologies used to ensure fast disintegration.</p> | <p>Drug delivered to the mouth cavity provides fast absorption of drugs which bypasses first pass metabolism ensuring enhanced bioavailability, especially for lipid soluble drugs. These systems are also effective at treating conditions within the oral cavity such as periodontal disease.</p> <p>However, factors such as the low permeability of the membranes that line the oral cavity results in a low flux of drug as well as the continual secretion and swallowing of saliva and mastication are unique problems which need to be considered during pre-formulation to ensure successful delivery of a drug via this route.</p> | <p>Rathbone <i>et al.</i>, 1994; Kararli, 1995; Seeley <i>et al.</i>, 1995, pg 798-799; Shojaei, 1998; Jacobsen <i>et al.</i>, 1999; Liang &amp; Chen, 2001; Giunchedi <i>et al.</i>, 2002; Baldi &amp; Malfertheiner; 2003; Attia <i>et al.</i>, 2004; Maffei <i>et al.</i>, 2004; Ameye <i>et al.</i>, 2005; Maggi <i>et al.</i>, 2005; Owens <i>et al.</i>, 2005; Abu-Huwajj <i>et al.</i>, 2007; Garg &amp; Kumar, 2007; Segale <i>et al.</i>, 2007; Goswami <i>et al.</i>, 2008; Messina <i>et al.</i>, 2008; Madhav <i>et al.</i>, 2009; Pinto, 2010.</p> |
| <b>Oesophagus</b> <ul style="list-style-type: none"> <li>• Length</li> <li>• Surface area</li> <li>• pH</li> <li>• Secretions</li> <li>• Transit Time</li> </ul>         | <ul style="list-style-type: none"> <li>• 25cm</li> <li>• <math>\pm 0.02\text{m}^2</math></li> <li>• <math>\pm 7.0</math></li> <li>• Mucus</li> <li>• 5-8sec</li> </ul>          | <p>There is a slight chance that a DDS may adhere to the oesophageal mucosa, but generally, they are propelled to the stomach via strong peristaltic contractions. These contractions have minimal effects on the physical properties of the DDS. The absence of enzymatic secretions prevents chemical modification of drugs.</p>  | <p>Bioadhesive liquid dosage forms are commonly employed to coat the oesophagus for protection against trauma or local delivery or alginate solutions for the treatment of GORD (Gastro-oesophageal reflux disease), while bioadhesive gels are employed for local drug delivery in the treatment of Barrett's Oesophagus. These bioadhesive systems contain cellulosic polymers, Carbopol® or Chitosan for prolonged adhesion to the oesophagus and the structure of these systems ensures that there is no blockage of the oesophagus, while the dislodging of the dosage form is minimised with further ingestion of foods.</p> <p>Other approaches for targeting the oesophagus have been suggested, including orally retained lozenges, chewing gums, films, as well as endoscopically delivered drugs.</p>  | <p>The oesophagus is generally not targeted for site-specific drug delivery due to the short transit time and low mucosal permeability. In addition bulky systems may cause discomfort and local irritation. However, it is a desirable organ to be targeted for local oesophageal disorders.</p> <p>Strictly speaking, retention of a DDS within the oesophagus can only be achieved by a medical device e.g. using photodynamic therapy for oesophageal cancer treatment.</p>  | <p>Swisher <i>et al.</i>, 1984; Kararli, 1995; Seeley <i>et al.</i>, 1995, pg 798-799; Overholt <i>et al.</i>, 1996; Batchelor <i>et al.</i>, 2002; Batchelor <i>et al.</i>, 2004; Tutuian and Castell, 2006; Collaud <i>et al.</i>, 2007; Zhang <i>et al.</i>, 2008; Pinto, 2010.</p>  |

**Table 1.1 continued**

|  |   |   |   |   |   |
|--|---|---|---|---|---|
| <p><b>Stomach</b></p> <ul style="list-style-type: none"> <li>• Length</li> <li>• Surface area</li> <li>• pH</li> <li>• Secretions</li> <br/> <li>• Transit Time</li> </ul> | <ul style="list-style-type: none"> <li>• 20cm</li> <li>• <math>\pm 0.11\text{m}^2</math></li> <li>• 1-3.5</li> <li>• Mucus, HCl, IF, Pepsin and Gastrin</li> <li>• 1.3-2.5 hours for liquids; 3-4 hours for solids</li> </ul>         | <p>Enzymes present in gastric fluid chemically modify some drugs, and proteins, to the extent that they are no longer able to exert the required effect.</p> <p>The low pH of the stomach region affects the ionisable state and hence dissolution and absorption qualities of drugs. Low pH ranges may cause degradation of some drugs.</p> <p>The presence of food prolongs the transit time within the gastric region, with detrimental effects on time-dependant colon targeted systems. However, food can enhance the dissolution of basic drugs as the volume of the gastric contents is larger than that of a fasting individual.</p> <p>The primary role of the stomach is the mixing of food with gastric fluid, promoting digestion, rather than absorption. A DDS should be designed to withstand such conditions.</p> | <p>Gastroretentive systems (GR) based on density related floating relies on the entrapment of air within the system or the use of highly porous structures, such as tablets, microparticles or hydrogels, which float upon contact with gastric fluid. These systems release drug in a controlled, chronotherapeutic or modified manner. The highly porous structures can be developed by lyophilisation.</p> <p>GR systems based on effervescent characteristics, such as tablets, microspheres, granules, which, upon contact with gastric fluid, generate gas to produce a low density matrix able to float upon contact with gastric fluid, releasing drug in a controlled or pulsatile manner. These systems require a base, generally sodium bicarbonate, and an acid such as citric acid for the effervescent properties of the system.</p> <p>GR systems developed by incorporating highly swellable polymers rely on the system, (i.e. tablet) swelling to decrease density and hence float, with the potential to release drug for up to 20 hours in the stomach. The size increase prevents the system from being prematurely evacuated from the stomach, and these systems generally incorporate highly swellable cellulosic polymers, which eventually decreases in size and is evacuated from the stomach.</p> <p>Mucoadhesive systems contain adhesive polymers such as Chitosan, Carbopol<sup>®</sup>, and other cellulosic polymers, and are administered in the form of microspheres, patches or tablets. These systems, upon swelling, are able to adhere to the gastric mucosa for prolonged periods of time, releasing drug in a controlled manner. Other adherents that are used as potential drug carriers include ion exchange resins.</p> <p>Enteric coated systems, generally used to protect gastric sensitive agents from the harsh gastric environment, are based on the use of pH-responsive polymers (Eudragit<sup>®</sup>) which dissolve and release drug only in the higher pH ranges of the intestine.</p> | <p>Stomach targeted systems generally exploit physiological factors such as the low pH, motility and gastric emptying time to ensure a system is retained and releases drug in the gastric region of the GIT for a prolonged period of time. However these factors are highly variable and vary with the presence of food, disease states or even other drugs, and hence will affect the release profiles of drug delivery systems.</p> <p>Stomach targeted systems are beneficial in the treatment of local disorders such as <i>H. Pylori</i> infections or ulcers.</p> <p>The surface area of the stomach is larger than the mouth or oesophagus aiding in absorption of acidic drugs absorbed through the gastric wall.</p> <p>Gastric retention provides advantages such as the delivery narrow absorption window drugs in the gastric or small intestinal region, for local action in the upper part of the small intestine, and improved bioavailability is expected for drugs absorbed readily upon release in the GIT.</p> | <p>Kawashima <i>et al.</i>, 1992; Desai and Bolton, 1993; Seeley <i>et al.</i>, 1995, pg 798-799; Kararli, 1995; Deshpande <i>et al.</i>, 1997; Baumgartner <i>et al.</i>, 1998; Krogel and Bodmeier, 1999; Jackson and Perkins, 2001; Eaimtrakarn <i>et al.</i>, 2003; Streubel <i>et al.</i>, 2003; Elkheshen <i>et al.</i>, 2004; Dhaliwal <i>et al.</i>, 2008; McConnell <i>et al.</i>, 2008; Zou <i>et al.</i>, 2008; Meka <i>et al.</i>, 2009; Chanda <i>et al.</i>, 2010; Pinto <i>et al.</i>, 2010; Surana and Kotecha, 2010; Yuen, 2010.</p> |
| <p><b>Small Intestine</b></p> <ul style="list-style-type: none"> <li>• Length</li> <li>• Surface area</li> <li>• pH</li> <li>• Secretions</li> </ul>                       | <ul style="list-style-type: none"> <li>• <math>\pm 625\text{cm}</math></li> <li>• <math>\pm 120.\text{m}^2</math></li> <li>• 5-7</li> <li>• Mucus, Enzymes (trypsin, peptidase, lactase, sucrose, amylase, lipase, gastrin</li> </ul> | <p>Enzymes present in intestinal fluid chemically modify some drugs and proteins to the extent that they are no longer effective.</p> <p>Basic drugs are better absorbed in the intestine due to its unionised state. The pH range of the intestine has a minimal effect on drug stability.</p> <p>The presence of food</p>   | <p>pH-sensitive polymers i.e. Eudragit<sup>®</sup> are commonly used as enteric coatings in tablets, capsules or microspheres to ensure that the drug is not released before reaching the intestinal area. These polymers, which are acidic in nature, disintegrate/dissolve at the relatively higher pH ranges of the intestine, only releasing the entrapped drug upon contact with intestinal fluids.</p> <p>Bioadhesive tablets, pellets and hydrogels incorporating polymers with mucoadhesive characteristics, including Carbopol<sup>®</sup>, methacrylic and cellulosic polymers, demonstrate maximal mucoadhesion in intestinal pH ranges, thereby bypassing the stomach without adhering to or releasing drug in the stomach.</p> <p>Remote controlled systems such as the IntelliSite<sup>®</sup> capsule</p>  | <p>Due to the large surface area and long length of the intestine, it is the major organ for absorption of many drugs. It should be noted that the mobility of the intestine, and thus its contents, is quite constant in comparison to other GIT organs, therefore not surprising that only a few strategies have been described to control the mobility of dosage forms within the small intestine.</p>   | <p>Seeley <i>et al.</i>, 1995, pg 798-799; Kararli, 1995; Pithavala <i>et al.</i>, 1998; Carelli <i>et al.</i>, 2000; Awad <i>et al.</i>, 2002; Bernkop-Schnurch <i>et al.</i>, 2004; Fedorak and Bistriz, 2005; Goto <i>et al.</i>, 2006; Hinderling <i>et al.</i>, 2007; Schellekens <i>et al.</i>, 2008; Pinto, 2010; Yuen, 2010</p>   |

**Table 1.1 continued**

|  |   |   |   |   |  |
|--|---|---|---|---|--|
| <ul style="list-style-type: none"> <li>• Transit Time</li> </ul>   | <p>secretin), bile, bicarbonate ions</p> <ul style="list-style-type: none"> <li>• 3-5 hrs</li> </ul>  | <p>within the intestinal region has not been associated with drastic changes in transit time, and its effects are said to be negligible.</p>  | <p>are able to release drugs at differing sites within the GIT using capsules which release drugs in the presence of a stimulus. These capsules can deliver drugs to a defined region of the intestine after application of a magnetic signal.</p>  |   |  |
| <b>Colon</b>   |   |   |   |   |  |
| <ul style="list-style-type: none"> <li>• Length</li> <li>• Surface area</li> <li>• pH</li> <li>• Secretions</li> <li>• Transit Time</li> </ul> | <ul style="list-style-type: none"> <li>• ±150cm</li> <li>• ±0.25m<sup>2</sup></li> <li>• 5.5-7</li> <li>• Mucus</li> <li>• 18-24 hrs</li> </ul> | <p>If a drug passes through the GIT intact, any remaining drug within a DDS will be embedded in semi-solid faecal matter, drastically limiting dissolution and hence absorption.</p>  | <p>Prodrugs delivered via the oral route require a specific enzyme, present only in the colon, for absorption or activation, and hence will pass through the stomach and small intestine unchanged. These systems have the potential for local delivery to the colon and include drugs such as sulphasalazine or dexamethasone glucoside.</p>   | <p>The colon is particularly useful to target not just for local diseases, but for the delivery of therapeutic proteins and vaccines sensitive to the stomach and small intestine environments. Furthermore, the colon has a long retention time and appears highly responsive to agents enhancing absorption of poorly absorbed drugs.</p>   | <p>Seeley <i>et al.</i>, 1995, pg 798-799; Kararli, 1995; Ahrabi <i>et al.</i>, 1997; Vandamme <i>et al.</i>, 2002; Yang <i>et al.</i>, 2002; Chourasia and Jain, 2003, Chourasia and Jain, 2004; McConnell <i>et al.</i>, 2008; Pinto <i>et al.</i>, 2010; Yuen, 2010; Kumar <i>et al.</i>, 2011a</p> |
|  |   | <p>Due to the strong contractions within the colon, DDSs targeted to the colonic area may rupture, detrimentally affecting the drug release profile.</p>  | <p>Polymeric coatings such as Pectin and galactomannan degrade in the presence of colonic microflora and have thus been utilised to protect the drug-containing core and prevent release of the DDS from the upper GIT conditions. The success of these systems has been further enhanced by promoting hydrophobicity within these polysaccharides via chemical modification, ensuring drug release only in the colon.</p>  | <p>However, there are more restrictive tight junctions in the colon rendering drug absorption more difficult via this route. In addition, due to the variations in the fluid volume distribution within the colon, colon targeted DDS can be exposed to anything between 1 and 100mls of fluid at any given time, causing significant variations in the bioavailability of these DDS. Absorption within the colon is significantly smaller than that of the small intestine, and due to the highly variable transit times in this region, absorption is generally incomplete and erratic.</p> |  |
|  |   | <p>The fluid volume and composition within the colon is quite variable, and further influenced by pathology. For instance, in individuals suffering with constipation, there is increased water resorption in the gut leading to more viscous or solid colonic contents. Its aetiology is usually related to delayed transit or obstruction to defecation and its presence may make drug dispersal or dissolution problematic, consequently affecting oral bioavailability.</p> | <p>pH responsive polymers (Eudragit<sup>®</sup> FS) dissolving at a pH &gt; 7 are also utilised as protective coatings over solid dosage forms such as tablets, capsules or pellets. The polymeric coating provides protection and until it reaches the colon where the polymer is dissolved, releasing the entrapped drug. These systems are similar to intestinal targeted enteric coated systems, but differ on the targeted site and polymers incorporated.</p>   | <p>It should be noted that the design of controlled release systems for optimal drug delivery to the colon requires comprehensive understanding of the relationship between particle size, colonic dispersion and colonic transit rates, in addition to other factors (e.g. disease or other drugs) which influence colonic transit rates and consequent drug bioavailability.</p>  |  |
|  |   |   | <p>Drug delivery systems which are time dependent are based on the principle of incorporating a lag time, which delays the release of the drug for 3-4 h after leaving the stomach. These systems generally incorporate multiple layers of coatings that may have pH responsive tendencies. However, most of these systems are based on the assumption that transit times within the GIT are consistent even though it is widely accepted that transit times differ considerably. If designed correctly, these systems can be useful in the therapy of diseases related to circadian rhythms.</p> |   |  |
|  |   |   | <p>Pressure controlled systems require high pressures caused by strong contractions, present only within the colon to collapse the DDS and hence release drug. Such systems include capsules, of which the outer shell collapses and releases drug in response to the increased pressure of the colon.</p>  |   |  |
|  |   |   | <p>Osmotically driven systems require the rapid uptake of water into the DDS, causing the forceful ejection of the drug, either by polymer swelling or fluid displacement. These systems, such as the OROS-CT (Alza Corporation), are intricately designed incorporating lag times and enteric coatings to ensure colon-targeted drug delivery for anything between 4-24 hours.</p>   |   |  |

### **1.3.2 pH as a stimulus employed for targeting in oral drug delivery**

As highlighted previously, each segment of the GIT varies from the other in pH, ranging from the acidic stomach, to the more alkaline duodenum and ileum. The use of pH as a stimulus triggering or retarding drug release is a commonly adopted approach to targeting or achieving organ-specific drug delivery. pH, as opposed to other methods including enzyme-responsive systems for drug targeting, is preferred in the formulation of the MMDDS due to the ease at which the system can be adapted for targeting within an alternative region of the GIT, simply by replacing the existing pH-responsive polymer to one responsive to more alkaline/acidic pH environments. These pH-responsive systems have been employed for achieving preferential release in a particular organ based on a drugs' sensitivity to a particular gastric environment or the local treatment of a disease. Furthermore, there is particular interest in applying pH-responsive systems for segregating interacting drugs (Gao *et al.*, 2010). A detailed review highlighting the polymers employed in pH-responsive drug delivery is outlined in *Chapter 2*.

In terms of oral drug delivery, it is desirable to select a polymer that requires a pH change falling within the physiological pH range of the GIT. In this manner, drug release from these systems would not necessitate the use of an external trigger, complicating oral drug delivery. Furthermore, if the externally applied trigger is removed, the stimuli-responsive polymer would revert back to its original state, changing the rate of drug release (Carrera *et al.*, 2010). Due to the pH of the differing areas within the GIT, the trigger for stimulating/retarding drug release is almost always present when required. In order to achieve prolonged release with a pH-responsive oral DDS, said system should be maintained at the site of absorption (through gastroretention) for a period of time sufficient to produce desired therapeutic concentrations.

### **1.3.3 Architectural strategy employed to exploit and overcome the GIT physiology**

Although many DDSs on the market today boast novel technologies which provide controlled release, these systems ultimately rely on dissolution/bio-erosion, diffusion or a combination thereof to instigate controlled release of drug at the desired site. Other factors including the drug's physicochemical properties, rate of absorption, metabolism, and elimination are integral in how a pharmaceutical dosage form should be designed to ensure optimal efficacy whilst ensuring minimal toxicity (Ranade, 1991). The MMDDS proposed by the present dissertation, illustrated in Figure 1.3, takes into account the GIT physiology and the drugs' properties, allowing the DDS to overcome many of the limitations in oral drug delivery.

The strategy employed, lies in the multi-layered design of the system (Figure 1.7), providing several functions and taking advantage of several aspects of the various components within the DDS, in particular the improved bioavailability offered from unidirectional release provided by the protective coating of the system. Furthermore, the mucoadhesive layer provides intimate contact between the DDS and the site of absorption, a driving force promoting passive uptake and absorption from the DDS which is not altered by variations in gastric transit time (Schmitz *et al.*, 2005). Targeting, achieved by pH dependant mucoadhesion, ensures that the drug/drugs incorporated are delivered to its specific site, avoiding any deleterious drug interactions or harmful GIT affects, thereby promoting bioavailability. To ensure segregated delivery of interacting drugs, two components were developed, each targeted to a different region of the GIT, differing solely on the drug incorporated and consequent pH-responsive polymer employed for drug targeting. The system is therefore versatile, in that it may be applied to a wide variety of drugs, each being targeted to the relative site of absorption, while multiple drugs can be incorporated in one system, easing therapeutic regimens.

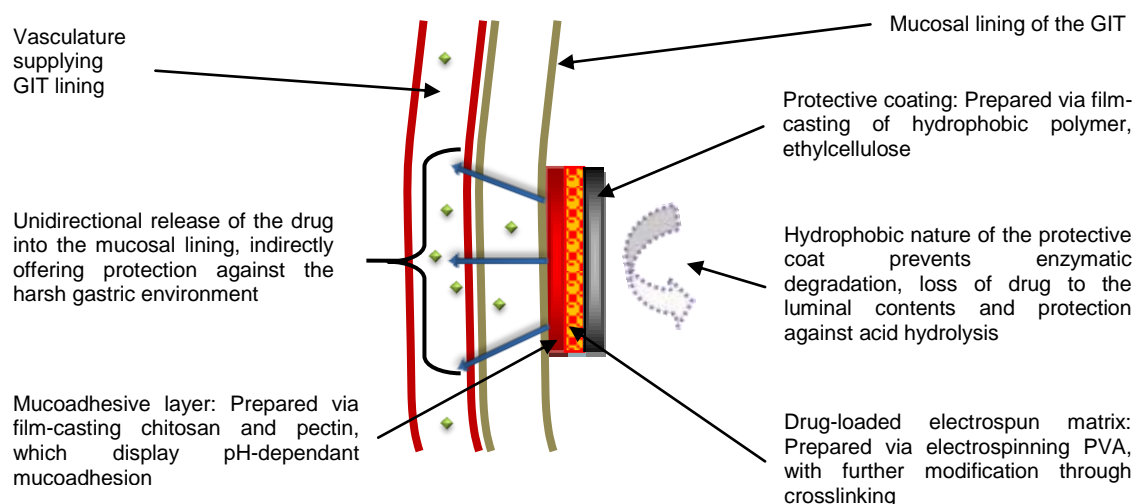


**Figure 1.7:** Simplified illustration of the proposed mode of drug delivery of the MMDDS with a depiction of the architectural strategy employed to overcome and exploit the human GIT physiology.

#### 1.4 Novelty of the Study

The novelty of this study lies in the mode of segregated drug delivery proposed, which was achieved through the use of pH-responsive mucoadhesion. The componential system was able to negate deleterious interactions even though the interacting drugs were administered in a single dosage form. Furthermore, it employs the technique of

electrospinning in order to create a fibrous, highly porous structure with an increased surface area able to effectively control the rate of drug release from the MMDDS. Furthermore, the electrospinning process is a simple and easily fabricated method for the production of nano- or microfibers, without the use of complex or costly equipment (Choi *et al.*, 2008). The crosslinking procedure was novel in that it ensures that there was no need for post-treatment of the nanofibrous matrices required to remove residual glutaraldehyde, substantially limiting its toxicity.

### **1.5 Aim and Objectives of the Study: Description of the Oral Multi-component Membranous Drug Delivery System**

In order to develop an ideal DDS, the aim of the study was to design and formulate a MMDDS for prolonged and site-specific drug delivery of two or more drugs in a single system. The proposed MMDDS ensures differentiated release of the incorporated drugs as illustrated in Figure 1.8.

The above aim was achieved by outlining the following objectives:

1. Identifying a novel means of segregating drug delivery by employing stimuli-responsive mucoadhesion and determining the most appropriate stimulus to be targeted for stimuli-responsive mucoadhesion.
2. Reviewing and evaluating various stimuli-responsive polymers and assessing their feasibility in segregated drug delivery.
3. Selection of appropriate polymer combinations and other excipients to formulate the mucoadhesive layer within the gastric targeted and intestinal targeted components.
4. Experimentally synthesizing variants of the preferred mucoadhesive layer for each component employing a 2-Factor Central Composite Design followed by physicochemical and physicomechanical analysis.
5. Determination of the optimum parameters required to synthesise the desired mucoadhesive layer for both components based on statistical optimisation implemented via the Response Surface Methodology.
6. Identifying suitable polymers and parameters employed during electrospinning for the development of drug-loaded electrospun nanofibrous matrices for both components.
7. Selection of suitable crosslinking agents and description of the crosslinking methodology for modification of the nanofibrous matrices required to achieve the preferred drug release profiles.

8. Performing *in vitro* drug release studies in order to determine the drug release behaviour from both components in the MMDDS in comparison to the marketed 'gold-standard' formulations of both drugs.
9. Undertaking *in vivo* animal studies on a pig model to determine the release behaviour and to assess the pharmacokinetics of the MMDDS in relation to the marketed 'gold-standard' formulations of both drugs.

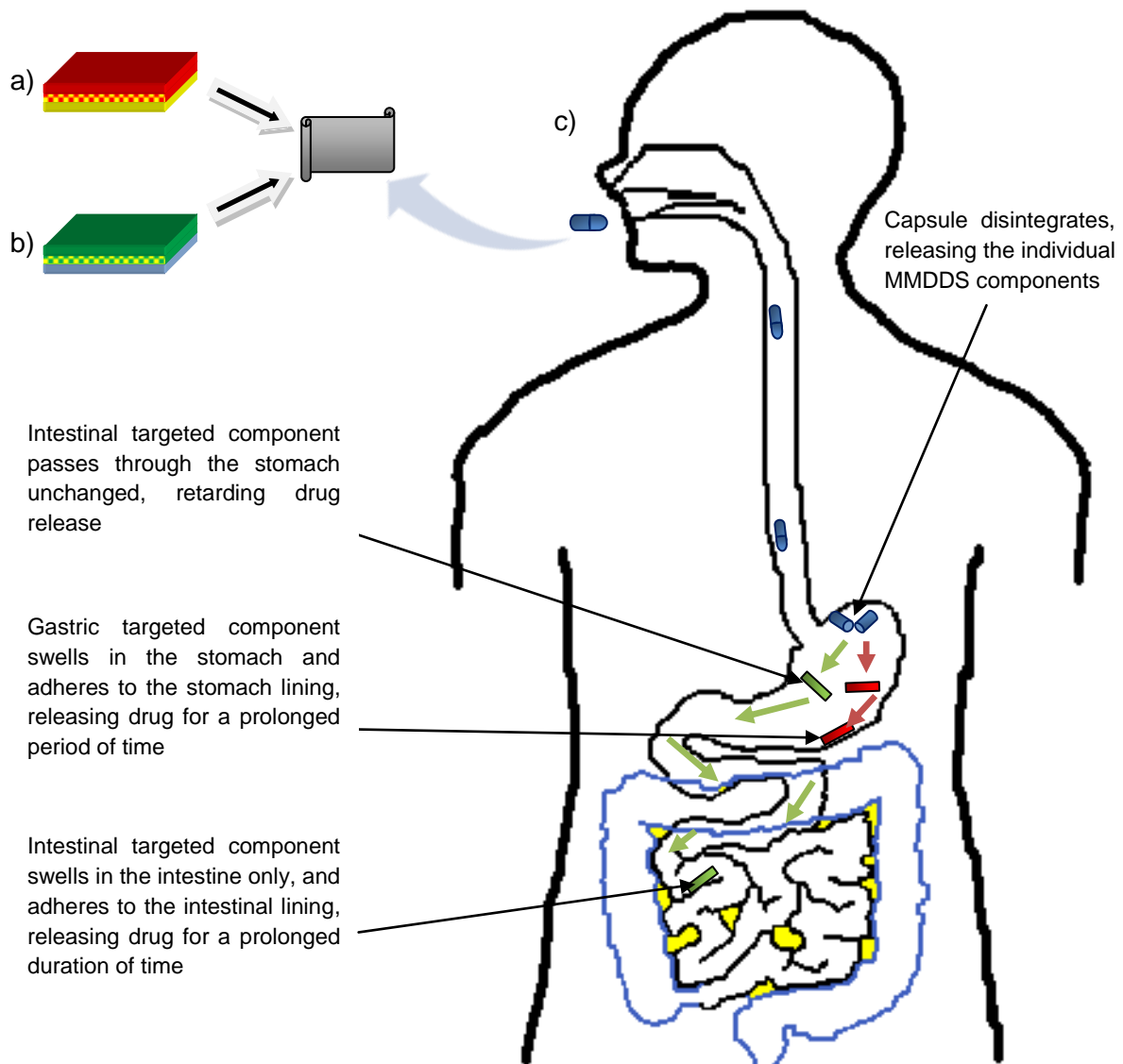


**Figure 1.8:** Schematic illustration depicting differential release, representing a) the gastric targeted component for the delivery of RIF to the stomach, containing a gastric targeted pH-responsive mucoadhesive layer, a RIF-loaded nanofibrous matrix and a protective coat; b) the intestinal targeted component for the delivery of INH to the intestine containing an intestinal targeted pH-responsive mucoadhesive layer, an INH-loaded electrospun matrix and a protective coat; and c) proposed strategy employed to ensure site-specific, segregated and prolonged delivery of both drugs.



## 1.6 Synopsis of the Dissertation

**Chapter One** of this dissertation provides a summary to the dissertation. It outlines an introduction to the study that covers the background, delineates the problems associated with oral drug delivery and highlights the rationale for the study. It briefly describes the architectural structure of the proposed drug delivery system and how it overcomes the limitations to oral drug delivery. Aspects of the gastric physiology are considered in terms selection of an appropriate stimulus employed for drug targeting within the GIT. A summary of the aim and objectives is included in this chapter.

**Chapter Two** of this dissertation provides a comprehensive literature survey, focusing on the use of smart polymers in drug delivery, specifically membranous systems. Furthermore, there is a detailed outline of the various methods in membrane fabrication, with impetus placed on the electrospinning method.

**Chapter Three** of this dissertation provides a brief introduction to mucoadhesion, including the different mechanisms responsible for mucoadhesion in the GIT. It describes the pre-formulation and development of the respective pH-responsive layers. Preliminary formulation methods investigated the ideal polymers and respective quantities required to ensure mucoadhesion was sustained over a prolonged period of time. In addition, formulation parameters were established to allow for the construction of a Central Composite Design.

**Chapter Four** of this dissertation describes the preparation of variants of the respective pH-responsive layers as constructed according to a randomized, Face-centered Central Composite Design, followed by optimization using Response Surface Methodology. The applicability of the respective design was analysed. Furthermore, physicochemical and physiochemical properties were analyzed in order to determine the influence of simulated gastro-intestinal conditions.

**Chapter Five** of this dissertation describes the preliminary formulation and development of the drug-loaded electrospun layer of the MMDDS. It describes the rational approach to selection of a suitable polymer for electrospinning. In addition, it includes a comprehensive outline of the electrospinning procedure and factors which affect the final morphology of resultant nanofibres.

**Chapter Six** of this dissertation is a comprehensive description *in vitro* analysis of the drug-loaded electrospun layer. An in depth analysis of the post-spun modification procedure is provided with the resultant alterations to the physicochemical and physiochemical properties of the electrospun layer. An ideal formulation based on the *in vitro* results was highlighted as a candidate formulation for further analysis.

**Chapter Seven** of this dissertation provides a comparative analysis of the MMDDS with a “gold-standard” marketed formulation in terms of both *in vitro* and *in vivo* drug release behaviour. Furthermore, it contains an explanation of the *in vivo* animal studies undertaken in the pig model. Assessment of the MMDDS biocompatibility and drug release behaviour were highlights of this chapter. In addition, dosage administration and sample collection of blood is described.

**Chapter Eight** of this dissertation presents the conclusions and recommendations for future work.

## 1.7 Concluding Remarks

This chapter sought to highlight the problems and challenges associated with the oral route of drug delivery, in particular, the effects of the gastric physiology on drug bioavailability, while the approaches to overcoming said limitations were identified. Furthermore, the rationale for drug targeting within the GIT was explored while aspects of the gastric physiology were considered in terms of the selection of an appropriate stimulus for drug targeting within the GIT. The focus of the chapter was a description of the MMDDS, with particular emphasis on the architectural structure and functioning of the different layers. The advantages in drug targeting were explored, with particular reference to interacting drugs rifampicin and isoniazid, which require segregated drug delivery.

## CHAPTER 2

### A REVIEW ENCOMPASSING STIMULI-RESPONSIVE POLYMERS WITH SPECIFIC APPLICATION IN MEMBRANOUS SYSTEMS AND THE FORMULATION THEREOF

---

#### 2.1 Introduction

The membrane industry is a rapidly growing field of research that has found extensive application in industrial and medical fields (Baker, 2004; Stamatialis *et al.*, 2008). Industrially, membranes have found application in ultrafiltration, microfiltration, reverse osmosis, gas separation, prevaporation and electro dialysis, while medically; applications include incorporation into artificial organs, haemodialysis, drug delivery systems, diagnostics, coatings for medical devices, tissue regeneration and biosensors amongst others (Baker, 2004; Stamatialis *et al.*, 2008). It is imperative to have an understanding of the method of membrane fabrication as it affects the final morphology, and hence the potential applications of the polymeric membranes.

The earliest application of membrane systems in drug delivery included osmotically controlled systems, developed by Rose and Nelson in 1955 that delivered medication to the gut of sheep and cattle in a zero-order release rate over a prolonged period. The Higuchi-Theeuwes pump, developed by the Alza Corporation, improved this technology by overcoming the limitations such as the short shelf-life and the need for immediate administration (Santus and Baker, 1995). Eventually, the Alza Corporation successfully managed to deliver drugs transdermally by developing an adhesive patch containing scopolamine, with a zero-order release rate, for the treatment of motion sickness (Lonsdale, 1982). The OROS<sup>®</sup> (osmotic-controlled release oral delivery system) technology (Alza Corporation) is used today for the delivery of many drugs including Adalat CR<sup>®</sup> (controlled-release nifedipine) and led to the development of various other prolonged release delivery systems for the delivery of drugs such as Acutrim<sup>®</sup> (phenylpropanolamine), Minipress XL<sup>®</sup> (prazosin) and Volmax<sup>®</sup> (salbutamol) (Santus and Baker, 1995). The potential for membrane technology in medical industry supersedes its other applications due to its versatility in medical applications (Stamatialis *et al.*, 2008).

Membranes have been vastly utilized in the medical and pharmaceutical fields, in particular drug delivery, due to their ability to control the permeation rate of chemical substances (Stamatialis *et al.*, 2008). Synthetic functional polymers have witnessed much

advancement in the last two decades, and said polymers are capable of responding in a desirable manner to a change in temperature, pH, electric or magnetic fields (Kumar, 2009). These stimuli-responsive polymers are also referred to as smart, intelligent, or environmentally-sensitive/responsive polymers (Lue *et al.*, 2008). Polymers with physical and chemical properties that can be manipulated by the surrounding environment, such as hydrogels, have potential applications in surgical implants, scaffolds for tissue engineering, supports for *in vitro* cell culture and biotechnological screening, as well as in drug delivery systems (Stamatialis *et al.*, 2008; Kumar, 2009). In drug delivery, they may be used to target drugs to specific sites in the body or as a 'smart' surface which can be switched from an adhesive to a non-adhesive state or from a hydrophilic to a hydrophobic state and thus can swell or shrink. The changes are reversible, implying that the polymer is capable of returning to its initial state upon removal of the trigger (Schmaljohann, 2006).

## **2.2 Membrane Applications in Drug Delivery**

Membranes are extensively employed in the medical field for drug delivery, haemodialysis artificial organs (oxygenators, pancreas etc) and tissue engineering. The development and formulation of these membranous systems requires biocompatible and sometimes biodegradable materials as the systems would ultimately be in contact with biological fluids and tissues. In addition, these materials require other imperative properties, such as blood compatibility, size, shape and porosity, to be carefully controlled. Controlled drug permeability and good release properties are the characteristics required for a membranous system to function as an efficient drug delivery system. Drug release is directly related to the degradation rate of the materials used i.e. the faster the material degrades, the higher the blood levels of the drug, resulting in toxic doses which may often be fatal. Therefore, for implantable drug delivery systems, erosion and degradability are key parameters. In addition, the swelling dynamics of certain polymers are also crucial for the mass transport of drug (diffusion) and also needs to be considered. This is also true for polymeric membranes utilized in tissue engineering (Stamatialis *et al.*, 2008). Incorporation of stimuli-responsive polymers in membranes systems can further widen their repertoire of application in drug delivery and biomedicine by improving key qualities such as the biocompatibility/biodegradability of the membrane system, providing site-specific and/or modified release drug delivery or improving tissue engineering features.

Conventional drug delivery systems available on the market i.e. tablets, injections, liquids and so forth often provide drug delivery with fluctuating plasma concentrations which results in sub-therapeutic or toxic plasma levels of the drug. An ideal drug delivery system

should ensure a sustained drug release pattern for a specific period of time at a specific site. A key advantage of site-specific drug delivery is that molecules that have problematic toxicology profiles, localized delivery can often mitigate such issues and is therefore a key driver for the development of biocompatible and/or biodegradable sustained release drug delivery systems. Membrane based drug delivery systems have the potential to ensure sustained drug release based on mechanisms of osmosis or diffusion (Stamatialis *et al.*, 2008).

Diffusion-controlled membrane drug delivery systems depend on drug diffusion across the membrane, operating according to Fick's law, and on membrane thickness (Stamatialis *et al.*, 2008). These systems have been applied in pills, implants and patches. Smart polymers are extensively used in membrane systems as permeation switches or "gates" (Discher and Ahmend, 2006). The pores within the membrane become blocked when swelling is initiated in response to a stimulus, thereby preventing the release of the drug. Conversely, they may open and release the drug when the polymeric surface collapses.

## **2.3 Methods Employed in the Fabrication of Polymeric Membranes**

Various methods have been employed in the preparation of polymeric membranes. The type of the polymer and method employed, as well as the conditions during formulation determines the final morphology, and hence potential application, of the membranes. Phase separation, electrospinning, foaming, particle leaching, emulsion freeze-drying and sintering are some of the common methods that have been used in the production of membranes (Witte *et al.*, 1996; Altinkaya *et al.*, 2005).

### **2.3.1 Phase separation**

Phase separation, a membrane fabrication technique, has been widely applied in the production of scaffold membranes typically employed in tissue engineering. This fabrication method may be applied to pure polymers as well as polymeric composites (Sun *et al.*, 2007a; Stamatialis *et al.*, 2008). The technique involves the formation of an initial homogenous polymeric solution that becomes thermodynamically unstable upon exposure to an external stimulus. Upon reaching thermodynamic instability, the polymeric solution divides into two phases, a high and low polymer concentration phase. The concentrated phase then solidifies after phase separation, resulting in the formation of a polymeric membrane structure (Stamatialis *et al.*, 2008). The resultant membrane often has pores which become filled by the less concentrated polymer phase. Studies have indicated that phase separation can be induced by a variety of external effects. These

effects have been divided into four key techniques based on the concept of phase separation. The fundamental difference between each technique is the desolvation ability (Witte *et al.*, 1996; Altinkaya *et al.*, 2005).

#### **2.3.1.1 Vapour-induced phase separation**

Vapour-induced phase separation (VIPS) is a phase separation technique that involves the penetration of non-solvent vapour into the polymeric solution. It is a dry-wet casting process where the vapour of the non-solvent (usually water) allows for the slow transfer of non-solvent molecules into the polymeric solution (Witte *et al.*, 1996). The polymeric membrane then forms as a result of thermodynamic instability caused from exposure of the polymeric solution to the non-solvent vapour (Witte *et al.*, 1996; Matsuyama *et al.*, 1999; Sun *et al.*, 2007a; Kao *et al.*, 2008). VIPS is frequently used in the production of asymmetric membranes, comprising of a dense skin layer and a porous sub-layer. These membranes are typically applied in the separation of gaseous and liquid mixtures.

#### **2.3.1.2 Thermal-induced phase separation**

Thermal-induced phase separation (TIPS) is applicable to polymers that cannot form membranes through other phase separation methods due to inadequate solubility (Witte *et al.*, 1996). The effects of temperature changes on the solvent used to initially dissolve the polymer leads to the formation of the polymeric membrane (Hanks and Lloyd, 2007). A polymer is initially mixed at high temperatures to form a homogenous solution, followed by casting of the hot polymeric solution onto a cold surface of desired dimensions. The decrease in the surrounding temperature causes a decrease in the quality of the solvent used. Subsequently, phase separation of the polymeric solution occurs forming a microporous membrane (Witte *et al.*, 1996; Matsuyama *et al.*, 2001a; Matsuyama *et al.*, 2003; Li *et al.*, 2006a, Hanks and Lloyd, 2007). Porous films of isotropic, anisotropic or asymmetric membrane structures can be formed, with high porosity percentages, using the TIPS method. Other methods of phase separation involve a multi-component mass transfer reaction for phase separation to occur. In the TIPS method, heat transfer primarily induces phase separation, and therefore this method can be adapted to a wider range of membrane applications (Li *et al.*, 2006a).

#### **2.3.1.3 Immersion precipitation**

This method involves the casting of a polymeric solution into a mould or support as a thin film. The thin film-like polymeric solution is then immersed into a non-solvent containing bath which eventually leads to the precipitation of the polymeric solution. This occurs through a series of liquid-solid and/or liquid-liquid phase separation events (Witte *et al.*,

1996). Solvent molecules from the polymeric solution are replaced by the non-solvent molecules, as illustrated in Figure 2.1, resulting in the formation of a porous polymeric membrane that is subsequently dried to remove the liquid phase (Witte *et al.*, 1996; Hester *et al.*, 2002; Lin *et al.*, 2006). Membranes produced via this method are widely applied in microfiltration/ultrafiltration.

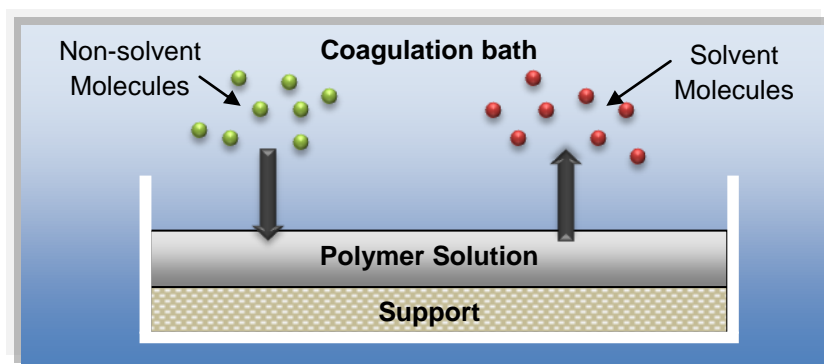


**Figure 2.1:** Schematic illustration of the mass transfer of solvent and non-solvent occurring during immersion precipitation (Adapted from Pereira *et al.*, 2000).

#### 2.3.1.4 Film/dry-casting technique

Film- or dry-casting essentially involves dissolving of the polymer in a volatile solvent and a less volatile non-solvent. The polymer becomes less soluble in the non-solvent as the solvent evaporates, culminating into phase separation that eventually results in the formation of a polymeric membrane (Witte *et al.*, 1996; Altinkaya *et al.*, 2005; Lai *et al.*, 2006). This technique can be successfully applied in the formation of coatings which require a stimulus to control the rate of drug release (Sun *et al.*, 2001).

The primary disadvantage of phase separation is that it involves the use of organic solvents in the formulation and development of membrane systems. Incomplete removal of these solvents may result in toxicity when these membrane systems are used in biomedical and pharmaceutical applications. The removal of organic solvents from these membranes is thus necessary; however, it is a costly exercise. Additionally, the formation of polymeric membranes using phase separation is a lengthy process with the solvents often being environmentally harmful. Furthermore, slight changes in the membrane fabrication process may significantly affect the final membrane morphology and hence drug release performance (Krause *et al.*, 2002; Altinkaya *et al.*, 2005; Sun *et al.*, 2007a).

### 2.3.2 Electrospinning

Electrospinning is based on charging a polymeric solution followed by ejecting the solution through a fine capillary tip or needle. The syringe pump forces the polymeric solution through a small-diameter capillary, thereby forming a pendant drop at the tip. A voltage is applied to the tip of the syringe in order to create a charge of certain polarity in the solution. The collecting surface is usually of opposite polarity. As a result of the applied electric field, a leading edge or Taylor cone forms, that eventually forms a fibre jet. The fibre jet then travels towards the collecting surface where solid fibres are deposited as the solvent evaporates. This ultimately leads to the formation of a membranous structure through the continuous deposition of polymeric fibres on the collecting surface. Figure 2.2 illustrates the polymer electrospinning process. The parameters during electrospinning including distance of the needle from the collecting surface, the applied voltage as well as the solution flow rate can be carefully manipulated and thus electrospun membranous matrices can be customized to achieve desired drug release patterns (Kim *et al.*, 2007; Sill and Von Recum, 2008).

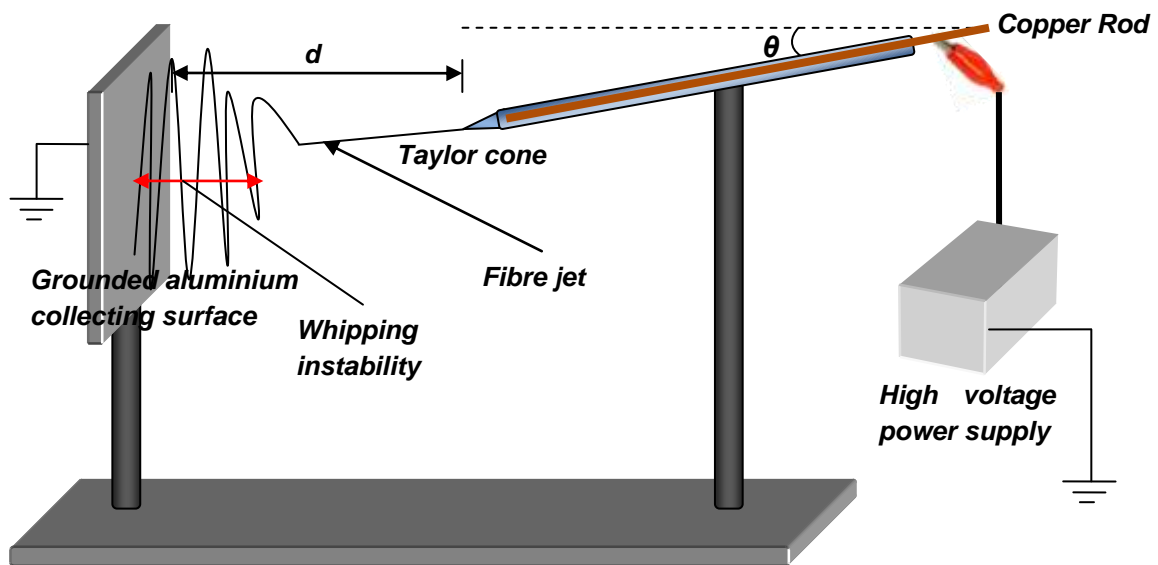


**Figure 2.2:** A schematic illustration of the electrospinning process, where  $d$  = distance between capillary tip and collecting surface and  $\theta$  = Capillary angle.

Electrospun nanofibrous membranes have many promising applications in the pharmaceutical industry, including tissue engineering, drug delivery and filtration. Thus far, several studies examined the potential of electrospun matrices for use as controlled drug delivery systems for the delivery of drugs such as antibiotics and anticancer drugs; as well as for tissue engineering applications (Sill and Von Recum, 2008). Approximately



one hundred polymers have successfully been manipulated through electrospinning to form nanofibrous matrices in a scaffold or membranous matrix-like structure. The various polymers that are used to form nanofibrous matrices currently used in the medical industry are depicted in *Chapter 5, Table 5.1*.

Electrospun nanofibrous matrices are able to modulate drug delivery due to their three dimensional porous structure that provides a relatively large surface area thus making them valuable scaffolds in tissue engineering. A key advantage of utilizing electrospinning in the formation of membrane systems is that the obtained membrane has high flexibility and good mechanical properties. Furthermore, the electrospun fibres can be aligned and functionalized to induce tissue alignment. However, a drawback associated with this technique arises during fabrication of electrospun membranes, there is a possibility that fibres may break, leading to the formation of poor quality nanofibrous membranes (Sill and Von Recum, 2008; Stamatialis *et al.*, 2008).

### **2.3.3 Foaming**

This method requires a soluble inert gas such as CO<sub>2</sub> or N<sub>2</sub>. The process involves the saturation of the polymer with the gas at a high pressure. The polymer and gas mixture is subsequently quenched into a supersaturated state either by a reduction of the pressure or an increase of the temperature. The properties of the formed membranes may be varied by changing the foaming process conditions. This technique is applicable to substances with high T<sub>g</sub> (glass transition) values such as pure polymers as well as polymer composites and ceramics. It does not require solvent use and thereby eliminates the risk of residues. However, the technique requires very high temperatures, which could lead to the degradation of the polymers employed and these membranes are not suitable for the application in tissue engineering due to their small pore size range (Matsuyama *et al.*, 2001b; Krause *et al.*, 2002; Matsuyama *et al.*, 2002; Sun *et al.*, 2007a; Stamatialis *et al.*, 2008).

### **2.3.4 Particle leaching**

Particle leaching is generally carried out in combination with other methods of membrane formation methods such as foaming and film-casting. The process involves the incorporation of salts, sugars, or other specifically prepared spheres into a polymer sample. The polymer is then processed into a membrane using an appropriate method (e.g. foaming, film-casting etc). The particles within the membrane are then dissolved and washed out to create additional pores in the membrane. This method ensures that membranes with highly controlled porosity and pore sizes are produced (Sanguanruksa *et*

*al.*, 2004). However, a drawback associated with this method is that it may not be applicable to all materials (e.g. soluble protein scaffolds). Furthermore, the washing out post-process is time-consuming and there is a risk of residues remaining from the method of processing (i.e. organic solvents) (Stamatialis *et al.*, 2008). Thus, this method is preferred for polymers that are not readily soluble in common organic solvents (Sanguanruksa *et al.*, 2004; RoyChowdhury and Kumar, 2005; Stamatialis *et al.*, 2008).

### **2.3.5 Emulsion freeze-drying**

This method involves an emulsification process which is attained through homogenization of a polymer-solvent and water system in which the polymer-rich phase is the continuous phase while water is the dispersed phase. The produced emulsion is cooled down rapidly and frozen, a process that results in the direct solidification of the polymer from the liquid phase, thus creating a porous polymeric structure or scaffold. Ultimately, the structure is freeze-dried in order to remove water and solvent. Studies indicated that this technique produces membranous scaffolds which are ideal for use in tissue engineering since the pores produced are large, and the membranes are relatively thicker than membranes formed through other methods (Ho *et al.*, 2004; Cheng *et al.*, 2008). Furthermore, incorporating proteins during fabrication is possible. However, there is a possibility of pores forming which are not highly interconnected. This creates a challenge when using certain ceramics as the resultant membranous scaffold becomes brittle (Cheng *et al.*, 2008; Stamatialis *et al.*, 2008).

### **2.3.6 Sintering**

This method involves heating powdered polymeric material causing the particles to adhere to one another, thereby forming a membranous scaffold. These kinds of membranous scaffolds show potential in tissue engineering applications, and separation processes. This technique is applied to certain polymers and their composites, and ceramic powders. The principle advantage of this method is that sintering allows for the production of polymeric membranes with a controlled and graded porosity (Stamatialis *et al.*, 2008). Sintering ceramic powders produces membranes with greater properties including higher thermal and mechanical stabilities and a better chemical and microbial resistance. In addition to their potential use in harsh environments (higher temperatures and exposure to various chemicals), ceramic membranes have a relatively long life of use, and are typically applied to separation processes due to their permeation characteristics. Pore size, porosity, and pore tortuosity can be carefully controlled by adjusting the conditions of the sintering procedure such as the temperature, pressure, particle size, green density and the addition of sintering additives (Qiu *et al.*, 2009). Liu

and Li (2005) investigated the effects of sintering temperature and time on the final membrane morphology. The study concluded that higher sintering temperatures result in membranes with lower porosities, whereas lower sintering temperatures produces highly porous membranes. Medically, sintering can be conducted to form three dimensional porous scaffolds by sintering polymeric microspheres onto existing moulds. Such porous scaffolds produced are widely applied in bone tissue engineering, with Bioglass® composite microspheres as a key component (Rezwan *et al.*, 2006).

## **2.4 Stimuli-responsive Polymers and their Application in Drug Delivery Systems**

Biopolymers are basic components found in all living organisms. Biopolymers, such as proteins, polysaccharides, and nucleic acids respond to changes in stimuli by undergoing a change in their properties. Stimuli-responsive polymers are able to mimic these biopolymers. Fundamentally, stimuli-responsive polymers are those polymers that when exposed to a slight change in the surrounding environment, undergo a relatively significant and immediate change in its properties. This change occurs as a result of the polymer recognizing a specific stimulus as a signal, judging the magnitude of this signal, and then changing its chain conformation in direct response (Gil and Hudson, 2004; Schmaljohann, 2006). These changes in response to stimuli, which are continuous throughout its polymer network, are exploited in many applications, specifically drug delivery for a plethora of applications, as illustrated in Figure 2.3. The driving force behind these changes include neutralization of charged groups by either a pH shift or addition of an oppositely charged polymer, changes in the efficiency of hydrogen bonding with an increase in temperature or ionic strength and collapse of hydrogels and interpenetrating polymeric networks. Electric, magnetic, light and radiation stimuli are also capable of inducing reversible phase transitions and are currently being considered as possible driving forces (Kumar, 2009).

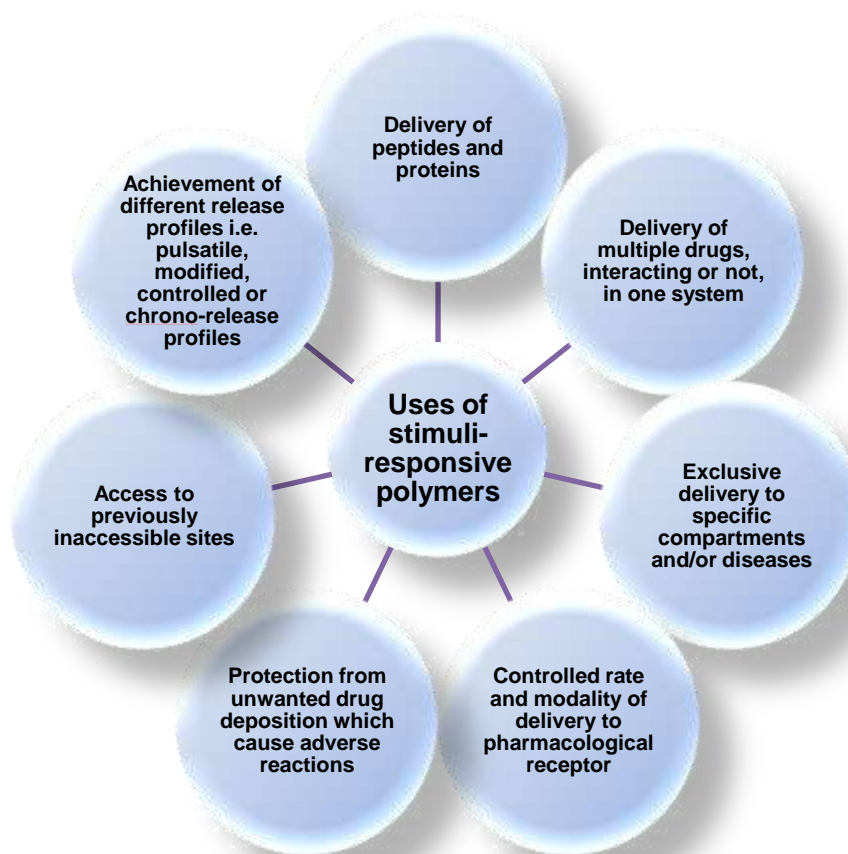


**Figure 2.3:** Common uses of stimuli-responsive polymers in terms of drug delivery (Adapted from Tomlinson, 1987).

In terms of drug delivery, smart polymers have been commonly used to achieve pulsatile or modulated release patterns which mimic biological demands, minimizing drug degradation and loss, the prevention of harmful side-effects and increasing drug bioavailability and the fraction of the drug accumulated in the required zone. Among the most important stimuli that are applicable in drug delivery systems are temperature and pH, however, external triggers, including electric current, photoirradiation or externally applied thermal changes, can be used to trigger the required change. Responses to stimuli may present as a change in physical conformation (size, shape, formation of an intricate molecular assembly), solubility (a sol-gel transition), mucoadhesion and surface characteristics, hydration state (swelling or shrinking), and increase or decrease in polymer permeability or release of a bioactive molecule (e.g. drug molecule) (Schmaljohann, 2006; Kumar *et al.*, 2007). These changes are typically reversible and can occur as a combination of several responses occurring simultaneously in response to one or more stimuli (i.e. dual responsiveness). Figure 2.4 illustrates the potential stimuli that may cause changes in the physical properties of stimuli-responsive polymers (Gil and Hudson, 2004; Schmaljohann, 2006; Kumar *et al.*, 2007; Kumar 2009).

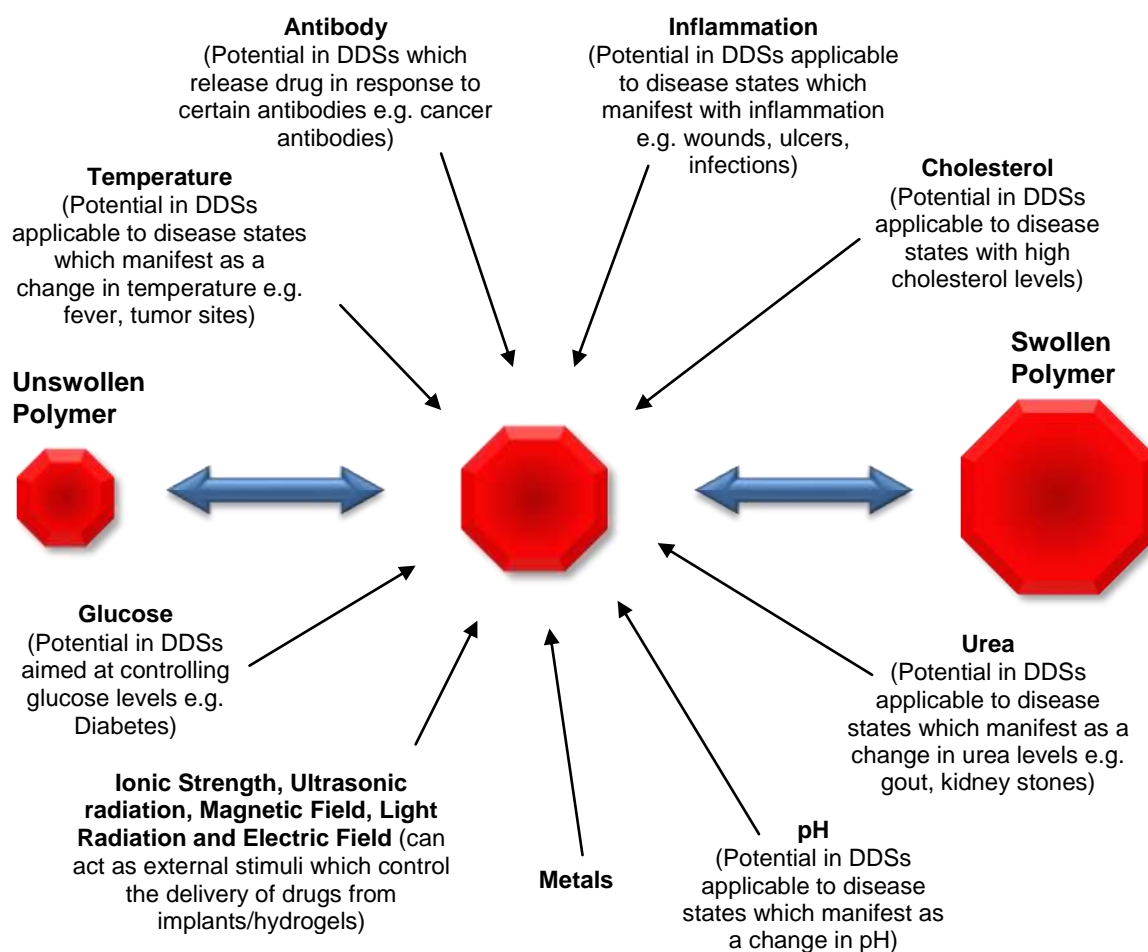


**Figure 2.4:** Factors that can transform unswollen polymer into swollen polymer (Adapted from Dispenza, 2009).

Some polymeric systems have been developed to combine two or more responsive mechanisms into one polymer (e.g. a polymer that responds to temperature may also be responsive to a change in pH). Simultaneous exposure to the stimuli is not always a prerequisite for the required response in these polymers (Gil and Hudson, 2004). These smart polymers in drug delivery have been applied in the delivery of proteins such as insulin (Chen *et al.*, 2005), and coenzyme A (Guo and Gao, 2007); anticancer drugs such as doxorubicin (Liu *et al.*, 2007) and paclitaxel (Liu *et al.*, 2005); and levonorgestrel (Chen and Singh, 2005a) among others.

Stimuli-responsive polymers can be used for intracellular delivery, exploiting the drop in pH from 6.2 in plasma and extracellular fluid to 5.0 in intracellular cytoplasm. Cellular absorption of polymers involves fluid-phase pinocytosis or receptor mediated endocytosis that leads into the formation of endosomes. Endosomes eventually fuse with lysosomes

which contain enzymes, causing a pH change which is utilized as a trigger for the release molecules into the cellular cytoplasm. These pH-responsive polymers are cationic in nature and can therefore be used for the intracellular delivery of nucleic acids. The cationic polymer binds to the negatively charged nucleic acid, and as this complex enters the endosomes, the cationic polymers are deprotonated. This deprotonation eventually leads to the disruption of the endosomal membrane, prior to the fusion with the lysosome, thereby allowing the release of drug molecules into the cytoplasm. Intracellular delivery of drugs using pH-responsive polymers may eventually lead to safer and more efficient drug delivery systems (Schmaljohann, 2006).

Polymers, silica and metal surfaces can be functionalised by stimuli-responsive polymers to produce highly responsive interfaces between two phases, usually a solid and a liquid. The modified interface produces a dynamic “on-off” system, through changing either the hydrophilic and/or hydrophobic balance of the surface. Table 2.1 provides the most commonly employed polymers used in pH-responsive and thermo-responsive systems which have been explored for drug delivery or other medical applications. Polymers may be conjugated to form polymeric conjugates with a modulated stimuli-responsive ability. Conjugation may also help in improving desirable properties such as mechanical strength and biodegradability of polymeric systems (Gil and Hudson, 2004).

Over the past two decades, there has been a great focus on research directed towards synthetic environmentally-responsive membranes (Obaidat and Park., 1997; Park *et al.*, 2001; Hester *et al.*, 2002; Ying *et al.*, 2004). These membranes are able to reversibly vary their own permeation characteristics in response to various environmental stimuli. They have potential applications in the treatment of wastewater streams, water softening, fractionation of macromolecules, drug delivery, cell encapsulation, electronic devices and sensors (Hester *et al.*, 2002).

Typically, drug release from membrane systems depends on various parameters such as initial drug-loading, membrane thickness, pH of the surrounding medium and the mechanism involved in membrane fabrication (Singh and Ray, 1999). Several of the membranous DDSs that have been developed respond to various stimuli including glucose concentration (Obaidat and Park, 1997; Chu *et al.*, 2004a), temperature (Ying *et al.*, 2004; Zhang *et al.*, 2006a), and pH (Park *et al.*, 2001; Varshosaz and Falamarzian, 2001; Hester *et al.*, 2002). These systems are further elaborated in this chapter.

**Table 2.1: Stimuli-responsive polymers and their drug delivery and other medical applications.**

| Polymer  | Drug delivery and other medical applications   | Reference                     |
|--|--|-------------------------------|
| <b>Thermo-responsive polymers</b>  |  |                               |
| <b>p(NIPAAm) copolymers</b>  |  |                               |
| p(NIPAAm-co-DMAAm-co-AMA)-b-PUA  | Doxorubicin and folic acid   | Liu <i>et al.</i> , 2007a     |
| P(NIPAAm-co-DMAAm)-b-poly(PLGA)  | Doxorubicin  | Liu <i>et al.</i> , 2005a     |
| Alginate-g-p(NIPAAm)   | Blue dextran   | Kim <i>et al.</i> , 2005b     |
| p(HEMA-g-NIPAAm)   | Theophylline and Inulin  | Ankareddi and Brazel, 2007    |
| p(NIPAAm)-HA   | Control of post-surgical tissue adhesions  | Ohya <i>et al.</i> , 2005     |
| p(NIPAM)-grafted gelatin (PNIPAM-g-gelatin).   | Haemostatic aid in uncontrolled bleeding during surgery  | Ohya <i>et al.</i> , 2005     |
| DMAEMA and p(NIPAAm)   | DNA delivery   | Hinrichs <i>et al.</i> , 1999 |
| <b>PEG / PLGA block copolymers</b>   |  |                               |
| PLGA-PEG-PLGA  | Delivery of proteins (model protein lysozyme used)   | Chen <i>et al.</i> , 2005     |
| PLGA-PEG-PLGA triblock copolymers with varying ratio of lactide/glycolide                      | Testosterone   | Chen and Singh; 2005b         |
| PLGA-PEG-PLGA microspheres   | Zinc crystalline recombinant human insulin   | Kwon and Kim, 2004            |
| PEG-PLGA-PEG triblock copolymers   | <i>In situ</i> generated implants  | Jeong <i>et al.</i> , 2000    |
| <b>Poly(organophosphazenes)</b>  |  |                               |
| Poly(organophosphazene) hydrogel   | Tissue engineering matrix (mouse pre-osteoblasts and collagen injected subcutaneously into nude mice forming an <i>in situ</i> gelation-injected site) | Yoon <i>et al.</i> ; 2007     |
| Poly(organophosphazene) hydrogel   | Tissue engineering (delivery of spheroidal hepatocytes).   | Park and Song, 2006           |
| Poly(organophosphazene) hydrogel   | Doxorubicin  | Kang <i>et al.</i> , 2006a    |
| Poly(organophosphazene) hydrogel   | Dextran and albumin  | Kang <i>et al.</i> , 2006b    |
| <b>PEG/biodegradable polyester copolymers</b>  |  |                               |
| P(HPMAmDL-b-PEG).  | Paclitaxel   | Soga <i>et al.</i> , 2005     |
| PEG and PPG  | <i>In situ</i> generated implants  | Cohn <i>et al.</i> , 2005     |
| PEG (Mw: 2000g/mol) with PLLA (PLLA/PEG/PLLA)  | Doxorubicin  | Na <i>et al.</i> , 2006       |
| Poly(PEG/PPG/PCL urethanes)  | Potential for application as a non-toxic polymer for use in biomedical applications  | Loh <i>et al.</i> , 2008      |
| <b>PEO / PPO block copolymers</b>  |  |                               |
| Pluronic <sup>®</sup> F127 (M <sub>w</sub> =12,600, 70wt% PEO) with hexamethylene diisocyanate | Delivery of an anti-restenosis model drug (RG-13577)   | Cohn <i>et al.</i> , 2003     |
| Pluronic <sup>®</sup> F127 (PEO99-PPO67-PEO99)   | Metronidazole and methylene blue   | Sosnik and Cohn, 2004         |
| Cross-linked PEO-PPO   | <i>In situ</i> generated implants produced by end-capping them with triethoxysilane or methacrylate reactive groups                                    | Cohn <i>et al.</i> , 2005     |
| Pluronic <sup>®</sup> F127   | <i>In situ</i> forming implant delivering of human growth hormone  | Chung <i>et al.</i> , 2008    |

**Table 2.1 continued**

| pH-responsive polymers  |  |   |
|---|--|---|
| <b>Methacrylic acid copolymers</b>  |  |   |
| Eudragit <sup>®</sup> L100-55 (pH 5.5)  | Mesalazine   | Khan <i>et al.</i> , 1999                                       |
| Eudragit <sup>®</sup> L100 (pH 6.0)   | Mesalazine   | Khan <i>et al.</i> , 2000                                       |
| Eudragit <sup>®</sup> S100 (pH 7.0)   | Mesalazine   | Khan <i>et al.</i> , 1999                                       |
| Eudragit <sup>®</sup> P-4135F   | (i) Norfloxacin<br>(ii) Ellagic acid   | (i) Hu <i>et al.</i> , 1999;<br>(ii) Jeong <i>et al.</i> , 2001 |
| GMD/PAA   | 5-aminosalicylic acid  | Kim and Oh, 2005  |
| MEMA/MAA copolymer  | Indomethacin and ephedrine HCl with the use of ethyleneglycol dimethacrylate as a cross-linker   | Varshosaz and Hajian, 2004                                      |
| p(MAA-EA)   | Procaine hydrochloride and Imipramine hydrochloride with diallyl phthalate (DAP) as a cross-linker   | Tan <i>et al.</i> , 2007  |
| p(MMA-DMA)  | Aminopyrine, caffeine and theobromine with divinylbenzene as a cross-linker  | Varshosaz and Falamarzian, 2001                                 |
| Poly(MMA)   | Microparticles incorporated into the hydrogel were grafted with PEG chains that are capable of complexing with the hydroxyl groups of the polyacid and interpenetrating into the mucus gel layer upon entry into the small intestine | Thomas <i>et al.</i> , 2007                                     |
| Copolymers composed of different aminoethyl methacrylate monomers synthesized from a PEG macroinitiator by ATRP | Heparin  | Dufresne and Leroux, 2004                                       |
| PEG-b-poly(alkyl acrylate-co-methacrylic acid)  | Fenofibrate and progesterone.  | Sant <i>et al.</i> , 2005                                       |
| p(HEMA)   | (i) Salicylic acid with tripropyleneglycol diacrylate (TPGDA) as a cross-linker;<br>(ii) Oral Insulin delivery with methacrylic acid   | (i) Ferreira <i>et al.</i> , 2000;<br>(ii) Mahkam, 2005         |
| p(HEMA)   | (i) Theophylline, proxiphylline and oxprenolol HCl combined with acrylic acid or methacrylic acid;<br>(ii) Insulin and Protamine with tetraethyleneglycol diacrylate (TEGDA) as a cross-linker                                       | (i) Khare and Peppas, 1993;<br>(ii) Brahim <i>et al.</i> , 2003 |
| Poly(EA/MAA/BDDA) and Poly(MMA/MAA/EGDMA)   | Biomaterials for structural support of soft connective tissues (degenerated intervertebral discs)  | Lally <i>et al.</i> , 2007                                      |
| Poly(MAA-g-EG)  | Comparison of complexed and uncomplexed hydrogels and their effects on the release of dextran and proxiphylline  | Lowman and Peppas, 1999   |
| PEG-b-p(AIA-co-tBMA)) block copolymers  | Poorly water-soluble model drugs: indomethacin, fenofibrate and progesterone   | Sant <i>et al.</i> , 2004                                       |
| Poly(HEMA-co-MAA) hydrogels   | Phenylpropanolamine with tetraethylene glycol dimethacrylate (TEGDMA) as a cross-linker  | Kou <i>et al.</i> , 1988  |
| PEG-b-poly(alkyl(meth)acrylate-co-MAA)  | Candesartan cilexetil  | Satturwar <i>et al.</i> , 2007                                  |
| poly(MMA-co-MAA)  | Oxprenolol HCl   | Kim and Lee, 1992   |



**Table 2.1 continued**

|   |  |  |
|---|--|--|
| Psyllium and methacrylamide<br>PCL-p(MAA-EG) hydrogel   | Tetracycline HCl<br>Hydrogels which swell at pH 7.2 and shrank at pH 1.2   | Singh <i>et al.</i> , 2007<br>Chao <i>et al.</i> , 2007  |
| <b>Poly(acrylate) derivatives</b><br>PVP and linear PAA<br>PA-g-guar gum<br>p(NPA)  | pH sensitivity in the pH range of 2.25 to 4.00 at 37°C<br>Diltiazem hydrochloride and nifedipine<br>Folic acid   | Jin <i>et al.</i> , 2006<br>Soppimath <i>et al.</i> , 2001<br>Sáez-Martínez <i>et al.</i> , 2008 |
| <b>Alginate derivatives</b><br>Alginate–guar gum hydrogel   | Delivery of proteins and peptides (i.e. BSA) with<br>glutaraldehyde as a cross-linker  | George and Abrahams,<br>2007   |
| <b>Chitosan</b><br>CHT-tetra ethyl ortho silicate (TEOS)<br>Polyphosphazenes<br>Polyphosphazene-PS, polyphosphazene-polysiloxane, and polyphosphazene-<br>ROMP of norbornene copolymers | Lidocaine HCl, sodium salicylate and 4-acetamidophenol<br>No drug delivery application. A dye Biebrich Scarlet was<br>used to test release from these copolymers | Park <i>et al.</i> , 2001<br>Allcock and Ambrosio, 1996  |

*P(NIPAAm)*: Poly(*N*-isopropylacrylamide); *DMAAm*: Dimethylacrylamide; *AMA*: 2-aminoethyl methacrylate; *PLGA*: Poly(*D,L*-lactide-co-glycolic acid); *HEMA*: 2-hydroxyethyl methacrylate; *HA*: Hyaluronan; *DMAEMA*: 2-(dimethylamino)ethyl methacrylate; *PEG*: poly(ethylene glycol); *HPMAmDL*: 2-hydroxypropyl methacrylamide lactate; *PPG*: Poly(propylene glycol); *PLLA*: Poly(*L*-lactic-acid); *PCL*: Poly(caprolactone); *PEO*: Poly(ethylene oxide); *PPO*: Poly(propylene oxide); *GMD*: Glycidyl methacrylate dextran; *PAA*: Poly(acrylic acid); *MAA*: Methacrylic acid; *MMA*: methyl methacrylate; *EA*: ethyl acrylate; *DMA*: dimethylaminoethyl methacrylate; *ATRP*: atom transfer radical polymerization; *BDDA*: butanediol diacrylate; *AIA*: alkyl acrylate; *EG*: ethylene glycol; *MA*: methacrylamide; *EGDMA*: ethyleneglycol dimethacrylate; *CL*: caprolactone; *tBMA*: *t*-butyl methacrylate; *AIMA*: alkyl (meth)acrylate; *PVP*: Poly(*N*-vinylpyrrolidone); *PA*: Polyacrylamide; *NPA*: *p*-nitrophenyl acrylate; *CHT*: Chitosan; *TEOS*: tetra ethyl ortho silicate; *PS*: Polystyrene.

### 2.4.1 Thermo-responsive polymers and their applications in membranous drug delivery systems

As of late, thermo-responsive DDSs have gained much attention since many disease states manifest themselves by a change in temperature, which can be employed to trigger conformational changes within the polymeric structure and hence affect drug release (Zhang *et al.*, 2006a). Thermo-responsive polymers exhibit a sol-gel behavior in response to temperature changes, and have been applied in drug and gene delivery, prevention of tissue adhesions, wound dressings, as cell carriers in tissue regeneration and *in situ*-forming systems (e.g. the “molecular condom” used in the prevention of STI’s and HIV transmission) (Ichikawa and Fukumori, 2000; Ohya *et al.*, 2005; Zhang and Misra, 2007; Ndesendo *et al.*, 2008). The change in the characteristics of the polymer arises from a lower critical solution temperature (LCST) behavior, where if a certain temperature threshold is surpassed; the polymer will undergo a reversible phase separation. These polymers are typically soluble in a solvent (usually water) at lower temperatures, however, once the LCST has been reached; the polymers begin to solidify and are rendered insoluble at temperatures above the LCST (Schmaljohann, 2006).

Drug delivery through these hydrogels usually occurs at the soluble stage of the polymer i.e. at temperatures lower than the LCST (Liang *et al.*, 1999; Ying *et al.*, 2004; Lue *et al.*, 2008). In principle, the LCST of a given polymer can be “tuned” to create the desired property by varying the hydrophilic or hydrophobic co-monomer content (Lue *et al.*, 2008). Thermo-responsive polymers commonly employed are listed in Table 2.1, with poly(*N*-isopropylacrylamide) [p(NIPAAm)] and its copolymers being the prevalent alternative. The majority of thermo-responsive polymer applications utilize the change from room to body temperature, or externally applied hyper/hypothermia to trigger the conformational change to a gel phase (Schmaljohann, 2006). These polymers are commonly grafted into the pores (Figure 2.5a) or surface (Figure 2.5b) of a membrane structure, controlling drug release in responses to changes in the surrounding temperature. Porous substrates are usually inert and provide physical strength and support, whereby the drug diffusion is controlled by the stimuli-responsive polymers present on the membrane surfaces or within pores (Chun and Kim, 1996; Ng *et al.*, 2001; Ying *et al.*, 2004; Lue *et al.*, 2007; Mizutani *et al.*, 2008).

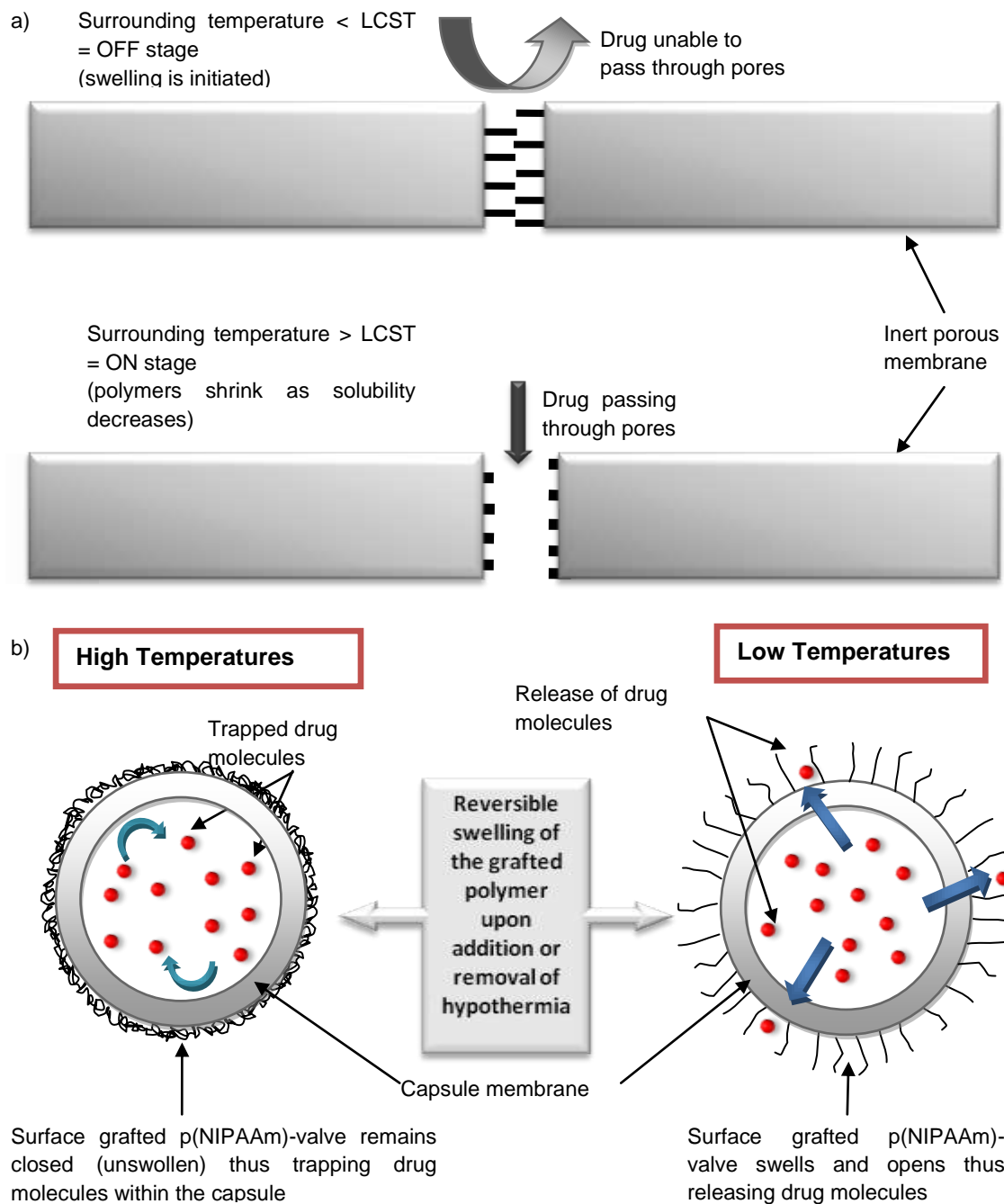


**Figure 2.5:** Schematic illustration of a) the ‘on-off’ valve mechanism of polymeric brushes grafted onto porous support, and b) the permeability changes occurring as a result of temperature changes of surface grafted polymeric chains (Adapted from Lue et al., 2008).

Commonly, p(NIPAAm) is grafted onto the surface of the pores in the form of polymeric brushes (Ying *et al.*, 2004; Lue *et al.*, 2008) forming an ‘on-off’ valve mechanism ideal for numerous applications (Table 2.2). The ‘off’ stage occurs when the polymeric brushes become soluble in water at temperatures below the LCST which leads to swelling that ultimately leads to closing of the membrane system pores, retarding drug release. The ‘on’ stage occurs when the polymer becomes insoluble in water at temperatures above

the LCST and shrinks, thus causing the opening of the pores within the membrane system, allowing drug release (Liang *et al.*, 1999; Ying *et al.*, 2004; Lue *et al.*, 2008). Alternatively, the pores in ‘on-off’ valve systems can be filled with liquid crystals which melt, thereby releasing drug at a certain temperature threshold (Dinarvand and Ansari, 2003; Makai *et al.*, 2003; Atyabi *et al.*, 2007); or by aminated polymers demonstrating improved and more sensitive thermo-responsive behaviour (Zhang *et al.*, 2006a). Such stimuli-responsive DDSs that release drug only above certain temperatures may be usefully applied as drug reservoir systems, specifically as implants (Ng *et al.*, 2001), transdermal patches (Csóka *et al.*, 2007; Dong *et al.*, 2008), and in wound healing (Ohya *et al.*, 2005). An area of vast potential is use of these systems chemotherapeutics delivery under local hyperthermia (Atyabi *et al.*, 2007).

**Table 2.2:** Application of thermo-responsive polymer p(NIPAAm) in ‘on-off’ valve mechanisms.

| <b>Grafting mechanism</b>   | <b>Porous membranes or substrate</b>  | <b>Drug delivery and Medical applications</b>              | <b>Reference</b>              |
|---|---------------------------------------|--|-------------------------------|
| Ultraviolet photopolymerization   | Hydrophilic microfiltration membranes | PP Solute separations                                      | Liang <i>et al.</i> , 1999    |
| Photoimmobilization via photoirradiation                                      | PC membranes                          | Permeation of Tryptophan                                   | Park <i>et al.</i> , 1998     |
| Irradiation   | PVDF membranes                        | Potential for polynucleotide, peptide and protein delivery | Åkerman <i>et al.</i> , 1998  |
| Photografting using UV light  | PET track membranes                   | None used  | Yang and Yang, 2003           |
| Plasma-induced graft polymerization   | PE membranes                          | Separation and filtration                                  | Huang <i>et al.</i> , 2002    |
| Plasma-induced graft polymerization   | Track-etched PC films                 | 4-acetamidophenol and ranitidine HCl                       | Lue <i>et al.</i> , 2007      |
| Plasma-induced graft polymerization   | PA microcapsules                      | NaCl and Vitamin B <sub>12</sub>                           | Chu <i>et al.</i> , 2001      |
| Radiation-induced graft polymerization  | PET and PP membranes                  | Separation and filtration                                  | Shtanko <i>et al.</i> , 2000  |
| Surface-initiated polymerization by aqueous FRP and ATRP                      | PET membranes                         | Separation and filtration                                  | Alem <i>et al.</i> , 2008     |
| <i>In situ</i> polymerization of hydrogel within pores of the sintered glass. | Disc-shaped sintered glass filter     | Permeation of salicylic acid and bovine albumin            | Li and D'Emanuele, 2001       |
| Surface initiated ATRP  | PS substrates                         | Cell-based therapy for severe disorders                    | Mizutani <i>et al.</i> , 2008 |

PP: polypropylene; PC: Polycarbonate; PVDF: Poly(vinylidene fluoride); PET: Polyethylene terephthalate; ; PE: Polyethylene; PA: Polyamide; FRP: free radical polymerization; ATRP: atom transfer radical polymerization; PS: Polystyrene

### **2.4.2 pH-responsive polymers and their applications in membranous drug delivery systems**

The use of pH-responsive hydrogels as stimuli-responsive drug delivery systems is based on the variability of the physiological pH is at different sites of the body, including the GIT, vagina and blood vessels (lemma *et al.*, 2006). pH-responsive polymers are used to target drug delivery to damaged, wounded or inflamed tissues and certain cancer cells. Table 2.3 lists commonly targeted drug delivery sites in the body and their respective pH ranges. For a polymer to portray pH-responsive properties, they should be ionisable and preferably have a  $pK_a$  value of 3-10 (lemma *et al.*, 2006; Schmaljohann, 2006). A change in pH results in a deviation in the ionisation state of these polymers (via protonation/deprotonation events thus imparting a charge over the molecule) and therefore a conformational change, which culminates in the changing of the solubility and swelling behavior of the polymer. This pH-responsive swelling ability has been exploited to induce the controlled release of drugs and proteins (lemma *et al.*, 2006; Schmaljohann, 2006; Kumar *et al.*, 2007).

The pH sensitivity of a pH-responsive polymer is a direct result of the presence of weakly acidic (e.g. carboxylic and sulfonic acids) and/or weakly basic (e.g. ammonium salts or amino groups) functional groups on the polymeric backbone, which allow for reversible swelling/deswelling behavior in acidic or basic media. These functional groups undergo protonation/deprotonation with changes in pH as small as 0.2-0.3 units, thus resulting in water uptake by the polymer, increasing the solubility of solutes within the polymeric matrix, thus releasing said solutes (Lee and Shim, 1997; Soppimath *et al.*, 2001). The ionisation of these polymers (which depends on the pH and ionic strength of the external medium), renders them pH-responsive thus making them useful in drug delivery systems known as pH-dependant 'switch-on and -off' systems (lemma *et al.*, 2006). Thus far, these pH-responsive hydrogels have shown vast potential in the delivery of drugs and therapeutic agents into various areas of the body (Lee and Shim, 1997; Soppimath *et al.*, 2001; Varshosaz and Falamarzian, 2001; lemma *et al.*, 2006). Table 2.2 summarizes certain pH-responsive polymers that have been employed in smart drug delivery systems.

**Table 2.3:** Variations in pH values in different tissue and cellular compartments (Adapted from Schmaljohann, 2006; Mania-Pramanik *et al.*, 2008).

| <b>Tissue/cellular compartment</b> | <b>pH</b> |
|------------------------------------|-----------|
| Blood                              | 7.35-7.45 |
| Stomach                            | 1.0-3.0   |
| Duodenum                           | 4.8-8.2   |
| Colon                              | 7.0-7.5   |
| Early endosome                     | 6.0-6.5   |
| Late endosome                      | 5.0-6.0   |
| Lysosome                           | 4.5-5.0   |
| Golgi                              | 6.4       |
| Tumour, extracellular              | 7.2-6.5   |
| Vagina                             | 3.5-5.0   |

Poly(vinyl alcohol) (PVA) and poly(acrylic acid) (PAA) have been used to prepare pH-responsive interpenetrating polymeric network (IPN) membranes by employing varying crosslinking ratios for application in drug and selective protein separation (Gudeman and Peppas 1995). Methacrylate based polymers are commonly employed as coatings, which control drug release over the physiological pH range. The permeability of such coatings, referred to as enteric coatings, differ over the physiological pH range, and hence is ideal for use in drug targeting (Sun *et al.*, 2001). Poly(ethylene-co-vinyl-alcohol) (EVAL) blended with PAA or glycine demonstrate potential for colonic drug delivery in the local treatment of ulcerative colitis (Shieh *et al.*, 2000) or colorectal cancer (Lai *et al.*, 2006). The 'on-off' valve mechanism can also be successfully achieved with pH-responsive hydrogels where drug permeability differs with changes in pH (Mika *et al.*, 1999; Kai and Min, 2001; Varshosaz and Falamarzian, 2001; Hu and Dickson, 2008). pH-responsive polymers can be grafted onto the surfaces of said membranes through a variety of mechanisms including UV irradiation (Kai and Min, 2001) and  $\gamma$ -ray irradiation (Singh and Ray, 1999).

### **2.4.3 Glucose-responsive polymers and their applications in membranous drug delivery systems**

Recently, studies have aimed at developing biomaterials that exhibit sensitivity to biomolecules, demonstrating potential in the development of drug delivery systems with improved therapeutic efficacies and a lower side effect profile. These systems have the potential to release the drug or bioactive only when the body requires it. Thus far, there is no sufficiently effective system for the control of blood glucose levels. In insulin-dependent diabetes, an increase in blood glucose levels requires the administration of insulin to effectively control blood glucose levels. Daily insulin injections cause discomfort and other complications and therefore improved and novel means of delivering insulin would be beneficial in diabetes treatment (Tang *et al.*, 2003).

Hydrogels, implantable or injectable, which respond to glucose by swelling or deswelling, have potential for a self-regulating insulin delivery system as an alternative in the treatment of diabetes. Typically, self-regulating glucose-responsive systems should mimic the physiological response of insulin release from the pancreas in response to blood glucose concentrations (Tang *et al.*, 2003). To date, competitive binding, substrate-enzyme reactions, pH-dependant polymer erosion or drug solubility are employed as glucose sensing mechanisms (Podual *et al.*, 2000; Miyata *et al.*, 2002; Zhang and Wu, 2002; Tang *et al.*, 2003).

Lectin incorporated systems rely on the concept of competitive binding, whereby insulin molecules are initially attached to a lectin molecule. The lectin molecules have a higher affinity for glucose molecules, and hence will detach from the insulin molecules in the presence of glucose and therefore releasing insulin as a function of free glucose concentration in the environment. The concept of competitive binding for insulin release has also been employed in phenylboronic acid incorporated systems. The phenylboronic acid is initially attached to polymeric molecules, illustrated in Figure 2.6, and in the presence of glucose, dissociates from the polymer, disrupting the polymeric network, and promoting insulin permeability (Kitano *et al.*, 1992; Obaidat and Park, 1996; Miyata *et al.*, 2002; Tang *et al.*, 2003).

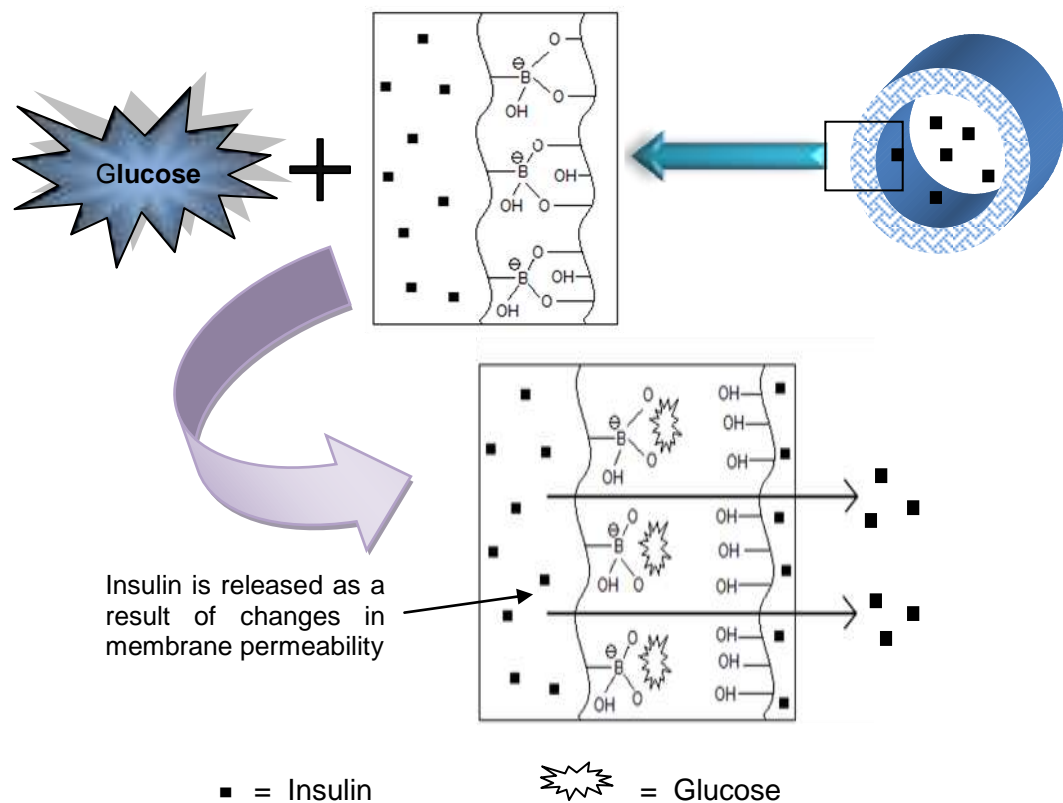


**Figure 2.6:** A glucose-responsive insulin releasing system based on PVA/poly(NVP-co-PBA) (Adapted from Kitano *et al.*, 1992).

In enzyme incorporated systems, the stimuli-responsive behaviour is not exclusive to the presence of glucose molecules, but rather from a change in pH caused by glucose oxidase enzymes in the presence of glucose molecules. Glucose oxidase converts glucose to gluconic acid and hydrogen peroxide, lowering the pH of the environment surrounding the DDS (Podual *et al.*, 2000; Chu *et al.*, 2004a). This pH change acts as a trigger for the incorporated pH-responsive polymeric chain grafts to undergo a conformational change leading to insulin release. As the pH of the body drops with increasing concentrations of glucose, insulin release increases (Podual *et al.*, 2000).

Catalase is incorporated into these glucose-responsive systems to eliminate hydrogen peroxide and therefore prevent toxicity, by ensuring that oxygen depletion is prevented (Zhang and Wu, 2002; Miyata *et al.*, 2002). Various polymers including polyacrylates, polymethacrylates, polyethylene, polypyrroles, silica, and poly(vinyl alcohol) have been successfully used as substrates for the immobilization of glucose oxidase (Podual *et al.*, 2000). The clinical efficacy of glucose-responsive systems was studied by Traitel and co-workers who reported that a poly(HEMA-co-N,N-dimethylaminoethyl methacrylate) [p(HEMA-co-DMAEMA)] hydrogel entrapped with glucose oxidase, catalase and insulin was both biocompatible and effective in reducing blood glucose levels in rats (Traitel *et al.*, 2000).

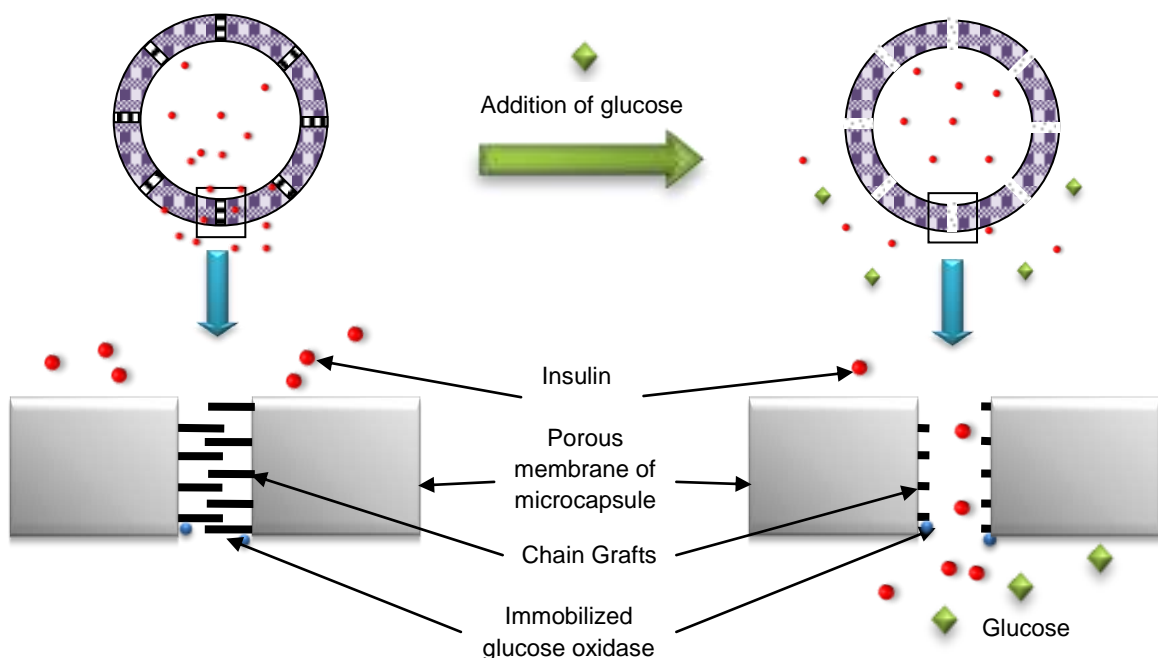


**Figure 2.7:** Schematic representation of a typical glucose-responsive microcapsule. The pores contain surface immobilised enzyme glucose oxidase with grafted pH-responsive PAA chains which, upon exposure to glucose, causes the pore opening and consequent insulin release (Adapted from Chu *et al.*, 2004b).



#### 2.4.4 Dual-responsive systems

The combination of two stimuli-responsive mechanisms in one polymeric system results in the development of a dual-responsive system that responds only when exposed to two stimuli simultaneously (Ashok *et al.*, 2007). Injections of thermo-responsive hydrogels into deep anatomical sites within the body are not suitable due to the premature gelling of the hydrogel within the catheter used to deliver the hydrogel (Shim *et al.*, 2006). This challenge can be overcome by combining a thermo-responsive polymer with a pH-responsive polymer to form a copolymer that is responsive to both pH and temperature changes, which gels only in response to simultaneous exposure to pH and temperature, preventing any premature gelation (Liu *et al.*, 2007b).

Shim and co-workers (2006) reported a novel pH- and thermo-responsive block copolymer prepared by adding pH-responsive sulfamethazine oligomer (SMO) to thermo-responsive poly(caprolactone-co-lactide)-PEG-poly(caprolactone-co-lactide) resulting in a copolymer solution which demonstrated a reversible sol-gel transition triggered by a change in the pH in the range of 7.2-8.0 at a temperature of 37°C (body temperature) (Shim *et al.*, 2006). Hoffman and Dong, (1992) crosslinked various ratios of p(NIPAAm) and poly(*N,N'*-dimethyl aminopropyl methacrylamide) to form a positively charged pH-/thermo-responsive hydrogel. Dual-responsive systems in the form of beads have also been developed by Kim and co-workers for the release of insulin. These beads were composed of poly(NIPAAm-co-butylmethacrylate-co-acrylic-acid) and PAA, which controlled rate of insulin release (pH 7.4; 37°C) (Kim *et al.*, 1994).

Dual-responsive membranes can be prepared by co-grafting thermo- and pH-responsive polymers, in the form of chains or nanoparticles, on porous membrane substrates. Porous polyamide membranes grafted with both PAA and p(NIPAAm) were found to be responsive to both temperature and pH. These were amongst the first dual-responsive membranes produced. Permeability of solutes (peptides, Leuprolide, vitamin B12, insulin, and lysozyme) across these membranes increased with increasing temperatures or particle concentration and decreased with increasing pH (Lee and Shim, 1997; Zhang and Wu, 2004).

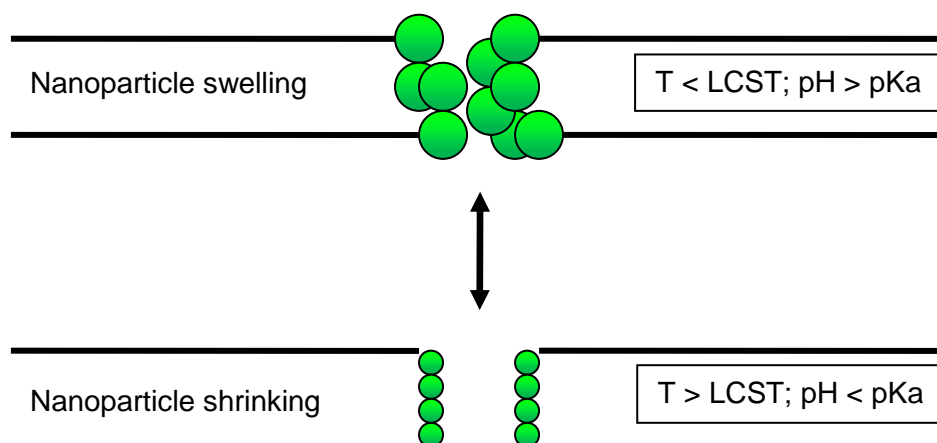


**Figure 2.8:** A simplified schematic illustrating the permeation of solutes through a nanoparticulate thermo- and pH-responsive membrane (Adapted from: Zhang and Wu, 2004).

Chitosan (CHT) based hydrogel films possessing both thermal and pH-sensitivity were prepared by blending CHT with p(NIPAAm) and polyethylene glycol (PEG). PEG was added to enhance thermo-mechanical and swelling properties of the film. The data obtained from the study revealed that the blended CHT/PEG/p(NIPAAm) films had a LCST at around 32°C due to the p(NIPAAm) component and demonstrated pH-responsiveness due to the amino groups of CHT component (Sun *et al.*, 2007b).

Membranes with dual-responsive systems not originating from pH- and/or thermo-responsive properties have also been investigated (Kontturi *et al.*, 1996; Zhang and Misra, 2007). In an attempt by Kontturi and co-workers, a PVDF hydrophobic membrane was grafted with PAA via radiation grafting. The resultant PVDF/PAA membranes demonstrated convective permeability which changed significantly with the pH and/or the salt concentration of surrounding fluids, thus representing an appropriate dual-responsive mechanism (Kontturi *et al.*, 1996). The effects of a thermo-responsive polymer combined with a magnetic drug-targeting carrier were also investigated (Zhang and Misra, 2007; Yang *et al.*, 2008).

These types of responsive systems offers substantial potential for application in the field of drug targeting such as delivery of anti-cancer drugs to tumour sites, and they are associated with reduced side-effects and controlled drug release in response to temperature changes, as well as magnetic flux. These microcapsules are directed to the target and remain there with the aid of the magnetic field. The permeability of the microcapsule membrane changes in response to environmental temperature, thus

controlling the rate of drug release (Zhang and Misra, 2007). Other applications of such dual-responsive systems include controlled-release of chemicals, and the production of biomedical and/or chemical sensors and microreactors (Yang *et al.*, 2008).

## **2.5 Concluding Remarks**

The focus of this chapter was placed on reviewing stimuli-responsive polymers, in particular pH- and thermo-responsive membranous systems. ‘Smart’ drug delivery systems have shown great potential in combating many disease states due to their targetability and in-built drug release mechanisms. Rather than acting exclusively as a drug carrier, these systems are able to respond to their environments, allowing drugs to be delivered solely to the target site and in response to a disease related stimulus. This, in turn, allows for safer and more potent therapeutic interventions in many disease states thus improving the health-related quality of life in countless patients. Commonly employed pH- and thermo-responsive polymers were identified and their applications in drug delivery were further elaborated. The concept of the ‘on-off’ gating mechanism was comprehensively reviewed with reference to stimuli-responsive polymers able to achieve said mechanism. The various methods employed in fabrication of membrane systems were briefly discussed, with impetus placed on the electrospinning method. Furthermore, the polymers and solvents employed in electrospinning were identified with their potential drug delivery and other medical applications. In conclusion, membranous drug delivery systems developed from the architecture of various drug delivery technologies have significant potential in solving the problem of uncontrolled and untargeted delivery of drugs to different body sites. Research should therefore be aimed at developing more refined membranous drug delivery systems with enhanced intelligent capabilities using stimuli-responsive polymers for the treatment of various diseases.

# CHAPTER 3

## PRELIMINARY DESIGN OF THE STIMULI-RESPONSIVE MUCOADHESIVE LAYERS OF THE MULTI-COMPONENT MEMBRANOUS DRUG DELIVERY SYSTEM

---

### 3.1 Introduction

As of late, there is growing interest in the development of drug delivery systems employing mucoadhesive polymers which are able to attach to a desired tissue (or to the surface coating of the tissue, mucin) within the human body, thereby providing a targeted system. As such, the bioavailabilities of existing drug molecules, especially those with narrow therapeutic absorption windows are enhanced, thereby maximising their therapeutic effectiveness ultimately improving their cost-effectiveness. Mucoadhesive systems in oral drug delivery promise the advantage of a prolonged gastric or small intestinal residence time, an intimate contact of the delivery system with the absorption site and the basis for interactions of multifunctional polymers with the mucosa such as permeation enhancement or enzyme inhibition. Mucoadhesive drug delivery systems (MDDSs) improve many administration routes, like the ocular, nasal, buccal and gingival, gastrointestinal (oral), vaginal and rectal routes, through the mechanisms illustrated in Figure 3.1. A polymer is mucoadhesive if it is able to adhere (for an extended duration of time) to a mucosal surface within the human body. Such mucoadhesion arises through interfacial molecular attractive forces present at the interface between a mucoadhesive polymer and a mucosal membrane (Harris *et al.*, 1990; Bernkop-Schnürch, 2005; Roy *et al.*, 2009; Khutoryanskiy, 2010; Yadav *et al.*, 2010; Mythri *et al.*, 2011).

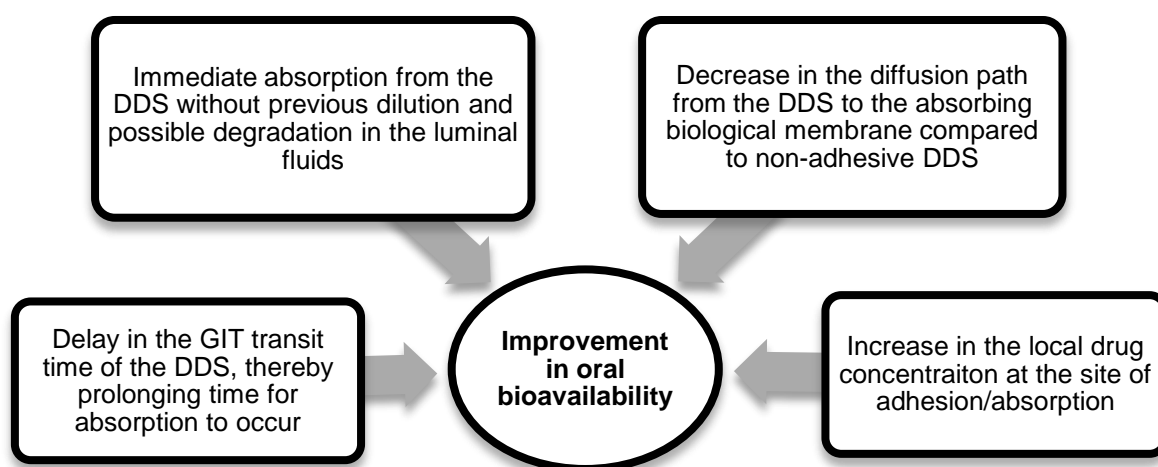


**Figure 3.1:** Mechanisms of which mucoadhesion improves oral bioavailability of drugs.

Although not entirely understood, the use of mucoadhesive polymers dates back as early as 1947, when Scrivener and Schantz reported the use of gum tragacanth combined with a dental adhesive to administer penicillin to the oral cavity (Scrivener and Schantz, 1947). This pioneering study ultimately led to further developments in MDDSs, using novel mucoadhesive polymers with varying molecular architectures in various drug delivery approaches. The repertoire of advantages associated with mucoadhesive polymers includes an increase in residence time of the MDDS at the site of absorption thus improving drug bioavailability and reducing dosage frequency, simplifying the administration of a dosage form and termination of a therapy (for transdermal, buccal or ocular systems), and the possibility of targeting particular body sites and tissues (Harding *et al.*, 1999; Roy *et al.*, 2009; Khutoryanskiy, 2010). Prior to the selection and identification of appropriate mucoadhesive polymers for the MMDDS, it was important to fully comprehend the mechanisms of mucoadhesion, define the various classes of mucoadhesives, and identify any factors that would affect the mucoadhesive properties of polymers.

### **3.1.1 Theories of mucoadhesion**

In spite of copious research, scientists cannot fully elucidate the phenomenon responsible for mucoadhesion. As a result, there are various theories attempting to account for mucoadhesion, as follows:

#### **3.1.1.1 The electronic theory**

*The electronic theory* postulates that attractive forces arise resulting from the transfer of electrons between the mucoadhesive polymer and mucus (having different electronic characteristics) causing the formation of an electrical double layer thereby giving rise to electrostatic attraction (Hogerstrom, *et. al.*, 2003; Dodou *et al.*, 2005; Khutoryanskiy, 2010; Mythri *et al.*, 2011).

#### **3.1.1.2 The adsorption theory**

*The adsorption theory* proposes that intermolecular forces such as hydrogen bonding, Van der Waals forces and chemisorption (through covalent bonds), provide the adhesive attraction between mucus and mucoadhesive polymers. Furthermore, the adsorption theory also considers that hydrophobic effects, especially in amphiphilic polymers, play an important role in mucoadhesion (Hogerstrom, *et. al.*, 2003; Dodou *et al.*, 2005; Khutoryanskiy, 2010; Mythri *et al.*, 2011).

### **3.1.1.3 The wetting theory**

*The wetting theory* correlates the surface tension of the mucus and the mucoadhesive polymer with its spreading ability. The lower the contact angle of the liquid on the mucus surface, the higher its affinity for that surface. This theory is mainly applicable to liquid mucoadhesive forms, but if two solid substrates are brought into contact in the presence of a liquid, the liquid may act as an adhesive between the two surfaces (Hogerstrom, et. al., 2003; Dodou *et al.*, 2005; Khutoryanskiy, 2010; Mythri *et al.*, 2011).

### **3.1.1.4 The diffusion theory**

*The diffusion theory* proposes that mucoadhesion depends on the formation of a networked or interpenetrated structure between the mucoadhesive polymeric chains and the mucus layer. Mucoadhesive macromolecules are able to penetrate the mucus layer and soluble mucins are able to diffuse into the dosage form or mucoadhesive system due to the presence of a concentration gradient between the two interfaces, forming a semi-permanent bond through physical entanglement. The theory further postulates that mucoadhesion is dependent on the molecular weight of mucoadhesive macromolecules, their hydrodynamic size and mobility, and that the depth of interpenetration is dependent on the diffusion coefficient and the contact time. It defines that efficient adhesion can be achieved when the interpenetration layer reaches 0.2-0.5mm in thickness (Hogerstrom, et. al., 2003; Dodou *et al.*, 2005; Khutoryanskiy, 2010; Mythri *et al.*, 2011).

### **3.1.1.5 The fracture theory**

*The fracture theory* elucidates that the difficulty of separation of two surfaces after adhesion is related to the adhesive bond strength of the mucoadhesive polymer. This theory is considered suitable in the calculation of the fracture strength of adhesive bonds which involve solid and rigid mucoadhesive materials. The fracture theory is considered to be the most widely accepted theory of mucoadhesion (Hogerstrom, et. al., 2003; Dodou *et al.*, 2005; Khutoryanskiy, 2010; Mythri *et al.*, 2011).

### **3.1.1.6 The mechanical theory**

*The mechanical theory* relates the effect of surface morphology such as micro-cracks and surface irregularities or roughness with an increase in contact area, thereby promoting mucoadhesion. Liquid or gel-like adhesives are able to diffuse into said micro-cracks and irregularities, forming an interlocked network which promotes adhesion (Dodou *et al.*, 2005; Smart, 2005; Roy *et al.*, 2009; Khutoryanskiy, 2010; Harsulkar *et al.*, 2011; Tangri and Madav, 2011).

Due to the complexity of the mucoadhesive process, none of these theories are able to fully describe the concept of mucoadhesion when they are considered in isolation. Mucoadhesion most probably results from a number of mechanisms combined. As a result, authors prefer to define the mucoadhesive process as sequential process of phases, each associated with a different mechanism. It has been reported that mucoadhesion can be divided into two phases, namely the contact and consolidation phases as illustrated in Figure 3.2 (Hogerstrom, et. al., 2003; Dodou *et al.*, 2005; Khutoryanskiy, 2010; Mythri *et al.*, 2011).

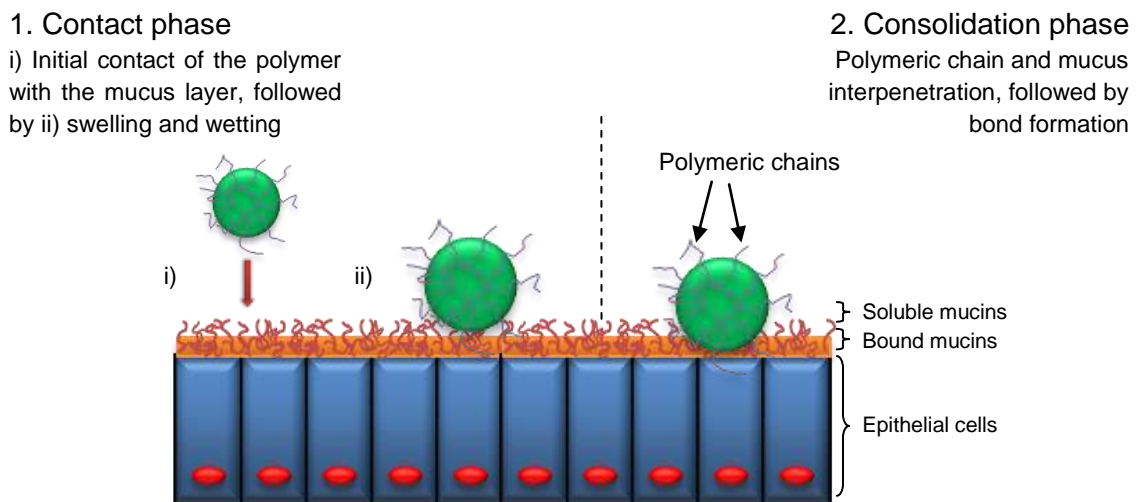


**Figure 3.2:** Schematic demonstration of the mucoadhesive process (divided into the contact and consolidation phases) (Adapted from Khutoryanskiy, 2010).

The contact phase is initiated with contact between the mucoadhesive polymer and the mucus membrane. This phase is characterised by swelling (wetting theory) and spreading of the polymer over the mucosal layer. As a result, deep or intimate contact between the polymeric network and the mucosal layer is achieved. The following consolidation phase is characterised by the presence of moisture which plasticizes the system, allowing polymer chains to interpenetrate with the mucus layer (diffusion theory) resulting in the free mucoadhesive molecules forming weak Van der Waals and hydrogen bonds (adsorption and electronic theories), thus maintaining mucoadhesion (Hogerstrom, et. al., 2003; Dodou *et al.*, 2005; Khutoryanskiy, 2010; Mythri *et al.*, 2011).

### 3.1.2 Classification and properties of mucoadhesive polymers

Mucoadhesives are generally classified using a variety of criteria, including charged state, source, binding ability or binding forces. The criteria employed in classifying mucoadhesives differs depending on the authors preferences, e.g. Grabovac and co-workers (2005) prefer to classify mucoadhesives into four broad categories based on

charge viz. anionic, cationic, non-ionic and thiolated polymers, while Helliwell and coworkers prefer to classify mucoadhesives into the specific and non-specific groups, based on their binding ability to various substrates (Helliwell *et al.*, 1992; Grabovac *et al.*, 2005). The various classification criteria commonly employed by authors are illustrated in Table 3.1.

For a polymer to exhibit sufficient mucoadhesive properties, it should contain strong hydrogen bonding groups, strong anionic or cationic charges, high molecular weight, chain flexibility, and surface energy properties favouring spreading on a mucosal layer while demonstrating suitable wetting and swelling of the polymer which favours mucoadhesion. Ideally, a mucoadhesive polymeric matrix should be biodegradable and rapidly adhere to the mucosal layer without any change in the physical characteristics of the DDS (with no impact on the bioactive release rate) while inhibiting enzymes present at the delivery site and enhancing the penetration of the active agent. Swelling and hydration permits mutual interpenetration and subsequent establishment of bonds and interactions between polymeric chains and mucin molecules. Generally, an increase in physical entanglement strengthens the network in the interfacial/contact area, improving mucoadhesion (Salamat-Miller *et al.*, 2005; Sudhakar *et al.*, 2006; Roy *et al.*, 2009).



**Table 3.1:** Classification of various mucoadhesive polymers (Adapted from Salamat-Miller *et al.*, 2005).

| Criteria                  | Categories                     | Comments  | Examples  | References   |
|---------------------------|--------------------------------|---|---|--|
| <b>Source</b>             | Natural/<br>Semi-<br>Synthetic | Majority of the natural polymers, or conventional mucoadhesives, typically display non-specific mucoadhesion, and relatively poorer mucoadhesive characteristics than their synthetic counterparts.   | Agarose, CHT, gelatin<br>Hyaluronic acid<br><i>Various gums:</i> guar, sodium alginate, hakea, gellan, pectin, xanthan, carrageenan   | Salamat-Miller <i>et al.</i> , 2005  |
|                           | Synthetic                      | Mucoadhesive polymers undergo chemical modification to further improve their targeting, mucoadhesive characteristics, toxicity profiles and biocompatibility.   | <i>Cellulosic derivatives:</i> CMC, thiolated CMC, NaCMC, HEC, HPC, HPMC, MC etc.<br><i>PAA-based polymers:</i> PAA, polyacrylates, P(MVE-MAA), pHEMA, PAA-EHA, PMA, PACA, PHCA, PBCA, copolymers of acrylic acid and PEG<br><i>Others:</i> PHPMAm, PVA, PVP, polyoxyethylene, thiolated polymers |  |
| <b>Aqueous Solubility</b> | Hydrophilic                    | Water-soluble polymers swell indefinitely in contact with water, eventually undergoing complete dissolution. Hydrogels, on the other hand are water swellable materials, usually a cross-linked polymer with limited swelling capacity. These hydrogels swell by absorbing water present in the mucus layer, hence interacting with the mucus by means of means of adhesion.  | <i>Hydrophilic polymers:</i> MC, HEC, HPMC, sodium CMC, carbomers, PAA and plant gums.<br><i>Hydrogels:</i> poly(acrylic acid-co-acrylamide) copolymers, carrageenan, sodium alginate, guar gum and modified guar gum.  | Chowdary and Srinivasa Rao, 2004; Salamat-Miller <i>et al.</i> , 2005; Sudhakar <i>et al.</i> , 2006 |
|                           | Hydrophobic                    | Water-insoluble polymers provide greater flexibility in dosage form design in comparison water-soluble polymers.  | CHT (soluble in dilute aqueous acids), EC, PC   |  |
| <b>Charge</b>             | Cationic                       | CHT is the most commonly employed cationic polymer due to its favourable biocompatibility, biodegradability and relatively lower toxicological properties. Furthermore, CHT has demonstrated permeation enhancing properties via the paracellular route through neutralisation of fixed anionic sites within the tight junctions between mucosal cells.   | Aminodextran, CHT, dimethylaminoethyl (DEAE)-dextran, trimethylated CHT, Selected synthetic polymethacrylates   | Grabovac <i>et al.</i> , 2005; Salamat-Miller <i>et al.</i> , 2005; Andrews <i>et al.</i> , 2009;    |
|                           | Anionic                        | Anionic polymers display the greatest interaction with mucus/mucosal layers and are commonly utilised due to their low toxicity. These polymers typically present with carboxyl and sulphate functional groups which provide a net overall negative charge at pH values exceeding the $pK_a$ of the polymer. Mucoadhesion arises from the presence of the carboxylic groups forming hydrogen-bonds with the oligosaccharide chains of mucins. | CHT-EDTA, CP, CMC, pectin, PAA, PC, sodium alginate, NaCMC, xanthan gum   | Khutoryanskiy <i>et al.</i> , 2010; Harsulkar <i>et al.</i> , 2011                                   |
|                           | Amphoteric                     | Mucoadhesive properties of polyampholytes (polymers simultaneously bearing cationic and anionic functional groups) have been explored only in few studies. Although boasting permeation enhancing properties, pH changes in the surrounding media cause structural and physicochemical  | Gelatin<br>N-carboxymethylchitosan  |  |

**Table 3.1 continued**

|                                  |                           |  |   |   |
|----------------------------------|---------------------------|--|---|---|
|                                  |                           | transformations which are expected to affect the mucoadhesive and penetration enhancing properties of polyampholyte-based formulations.  |   |   |
|                                  | Non-ionic                 | Non-ionic polymers typically display poorer mucoadhesive tendencies than their charged counterparts. Mucoadhesion typically arises through diffusion of their macromolecules and formation of an interpenetration layer with mucus gel (diffusion theory).   | Hydroxyethyl starch, HPC, PEO, PVA, PVP, scleroglucan   |   |
| <b>Potential adhesive forces</b> | Covalent                  | Polymers demonstrating mucoadhesive characteristics based on covalent bonding demonstrate significantly enhanced mucoadhesive characteristics than conventional mucoadhesives. Thiolated polymers are capable of forming covalent bonds (disulfide bridges) with cysteine-rich subdomains of mucus glycoproteins either via thiol/disulfide exchange reactions or through a simple oxidation of free thiol groups. | Cyanoacrylate, thiolated polymers, Polymers with acrylate end groups  | Dodou <i>et al.</i> , 2005; Salamat-Miller <i>et al.</i> , 2005; Andrews <i>et al.</i> , 2009; Khutoryanskiy <i>et al.</i> , 2010 |
|                                  | Hydrogen Bond             | These polymers generally contain functional groups which form hydrogen bonds with mucus. For sufficient hydrogen bonding to occur, flexibility of the polymer is vital, and can further improve mucoadhesion by providing further hydrogen bonding potential.  | Acrylates: hydroxylated methacrylate, p(MAA), CP, PC, PVA   |   |
|                                  | Electrostatic Interaction | CHT has been reported to bind via ionic interactions between primary amino functional groups and the sialic acid and sulphonic acid substructures of mucus. The electrostatic attraction arises from the difference in electrostatic charge between CHT (cationic) and mucus (anionic).  | CHT   |   |
| <b>Substrate binding ability</b> | Specific                  | Mucoadhesion is generally achieved by means of specific, receptor mediated interactions between the mucosal cell surface and the mucoadhesive. Such polymers are able to produce mucoadhesive DDSs with highly specific and targeting capabilities, and hence reduced side effect profiles.  | Antibodies, lectins, fimbrial proteins, liposomes, many chemically modified or synthesized polymers, in particular, thiolated polymers        | Helliwell <i>et al.</i> , 1993; Andrews <i>et al.</i> , 2009  |
|                                  | Non-specific              | Non-specific polymers are those that bind to mucin or mucus throughout the human body rather than at specific sites. The major disadvantage in using non-specific mucoadhesive polymers is that adhesion may occur at sites other than those intended, causing undesirable side effects.   | Traditional mucoadhesives such as alginates, cellulose derivatives, dextrans, gelatin, pectin, chitosan, poly(acrylic acids) and xanthan gum. |   |

CHT: Chitosan; CMC: Carboxymethyl cellulose; NaCMC: Sodium carboxy methylcellulose; HEC: Hydroxyethyl cellulose; HPC: Hydroxypropyl cellulose; HPMC: Hydroxypropyl methylcellulose; MC: Methylcellulose; PAA: Polyacrylic acid; P(MVE-MAA): poly(methylvinylether-co-methacrylic acid); pHEMA: poly(2-hydroxyethyl methacrylate); PAA-EHA: poly(acrylic acid-co-ethylhexylacrylate); PMA: poly(methacrylate); PACA: poly(alkylcyanoacrylate); PHCA: poly(isohexylcyanoacrylate); PBCA: poly(isobutylcyanoacrylate); PEG: Poly(ethylene glycol); PHPMAm: Poly(N-2-hydroxypropyl methacrylamide); PVA: Polyvinyl alcohol; PVP: Polyvinylpyrrolidone; PEO: poly(ethylene oxide); p(MAA): Poly(methacrylic acid).

### **3.1.3 Factors affecting mucoadhesion**

There are several factors that influence one or more material properties of mucoadhesive polymers, causing either an improvement or a decrease in their mucoadhesive abilities. Structural characteristics, also known as intrinsic factors, such as the molecular weight, crosslinking extent, the presence of functional groups and the concentration of the mucoadhesive dispersion, are usually manipulated during the polymerization process to improve mucoadhesive characteristics. External or environmental factors known to cause variations in mucoadhesive abilities include the surrounding pH, the temperature, the shear rate and the contact time with the mucosal membrane (Dodou *et al.*, 2005). If the polymer undergoes a change in its properties, in this case mucoadhesion, as a result of a change in environmental conditions, one can conclude that these polymers display stimuli-responsive tendencies.

When considering the differences in pH along the GIT, it is of particular importance to determine the effects it would have on MDDSs delivered via the peroral route. According to Dodou and co-workers, pH affects the material properties of mucoadhesive polymers such as swelling, molecular bonding, spatial conformation and rheological properties, ultimately affecting the mucoadhesive characteristics of the respective polymers and DDSs (Dodou *et al.*, 2005). Thus, the mucoadhesion of various polymers varies as a function of pH, which is exploited by the present study to produce a targeted MMDDS, aimed at improving poor oral bioavailability.

### **3.1.4 Preliminary formulation design**

The rational identification of a candidate system for further optimisation was the primordial focus of the current chapter. The ensuing experimental investigations were conducted to provide a logical comparison of the mucoadhesive properties of the various formulations developed, and determine their potential in designing a targeted drug delivery system.

Preliminary formulation studies involved, initially selecting and evaluating various mucoadhesive polymers for their pH-responsive, mucoadhesive and film-forming properties. Further modification and inclusion of excipients/other polymers was then undertaken to develop a candidate system. The identification of variables with upper and lower limits was paramount for further optimisation of both the gastric-responsive and intestinal-responsive mucoadhesive layers of the MMDDS.

## 3.2 Materials and Methods

### 3.2.1 Materials

Biocompatible and mucoadhesive polymers investigated included poly(acrylic acid) (PAA) ( $M_w$ : 1800g/mol) and chitosan (CHT) (medium molecular weight) obtained from Sigma Aldrich (Pty) Ltd (St Louis, MO, USA), Pectin Classic CU 701 (PEC) (Herbstreith & Fox KG, Neuenbürg/Württ, Germany), hydroxypropyl cellulose (HPC) (Merck-Schuchardt<sup>®</sup>, Hohenbrunn, Germany) and polyvinylpyrrolidone-40 (PVP-40;  $M_w$ : 40000g/mol) (Sigma-Aldrich Chemie GmbH, Steinheim, Germany). Poly(vinyl alcohol) (PVA) (Avg  $M_w$ =146000-186000g/mol; 98-99% hydrolyzed) was purchased from Sigma Aldrich (Pty) Ltd (Milwaukee, WI, USA).

Glycerol purchased from Associated Chemical Enterprises (Pty) Ltd. (Southdale, South Africa) was employed as a plasticizer, while an antifoaming agent, silicone, (BDH, VWR International Ltd, London, UK) was employed to prevent entrapment of air bubbles within the membranes. Solvent acetic acid was obtained from Sigma Aldrich Chemie GmbH (Steinheim, Germany). All other reagents employed were of analytical grade and used without further purification. De-ionized water was obtained from a Milli-Q water purification system (Milli-Q, Millipore, Billerica, MA, USA). Simulated gastric and intestinal membranes employed were dialysis flat sheet membranes ( $M_w$ =12,000-14,000g/mol) purchased from Spectrum Laboratories Inc. (Rancho Dominguez, CA, USA). Phosphate buffered saline (PBS) was prepared using sodium hydroxide (NaOH,  $M_w$ =40.00g/mol) and sodium chloride (NaCl,  $M_w$ =58.44g/mol) obtained from Saarchem (Wadeville, Gauteng, South Africa), hydrochloric acid (HCl, 32%<sup>w/v</sup>) purchased from Rochelle Chemicals (Johannesburg, South Africa) and potassium dihydrogen phosphate ( $KH_2PO_4$ ,  $M_w$ =136.09g/mol) obtained from Riedel-de Haen (Sigma-Aldrich Laborchemikalein GmbH, Germany) in double-deionised water (Milli-Q System, Millipore, Bedford MA, USA). Paraffin liquid, employed as a lubricant to facilitate membrane removal from moulds was obtained from Saarchem (Wadeville, Gauteng, South Africa).

### 3.2.2 Formulation and evaluation of various mucoadhesive polymers for their pH-responsive properties

Polymers selected for the pH-responsive, mucoadhesive layer (Figure 3.3) were representative of the various classes of mucoadhesive polymers (Table 3.1). The mucoadhesive layer was fabricated using the film casting technique of membrane fabrication. Film-casting was selected as membranes formed via this technique are relatively more elastic and the technique avoids the use of toxic solvents and costly

equipment as compared to other methods of membrane fabrication. Furthermore, the method is relatively cost-effective, versatile with application in a wide range of polymers, demonstrating potential in scale-up procedures, which may ultimately facilitate bulk-manufacturing and marketing measures.

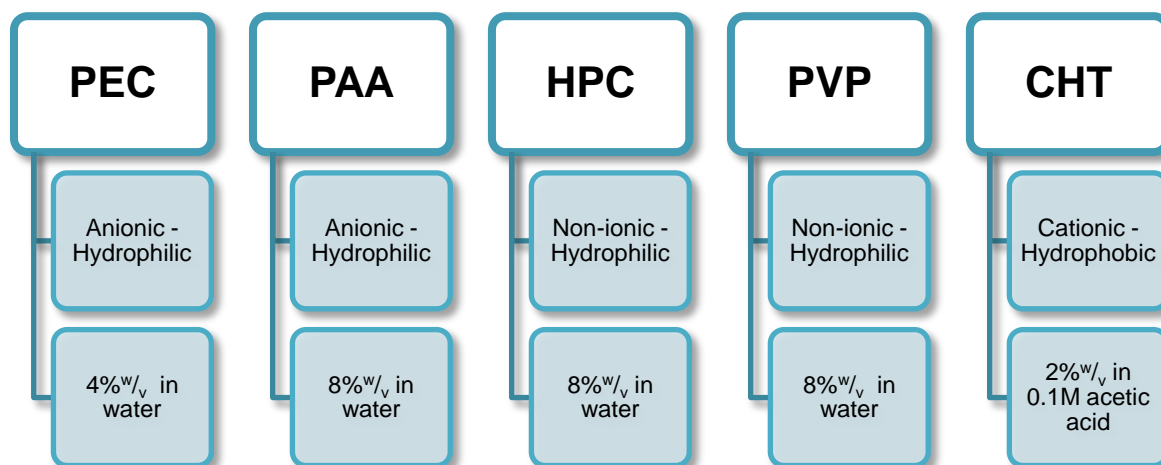


**Figure 3.3:** Mucoadhesive polymers, their respective concentrations and solvents employed in the preliminary design of the pH-responsive mucoadhesive layer.

Briefly, the film-casting method included solubilising the polymers in their respective concentrations and solvents followed by addition of glycerol as a plasticizer (2:1 of polymer: plasticizer) and the antifoaming agent, silicone (1 drop per 100mL). 40mL aliquots of the clear, homogenous polymeric solution were then film-cast into moulds (dimensions: of 120x120mm) and subject to ambient conditions for 24 hours. Phase separation, occurring as the solvent (water) evaporates, resulted in the formation of a thin, transparent and uniform polymeric membrane. To facilitate the removal of membranes upon drying, moulds were lubricated with liquid paraffin prior to film-casting to prevent any physical alteration incurred on the membrane during the removal process. Membranes were then cut into 18x30mm dimensions and stored with desiccants in airtight containers until further testing was completed. The size range selected for the mucoadhesive layer was based on the dimensions of a typical capsule since the MMDDS would be incorporated into a capsule to ease oral administration.

### 3.2.3 The effect of employing a combination of mucoadhesive polymers in the development of the pH-responsive mucoadhesive layer

Following the identification of the polymers demonstrating the highest potential in the development of the pH-responsive mucoadhesive layers, studies were undertaken to elucidate the effect of adding a hydrophilic, mucoadhesive polymer for further improving pH-responsive mucoadhesion, while their effects on the pH-responsive nature of the

formulations investigated were carefully monitored. Polymers were dissolved in their respective concentrations and solvents illustrated in Figure 3.3 and combined in accordance with the ratios depicted in Table 3.2, followed by the film-casting method described in *Chapter 3, Section 3.2.2*.

**Table 3.2:** Experimental formulations evaluated for the identification of the optimal combination of mucoadhesive polymers for application in the respective pH-responsive mucoadhesive layers.

| <b>Formulation No</b>                            | <b>Concentration of Polymer 1 (%<sup>w</sup>/v)</b> | <b>Concentration of Polymer 2 (%<sup>w</sup>/v)</b> | <b>Ratio*</b>   |
|--|---|---|-----------------|
| <b>Gastric-targeted component<sup>1</sup></b>    |   |   |                 |
|  | <b>CHT</b>  | <b>PAA</b>  | <b>CHT:PAA</b>  |
| GT1  | 1.60  | 1.60  | 1:1             |
| GT2  | 1.33  | 2.66  | 1:2             |
| GT3  | 1.00  | 4.00  | 1:4             |
| GT4  | 0.66  | 5.34  | 1:8             |
| GT5  | 0.40  | 6.40  | 1:16            |
|  | <b>CHT</b>  | <b>HPC</b>  | <b>CHT: HPC</b> |
| GT6  | 1.60  | 1.60  | 1:1             |
| GT7  | 1.33  | 2.66  | 1:2             |
| GT8  | 1.00  | 4.00  | 1:4             |
| GT9  | 0.66  | 5.34  | 1:8             |
| GT10   | 0.40  | 6.40  | 1:16            |
| <b>Intestinal-targeted component<sup>2</sup></b> |   |   |                 |
|  | <b>PEC</b>  | <b>PAA</b>  | <b>PEC: PAA</b> |
| IT1  | 2.67  | 2.67  | 1:1             |
| IT2  | 2.00  | 4.00  | 1:2             |
| IT3  | 1.33  | 5.34  | 1:4             |
| IT4  | 0.80  | 6.40  | 1:8             |
| IT5  | 0.45  | 7.20  | 1:16            |
|  | <b>PEC</b>  | <b>HPC</b>  | <b>PEC: HPC</b> |
| IT6  | 2.67  | 2.67  | 1:1             |
| IT7  | 2.00  | 4.00  | 1:2             |
| IT8  | 1.33  | 5.34  | 1:4             |
| IT9  | 0.80  | 6.40  | 1:8             |
| IT10   | 0.45  | 7.20  | 1:16            |

\* The ratios selected were based on the ability to combine the highest polymer concentrations without producing a polymeric solution too viscous to film-cast.

<sup>1</sup> Results obtained from preliminary mucoadhesive evaluation studies indicated that CHT demonstrated the highest potential in gastric targeting.

<sup>2</sup> results obtained from preliminary mucoadhesive evaluation studies indicated that PEC demonstrated the highest potential in intestinal targeting.

### 3.2.4 The influence of PVA addition to develop a durable mucoadhesive layer able to withstand the conditions of the GIT

Following the identification of the most effective polymer combinations for the gastric- and intestinal-targeted components demonstrating the most promising mucoadhesive properties, studies were undertaken to elucidate the influence of the incorporation of various quantities of PVA on the mucoadhesive properties of the experimental formulations. PVA was incorporated to ensure the mucoadhesive layer is able to

withstand the conditions of the GIT without premature erosion. The incorporation of PVA was essentially performed by dissolving PVA in differing concentrations, combining the polymers in their various ratios depicted in Table 3.3, followed by film-casting according to the method depicted in *Chapter 3, Section 3.2.2*.

**Table 3.3:** Experimental formulations evaluated for the optimal PVA quantity required to impart enduring mucoadhesive properties.

| <b>Experimental Formulation</b> | <b>Concentration of pH-responsive polymer (%<sup>w</sup>/<sub>v</sub>)</b> | <b>Concentration of mucoadhesive polymer (%<sup>w</sup>/<sub>v</sub>)</b> | <b>Concentration of poly(vinyl alcohol) (%<sup>w</sup>/<sub>v</sub>)</b> | <b>Ratio*</b>      |
|---------------------------------|--|---|--|--------------------|
| <b>Gastric-targeted</b>         |  |   |  |                    |
| <b>component</b>                | <b>CHT</b>   | <b>PAA</b>  | <b>PVA</b>   | <b>CHT:PAA:PVA</b> |
| GT11                            | 1  | 8   | 4.68   | 1:8:4.68           |
| GT12                            | 1.5  | 4   | 3.2  | 1:2.67:2.1         |
| GT13                            | 2  | 4   | 2.3  | 1:2:1.15           |
| <b>Intestinal-targeted</b>      |  |   |  |                    |
| <b>component</b>                | <b>PEC</b>   | <b>PAA</b>  | <b>PVA</b>   | <b>CHT:PAA:PVA</b> |
| IT11                            | 1.3  | 8   | 4.68   | 1:6.15:3.6         |
| IT12                            | 2  | 4   | 3.2  | 1:2:1.6            |
| IT13                            | 2.6  | 4   | 2.3  | 1:1.5:0.88         |

\* The ratios selected were based on the ability to combine the highest polymer concentrations without producing a polymeric solution too viscous to film-cast.

### 3.2.5 The influence of PAA substitution with PVP for the further improvement of mucoadhesive properties over a prolonged period of time

Following the incorporation of PVA in experimental formulations, the influence of poly(vinyl pyrrolidone) (PVP), a non-ionic mucoadhesive polymer as a substitute for PAA was investigated. Substitution with PVP was attempted to ensure that the membranes were viable for longer durations within the GIT, while imparting pH-responsive mucoadhesive properties. The incorporation of PVP was essentially performed by dissolving PVP in differing concentrations, combining the polymers in their various ratios (Table 3.4), followed by film-casting according to the method depicted in *Section 3.2.2*.

**Table 3.4:** Experimental formulations investigating the effects of substitution with PVP on mucoadhesive characteristics.

| <b>Experimental Formulation</b>      | <b>Concentration of pH-responsive polymer (%<sup>w</sup>/<sub>v</sub>)</b> | <b>Concentration of mucoadhesive polymer (%<sup>w</sup>/<sub>v</sub>)</b> | <b>Concentration of PVA (%<sup>w</sup>/<sub>v</sub>)</b> | <b>Ratio*</b>      |
|--------------------------------------|--|---|--|--------------------|
| <b>Gastric-targeted component</b>    |  |   |  |                    |
|                                      | <b>CHT</b>   | <b>PVP</b>  | <b>PVA</b>   | <b>CHT:PAA:PVA</b> |
| GT14                                 | 1  | 8   | 4.68   | 1:8:4.68           |
| GT15                                 | 1.5  | 4   | 3.2  | 1:2.67:2.1         |
| GT16                                 | 2  | 4   | 2.3  | 1:2:1.15           |
| <b>Intestinal-targeted component</b> |  |   |  |                    |
|                                      | <b>PEC</b>   | <b>PVP</b>  | <b>PVA</b>   | <b>CHT:PAA:PVA</b> |
| IT14                                 | 1.3  | 8   | 4.68   | 1:6.15:3.6         |
| IT15                                 | 2  | 4   | 3.2  | 1:2:1.6            |
| IT16                                 | 2.6  | 4   | 2.3  | 1:1.5:0.88         |

\* The ratios selected were based on the ability to combine the highest polymer concentrations without producing a polymeric solution too viscous to film-cast.

### 3.2.6 Determining the upper and lower variables of the formulation required for input into the Central Composite Design

Following the identification of the most appropriate polymer combinations to be employed in the respective pH-responsive DDS, upper and lower limits of the formulation variables were determined for input into the Central Composite Design. Determination of the variables involved combining the polymers in various ratios and film-casting as detailed in Chapter 3, Section 3.2.2 and thereafter assessing whether the formulations fulfilled the following criteria:

- demonstrated good film-forming properties
- demonstrated promising mucoadhesive properties
- maintained pH-responsive mucoadhesion
- did not prematurely disintegrate/erode when subject to prolonged exposure to simulated GIT conditions.

### 3.2.7 Determination of mucoadhesive properties through textural analysis

In order to evaluate the mucoadhesive properties of the mucoadhesive layer, the Work of Adhesion (WA) and the Maximum Detachment Force (MDF) required to detach a hydrated mucoadhesive layer from a portion of Simulated Gastric Membrane (SGM) was determined, using Texture Analyser TA.XTplus (Stable Microsystems, England), employing the test parameters depicted in Table 3.5. Portions of SGMs were secured to a flat-tipped probe (diameter: 15mm), while a hydrated section of the mucoadhesive layer was secured to the stand as illustrated in Figure 3.4. Polymeric SGMs were pre-impregnated with PBS; pH 1.2±0.1 or pH 6.8±0.1 prior to mucoadhesive testing;



simulating the gastric or intestinal regions respectively. The probe was lowered to make contact with the SGM mount inducing a test force, and thereafter raised, while simultaneously measuring the MDF. Data was captured at a rate of 200pps via the Texture Expert Software v3.2, producing a force: distance curve.

**Table 3.5:** Textural analysis settings for mucoadhesive test sequence.

| <b>Mucoadhesive test parameter</b> | <b>Mucoadhesive test settings</b> |
|------------------------------------|-----------------------------------|
| Pre-test speed                     | 0.5mm/sec                         |
| Test speed                         | 0.5mm/sec                         |
| Post-test speed                    | 10mm/sec                          |
| Applied force                      | 5N                                |
| Contact time                       | 10 seconds                        |
| Trigger force                      | 0.05N                             |

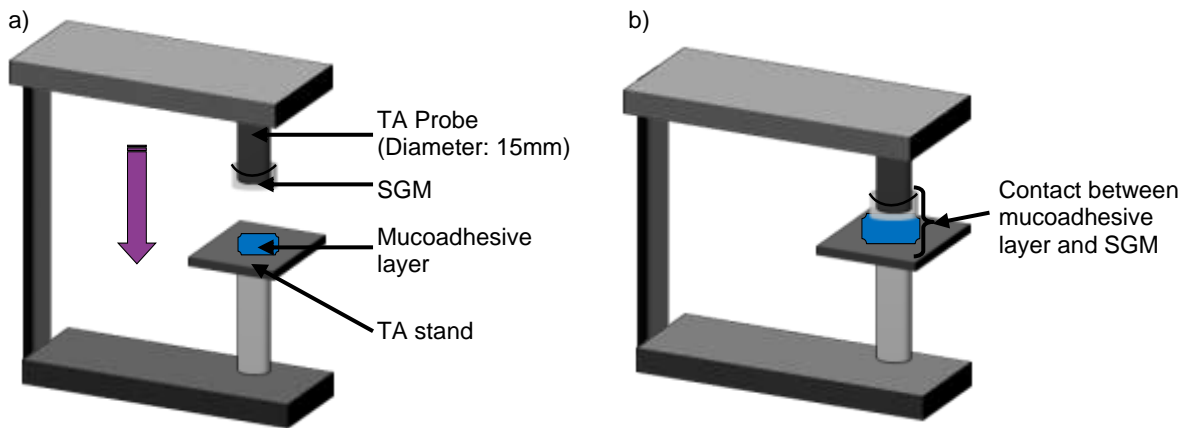


**Figure 3.4:** Schematic illustration of the textural analysis method employed to generate force: distance profiles for mucoadhesive analysis, where a) is lowering of the probe onto the mucoadhesive layer, and b) is the contact between the SGM and mucoadhesive layer.

The WA (mJ) was determined from the Area Under the Curve of the force: distance curve ( $AUC_{FD}$ ) and the MDF (N) required to detach the polymeric layer from the SGM was determined by measuring the maximum peak force from the resultant force: distance curve. The Work of Adhesion per unit area ( $WA_{\alpha\beta\delta}$ ), was characterized by the work executed on the matrices when the two contact phases i.e. the SGM ( $\alpha$ ) and the mucoadhesive layer ( $\beta$ ), formed an interface of unit area which were subsequently separated reversibly to form unit areas of each of the  $\alpha\delta$ - and  $\beta\delta$ - interfaces. This relationship is mathematically described by Equation 3.1.

$$WA_{\alpha\beta\delta} = \gamma_{\alpha\delta} + \gamma_{\beta\delta} - \gamma_{\alpha\beta}$$

Equation 3.1

where,  $\gamma_{\alpha\beta}$ ,  $\gamma_{\alpha\delta}$  and  $\gamma_{\beta\delta}$  are the surface tensions between the two bulk phases comprising the SGM and the mucoadhesive layer,  $\alpha$ ,  $\beta$ ;  $\alpha$ ,  $\delta$  and  $\beta$ ,  $\delta$  respectively.

The tensile related mucoadhesive test described is able to reproduce *in vivo*-occurring processes to some extent. This form of tensile testing provides information on the *relative* mucoadhesiveness of dosage forms and thus allows classifying mucoadhesive properties based on their performance. It is now recognised that detachment between the dosage form and substrate is a complex physical process, depending on both the deformation and mechanical properties of both the dosage form and the substrate (characterised by the WA), as well as the adhesiveness (characterised by the MDF) (Khutoryanskiy, 2010). Although many studies report the use of biological substrates in mucoadhesive analysis (Park and Robinson, 1987; Rathi *et al.*, 1991), the results obtained from these studies are often characterized by relatively poor reproducibility due to variable properties of biological substrates. It is thus important to make use of an alternative testing method, which does not involve biological substrates in assessment of mucoadhesives (Merkle *et al.*, 1990; Khutoryanskiy, 2010) and thus several studies have reported the use of dialysis flat sheet membranes in mucoadhesive analysis as a surrogate environment simulating *in vivo* conditions. This prompted the use of dialysis flat sheet membranes as a substrate in the present study as a simulated gastric or intestinal membrane (Lele and Hoffman, 2000; Ndesendo *et al.*, 2009; Murphy *et al.*, 2011).

### **3.2.8 Evaluation of variations in mucoadhesive properties as a function of time**

In order to determine the effects of the GIT on the mucoadhesive characteristics, the mucoadhesive layers were subject to conditions typical of *in vitro* drug release studies in a six station USP Dissolution Apparatus (Erweka DT 700 GmbH Germany). The USP 25 rotating paddle method of dissolution was selected where the mucoadhesive layers were exposed to 900mL of PBS (pH 1.2±0.1 or pH 6.8±0.1) for 12 hours at 37±0.5°C at 50rpms. At two hour intervals (0, 2, 4, 6, 8, 10, 12), the layers were removed from the dissolution media and subject to mucoadhesive analysis as described in *Chapter 3, Section 3.2.7*. Fresh samples were used for each individual time point.

## **3.3 Results and Discussion**

### **3.3.1 Most appropriate mucoadhesive polymer demonstrating pH-responsive properties for the respective mucoadhesive layers**

Film-casting produced membranes that were clear, flexible and uniform throughout its structure for PEC, HPC and CHT membranes. Solutions of PAA and PVP, when film-cast, did not produce membranes or films, but rather a semi-solid hydrogel type structure upon which further mucoadhesive analysis could not be undertaken, and therefore results for these polymers are not represented. Figure 3.5 illustrates a typical force: distance curve

obtained through mucoadhesive textural analysis. The MDF (N) (highlighted in green) and the WA (mJ) (highlighted in red) are related to mucoadhesive properties, where the higher the WA and MDF, the stronger the mucoadhesive properties.

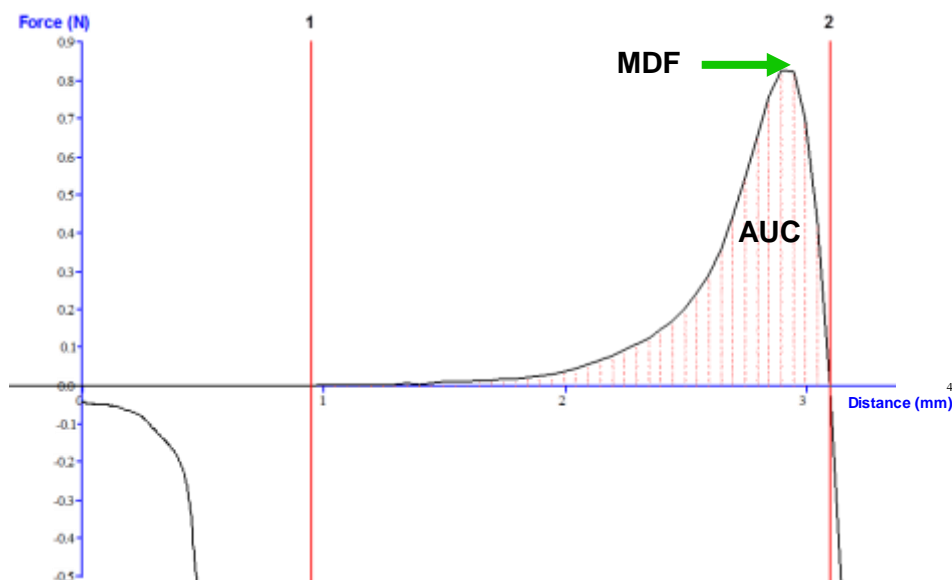


**Figure 3.5:** Typical textural profiles elucidating the MDF (N) and WA ( $AUC_{FD}$ ) (mJ).

pH-responsive mucoadhesion was achieved from the CHT and PEC membranes in acidic and more alkaline pH ranges respectively (Figure 3.6a-b). Although mucoadhesion in HPC membranes were not poor, they were relatively consistent with variations in pH (Figure 3.6a-b), and hence HPC membranes were unable to demonstrate pH-responsive mucoadhesion. It is speculated that mucoadhesive properties of non-ionic polymers (Table 3.1) arises from the diffusion theory, where polymeric chains interpenetrate within the mucin layer, promoting adhesion, which based on the results elaborated below, does not seem to be drastically affected by changes in the surrounding pH range. As the proposed DDS requires pH-responsive mucoadhesion to ensure site-specific drug delivery, it was concluded that HPC demonstrated little, if not, no potential as a candidate polymer, and no further studies were conducted employing HPC as the primary polymer in the development of the mucoadhesive layer.

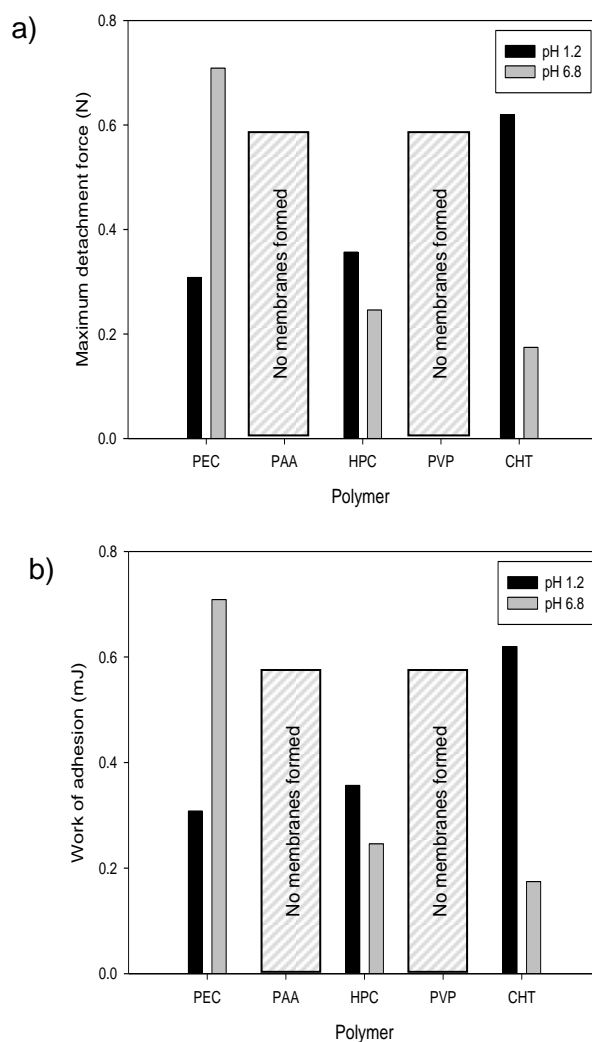


**Figure 3.6:** A comparison of a) the Maximum Detachment Force (MDF) (N) and b) Work of Adhesion (AUC<sub>FD</sub>) (mJ) of the preliminary mucoadhesive layers in acidic and alkaline pH ranges (n=3; SD < 0.028 in all cases).

Mucoadhesive analysis revealed that CHT displayed higher mucoadhesion in acidic pH ranges (MDF=0.61975±0.00415N; AUC<sub>FD</sub>=0.899±0.001mJ) as compared to alkaline pH ranges (MDF=0.1744±0.0224N; AUC<sub>FD</sub>= 0.0685±0.0035mJ) (Figure 3.6a-b). The pH-responsive nature of CHT can be related to its state of ionisation in the respective pH range. Since CHT (pK<sub>a</sub>=6.3) is cationic in nature, mucoadhesion typically arises from an electrostatic interaction between the CHT and negatively charged mucin (Sogias *et al.*, 2008). Furthermore, a sufficient quantity of water is necessary to allow proper hydration and expansion (swelling) of the mucoadhesive network, which occurs only in low pH ranges, to expose available adhesive sites (promoting bond formation) and facilitate polymer chain relaxation (promoting chain interpenetration) (Leung and Robinson, 1990). The drastic change in the mucoadhesive properties of CHT occurring during variations in the pH of the surrounding medium is related to its ionisation state as is illustrated in Figure 3.7.

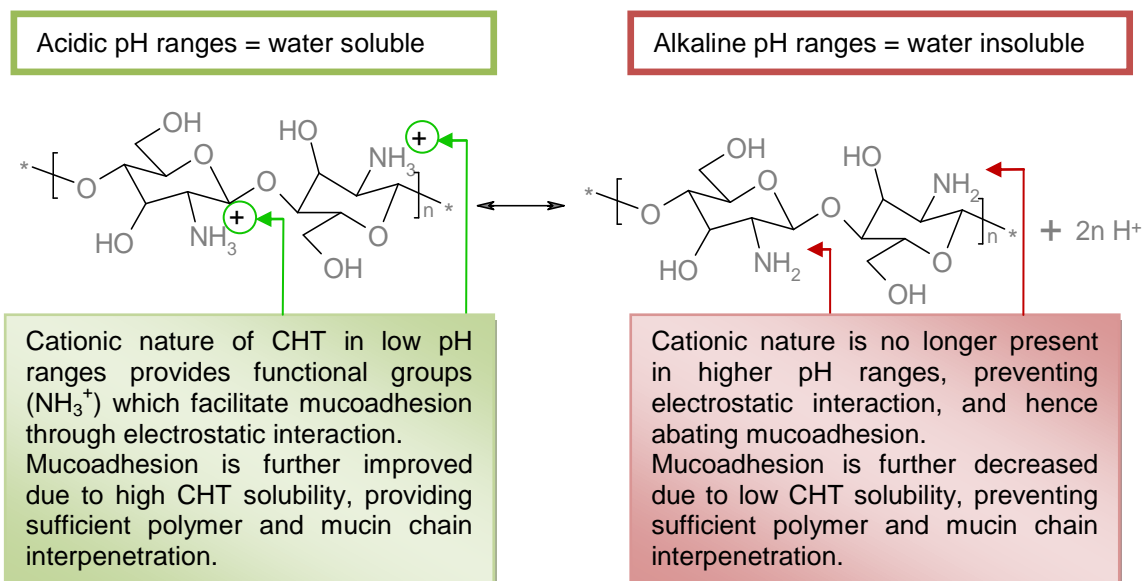


**Figure 3.7:** Variations in the ionisation state of the CHT molecules as a function of changes in the pH range (Adapted from Luo et al., 2010).

As illustrated in Figure 3.6, PEC displayed superior mucoadhesive properties in alkaline pH ranges ( $\text{MDF} = 0.70885 \pm 0.10145\text{N}$ ;  $\text{AUC}_{\text{FD}} = 1.0125 \pm 0.0265\text{mJ}$ ) as compared to acidic pH ranges ( $\text{MDF} = 0.3081 \pm 0.0598\text{N}$ ;  $\text{AUC}_{\text{FD}} = 0.218 \pm 0.035\text{mJ}$ ), the difference of which, once again, can be attributed to the change in ionisation state occurring as a function of pH. The mucoadhesive properties of PEC ( $\text{pK}_a$  of 3-4), an anionic polysaccharide, arises from the presence of carboxylic functional groups which interact with the oligosaccharide chains of mucin via hydrogen bonds (Table 3.1). Typically, in alkaline pH ranges, the carboxylic group of PEC is ionised, improving both mucoadhesion (through bond formation) and hydration (promoting interpenetration between PEC and mucin chains) (Peppas and Sahlin, 1996; Sriamornsak *et al.*, 2007; Hodges *et al.*, 2009). However, in acidic pH ranges, illustrated in Figure 3.8, PEC is rapidly converted from its anionic nature to unionised forms, lowering the mucoadhesive characteristics through both a reduction in hydration and the presence of functional groups required for hydrogen bonding (Sriamornsak *et al.*, 2007).

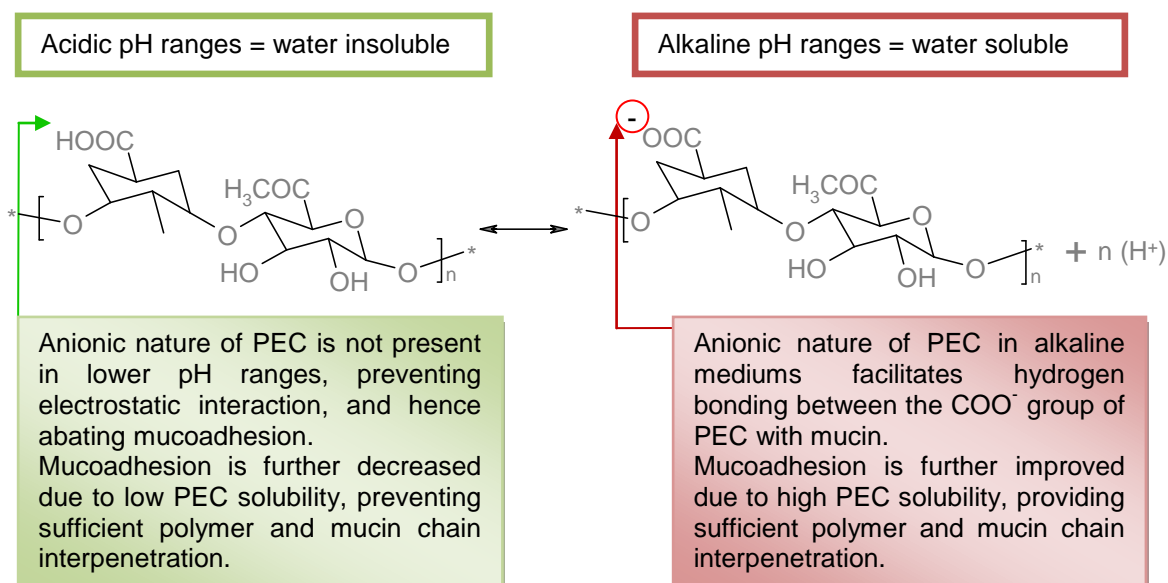


**Figure 3.8:** Variations in the ionisation state of the PEC molecules as a function of changes in the pH range.

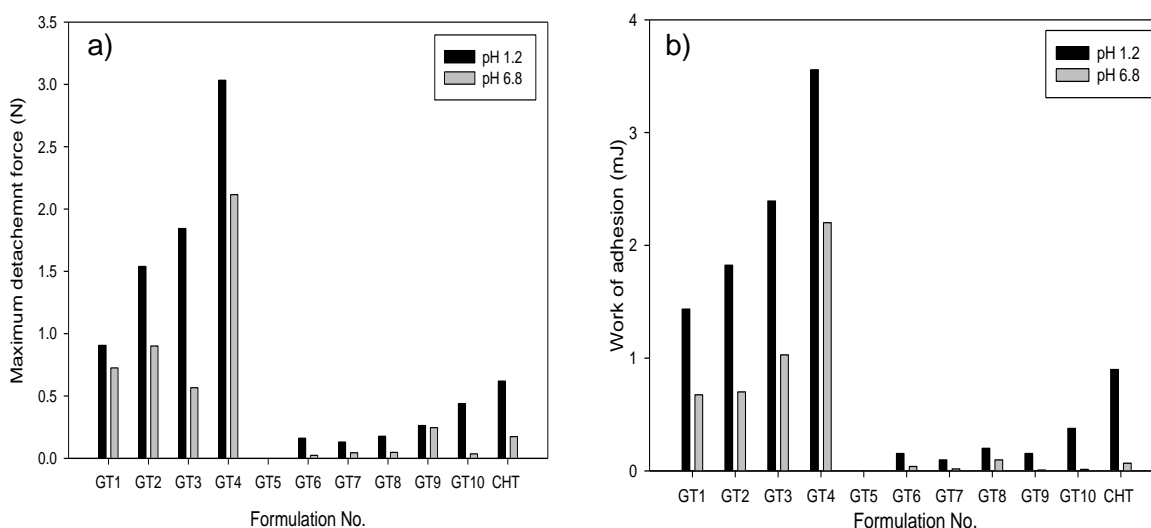
### 3.3.2 Identification of the most effective polymer combination in the respective pH-responsive mucoadhesive layers

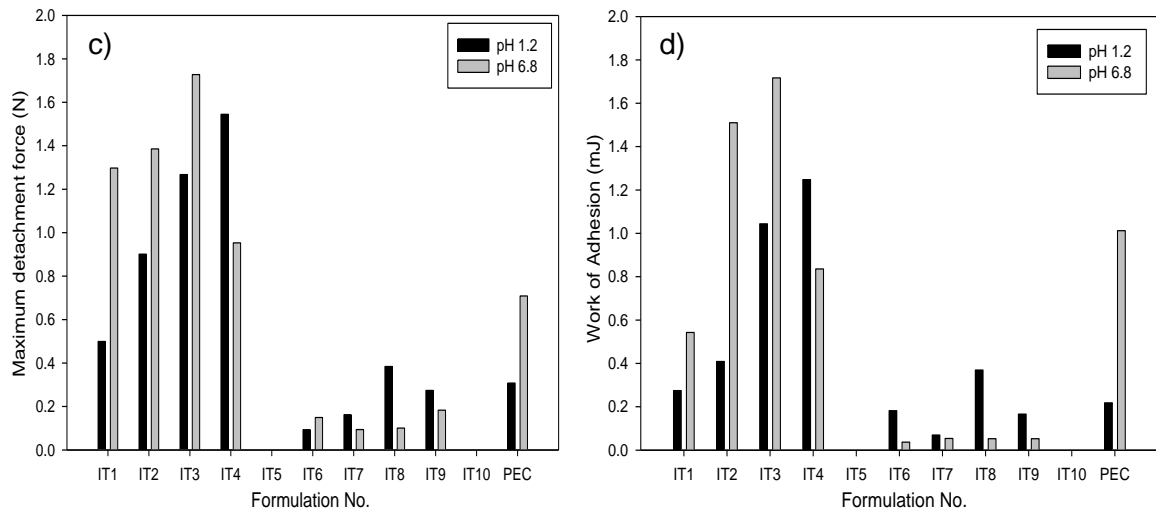
The addition of hydrophilic polymers had vastly different effects on the mucoadhesive properties of the experimental formulations, depending on the polymer employed. Formulations GR5, IR5 and IR10; comprising of extremely high concentrations of the hydrophilic polymer relative to the pH-responsive polymer resulted in the formation of membranes that were extremely sticky and difficult to handle, thus averting mucoadhesive analysis. Typically, the addition of HPC to CHT- and PEC-based formulations caused surprisingly poorer mucoadhesive characteristics (Figure 3.9).

The resultant decrease in mucoadhesive properties of CHT-based formulations can be attributed to the formation of hydrogen bonds between the functional groups (amino and amide groups) of CHT and HPC. Since the cationic nature of CHT is lost, there are fewer electrostatic interactions occurring between the polymer chains and mucin, causing an overall decrease in mucoadhesion (Pawlak and Mucha, 2003). It was speculated by Satoh and co-workers that combining HPC with anionic polymers, results in the formation of a complex between the carboxylic groups of the anionic polymer with HPC molecules. As such, the carboxylic groups of the anionic polymer (e.g. PEC) are no longer able to form hydrogen bonds with the mucin molecules, causing the resultant reduction in mucoadhesion (Satoh *et al.*, 1989).

PAA and its derivatives are known to possess exceptional mucoadhesive properties (Lehr *et al.*, 1992; Helliwell, 1993) and hence it is no surprise that the addition of PAA caused a drastic increase in the mucoadhesive properties of the both the CHT- and PEC-based formulations (for the gastric- and intestinal-targeted components respectively) (Figure 3.9a-b). Although an increasing trend in mucoadhesion was observed with an increase in the PAA ratio, a gradual decline in the pH-responsive nature of CHT-based formulations was observed. Granted, higher mucoadhesion would result in the formulation of a DDS with superior properties, however, the cost of losing its site-specificity would be detrimental for the proposed MMDDS (i.e. it would be unable to segregate drugs).

A similar trend was observed in PEC-based formulations (Figure 3.9c-d), where the pH-responsive nature of the experimental formulations investigated was lost with an increase in the PAA ratio. PAA typically demonstrates highest mucoadhesion in more neutral pH ranges, where the carboxyl groups are ionised (COO<sup>-</sup>), thus facilitating electrostatic interactions. However, at low pH ranges, mucoadhesion is promoted by H-bond formation between the unionised carboxyl groups (COOH) of PAA and mucus (Helliwell, 1993). Therefore, PAA displays superior mucoadhesion in both pH ranges investigated, accounting for the loss in the pH-responsive nature of the experimental formulations analysed. As such, it was imperative to obtain a balance between both the pH-responsive and mucoadhesive polymers that would provide optimum mucoadhesion without compromising site-specific drug delivery of both components.

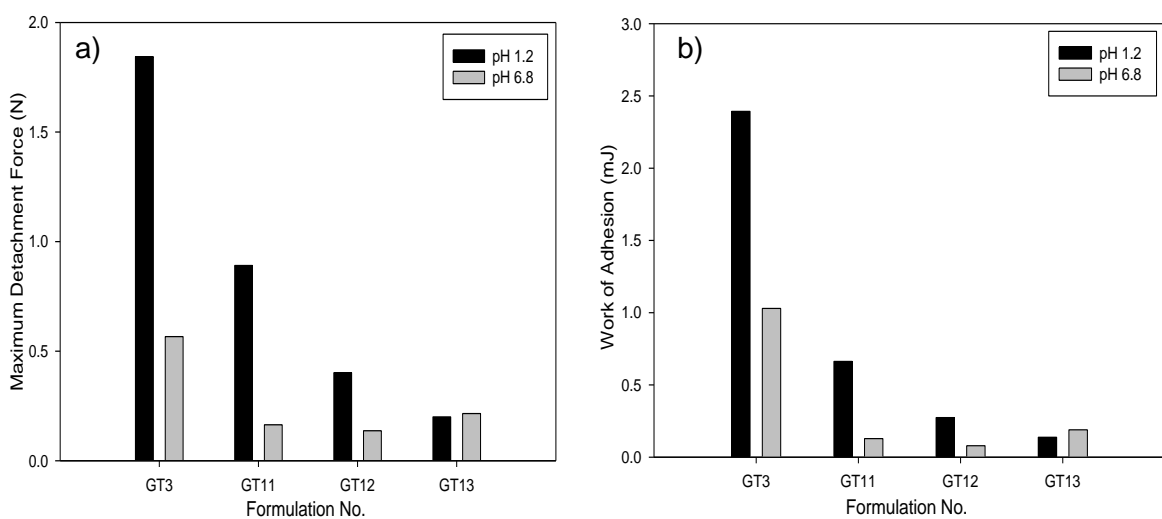




**Figure 3.9:** A comparison of a) the Maximum Detachment Force (MDF) (N) and b) Work of Adhesion ( $AUC_{FD}$ ) (mJ) of the experimental CHT-based formulations; and c) the Maximum Detachment Force (MDF) (N) and d) Work of Adhesion ( $AUC_{FD}$ ) (mJ) of the experimental PEC-based formulations ( $n=3$ ;  $SD < 0.037$  in all cases).

### 3.3.3 Effect of PVA incorporation in the respective pH-responsive mucoadhesive layers

When attempting to evaluate the variations of the mucoadhesive characteristics as a function of time, it was revealed that experimental Formulations GT1-10 and IT1-10 were unable to withstand the conditions of *in vitro* dissolution testing (all formulations dissolved or disintegrated within the first two hours of analysis). PVA was thus incorporated into the experimental formulations to retard premature disintegration of the respective pH-responsive layers within the GIT. As illustrated in Figure 3.10a-d, although the addition of the PVA in the experimental formulations had little effect on the pH-responsive nature of the formulations, a decrease in both the MDF and  $AUC_{FD}$  was observed.





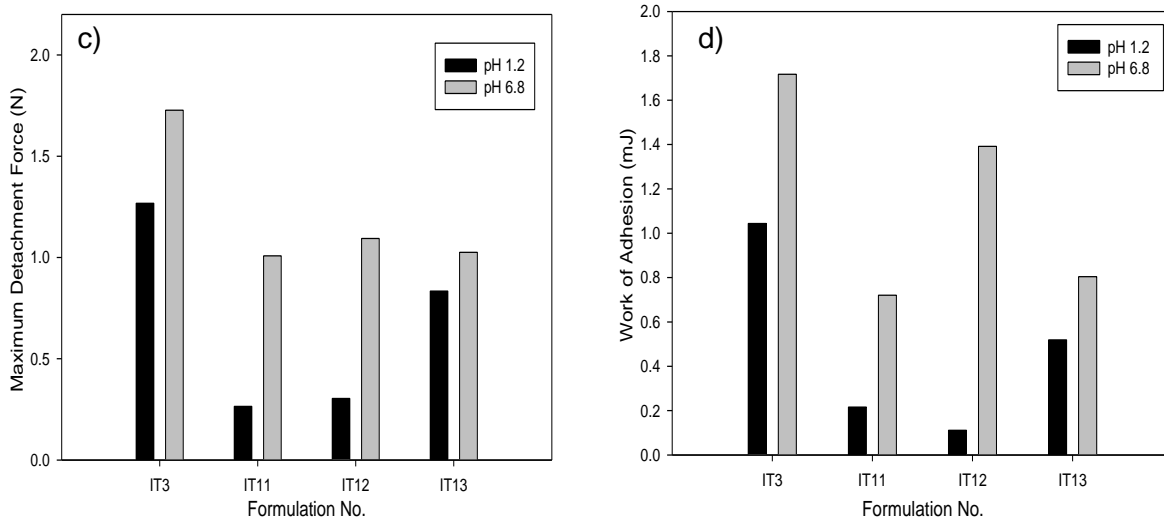


**Figure 3.10:** A comparison of the effect of PVA incorporation on a) the Maximum Detachment Force (MDF) (N) and b) Work of Adhesion (AUC<sub>FD</sub>) (mJ) of the experimental CHT-based formulations; and c) the Maximum Detachment Force (MDF) (N) and d) Work of Adhesion (AUC<sub>FD</sub>) (mJ) of the experimental PEC-based formulations (n=3; SD < 0.075 in all cases).

The interaction of functional groups between PAA and PVA may be accountable for the decline in mucoadhesive properties. It was postulated by Daniliuc and coworkers that when in solution, PVA and PAA tend to form inter- and intra-molecular hydrogen bonds, resulting in poorer solubility characteristics (Daniliuc *et al.*, 1992; Daniliuc and David, 1996). Theoretically, any interaction which decreases solubility would decrease mucoadhesive properties by retarding swelling and ultimately hindering chain interpenetration between the DDS and mucus. Furthermore, it is theoretically possible that the hydrogen bonding between the polymer molecules further impedes mucoadhesion as the polymers no longer contain free functional groups able to form hydrogen bonds with mucus molecules. CHT-based formulations displayed a notably larger drop in mucoadhesive characteristics than PEC-based formulations. This may be attributed to the cationic nature of CHT forming electrostatic interactions with anionic PAA, decreasing the solubility and sites available for adhesion, and hence mucoadhesive characteristics of the formulations.

PVA incorporation did, however, provide the qualities necessary to ensure that the CHT-based experimental formulations, specifically Formulations GR12 and GR13, would withstand the conditions of the GIT (Table 3.6). Granted the formulations containing PVA still displayed mucoadhesive characteristics, they were remarkably lower than that of the formulations without PVA due to the PVA/PAA interaction. PEC-based formulations, however, were unable to withstand the conditions of the GIT. In all cases, the PEC-based

mucoadhesive layers eroded within two hours of the study, regardless of PVA quantity (Table 3.6). The variations in the durability of PEC- and CHT-based formulations can be attributed to the electrostatic interaction taking place between CHT and PAA, which further decreases solubility as opposed to the electrostatic repulsion between anionic PEC and anionic PAA, which increases the rate of dissolution of the polymer structure. Typically, formulations containing higher concentrations of PAA did not last longer than 2-4 hours when exposed to simulated GIT conditions.

**Table 3.6:** Periods of which the experimental formulations were able to withstand the GIT conditions.

| <b>Experimental Formulation</b>      | <b>Ratio</b>       | <b>Time (hours)*</b> |               |
|--------------------------------------|--------------------|----------------------|---------------|
|                                      |                    | <b>pH 1.2</b>        | <b>pH 6.8</b> |
| <b>Gastric-targeted component</b>    | <b>CHT:PAA:PVA</b> |                      |               |
| GT1-GT10                             | Varying            | 2-4                  | >10           |
| GT11                                 | 1:8:4.68           | 2-4                  | >10           |
| GT12                                 | 1:2.67:2.1         | >10                  | >10           |
| GT13                                 | 1:2:1.15           | >10                  | >10           |
| <b>Intestinal-targeted component</b> | <b>CHT:PAA:PVA</b> | <b>pH 1.2</b>        | <b>pH 6.8</b> |
| IT1-IT10                             | Varying            | >10                  | <2            |
| IT11                                 | 1:6.15:3.6         | >10                  | <2            |
| IT12                                 | 1:2:1.6            | >10                  | <2            |
| IT13                                 | 1:1.5:0.88         | >10                  | <2            |

\* Duration the experimental formulation was able to withstand the conditions of the GIT without showing any visible signs of erosion or disintegration and were able to undergo mucoadhesive analysis.

Despite the initial mucoadhesive characteristics (at t=0 hours) of PVA incorporated membranes being relatively low, the subsequent increase in swelling over time promoted mucoadhesion via polymer chain interpenetration (diffusion theory) and the resultant expansion in the polymeric network exposed additional adhesive sites which were initially unable to interact with mucus. Figure 3.11a-b illustrates the variations in the mucoadhesive properties which was typical for both GT12 and GT13. The initial rise in mucoadhesion can be attributed to the increase in swelling, thereby promoting mucoadhesion, followed by a more consistent level of mucoadhesive characteristics. The eventual decrease in the mucoadhesive characteristics can possibly be attributed to the slow erosion or dissolution of the mucoadhesive polymer out of the mucoadhesive layer. It is important to note, however, that the pH-responsive characteristics are maintained throughout the duration of the study.

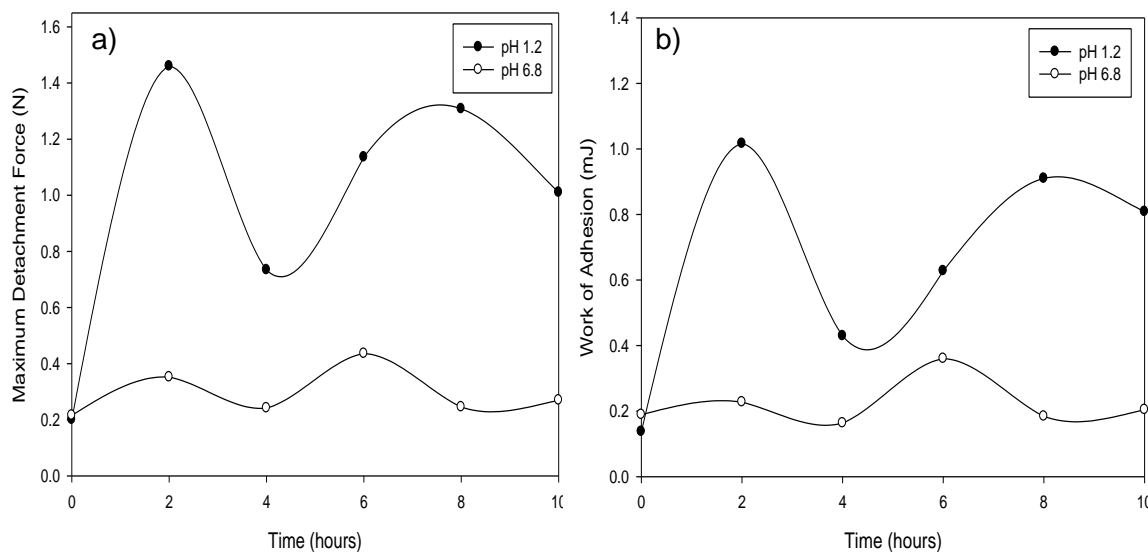


**Figure 3.11:** Variations in a) the Maximum Detachment Force (MDF) (N), and b) Work of Adhesion ( $AUC_{FD}$ ) (mJ) (mJ) of experimental Formulation GT12 as a function of time ( $n=3$ ;  $SD < 0.034$  in all cases).

### 3.3.4 Effect of PAA substitution with PVP in the pH-responsive mucoadhesive layer

Although the incorporation of PVA produced mucoadhesive membranes that were able to withstand simulated GIT conditions for some CHT-based formulations, PEC-based formulations containing PAA did not last for periods greater than 2 hours due to the possibility of the electrostatic repulsion increasing the dissolution rate. Therefore, in order to ensure the mucoadhesive membranes would remain viable for longer periods within the GIT, the effects of PAA substitution with a non-ionic polymer, PVP was determined. Substitution with PVP was conducted to prevent any electrostatic-related interactions from affecting either the mucoadhesive characteristics or the durability of the membranes from being detrimentally affected. As illustrated in Figure 3.12a-b substitution of PVA with PVP improved both the  $AUC_{FD}$  and the MDF of the CHT-based formulations while maintaining the pH-responsive nature.

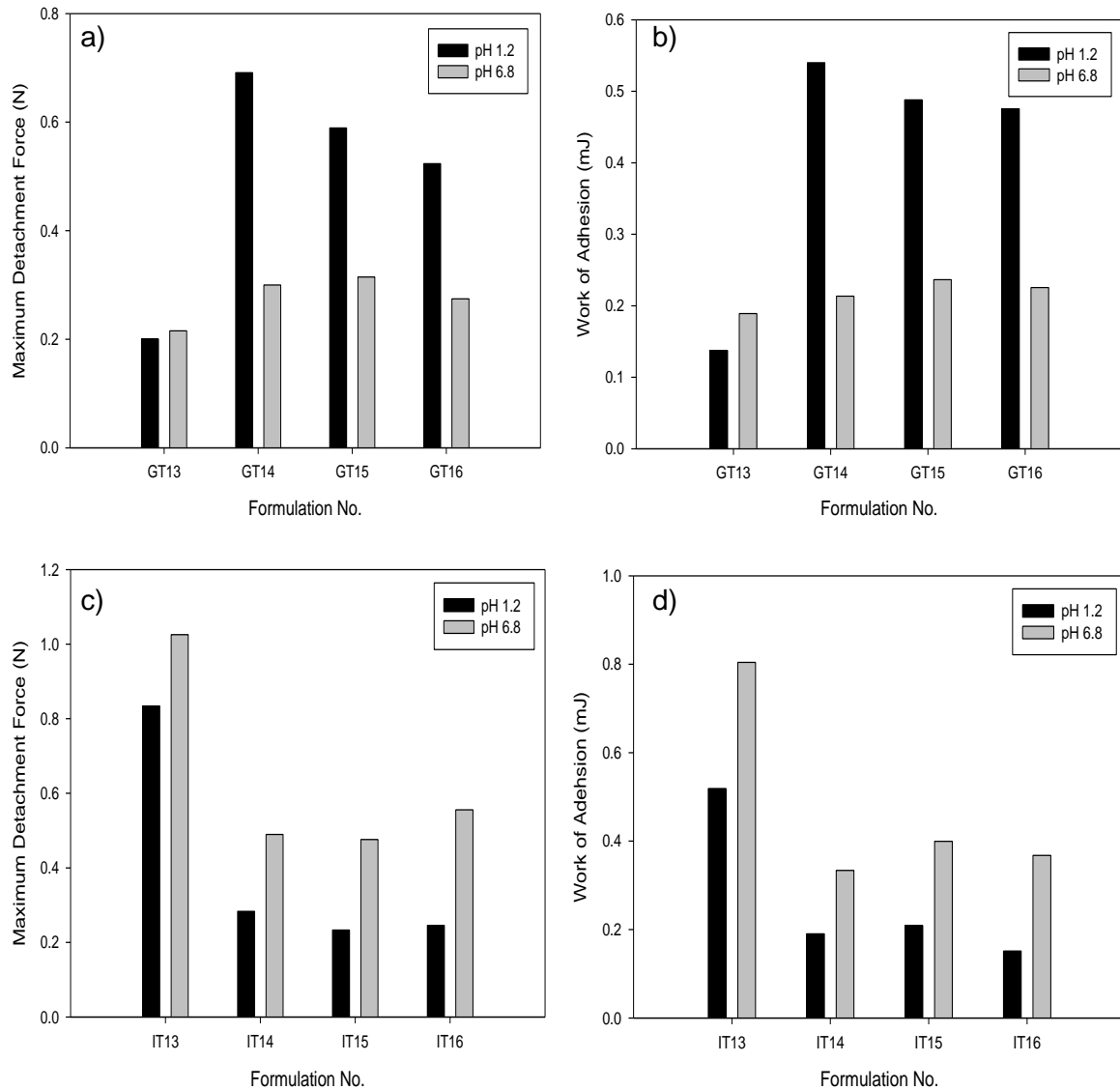


**Figure 3.12:** A comparison of the effect of PAA substitution with PVP on a) the Maximum Detachment Force (MDF) (N) and b) Work of Adhesion ( $AUC_{FD}$ ) (mJ) of the experimental CHT-based formulations; and c) the Maximum Detachment Force (MDF) (N) and d) Work of Adhesion ( $AUC_{FD}$ ) (mJ) of the experimental PEC-based formulations ( $n=3$ ;  $SD < 0.023$  in all cases).

Although the mucoadhesive characteristics of PEC-based formulations dropped with PVP substitution (Figure 3.12c-d), these membranes were more likely to remain viable for prolonged periods of exposure to the GIT (Figure 3.13c-d). Furthermore, the mucoadhesive characteristics of all experimental formulations containing PVP improved as the formulations swelled, causing expansion of the polymeric network thus promoting mucoadhesion through polymer chain interpenetration and exposure of additional adhesive sites within the network (Figure 3.13a-d).

The eventual decline in mucoadhesion can be attributed to the slow dissolving of the mucoadhesive polymer, PVP. Experimental formulations containing PVP successfully met the criteria of good film-forming properties, while remaining viable during prolonged periods of exposure to simulated GIT conditions and maintaining pH-responsive mucoadhesion. Overall, substitution with PVP led to the identification of the most appropriate combination of polymers required to develop a candidate system for further development and optimisation (of both the gastric-targeted and intestinal-targeted components of the MMDDS).

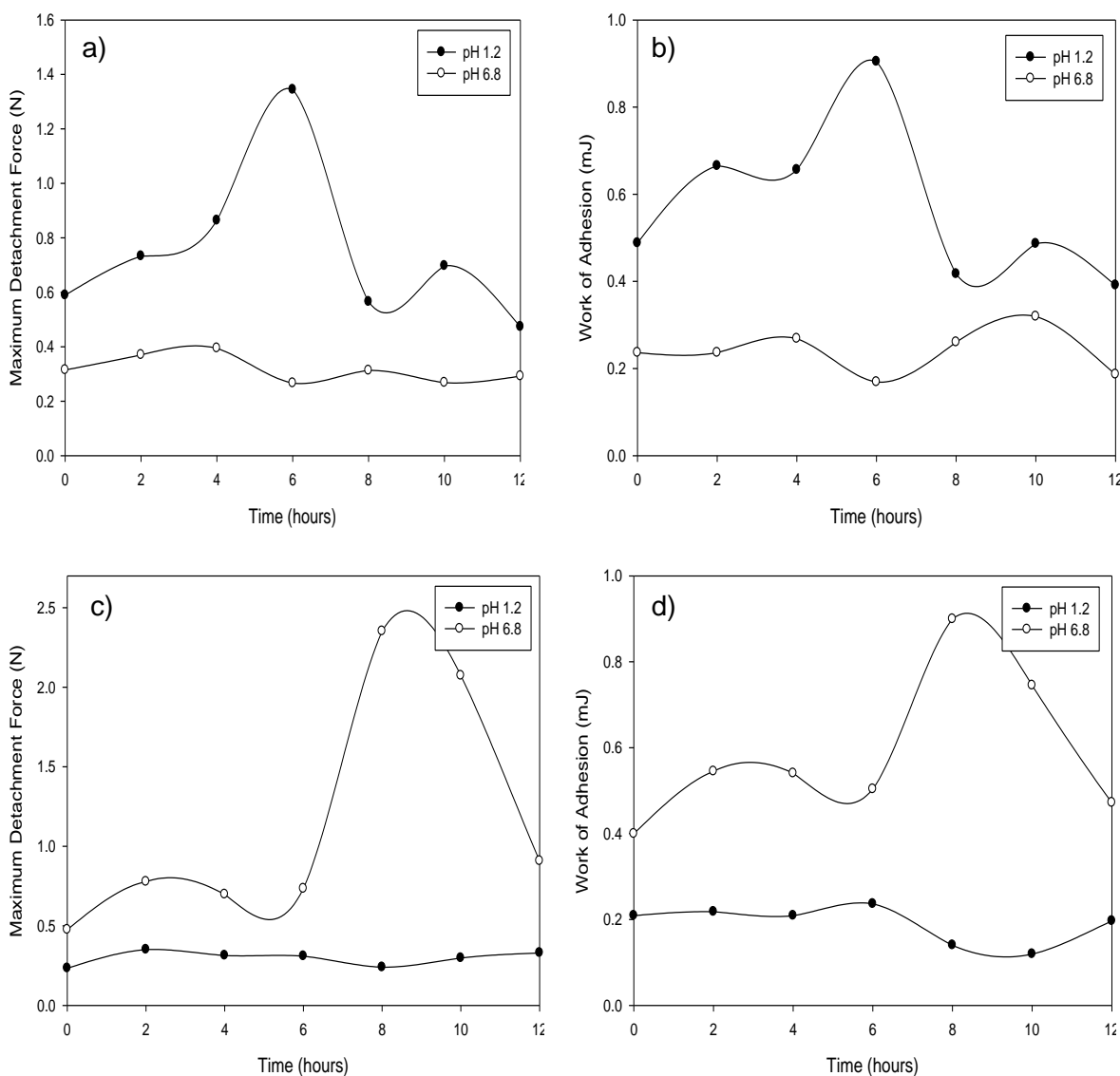


**Figure 3.13:** Variations in a) the MDF (N), and b) the  $AUC_{FD}$  (mJ) of experimental Formulation GT15 and c) the MDF (N), and d) the  $AUC_{FD}$  (mJ) of experimental Formulation IT15 as a function of time ( $n=3$ ;  $SD < 0.088$  in all cases).

### 3.3.5 Determining the upper and lower limits of the formulation variables required for input into the Central Composite Design

Following the identification of the polymer combinations for the gastric- and intestinal-targeted components respectively, the upper and lower limit variables of the formulation was determined. The resultant variables are illustrated in Table 3.7. The limits were determined by ensuring the membranes formed met the criteria identified in *Section 3.2.6, Chapter 3*. For optimization purposes, further elaborated in *Chapter 4*, the ratio of PVP to CHT was kept constant at a ratio of 1:4, while for PEC-based formulations; the ratio was maintained at 1:3. Any further increase in the ratio was detrimental to the pH-responsive nature and any decrease in the ratio demonstrated relatively poorer characteristics.

**Table 3.7:** The identified variables and their corresponding upper and lower limits for input into the Central Composite Design.

| <b>Polymer</b>   | <b>Lower Limit (%<sup>w</sup>/<sub>v</sub>)</b>  | <b>Upper Limit (%<sup>w</sup>/<sub>v</sub>)</b>   |
|--|--|---|
| <b>Gastric-targeted component</b>  |  |   |
| <b>CHT</b>   | <ul style="list-style-type: none"> <li>1%<sup>w</sup>/<sub>v</sub></li> <li>Anything &lt;1%<sup>w</sup>/<sub>v</sub> did not demonstrate a satisfactory pH-responsive nature. Furthermore, these formulations tended to erode prematurely and were thus not viable for a sufficient period.</li> </ul>     | <ul style="list-style-type: none"> <li>2%<sup>w</sup>/<sub>v</sub></li> <li>Formulations containing &gt;2%<sup>w</sup>/<sub>v</sub> resulted in solutions that were too viscous to film-cast properly, and membranes formed were not uniform and consistent in structure.</li> </ul>  |
| <b>PVP</b>   | <ul style="list-style-type: none"> <li>4%<sup>w</sup>/<sub>v</sub></li> <li>Formulations containing less than &lt;4%<sup>w</sup>/<sub>v</sub> demonstrated relatively poorer mucoadhesive properties.</li> </ul>   | <ul style="list-style-type: none"> <li>8%<sup>w</sup>/<sub>v</sub></li> <li>Formulations containing &gt;8%<sup>w</sup>/<sub>v</sub> did not form viable membranes (the structure was too sticky to handle). Furthermore, the pH-responsive nature was being lost as PVP concentration increased.</li> </ul>   |
| <b>PVA</b>   | <ul style="list-style-type: none"> <li>2%<sup>w</sup>/<sub>v</sub></li> <li>Formulations containing less than &lt;2%<sup>w</sup>/<sub>v</sub> eroded or disintegrated prematurely, and were thus not viable for a sufficient period.</li> </ul>  | <ul style="list-style-type: none"> <li>4.75%<sup>w</sup>/<sub>v</sub></li> <li>Formulations containing &gt;4.75%<sup>w</sup>/<sub>v</sub> resulted in solutions that were too viscous to film-cast properly, and membranes formed were not uniform and consistent in structure. Furthermore, poor mucoadhesion was demonstrated by these formulations.</li> </ul> |
| <i>Ratio between CHT and PVP was kept constant at 1:4. If the ratio increased, detrimental effects to the pH-responsive nature of the formulation were observed.</i> |  |   |
| <b>Intestinal-responsive component</b>   |  |   |
| <b>PEC</b>   | <ul style="list-style-type: none"> <li>1.3%<sup>w</sup>/<sub>v</sub></li> <li>Anything &lt;1.3%<sup>w</sup>/<sub>v</sub> did not demonstrate a satisfactory pH-responsive nature. Furthermore, these formulations tended to erode prematurely and were thus not viable for a sufficient period.</li> </ul> | <ul style="list-style-type: none"> <li>2.7%<sup>w</sup>/<sub>v</sub></li> <li>Formulations containing &gt;2.7%<sup>w</sup>/<sub>v</sub> resulted in solutions that were too viscous to film-cast properly, and membranes formed were not uniform and consistent in structure.</li> </ul>  |
| <b>PVP</b>   | <ul style="list-style-type: none"> <li>3.9%<sup>w</sup>/<sub>v</sub></li> <li>Formulations containing less than &lt;3.9%<sup>w</sup>/<sub>v</sub> demonstrated relatively poorer mucoadhesive properties.</li> </ul>   | <ul style="list-style-type: none"> <li>8.1%<sup>w</sup>/<sub>v</sub></li> <li>Formulations containing &gt;8.1%<sup>w</sup>/<sub>v</sub> did not form viable membranes (the structure was too sticky to handle). Furthermore, the pH-responsive nature was being lost as PVP concentration increased.</li> </ul>   |
| <b>PVA</b>   | <ul style="list-style-type: none"> <li>2%<sup>w</sup>/<sub>v</sub></li> <li>Formulations containing less than &lt;2%<sup>w</sup>/<sub>v</sub> eroded or disintegrated prematurely, and were thus not viable for a sufficient period.</li> </ul>  | <ul style="list-style-type: none"> <li>4.75%<sup>w</sup>/<sub>v</sub></li> <li>Formulations containing &gt;4.75%<sup>w</sup>/<sub>v</sub> resulted in solutions that were too viscous to film-cast properly, and membranes formed were not uniform and consistent in structure. Furthermore, poor mucoadhesion was demonstrated by these formulations.</li> </ul> |
| <i>Ratio between PEC and PVP was kept constant at 1:3. If the ratio increased, detrimental effects to the pH-responsive nature of the formulation were observed.</i> |  |   |

### 3.4 Concluding Remarks

Preliminary studies led to the rational identification of the formulation variables most suited for the development and further optimization of the gastric- and intestinal-targeted mucoadhesive systems respectively. Due to their pH-responsive nature, CHT (1-2%<sup>w/v</sup>) and PEC (1.3-2.7%<sup>w/v</sup>) were identified as the primary polymers necessary for the development of the gastric- and intestinal-targeted systems respectively. Screening of various mucoadhesive polymers led to the selection of PVP (4-8%<sup>w/v</sup> and 3.9-8.1%<sup>w/v</sup> for the gastric- and intestinal-targeted components respectively) as the most ideal polymer able to further improve the mucoadhesive characteristics of the respective mucoadhesive layers without impacting the pH-responsive nature of the formulations. The ratio between the pH-responsive polymer and PVP was found to be optimal if kept at 1:4 and 1:3 for the gastric- and intestinal-targeted components respectively.

An important outcome of this chapter was to ensure that the mucoadhesive membranes maintained their pH-responsive mucoadhesive characteristics, while not undergoing premature disintegration with prolonged periods of exposure to simulated GIT conditions. Inclusion of PVA (2-4.75%<sup>w/v</sup>) was thus beneficial, as the mucoadhesive membranes were able to withstand prolonged periods of exposure to simulated GIT conditions, while still maintaining both the mucoadhesive and pH-responsive nature of the mucoadhesive membranes. This chapter served to identify the candidate formulation which led to the identification of 2 variables, with their corresponding upper and lower limits, for input into a Central Composite Design. The Central Composite Design, detailed in *Chapter 4*, was conducted for further optimization of gastric-targeted and intestinal-targeted components respectively.

## CHAPTER 4

### FABRICATION AND STATISTICAL OPTIMIZATION OF THE STIMULI-RESPONSIVE MUCOADHESIVE LAYERS OF THE MULTI-COMPONENT MEMBRANOUS DRUG DELIVERY SYSTEM EMPLOYING AN EXPERIMENTAL DESIGN STRATEGY

---

#### 4.1 Introduction

Statistical formulation optimization approaches, employing a systematic Design of Experiments (DoE), are extensively practiced to improve the outcomes of formulation design in DDS development, as it is an efficient and cost-effective tool that is able to provide the most optimal formulation in response to the most desired characteristics. In order to ensure the successful implementation of an experimental design, the objectives of the experiment and the factors to be investigated need to be clearly defined (Singh *et al.*, 2004). Through extensive preliminary studies, detailed in *Chapter 3*, a prototypical formulation led to the identification of independent variables (polymer quantity) which impacted the measured responses (i.e. mucoadhesive characteristics).

In order to achieve the preferred characteristics and qualities of a DDS, it is necessary to recognize whether the factors included in the formulation will impact any characteristics of the formulation. During preliminary studies, one or more process variables or factors were deliberately changed to determine the effect that the change may have on measured responses (the-one-variable-at-a-time or OVAT approach). Results indicated that varying any of the components, specifically, the polymer quantity of the system caused interactions that would impact the mucoadhesive characteristics of the system. However, utilising the OVAT approach in designing a formulation is a costly and time-consuming process and achieving the optimized formulation is not guaranteed. This was overcome by employing a statistically robust experimental Central Composite Design, an optimization procedure which utilizes fewer experimental runs, is less time consuming and provides a true optimized formulation by a systematic approach (Singh *et al.*, 2004).

The Response Surface Methodology (RSM) was selected in design implementation as the factors affecting the formulation characteristics were already identified in *Chapter 3*, therefore facilitating the optimization process. The ultimate goal of employing the RSM was to identify the best combination of the formulation components that would achieve an optimal formulation for both the gastric-targeted and intestinal-targeted mucoadhesive



layers. RSM is useful for the elucidation of complex processes in many fields (chemical and engineering processes, industrial research, biological investigations and agricultural processes) with the final goal of optimizing a system and is commonly employed in Central Composite Designs to enable the investigator to identify the optimal settings of the experimental factors that give the maximum (or minimum) value of the response (He *et al.*, 2005; Kumar *et al.*, 2011b). Essentially, RSM is a collection of mathematical and statistical techniques for empirical model building based on physical experiments or experimental observations (Raissi and Eslami Farsani, 2009).

#### **4.1.1 Selection of independent variables for input into a Central Composite Design**

Based on the preliminary results obtained from *Chapter 3*, the formulation components (input variables) that impacted the mucoadhesive characteristics of the formulation (measured response) were identified along with their upper and lower limits. Factors along with the factor levels were selected for each of the mucoadhesive layers of the MMDDS such that individualised mathematical models were generated. The primary difference between the gastric-and intestinal-targeted components included the type of pH-responsive polymer employed, i.e. CHT or PEC.

CHT, a natural polysaccharide with low toxicity, was employed as the pH-responsive component of the gastric-targeted component. The myriad of pharmaceutical uses, including disintegrant, binder, mucoadhesive and permeation enhancing effects of CHT arises from the variations in the different grades of CHT, each differing in the degree of deacetylation (40-98%), molecular weight (50 kDa to 2000 kDa), viscosity and pKa. It is produced via the partial deacetylation of chitin, producing a polysaccharide copolymer of glucosamine and N-acetyl glucosamine (Singla and Chawla; 2001). The pH-dependant solubility of CHT has been exploited in the present study to ensure pH-dependent mucoadhesion, as in acidic mediums, the amine groups ( $\text{NH}_3^+$ ) are protonated which promotes mucoadhesion in the gastric pH-range. The concentration range selected for optimization of the gastric-targeted component was based on preliminary studies (*Chapter 3*) and determined to be 1-2%<sup>w/v</sup>.

PEC, a high-molecular-weight, complex polysaccharide, was employed as the pH-responsive polymer for the intestinal-targeted component. PEC consists primarily of chains of esterified D-galacturonic acid units linked as 1,4- $\alpha$ -glucosides, with a molecular weight of 30 000–100 000g/mol. It is typically used as an adsorbent, emulsifying agent, gelling agent, thickening agent, or stabilizing agent, and is commonly employed in oral

formulations due to its non-toxic and non-irritant nature. It is often employed as pH-sensitive polymeric coating, which retards drug release in the upper GIT region, due to its limited solubility in lower pH ranges. This pH-dependant solubility is exploited in the present study to ensure pH-dependent mucoadhesion, as in alkaline pH ranges, the carboxyl groups ( $\text{COO}^-$ ) are ionised, which promotes mucoadhesion in the intestinal pH-range (Rowe *et al.*, 2009). The concentration range selected for optimization of the intestinal-targeted component was based on preliminary studies (*Chapter 3*) and determined to be 1.3-2.7% $^w/v$ .

Polyvinyl alcohol (PVA), a water-soluble synthetic polymer represented by the formula  $(\text{C}_2\text{H}_4\text{O})_n$ , was utilized to prevent premature erosion and disintegration of both the gastric-targeted and intestinal-targeted mucoadhesive layers. The concentration range selected for optimization was based on preliminary studies (*Chapter 3*) and determined to be 2-4.75% $^w/v$  (Rowe *et al.*, 2009).

Poly(vinylpyrrolidone) (PVP), a synthetic polymer consisting essentially of linear 1-vinyl-2-pyrrolidinone groups, is highly biocompatible and commonly used as a mucoadhesive (Rowe *et al.*, 2009; Alsarra *et al.*, 2011). For the purposes of this study, PVP was incorporated to further improve the mucoadhesive characteristics of the formulations on a fixed ratio of 1:4 and 1:3 of CHT:PVP and PEC:PVP respectively, ranging in concentrations of 4-8% $^w/v$  for further optimization.

The focus of this chapter lies in development and optimization of both pH-responsive mucoadhesive layers through a systematic approach of experimental runs, employing a two-level, two-factorial, randomized Central Composite Design for each component. The optimized formulation of each component will provide the most ideal mucoadhesive characteristics over a prolonged period of time. The present chapter is divided into three Sections to facilitate a sequential and logical representation of the data obtained as follows: Part I: Fabrication and statistical optimization of gastric-responsive layer of the MMDDS; Part II: Fabrication and statistical optimization of intestinal-responsive layer of the MMDDS and Part III: Physicochemical and physicomechanical characterization of the optimized gastric- and intestinal-targeted mucoadhesive layers of the MMDDS.

## **Part I – Fabrication and statistical optimization of gastric-targeted mucoadhesive layer of the MMDDS**

### **4.2 Material and Methods**

#### **4.2.1 Materials**

The materials including chitosan (CHT), polyvinylpyrrolidone-40 (PVP), polyvinyl alcohol (PVA), glycerol, silicone, acetic acid, dialysis flat sheet membranes, sodium chloride, hydrochloric acid and liquid paraffin were obtained as described in *Section 3.2.1*. All other reagents employed were of analytical grade and used as purchased without further purification. Double-deionised water was obtained from a Milli-Q Water Purification System (Millipore, Bedford MA, USA).

#### **4.2.2 Construction of a randomized Central Composite Design for the optimization of the gastric-targeted component**

A Face-centered Central Composite Experimental Design (FCCCD) with 2 factors and cube points was generated by Minitab<sup>®</sup>, V15 (Minitab<sup>®</sup> Inc, Pennsylvania, USA) in order to statistically optimize the gastric-targeted mucoadhesive layer of the MMDDS. The input factors or independent variables, concentration of CHT: PVP, and concentration of PVA, were studied at two levels each, and the DoE generated 13 experimental runs (or formulations), consisting of the design points illustrated in Table 4.1. These experimental runs aimed to produce a minimum amount of runs that would ascertain maximum efficacy of information for prediction of responses. Table 4.2 represents the independent variables and their corresponding levels in the design. The dependent variable was identified as the Area Under the Curve (AUC) of the Work of Adhesion (WA) profile plotted against a time of 12 hours. RSM based on the constructed FCCCD was employed to evaluate the formulation factors that affected the dependant variable, the AUC of the WA (mJ) against time (hours) curve. The experimental range of each variable was selected based on the results of preliminary experiments detailed in *Chapter 3*. To reduce systematic errors, the experiments were completely randomized. All experiments were conducted in triplicate (n=3).

**Table 4.1:** Design points employed in the generation of the 2 factor, face-centred central composite design.

| <b>Two-level full factorial design</b>   |   |
|--|---|
| Cube points  | 4 |
| Centre points in cube  | 5 |
| Axial points (points parallel to each variable axis on a circle of radius equal to 1.0 and origin at the centre-point) | 4 |
| Centre points in axial   | 0 |
| Alpha ( $\alpha$ )   | 1 |

#### 4.2.3 Fabrication of the gastric-targeted mucoadhesive layer

The mucoadhesive layer was fabricated using the film-casting technique of membrane fabrication, as described in *Section 3.2.2*. Briefly, the film-casting method included solubilising the required quantity of the polymers in accordance with the randomized Central Composite Design template (Table 4.2), followed by glycerol (2:1 of polymer: plasticizer) and the antifoaming agent, silicone (1 drop per 100mL) addition. 40mL aliquots of the polymeric solution was then film-cast into moulds and subject to ambient conditions for 24 hours, resulting in the formation of thin, transparent and uniform polymeric membranes, which were cut into 20x30mm dimensions. Membranes were stored with desiccants in airtight containers until further testing was completed.

**Table 4.2:** Central composite design template of the 13 statistically derived formulations for the fabrication of the gastric-responsive mucoadhesive layer of the MMDDS.

| <b>Experimental Formulation</b> | <b>Independent variables</b>   |  |
|---------------------------------|--|--|
|                                 | <b>CHT(%<sup>w</sup>/<sub>v</sub>) : PVP(%<sup>w</sup>/<sub>v</sub>)</b> | <b>PVA(%<sup>w</sup>/<sub>v</sub>)</b> |
| 1                               | 2.0 : 8.0  | 2.000                                  |
| 2                               | 2.0 : 8.0  | 3.375                                  |
| 3                               | 1.0 : 4.0  | 3.375                                  |
| 4                               | 1.5 : 6.0  | 3.375                                  |
| 5                               | 1.5 : 6.0  | 4.750                                  |
| 6                               | 1.0 : 4.0  | 4.750                                  |
| 7                               | 2.0 : 8.0  | 4.750                                  |
| 8                               | 1.5 : 6.0  | 3.375                                  |
| 9                               | 1.5 : 6.0  | 2.000                                  |
| 10                              | 1.0 : 4.0  | 2.000                                  |
| 11                              | 1.5 : 6.0  | 3.375                                  |
| 12                              | 1.5 : 6.0  | 3.375                                  |
| 13                              | 1.5 : 6.0  | 3.375                                  |

#### **4.2.4 Mucoadhesive analysis through textural profiling**

In order to evaluate the mucoadhesive properties of the mucoadhesive layer, the Work of Adhesion (WA) required to detach a hydrated mucoadhesive layer from a portion of Simulated Gastric Membrane (SGM) was determined, using Texture Analyser *TA.XTplus* (Stable Microsystems, England), as described in *Section 3.2.7*. The polymeric and simulated gastric membranes were pre-impregnated with PBS; pH  $1.2\pm 0.1$  prior to mucoadhesive testing; simulating the gastric region of the GIT.

#### **4.2.5 Variations in mucoadhesive characteristics of the gastric-targeted experimental formulations as a function of time**

In order to determine the effects of the GIT on the mucoadhesive characteristics of the formulation as a function of time, the formulations were subject to conditions typical of *in vitro* drug release or dissolution studies in a USP Dissolution Apparatus (Erweka DT 700 GmbH Germany). The USP 25 rotating paddle method of dissolution was selected where the mucoadhesive layers were exposed to 900mL of PBS (pH  $1.2\pm 0.1$ ) for 12 hours at  $37\pm 0.5^\circ\text{C}$  and 50rpm. At two hour intervals, the layers were removed from the dissolution media and subject to mucoadhesive analysis as described in *Chapter 3, Section 3.2.7*. Fresh samples were used for each individual time point.

#### **4.2.6 Constrained statistical optimization of the gastric-targeted mucoadhesive layer of the MMDDS**

Following generation of the polynomial equations relating the dependent and independent variables, the formulation components were optimized under constrained conditions for the measured response using RSM. Simultaneous equation solving for optimization of the formulation process was performed to obtain the levels of independent variables, which would accomplish the most desired mucoadhesive characteristics. The factor levels or the polymer quantity represented the independent variables while the mucoadhesive characteristics (specifically the Work of Adhesion in mJ) represented the dependent variables (i.e. the response parameters). The Work of Adhesion (mJ) was identified as the dependant variable to be optimized, since it offers a truer representation of the adhesion process than the Maximum Detachment Force (N). Analysis of Variance (ANOVA), correlation analysis and regression analysis was employed for data analysis and determination of the statistical acceptability of the models proposed.

## 4.3 Results and Discussion

### 4.3.1 Central Composite Experimental Design for optimization of the gastric-targeted mucoadhesive layer of the MMDDS

#### 4.3.1.1 Measured responses for experimental optimization

The mucoadhesive layer experimental design formulations demonstrated relatively consistent mucoadhesion over the duration of the study, as illustrated in Figure 4.1a-d. Typically, formulations containing large concentrations of the incorporated polymers demonstrated relatively poorer mucoadhesive characteristics. This finding may be attributed to the large degree of chain entanglements (present from higher polymeric concentrations) which reduces the rate and degree of swelling, ultimately mitigating mucoadhesion. The measured response selected for optimization was determined from the Area Under the Curve (AUC) of the Work of Adhesion (mJ) vs. Time (hours) curve. The AUC, calculated employing SigmaPlot® V10.0 software, are depicted in Table 4.3.

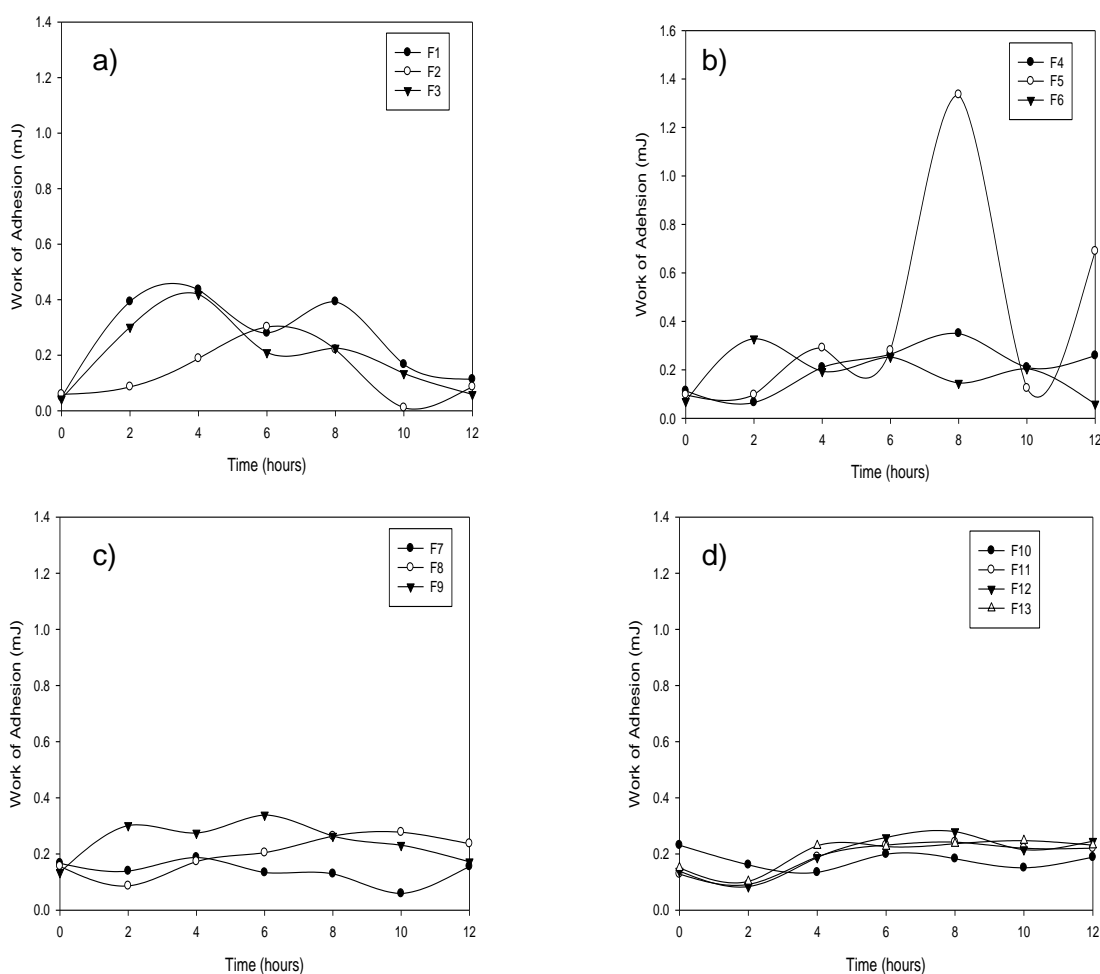


**Figure 4.1:** Variations in  $AUC_{FD}$  of the Experimental Formulations a) 1-3; b) 4-6; c) 7-9; and d) 10-13 as a function of time ( $n=3$ ;  $SD < 0.072$  in all cases).

**Table 4.3:** Measured responses of the experimental runs for the optimization of the gastric-targeted mucoadhesive layer of the MMDDS.

| <b>Formulation</b> | <b>CHT:PVP<br/>(%w/v)</b> | <b>PVA<br/>(%w/v)</b> | <b>Measured<br/>Response (AUC)</b> |
|--------------------|---------------------------|-----------------------|------------------------------------|
| 1                  | 2.0 : 8.0                 | 2.000                 | 3.5003                             |
| 2                  | 2.0 : 8.0                 | 3.375                 | 1.7609                             |
| 3                  | 1.0 : 4.0                 | 3.375                 | 2.6871                             |
| 4                  | 1.5 : 6.0                 | 3.375                 | 2.5686                             |
| 5                  | 1.5 : 6.0                 | 4.750                 | 5.0404                             |
| 6                  | 1.0 : 4.0                 | 4.750                 | 2.3802                             |
| 7                  | 2.0 : 8.0                 | 4.750                 | 1.6213                             |
| 8                  | 1.5 : 6.0                 | 3.375                 | 2.4040                             |
| 9                  | 1.5 : 6.0                 | 2.000                 | 3.1287                             |
| 10                 | 1.0 : 4.0                 | 2.000                 | 2.0786                             |
| 11                 | 1.5 : 6.0                 | 3.375                 | 2.3017                             |
| 12                 | 1.5 : 6.0                 | 3.375                 | 2.4354                             |
| 13                 | 1.5 : 6.0                 | 3.375                 | 2.4674                             |

#### 4.3.1.2 Correlation of the experimental and fitted response values

A comparative analysis of the experimental vs. the fitted response values, i.e. the mucoadhesive characteristics, was plotted to establish the applicability of the regression models and the robustness of the Central Composite Design employed for the optimization of the gastric-targeted mucoadhesive layer. The plot depicting the AUC (of the Work of Adhesion vs. Time profiles) of the experimental vs. the fitted values of each formulation show a general conformity with a correlation coefficient ( $R^2$ ) of 0.714 (Figure 4.2). An acceptable correlation between the experimental and fitted responses was determined verifying the central composite experimental design for the responses of mucoadhesive properties, aiding in the determination of an optimized gastric-targeted mucoadhesive layer.

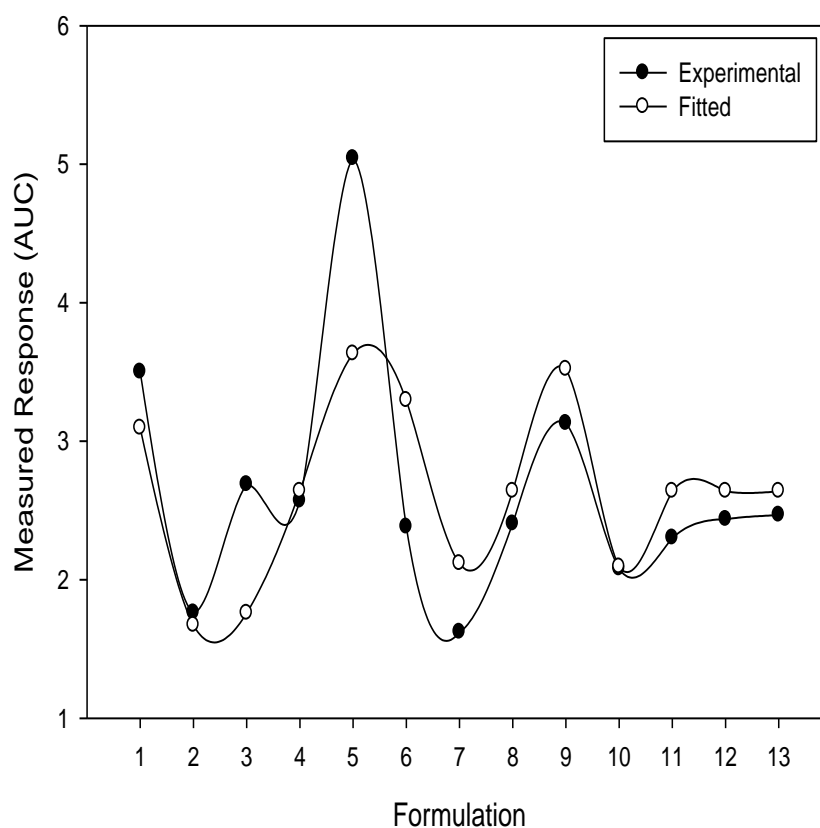


**Figure 4.2:** Regression plots of Area Under the Curve of the Work of Adhesion (mJ) vs. Time (hours) profile for the determination of the correlation between the experimental vs. the fitted response values.

#### 4.3.1.3 Analysis of the Central Composite Surface Design

The AUC (of the Work of Adhesion (mJ) vs. Time profile) was the response measured for the gastric-targeted mucoadhesive system. Surface plot analysis validated the relationship between the independent variables PVA and CHT:PVP concentrations on the response of AUC in Figure 4.3a. A positive or maximal response of the AUC ( $\pm 3.5$ ) was established from the response curve at concentrations of 1-1.5%<sup>w/v</sup> of CHT:PVP and 4.750%<sup>w/v</sup> of PVA. For PVA concentrations ranging from 3-4%<sup>w/v</sup>, a minimal response on the AUC was observed. However, formulations containing greater than 4%<sup>w/v</sup> PVA also demonstrated a maximal response on the AUC. Any increase in the CHT:PVP concentration to a point of  $\pm 1.75\%$ <sup>w/v</sup> influenced a positive effect on the measured response. Any further increase beyond this point influenced a negative effect on the response. For the purposes of optimizing the response of AUC, manipulation of the PVA concentrations had a more positive effect. These responses are also evident in the contour plot (Figure 4.3b), where a positive effect on the AUC was observed at concentrations of PVA > 4%<sup>w/v</sup> and between 1-1.5%<sup>w/v</sup> CHT:PVP.



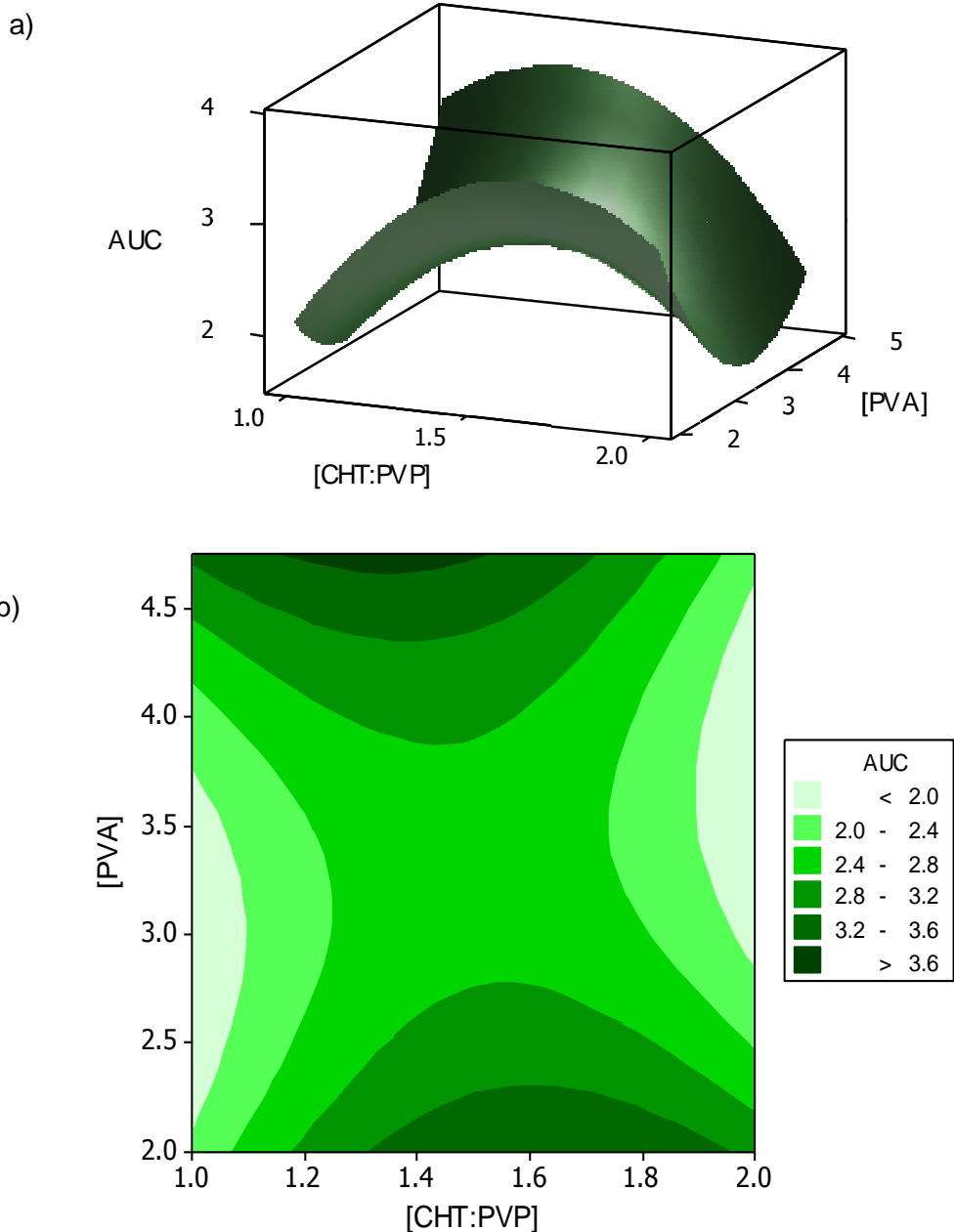


**Figure 4.3:** Illustration of the relationship between independent variables and the response of mucoadhesive properties through a) 3-D surface plots and b) contour plots for the gastric-targeted mucoadhesive layer.

In contrast to preliminary studies, increasing the PVA concentration proved to provide the maximal response required for the AUC. Upon analysis of the Work of Adhesion vs. time profiles of the experimental design formulations (Figure 4.1), a decrease in the WA was observed over time in formulations containing less than 4.75%<sup>w/v</sup> of PVA. These findings can be attributed to the mucoadhesive polymers diffusing or dissolving out of the mucoadhesive membranes. With the increase in chain entanglements occurring as PVA concentration increases, the mucoadhesive characteristics remain constant for longer durations of time since the mucoadhesive polymer is no longer able to diffuse or erode

out of the mucoadhesive layer as easily. However, increasing the concentration of the CHT beyond 1.5%<sup>w/v</sup> caused an even higher degree of chain entanglements to occur, thus abating mucoadhesion (due to the resultant decrease in swelling and thus preventing accessibility of the adhesive sites on the mucoadhesive polymer).

#### **4.3.1.4 Residual Analysis of the Central Composite Experimental Design for the optimization of the gastric-targeted mucoadhesive layer**

The suitability of the model was assessed employing residual analysis. A comparison between observed and fitted responses of the model was linearly compared, and the fit of the model was determined employing regression models. Ideally, response values should be normally distributed with constant variance and means (Deschepper *et al.*, 2006; Larsen and McCleary, 1972).

As illustrated in Figure 4.4, the normal probability plots of the residuals fell on a straight line indicating that the data was normally distributed with no evidence of unidentified variables. The plot of residuals vs. the fitted values tests the assumption of constant variance. A random arrangement of data points was demonstrated, with the presence of a small cluster, signifying an acceptable and normal fit with a linear regression model. The data points were plotted close to the zero axis, while demonstrating no discernible pattern, thus validating the assumption of constant variance. These assumptions were further validated by the histogram of residuals, where a constant variance was observed and that the residuals had a normal distribution. Furthermore, the residuals vs. the order of data plot, demonstrated a random distribution between the consecutive points, with some clustering of Formulations 6-9 and 10-13.

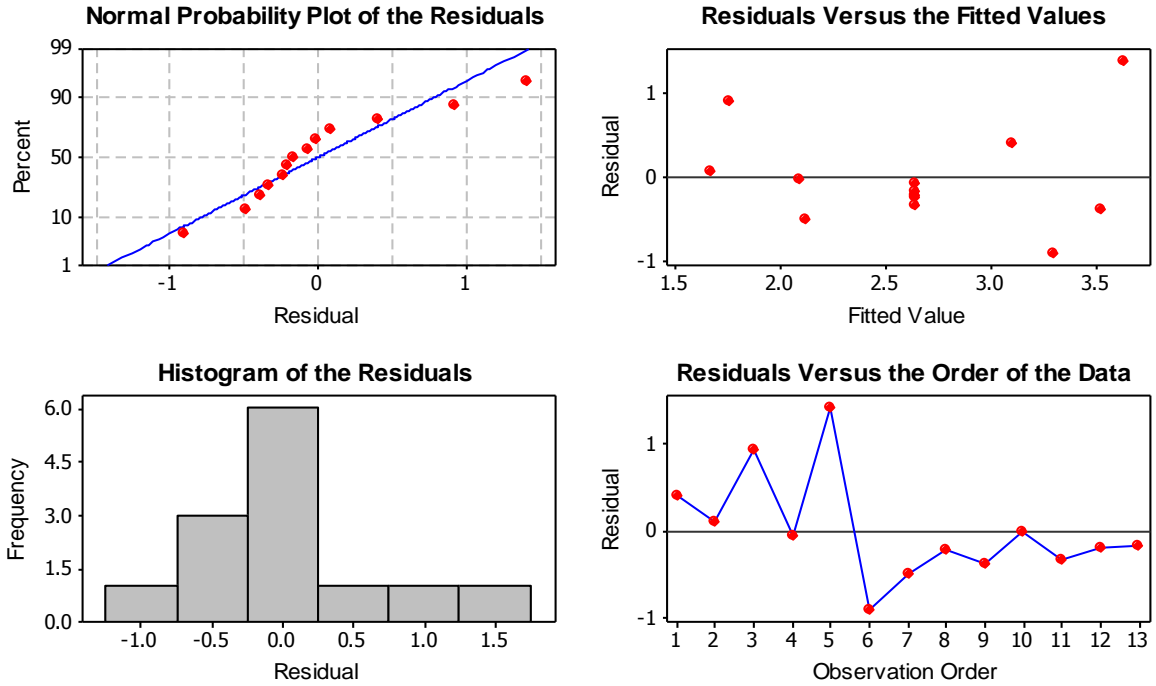


**Figure 4.4:** Residual plots of AUC of the Work of Adhesion (mJ) vs. Time (hours) profile for the gastric-targeted mucoadhesive layer of the MMDDS.

Based on a full ANOVA analysis of the measured formulation responses it was determined that none of the factors exhibited any significant influence ( $p \leq 0.05$ ). Only the PVA\*PVA ( $p=0.097$ ) term of the AUC response possessed a notable effect, even though  $p \geq 0.05$  (Table 4.4). The complete regression equations generated for AUC of the WA vs. Time profile is depicted in Equation 4.1.

**Table 4.4:** Estimated p-values for the response: AUC of the WA: Time profile.

| <b>Term</b>         | <b>Coef</b>     | <b>SE Coef</b> | <b>T</b>      | <b>p-value</b> |
|---------------------|-----------------|----------------|---------------|----------------|
| [CHT:PVP]           | -0.04390        | 0.3274         | -0.134        | 0.897          |
| [PVA]               | +0.05572        | 0.3274         | +0.170        | 0.870          |
| [CHT:PVP]*[CHT:PVP] | -0.92495        | 0.4826         | -1.917        | 0.097          |
| [PVA]*[PVA]         | +0.93560        | 0.4826         | +1.939        | 0.094          |
| [CHT:PVP]*[PVA]     | -0.54515        | 0.4010         | -1.360        | 0.216          |
| <b>Constant</b>     | <b>+2.63929</b> | <b>0.3330</b>  | <b>+7.926</b> | <b>0.000</b>   |

$$\text{AUC} = -4.06784 + 13.6878 [\text{CHT : PVP}] - 2.11038 [\text{PVA}] - 3.69981 [\text{CHT : PVP}]^2 + 0.494862 [\text{PVA}]^2 - 0.792945 [\text{CHT : PVP} * \text{PVA}]$$

Equation 4.1

#### 4.3.1.5 Constrained optimization of the gastric-targeted mucoadhesive layer

Optimization of the gastric-targeted mucoadhesive layer was performed employing Minitab® V15 statistical software (Minitab® Inc., PA, USA) to determine the optimum level for each variable. The optimization approach resulted in the attainment of a formulation with a desirability of 0.999 and the fabrication of this formulation included the employment of a 1.0014%<sup>w/v</sup> of CHT and a PVA concentration of 4.750%<sup>w/v</sup>, as depicted in Figure 4.5. Since the ratio of CHT:PVP was kept constant at 1:4, the final PVP concentration employed was 4.004%<sup>w/v</sup> in the optimized formulation. The resultant fitted and experimental values for the response parameters are provided in Table 4.5.

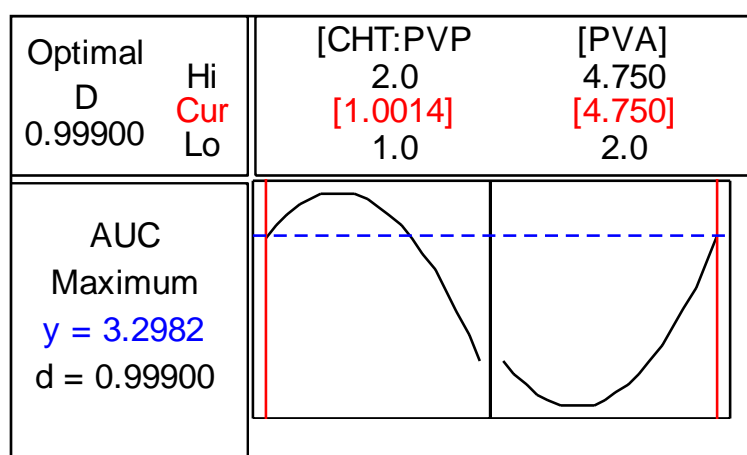


**Figure 4.5:** Optimization plots displaying factor levels and desirability values for the optimized gastric-targeted mucoadhesive layer of the MMDDS.

**Table 4.5:** Comparison of the fitted and experimental values of the response parameter.

| <b>Response parameter</b> | <b>Fitted</b> | <b><sup>1</sup>Desirability (%)</b> | <b>Experimental</b> | <b><sup>2</sup>Deviation (%)</b> |
|---------------------------|---------------|-------------------------------------|---------------------|----------------------------------|
| <b>AUC</b>                | 3.2982        | 0.999                               | 3.2310              | 2.037                            |

<sup>1</sup> Statistical desirability values of the fitted optimized formulation (%)

<sup>2</sup> Deviation of the experimental response values from the fitted

The fitted optimized formulation had a statistical desirability of ≥90% for the response parameter. An experimental AUC of 3.210 was achieved with the optimized formulation, with a deviation of 2.037% from the fitted response value of 3.2982, thereby demonstrating that the experimental response parameters achieved with the constrained settings for the optimized formulation were in close agreement with the fitted response values. This identified the reliability of the optimization process in predicting the maximal AUC and identifying an optimized formulation. Figure 4.6 represents the variations in the WA as a function of time. The shape of the curve was observed to possess a similar trend

that was typical of the experimental design formulations analyzed (Figure 4.1a-d), thus demonstrating that similar processes occur which promote or mitigate mucoadhesion as for the experimental design formulations. The variations in the mucoadhesion of the formulation can be attributed to the simultaneous swelling and erosion, which is further elaborated in Part III of the present chapter.

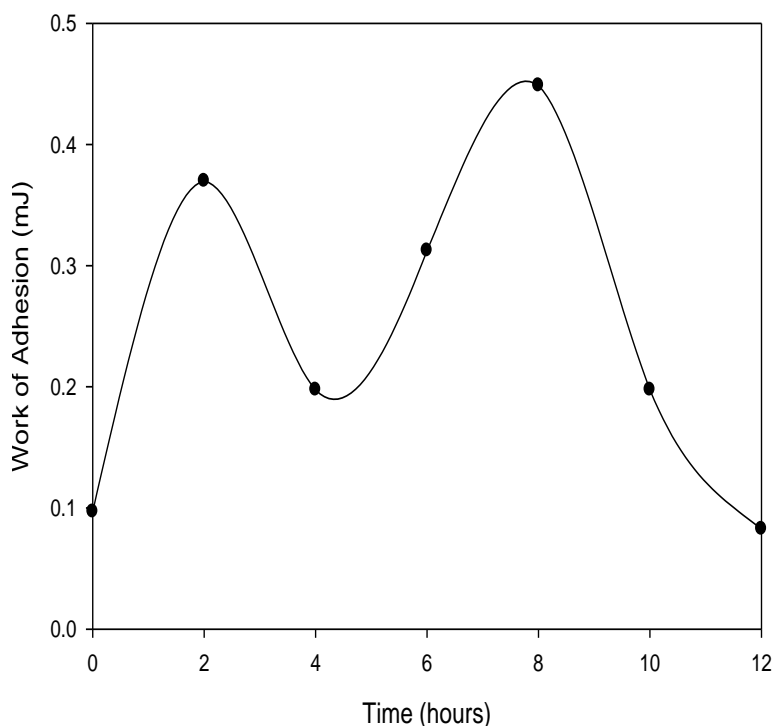


**Figure 4.6:** Variations in  $AUC_{FD}$  of the optimized gastric-targeted mucoadhesive layer as a function of time ( $n=3$ ;  $SD < 0.071$  in all cases).

## Part II – Fabrication and statistical optimization of the intestinal-targeted mucoadhesive layer of the MMDDS

### 4.4 Materials and Methods

#### 4.4.1 Materials

The materials included pectin (PEC), polyvinylpyrrolidone-40 (PVP), polyvinyl alcohol (PVA), glycerol, silicone, dialysis flat sheet membranes, sodium hydroxide, potassium dihydrogen phosphate and liquid paraffin, were obtained as described in *Section 3.2.1*. All other reagents employed were of analytical grade and used as purchased without further purification. Double-deionised water was obtained from a Milli-Q Water Purification System (Millipore, Bedford MA, USA).

#### 4.4.2 Construction of a randomized central composite design for the optimization of the intestinal-targeted component

A Face-centered Central Composite experimental Design (FCCCD), as detailed in *Section 4.2.2*, was generated to statistically optimize the intestinal-targeted mucoadhesive layer of the MMDDS. The input factors or independent variables, concentration of PEC:PVP, and concentration of PVA, generated 13 experimental runs (or formulations), as illustrated in Table 4.6. The experimental range of each variable was selected based on the results of preliminary experiments detailed in *Chapter 3*. The dependent variable was identified as the Area Under the Curve (AUC) of the Work of Adhesion (WA) profile plotted against a time of 12 hours.

#### 4.4.3 Fabrication of the intestinal-targeted mucoadhesive layer

The mucoadhesive layer was fabricated using the film-casting technique of membrane fabrication, as detailed in *Section 3.2.2*. Briefly, the film-casting method included solubilising the required quantity of the polymers in accordance with the randomized central composite design template (Table 4.6), followed by glycerol and silicone addition. 40mL aliquots of the polymeric solution was then film-cast into moulds and subject to ambient conditions for 24 hours, resulting in the formation of thin, transparent and uniform polymeric membranes, which were cut into 20x30mm dimensions. Membranes were stored with desiccants in airtight containers until further testing was completed.

**Table 4.6:** Central composite design template of the 13 statistically derived formulations for the fabrication of the intestinal-responsive mucoadhesive layer of the MMDDS.

| <i>Experimental Formulation</i> | <i>Independent Variables</i>   |  |
|---------------------------------|--|--|
|                                 | <i>PEC(%<sup>w</sup>/<sub>v</sub>) : PVP(%<sup>w</sup>/<sub>v</sub>)</i> | <i>PVA(%<sup>w</sup>/<sub>v</sub>)</i> |
| 1                               | 2.7 : 8.1  | 2.000                                  |
| 2                               | 2.7 : 8.1  | 3.375                                  |
| 3                               | 1.3 : 3.9  | 3.375                                  |
| 4                               | 2.0 : 6.0  | 3.375                                  |
| 5                               | 2.0 : 6.0  | 4.750                                  |
| 6                               | 1.3 : 3.9  | 4.750                                  |
| 7                               | 2.7 : 8.1  | 4.750                                  |
| 8                               | 2.0 : 6.0  | 3.375                                  |
| 9                               | 2.0 : 6.0  | 2.000                                  |
| 10                              | 1.3 : 3.9  | 2.000                                  |
| 11                              | 2.0 : 6.0  | 3.375                                  |
| 12                              | 2.0 : 6.0  | 3.375                                  |
| 13                              | 2.0 : 6.0  | 3.375                                  |

#### **4.4.4 Mucoadhesive analysis through textural profiling**

In order to evaluate the mucoadhesive properties of the mucoadhesive layer, the Work of Adhesion (WA) and the Maximum Detachment Force (MDF) required to detach a hydrated mucoadhesive layer from a portion of Simulated Intestinal Membrane (SIM) was determined, using Texture Analyser TA.XTplus (Stable Microsystems, England), as described in Section 3.2.7. The polymeric and SIMs were pre-impregnated with PBS; pH  $6.8 \pm 0.1$  prior to mucoadhesive testing; simulating the intestinal region of the GIT.

#### **4.4.5 Variations in the mucoadhesive characteristics of the intestinal-targeted experimental formulations as a function of time**

In order to determine the effects of the GIT on the mucoadhesive characteristics of the formulation as a function of time, the formulations were subject to conditions typical of *in vitro* drug release or dissolution studies, as described in Section 3.2.8. The USP 25 rotating paddle method of dissolution was selected where the mucoadhesive layers were exposed to 900mL of PBS (pH  $6.8 \pm 0.1$ ) for 12 hours at  $37 \pm 0.5^\circ\text{C}$  and 50rpm. At two hour intervals, the layers were removed from the dissolution media and subject to mucoadhesive analysis as described in Chapter 3, Section 3.2.7. Fresh samples were used for each individual time point.

#### **4.4.6 Constrained statistical optimization of the intestinal-targeted mucoadhesive layer of the MMDDS**

Following generation of the polynomial equations relating the dependent and independent variables, the formulation components were optimised under constrained conditions for the measured response using response surface methodology. Simultaneous equation solving for optimisation of the formulation process was performed to obtain the levels of independent variables, which would accomplish the most desired mucoadhesive characteristics. The factor levels or the polymer quantity represented the independent variables while the mucoadhesive characteristics in terms of the Work of Adhesion (mJ) represented the dependent variables (i.e. the response parameters).

## 4.5 Results and Discussion

### 4.5.1 Central Composite Experimental Design for optimization of the gastric-targeted mucoadhesive layer of the MMDDS

#### 4.5.1.1 Measured responses for experimental optimization

The mucoadhesive layer experimental design formulations demonstrated relatively consistent mucoadhesion over the duration of the study, as illustrated in Figure 4.7a-d. Typically, formulations containing large concentrations of the incorporated polymers demonstrated relatively poorer mucoadhesive characteristics. This finding may be attributed to the large degree of chain entanglements (present from higher polymeric concentrations) which reduces the rate and degree of swelling, ultimately mitigating mucoadhesion. The measured response selected for optimization was determined from the Area Under the Curve (AUC) of the Work of Adhesion (mJ) vs. Time (hours) curve. The AUC, calculated employing SigmaPlot® V10.0 software, are depicted in Table 4.7.

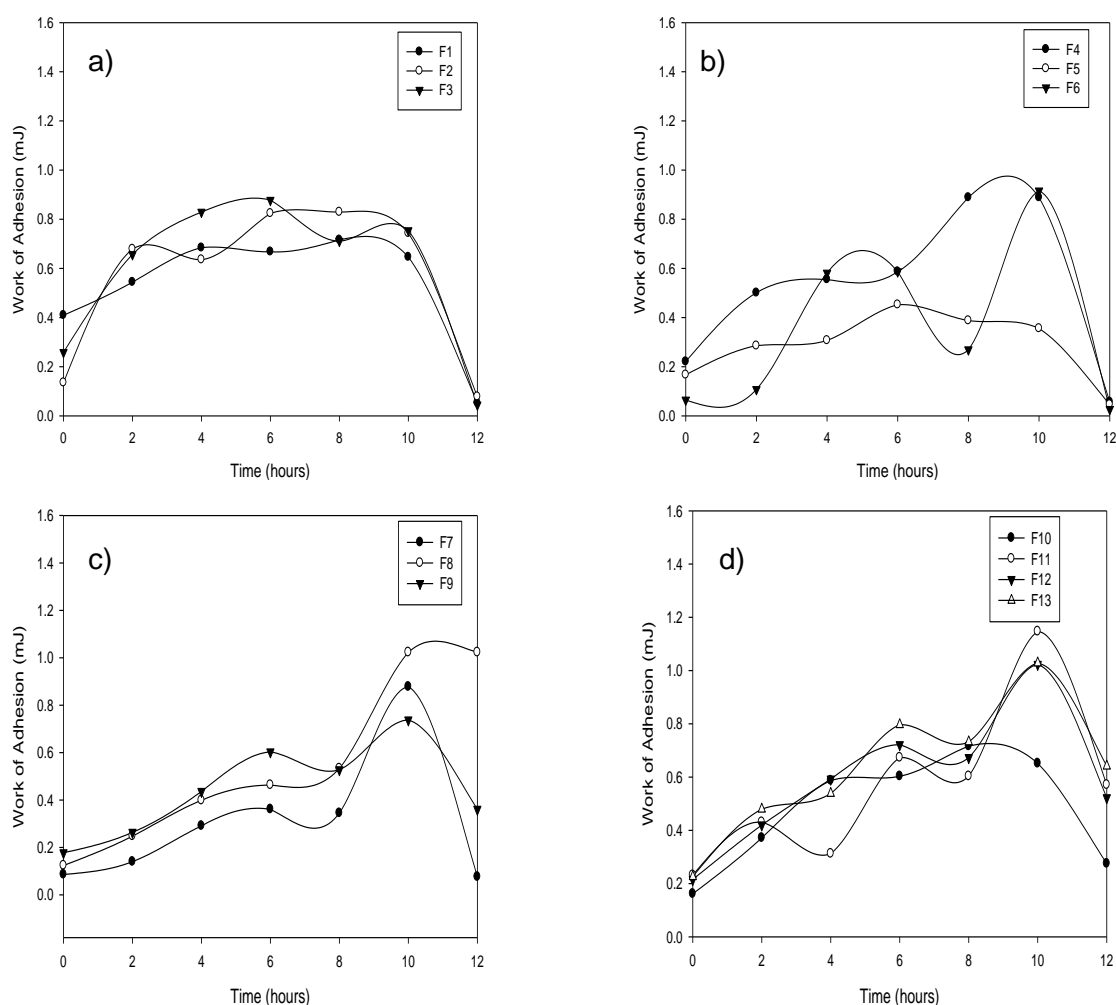


**Figure 4.7:** Variations in  $AUC_{FD}$  of the Experimental Formulations a) 1-3; b) 4-6; c) 7-9; and d) 10-13 as a function of time ( $n=3$ ;  $SD < 0.067$  in all cases).



**Table 4.7:** Measured responses of the experimental runs for the optimization of the gastric-targeted mucoadhesive layer of the MMDDS.

| <b>Experimental Formulation</b> | <b>PEC:PVP (%<sup>w</sup>/v)</b> | <b>PVA (%<sup>w</sup>/v)</b> | <b>Measured Response (AUC)</b> |
|---------------------------------|----------------------------------|------------------------------|--------------------------------|
| 1                               | 2.7 : 8.1                        | 2.000                        | 6.9781                         |
| 2                               | 2.7 : 8.1                        | 3.375                        | 7.6332                         |
| 3                               | 1.3 : 3.9                        | 3.375                        | 7.9610                         |
| 4                               | 2.0 : 6.0                        | 3.375                        | 7.1162                         |
| 5                               | 2.0 : 6.0                        | 4.750                        | 3.7886                         |
| 6                               | 1.3 : 3.9                        | 4.750                        | 5.0135                         |
| 7                               | 2.7 : 8.1                        | 4.750                        | 4.1901                         |
| 8                               | 2.0 : 6.0                        | 3.375                        | 6.4782                         |
| 9                               | 2.0 : 6.0                        | 2.000                        | 5.6758                         |
| 10                              | 1.3 : 3.9                        | 2.000                        | 6.2951                         |
| 11                              | 2.0 : 6.0                        | 3.375                        | 7.1351                         |
| 12                              | 2.0 : 6.0                        | 3.375                        | 7.5982                         |
| 13                              | 2.0 : 6.0                        | 3.375                        | 8.0183                         |

#### 4.5.1.2 Correlation of the experimental and fitted response values

A comparative analysis of the experimental vs. the fitted response values, i.e. the mucoadhesive characteristics, was plotted to establish the applicability of the regression models and the robustness of the Central Composite Design employed for the optimization of the intestinal-targeted mucoadhesive layer. The plot depicting the AUC (of the Work of Adhesion vs. Time profiles) of the experimental vs. the fitted values of each formulation show a general conformity with a correlation coefficient ( $R^2$ ) of 0.968 (Figure 4.8). The  $R^2$  values provide evidence of the success and robustness of the Central Composite Experimental Design and thus the efficiency of the design in aiding the determination of an optimized intestinal-targeted mucoadhesive layer.

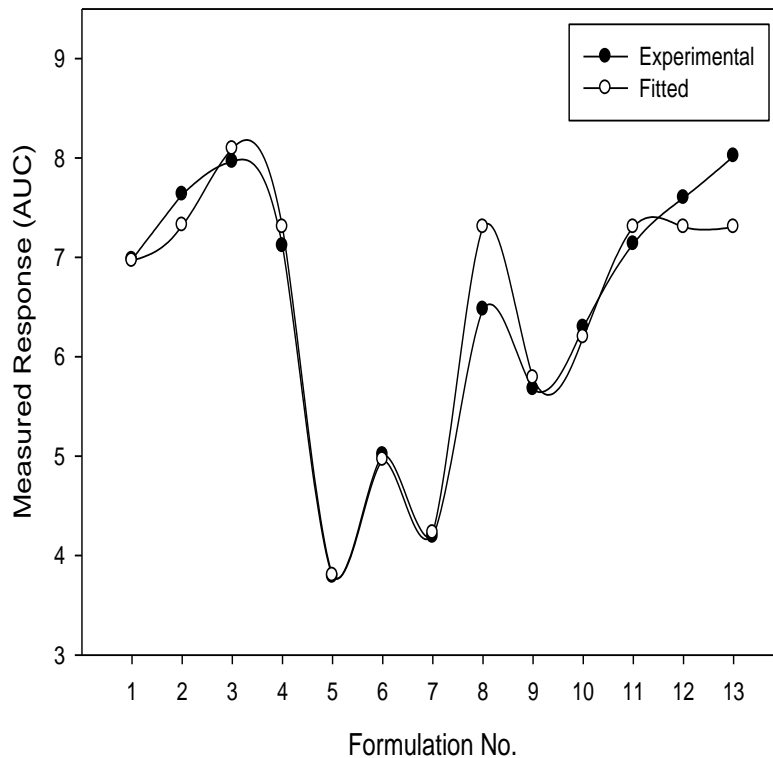


**Figure 4.8:** Regression plots of Area Under the Curve of the Work of Adhesion (mJ) vs. Time (hours) profile for the determination of the correlation between the experimental vs. the fitted response values.

#### 4.5.1.3 Analysis of the central composite surface design

The AUC (of the Work of Adhesion (mJ) vs. Time profile) was the response measured for the intestinal-targeted mucoadhesive system. Surface plot analysis validated the relationship between the independent variables PVA and PEC:PVP concentrations on the response of AUC in Figure 4.9a. A positive or maximal response of the AUC (>7.5) was established from the response curve at concentrations of  $\pm 3.375\% w/v$  of PVA at differing PEC:PVP concentrations. Any further increase beyond this point influenced a negative effect on the response. For the purposes of optimizing the response of AUC, manipulation of the PVA concentrations had a more pronounced effect on the AUC, which is clearly illustrated in Figure 4.9. These responses are also evident in the contour plot (Figure 4.9b), where a positive effect on the AUC was observed at concentrations of PVA  $= 3.375\% w/v$ .

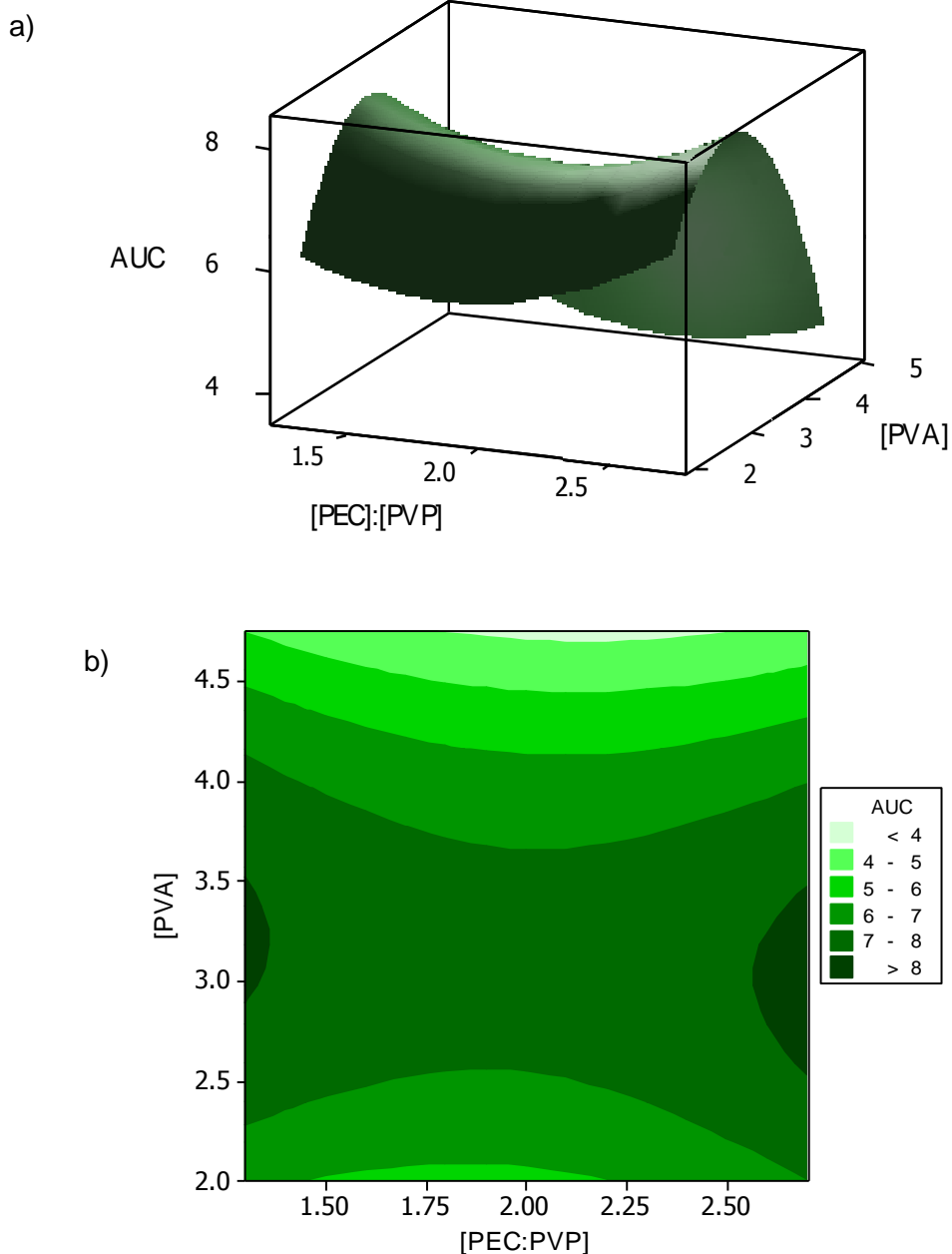


**Figure 4.9:** Illustration of the relationship between independent variables and the response of mucoadhesive properties through a) 3-D surface plots and b) contour plots for the intestinal-targeted mucoadhesive layer.

#### 4.5.1.4 Residual Analysis of the Central Composite Experimental Design for the optimization of the intestinal-targeted mucoadhesive layer

The normal probability plots of the residuals fell on a straight line (Figure 4.10), with 2 outliers, indicating that the data was normally distributed with no evidence of unidentified variables. The residuals vs. fitted values plots demonstrated a random arrangement of data points, with the presence of a small cluster, signifying an acceptable and normal fit with a linear regression model. The data points were plotted close to the zero axis, demonstrating no discernible pattern, validating the assumption of constant variance.

These assumptions were further validated by the histogram of residuals, where a constant variance with normal distribution of the residuals was observed. Furthermore, the residuals vs. the order of data plot demonstrated a random distribution between the consecutive points, rapidly alternating between positive and negative values, was observed.

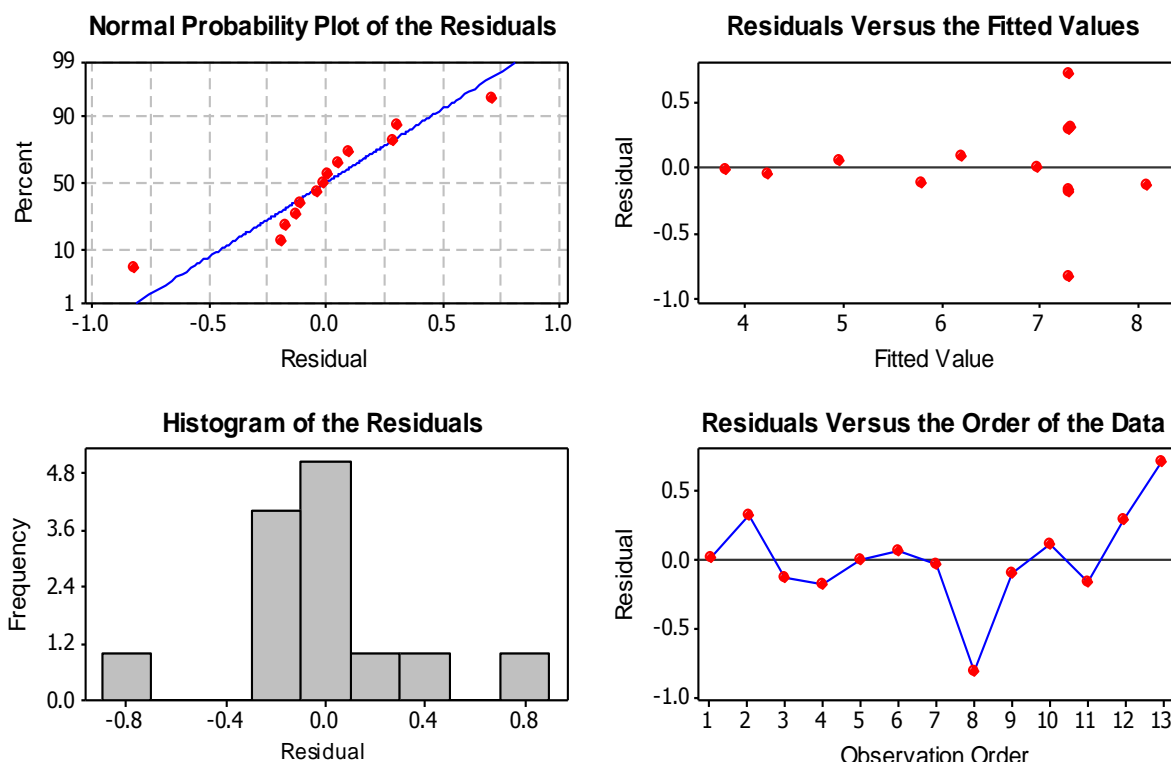


**Figure 4.10:** Residual plots of AUC of the Work of Adhesion (mJ) vs. Time (hours) profile for the intestinal-targeted mucoadhesive layer of the MMDDS.

Based on a full ANOVA analysis of the measured formulation responses it was determined that the PVA and PVA\*PVA factors had statistically significant effects ( $p < 0.05$ ) (Table 4.8) on the measured response (AUC). The complete regression equations generated for AUC of the WA vs. Time profile is depicted in Equation 4.2.

**Table 4.8:** Estimated p-values for the response: AUC of the WA: Time profile.

| Term                | Coef     | SE Coef | T       | p-value |
|---------------------|----------|---------|---------|---------|
| [PEC:PVP]           | +0.00850 | 0.2153  | +0.039  | 0.970   |
| [PVA]               | -0.99280 | 0.1879  | -5.284  | 0.001   |
| [PEC:PVP]*[PEC:PVP] | +0.79423 | 0.3230  | +2.459  | 0.044   |
| [PVA]*[PVA]         | -2.51125 | 0.3113  | -8.066  | 0.000   |
| [PEC:PVP]*[PVA]     | -037660  | 0.2301  | -1.637  | 0.146   |
| Constant            | +7.30529 | 0.1803  | +40.517 | 0.000   |

$$\text{AUC} = -1.56942 - 5.15084[\text{PEC} : \text{PVP}] + 9.02628[\text{PVA}] + 1.62088[\text{PEC} : \text{PVP}]^2 - 1.32826[\text{PVA}]^2 - 0.391273[\text{PVP} * \text{PVA}]$$

Equation 4.2

#### 4.5.1.5 Constrained optimization of the intestinal-targeted mucoadhesive layer of the MMDDS

Optimization of the intestinal-targeted mucoadhesive layer was performed employing Minitab<sup>®</sup> V15 statistical software (Minitab<sup>®</sup> Inc., PA, USA) to determine the optimum level for each variable. The optimization approach resulted in the attainment of a formulation with a desirability of 1.000 and the fabrication of this formulation included the employment of a 2%<sub>w/v</sub> of PEC and a PVA concentration of 3.3750%<sub>w/v</sub> as depicted in Figure 4.11. Since the ratio of PEC:PVP was kept constant at 1:3, the final PVP concentration employed was 6%<sub>w/v</sub> in the optimized formulation. The resultant fitted and experimental values for the response parameters are provided in Table 4.9.

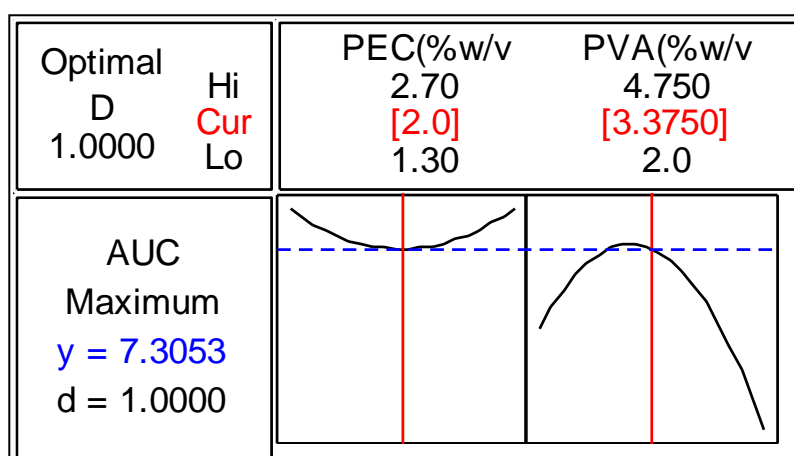


**Figure 4.11:** Optimization plots displaying factor levels and desirability values for the optimized gastric-targeted mucoadhesive layer of the MMDDS.

**Table 4.9:** Comparison of the fitted and experimental values of the response parameter.

| <b>Response parameter</b> | <b>Fitted</b> | <b><sup>1</sup>Desirability (%)</b> | <b>Experimental</b> | <b><sup>2</sup>Deviation (%)</b> |
|---------------------------|---------------|-------------------------------------|---------------------|----------------------------------|
| <b>AUC</b>                | 7.3053        | 1.000                               | 7.6332              | 4.488                            |

<sup>1</sup> Statistical desirability values of the fitted optimized formulation (%)

<sup>2</sup> Deviation of the experimental response values from the fitted

The fitted optimized formulation had a statistical desirability of 100% for the response parameter. An experimental AUC of 7.6332 was achieved with the optimized formulation, with a deviation of 4.488% from the fitted response value of 7.3053, thereby demonstrating that the experimental response parameters achieved with the constrained settings for the optimized formulation were in close agreement with the fitted response values. This identified the reliability of the optimization process in predicting the maximal AUC and identifying an optimized formulation. Figure 4.12 represents the variations in the WA as a function of time. Mucoadhesive characteristics were successfully maintained throughout the duration of the study. The shape of the curve was observed to possess a similar trend that was typical of the experimental design formulations analyzed (Figure 4.1a-d), thus demonstrating that similar processes occur which promote or mitigate mucoadhesion as for the experimental design formulations, which is further elaborated in Part III of the present chapter.

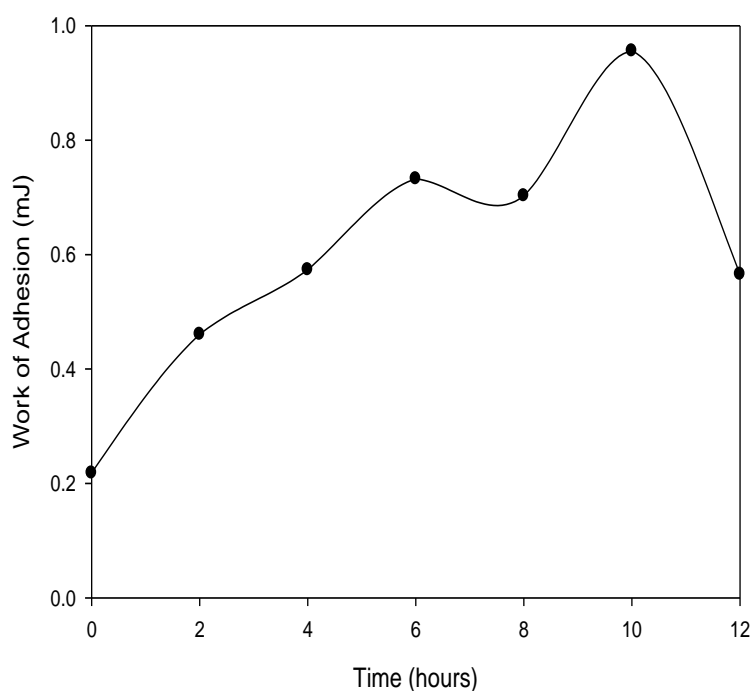


**Figure 4.12:** Variations in  $AUC_{FD}$  of the optimized intestinal-targeted mucoadhesive layer as a function of time ( $n=3$ ;  $SD < 0.094$  in all cases).

### **Part III: Physicochemical and physicomechanical characterization of the optimized gastric- and intestinal-targeted mucoadhesive layers**

#### **4.6 Materials and Methods**

##### **4.6.1 Materials**

The materials employed were as described in *Section 4.2.1* and *Section 4.4.1* for the optimized gastric- and intestinal-targeted mucoadhesive layers.

##### **4.6.2 Fabrication of the optimized mucoadhesive layers**

Membranes were fabricated as described in *Section 4.2.3* and *Section 4.4.3* for the optimized gastric- and intestinal-targeted mucoadhesive layers respectively. The polymers were combined in the ratios defined via optimization studies and included: 1.001%<sup>w/v</sup> of CHT, 4.750%<sup>w/v</sup> PVA and 4.004%<sup>w/v</sup> of PVP for the gastric-targeted mucoadhesive layer and 2%<sup>w/v</sup> of PEC, 3.375%<sup>w/v</sup> of PVA and 6%<sup>w/v</sup> of PVP for the intestinal-targeted mucoadhesive layer. Membranes were cut into dimensions of 20x30mm and thereafter stored with desiccants in airtight containers until further testing was completed.

##### **4.6.3 Physical characterization of the optimized mucoadhesive layers: Evaluation of membrane uniformity**

The uniformity of the mucoadhesive layer was determined by accurately weighing a number of samples (n=10) on a calibrated Mettler Toledo Balance (Model AB104-S, Mettler Toledo, Switzerland). The average mass was then calculated followed by determination of the standard deviation. The thickness of the membranes was determined using an electronic digital calliper (n=10). Different points within a single membrane was also measured for thickness to determine the consistency of individual membranes (n=10). Similarly, the average thickness was then determined and the standard deviation calculated. All samples were previously cut into 20x30mm dimensions. Membranes were also visually assessed for colour, formation of air bubbles, and clarity.

##### **4.6.4 Determination of the tensile properties and Young's Modulus of the optimized gastric-targeted mucoadhesive layer**

Young's Modulus and other tensile properties of the optimized mucoadhesive layers were determined using the nanoTensile<sup>®</sup> 5000 (Hysitron Inc. Nanomechanical Test Instrument, Minneapolis, MN). The nanotensile (NT) apparatus was calibrated before samples were tested to ensure accuracy. Samples, cut into approximately 2x15mm strips, were

mounted on the specially designed NT mounting brackets, as illustrated in Figure 4.13. The brackets were held together with a rigid cardboard frame, aiding in sample alignment, and the samples were attached to the brackets using a rigid cyanoacrylate-based adhesive, thus holding the sample firmly in place during the test procedure. Samples were allowed to cure and accurate measurements of the sample width, thickness and length were recorded using digital callipers.

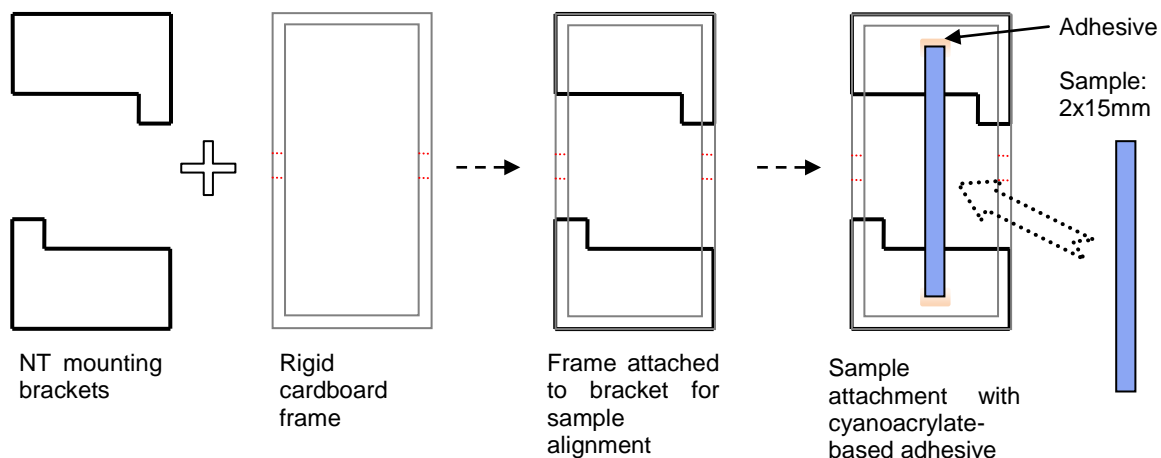


**Figure 4.13:** Sample preparation procedure for analysis on a Hysitron nanoTensile® analyzer.

The upper sample bracket was secured to the upper sample gripper of the NT head, the cardboard frame was snipped at the points demarcated in red in Figure 4.13 (to prevent any interference from the frame during analysis), and the mass measured. The NT head was lowered and the lower sample bracket secured to the lower sample gripper on the NT stage. The mounting brackets were moved apart at a constant rate of displacement of 100 $\mu$ m/sec and the tensile properties of the sample were measured and recorded.

#### 4.6.5 Simultaneous qualitative and quantitative analysis of the mucoadhesive layer surface morphology and porosity

The surface area and porosity of the optimized mucoadhesive layers were analyzed on a Micromeritics Porosimeter (Micromeritics ASAP 2020, GA, USA) by employing the Brunauer-Emmett-Teller (BET) isotherm of adsorption/ desorption of nitrogen. Samples were initially degassed, which includes an evacuation and heating phase (Table 4.10). Approximately 0.285g and 0.275g of the gastric- and intestinal-targeted mucoadhesive layers was inserted into sample tubes, degassed and thereafter subject to the adsorptive properties listed in for analysis. Amongst the porositometric profiles the following were analyzed: i) the single point surface area (at point P.Po); and ii) the Barrett-Joiner-Halenda (BJH) computation that allowed for the determination of the mesopore



volume/area and size distribution which accounts for both the change in adsorbate layer thickness and the liquid condensed in the membrane pore cores. All analyses were conducted in triplicate (n=3).

**Table 4.10:** Parameters and settings employed during degassing and analysis of the optimized mucoadhesive layers.

| <b>Parameters</b>  | <b>Settings</b>                |
|--|--------------------------------|
| <b><i>Degassing Conditions during the Evacuation Phase</i></b>       |                                |
| Temperature ramp rate  | 10°C/min                       |
| Target temperature   | 30°C                           |
| Evacuation rate  | 50.0mmHg/s                     |
| Unrestricted evacuation from   | 30.0mmHg                       |
| Vacuum set-point   | 500µmHg                        |
| Evacuation time  | 60 min                         |
| <b><i>Degassing Conditions during the Heating Phase</i></b>          |                                |
| Ramp rate  | 10°C/min                       |
| Hold temperature   | 30°C                           |
| Hold time  | 900min                         |
| <b><i>Hold pressure during the evacuation and heating phases</i></b> | 100mmHg                        |
| <b><i>Analysis Conditions (Adsorptive Properties)</i></b>            |                                |
| Adsorptive   | Nitrogen gas (N <sub>2</sub> ) |
| Maximum manifold pressure  | 925kPa                         |
| Non-ideality factor  | 0.0000620                      |
| Density conversion factor  | 0.0015468                      |
| Hard sphere diameter   | 3.860Å                         |
| Molecular cross-sectional area                                       | 0.162nm <sup>2</sup>           |

Surface morphology of the mucoadhesive layers were analyzed on a Phenom™ Scanning Electron Microscope (SEM) (FEI Company, Hillsboro, Oregon, USA). Different magnifications at 10kV were employed to view the overall and in-depth surface structure to qualitatively elucidate the surface morphology of the mucoadhesive layer in relation to its surface area and porosity. The photomicrographs were then placed as insets on the porositometric profiles for the simultaneous qualitative and quantitative analysis of the mucoadhesive layer surface morphology and porosity.

#### **4.6.6 Evaluation of the polymeric structural and vibrational frequency variations of the mucoadhesive layer relative to its exposure to simulated GIT conditions**

The vibrational molecular transitions of the mucoadhesive layer relative to exposure in simulated gastro-intestinal conditions was characterized for the attainment of important

micro-structural data via an Attenuated Total Reflectance Fourier-Transform Infrared (ATR-FTIR) spectroscopy, recorded on a PerkinElmer® Spectrum 100 Series fitted with a universal ATR polarization accessory (PerkinElmer Ltd., Beaconsfield, UK). Samples required no further modification for analysis, and were placed in direct contact with the ATR crystal. Spectra were recorded over the range of 4000-650cm<sup>-1</sup>, with a resolution of 4cm<sup>-1</sup> and 32 iterations.

#### **4.6.7 Evaluation of the degree of swelling and polymeric erosion on the mucoadhesive characteristics of the optimized formulation relative to GIT exposure**

The variations in the swelling and erosion of the optimized formulations were evaluated by exposing the respective mucoadhesive layer to simulated gastro-intestinal conditions as described in *Sections 4.2.5 and 4.4.5* for the gastric- and intestinal-targeted mucoadhesive layers respectively. The mucoadhesive characteristics, as well as the degree of swelling and erosion were determined at 0, 2, 4, 6, 8, 10 and 12 hours. Fresh samples were assessed for mucoadhesion, swelling and erosion at each time point.

Swelling of a DDS is known to affect the mucoadhesive properties of the system. If the polymer is hydrated and expands, additional adhesive sites are exposed to improve mucoadhesion. Furthermore, swelling promotes chain entanglement between the mucoadhesive layer of the system and mucin in the GIT (Dodou *et al.*, 2005; Smart, 2005; Roy *et al.*, 2009; Khutoryanskiy, 2010; Harsulkar *et al.*, 2011; Tangri and Madav, 2011). The degree of swelling was expressed as water absorption capacity or PBS uptake.

Gravimetric analysis was conducted whereby the mucoadhesive layer was subject to the conditions identical to those employed in *Section 3.2.8*. Each mucoadhesive layer was removed from the dissolution apparatus at predetermined time intervals (0, 2, 4, 6, 8, 10, and 12 hours). Excess phosphate buffer was removed by allowing samples to drip dry for a period of 1 minute prior to gravimetric analysis. Fresh samples were used for each individual time point. The degree of swelling at each time point, expressed as a percentage of PBS uptake, was then determined based on the increase in weight of the formulation, and was calculated according to Equation 4.3.

$$PBS_{uptake} = \frac{(W_t - W_0)}{W_0} \times 100 \quad \text{Equation 4.3}$$

where  $PBS_{uptake}$  is the percentage of PBS uptake by the mucoadhesive layer at the relevant time point,  $W_t$  is the weight of the mucoadhesive layer at the relevant time point, and  $W_0$  is the initial weight of the mucoadhesive layer.

Subsequent to establishing the degree of fluid uptake by the mucoadhesive layer, the hydrated samples were dried at ambient room conditions for 24 hours after which they were re-weighed. The polymers employed in the mucoadhesive layer typically absorb a significant quantity of fluid thereby masking the degree of polymeric erosion. Therefore re-weighing the dried samples enabled the determination of the degree of polymeric erosion from the mucoadhesive layer. The degree of erosion, expressed as a percentage, at each time point was calculated according to Equation 4.4.

$$Erosion (\%) = \frac{(W_0 - W_t)}{W_0} \times 100$$

Equation 4.4

where  $W_t$  is the weight of the dehydrated mucoadhesive layer at the relevant time point, and  $W_0$  is the initial weight of the mucoadhesive layer.

#### **4.6.8 Evaluation of the surface morphology variations of the optimized mucoadhesive layers relative to exposure to simulated gastro-intestinal conditions**

Surface morphology of the mucoadhesive layer was analyzed on a Phenom™ Scanning Electron Microscope (SEM) (FEI Company, Hillsboro, Oregon, USA). Different magnifications at 10kV were employed to view the overall and in-depth surface structure to qualitatively elucidate the variations in the surface morphology of the mucoadhesive layer as a function of time. The optimized gastric-targeted and intestinal-targeted mucoadhesive layers were exposed to conditions detailed in *Section 3.2.8, Chapter 3* to simulate the gastric and intestinal conditions of the GIT respectively. The mucoadhesive layer was removed at two-hour intervals, allowed to dry at ambient conditions and thereafter subject to SEM analysis as follows. Samples were firmly mounted on aluminium stubbs with carbon tape. They were subject to a gold sputter coating under a vacuum of 0.1Torr with argon gas in a SPI-Module™ Sputter Coater and SPI-Module™ Control (SPI Supplies, Division of Structure Probe Inc., West Chester, PA, USA). Each sample required 90 seconds of coating to ensure complete coverage of the sample. Subsequent viewing was thereafter performed at various magnifications under the Phenom™ SEM.

#### **4.6.9 Magnetic Resonance Imaging (MRI) of the swelling behaviour of the optimized formulations**

A digital MARAN-ip magnetic resonance system configured with a DRX2 HF Spectrometer console (Oxford Instruments Magnetic Resonance, Oxon, UK) was employed to confirm the swelling behaviour occurring with exposure to simulated GIT conditions. The Maran-ip was equipped with a compact 0.5 Tesla permanent magnet

stabilized at 37°C and a dissolution flow through cell. The image acquisition parameters are depicted in Table 4.11.

**Table 4.11:** Image acquisition parameters applied during magnetic resonance imaging using MARAN-ip.

| <b>S. No.</b> | <b>Parameter</b>     | <b>Value</b> |
|---------------|----------------------|--------------|
| 1             | Imaging protocol     | FSHEF        |
| 2             | Requested gain (%)   | 3.31         |
| 3             | Signal strength (%)  | 68.20        |
| 4             | Average              | 2            |
| 5             | Matrix size          | 128          |
| 6             | Repetition time (ms) | 1000.00      |
| 7             | Spin Echo Tau (ms)   | 6.00         |
| 8             | Image acquired after | 15min        |
| 9             | Total scans          | 64           |

A laminar flow of 16mL/min was achieved with the presence of glass beads present in the cell. The solvent utilized was PBS (pH 1.2±0.5; 37°C for the gastric-targeted component and pH 6.8±0.5; 37°C for the intestinal-targeted component). The mucoadhesive layer (20x30mm dimensions) was rolled and placed in position within the cell which in turn was positioned in a magnetic core of the system. Magnetic resonance images were acquired every 15 minutes over 24 hours with MARAN-ip version V1.0 software. The image was acquired after setting the frequency offset and testing gain employing RINMR v5.7 under continuous solvent flow conditions. MARAN-ip software comprises image acquisition software and image analysis software.

## 4.7 Results and Discussion

### 4.7.1 Physical characterization of the optimized mucoadhesive layers: Characterization of membrane uniformity

Uniformity assessment of the mucoadhesive layer provided an indication of the inter- and intra-formulation variability. Consistency and uniformity of the mucoadhesive layer were important attributes to evaluate as these parameters ultimately influence the mucoadhesive characteristics. The average weight and thickness, along with their standard deviations are depicted in Figure 4.14. With the standard deviation being <10% for all parameters investigated, it was determined that the mucoadhesive layers were relatively consistent and uniform in nature with limited inter- and intra-formulation

variability. The optimized gastric-targeted membranes were clear with a yellow tint, while the optimized intestinal-targeted membranes were clear, both displaying limited air bubble formation.

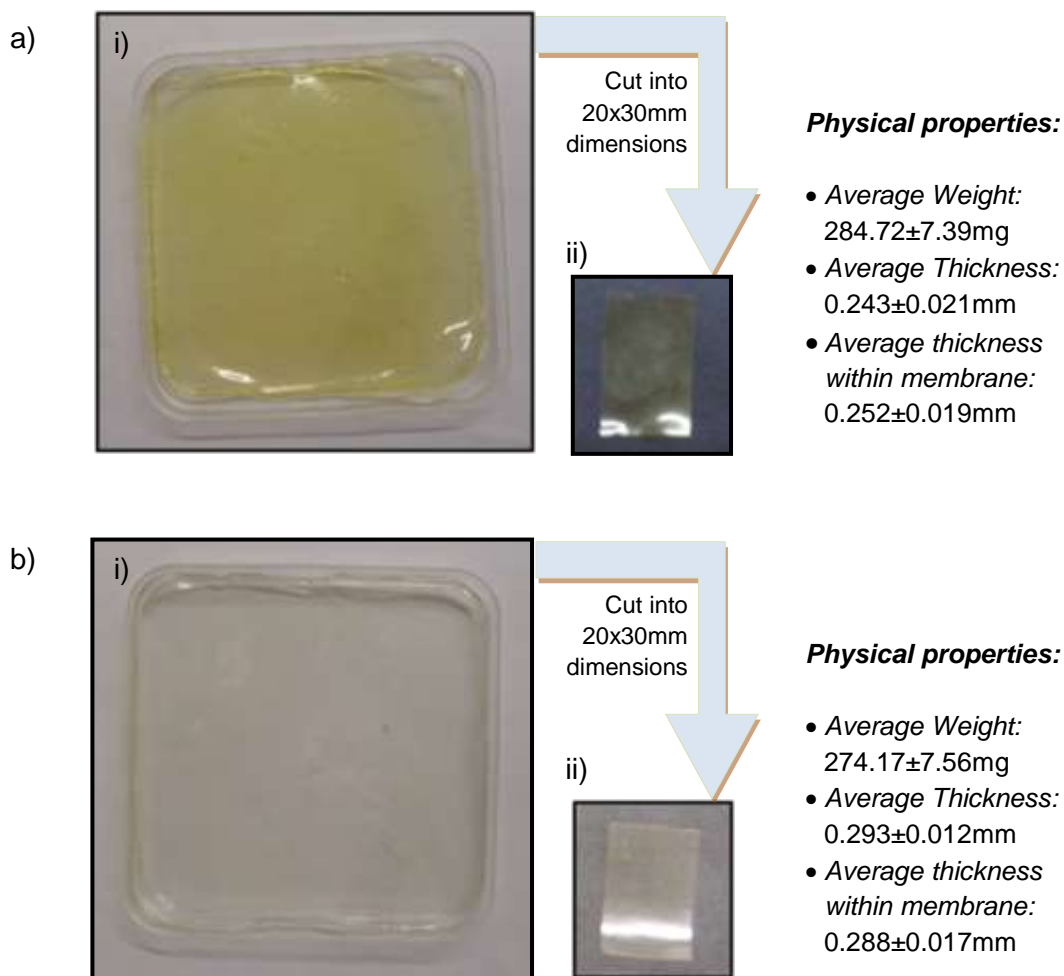


**Figure 4.14:** Digital images of a) the optimized gastric-targeted formulation and b) the optimized intestinal-targeted formulation i) upon removal from the mould, and ii) when cut into predetermined dimensions.

#### 4.7.2 Determination of the tensile properties and Young's Modulus of the optimized mucoadhesive layers

The stress-strain relationship of a material is highly dependent on the flexibility of the polymer chains and the strength of the material. When only a small amount of stress is required to produce a large amount of strain, the material is considered to be flexible and the Young's Modulus, which is the slope of the linear portion of the stress-strain curve, highlighted in green in Figure 4.15, will be relatively small (Leung and Ko, 2011). Tensile properties were determined as the MMDDS would be ultimately rolled and inserted into a capsule to ease oral administration. The average experimental values for Young's

Modulus (E), yield stress ( $\sigma_y$ ) (magnitude of stress on the stress-strain curve at which appreciable deformation takes place without any appreciable increase in the stress), ultimate strength ( $\sigma_u$ ) (the maximum stress a material can withstand), ultimate strain ( $\epsilon_u$ ) and toughness ( $u_f$ ) are outlined in Table 4.12.

**Table 4.12:** Experimental values obtained from nanotensile analysis of the optimized gastric-targeted mucoadhesive layer.

| <b>Formulation</b>                               | <b>E (MPa)</b> | <b><math>\sigma_y</math> (MPa)</b> | <b><math>\sigma_u</math> (MPa)</b> | <b><math>\epsilon_u</math></b> | <b><math>u_f</math> (J/cm<sup>3</sup>)</b> |
|--|----------------|------------------------------------|------------------------------------|--------------------------------|--|
| <b>Optimized gastric-targeted formulation</b>    | 11.5167±       | 1.2133±                            | 6.7833±                            | 0.9063±                        | 3.55±                                      |
|  | 0.249043       | 0.06549                            | 1.6481                             | 0.1281                         | 1.1870                                     |
| <b>Optimized intestinal-targeted formulation</b> | 49.7933±       | 1.1967±                            | 7.7233±                            | 0.365±                         | 1.6533±                                    |
|  | 3.502688       | 0.162138                           | 0.6623                             | 0.0054                         | 0.1580                                     |

The Young's Modulus values were relatively low indicating that the membranes demonstrated good elasticity. The gastric-targeted membranes, containing CHT, demonstrated higher elasticity values (a lower Young's Modulus) than the intestinal-targeted membranes containing PEC. Membranes displayed adequate strength and toughness to be able to withstand rolling and insertion into capsules for administration as depicted in Figure 4.15.

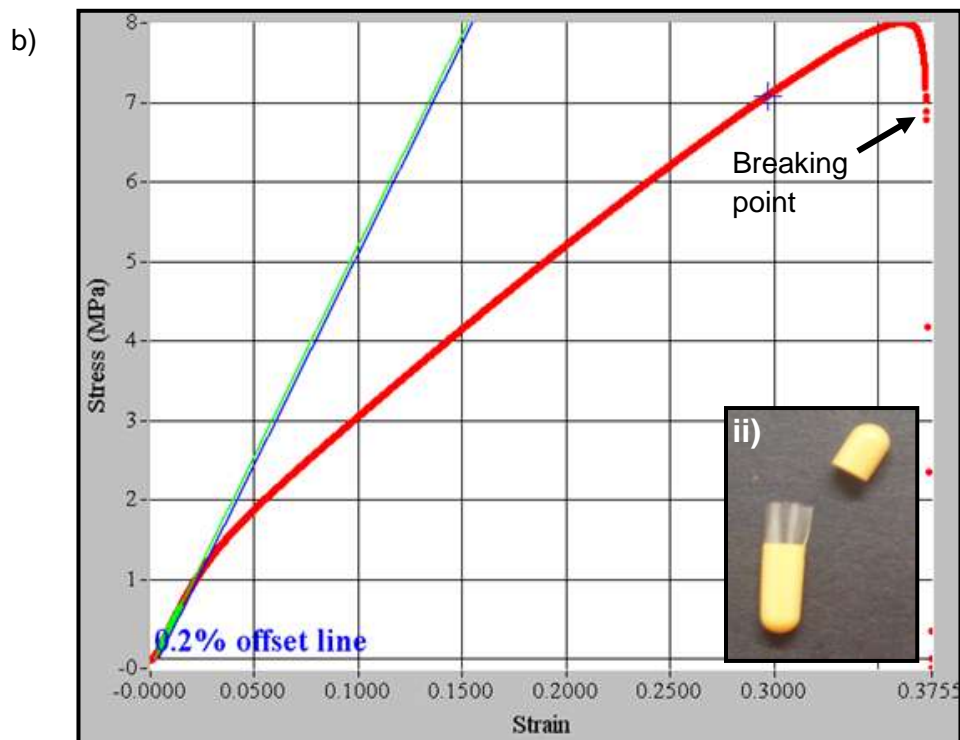
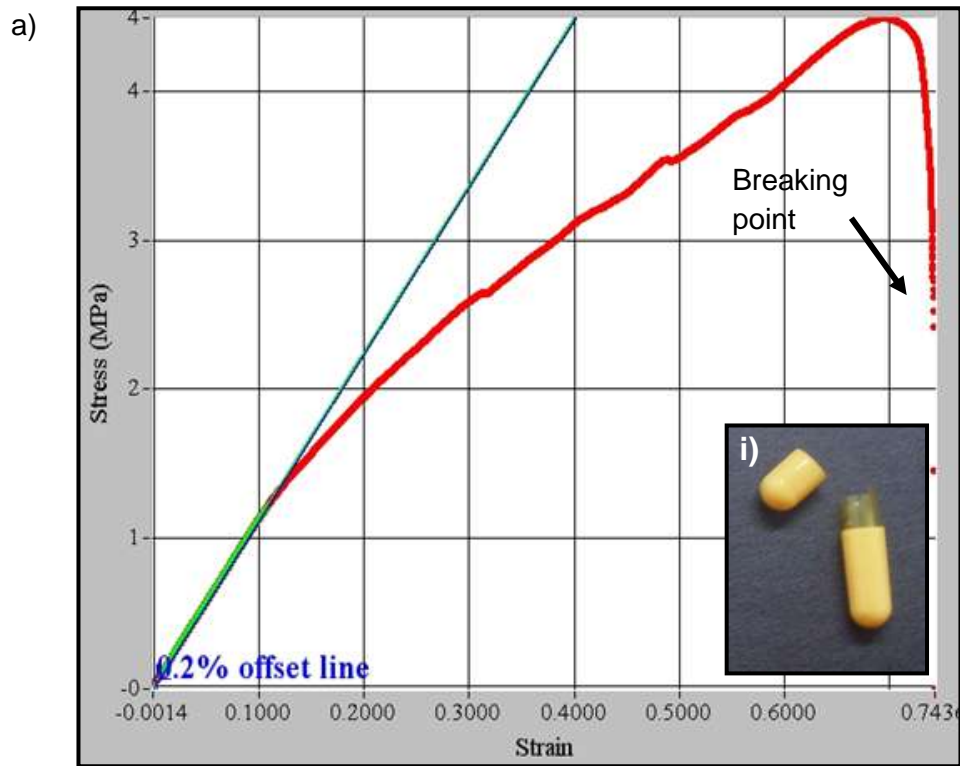


**Figure 4.15:** Typical stress-strain nanotensile profile of a) the optimized gastric-targeted component with inset i) digital image illustrating insertion into a capsule, and b) the optimized intestinal-targeted component, with inset ii) digital image illustrating insertion into a capsule.

### 4.7.3 Simultaneous qualitative and quantitative analysis of the mucoadhesive layer surface morphology and porosity

Studies were conducted to determine the volume of distribution of pores and pore sizes. As discussed previously, micro-cracks or pores promote mucoadhesion by forming an interlocked network which promotes adhesion (Dodou *et al.*, 2005; Smart, 2005; Roy *et al.*, 2009; Khutoryanskiy, 2010; Harsulkar *et al.*, 2011; Tangri and Madav, 2011). In order to insert membranes into the porosimeter analysis tubes, they required cutting of the membrane, and therefore altered the surface area of the membranes. For characterization purposes, it was thus determined that the single point surface area would provide a more reliable indication of the surface area. The single point selected for analysis of surface area was at  $P/P_0 = 0.200450676$  and  $0.204257893$  for the gastric- and intestinal-targeted membranes respectively. The resultant single point surface area, and pore volume, surface area and diameter are depicted in Table 4.13. The larger pore size of the intestinal-targeted membranes may be a potential contributing factor to the mucoadhesive properties of the formulation being higher as compared to the gastric-targeted formulation.

**Table 4.13:** Quantitative properties of the optimized formulations' surface structure.

| <i>Measured characteristic</i>              | <i>Optimized gastric-targeted formulation</i>  | <i>Optimized intestinal-targeted formulation</i>   |
|---|--|--|
| Single Point Surface area                   | 0.8053m <sup>2</sup> /g  | 0.4688m <sup>2</sup> /g  |
| BJH: cumulative surface area of pores       | Adsorption: 1.048m <sup>2</sup> /g<br>Desorption: 1.0339m <sup>2</sup> /g                                      | Adsorption: 1.019m <sup>2</sup> /g<br>Desorption: 1.0508m <sup>2</sup> /g                                      |
| BJH: cumulative volume of pores             | Adsorption: 1.098x10 <sup>-3</sup> cm <sup>3</sup> /g<br>Desorption: 0.996x10 <sup>-3</sup> cm <sup>3</sup> /g | Adsorption: 1.162x10 <sup>-3</sup> cm <sup>3</sup> /g<br>Desorption: 1.162x10 <sup>-3</sup> cm <sup>3</sup> /g |
| BJH Adsorption average pore diameter (4V/A) | Adsorption: 41.892Å<br>Desorption: 38.521Å   | Adsorption: 45.609Å<br>Desorption: 44.221Å   |

The mechanical theory of mucoadhesion (*Section 3.1.1.6*) postulates that surface irregularities and roughness promotes mucoadhesion through an increase in contact area. As illustrated in the SEM images at a magnification of x4000 (Figure 4.16), both the gastric- and intestinal-targeted formulations possess surface morphology ideal for promoting mucoadhesion. It was also noted that there were no large variations in the surface morphology that would cause drastic differences in the overall membrane performance, either within an individual membrane or between differing membranes.



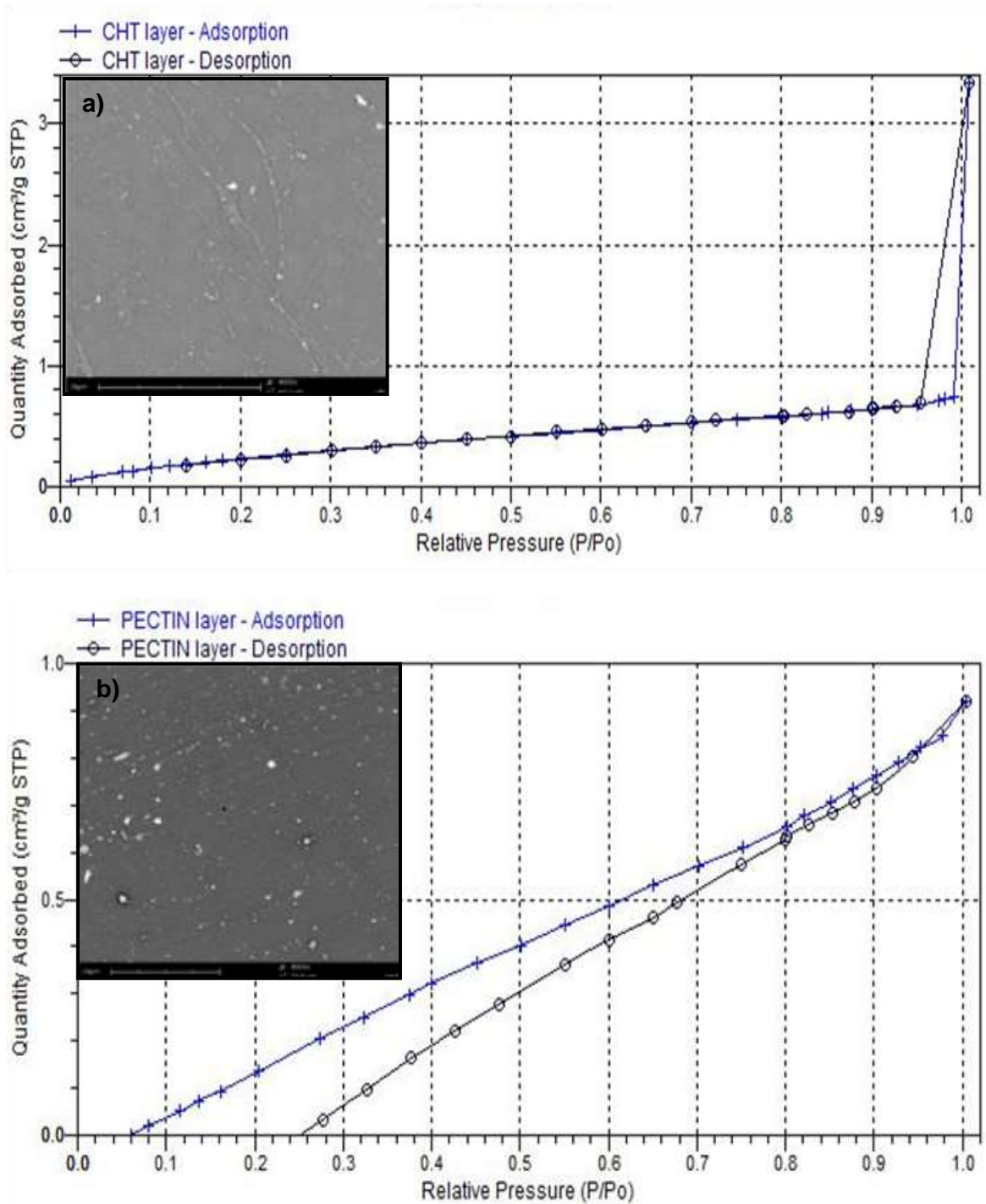
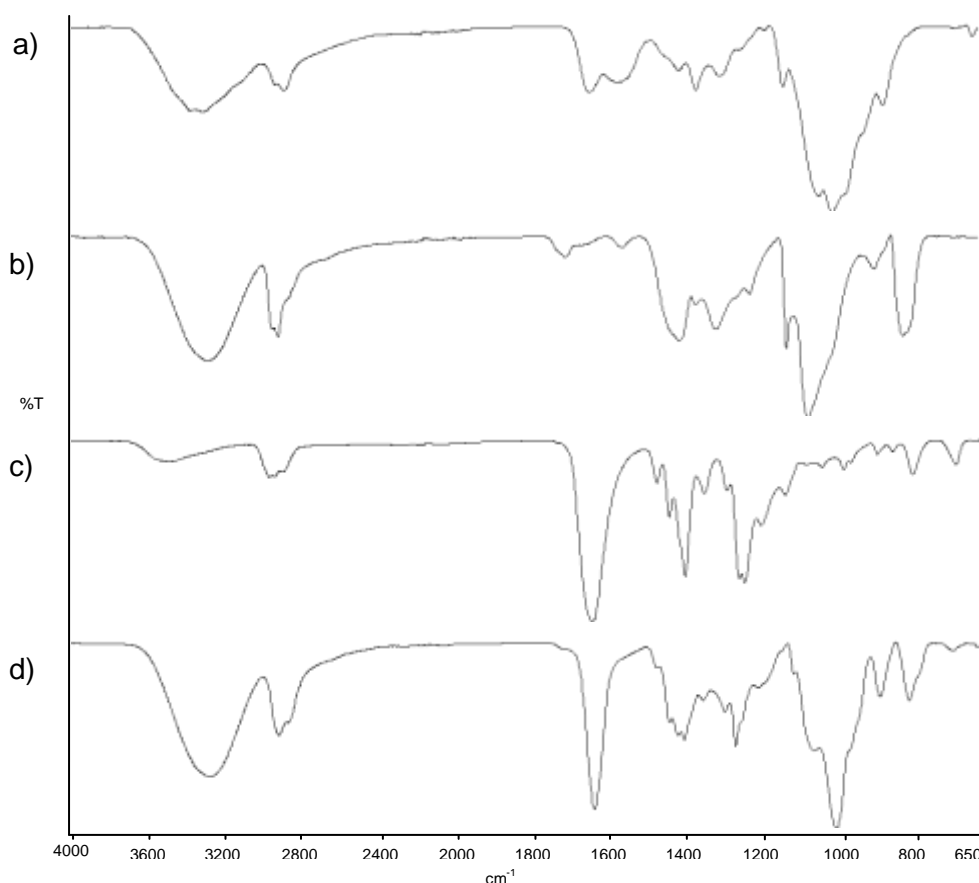


**Figure 4.16:** Isotherm plots and scanning electron micrographs depicting the surface morphology of a) the optimized gastric-targeted formulation and b) the optimized intestinal-targeted formulations.

#### 4.7.4 Evaluation of the polymeric structural and vibrational frequency variations of the mucoadhesive layer relative to its exposure to simulated GIT conditions

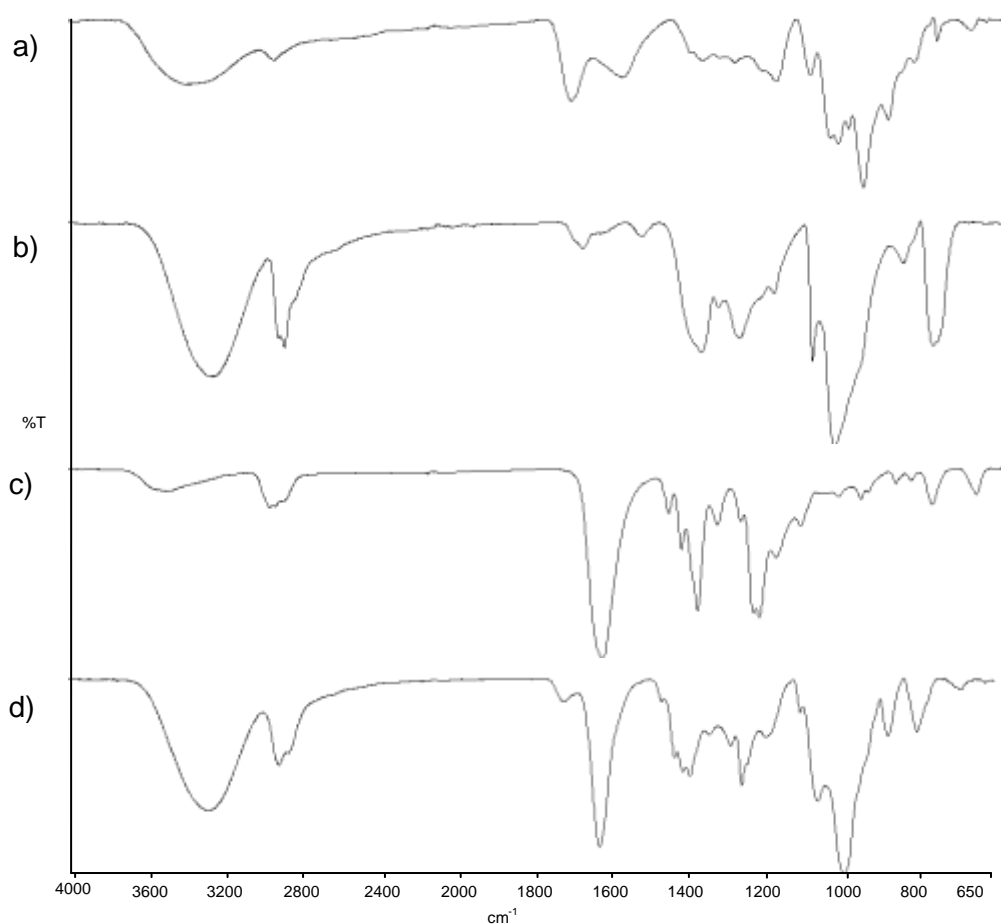
FTIR spectra of the native polymers employed in the respective mucoadhesive layers were analyzed in relation to the spectrum attained of the optimized formulations, to

determine whether any constituents within the formulation interacted as a result of the polymer blending and film-casting procedure. CHT (Figure 4.17a) demonstrates a characteristic peak at  $1650\text{cm}^{-1}$  corresponding to the amide groups; the hydroxyl groups at  $3440\text{cm}^{-1}$  and the C–O stretching at  $1060\text{cm}^{-1}$ . The FTIR spectra of PVA (Figure 4.17b) depicts a characteristic C–H broad alkyl stretching band ( $2850\text{--}3000\text{cm}^{-1}$ ), a strong transmittance band associated with hydroxyl groups stretching at  $3200\text{--}3600\text{cm}^{-1}$  and the transmittance band at  $1060\text{cm}^{-1}$  is indicative of C–OH bonding of PVA. In the FTIR spectra of PVP (Figure 4.17c) a CH stretching at  $2900\text{cm}^{-1}$ , C–O stretching at  $1650\text{cm}^{-1}$ ,  $\text{CH}_3$  scissoring at  $1420\text{--}1500\text{cm}^{-1}$ , C–C ring stretching at  $1300\text{cm}^{-1}$  and tertiary amine C–N stretching at  $1290\text{cm}^{-1}$  are the characteristic absorbance bands of PVP (Koo *et al.*, 2003). Analysis of the optimized gastric-targeted formulation (Figure 4.17d) revealed that all characteristic peaks present in the spectra of the native polymers were unaltered proving no covalent interactions between the polymers, thus causing no detrimental effects on the mucoadhesive properties of the system.



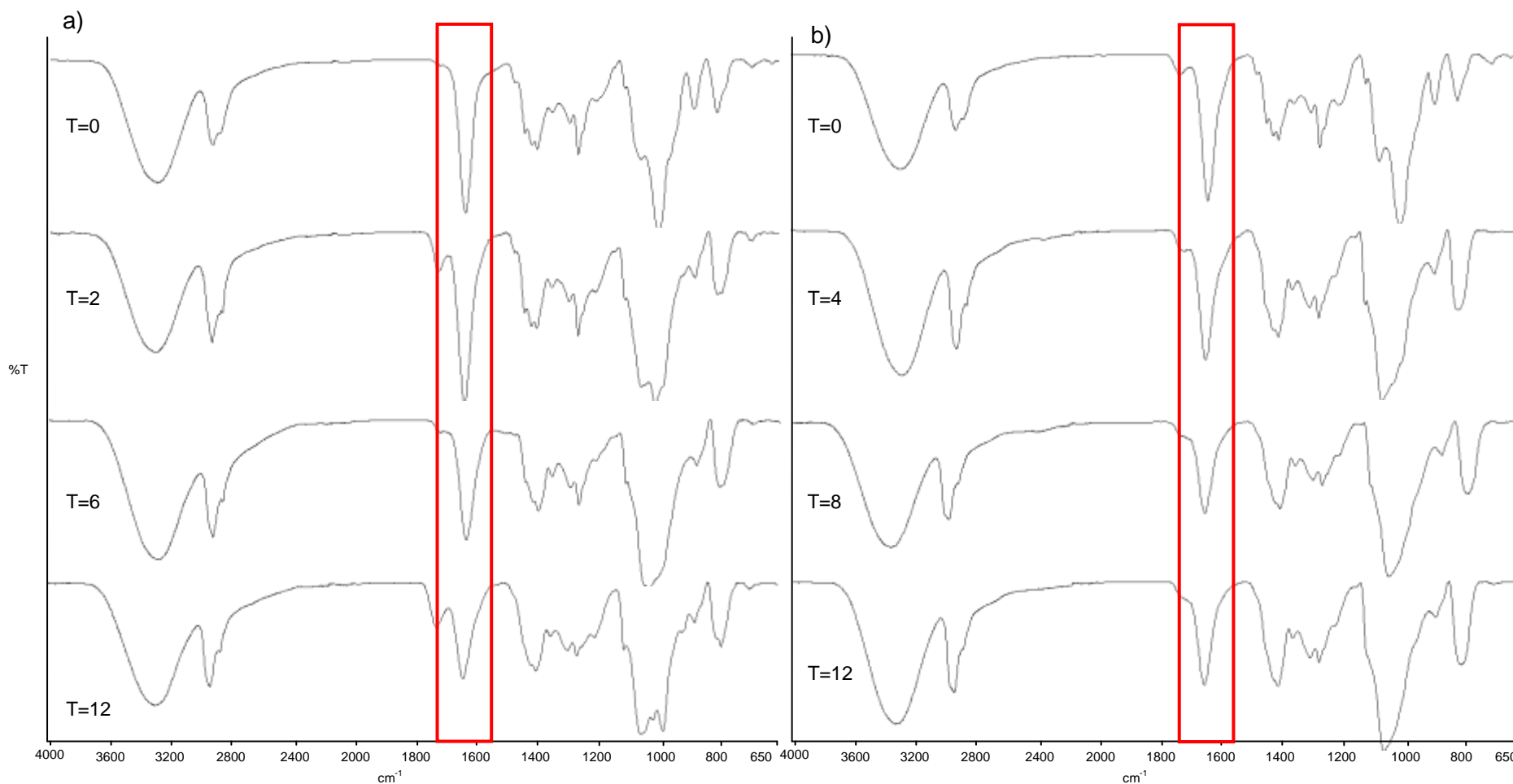
**Figure 4.17:** FTIR spectra of the native polymers a) CHT; b) PVA; and c) PVP employed in the fabrication of d) the optimized gastric-targeted component.

Figure 4.18a illustrates the FTIR spectra of PEC. The characteristic peaks associated with PEC includes the carboxylate groups associated with the  $1607\text{cm}^{-1}$  peak and the ester group with transmittance band at  $1740\text{cm}^{-1}$ . In a similar fashion, analysis of the native polymer spectra (Figure 4.18a-c) with the optimized intestinal-targeted formulation (Figure 4.18d) revealed that there were no alterations to the characteristic peaks of the native polymers, proving that no interactions occurred.



**Figure 4.18:** FTIR spectra of the native polymers a) PEC; b) PVA; and c) PVP employed in the fabrication of d) the optimized intestinal-targeted formulation.

FTIR spectra (Figure 4.19) of both the optimized gastric- and intestinal-targeted formulations illustrated that upon exposure to simulated GIT conditions, the characteristic C-O stretching of PVP (highlighted in red at  $1650\text{cm}^{-1}$ ) decreased in intensity with increase in exposure time. The gradual disappearance of the band highlighted in red, can be attributed to PVP eroding out of the optimized membrane with time, accounting for the eventual decrease in the mucoadhesive characteristics of the formulations (revealed after  $t=8$  hours and  $t=10$  hours for the gastric- and intestinal-targeted component in Figure 4.21a).



**Figure 4.19:** FTIR spectra demonstrating the changes in band intensities of the formulation in relation to exposure to simulated gastrointestinal conditions of a) the optimized gastric-targeted formulation and b) the optimized intestinal-targeted formulation with the characteristic C-O peak of PVP highlighted in red.

#### 4.7.5 The influence of exposure to simulated gastro-intestinal conditions on the degree of swelling and polymeric erosion

Through gravimetric analysis it was revealed that with increased exposure to simulated gastro-intestinal conditions, the optimized formulations tended to swell, resulting in an increase in the weight of the mucoadhesive layer. The expanded or hydrated nature of the polymeric network permits mutual interpenetration between the mucoadhesive membrane and mucin molecules, subsequently establishing stabilizing interactions and thus strengthening the mucoadhesive characteristics of the formulations (Salamat-Miller *et al.*, 2005; Sudhakar *et al.*, 2006; Roy *et al.*, 2009). With exposure of the surface layer of the mucoadhesive membrane to simulated gastro-intestinal conditions, polymeric chains present on the surface, swelled, promoting both mucoadhesion and weight gain (Figure 4.20a). With continuous exposure, the surface layer eventually disintegrates and erodes out of the membrane, causing a decrease in both the mucoadhesion and weight gain (swelling) (Figure 4.20b). The underlying polymeric chains would then become exposed to the surrounding fluid (Figure 4.20c), and swell further, promoting swelling and hence mucoadhesion (Figure 4.20d). As a result, fluctuating degrees of swelling was observed at different time points, causing the resultant variations in the mucoadhesive characteristics of the respective formulations, as illustrated in Figure 4.21.

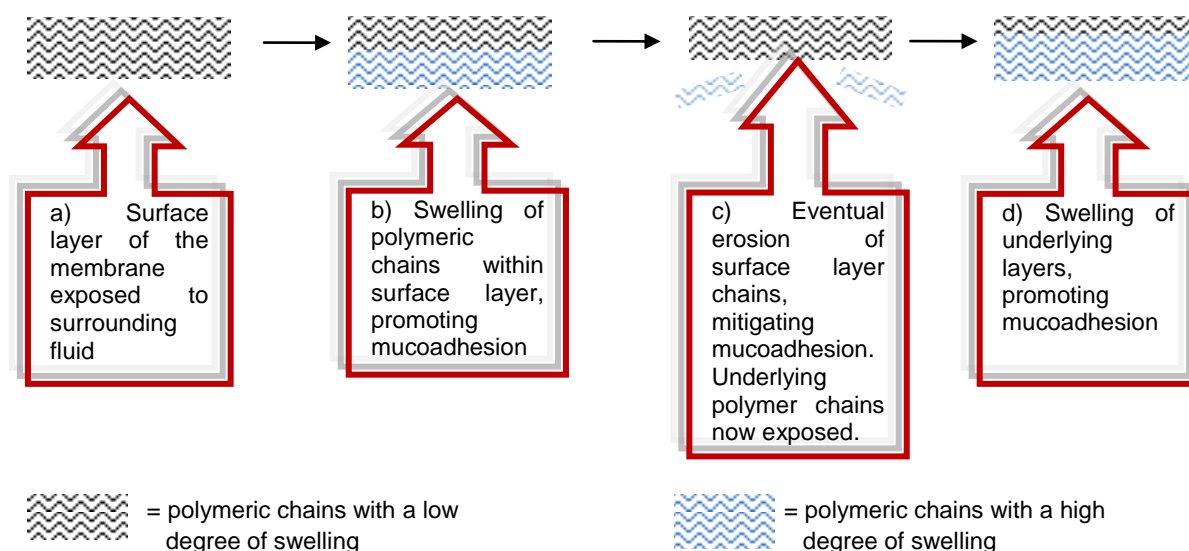


**Figure 4.20:** Schematic illustration of the proposed processes causing the fluctuations observed in the swelling and hence mucoadhesive characteristics of the formulations.

For the intestinal-targeted component, the rate of erosion was considerably higher than that of the gastric-targeted formulation. As a result, an overall decrease in the weight and

hence swelling was observed as a function of time. However, the decrease in swelling did not affect the mucoadhesive characteristics of the formulation, as results indicated a consistent increase in the mucoadhesion of the formulation over time (Figure 4.21a). It can therefore be deduced that the mucoadhesive characteristics optimized intestinal-targeted formulation is not detrimentally affected by GIT conditions, ensuring that the optimal mucoadhesion over prolonged periods of time.

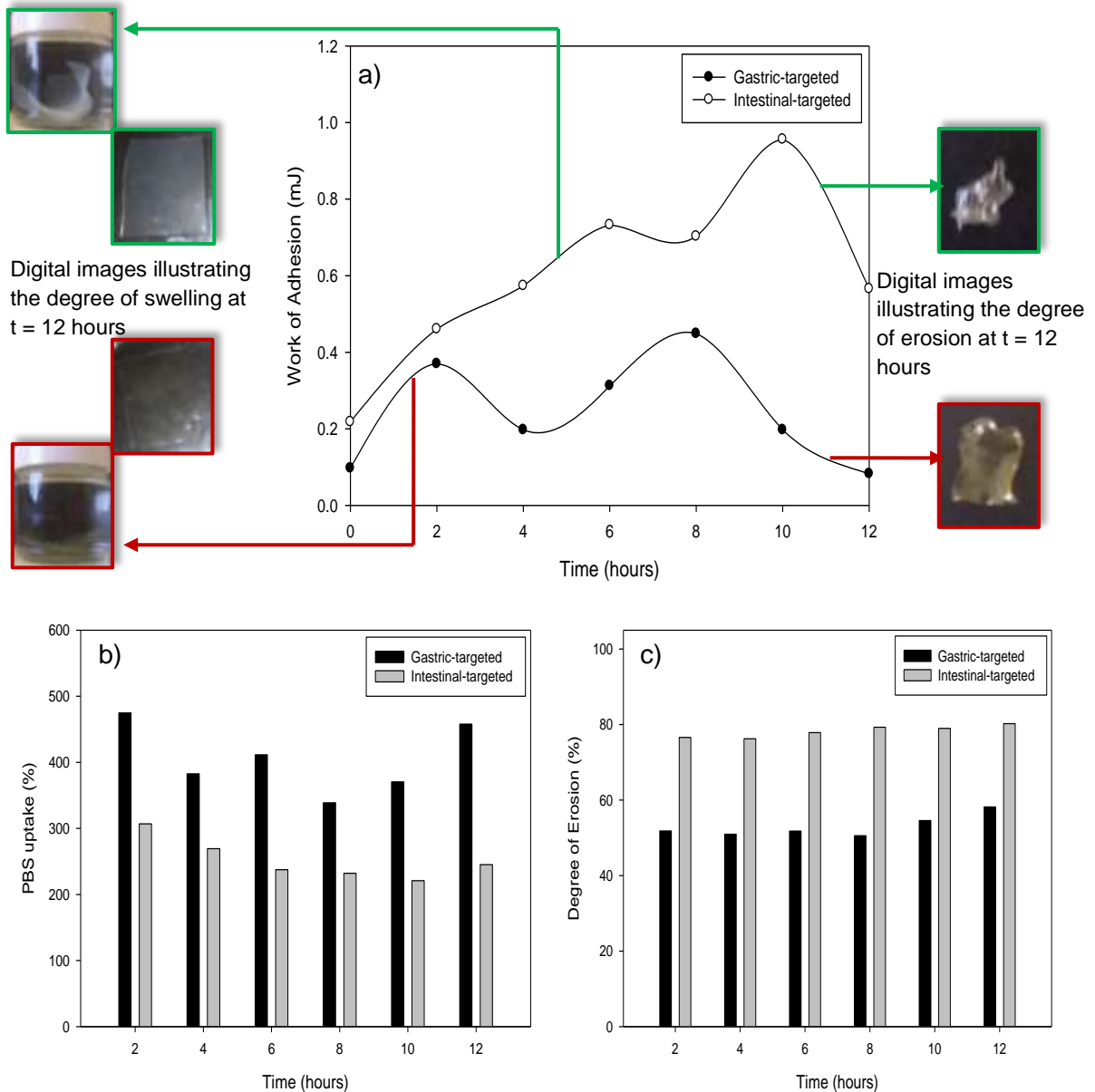


**Figure 4.21:** Graphic illustration of the variations in a) the  $AUC_{FD}$  ( $n=3$ ;  $SD < 0.094$  in all cases); b) the degree of swelling ( $n=3$ ;  $SD < 11.5\%$  in all cases) and c) degree of erosion ( $n=3$ ;  $SD < 7.25\%$  in all cases) of optimized gastric-(highlighted in red) and intestinal-targeted (highlighted in green) mucoadhesive formulations as a function of time.

#### **4.7.6 Analysis of the surface morphology variations of the optimized mucoadhesive layers relative to exposure to simulated gastro-intestinal conditions**

Scanning electron micrographs revealed that with exposure to simulated GIT conditions, drastic alterations were observed in the surface morphology of the gastric-targeted mucoadhesive layer (Figure 4.22a). At  $t=2$  hours, a fissure-like surface appearance of the mucoadhesive layer was observed. As these fissures were not seen at the other time point, and considering that the main physical alteration occurring with exposure to simulated GIT conditions between 0 and 2 hours is swelling, it can be concluded that the fissuring may be attributed to the swelling process. The fissures may have resulted with slower swelling areas of the layer forming the troughs of the fissures while the faster swelling areas forming the higher regions or peak areas as illustrated in Figure 4.22a. After six hours of exposure to simulated gastro-intestinal conditions, pores began to develop in the surface structure of the formulation, resulting from polymeric erosion from the mucoadhesive membrane. The pore distribution and depth increased with time as observed after 12 hours (Figure 4.22a).

A similar phenomenon is observed in the optimized intestinal-targeted mucoadhesive layer, where the swelling process caused an irregular surface appearance with areas of larger degrees of swelling (Figure 4.22b). Polymer erosion from the membrane may be a potential contributing factor to the tearing and pore formation occurring after six hours of exposure to simulated gastro-intestinal conditions as illustrated in Figure 4.22. After 12 hours of exposure, the surface morphology was drastically altered, with numerous pores and tears present. With the resultant polymer erosion from the mucoadhesive layer, it would be postulated that a decline in the mucoadhesion should be observed. Since the mucoadhesion was not drastically affected (a small loss in the mucoadhesive characteristics was observed after 10 hours) it can be concluded that these pores may improve the mucoadhesion of the mucoadhesive layer due to the increase in the contact area available for mucoadhesion.

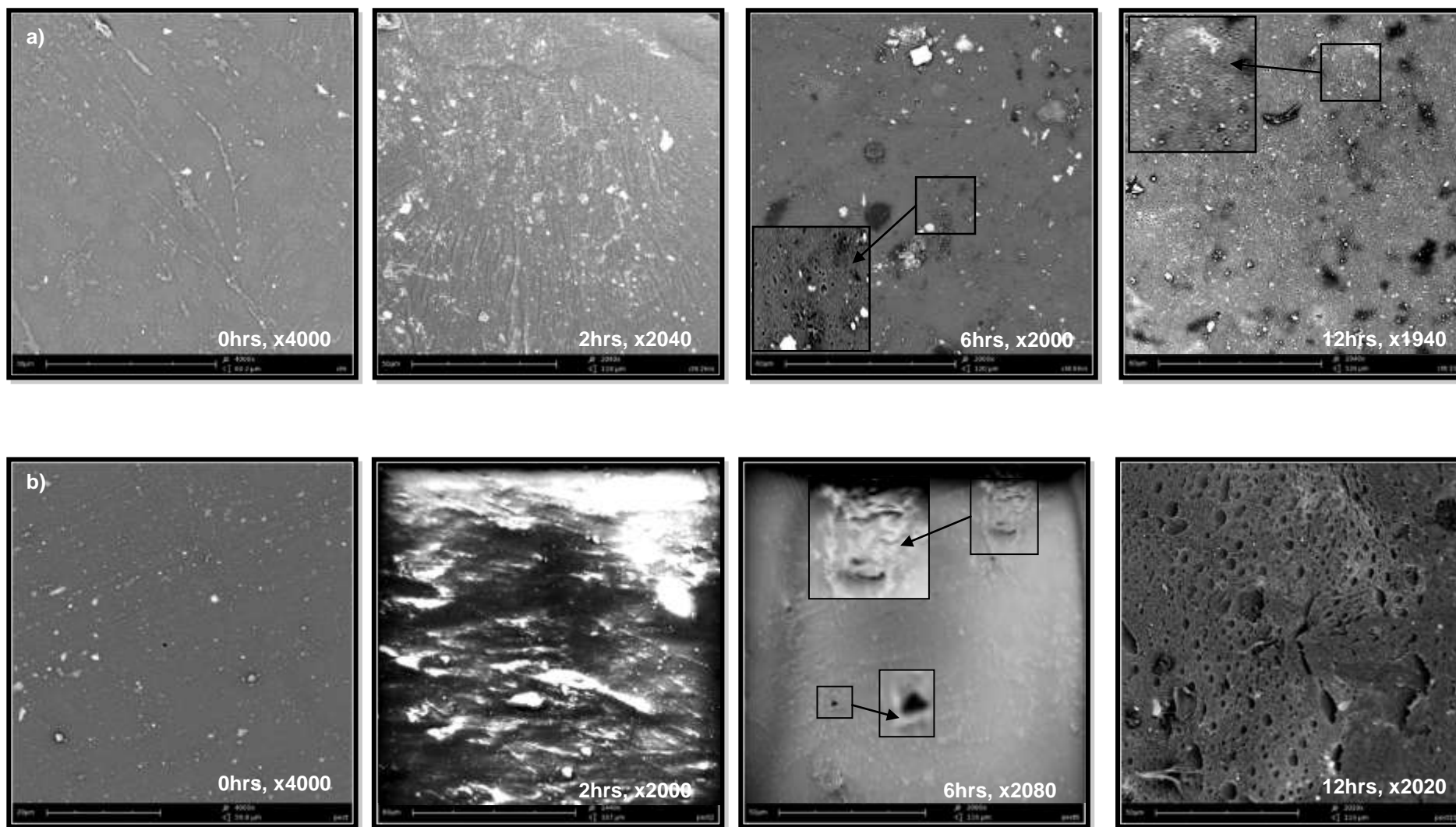


**Figure 4.22:** Scanning electron micrographs of a) the optimized gastric-targeted formulation in simulated gastric conditions and b) the optimized intestinal-targeted formulation at various time points and magnifications in simulated intestinal conditions.



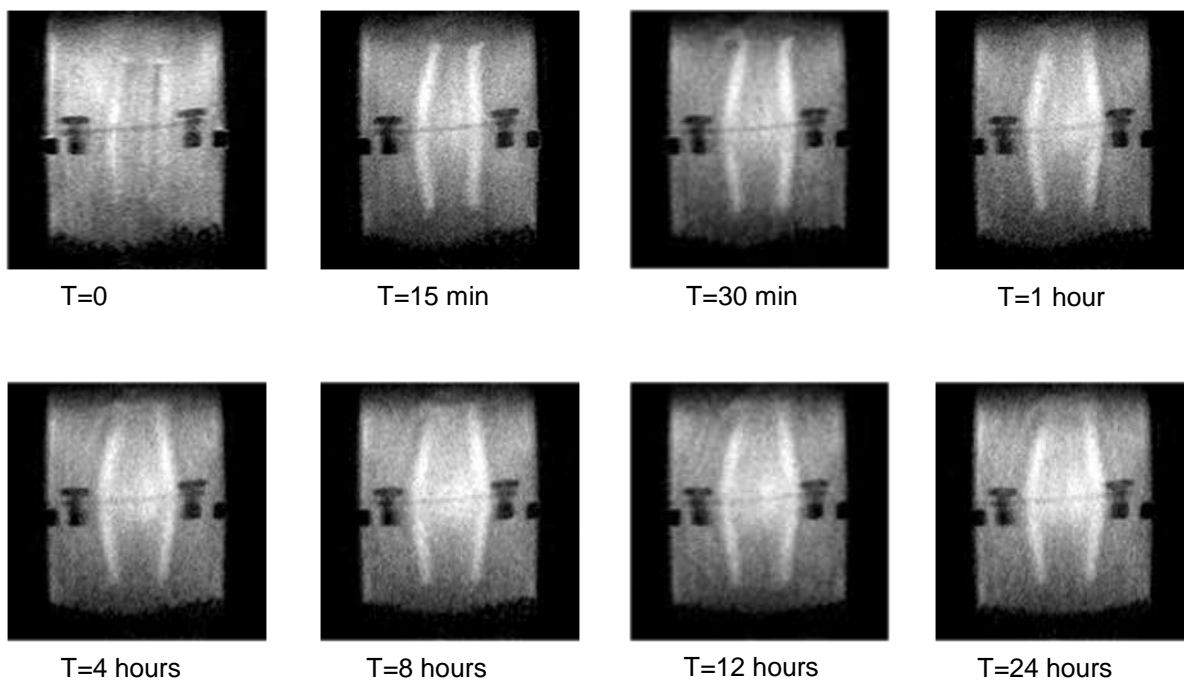
#### **4.7.7 Magnetic Resonance Image analysis of the swelling behaviour of the optimized formulations**

Magnetic resonance imaging (MRI) was also employed to observe and confirm the swelling and erosion behaviours that occurred during mucoadhesive studies. Figure 4.23 displays the images obtained for the optimized gastric-targeted and intestinal-targeted formulations, where the displayed images were obtained at zero, 15 and 30 minutes, 1, 4, 8, 12 and 24 hours. The light grey part surrounding the formulation is the dissolution medium (PBS: pH  $1.2\pm 0.1$ ; or  $6.8\pm 0.1$ ). As the optimized gastric- or intestinal-targeted formulation swelled, the darker grey, un-hydrated portions of the formulation turned white due to hydration.

As illustrated in Figure 4.23a, the optimized gastric-targeted formulation became progressively larger in size between the zero to one hour time points. Thereafter the formulation remained relatively consistent in size throughout the study, with slight size variations as a result of the simultaneous swelling and erosion processes occurring within the polymeric structure. The simultaneous swelling and erosion occurring with the gastric-targeted formulation with time, caused significant variations in the hydration state of the formulation in relation to time, thus causing variations in the mucoadhesive properties of the formulation, as confirmed in *Section 4.7.5*.

A clear succession of swelling was observed between zero to one hour of the optimized intestinal-targeted formulation, followed by an observed decline in the formulation size, as illustrated in Figure 4.23b,. As confirmed in previous studies, (*Section 4.7.5*) erosion occurred at a fairly larger degree in the intestinal-targeted formulation. The rapid erosion did not, however, detrimentally affect the mucoadhesive properties of the intestinal-targeted formulation. Therefore, MRI scans confirmed the swelling and erosion behaviour of the optimized mucoadhesive formulations.

a)



b)

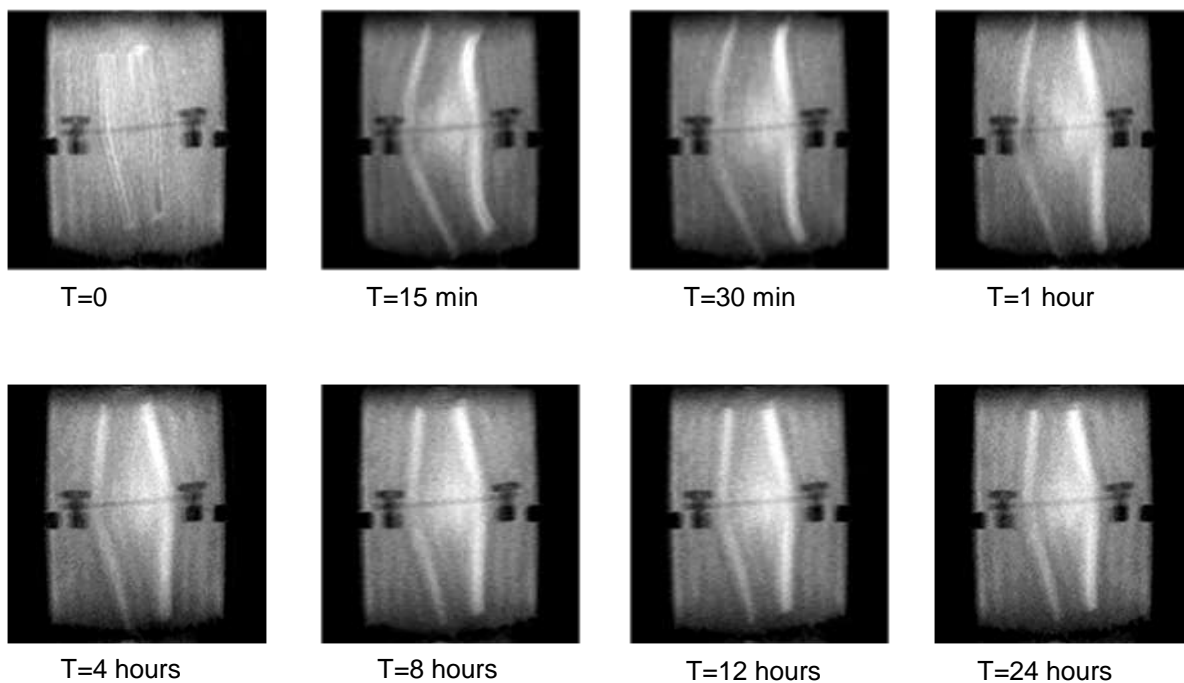


**Figure 4.23:** Magnetic resonance images of the hydration state and accompanying weight changes of the a) optimized gastric-targeted formulation and b) the optimized intestinal formulation when exposed to simulated gastro-intestinal conditions at different time points.

#### 4.8 Concluding Remarks

The mucoadhesive layer of both the gastric- and intestinal-targeted components of the MMDDS were successfully developed, optimized and characterized. The Face-centered Central Composite Experimental Design generated 13 test formulations, of which effects of the independent variables on the dependent response variable was analyzed and an optimized formulation was mathematically produced. The experimental and fitted values (generated during optimization studies) achieved good correlation, demonstrating a good fit of the design model. Analysis of Variance (ANOVA), correlation analysis, and regression analysis was used to analyze the dataset, proving the statistical acceptability of the models proposed. Both the optimized formulations provided the necessary mucoadhesive properties required in their respective pH ranges, ensuring that the formulations will provide site-specific drug delivery. Both optimized formulations achieved a high desirability with optimization.

Furthermore, this chapter demonstrated the manner in which the optimized formulations would react upon exposure to simulated GIT conditions, providing useful information required to predict the formulations' *in vivo* performance. Tensile analysis revealed that the optimized formulations possess suitable elasticity and flexibility, required for insertion into capsules. Vibrational and SEM analysis demonstrated that the mucoadhesive polymer PVP eroded out of the membranes with extended exposure to simulated GIT conditions, which was further confirmed by swelling and erosion studies and MRI analysis. The variations observed in the mucoadhesive characteristics were related to the physical alteration (i.e. simultaneous swelling and erosion) of the system occurring with exposure to simulated gastro-intestinal conditions.

## CHAPTER 5

### PRELIMINARY DESIGN OF THE DRUG-LOADED NANOFIBROUS MATRICES OF THE MULTI-COMPONENT MEMBRANOUS DRUG DELIVERY SYSTEM

---

#### 5.1 Introduction

Electrospinning has gained much popularity in recent years as a versatile and relatively simple technique that produces nanofibrous matrices or membranes with fibres ranging in the submicron (micrometre) to nanometre size range. The electrospun product, a nanofibrous matrix of polymeric fibres, has been investigated extensively for application in areas of protective clothing, catalysis, electronic systems, biomedical devices, filtration systems, agriculture and composites (Xie and Wang, 2006). These polymeric fibres can be utilized in health care as carriers for drug delivery (Zeng *et al.*, 2003), prevention of post-surgical adhesions and infections or wound healing in the form of medicated scaffolds (Kim *et al.*, 2004; Jia *et al.*, 2007) or as implantable systems containing nanofibres for delivery of bioactive agents over prolonged periods of time (Xie and Wang, 2006). Other common uses for polymeric nanofibres or nanofibrous matrices are depicted in Figure 5.1.

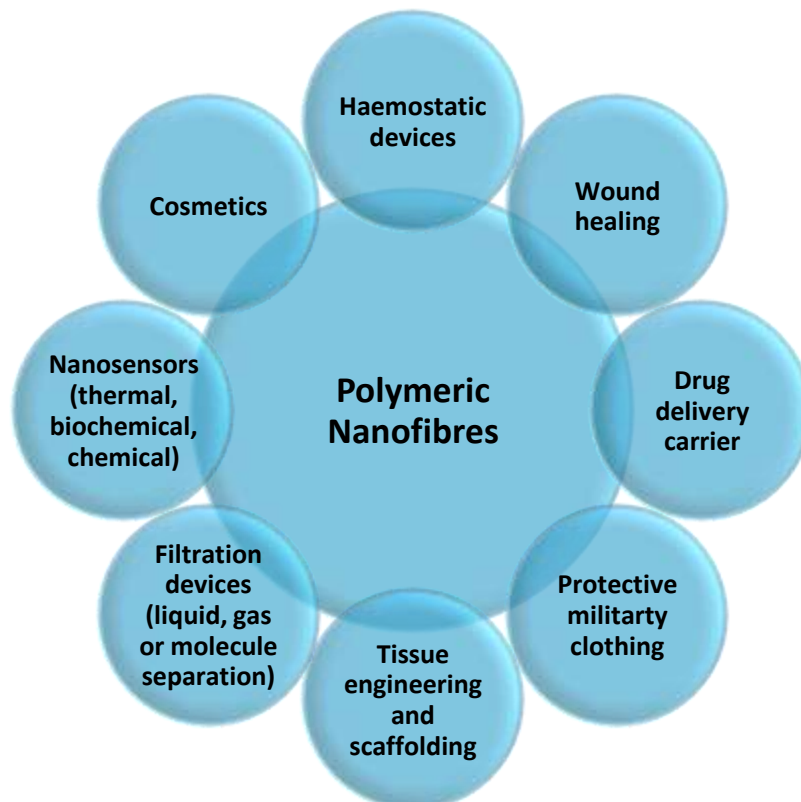


**Figure 5.1:** Common nanofibre applications (Sourced from Huang *et al.*, 2003; Venugopal *et al.*, 2004; Lu and Ding, 2008; Sill and Von Recum, 2008).

Granted there are other methods of producing ultra-thin fibres such as mechanical drawing or conventional spinning which rely on rheological, gravitational, tensile, inertial and aerodynamic forces (Reneker and Chun, 1996) or template synthesis, self-assembly and phase separation, it should be noted that these methods require specialized equipment, can only be applied to certain materials, cannot always produce continuous fibres or are extremely time-consuming (Huang *et al.*, 2003). The electrospinning method on the other hand, is a relatively versatile and simpler technique that is able to produce thinner, continuous nanofibres by applying an electrical potential to a polymeric solution (Reneker and Chun, 1996; Li and Xia, 2004; Li *et al.*, 2006b, Baji *et al.*, 2010).

Electrospun fibrous matrices possess a three dimensional porous structure ideal for controlling drug delivery due to their relatively large surface area and porosity. Several studies have examined the possibility of utilizing electrospun matrices as a controlled release system for the delivery of antibiotics, anti-cancer drugs, vitamins and proteins or DNA (tissue engineering applications) (Luu *et al.*, 2003; Kim *et al.*, 2004; Casper *et al.*, 2005; Chew *et al.*, 2005; Zeng *et al.*, 2005a; Taepaiboon *et al.*, 2007). Electrospun membranous matrices have been fabricated using various polymers and solvents, (Table 5.1), with the necessary physicochemical/physicomechanical properties to achieve the desired application (Kim *et al.*, 2007).

**Table 5.1:** Polymers electrospun drug for delivery applications (Adapted from Sill and Von Recum, 2008).

| <b>Polymer</b>   | <b>Solvents</b>                     | <b>Applications</b>   |
|--|-------------------------------------|---|
| Poly(D,L-lactic-co-glycolic acid), PEG- <i>b</i> -PLA, and PLA               | DMF                                 | Electrospun fibres for the sustained delivery of drugs (Mefoxin <sup>®</sup> and cefoxitin sodium) with successful retention of the structure and bioactivity of the drug molecules (Kim <i>et al.</i> , 2004). |
| Poly(D,L-lactic-co-glycolic acid)  | DCM                                 | An implantable electrospun device for the delivery of Paclitaxel to cancer cells <i>in vitro</i> (Xie and Wang, 2006).  |
| Poly(L-lactide-co-glycolide) and PEG-PLLA                                    | Chloroform                          | An implantable electrospun device for the delivery of BCNU (Xu <i>et al.</i> , 2006).   |
| (a) Poly( $\epsilon$ -caprolactone)<br>(b) Poly(ethylene glycol)             | (a) TFE<br>(b) Water                | TE and drug delivery of BSA, core/shell nanofibres were prepared via coaxial spinning capable of higher protein loading (Zhang <i>et al.</i> , 2006b).  |
| (a) Poly( $\epsilon$ -caprolactone) and Poly(ethylene glycol)<br>(b) Dextran | (a) Chloroform and DMF<br>(b) Water | Drug delivery of BSA, core/shell nanofibres were prepared via coaxial spinning capable of higher protein loading, PEG addition improved control over protein release (Jiang <i>et al.</i> , 2006).              |
| (a) Poly( $\epsilon$ -caprolactone)<br>(b) Poly(ethylene glycol)             | (a) Chloroform and DMF<br>(b) Water | Drug delivery of BSA and lysozyme, core/shell nanofibres were prepared via coaxial spinning (Jiang <i>et al.</i> , 2005).   |
| Poly( $\epsilon$ -caprolactone-co-ethyl ethylene phosphate)                  | DCM and PBS                         | Core/shell nanofibres were prepared via coaxial spinning for delivery of $\beta$ -nerve growth factor and BSA, PEG addition improved control over protein release (Chew <i>et al.</i> , 2005).                  |

DDS: Drug Delivery Systems; DCM: dichloromethane; THF: Tetrahydrofurane; PBS: Phosphate buffered saline; DMF: Dimethyl Formamide; HFP: 1,1,1,3,3,3-hexafluoro-2-propanol; TFE: 2,2,2-trifluoroethanol; BSA: Bovine serum albumin

The focus of this chapter lies in the selection of a suitable polymer for electrospinning, as well as the appropriate parameters employed in the electrospinning procedure. The nanofibrous matrix was investigated for its drug release characteristics of both rifampicin and isoniazid. Prior to the selection and identification of appropriate polymers for the development of the electrospun matrices, it was important to fully comprehend the electrospinning procedure, any parameters which would affect electrospinning and the ultimate fibre morphology as well as the different methods of drug-loading.

### **5.1.1 The electrospinning procedure**

Electrospinning is fundamentally based on inducing an electric charge into a polymeric solution followed by ejecting the charged solution through a fine capillary tip. The force generated by the syringe pump or gravitational forces allows the polymeric solution to pass through a capillary of small-diameter, resulting in the formation of a pendant drop at the tip. When an electrical potential is applied to the pendant drop the rounded drop elongates, becoming conical in shape (Baumgarten, 1971; Doshi and Reneker, 1995; Sill and Von Recum, 2008), which is now termed the Taylor cone as illustrated in Figure 5.2 (Sill and Von Recum, 2008). A fine fibre jet is eventually ejected from the tip of the Taylor cone, particularly when the electrical field exceeds the polymeric solution's surface tension (Zeleny, 1935; Liang *et al.*, 2007; Sill and Von Recum, 2008; Baji *et al.*, 2010). The fibre jet travels towards the collecting surface, which is typically of opposite polarity. Electric forces then accelerate and stretch the fibre jet, causing a reduction in diameter and a subsequent increase in length. As the fibre travels through the atmosphere, the high electric fields cause the jet to become unstable, which begins to whip at a high frequency, and the fibre undergoes further bending and stretching. The solvent then evaporates and the resultant solid fibres are deposited on the collecting surface. This eventually leads to the formation of a membranous structure through the continuous deposition of polymeric fibres on the collecting surface, closing the electrical circuit (Deitzel *et al.*, 2001; Pham *et al.*, 2006; Sill and Von Recum, 2008; Baji *et al.*, 2010). The resultant product is typically a highly porous matrix or matrix-like structure, possessing a high surface area to volume ratio (Liang *et al.*, 2007; Reneker and Yarin, 2008).

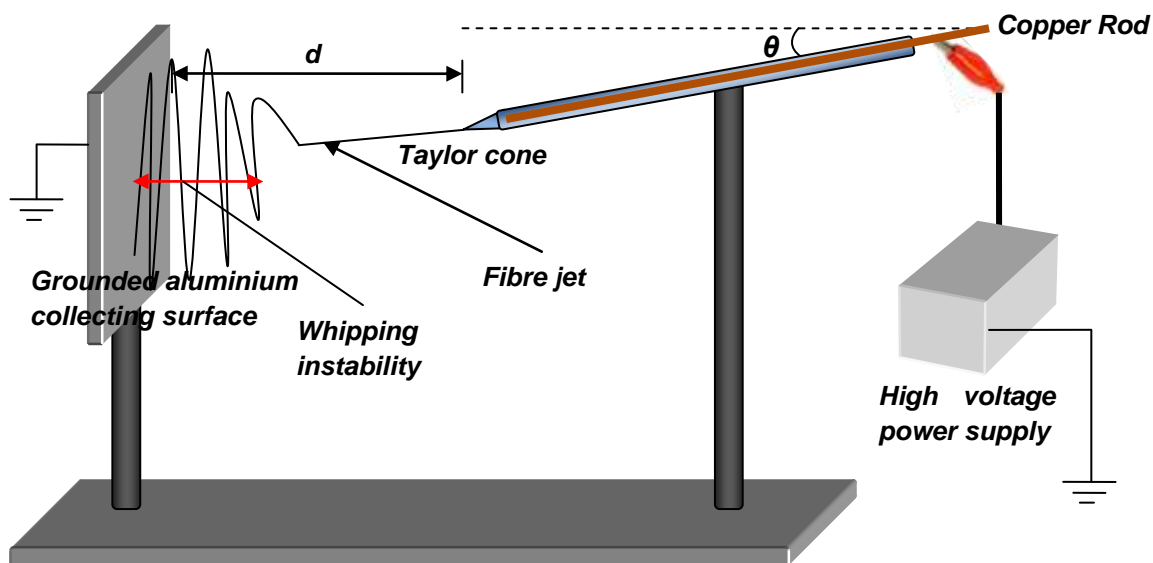


**Figure 5.2:** Schematic illustration of the horizontal electrospinning process, where  $d$  = distance between capillary tip and collecting surface and  $\theta$  = Capillary angle.

For successful determination of the optimal parameters for the preparation of membranous matrices, processing parameters (i.e. the distance of the needle from the collecting surface, applied voltage, solution flow-rate) and solution parameters, (i.e. viscosity, elasticity, surface tension, solution conductivity) must be carefully manipulated, and thus electrospun membranous matrices can be customized to achieve desired drug release patterns or other physicochemical properties (Kim *et al.*, 2007; Sill and Von Recum, 2008).

### 5.1.2 Parameters affecting the electrospinning procedure

In order to successfully apply any electrospun product to a specific target, the nanofibrous scaffold must exhibit suitable physical and biological properties closely matching the desired application requirements (Liang *et al.*, 2007). As discussed previously, there are various factors which affect the ultimate fibre morphology, which can be carefully manipulated to achieve electrospun products with finely tuned properties and characteristics. These factors can be classified into three broad categories, i.e. solution, processing and ambient parameters. These parameters have varying degrees of effects on the final fibre morphology as illustrated in Table 5.2.

**Table 5.2:** Effects of electrospinning parameters on fibre morphology.

| Parameter                                    | Effects on fibre morphology  | References  |
|--|--|---|
| <b>Solution Parameters</b>                   |  |   |
| <b>Viscosity or polymer concentration</b>    | The ability of a solution to form a fibre jet or the electrospinnability of a solution ultimately relies on the polymer concentration. Dependant on the viscosity, is the degree of chain entanglements, which is responsible for ensuring that the fibre jet remains stable during the electrospinning procedure, without breaking up into droplets before deposition on the collecting surface. Very dilute solutions cause the fibre jet to break up into droplets before reaching the collector due to the effects of surface tension and a lower degree of chain entanglements. Very high concentrations cause very high viscosities, resisting fibre jet formation. Within the optimal range of concentrations, electrospun fibre diameter increases with increases in the polymer concentration, however with concentrations at the lower end of the range, there is incomplete drying of the fibre which leads the presence of junctions and bundles. Doshi and Reneker (1995) reported that solution viscosities of less than 800 centipoises broke up into droplets before reaching the collecting surface while solutions with viscosity greater than 4000 centipoises were too thick to electrospin. Thus the concentration of the polymer solution should ideally be high enough, causing an adequate degree of chain entanglements, while the viscosity should be low enough to allow fibre jet formation. | Doshi and Reneker, 1995; Hohman <i>et al.</i> , 2001; Yao <i>et al.</i> , 2003; Mit-Uppatham <i>et al.</i> , 2004, Casper <i>et al.</i> , 2005; Gupta <i>et al.</i> , 2005; Lu and Ding <i>et al.</i> , 2006; Pham <i>et al.</i> , 2006; Sawicka and Gouma, 2006; Liu <i>et al.</i> , 2008; Sill and Von Recum 2008; Kriegel <i>et al.</i> , 2009; Bhardwaj and Kundu, 2010 |
| <b>Conductivity/ solution charge density</b> | Generally, solutions with a high conductivity tend to have greater charge carrying capacity than solutions with low conductivity, subjecting the fibre jet to greater tensile forces. Highly conductive solutions are extremely unstable when subject to strong electric fields, ultimately leading to dramatic bending instability as well as a broad diameter distribution. However, manipulating the charge density within an optimal range may result in the formation of more uniform fibres with lower incidence of bead defects and smaller fibre diameters. Solution conductivity can be altered by the addition of alcohol or salts.  |   |
| <b>Surface tension</b>                       | Surface tension is more likely to be a function of solvent composition rather than the polymer. Typically, solutions with lower surface tensions prevent the formation of bead defects. However, solutions with extremely low surface tensions cause the fibre jet to break down into drops before reaching the collecting surface, resulting in the formation of beaded fibres and droplets. If the solution has a high surface tension, the fibre jets become unstable and eventually breaks up, depositing on the collecting surface as droplets. Surface tension can successfully be lowered by addition of surfactants.   |   |
| <b>Polymer molecular weight</b>              | As the molecular weight of a polymer increases, the optimal concentration range for electrospinning is lowered. Gupta and co-workers (2005) managed to isolate the effect of the molecular weight on electrospinning while maintaining other parameters constant. Their studies revealed that as the molecular weight increased, a reduction in bead defects was observed. Typically, fibres with high molecular weights have larger fibre diameters. Furthermore, polymers with lower molecular weight distributions resulted in uniform fibres at a lower concentration than those with larger molecular weight distributions. The polymers molecular weight may have an effect on surface tension and conductivity.   |   |



**Table 5.2 continued**

|   |  |
|---|--|
| <b>Solvent volatility</b>                         | Typically, solutions containing solvents with higher volatilities produce fibres with higher densities of pores. On the other hand, for successful electrospinning the solvent requires adequate volatility to ensure adequate drying of the fibre before it deposits on the collecting surface.   |
| <b>Controlled Variables</b>                       |  |
| <b>Flow rate</b>                                  | Polymer flow rate can impact on fibre sizes, shape and porosity. Fibre diameters and porosity tend to increase with higher flow rates. Bead defects may also occur at extremely high flow rates, due to incomplete drying. Flattened or ribbon-like fibre shapes are also achieved with incomplete drying as opposed to fibres with circular cross-sections. With extremely slow flow rates, the Taylor cone cannot be maintained as there is insufficient solution to replace what has been ejected as the fibre jet.             |
| <b>Applied voltage</b>                            | Suboptimal field strengths lead to bead defects in the spun fibres or even failure in jet formation. Typically, fibre diameters decrease in diameter with an increase in the applied voltage until a threshold is reached. When the threshold is surpassed, fibre diameters increase with greater likelihood of bead defects. Many authors agree that an optimal range of applied voltage is required for any polymer and solvent system.  |
| <b>Capillary-collector distance</b>               | Fibre diameters tend to decrease with increased distances. If the distance is not sufficient, incomplete drying may lead to bead defects within the polymer fibres, clumping or droplet formation.   |
| <b>Collector composition, motion and geometry</b> | Collectors (metals) with a high conductivity dissipate the charge of fibre jets, allowing nanofibres to pack more densely. When non-conductive collectors are used, this charge is not dissipated and the fibres repel one another, yielding a more porous structure. Porous collectors, such as paper and copper mesh, produce less-packed nanofibrous structures as compared to fibres collected on aluminium foil. If the collecting surface rotates, i.e. a rotating drum collector, the fibres collect in an aligned fashion. |
| <b>Ambient parameters</b>                         |  |
| <b>Temperature</b>                                | If the surrounding temperature is increased, the polymeric solution viscosity decreases, causing a reduction in the fibre diameters.   |
| <b>Humidity</b>                                   | An increase in the surrounding humidity may result in the appearance of small circular pores on the surface of fibres produced.  |

Doshi and Reneker, 1995; Hohman *et al.*, 2001; Yao *et al.*, 2003; Mit-Uppatham *et al.*, 2004, Casper *et al.*, 2005; Gupta *et al.*, 2005; Lu and Ding *et al.*, 2006; Pham *et al.*, 2006; Sawicka and Gouma, 2006; Liu *et al.*, 2008; Sill and Von Recum 2008; Kriegel *et al.*, 2009; Bhardwaj and Kundu, 2010

### 5.1.3 Methods of drug incorporation

There are various methods employed to incorporate drug into nanofibres for drug delivery applications (Chew *et al.*, 2005; Luong-Van *et al.*, 2006; Natu *et al.*, 2010). The method of drug incorporation, which impacts the drug release behaviour, depends on both the polymer and drug solubility. Furthermore, the drug compatibility with the polymer solution can potentially affect the release behaviour, i.e. lipophilic drugs should be incorporated in lipophilic polymers in order to prevent surface deposition of drug which causes burst release characteristics (Natu *et al.*, 2010; Zeng *et al.*, 2005b). Nevertheless, any interaction occurring between the drug and the polymer can provide sustained release of the drugs, due to changes in the crystallinity of the drug molecules (Taepaiboon *et al.*, 2006; Yu *et al.*, 2009a; Natu *et al.*, 2010). The various methods of drug incorporation are illustrated in Figure 5.3 with the resultant nanofibre morphology.

As discussed in *Section 1.2*, rifampicin (RIF) and isoniazid (INH) were selected as model drugs to determine the efficacy of the drug delivery system. RIF and INH are prescribed concurrently in the treatment of TB. However, these drugs are not compatible when administered simultaneously, since RIF bioavailability is detrimentally affected by the presence of INH. The above and many other drugs would therefore benefit from site-specific drug delivery (Singh *et al.*, 2000a; Singh *et al.*, 2000b; Singh *et al.*, 2001; Shishoo *et al.*, 2001; Mohan *et al.*, 2003; Mariappan *et al.*, 2004; Gohel and Sarvaiya, 2007; du Toit *et al.*, 2008; Tanno *et al.*, 2008; Pund *et al.*, 2010; Pund *et al.*, 2011 *et al.*, 2011).

The proposed MMDDS will ensure segregated drug delivery, by delivering RIF to the upper gastric region of the GIT, while INH is delivered exclusively to the intestinal areas of the GIT. The sites selected were based on RIF being well absorbed from the stomach, while INH is relatively well absorbed in the intestinal region of the GIT (Mariappan and Singh, 2003). By incorporating the drug into the polymer solution before electrospinning, as illustrated in Figure 5.3, a simplistic approach was employed achieving a single step drug-loading procedure, while even drug distribution was achieved.

Drug can be incorporated by dissolving the drug into the polymer solution prior to electrospinning. Even drug encapsulation is achieved. However, drug solubility and compatibility with the solvent is important to ensure minimal surface deposition of drug, thus avoiding burst release characteristics (Zeng et al., 2005b).

When the drug and polymer are not soluble in the same solvent, the drug is solubilised prior to addition to the polymer solution and thereafter electrospun. Drug is generally encapsulated within the fibre, with some surface deposition that may cause burst release (Zeng et al., 2005b; Kim et al., 2007; Natu et al., 2010).

The drug and polymer solutions can be kept separate and subjected to co-axial spinning. The drug solution is fed through an inner capillary tip, while polymer solution is ejected from the outer tip. During electrospinning, the drug is encapsulated within the polymer fibre. No burst release is observed due to the absence of surface drug (He et al., 2006; Huang et al., 2006).

If the drug and polymer is not soluble in the same solvent, and the respective solvents are not miscible, an emulsion is produced which is subject to electrospinning. Complete drug encapsulation is achieved and controlled drug release is achieved by diffusion of the drug molecules out of the fibres (Xu et al., 2005; Qi et al., 2006; Maretschek et al., 2008).

Drug loading can be conducted after electrospinning has occurred. The electrospun product is submerged in a drug solution and the drug is adsorbed onto the surface of the fibres. Typically, positive or negative ions are initially adsorbed onto the surfaces, followed by immersion into the drug solution. The drug would then form and electrostatic interaction with the ions. Release is achieved as the interaction is weakened (Chunder et al., 2007).

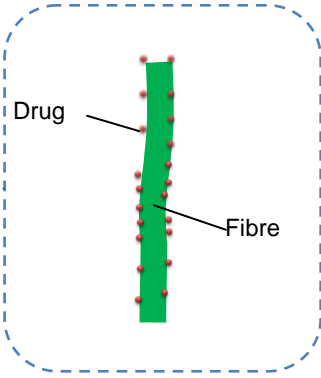
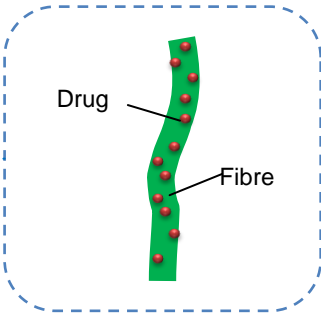
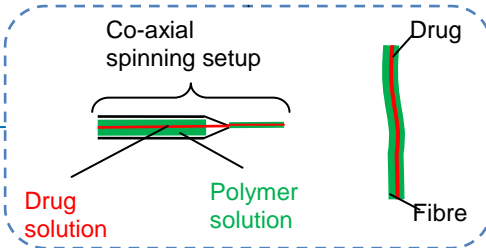
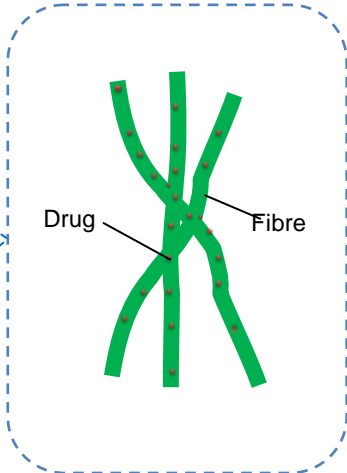


**Figure 5.3:** Methods of nanofibre drug incorporation and resultant fibre morphology, where the red particles indicate the drug molecules and the green indicates the nanofibre.

#### **5.1.4 Preliminary formulation design**

The rational identification of a candidate system for further development was the principle focus of the current chapter. The ensuing experimental investigations were conducted to provide a logical comparison of the electrospinnability of various polymers, identify the most appropriate drug-loading method and determining the need for post-treatments. Preliminary formulation studies (Part I) involved, initially selecting and evaluating various potential polymers for electrospinning potential and identifying the optimal parameter range. Further modification and inclusion of excipients/other polymers was then undertaken to develop a candidate system (Part II). This led to the identification of candidate formulations of both the rifampicin and isoniazid-loaded nanofibres that would achieve the most desirable drug release characteristics.

### **PART I: Identification of a suitable polymer for electrospinning followed by determination of the optimal electrospinning parameters**

## **5.2 Materials and Methods**

### **5.2.1 Materials**

Polymers investigated for electrospinning included poly(vinyl alcohol) ( $M_w$  146000-186000g/mol, 87-89% hydrolyzed) (PVA), ethylcellulose (Ph Eur viscosity 9m.Pa.sS), chitosan (medium molecular weight), cellulose acetate phthalate (CAP) obtained from Sigma-Aldrich (Milwaukee, WI, USA); poly(ethylene oxide) (PEO) (Polyox<sup>TM</sup> WSR 205-NF grade) obtained from The Dow Chemicals Company, (Danbury, CT, USA); hydroxypropylcellulose (HPC) (Klucel Type EF) purchased from Hercules (Wilmington, Delaware, USA); poly(ethylene glycol) (4000; 6000) (PEG) purchased from Merck chemicals (Halfway House, Gauteng, South Africa), Eudragit<sup>®</sup> RS 100 (Röhm GmbH, Pharma Polymers, Kirschenallee, Darmstadt, Germany), carboxymethylcellulose sodium salt and cellulose acetate (CA) obtained from Fluka<sup>®</sup>, (Sigma-Aldrich, GmbH Chemie, Steinheim, Germany). Diphenhydramine HCl (DPH) obtained from Sigma-Aldrich (St. Louis, Missouri, USA) was employed as a model drug to determine the drug entrapment efficiency of the nanofibrous matrices (DPH was initially employed in preliminary studies not only to reduce costs associated with INH and RIF use, but also to ensure the versatility in application of the MMDDS in terms of drug incorporation). Solvents employed included isopropanol purchased from Rochelle Chemicals (Johannesburg, South Africa), acetone obtained from Merck (Pty) Ltd. (Merck, Wadeville, Gauteng, South Africa), acetic acid purchased from (Sigma Aldrich Chemie GmbH (Steinheim, Germany) and water obtained from a Milli-Q water purification system (Milli-Q, Millipore, Billerica, MA, USA).

### 5.2.2 Preparation of nanofibrous matrices by electrospinning

Homogenous polymeric solutions, employing the solvents and polymer concentrations detailed in Table 5.3, were electrospun as follows: The electrospinning setup, as illustrated in Figure 5.2, involved applying 5-20kV, supplied by a Glassman High Voltage, INC (High Bridge, NJ, USA) to the polymer solutions via a copper rod. The polymer solution, placed in 5mL Goldline glass pipettes, was mounted at varying distances from the collecting surface. The distance between the capillary tip to collector and applied potentials were selected based on Taylor cone formation, and were adjusted accordingly during the process of electrospinning to ensure fine fibre jet formation. The solution was fed through a capillary size of  $\pm 1.2$ mm from a horizontal electrospinning setup, with differing capillary angles ( $\theta$ ) from the horizontal surface. The electrospun fibres were collected on an aluminium sheet connected to a grounded counter electrode. Electrospinning was carried out at ambient room conditions for periods ranging between 5-8 hours. The fibres were carefully removed from the aluminium collector and stored in air-tight containers, in the presence of a desiccant, until further testing was conducted.

**Table 5.3:** Polymers and their respective parameters investigated for the development of a nanofibrous matrix.

| Polymer                      | Polymer Concentration (%w/v) | Solvent                  | Electrospinning variables |                      |
|------------------------------|------------------------------|--------------------------|---------------------------|----------------------|
|                              |                              |                          | Distance (cm)             | Applied Voltage (kV) |
| CMC                          | 3.5-5.0                      | Water                    | 18-25                     | 5-20                 |
| PEG 4000                     | 80                           | Water                    | 15-28                     | 5-20                 |
| PEG 6000                     | 80                           | Water                    | 15-28                     | 5-20                 |
| CHT                          | 0.5-2.0                      | 0.1M acetic acid         | 10-30                     | 5-20                 |
| HPC                          | 15                           | Water: Isopropanol (1:1) | 20-25                     | 20                   |
| CA                           | 5-10                         | Water: Acetone (1:3)     | 18-25                     | 20                   |
| CAP                          | 5-10                         | Water: Acetone (1:3)     | 18-25                     | 20                   |
| Eudragit <sup>®</sup> RS 100 | 30                           | Water: Acetone (1:1)     | 18-25                     | 20                   |
| PVA                          | 6-12                         | Water                    | 17-20                     | 20                   |
| PEO                          | 3-5                          | Water                    | 18                        | 5-20                 |

CMC: Carboxymethylcellulose; PEG: Poly(ethylene glycol); CHT: Chitosan; PVA: Poly(vinyl alcohol); PEO: Poly(ethylene oxide); HPC: Hydroxypropyl cellulose; CA: Cellulose acetate; CAP: Cellulose acetate phthalate

### 5.2.3 Analysis of nanofibre morphology employing scanning electron microscopy

Surface morphology of the nanofibrous matrices was analyzed on a Phenom<sup>™</sup> Microscope (FEI Company, Hillsboro, Oregon, USA). Samples were firmly mounted on aluminium stubbs with carbon tape. They were subject to a gold sputter coating under a vacuum of 0.1Torr with argon gas in a SPI-Module<sup>™</sup> Sputter Coater and SPI-Module<sup>™</sup> Control (SPI Supplies, Division of Structure Probe Inc., West Chester, PA, USA). Each

sample required 90 seconds of coating to ensure complete coverage of the sample. Subsequent viewing was thereafter performed at various magnifications under the Phenom™ desktop Scanning Electron Microscope. Different magnifications at 10kV were employed to view the overall and in-depth surface structure to qualitatively elucidate factors such as the nanofibre shape, size range and fibre packing density. The presence of bead defects was also determined from the resultant micrographs.

#### **5.2.4 Construction of a calibration curve for UV spectroscopic determination of DPH**

A calibration curve for DPH was conducted in PBS (pH 1.2; 37°C) by analysing a known series of concentrations of DPH (0-0.7mg/mL) in PBS on a UV spectrophotometer (Lambda 25, UV/VIS Spectrometer, PerkinElmer®, Waltham, MA, USA) at a wavelength of 254nm. A linear curve was generated with the observed absorbance plotted on the y-axis and the corresponding concentrations (mg/mL) on the x-axis. With the intercept set at 0, the  $R^2$  value was determined to be 0.998.

#### **5.2.5 Drug entrapment efficiency**

DPH was employed as a model drug to determine the drug entrapment efficiency (DEE) of the resultant nanofibrous matrices, therefore identifying the polymer with the highest drug entrapment potential. DPH was incorporated into the polymeric solutions in a 1%<sub>w/v</sub> concentration prior to electrospinning. Accurately weighed samples of DPH-loaded nanofibres were dissolved in 100mLs of phosphate buffered saline (PBS) (37°C; pH 1.2). The drug content was analyzed by UV spectrophotometry (Lambda 25, UV/VIS Spectrometer, PerkinElmer®, Waltham, MA, USA) and computed from a standard linear curve of the drug in PBS (pH 1.2) at a  $\lambda_{max}$  of 254nm for determination of drug content. All tests were performed in triplicate (n=3) and presence of the polymer was taken into account. Equation 5.1 was used to compute the DEE, where the theoretical drug (mg) in the formulation was determined as a function of the fibre weight. In order to ensure that the nanofibers were completely dissolved, the solution was subject to agitation with the Sonics Vibra Cell™ Sonicator (Sonics and Materials Inc, Newtown, CT, USA) for 15 minutes at a 60% amplitude.

$$\%DEE = \frac{D_a}{D_t} \times 100$$

Equation 5.1

where %DEE = Percentage of drug entrapped;  $D_a$  = Actual drug quantity (mg) measured by UV spectrophotometry and  $D_t$  = Theoretical drug (mg) added to the formulation.

## 5.3 Results and Discussion

### 5.3.1 Analysis of the degree of success of polymers investigated for electrospinning

The polymers investigated for electrospinning had varying degrees of success in nanofibre fabrication. Successful electrospinning was determined by the fulfilment of two factors, namely,

- a) The deposition of continuous nanofibres, thus forming a three dimensional matrix;
- b) Achieving consistent electrospinning over a prolonged duration of time, without the need for repeated unblocking of the pipette tip.

Generally, when employing solvents with higher volatility, the Taylor cone tended to solidify frequently during the electrospinning procedure, preventing any fibre jet formation. As a result, electrospinning could not proceed until the blockage was manually removed. Furthermore, as the nanofibrous matrix is ultimately rolled and inserted into a capsule, a denser packed nanofibrous matrix was preferred as opposed to the more porous matrices. The porous nanofibrous matrices were brittle and prone to breakage when removed from the collecting surface. Microscopic and scanning electron micrographic analysis distinguished polymer electrospinning from electro spraying, and identified any deposition of droplets within the nanofibre structure. Droplets typically deposit on the collecting surface in a more hydrated state than the nanofibres, and thus cause agglomeration of the fibres surrounding the area of droplet deposition. This defect has the potential to drastically alter the release characteristics of the nanofibrous matrix, due to vastly differing shapes or sizes, and was thus deemed undesirable. Polymers which were unable to form three dimensional nanofibrous matrices may be as a result of improper solvent choice, polymer concentration or solution viscosity, very low or high surface tension or conductivity.

#### 5.3.1.1 Carboxymethyl cellulose

When attempting to electrospin higher concentrations of the carboxymethylcellulose (CMC) solution (5%<sup>w/v</sup>), a fibre jet was unable to form due to the high viscosity of the solution. However, when attempting to electrospin the 3.5%<sup>w/v</sup> CMC solution, some form of electro spraying intermingled with electrospinning occurred, depositing droplets on the collecting surface in a very random and erratic manner. Furthermore, an insufficient quantity of the droplets was obtained regardless of electrospinning duration. Upon microscopic analysis (Figure 5.4), it was revealed that the CMC solution did not produce

any continuous fibres, but rather a collection of randomly scattered bead-like particles of varying sizes and shapes. Further alterations in the solution or processing parameters demonstrated no success fibre formation. Further electrospinning investigations employing CMC as a polymer for the production of nanofibrous matrices were thus not conducted.

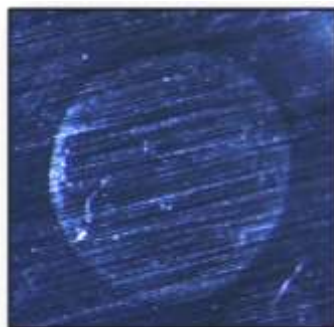


**Figure 5.4:** Microscopic analysis of CMC electrospun at a concentration of 3.5%<sup>w/v</sup> CMC.

### 5.3.1.2 Poly(ethylene glycol) 4000

Electrospinning of poly(ethylene glycol) (PEG) 4000 solutions required significantly prolonged electrospinning periods before a sufficient quantity of the electrospun product was obtained. Furthermore, the product was very randomly distributed, with no formation of a three dimensional matrix structure. The resultant electrospun product was rather powdery in nature and extremely prone to disintegrating when handled for further analysis. Altering the processing parameters demonstrated no success in improvement fibre formation. Microscopic and scanning electron micrographic analysis (Figure 5.5) revealed that continuous fibres were not formed, but rather highly porous and elongated bead-like particles about 500 $\mu$ m in length were randomly deposited. Further electrospinning investigations employing PEG 4000 were therefore not conducted.

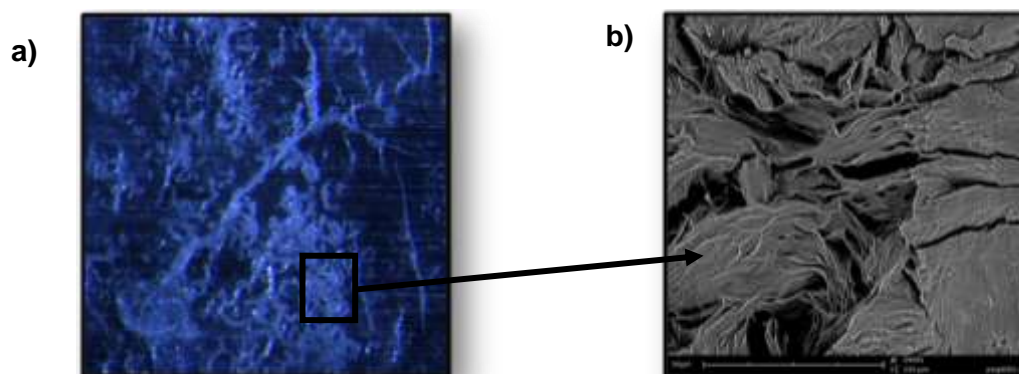


**Figure 5.5:** a) Microscopic and b) Scanning electron micrographic analysis at a magnification of 2400x depicting the surface morphology of PEG 4000 electrospun at a concentration of 60%<sup>w/v</sup>.



### 5.3.1.3 Poly(ethylene glycol) 6000

Electrospinning PEG 6000 for significant periods of time did not produce a sufficient quantity of the electrospun product. Furthermore, the quantity that was present was randomly and erratically distributed, which did not form any sort of three dimensional matrix or structure. The product had a waxy feel and appearance, and was very brittle and prone to breakage and/or disintegration. Altering the processing parameters demonstrated no success in fibre formation. Microscopic and SEM analysis (Figure 5.6) revealed irregular-shaped porous structures with random distribution and with size ranges of 100-200 $\mu\text{m}$  in diameter. Further electrospinning investigations employing PEG 6000 were thus absolved.

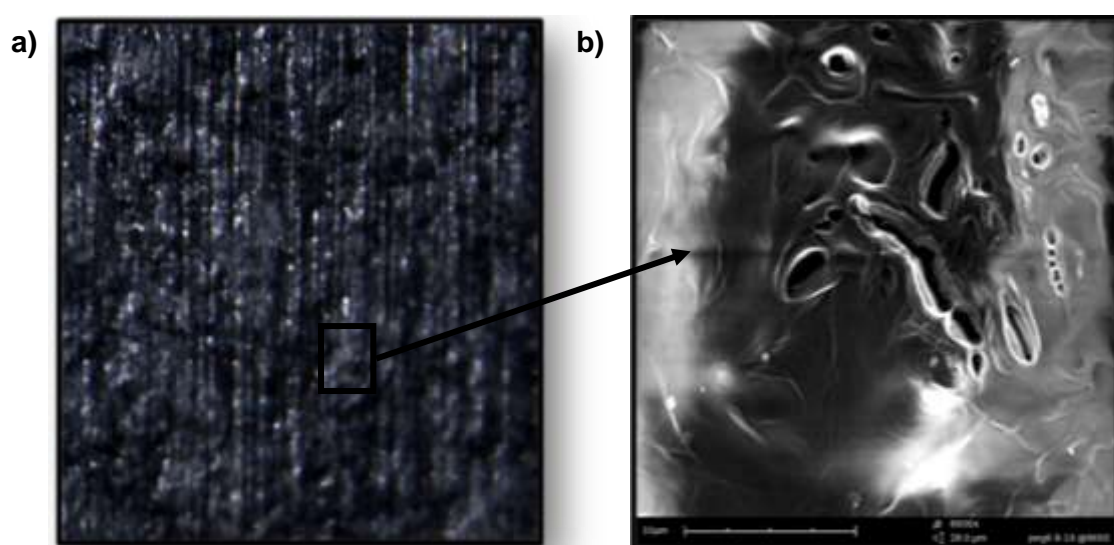


**Figure 5.6:** a) Microscopic analysis and b) Scanning electron micrographic analysis at a magnification of 8600x depicting the surface morphology of PEG 6000 electrospun at a concentration of 80%<sup>w</sup>/<sub>v</sub>.

### 5.3.1.4 Chitosan

Typically, high concentrations of chitosan (CHT) were unable to form any type of Taylor cone, and could thus not be electrospun. However, during electrospinning of lower concentrations of CHT solutions, the fibre jet that was able to form, was extremely unstable, producing erratic periods of electrospaying rather than electrospinning. Attempts at altering the processing and solution parameters demonstrated no success in improving fibre formation. However, some large and randomly scattered droplets were deposited on the collecting surface. CHT was thus deemed to be unsuitable for further electrospinning investigations.

### 5.3.1.5 Hydroxypropyl cellulose

Electrospinning of hydroxypropyl cellulosic (HPC) solutions was consistent, with uniform and even deposition of the electrospun product (Figure 5.7). However, frequent blocking of the pipette tip occurred, necessitating manual removal of the blockage before the electrospinning process could continue. Although macroscopically it appeared as if the polymer was being electrospun into fibres, microscopic and SEM evaluation revealed that no fibres, but rather many bead-like particles were deposited on the collecting surface. The size range of the particles varied drastically, from the deposition of extremely fine particles, to larger particles of 3-6 $\mu\text{m}$  in diameter. The particles were typically spherical in shape, however, some particles collapsed as it was deposited, concaving in certain areas of the particle surface. Further electrospinning investigations employing HPC were thus absolved.

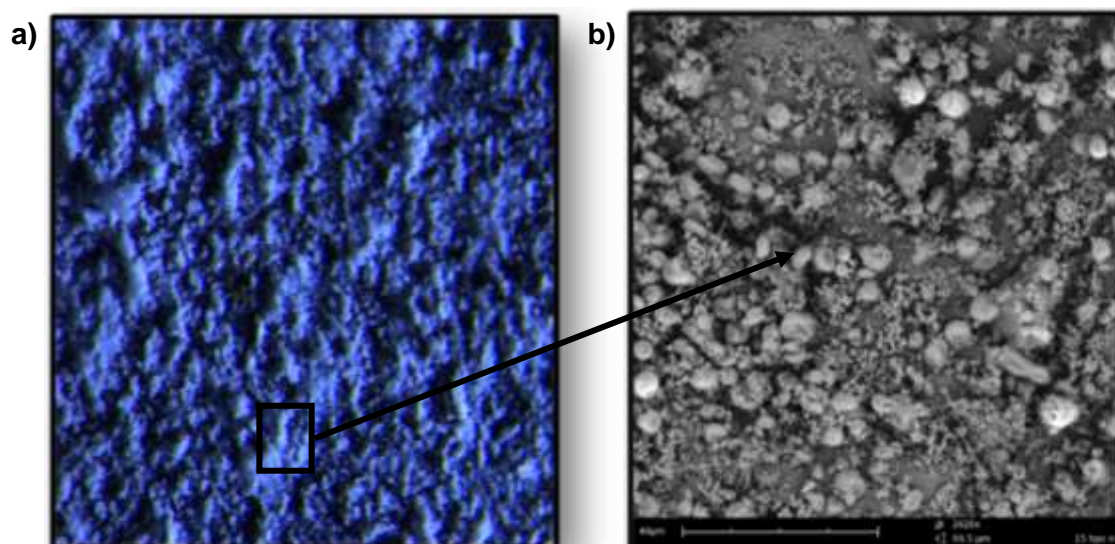


**Figure 5.7:** a) Microscopic analysis and b) Scanning electron micrographic analysis at a magnification of 8600x depicting the surface morphology of HPC electrospun at a concentration of 15% $w/v$ .

### 5.3.1.6 Cellulose acetate

Cellulose acetate (CA) electrospun as a 5% $w/v$  solution demonstrated very random and erratic deposition of bead-like particles with the presence of some fibres. Blockage of the pipette tip was extremely frequent due to rapid evaporation of the solvent, and therefore prevented any further solution from being electrospun. Microscopic analysis revealed that some fibres were present with diameters of less than 1 $\mu\text{m}$ . However, these fibres demonstrated beaded defects as depicted in Figure 5.8. Furthermore, the fibres were not continuous in its length, and no three dimensional structure or matrix was obtained.

Microscopic and SEM analysis revealed that the particles deposited were extremely porous in nature, which can be attributed to rapid evaporation of the solvent, and varied drastically in both size (smaller particles ranging in 2-5 $\mu\text{m}$  in diameter and larger particles ranging from 100-300 $\mu\text{m}$  in diameter) and shape (spherical to elongated particles), with no clear pattern of deposition, where large amounts of deposition occurred in some regions while little or no deposition occurred in other areas. CA was therefore not included in further electrospinning investigations.

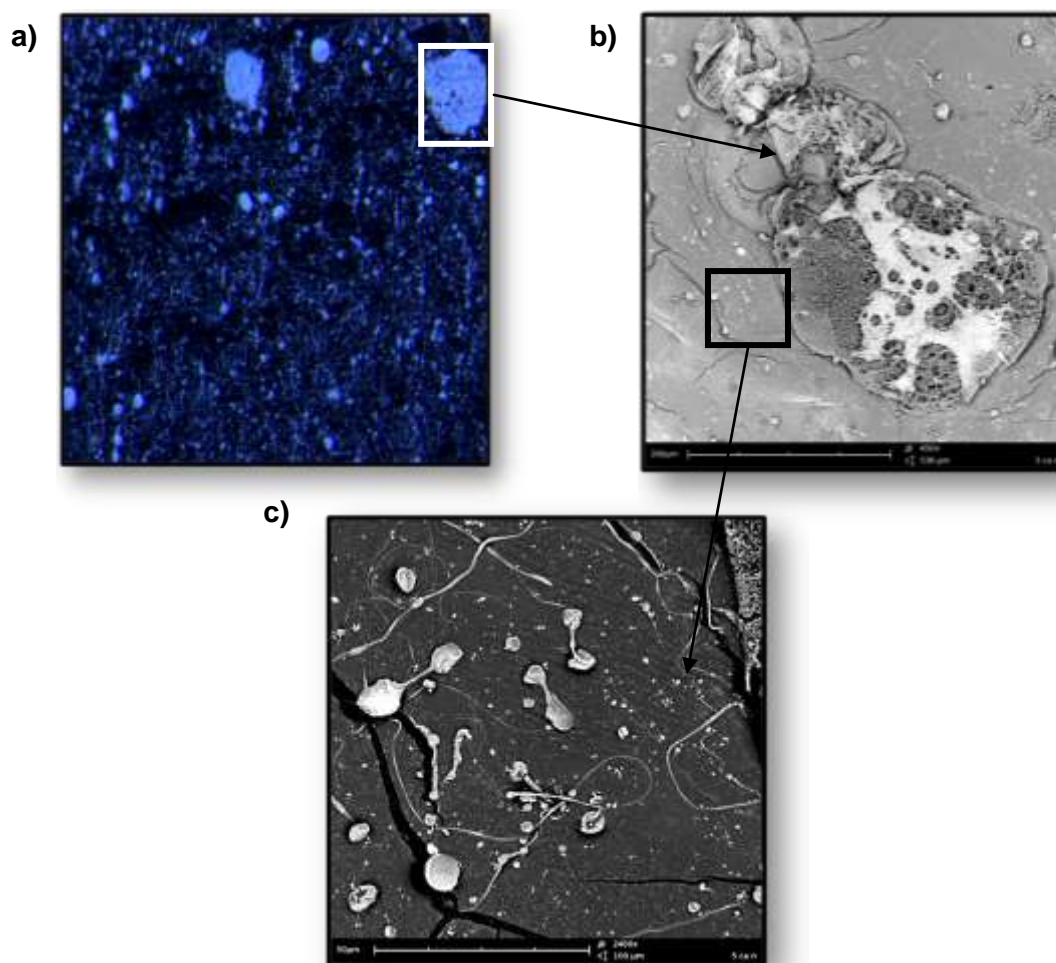


**Figure 5.8:** a) Microscopic; and scanning electron micrographic analysis at magnifications of b) 445x and c) 2400x depicting the surface morphology of CA electrosun at a concentration of 5%<sup>w/v</sup>.

### 5.3.1.7 Cellulose acetate phthalate

A larger degree of electrospaying rather than electrospinning occurred with the 5%<sup>w/v</sup> solution of cellulose acetate phthalate (CAP) as depicted in Figure 5.9a-b. The particles deposited were extremely porous, with the larger particles ranging in diameters of 30-60 $\mu\text{m}$ , while the smaller particles possessed diameters of <10 $\mu\text{m}$ . Increasing the

concentration to 10%<sup>w/v</sup> caused some degree of fibre deposition as illustrated in Figure 5.9c-d while a reduction in the larger particle size to 15-30 $\mu$ m was observed. The fibres however, were not continuous in length and erratically deposited. The quantity of fibres deposited was not sufficient to ensure adequate drug-loading and therefore, an increase in the polymer concentration was attempted to obtain greater quantities of fibres. However, these solutions were too viscous to electrospin and blockages occurred almost instantaneously. Furthermore, electrospinning of CAP failed to produce the three-dimensional structure required for drug delivery applications. Further electrospinning investigations employing CAP were thus absolved.

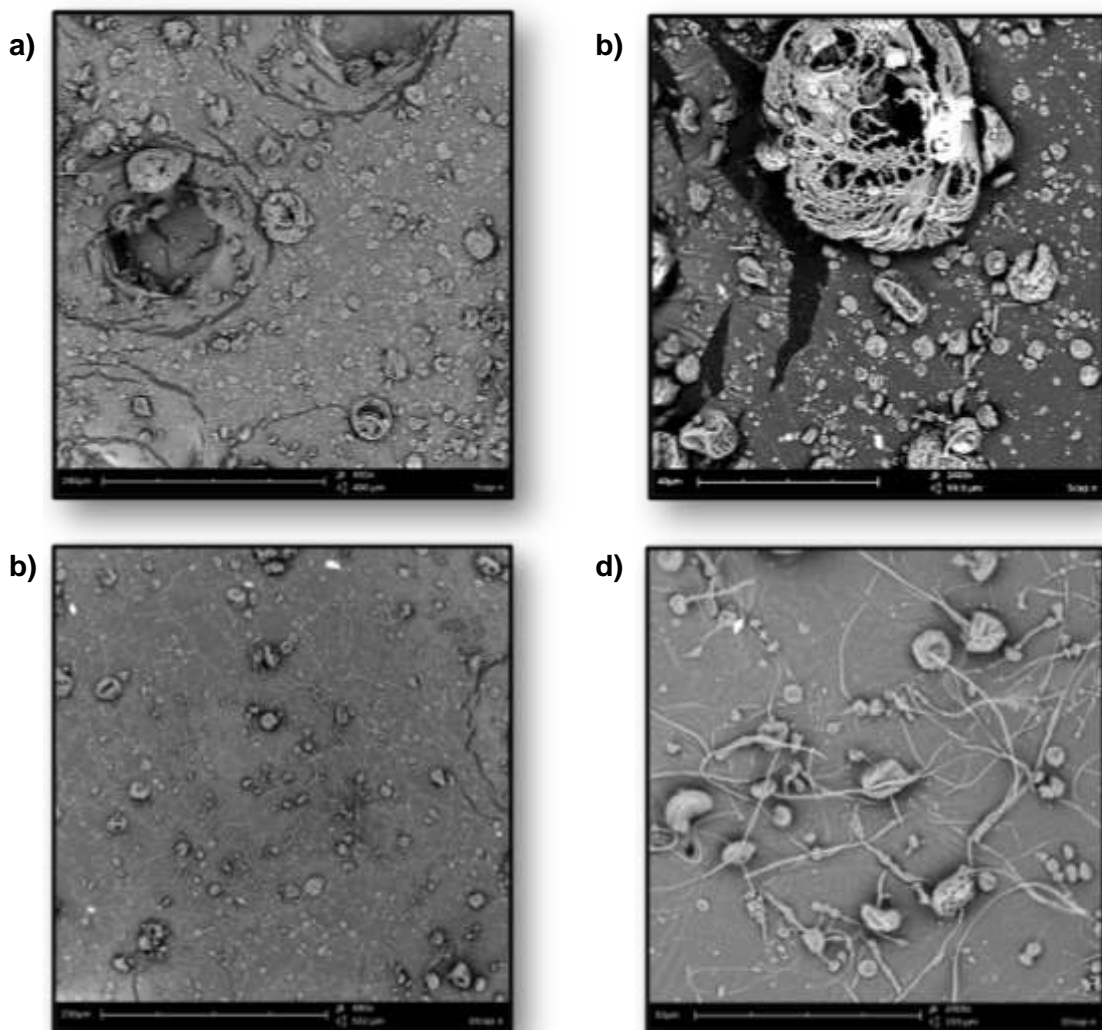


**Figure 5.9:** Scanning electron micrographic analysis depicting the surface morphology of the 5%<sup>w/v</sup> CAP at magnifications of a) 495x and b) 2400x; and 10%<sup>w/v</sup> CAP at magnifications of c) 480x and d) 2400x.

### 5.3.1.8 Eudragit® RS 100

Electrospinning of a 30%<sup>w/v</sup> solution of Eudragit® RS 100 was extremely rapid and erratic, producing a highly porous, three dimensional matrix with a ‘candyfloss’ appearance. Although electrospinning was rapid, blockages tended to occur often, halting the electrospinning process intermittently. The resultant matrix was extremely brittle and prone to breakage. Microscopic and SEM analysis (Figure 5.10) revealed that the fibres produced were flat and ribbon-shaped (due to inadequate drying prior to deposition), with a very wide diameter distribution of 2-50µm. The fibres appeared to have a crystalline appearance, which may be attributed to the brittle nature of the matrix. Alterations to the solution or processing parameters provided no further improvement in fibre formation. Eudragit® was thus not employed in any further studies.

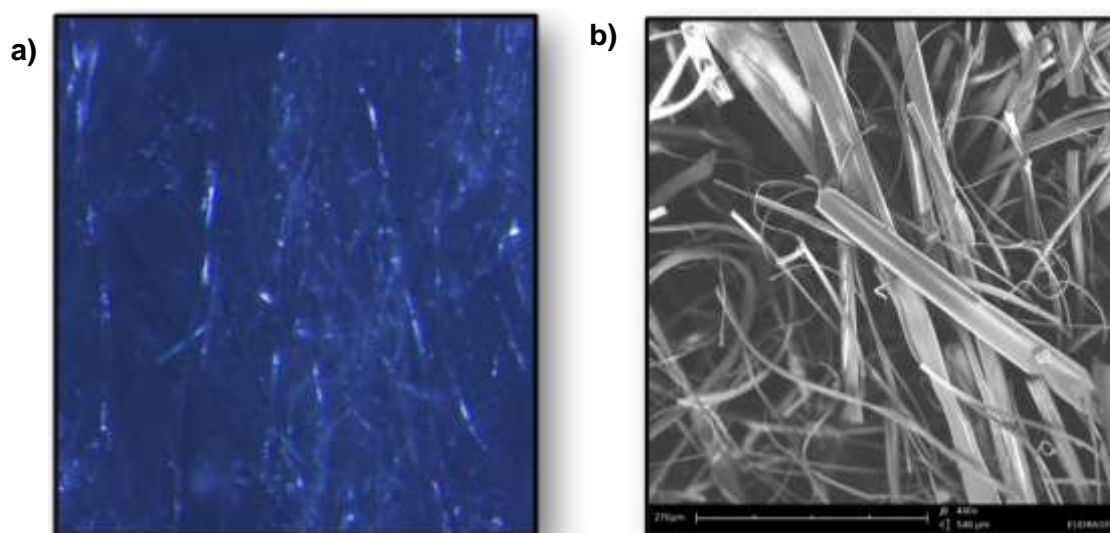


**Figure 5.10:** a) Microscopic analysis and b) scanning electron micrograph at a magnification of 440x depicting the surface morphology of electrospun Eudragit® RS 100 at a 30%<sup>w/v</sup> solution.

### 5.3.1.9 Poly(vinyl alcohol)

Electrospinning of poly(vinyl alcohol) (PVA) proved to be the most successful in producing a uniform and consistent three dimensional matrix. The electrospinning procedure was rarely halted by blocking of the pipette tip. An optimal concentration range of 7-12%<sup>w/v</sup> of PVA for electrospinning was identified, with a 10%<sup>w/v</sup> solution providing the most consistent nanofibrous matrix. The matrix was relatively consistent and densely packed. Electrospinning for periods of 3-5 hours produced an adequate quantity of fibres in the form a nanofibrous matrix. The matrix was relatively easy to handle, and did not disintegrate easily when handled. Furthermore, fibres were successfully produced, regardless of alterations in the solution or processing parameters. Therefore PVA was

identified as the most suitable and versatile polymer to be employed in the development of the drug-loaded nanofibrous matrix. Scanning electron microscopic analysis revealed that thin, cylindrical, continuous and uniform fibres were deposited as depicted in Figure 5.11. There was however, deposition of some large, wet droplets which caused fusing of the nanofibres in certain regions, therefore necessitating minor adjustments to the solution and/or processing parameters. The fibre diameter was determined to be within a range of 400nm.

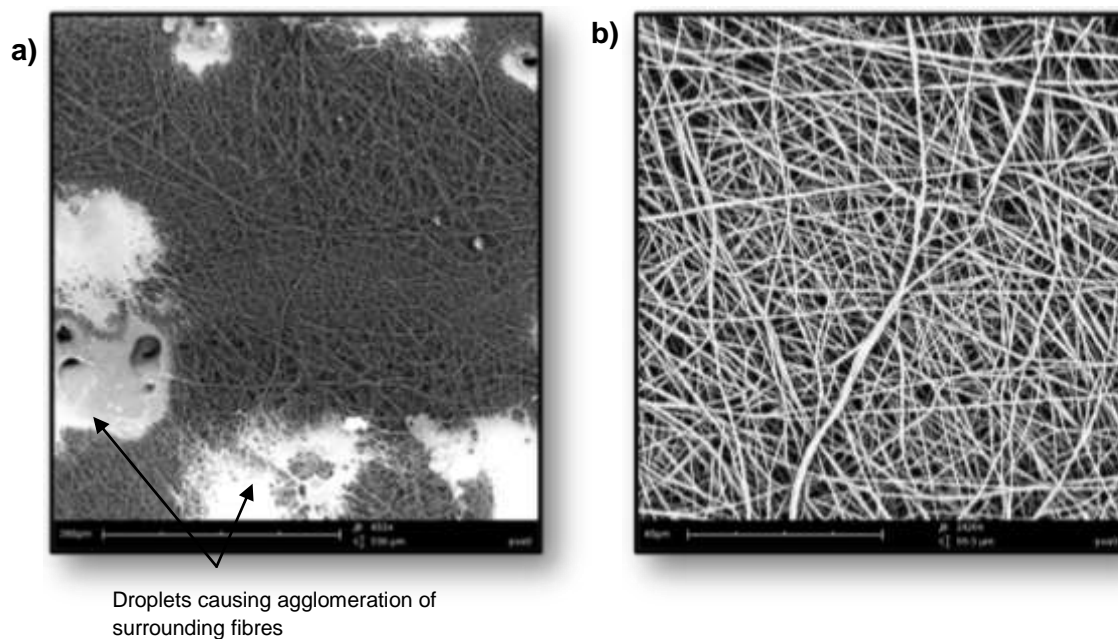


**Figure 5.11:** Scanning electron micrographs at magnifications of a) 455x and b) 2420x depicting the surface morphology of PVA electrospun at a 10%<sup>w/v</sup> concentration.

#### 5.3.1.10 Poly(ethylene oxide)

Attempts at electrospinning of poly(ethylene oxide) (PEO) solutions at concentrations of 3, 4 and 5%<sup>w/v</sup> were successful in the production of three dimensional nanofibrous matrices. However, fibres were deposited in an inconsistent manner, with some areas of larger fibre accumulation than others. In comparison to electrospinning of PVA solutions, there was a greater frequency in blockages occurring which necessitated manual removal before electrospinning could proceed. Furthermore, the quantity of the electrospun quantity obtained for the duration of electrospinning of a 3%<sup>w/v</sup> or 5%<sup>w/v</sup> PEO solution was not feasible for scale-up procedures. However, a 4%<sup>w/v</sup> solution produced a sufficient quantity of fibres during the electrospinning procedure. The resultant matrix was, nevertheless, extremely prone to disintegration when being handled for further processing. Scanning electron microscopic analysis (Figure 5.12) revealed that only the 5%<sup>w/v</sup> produced a nanofibrous matrix containing fibres with consistent diameters of 200-

300nm. There was a notable absence of bead defects and droplet deposition in the resultant matrix, resulting in the production of a uniform and consistent three-dimensional nanofibrous matrix.

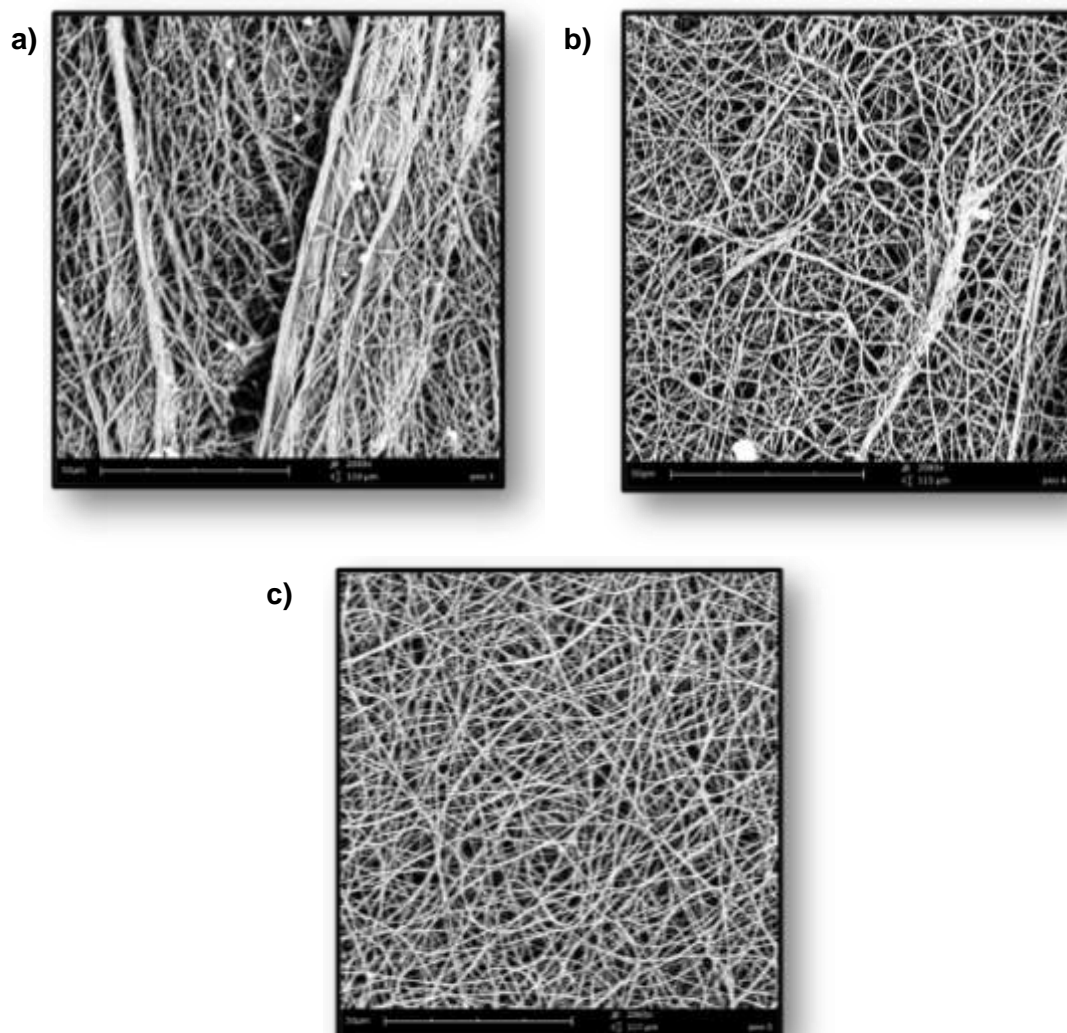


**Figure 5.12:** Scanning electron micrographs depicting the surface morphology of PEO electrospun at concentrations of a) 3%<sup>w/v</sup> at a magnification of 2040x; b) 4%<sup>w/v</sup> at a magnification of 2080x and c) 5%<sup>w/v</sup> at a magnification of 2060x.

### 5.3.2 Calibration curves for UV spectrophotometric determination of DPH

Figure 5.13 displays the calibration curve obtained for DPH in PBS (pH 1.2; 37°C), with an  $R^2$  value of 0.998, demonstrating good linearity, and the equation determined as  $y=1.304x$ .

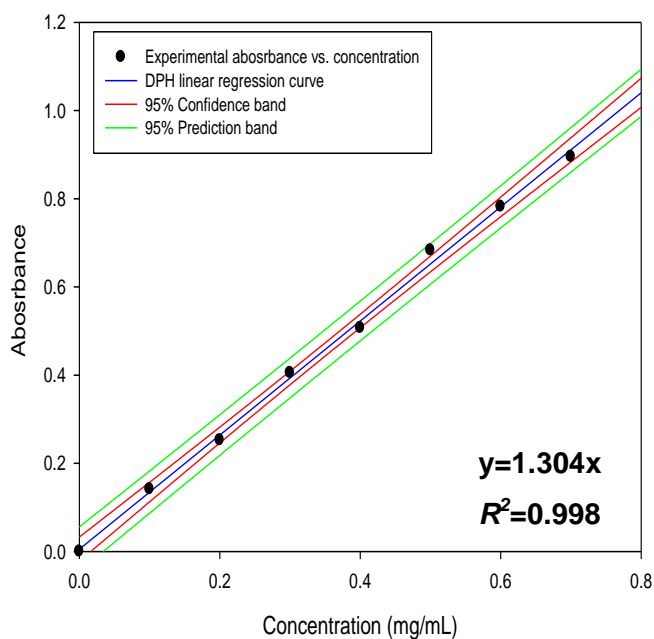


**Figure 5.13:** Diphenhydramine HCl calibration curves in PBS (pH 1.2 at 37°C).

### 5.3.3 Drug entrapment efficiency of electrospun nanofibres

Studies indicated that the DEE value was considerably higher in PVA nanofibres (93.5±2.12%) as compared to PEO nanofibres (54±1.41%) (Figure 5.14), thus indicating that PVA possessed a greater potential for entrapping DPH due to its hydrophilic nature. Furthermore, high drug entrapment was achieved with a single step drug-loading and electrospinning process, identifying the method of drug incorporation suitable for scale-up purposes.

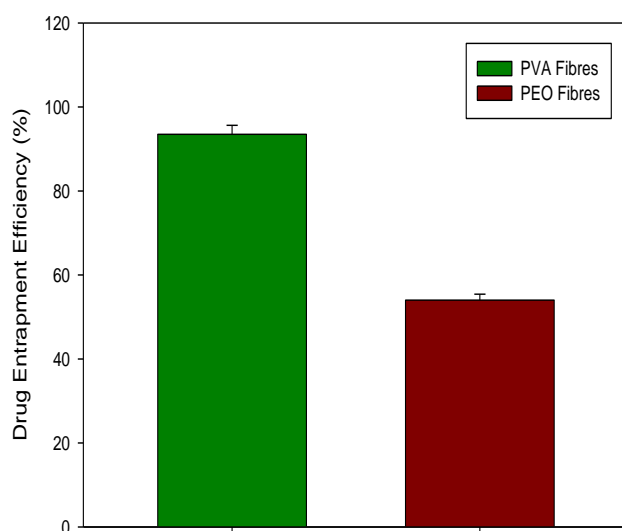


**Figure 5.14:** Comparison of Diphenhydramine HCl entrapment efficiency within PVA and PEO nanofibres.



Following the identification of PVA possessing superior DEE properties, it was determined the PVA would be selected as a suitable polymer for electrospinning. Granted, some droplets were observed within the nanofibrous matrix; however, minor adjustments to the solution and or processing parameters can be made to reduce such defects. Although electrospinning of PEO produced uniform nanofibres, the resultant matrix demonstrated poorer drug entrapment properties, while the matrix possessed inferior physical characteristics (i.e. disintegrated when being handled); thus mitigating any further studies employing PEO for electrospinning.

## **Part II: Improving the electrospinnability of poly(vinyl alcohol) solutions with the incorporation of excipients**

### **5.4 Materials and Methods**

#### **5.4.1 Materials**

All electrospinning experiments conducted employed the polymer PVA (Sigma Aldrich, Milwaukee, WI, USA), with a typical average molecular weight ( $M_w$ ) of 146000-186000 and degree of hydrolysis of 87-89%. Isoniazid (INH) and rifampicin (RIF) purchased from Sigma (Sigma Aldrich Chemie GmbH, Steinheim, Germany) were utilized as the model drugs to determine drug entrapment and drug release. Excipients investigated for improving PVA electrospinning included silicone antifoaming agent (BDH, VWR International Ltd, London, UK); Tween<sup>®</sup> 80 (polysorbate) and Span<sup>®</sup> 80 (sorbitan oleate) uniLAB<sup>®</sup> (Merck Chemicals (Pty) Ltd, Wadeville, Gauteng, RSA); sodium chloride (NaCl,  $M_w=58.44\text{g/mol}$ ; Saarchem, Wadeville, Gauteng, South Africa); poly(ethylene oxide) (Polyox<sup>™</sup> WSR 205-NF grade) obtained from The Dow Chemicals Company, (Danbury, CT, USA); silicone antifoaming agent, Silicone, purchased from BDH (BDH, VWR International Ltd, London, UK and glycerol (Associated Chemical Enterprises (Pty) Ltd. Southdale, South Africa).

Hydrochloric acid (32%<sup>w/v</sup>), used to dissolve RIF, was purchased from Merck Chemicals (Merck Chemicals (Pty) Ltd, Wadeville, Gauteng, RSA). All chemicals utilised were of analytical grade and used without further purification. Phosphate buffered saline (PBS) was prepared using sodium hydroxide (NaOH,  $M_w=40.00\text{g/mol}$ ) and sodium chloride (NaCl,  $M_w=58.44\text{g/mol}$ ; Saarchem, Wadeville, Gauteng, South Africa), hydrochloric acid (HCl, 32%<sup>w/v</sup>) purchased from Rochelle Chemicals (Johannesburg, South Africa) and potassium dihydrogen phosphate ( $\text{KH}_2\text{PO}_4$ ,  $M_w=136.09\text{g/mol}$ ) obtained from Riedel-de

Haen (Sigma-Aldrich Laborchemikalein GmbH, Germany) in double-deionised water (Milli-Q System, Millipore, Bedford MA, USA).

#### **5.4.2 Preparation of PVA nanofibrous matrices by electrospinning**

Preliminary studies identified PVA as the most suitable polymer to be employed for the preparation of the nanofibrous matrices. Differing concentrations (6, 7, 8, 10 and 12%<sup>w/v</sup>) of PVA were dissolved in water. The clear PVA solution was thereafter electrospun according to the method depicted in *Section 5.2.2*. Briefly, a horizontal electrospinning setup was employed while the electrospun fibres were collected on an aluminium sheet connected to a grounded counter electrode. Electrospinning was carried out at ambient room conditions for periods ranging between 5-8 hours. The fibres were carefully removed from the aluminium collector, cut into 20x30mm dimensions and stored in air-tight containers, in the presence of a desiccant, until further testing was conducted.

#### **5.4.3 Influence of sodium chloride addition on the electrospinnability PVA**

Following the identification of the optimal concentration for PVA, the effects of sodium chloride (NaCl) addition on the electrospinnability of PVA was investigated. NaCl was incorporated to the PVA solution at a concentration of 2%<sup>w/v</sup> to investigate the effects of conductivity variations on the electrospinning potential. The solution was then electrospun according to the method described in *Section 5.4.2*. The influence of NaCl on nanofibre formation was investigated by scanning electron microscopic analysis.

#### **5.4.4 Influence of Tween<sup>®</sup> 80 addition on the electrospinnability of PVA**

Lowering the surface tension of the PVA solution by incorporating surfactants mitigates the formation of bead defects (Table 5.2). Furthermore, it stabilizes the fibre jet, ensuring fibre, rather than droplet deposition. Tween<sup>®</sup> 80, a hydrophilic surfactant, was incorporated into the PVA solution at a concentration of 5%<sup>w/v</sup> and the resultant homogenous solution was electrospun according to the method depicted in *Section 5.4.2*. The influence of Tween<sup>®</sup> 80 on nanofibre formation was investigated by scanning electron microscopic analysis.

#### **5.4.5 Influence of Span<sup>®</sup> 80 addition on the electrospinnability of PVA**

Span<sup>®</sup> 80, a hydrophobic surfactant was incorporated into the PVA solution to determine the effect of a hydrophobic surfactant on the electrospinnability of PVA solutions as opposed to a hydrophilic surfactant. Span<sup>®</sup> 80 at a concentration of 5%<sup>w/v</sup> was initially dissolved in the solvent (water), followed by addition of PVA. When a homogenous solution was obtained, it was subject to the electrospinning method depicted in *Section*

5.4.2. The influence of Span<sup>®</sup> 80 on nanofibre formation was investigated by scanning electron microscopic analysis.

#### **5.4.6 Influence of silicone addition on the electrospinnability of PVA**

Addition of an antifoaming agent, silicone was also investigated for potentially improving the electrospinnability of the PVA solution. Silicone was added in a concentration of 0.1%<sup>w/v</sup> to the solvent, water, prior to PVA addition. When silicone was satisfactorily distributed throughout the solvent, PVA was then incorporated and the solution was agitated until a clear and homogenous solution was obtained. The silicone-PVA solution was electrospun according to the method described in *Section 5.4.2*. The influence of silicone addition on nanofibre formation was analyzed employing scanning electron microscopy.

#### **5.4.7 Influence of glycerol addition on the electrospinnability of PVA**

The effects of plasticizer addition on the electrospinnability of PVA solution was investigated by the addition of glycerol. Glycerol was added to the solvent (water) at a concentration of 5%<sup>w/v</sup>, followed by PVA addition. When a clear solution was obtained it was subject to electrospinning as detailed in *Section 5.4.2*. The influence of glycerol addition on nanofibre formation was analyzed employing scanning electron microscopy.

#### **5.4.8 Influence of drug incorporation on the electrospinnability of PVA**

Drug-polymer solutions were prepared by initially dissolving the drug in their respective solvents (RIF in 0.01M HCl; INH in water) at concentration of 2%<sup>w/v</sup>. PVA was then added and the solution was agitated. The homogenous drug-polymer solution was then subject to electrospinning as described in *Section 5.4.2*. The variations arising from the addition of drugs RIF and INH on the electrospinnability of PVA was identified and alterations to the solution and processing parameters were made accordingly. Various excipients including Tween<sup>®</sup> 80 (5%<sup>w/v</sup>) and silicone (0.1%<sup>w/v</sup>) were added to PVA solutions to improve the electrospinning procedure and outcome. The influence of drug addition on nanofibre formation was analyzed employing scanning electron microscopy.

#### **5.4.9 Elucidation of pertinent rheological properties of the polymer solutions employed in electrospinning**

The variations in the rheological properties of PVA solutions with excipient addition were determined with the use of a Modular Advanced Rheometer System (ThermoHaake MARS Rheometer, Thermo Fischer Scientific, Karlsruhe, Germany). The stress-strain rheological parameters of the polymer solution have an influence on electrospinning, and

are important factors when considering the desired characteristics of a solution to be electrospun. In particular, changes in the viscosity of the solution to be electrospun results in variations in nanofibre diameter. Samples were analyzed by placing the polymer solution on the sample stage and immersing the C35/1° titanium rotor in the polymeric solution while the temperature was maintained at 24°C. The shear rate was maintained at 100/s for 360 seconds and the viscosity was quantified for each solution.

#### **5.4.10 Determination of the electrical conductivity of the polymer solutions employed in electrospinning**

The variations in the electrical conductivity of the PVA solutions with excipient addition were determined with the use of an OAKTON® TDS Tester™ (Model UD-35661-70, Solon, OH, USA). The electrode was immersed in the polymer solution at 25°C and the electrical conductivity, measured in  $\mu$ Siemens, was determined.

### **5.5 Results and Discussion**

#### **5.5.1 Determination of the optimal PVA concentration for the electrospinning of three-dimensional nanofibrous matrices**

Solution concentrations of 8-10%<sup>w/v</sup> PVA exhibited the most desirable electrospinning properties and outcomes. The resultant matrices were uniform and consistent, and fibre diameters increased from 297.5±29.47nm to 345.00±30.41nm with an increase in PVA concentration from 8%<sup>w/v</sup> to 10%<sup>w/v</sup>. Minimal droplet formation was observed when electrospinning PVA solution concentrations within said range as opposed to other solution concentrations. Furthermore, the quantity of electrospun fibres produced within the same time frame was considerably greater than those produced at other concentrations, with a PVA concentration of 10%<sup>w/v</sup> producing the largest quantity of fibres that possessed the highest packing density. Scanning electron micrographic analysis (Figure 5.15) revealed that electrospinning of PVA concentrations less than that of 8%<sup>w/v</sup> caused a large degree of droplet formation within the nanofibrous structure due to the decreased incidence of chain entanglements. As a result, the degree of chain entanglements was not adequate to allow the fibre to maintain a fibre while travelling to the collecting surface. It was thus deduced that the viscosity of these solutions was not conducive to electrospinning. PVA solutions of concentrations greater than 10%<sup>w/v</sup> produced fibres that demonstrated a wide diameter distribution (less than 1 $\mu$ m to 5.5 $\mu$ m). Furthermore, fibre deposition was extremely haphazard and erratic, with areas of larger fibre deposition than others. Electrospinning of a 10%<sup>w/v</sup> PVA solution demonstrated the greatest success in the formation of a uniform and consistent three-dimensional

nanofibrous matrix, and was thus selected as the optimal concentration for the fabrication of the drug-loaded layer of the MMDDS.

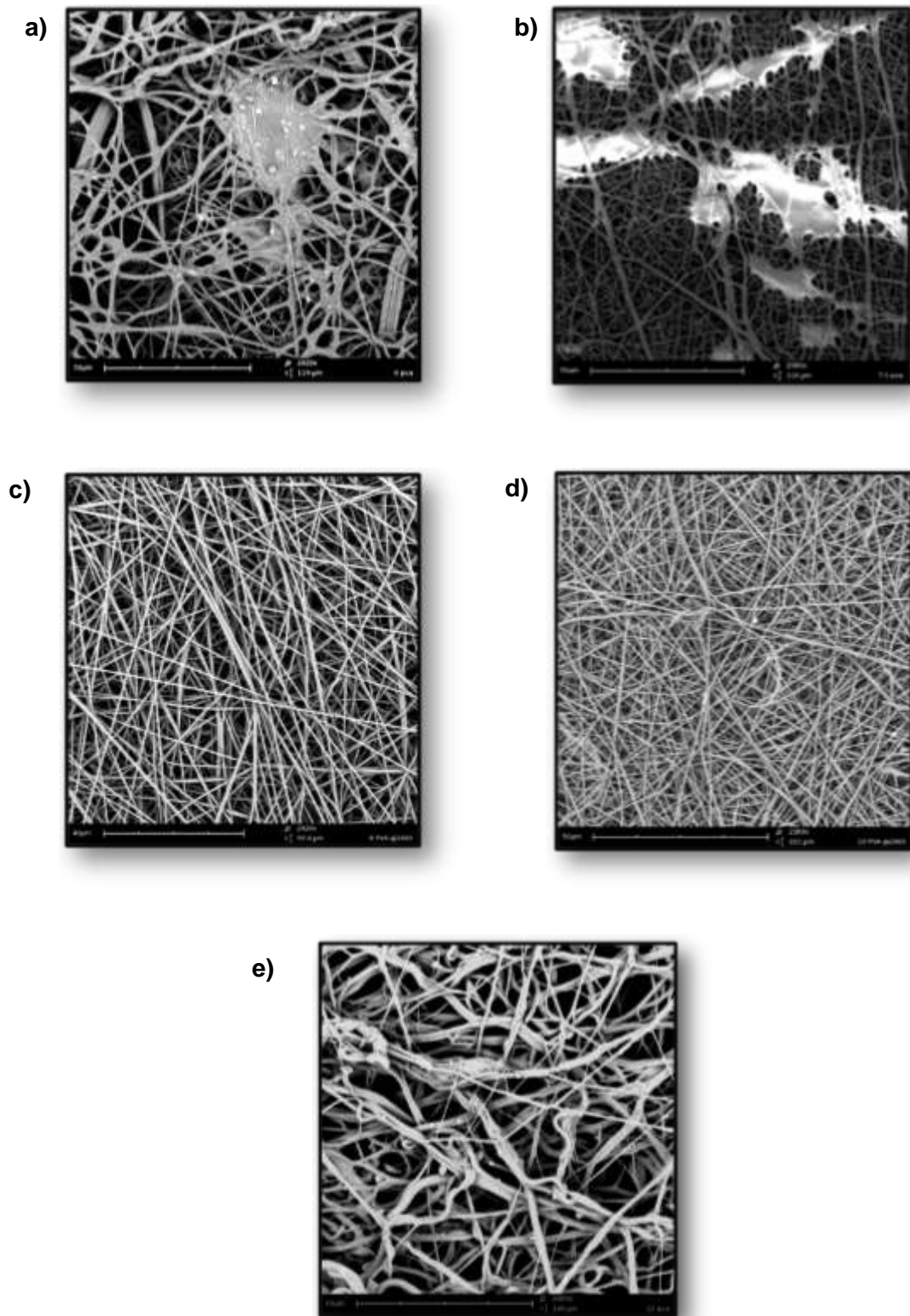


**Figure 5.15:** Scanning electron micrographs illustrating the surface morphology of PVA electrospun at concentrations of a) 6%<sup>w/v</sup>; b) 7.5%<sup>w/v</sup>; c) 8%<sup>w/v</sup>; d) 10%<sup>w/v</sup> and e) 12%<sup>w/v</sup> at magnifications of 2020x, 2080x, 2420x, 2380x, 2000x respectively.

### 5.5.2 Effect of excipient addition on the electrospinnability of PVA

Typically, addition of excipients caused undesirable alterations in the surface morphology of the PVA nanofibres. Some viscosity and electrical conductivity changes (Table 5.4) were also observed which caused the variations in the both the electrospinnability of the solution and surface morphology of the resultant nanofibrous matrix.

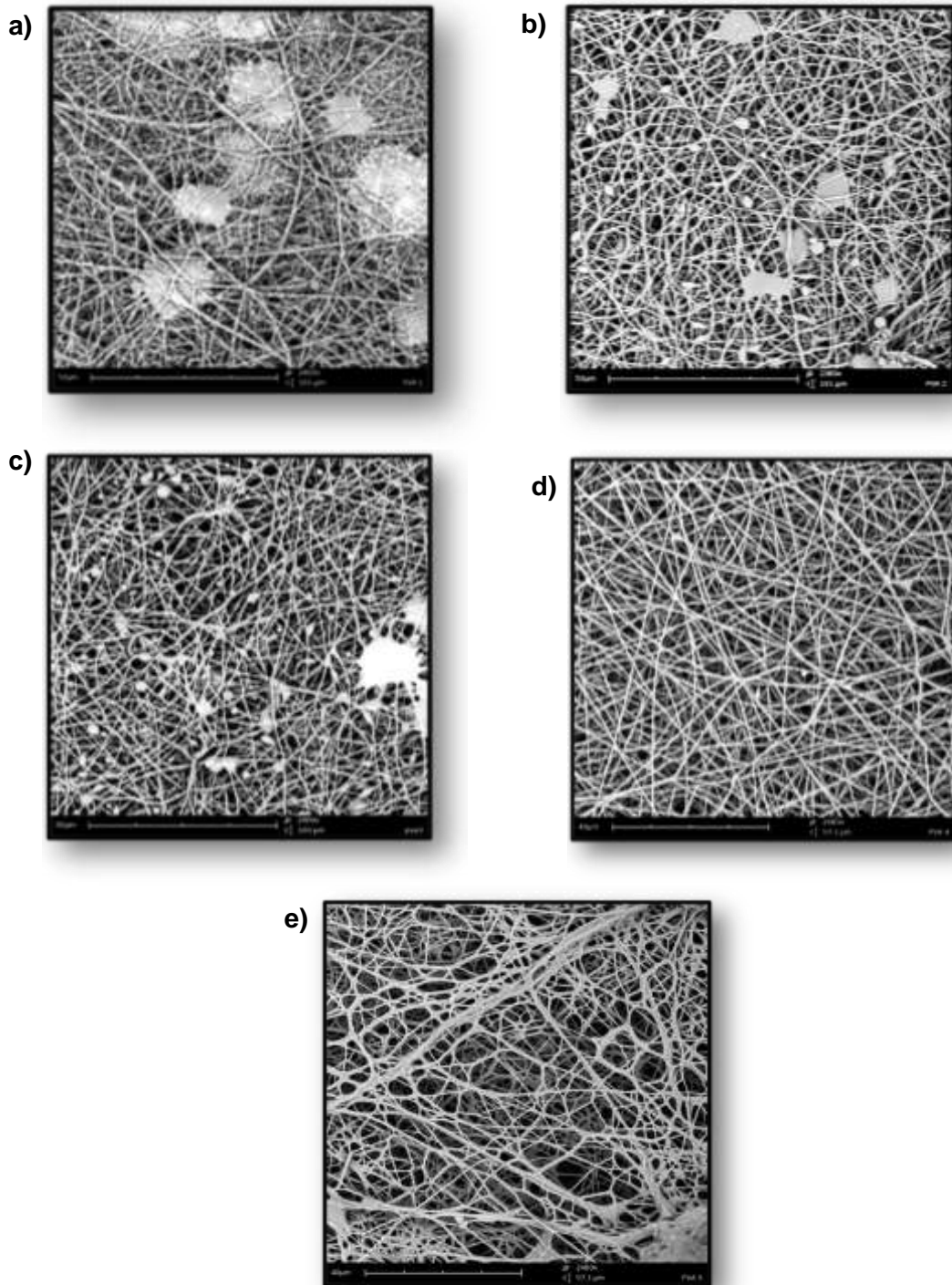


**Figure 5.16:** Scanning electron micrographs depicting the changes in surface morphology of PVA nanofibres with the addition of a) sodium chloride at 2400x; b) Tween® 80 at 2380x; c) Span® 80 at 2400x, d) silicone at 2480x and e) glycerol at 2480x.

**Table 5.4:** Effects of excipient addition on the viscosity of PVA solutions.

| <b>Electrospinning solution parameters</b>                       | <b>Viscosity at shear rate of 100/s (mPas)</b> | <b>Conductivity of Solution (<math>\mu</math>Siemens)</b> |
|--|--|---|
| 10% <sup>w/v</sup> PVA   | 830.53 $\pm$ 26.41                             | 635   |
| 10% <sup>w/v</sup> PVA + 2% <sup>w/v</sup> NaCl                  | 1137.29 $\pm$ 4.40                             | 484 (after a 1:100 dilution)                              |
| 10% <sup>w/v</sup> PVA + 5% <sup>w/v</sup> Tween <sup>®</sup> 80 | 351.59 $\pm$ 13.78                             | 740   |
| 10% <sup>w/v</sup> PVA + 5% <sup>w/v</sup> Span <sup>®</sup> 80  | 838.77 $\pm$ 8.08                              | 646   |
| 10% <sup>w/v</sup> PVA + 0.1% <sup>w/v</sup> Silicone            | 1098.46 $\pm$ 9.91                             | 692   |
| 10% <sup>w/v</sup> PVA + 5% <sup>w/v</sup> Glycerol              | 748.68 $\pm$ 3.93                              | 500   |

Attempts to increase the conductivity of the solution with the addition of salts caused an increase in the incidence of droplet formation (Figure 5.16a). Furthermore, fibre deposition was erratic, with varying degrees of accumulation. This can be attributed to the increase in the electric potential (Table 5.4) caused by the addition of salts, resulting in the formation of an unstable fibre jet during electrospinning. This instability is known to cause an increased incidence of defects such as beaded fibre morphology and droplet formation (Table 5.2). Furthermore, the resultant fibres typically possess a wide fibre distribution as illustrated in Figure 5.16a, which is related to the increase in the viscosity of the solution with NaCl addition (Table 5.4).

Both Tween<sup>®</sup> 80 and Span<sup>®</sup> 80 were investigated as potential non-ionic surfactants which may improve the electrospinnability of the PVA solution. Surfactants typically lower the surface and interfacial tension of the solution, preventing the formation of both droplets and beaded fibre morphology (Table 5.2). However, scanning electron micrographic analysis revealed the presence of bead defects and formation of droplets within the nanofibrous matrix with surfactant addition (Figure 5.16b-c), with a larger degree of defects occurring with Tween<sup>®</sup> 80 addition. Therefore the addition of the surfactants caused a reduction in the surface tension of the solution to a suboptimal level, causing the fibre jet to break up into droplets before reaching the collecting surface (Table 5.2).

Rheological and conductivity analysis of the surfactant incorporated solutions provides further evidence that surfactant addition caused detrimental effects on the electrospinnability of the solutions. As depicted in Table 5.4, the conductivity of the solution increased slightly with Tween<sup>®</sup> 80 addition, thus promoting fibre jet instability and hence the presence of defects increased. Furthermore, rheological analysis revealed that a dramatic decrease in the viscosity of the PVA solution occurred with the addition of Tween<sup>®</sup> 80 (from 830.53 $\pm$ 26.41 to 351.59 $\pm$ 13.78mPas) detrimentally affecting the electrospinnability of the solution. This resulted in a higher incidence of bead defects relative to Span<sup>®</sup> 80 addition, where an increase in the viscosity was observed. The

increase in the viscosity after the addition of Span<sup>®</sup> 80 can be related to the likelihood of the surfactant associating with the polymer molecules via electrostatic and/or hydrophilic/hydrophobic interactions, causing the notable increase solution viscosity (Goddard and Hannan, 1976; Manglik *et al.*, 2001; Jung *et al.*, 2005). As a result, the presence of a larger degree of chain entanglements causes the fibre jet to deposit as droplets and not continuous fibres (Table 5.2). Furthermore, fibre deposition was highly erratic and haphazard, with a reduced quantity of nanofibres collected.

In contrast, silicone addition improved the electrospinnability of the PVA solution by preventing both droplet deposition and the incidence of beaded fibre morphology. Furthermore, consistent, uniform fibres were deposited with random orientation, while the fibre diameters were maintained within a small range (350-400nm). A sufficient quantity of nanofibres were formed which were deposited as a consistent, uniform three dimensional matrix. Antifoaming agents, such as silicone are able to prevent foam formation through several forces resulting from its inherently low surface tension. To successfully displace foam, the antifoaming agent spreads over the liquid surface and displaces the foam stabilizing film surrounding the surface, while causing an increase in the film elasticity of foam (Kulkarni *et al.*, 1977; Pape, 1983).

Therefore, it can be postulated that during electrospinning, these forces may allow easier fibre jet formation by destabilizing the film surrounding the Taylor cone, thus increasing the rate of fibre deposition (i.e. less effort is required to induce and maintain the fibre jet, increasing fibre jet production). Furthermore, increasing the elasticity of the film surrounding the Taylor cone ensures that the film surrounding the fibre jet possess a higher elasticity, and when subject to whipping instability, forms fibres with uniform diameter distribution. In drug delivery systems, a uniform structure and size distribution are important factors to ensure that reproducible and consistent rates of drug release are achieved (Liu *et al.*, 2010). Therefore, the resultant nanofibrous matrix was deemed suitable for the delivery of RIF and INH, and further studies employed the use of silicone (0.1%<sup>w/v</sup>) in the formation of the drug-loaded nanofibrous matrices.

Glycerol addition resulted in the formation of an extremely porous matrix with an increased incidence of beaded fibre morphology. Addition of plasticizers such as glycerol typically breaks down any inter- and intra-molecular interactions of the polymer chains, hence facilitating their flow by decreasing the degree of chain entanglements. As a result, the viscosity of the solution is lowered (Pakraven *et al.*, 2011). Rheological evaluation of the glycerol incorporated solution reveals said viscosity decrease (from 830.53±26.41 to



748.68±3.93mPas), causing a detrimental effect on the electrospinnability of the PVA solution by decreasing the degree of chain entanglements which preventing the formation of a stable fibre jet. Furthermore, the decrease in the conductivity occurring after glycerol addition affected the whipping instability of the fibre jet. This in turn, affected the dimensions of the nanofibres formed (Table 5.2). The effects of both the reduction in viscosity and conductivity caused a non-uniform deposition of the nanofibres on the collecting surface, while an increased incidence of beaded defects was also observed.

### **5.5.3 Effect of drug incorporation on the electrospinnability of PVA solutions**

Electrospinning of a solution containing RIF (2%<sup>w/v</sup>) and PVA (10%<sup>w/v</sup>) was unsuccessful. Through qualitative assessment, the viscosity of the solution was observed to dramatically increase with drug incorporation. This viscosity increase detrimentally affected the electrospinning process, causing failure in fibre jet formation. When a fibre jet did form, it was highly unstable, with erratic deposition tendencies. Furthermore, a higher incidence of beaded defects was observed. PVA was thus reduced to a concentration of 8%<sup>w/v</sup> to ensure a lower viscosity, thus improving the electrospinnability of the RIF-PVA solution. Although the RIF-PVA solution was successfully electrospun (Figure 5.17b), it was observed that fibre deposition was highly erratic with a high incidence of beaded defects. As illustrated in Figure 5.17c, addition of Tween<sup>®</sup> 80 (5%<sup>w/v</sup>) dramatically improved the electrospinnability of the RIF-PVA solution, and uniform, consistent fibres were deposited with minimal beaded defects and droplet formation. A solution containing 10%<sup>w/v</sup> PVA and 2%<sup>w/v</sup> INH was successfully electrospun (Figure 5.17e). Silicone addition improved the electrospinnability of the solution by preventing droplet formation and producing a consistent and uniform three-dimensional structure. The quantity of nanofibres obtained was sufficient to ensure an adequate drug quantity was obtained.

The effects of incorporating drugs RIF and INH on the viscosity of the electrospinning solution as well as the tensile, fibre diameter distribution and drug entrapment efficiency of the resultant nanofibrous matrices are further detailed in *Chapter 6* of the present dissertation.

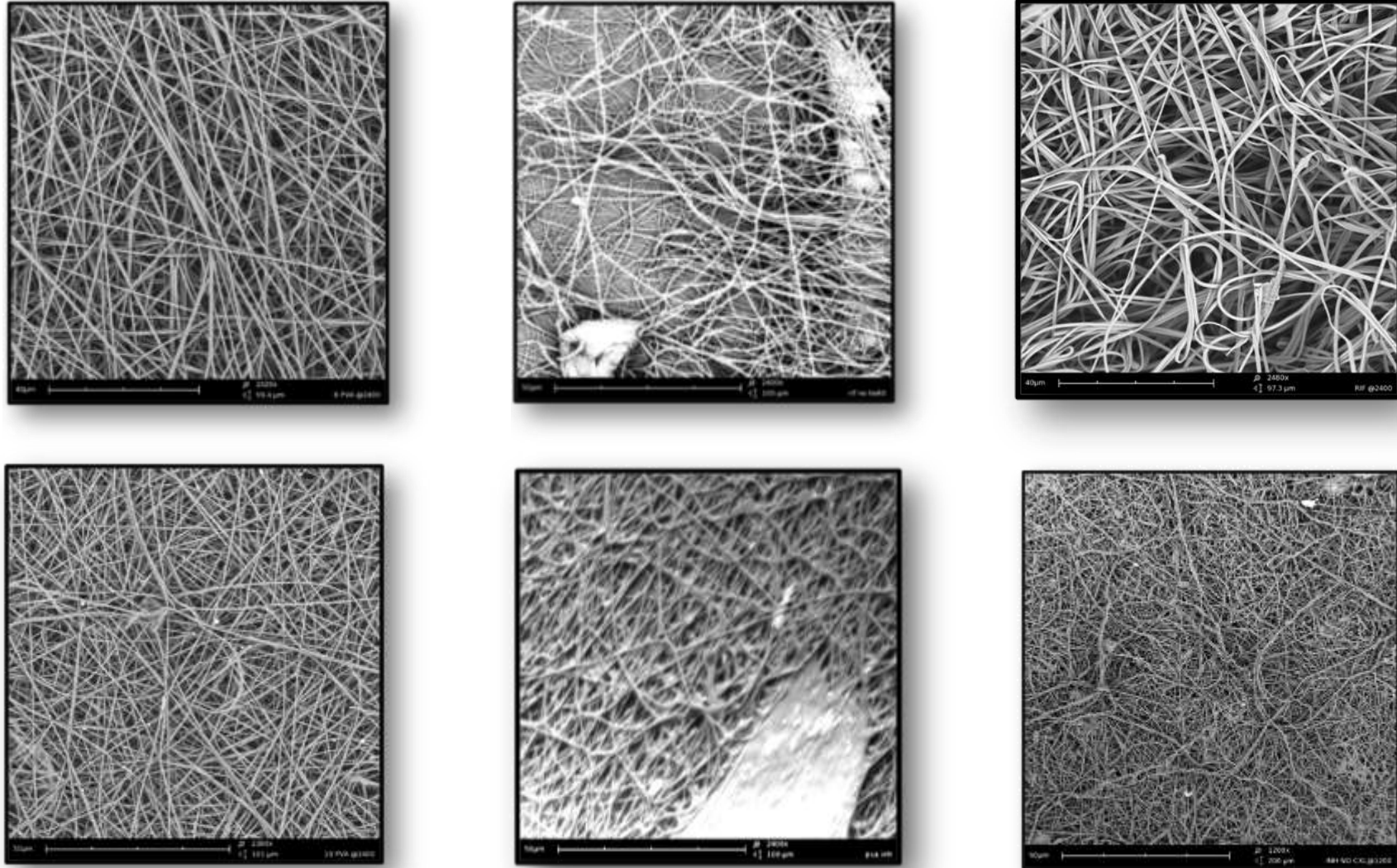


**Figure 5.17:** Scanning electron micrographs depicting the surface morphology of a) an 8%<sup>w/v</sup> PVA solution; b) an 8%<sup>w/v</sup> PVA solution containing 2%<sup>w/v</sup> RIF; c) an 8%<sup>w/v</sup> PVA solution containing 2%<sup>w/v</sup> RIF and 5%<sup>w/v</sup> Tween 80; d) 10%<sup>w/v</sup> PVA solution; e) a 10%<sup>w/v</sup> PVA solution containing 2%<sup>w/v</sup> INH, and f) a 10%<sup>w/v</sup> PVA solution containing 2%<sup>w/v</sup> INH and 0.1%<sup>w/v</sup> silicone at magnifications of 2420x, 2400x, 2480x, 2380x, 2400x, and 1200x respectively.

## 5.6 Concluding Remarks

Electrospun membranous systems have the advantage of increasing the surface area available for drug release due to the porous, nonwoven structure of the membranous system. Nanofibrous structures are produced with relative ease ensuring a single step drug entrapment process. Porosity, strength, surface functionality and fibre diameter, and hence drug release, can be manipulated by varying certain parameters during electrospinning, i.e. such as polymer and concentration or applied voltage (Frenot and Chronakis, 2003; Kim *et al.*, 2007).

Various polymers were investigated in order to develop the drug-loaded nanofibrous layer for application in the MMDDS. PVA and PEO demonstrated the most success in forming a relatively consistent three-dimensional nanofibrous matrix. Drug entrapment efficiency studies revealed that PVA demonstrated a greater efficiency for entrapping DPH molecules when electrospun. Therefore, based on both the electrospinnability and drug entrapment efficiency, PVA was identified as the most suitable polymer and further studies were therefore undertaken to improve the electrospinnability of the PVA solution. An optimal concentration range of 8-10%<sup>w/v</sup> for PVA electrospinning was identified, and any increase within the optimal range caused an increase in the nanofibre diameter. Ineffective solution parameters were also identified by determining the effects of excipient incorporation prior to electrospinning. Silicone was identified as the only excipient that improved the electrospinning characteristics of the PVA solution by minimizing both bead defects and the deposition of droplets. A RIF-PVA (2-8%<sup>w/v</sup>) solution containing 5%<sup>w/v</sup> Tween<sup>®</sup> 80 was identified as the candidate formulation for the production of RIF-loaded nanofibrous matrices, while an INH-PVA solution (2-10%<sup>w/v</sup>) containing 0.1%<sup>w/v</sup> silicone was selected as a candidate formulation for the development of the INH-loaded nanofibres matrices to be incorporated in the MMDDS.

## CHAPTER 6

### FABRICATION, MODIFICATION AND CHARACTERIZATION OF THE DRUG-LOADED NANOFIBROUS MATRICES OF THE MULTI-COMPONENT MEMBRANOUS DRUG DELIVERY SYSTEM

---

#### 6.1 Introduction

Many synthetic and natural polymers have been investigated for their potential in developing electrospun drug delivery devices. Amongst these polymers includes poly(vinyl alcohol) (PVA), which has been widely investigated in the production of electrospun nanofibres intended for water filtration or solvent separation applications (Wang *et al.*, 2006), fuel cells (Lin *et al.*, 2010), tissue engineering (Kim *et al.*, 2008) and drug and protein delivery (Zeng *et al.*, 2005a). PVA is exploited for use in drug delivery due to its high hydrophilicity, ease of processing, good mechanical and thermal stability, high biocompatibility, and its non-toxic and biodegradable nature (Koski *et al.*, 2004). This chapter focuses on the use of PVA nanofibres as potential drug delivery devices, for the prolonged release of model drugs RIF and INH.

Depending on the processing parameters, electrospun PVA fibres may dissolve instantly upon contact with aqueous mediums. As a result, there has been limited use of electrospun PVA nanofibres in biomedical applications and in particular, controlled drug release systems (Liu *et al.*, 2009; Cai *et al.*, 2010). However, nanofibres can be modified after the electrospinning procedure through various post-treatments to alter the physicochemical properties of the nanofibres or to functionalize nanofibre surfaces to provide various functionalities (Yu *et al.*, 2009b). Several studies have investigated the potential of crosslinking PVA membranes post-electrospinning, thereby producing a structure with poorer solubility characteristics and increased mechanical properties, which is ideal for both water filtration systems and biomedical devices (Bolto *et al.*, 2009; Liu, *et al.*, 2009; Tang *et al.*, 2010).

Glutaraldehyde (GA) solutions are commonly used to crosslink PVA, thereby retarding dissolution in physiological fluids. The mechanism of crosslinking (Figure 6.1) involves the chemical bonding of the hydroxyl groups present in PVA with the aldehyde groups of GA. A strong acid acts as a catalyst in this reaction (Tang *et al.*, 2010). However, GA is highly toxic to physiological tissues and therefore post-treatment and other methods of detoxification are required to prevent the harmful effects of residual GA. A study by

Ramires and Milella (2002) confirmed that crosslinking PVA using GA vapours produced membranes with no residual GA. This allows for safer alternative in producing a biocompatible crosslinked PVA intended for biomedical applications without necessitating post detoxification processes (Ramires and Milella, 2002). Many studies have been performed investigating the potential applications of GA vapour-induced crosslinking of polymers and are summarized in Table 6.1.

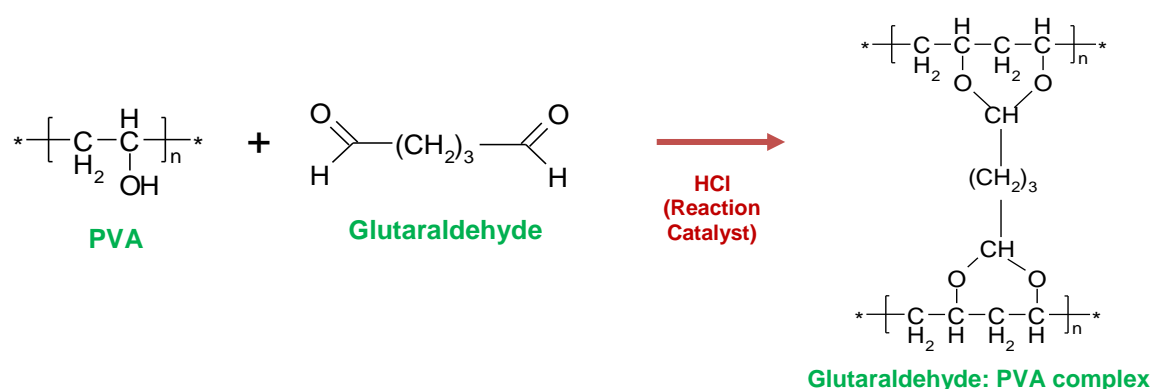


**Figure 6.1:** Crosslinking reaction occurring between PVA and Glutaraldehyde in the presence of HCl.

**Table 6.1:** Polymers crosslinked with GA vapours and their intended application.

| <b>Substrate crosslinked</b>                    | <b>Intended application</b>                             | <b>Reference</b>              |
|---|---|-------------------------------|
| Hard and Soft Gelatin Capsules                  | Modified capsules for DD                                | Meyer <i>et al.</i> , 2000    |
| PVA-HA and PVA-GEL membranes                    | Biocompatibility assessments                            | Ramires and Milella; 2002     |
| Electrospun PVA membrane                        | Investigation of enzyme (cellulase) immobilization (TE) | Wu <i>et al.</i> , 2005       |
| Electrospun PVA scaffolds                       | UF membranes  | Wang <i>et al.</i> , 2006     |
| Electrospun Gelatin fibres                      | Biomedical Applications particularly TE, WH and DD      | Zhang <i>et al.</i> , 2006c   |
| Electrospun PLGA, PLLA, PCL, and PLCL scaffolds | Vascular grafts in TE                                   | Lee <i>et al.</i> , 2007      |
| Electrospun COL-GAG scaffold                    | TE Scaffolds  | Zhong <i>et al.</i> , 2007    |
| Electrospun CHT-PLA mats                        | WD and WH applications                                  | Ignatova <i>et al.</i> , 2009 |
| Electrospun PAN/HEC membranes                   | UF membranes  | Zhang <i>et al.</i> , 2009    |
| Electrospun CHT-SF composites                   | WD and WH applications                                  | Cai <i>et al.</i> , 2010      |

*PVA: Polyvinyl alcohol; HA: Hyaluronic acid; GEL: Gellan; PLGA: Poly (D,L-lactide-co-glycolide); PLLA: poly(L-lactide); PCL: poly(ε-caprolactone); PLCL: poly(D,L-lactide-co-ε-caprolactone); COL: Collagen; PAN/HEC: polyacrylonitrile/hydroxyethyl cellulose; CHT: Chitosan; PLA: Poly[(L-lactide)-co-(D,L-lactide)]; SF: Silk Fibroin; TE: Tissue Engineering; WH: Wound Healing; WD: Wound dressing; DD: Drug Delivery; UF: Ultrafiltration; GAG: glycosaminoglycan*

## 6.2 Materials and Methods

### 6.2.1 Materials

All electrospinning experiments conducted employed the polymer PVA (Sigma Aldrich, Milwaukee, WI, USA), with a typical average molecular weight ( $M_w$ ) of 146000-186000 and degree of hydrolysis of 87-89%. Isoniazid (INH) and rifampicin (RIF) purchased from Sigma (Sigma Aldrich Chemie GmbH, Steinheim, Germany) were utilized as the model drugs to determine drug entrapment and drug release. An antioxidant, ascorbic acid (Sigma Ultra, Sigma Aldrich, St Louis, MO, USA), was incorporated in the nanofibres to prevent degradation of RIF. An antifoaming agent, Silicone, purchased from BDH (BDH, VWR International Ltd, London, UK) was utilized to enhance electrospinning of INH-loaded nanofibres while Tween<sup>®</sup> 80 uniLAB<sup>®</sup> (Merck Chemicals (Pty) Ltd, Wadeville, Gauteng, RSA) was used to improve the electrospinnability of RIF-loaded nanofibres. Hydrochloric acid (32%<sup>w/v</sup>), used to dissolve RIF, was purchased from Merck Chemicals (Merck Chemicals (Pty) Ltd, Wadeville, Gauteng, RSA). Glutaraldehyde Solution Grade II 25%<sup>w/v</sup> was purchased from Sigma Aldrich Co (St Louis, MO, USA). All chemicals utilised were of analytical grade and used without further purification. Water was purified and deionised using an Elix 5UV Millipore Filter.

### 6.2.2 Electrospinning of drug-loaded nanofibres

Drug solutions were prepared at ambient room conditions in their respective solvents at concentrations illustrated in Table 6.2. When a clear and homogenous drug solution was obtained, the antioxidant, ascorbic acid was added. The antioxidant-drug solution was then further agitated to produce a homogenous solution, followed by the addition of silicone/Tween<sup>®</sup> 80. Lastly PVA was incorporated into the solution in its respective concentrations. The homogenous drug-polymer solution was then electrospun as follows: The electrospinning setup, as illustrated in Figure 5.2, involved applying 20kV, supplied by a Glassman High Voltage, INC (High Bridge, NJ, USA) to the drug-polymer solutions via a copper rod. The drug-polymer solution, placed in 5mL Goldline glass pipettes, was mounted at distances of 21-28cm from the collecting surface. The solution was fed through a capillary size of  $\pm 1.2$ mm from a horizontal electrospinning setup, with the capillary being angled at 10°-11.5° from the horizontal surface. The electrospun fibres were collected on an aluminium sheet connected to a grounded counter electrode. Electrospinning was carried out at ambient room conditions for periods ranging between 5-8 hours. The fibres were carefully removed from the aluminium collector and stored in air-tight containers, in the presence of a desiccant, until further processing was carried out.

**Table 6.2:** Electrospinning parameters of INH- and RIF-loaded nanofibres.

| <b>Parameters</b>  | <b>RIF-loaded nanofibres</b>               | <b>INH-loaded nanofibres</b>                       |
|--|--|--|
| <b>Solution Parameters</b>   |  |  |
| PVA Concentration  | 8% <sup>w/v</sup>                          | 10% <sup>w/v</sup>                                 |
| Drug concentration   | 2% <sup>w/v</sup>                          | 2% <sup>w/v</sup>                                  |
| Solvent  | Weak HCl solution                          | Deionised water                                    |
| Surfactant   | Tween <sup>®</sup> 80 at 5% <sup>w/v</sup> | None added   |
| Antioxidant  | Ascorbic acid at 1% <sup>w/v</sup>         | None added   |
| Anti-foaming agent   | None added                                 | Silicone anti-foaming agent (0.1% <sup>w/v</sup> ) |
| <b>Electrospinning Parameters</b>                                  |  |  |
| Voltage Supplied   | 20kV                                       | 20kV   |
| Distance between capillary tip and collecting surface ( <i>d</i> ) | 28cm                                       | 21-24cm  |
| Capillary size   | 1.2mm                                      | 1.2mm  |
| Capillary angle ( $\theta$ )                                       | 11.5°                                      | 10°  |

### 6.2.3 Modification of the drug-loaded nanofibrous matrices through crosslinking

Crosslinking was carried out in the presence of GA vapours. HCl (32%<sup>w/v</sup>), as a catalyst, was added to the GA solution on a 3:1 ratio of GA:HCl. The GA-HCl was placed in the lower portion of desiccant jars while accurately weighed samples of drug-loaded PVA nanofibres were suspended approximately 5cm over the solution using a fine mesh sieve. Formulations were crosslinked according to parameters illustrated Table 6.3. The system was kept closed to impart a vapour-rich environment as illustrated in Figure 6.2. Drug-loaded membranes were allowed to crosslink in the vapour-rich environment for periods ranging from 6 to 24 hours at ambient room conditions, and thereafter stored in airtight containers with the presence of a desiccant until further testing was performed.

**Table 6.3:** Crosslinking variables of non-drug and drug-loaded PVA nanofibres.

| <b>Formulation</b> | <b>Drug Concentration</b> | <b>PVA Concentration</b> | <b>Concentration GA:HCl (mL)</b> | <b>Time (hours)</b> |
|--------------------|---------------------------|--------------------------|----------------------------------|---------------------|
| 1                  | -                         | 10% <sup>w/v</sup>       | -                                | -                   |
| 2                  | INH : 2% <sup>w/v</sup>   | 10% <sup>w/v</sup>       | -                                | -                   |
| 3                  | INH : 2% <sup>w/v</sup>   | 10% <sup>w/v</sup>       | 15: 5                            | 24                  |
| 4                  | INH : 2% <sup>w/v</sup>   | 10% <sup>w/v</sup>       | 30:10                            | 12                  |
| 5                  | INH : 2% <sup>w/v</sup>   | 10% <sup>w/v</sup>       | 60: 15                           | 6                   |
| 6                  | -                         | 8% <sup>w/v</sup>        | -                                | -                   |
| 7                  | RIF : 2% <sup>w/v</sup>   | 8% <sup>w/v</sup>        | -                                | -                   |
| 8                  | RIF : 2% <sup>w/v</sup>   | 8% <sup>w/v</sup>        | 15: 5                            | 24                  |
| 9                  | RIF : 2% <sup>w/v</sup>   | 8% <sup>w/v</sup>        | 30:10                            | 12                  |
| 10                 | RIF : 2% <sup>w/v</sup>   | 8% <sup>w/v</sup>        | 60: 15                           | 6                   |

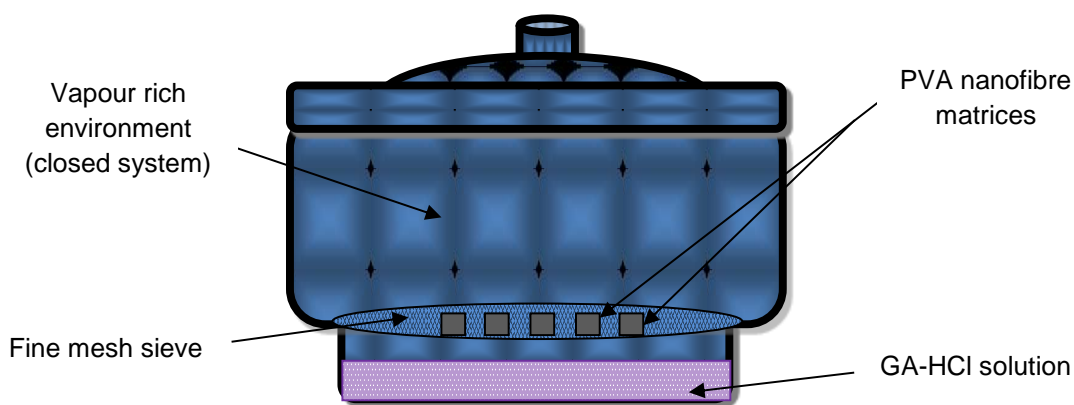


**Figure 6.2:** Schematic illustration of the crosslinking procedure of PVA nanofibre membranes.

#### 6.2.4 Construction of calibration curves for the UV spectroscopic determination of RIF and INH

A calibration curve for RIF and INH was conducted in PBS (pH 1.2 and pH 6.8 respectively) by analysing a known series of concentrations of the respective drug in PBS on a UV spectrophotometer (Lambda 25, UV/VIS Spectrometer, PerkinElmer®, Waltham, MA, USA). The content of RIF and INH was analyzed at wavelengths of 237 and 263nm. A linear curve was generated with the observed absorbance plotted on the y-axis and the corresponding concentrations (mg/mL) on the x-axis. With the intercept set at 0, the  $R^2$  values were determined to be 0.998 for RIF and 1.00 for INH.

#### 6.2.5 Determination of the Drug Entrapment Efficiency of PVA nanofibres

In order to determine the DEE of RIF- and INH-loaded PVA nanofibres, accurately weighed samples of INH- and RIF-loaded nanofibres were dissolved in 100mLs of phosphate buffered saline (PBS) (37°C) at pH 1.2 and 6.8 respectively. In order to ensure that the nanofibres were completely dissolved, the solution was subject to agitation with the Sonics Vibra Cell™ Sonicator (Sonics and Materials Inc, Newtown, CT, USA) for 15 minutes at a 60% amplitude. The drug content was analyzed by UV spectrophotometry (Lambda 25, UV/VIS Spectrometer, PerkinElmer®, Waltham, MA, USA) (parameters illustrated in Table 6.4) and computed from a standard linear curve of the drug in PBS. All tests were performed in triplicate (n=3) and presence of the polymer was taken into account. The DEE equation depicted in Section 5.2.5 was used to compute the DEE.

**Table 6.4:** Parameters employed to determine DEE of drug-loaded PVA nanofibres.

| Drug                  | RIF                       | INH                       |
|-----------------------|---------------------------|---------------------------|
| PBS                   | pH 1.2; 37°C              | pH 6.8; 37°C              |
| Wavelength            | 237nm                     | 263nm                     |
| Standard linear curve | RIF in PBS (pH 1.2; 37°C) | INH in PBS (pH 6.8; 37°C) |
| $R^2$ value           | $R^2=0.9998$              | $R^2=1.00$                |



### **6.2.6 *In vitro* drug release studies**

*In vitro* drug release studies were conducted using a six-station USP apparatus II (Erweka DT 700 GmbH Germany), in which a single nanofibrous membrane of known mass was placed within the vessel under a stainless steel ring mesh assembly. This prevents the paddle inflicting physical/mechanical damage to the nanofibrous matrices which can potentially alter the drug release characteristics, in addition to preventing any erratic fluctuation due to unstable hydrodynamics (Pillay and Fassihi, 2000). Each vessel contained 900mL of PBS at pH 6.8 or pH 1.2 for INH- and RIF-loaded nanofibres respectively. The PBS was heated to a temperature of 37°C prior to the addition of the nanofibrous membranes and the stainless steel ring mesh assembly. The apparatus was calibrated for a 12 hour run, and the rotating paddle method was selected with a rotational speed of 50rpm. Sampling occurred at hourly intervals and involved the drawing of 5mL of now drug incorporated solution from the dissolution vessel. An equal quantity of the removed buffer was replaced with fresh buffer to maintain sink conditions. Samples were then subject to UV spectrophotometry and drug quantity was determined using a standard calibration curve.

### **6.2.7 Influence of drug-loading and crosslinking on the surface morphology and network density of the nanofibrous membranes**

Surface morphology of the nanofibrous matrices were analyzed on a Phenom™ Microscope (FEI Company, Hillsboro, Oregon, USA). Samples were firmly mounted on aluminium stubbs with carbon tape. They were subject to a gold sputter coating under a vacuum of 0.1Torr with argon gas in a SPI-Module™ Sputter Coater and SPI-Module™ Control (SPI Supplies, Division of Structure Probe Inc., West Chester, PA, USA). Each sample required 90 seconds of coating to ensure complete coverage of the sample. Subsequent viewing was thereafter performed at various magnifications under the Phenom™ desktop scanning electron microscope. Different magnifications at 10kV were employed to view the overall and in-depth surface structure to qualitatively elucidate factors such as the nanofibre size range and density, as these factors affect drug release from the nanofibrous membrane system. Denser nanofibrous networks tend to entrap drug particles within its network structure and these molecules may only be released upon slow disentanglement of the network system.

### **6.2.8 Image processing using Mathematica™ 8.0**

SEM (.tif) images of electrospun nanofibres were processed using Mathematica™ 8.0 (Wolfram Research, Champaign, IL) using a sequential procedure of blurring, colorquantizing and generating an image histogram. Initially, the area of interest was

cropped to restrict image content to that of the scaffold. The whole analysis was performed on an HP Pavilion dv5-1102TU with an Intel Pentium Dual-Core (2.0 GHz, 3 GB RAM) running Microsoft Vista Basic.

#### **6.2.9 Determination of PVA:GA structural interactions as a result of nanofibre crosslinking with GA**

The vibrational molecular transitions of the non-crosslinked and crosslinked electrospun nanofibrous membrane systems were characterized for the attainment of important micro-structural data via an Attenuated Total Reflectance Fourier-Transform Infrared (ATR-FTIR) spectroscopy, recorded on a PerkinElmer<sup>®</sup> Spectrum 100 Series fitted with a universal ATR polarization accessory (PerkinElmer Ltd., Beaconsfield, UK). Spectra were recorded over the range of 4000-625cm<sup>-1</sup>, with a resolution of 4cm<sup>-1</sup> and 32 iterations. Furthermore, the FTIR spectra of the native polymer (PVA), and drugs RIF and INH were analyzed in relation to the electrospun and crosslinked formulations to determine whether the electrospinning or crosslinking procedure caused any structural changes or interactions between the drug and native polymer.

#### **6.2.10 Elucidation of pertinent rheological properties of the polymer solutions employed in electrospinning**

The rheological properties of PVA solutions at various concentrations were determined with the use of a Modular Advanced Rheometer System (ThermoHaake MARS Rheometer, Thermo Fischer Scientific, Karlsruhe, Germany). The stress-strain rheological parameters of the polymer solution have an influence on electrospinning, and are important factors when considering the desired characteristics of a solution to be electrospun. In particular, changes in the viscosity of the solution to be electrospun results in variations in nanofibre diameter. Samples were analyzed by placing the polymer solution on the sample stage and immersing the C35/1° titanium rotor in the polymeric solution while the temperature was maintained at 24°C. The shear rate was maintained at 100/s for 360 seconds and viscosity was quantified for each solution. The aforementioned shear rate was selected for comparative purposes only and a constant shear rate was selected to reduce sample variability.

#### **6.2.11 Determination of the tensile properties and Young's Modulus of crosslinked and non-crosslinked nanofibrous membranes**

Young's Modulus and other tensile properties of the crosslinked and non-crosslinked nanofibres were determined using the nanoTensile<sup>®</sup> 5000 (Hysitron Inc. Nanomechanical Test Instrument, Minneapolis, MN). The nanotensile (NT) apparatus was calibrated before

samples were tested to ensure accuracy. Samples, cut into approximately 2x15mm strips, were mounted on the specially designed NT mounting brackets as illustrated in *Chapter 4*, Figure 4.13. The brackets were held together with a rigid cardboard frame, aiding in sample alignment, and the samples were attached to the brackets using a rigid cyanoacrylate-based adhesive, thus holding the sample firmly in place during the test procedure. Samples were allowed to cure and accurate measurements of the sample width, thickness and length were recorded using digital callipers. The upper sample bracket was secured to the upper sample gripper of the NT head and the mass measured. The NT head was lowered and the lower sample bracket secured to the lower sample gripper on the NT stage. The mounting brackets were moved apart at a constant rate of displacement of 100 $\mu$ m/sec and the tensile properties of the sample were measured and recorded. The test was performed in triplicate (n=3).

#### **6.2.12 Static lattice atomistic simulations**

All modelling procedures and calculations, including energy minimizations in molecular mechanics, were performed using the HyperChem<sup>TM</sup> 8.0.8 Molecular Modeling System (Hypercube Inc., Gainesville, Florida, USA) and ChemBio3D Ultra 11.0 (CambridgeSoft Corporation, Cambridge, UK) on an HP Pavilion dv5 Pentium Dual CPU T3200 workstation. The structure of PVA (ten monomer units) was generated from standard bond lengths and angles employing polymer builder tools using ChemBio3D Ultra in its syndiotactic stereochemistry as 3D models and was saved in .skc file format readable to HyperChem<sup>TM</sup> 8.0.8. Structures of GA, INH and RIF were built up with natural bond angles as defined in the HyperChem<sup>TM</sup> software. The models were initially energy-minimized using MM+ force field and the resulting structures were again energy-minimized using the AMBER 3 (Assisted Model Building and Energy Refinements) force field. The conformers having the lowest energy were used to create the polymer-crosslinker and polymer-drug complexes. A complex of one molecule with another was assembled by disposing the molecules in a parallel way, and the same procedure of energy-minimization was repeated to generate the final models: PVA-PVA, PVA<sub>2</sub>-INH, PVA<sub>2</sub>-RIF and PVA<sub>2</sub>-GA<sub>3</sub>. Full geometry optimization was carried out in vacuum employing the Polak-Ribiere conjugate gradient algorithm until an RMS gradient of 0.001kcal/mol was reached. Force field options in the AMBER (with all hydrogen atoms explicitly included) and MM+ (extended to incorporate non-bonded cut-offs and restraints) methods were the HyperChem<sup>TM</sup> 8.0.8 defaults (Kumar *et al.*, 2011b).

## 6.3 Results and Discussion

### 6.3.1 Calibration curves for UV spectrophotometric determination of RIF and INH

Figure 6.3a displays the calibration curve obtained for RIF in PBS (pH 1.2; 37°C); and Figure 6.3b displays the calibration curve obtained for INH in PBS (pH 6.8; 37°C), with an  $R^2$  value of 0.9998 and 1.00 respectively. The regression equations were determined to be  $y=33.905x$  and  $y=29.947x$  for the RIF and INH calibration curves respectively.

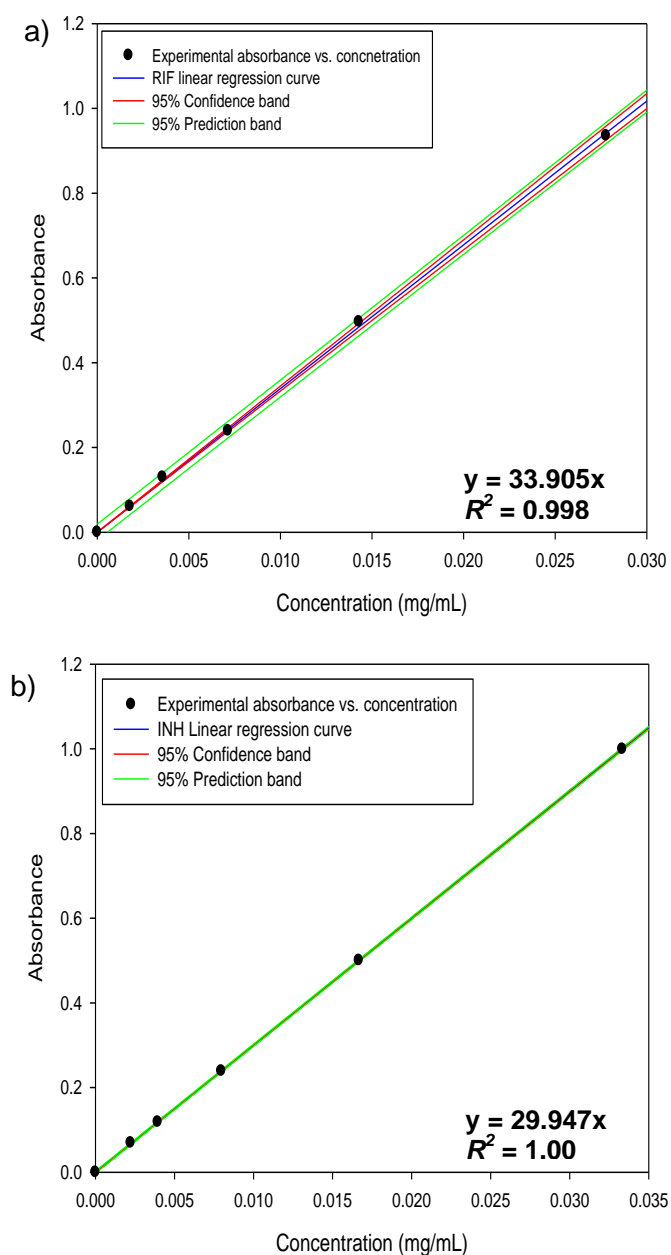


**Figure 6.3:** Constructed calibration curves of a) RIF in PBS (pH1.2; 37°C) at a wavelength of 237nm and b) INH in PBS at a wavelength of 263nm (pH 6.8; 37°C).

### 6.3.2 Drug Entrapment Efficiency (DEE) of PVA nanofibres

A drug entrapment value of  $98.77 \pm 1.384\%$  and  $95.07 \pm 1.988\%$  was calculated for the INH- and RIF-loaded PVA nanofibres respectively (Figure 6.4). DEE results indicate that drug-loading of nanofibres, as opposed to other nanoparticulate structures, is considerably higher. This can be attributed to the method of nanofibre formation, where electrospinning of the drug-polymer solution ensures that drug is entrapped within the nanofibres during fibre formation and therefore drug is embedded within the solid nanofibres. Various other nanoparticulate systems involve drug loading after the nanoparticulate structure is formed, and thus drug-loading is dependent on the diffusion of the drug through the nanoparticulate structure into the core. This results in variable drug-loading capacities between drugs of differing sizes and solubility. As RIF and INH have differing solubility's but similar DEE, it should be noted that DEE of PVA nanofibres is not determined by the solubility of the drugs, but rather through the process of electrospinning, and the parameters employed during this process.

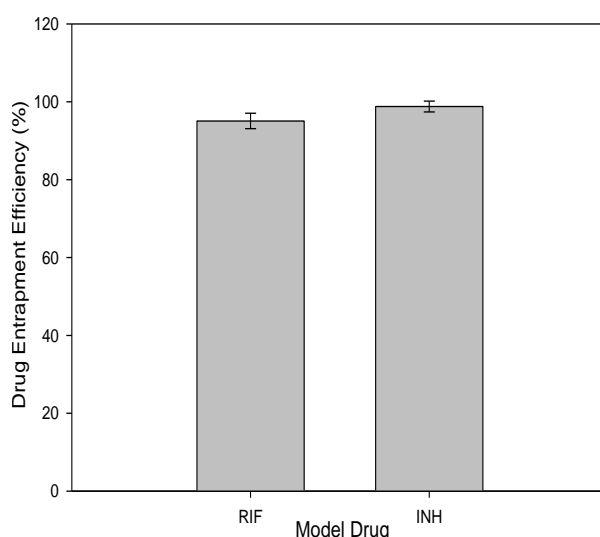


**Figure 6.4:** Graphical representation of the Drug Entrapment Efficiency of RIF- and INH-loaded nanofibres.

### 6.3.3 *In vitro* drug release from crosslinked nanofibrous matrices

Non-crosslinked nanofibrous matrices dissolve instantaneously upon contact with a dissolution medium. As a result, drug release from these matrices is immediate (Formulations 2 and 7). Vapour-induced crosslinking of the PVA fibres imparted water-insoluble properties on the fibrous network, resulting in slower drug release rates. Drug release from nanofibrous membranes is typically a biphasic process, with initial desorption of drugs from the fibre surface occurring alongside fast diffusion into the

aqueous phase (burst release), followed by solid-state diffusion of drug from within the solid nanofibres (slower release rate) (Leung and Ko, 2011).

The burst release of INH and RIF, demonstrated in all formulations investigated for drug release, can be attributed to the initial desorption and fast diffusion of drug from the nanofibre surface into the dissolution medium (Figure 6.5). This is followed by a reduced rate of drug release due to the solid-state diffusion of drugs through the solid PVA nanofibres. INH-loaded nanofibrous matrices demonstrated slower drug release over 12 hours in formulations crosslinked for longer durations, indicating that sufficient time is required to ensure adequate crosslinking of the PVA nanofibres. Formulation 3 demonstrated the most ideal drug release characteristics with  $81.11 \pm 2.35\%$  of the total drug being released in a controlled manner over 12 hours. Since a longer duration of crosslinking was required to ensure the most ideal release properties, it can be concluded that crosslinking time, rather than crosslinker quantity, was integral to modify nanofibrous matrices with appropriate degree of crosslinking required to achieve the desired drug release characteristics. The total quantity of drug release of Formulation 4 and Formulation 5 ( $94.95\% \pm 0.0011$   $98.653\% \pm 0.0086$  respectively) occurred at a relatively quicker rate than Formulation 1 (60% of drug was released by the third hour in Formulation 4 and 5 as compared to Formulation 3, where seven hours were required to release 60% of the total drug quantity). These findings further reiterate the conclusion that the duration of crosslinking was a more important factor than quantity of crosslinker for modifying PVA nanofibres.

Of the RIF-loaded formulations, Formulation 9 demonstrated optimal drug release kinetics with  $59.31 \pm 2.57\%$  being release over 12 hours in a controlled manner. Formulations crosslinked for longer durations than 12 hours (Formulation 8) released notably lower quantities of drug ( $46.34\% \pm 0.0336$ ) during the study period. As a result, PVA nanofibres had crosslinked to a degree that was beyond necessary, and the remainder drug was entrapped within the formulation, rather than being released. As such, it was determined that the duration of crosslinking for RIF-loaded nanofibres should not be greater than 12 hours to ensure maximum drug quantities are released in a controlled manner.

The variations in the drug release between the INH-loaded and RIF-loaded nanofibrous membranes can be attributed to the hydrophilicity of the respective drug molecules. INH, a hydrophilic drug molecule, required longer crosslinking periods as compared to RIF, which has a hydrophobic nature, to obtain prolonged drug release characteristics. The hydrophobic nature of RIF ultimately resulted in slower drug release of RIF-loaded

nanofibrous membranes than INH-loaded formulations of the same crosslinking quantity and time. These findings are depicted in Figure 6.5 where Formulation 3 released  $81.11 \pm 2.35\%$  of INH over 12 hours as opposed to Formulation 8 where only  $46.34 \pm 3.35\%$  of RIF was released over 12 hours.

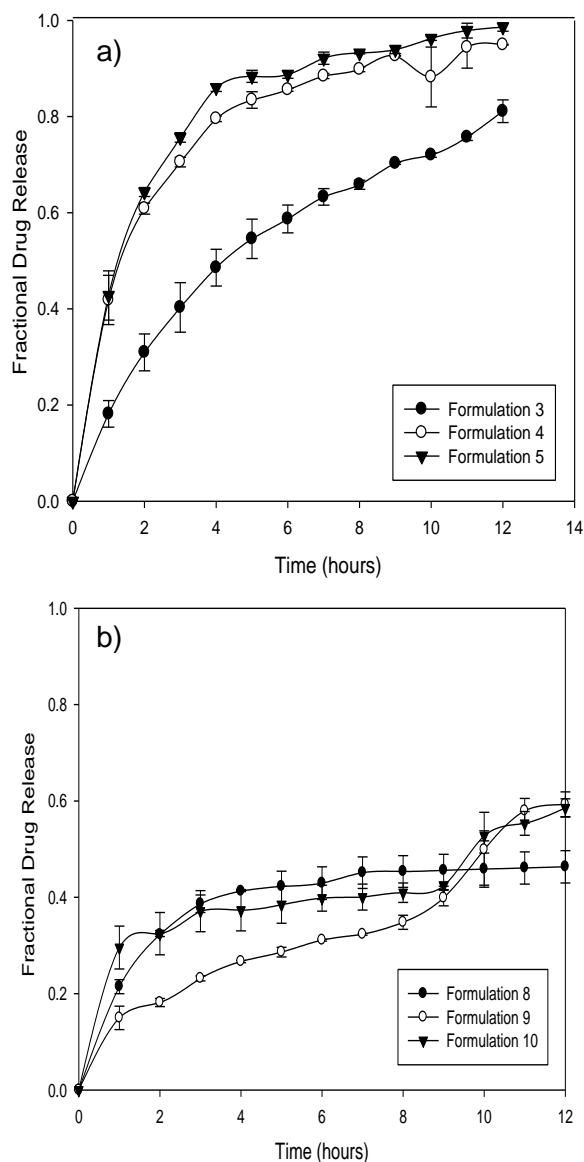


**Figure 6.5:** *In vitro* fractional drug release of a) Formulations 3-5 in PBS (pH 1.2) at 37°C and b) Formulations 8-10 in PBS (pH 6.8) at 37°C.

### 6.3.4 Surface Morphology and network density of the nanofibrous membranous system

Scanning electron microscopic evaluation revealed the formation of solid, uniform, cylindrical nanofibres of a non-porous surface with random orientation. The absence of pores on the surface of the nanofibres is principally dependant on the type of solvent used. In this case water was the solvent employed, and with its relatively low volatility

prevented the formation of pores. The absence of surface pores on the nanofibres aided in slowing the release rate of the incorporated drugs (Leung and Ko, 2011). As discussed in *Section 6.3.7*, the effects of increasing the polymer concentration on the diameter of the nanofibres is clearly illustrated on comparison of Figure 6.6a and Figure 6.7a. Increasing the polymer concentration from 8%<sup>w/v</sup> (Figure 6.7a) to 10%<sup>w/v</sup> PVA (Figure 6.6a) caused an increase in the fibre diameter from 297.5±29.47nm to 345.00±30.41nm as was demonstrated.

Figure 6.6a and Figure 6.6b demonstrates that the addition of INH had negligible effects in the fibre morphology and fibre diameter. A relatively smaller increase in the diameter from 345.00±30.41nm to 372.5±28.61nm was observed. However, the addition of RIF caused a drastic increase in the fibre diameter of 297.5±29.47nm to 631±57.78nm (Figure 6.7a-b). The increase in diameter correlates to the large increase in the viscosity of the RIF-loaded PVA solution (*Section 6.3.7*). Furthermore, RIF-loaded nanofibres were deposited on the aluminium collector in a rather haphazard fashion with many bends and kinks in the fibre structure, as opposed to straighter and more uniform fibres deposited in non-drug loaded nanofibres.

Crosslinking “contracted” nanofibres within the nanofibre matrices, producing a denser structure with closely packed nanofibres (Figure 6.6c-d and Figure 6.7c-d). The change in the nanofibre structure may also contribute to delaying drug release due to the decrease in surface area available for dissolution.



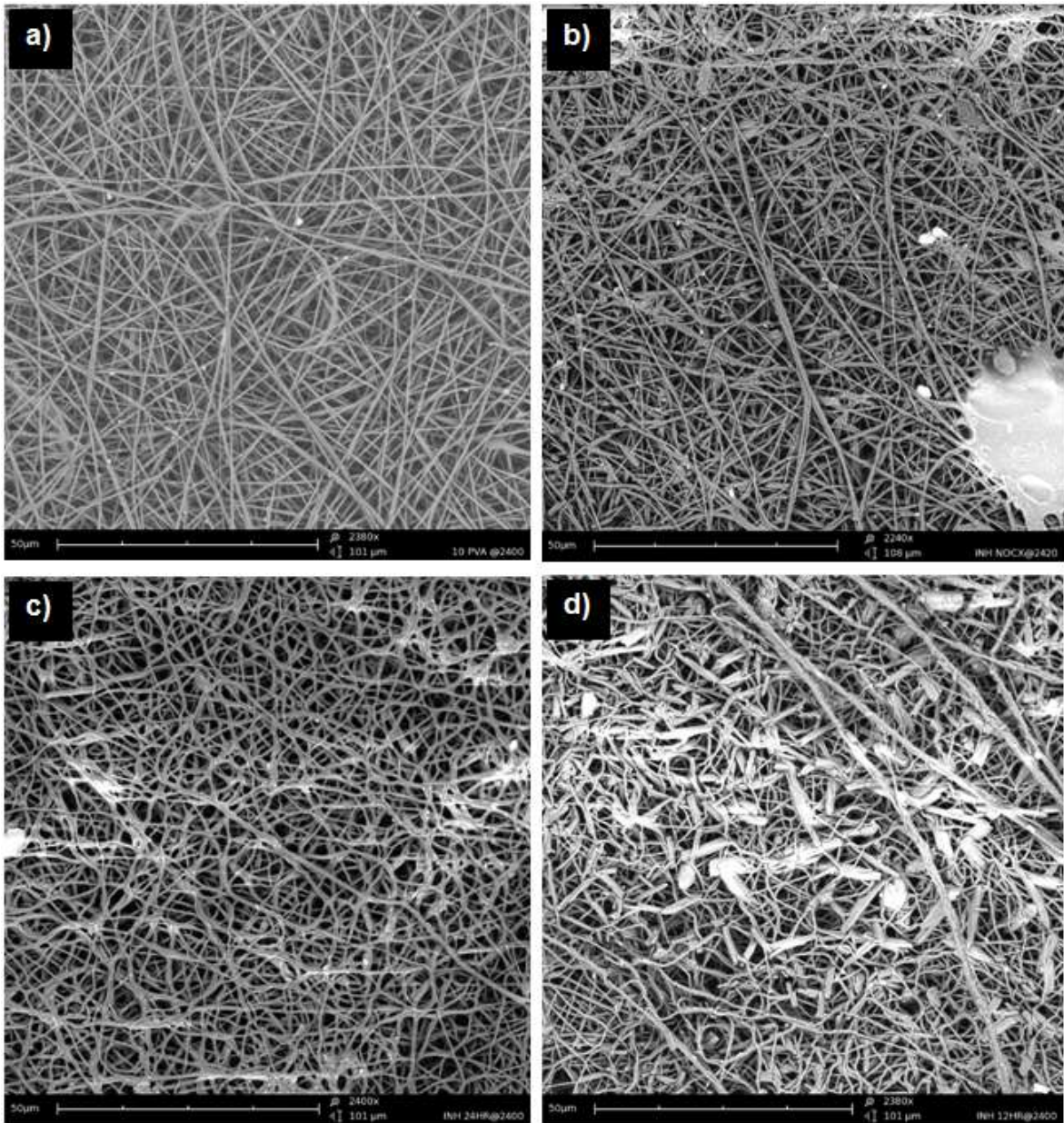


**Figure 6.6:** Scanning electron micrographs of a) Formulation 1; b) Formulation 2; c) Formulation 3; and d) Formulation 4.

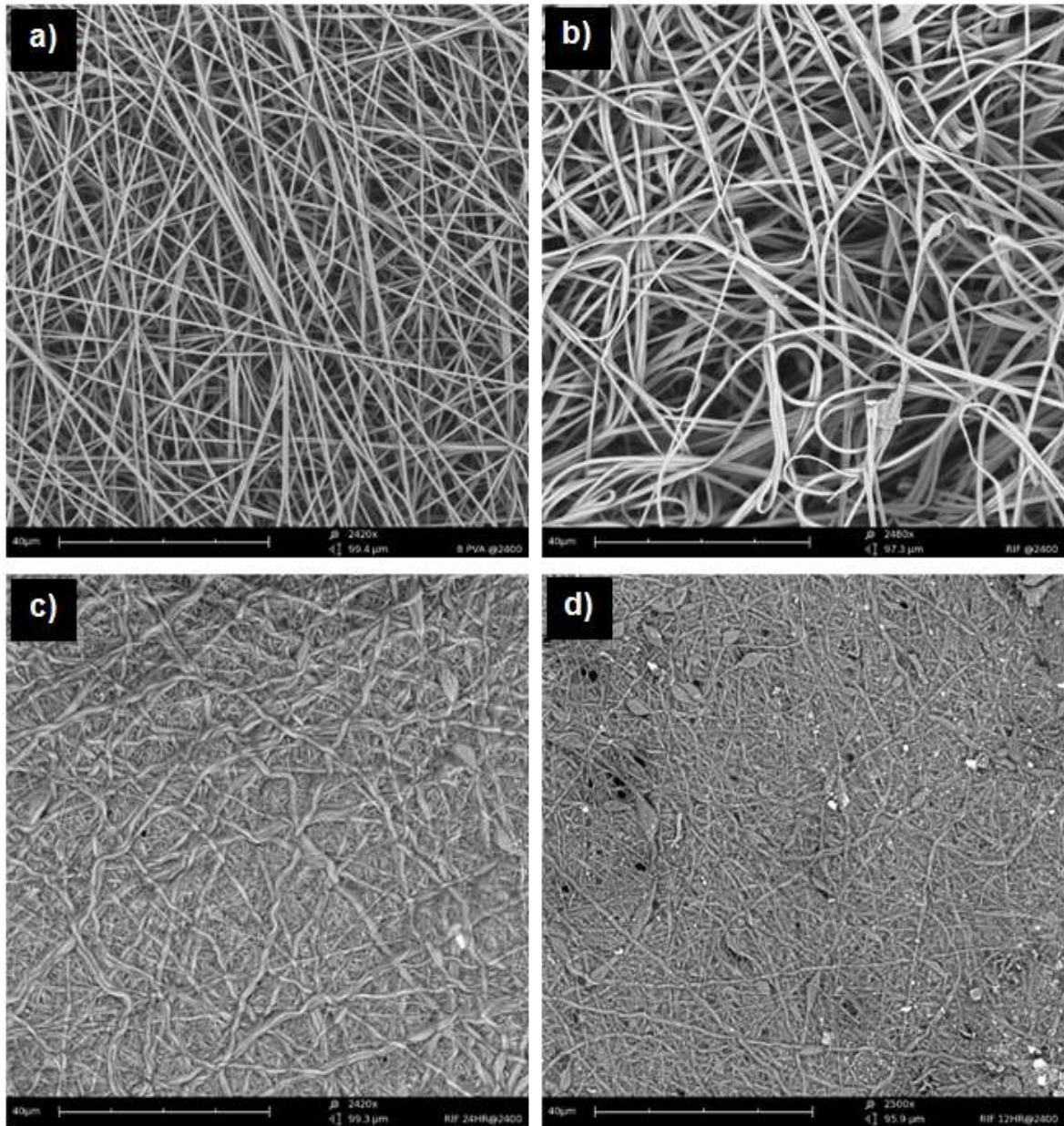


**Figure 6.7:** Scanning electron micrographs of a) Formulation 6; b) Formulation 7; c) Formulation 8; and d) Formulation 9.

### 6.3.5 Image processing algorithm for electrospun nanofibres

According to Wolfram Research Inc., “*Mathematica*<sup>TM</sup> provides broad and deep built-in support for both programmatic and interactive modern industrial-strength image processing—fully integrated with *Mathematica*'s powerful mathematical and algorithmic capabilities. *Mathematica*'s unique symbolic architecture and notebook paradigm allow images in visual form to be included and manipulated directly both interactively and in programs.” (Mathematica<sup>TM</sup> Image Processing and Analysis Guide, 2011). Here we used Mathematica<sup>TM</sup> to evaluate the influence of addition of drugs and crosslinking on the morphological characteristics of PVA electrospun nanofibres. Gray level images show a

complex structure in which, either an uneven illumination, or a lack of contrast or other sources of noise, hide the real pattern. In order to carry out the surface and fibre density analysis, fibre edges were extracted from the gray level images and histogramical analysis was carried out for the modified images (Figure 6.8a-d).

Sixteen-bit greyscale images obtained by SEM polymeric scaffolds were low in contrast (Figure 6.6 and Figure 6.7). This may have happened due to the non-uniform gold coating. In addition, the background appeared uneven due to inconsistent illumination across the field of view. Since thresholding of such images was unable to capture all of the required details, we employed some image-processing steps to even out the background and increase contrast between the fibres, pores in the fibrous matrix and the rest of the image. Images in .tif format were imported as shown in Expression 1 (Exp1) and converted to Mathematica™ 8.0 format (Figure 6.8a-d original):

```
Exp1: SEMimage = Import["X:\\directory\\folder\\filename.tif"];
```

The first processing step, blurring the image, created an unfocused image, which can be obtained by convolving the image with a low pass filter. In this work, the amount of blurring is increased by increasing the pixel radius (r) to 10 without compromising image detail. This was achieved in Mathematica™ 8.0 by applying a custom blurring function (Exp2) (Figure 6.8a-d blurred):

```
Exp2: BLURimage = Blur[SEMimage,10];
```

After blurring the image, the next step was to ColorQuantize the blurred image at 5 which provided an approximation to the image that uses only 5 distinct colours. This was achieved in Mathematica™ 8.0 by applying a custom colorquantize function (Exp3) (Figure 6.8a-d colorquantized):

```
Exp3: CQimage = ColorQuantize[BLURimage,5];
```

The third step consisted of analysing the images by plotting a histogram (Figure 6.9). The histogram expressions for original and processed images are denoted as OrgHistoSep and ProHistoSep, respectively. This default function plots a histogram of the pixel levels for each channel in image. Furthermore, separate histograms for each color channel were also constructed. This was achieved in Mathematica™ 8.0 by applying the custom ImageHistogram functions for default and separated algorithms as displayed in Exp 4:

```
Exp4:OrgHistoSep = ImageHistogram[SEMImage,Appearance->"Transparent"]
```

```
Exp5:ProHistoSep = ImageHistogram[CQImage,Appearance->"Transparent"]
```

The comparative analysis of histograms obtained before (Figure 6.9a-d) and after (Figure 6.9e-h) image processing revealed the striking effect of these steps on image histogram's clarity such that the presence of fibre uniformity and distribution is more obvious.

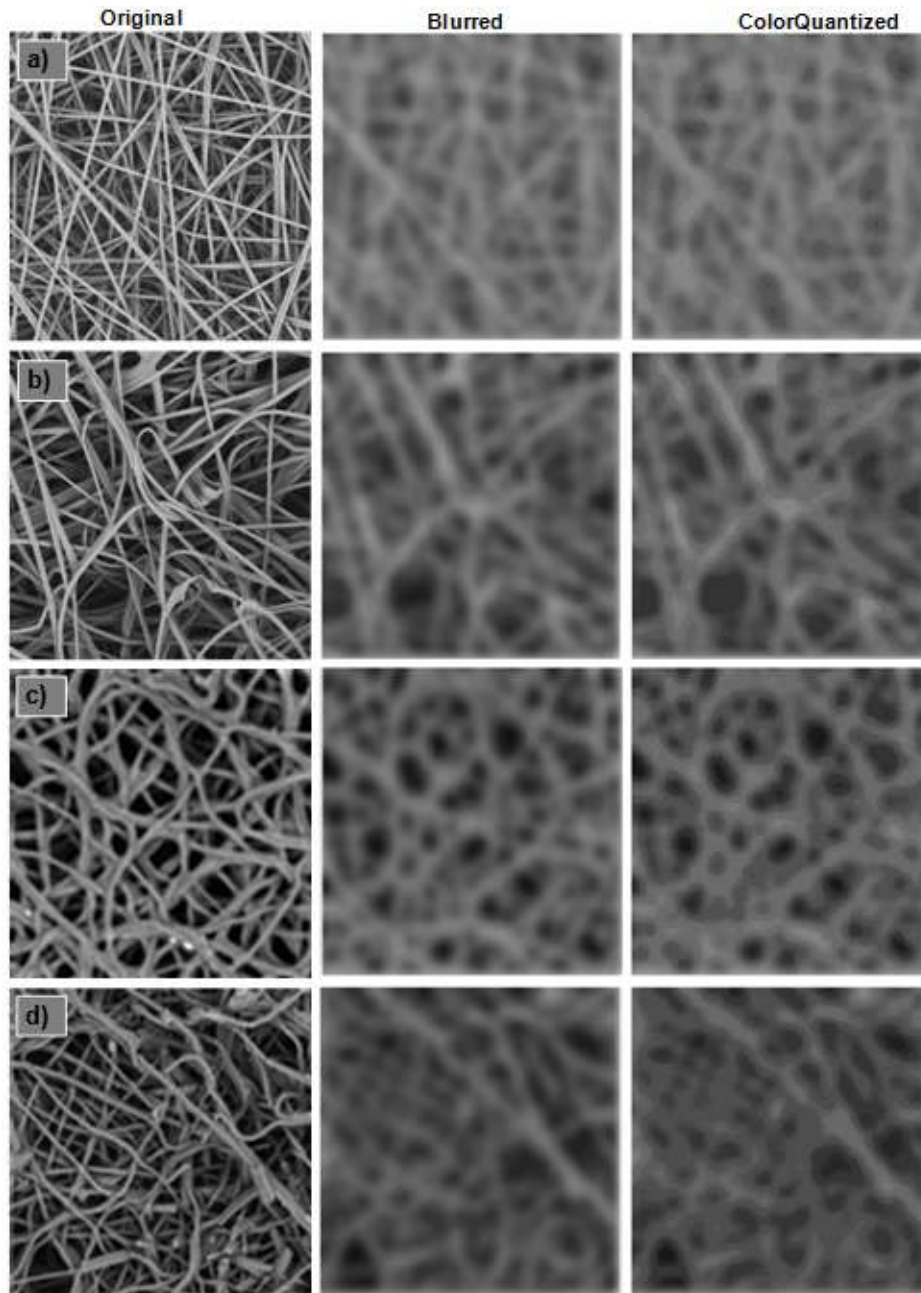


**Figure 6.8:** Image processing of PVA nanofibre micrographs representing a) Formulation 6; b) Formulation 7; c) Formulation 3; and d) Formulation 4 in Mathematica™ 8.0 format.

An analysis of the histogram is essential for the best choice of the threshold for discriminating between different morphological features seen in the SEM of electrospun nanofibres. Figure 6.9e (placebo nanofibres) displays a tetramodal distribution having peaks at 103, 119, 141 and 158 (voxel intensities) representing voxels for air-filled deep pores (porous throughout), pores reaching the second or third layer of the fibrous matrix, solid fibres in second or third layers and solid fibres in the top layer, respectively, in the order of increasing linear absorption coefficients. The peaks on either side of these pores and solid interfaces are blurred because of the finite spatial resolution of the scanning system creating an undesirable partial-volume effect. We assumed that the probability of finding intensity at a pore-fibre boundary should be equal for both the features. Therefore, the average of these peaks was chosen as the threshold (i.e., intensity ~130), implying that the voxels with an intensity equal to or smaller than 130 are pores. It is true for 103 and 119 which we assumed as pores earlier. This very assumption was used for the interpretation of the effect of addition of RIF to the nanofibres (Figure 6.9f) where the distribution became pentamodal with peaks at 63, 88, 104, 128 and 158 voxel intensities. The new threshold shifted from 130 voxel (original) to 108 voxel implying that intensities below 108 will represent porous structure. The above shifts towards air-filled pores may be attributed to an increase in fibre diameter (decreased solid area covered) leading to formation of larger pores causing an increase size of pores (increased porosity).

In the next part of ImageAnalysis, effect of variation of crosslinking on the morphological features of electrospun scaffold was evaluated. As evident from Figure 6.9g, the histogram of SEM image of fibres exposed to 15mL of glutaraldehyde represented a trimodal distribution having peaks at 64, 93 and 127 (voxel intensities) corresponding to voxels for air-filled deep pores and the solid fibrous matrix, in the order of increasing linear absorption coefficients. As in previous case, the peaks on either side of these pores and solid interfaces are blurred because of the finite spatial resolution of the scanning system creating an undesirable partial-volume effect. The average of these peaks was chosen as the threshold (i.e., intensity ~94), implying that the voxels with an intensity equal to or smaller than 94 are pores and greater ones are solid fibres. However in case of Figure 6.9, corresponding to SEM image of fibres exposed to 30mL of glutaraldehyde, the trimodal distribution culminated in a threshold value of 119 (average of voxel intensities of 68, 122 and 168). This means that there are more pores in Figure 6.9g than Figure 6.9h and Figure 6.9h is more fibrous than Figure 6.9g. Furthermore, the shift of histogram threshold from 94 to 119 may be attributed to the presence of dense network of fibres and hence less porous structure when amount of crosslinking agent is increased.

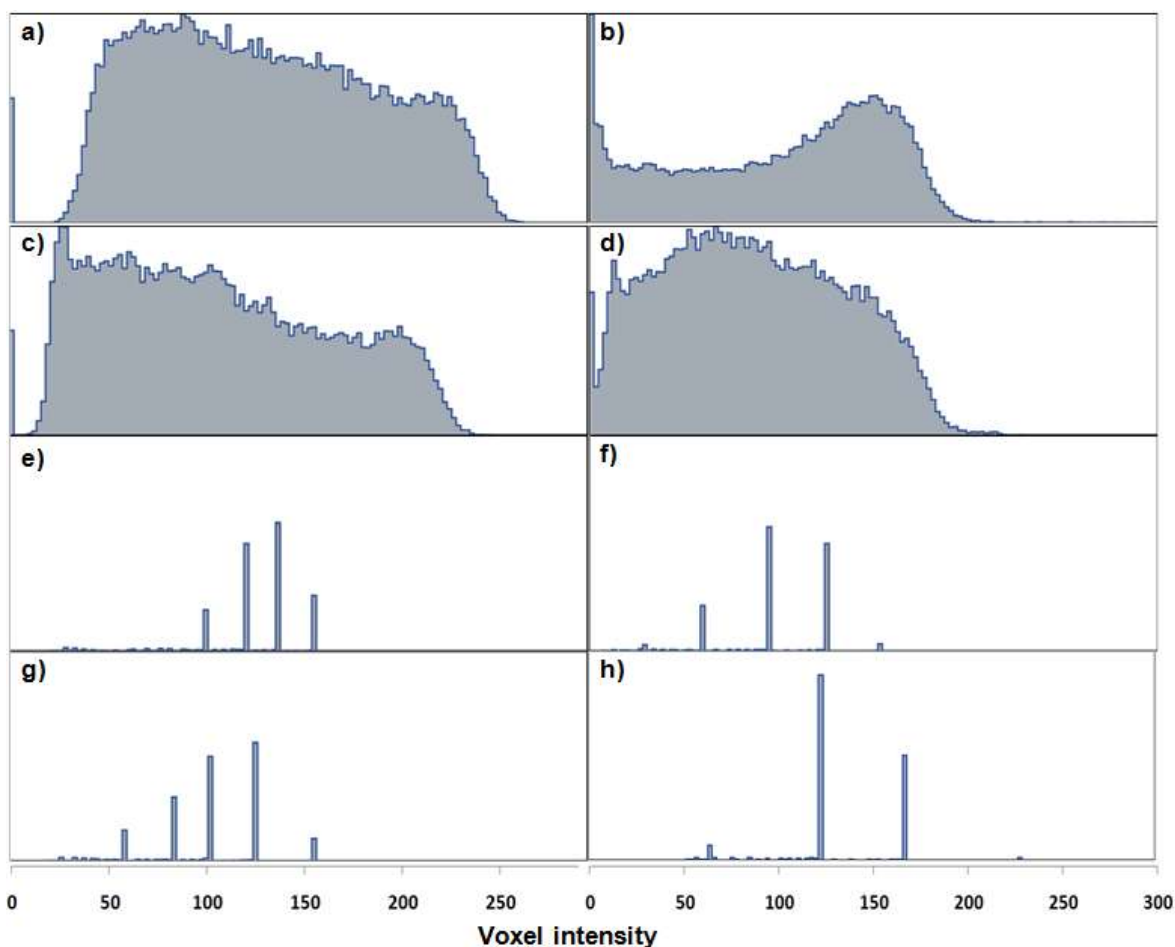


**Figure 6.9:** ImageHistograms of scanning electron micrographs representing a) Formulation 6-original, b) Formulation 7-original, c) Formulation 3-original, d) Formulation 4-original; e) Formulation 6-processed, f) Formulation 7-processed, g) Formulation 3-processed and h) Formulation 4-processed. Note that each channel is only capable of highlighting most of the pores and fibres.

### 6.3.6 PVA:GA structural interactions as a result of nanofibre crosslinking

The possibilities of chemical and physical interactions as a result of crosslinking were evaluated using FTIR. Furthermore, if one considers the process of electrospinning of aqueous polymer solutions, it is of interest to ascertain to what extent the nature of the native polymer is modified. Examination of the FTIR spectra generated for the non drug-loaded PVA nanofibres (Figure 6.10) demonstrated that the electrospinning procedure had a minimal impact on conferring inter- or intra-molecular arrangements, with no band shifts or enhancements observed as compared to pure PVA (Figure 6.10).

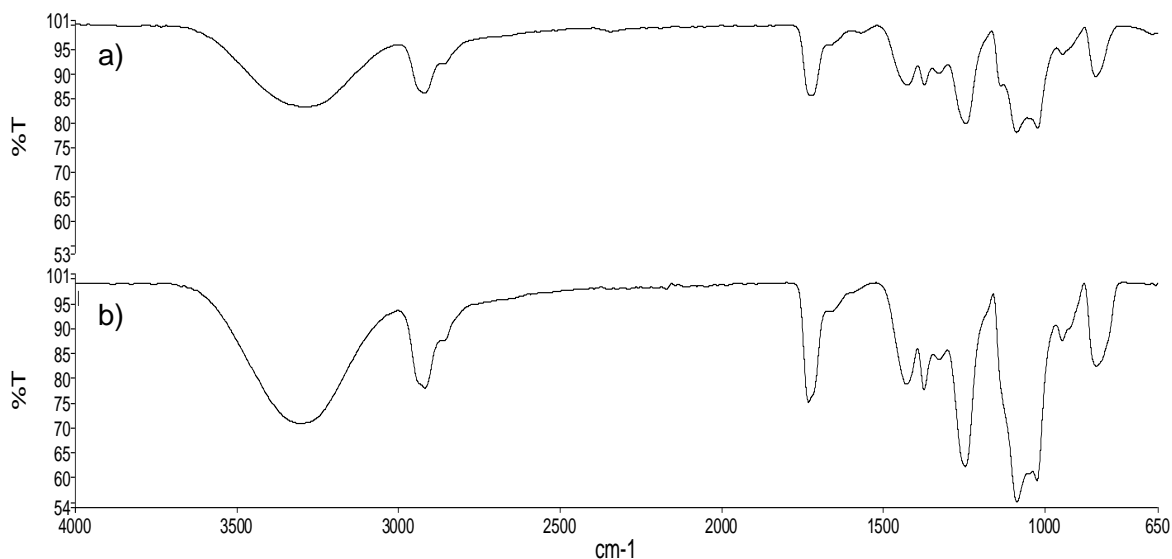


**Figure 6.10:** FTIR spectra of a) Pure PVA and b) an electrospun PVA nanofibrous matrix.

Crosslinking, on the other hand, had an impact on the establishment of inter- or intra-molecular crosslinks and is demonstrated by the variations in band intensities. The crosslinking of PVA with GA generally occurs through the formation of a  $-C-O-C-$  between the  $-OH$  of a typical PVA structure and the  $-C-$  of a GA molecule. As illustrated in Figure 6.11a-b, the transmittance bands at  $1380\text{cm}^{-1}$  and  $1030\text{cm}^{-1}$  (highlighted with a red arrow), indicative of  $C-OH$  bonding and the transmittance band at  $3348\text{cm}^{-1}$  (highlighted by green arrows), indicative of an  $O-H$  bond decreases in intensity after crosslinking. The appearance of a peak/shoulder at  $1150\text{cm}^{-1}$  (highlighted by a blue arrow) is indicative of  $-C-O-C-$  bonds which are formed during the crosslinking reaction. Furthermore, the strengthening of the transmittance band at  $800\text{cm}^{-1}$  and  $1720\text{cm}^{-1}$  is indicative of  $CH$  out of plane bending and  $C=O$  bonds respectively, which is characteristic of GA. These results indicate the decrement of  $C-OH$  bonds in the PVA molecular structure allowing for the increment of  $C-H$  alkyl groups, thereby confirming that crosslinking between PVA and GA occurs.

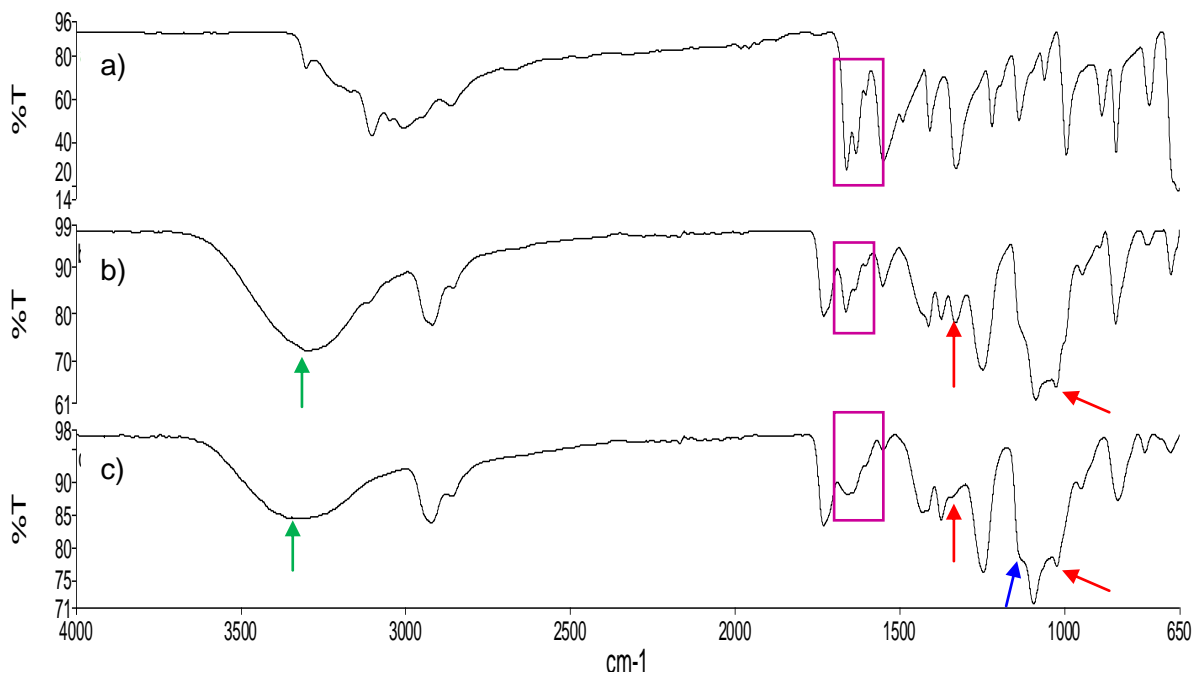


**Figure 6.11:** FTIR spectra of a) INH, b) INH-loaded nanofibres (Formulation 2) and c) crosslinked INH-loaded nanofibres (Formulation 4). The red arrow indicates transmittance bands at  $1380\text{cm}^{-1}$  and  $1030\text{cm}^{-1}$  associating with C–OH stretching of PVA; the green arrow indicates transmittance band at  $3348\text{cm}^{-1}$  associating with O–H bonding in PVA, the blue arrow indicates transmittance band  $1150\text{cm}^{-1}$  associating with C–O–C groups formed through crosslinking. The areas highlighted in purple demonstrate minimal change, before and after crosslinking, to the  $-\text{NH}_2$  related transmittance bands of INH.

The drug molecules contain functional groups which are also known to crosslink with the  $-\text{CHO}$  groups of glutaraldehyde. Figure 6.11 displays that the FTIR spectra of the INH in the formulation, before and after crosslinking, were analogous to each other. The amine group of INH within the nanofibrous matrix is represented by the transmittance bands at  $1665\text{cm}^{-1}$ ;  $1633\text{cm}^{-1}$  and  $1601\text{cm}^{-1}$  (Figure 6.11b). Nanofibrous matrices that were crosslinked, displayed no shift in the amine related transmittance bands. It was thus postulated that the mechanism of drug incorporation ensured that the drug molecules were embedded within the nanofibrous matrix, restricting exposure of the drug to the vapours. Furthermore, once the surface is crosslinked, the vapours may not be able to access the drug efficiently. Similarly, Figure 6.12 illustrates that the FTIR spectra of RIF-loaded nanofibres, before and after crosslinking were comparable with each other. The C–OH groups of RIF which interact with glutaraldehyde indicated by the transmittance bands at  $1646\text{cm}^{-1}$  and  $1371\text{cm}^{-1}$  did not shift or change in intensity after exposure to the GA vapours, indicating that minimal interactions occurred between RIF and GA. The decrease in the band intensities at  $3348\text{cm}^{-1}$ ,  $1347\text{cm}^{-1}$  and  $1023\text{cm}^{-1}$ , as well as the appearance of the shoulder at  $1150\text{cm}^{-1}$  reaffirms that crosslinking has occurred between GA vapours and PVA molecules.



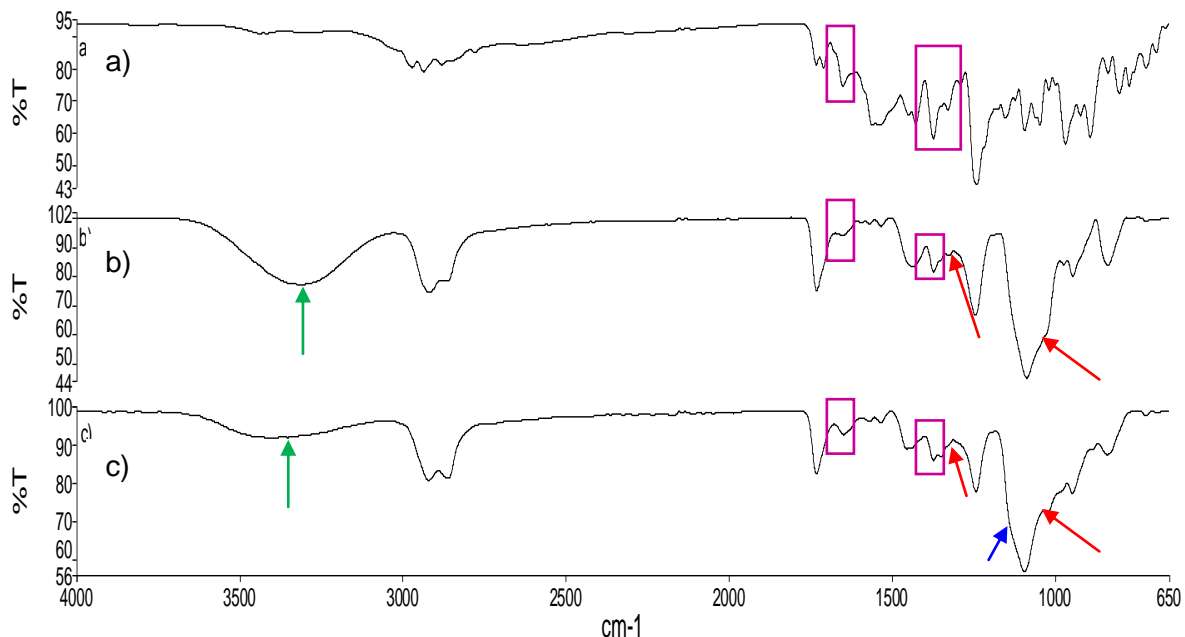


**Figure 6.12:** FTIR spectra of a) RIF, b) RIF-loaded nanofibres (Formulation 7) and c) crosslinked RIF-loaded nanofibres (Formulation 9). The red arrow indicates transmittance bands at  $1347\text{cm}^{-1}$  and  $1023\text{cm}^{-1}$  associating with C–OH stretching of PVA; the blue arrow indicates transmittance band  $1150\text{cm}^{-1}$  associating with C–O–C groups formed through crosslinking. The green arrow indicates the transmittance bands at  $3348\text{cm}^{-1}$ , associated with the –OH bonding of PVA. The areas highlighted in purple demonstrate minimal change, before and after crosslinking, to the –OH related transmittance bands of RIF.

The degree of crosslinking can be associated with the extent of change in the band intensities. As illustrated in Figure 6.13, the transmittance band at  $3348\text{cm}^{-1}$  (green arrows) indicative of the O-H functionality of PVA (responsible for crosslinking with GA), consistently decreases as the duration of crosslinking increased. The transmittance bands at  $1023\text{cm}^{-1}$  indicating the C-OH stretching of PVA also appears to decrease as the duration of crosslinking increased. Furthermore the shoulder at  $1150\text{cm}^{-1}$ , indicating the formation of the –C-O-C- bond appears to increase in intensity as the duration of crosslinking increased. The formulations displaying the highest extent of change in their band intensities corresponds to having the highest degree of crosslinking. Hence, it can be concluded that the degree of crosslinking was affected largely by the duration of crosslinking, rather than the quantity of crosslinker employed.

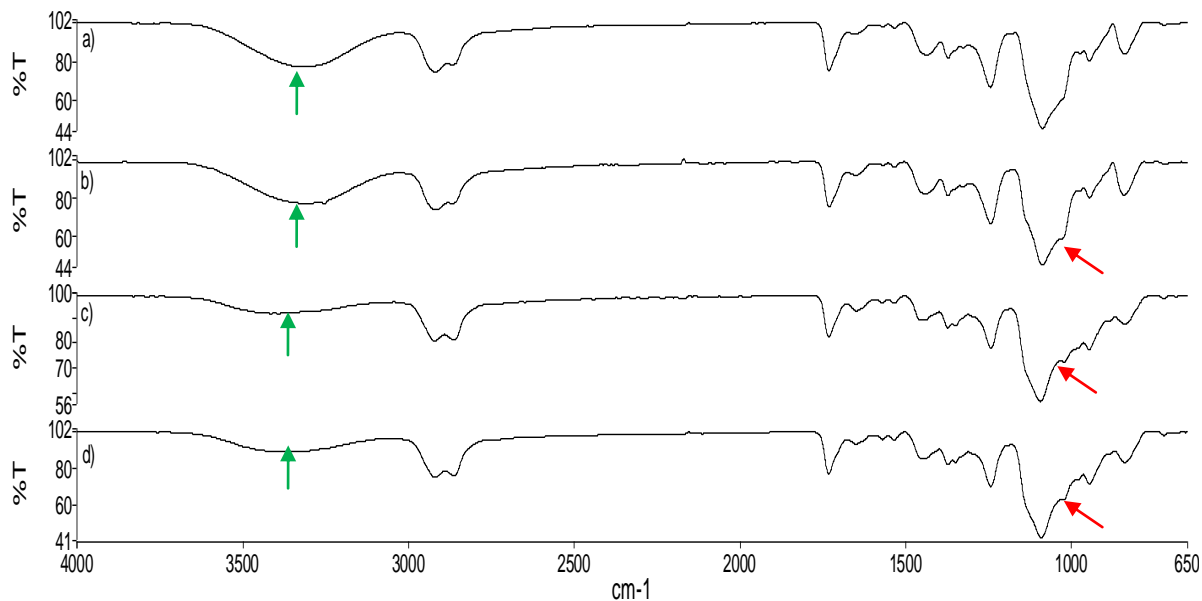


**Figure 6.13:** FTIR spectra of a) RIF-loaded nanofibres (Formulation 7); b) Formulation 8 (crosslinking for 6 hours); c) Formulation 9 (crosslinked for 12 hours) and d) Formulation 10 (crosslinked for 24 hours). The red arrow indicates transmittance bands at  $1023\text{cm}^{-1}$  associating with C–OH stretching of PVA; the blue arrow indicates transmittance band  $1150\text{cm}^{-1}$  associating with C–O–C groups formed through crosslinking. The green arrow indicates the transmittance bands at  $3348\text{cm}^{-1}$ , associated with the –OH bonding of PVA. The areas highlighted in purple demonstrate minimal change, before and after crosslinking, to the –OH related transmittance bands of RIF.

### 6.3.7 Rheological characteristics of the non-drug loaded and drug loaded polymeric solutions employed in electrospinning

The rheological characteristics, and in particular the viscosity, of polymeric solutions determines whether the solution can be electrospun, and further influences the fibre morphology (such as size) and quality once electrospun. Several studies have demonstrated that polymeric solutions can be electrospun only within an optimal range of polymer concentrations or solution viscosity. If a polymer solution is too dilute, the polymeric fibre breaks up into droplets before reaching the collecting surface. When solutions are too concentrated, fibres are unable to form due to very high viscosities (Tao and Shivkumar, 2007; Sill and Von Recum, 2008). Increasing the polymer concentrations within said range causes an increase in the diameter of the nanofibres formed (Sill and Von Recum, 2008).

The respective viscosities, determined through rheological analysis of the drug-loaded and non-drug loaded polymeric solutions, are listed in Table 6.5. As illustrated in the table, addition of RIF causes a drastic increase in the viscosity of the  $8\%_{\text{w/v}}$  PVA solution. During preliminary investigations, when RIF was added to a  $10\%_{\text{w/v}}$  solution, the viscosity increase fell outside the optimal viscosity range for electrospinning of PVA solutions. This

necessitated lowering the PVA concentration in RIF-loaded solutions from 10%<sup>w/v</sup> PVA to 8%<sup>w/v</sup> PVA solution, which had better electrospinnable characteristics. In addition, incorporation of Tween<sup>®</sup> 80 to the RIF-loaded PVA solutions caused a further decrease in the viscosity, further improving the electrospinning characteristics of the solution. INH addition demonstrated a minor increase in the polymer concentration, which had no drastic changes in the morphology or diameters of the fibres formed.

**Table 6.5:** Effect of drug and/or excipient addition on the viscosity of PVA solutions employed during electrospinning.

| <b>Solution Parameters</b>   | <b>Viscosity at shear rate of 100/s (mPas)</b> |
|--|--|
| 10% <sup>w/v</sup> PVA   | 830.53±26.41                                   |
| 10% <sup>w/v</sup> PVA + 2% <sup>w/v</sup> INH                       | 945.29±5.62                                    |
| 8% <sup>w/v</sup> PVA  | 443.14±13.90                                   |
| 8% <sup>w/v</sup> PVA + 2% <sup>w/v</sup> RIF                        | 707.27±13.60                                   |
| 8% <sup>w/v</sup> PVA; 2% <sup>w/v</sup> RIF + Tween <sup>®</sup> 80 | 647.92±10.31                                   |

### 6.3.8 Tensile properties and Young's Modulus of crosslinked and non-crosslinked nanofibrous membranes

The stress-strain relationship of a material is highly dependent on the flexibility of the polymer chains and the strength of the material. When only a small amount of stress is required to produce a large amount of strain, the material is considered to be flexible and the Young's Modulus, which is the slope of the linear portion of the stress-strain curve, as illustrated in Figure 6.14, will be relatively small (Wu and McGinity, 2000). A material is considered to be considerably stronger than another when the ultimate strength, which is the maximum point on the stress-strain curve, is relatively higher. The average experimental values for Young's Modulus (E), yield stress ( $\sigma_y$ ) (magnitude of stress on the stress-strain curve at which appreciable deformation takes place without any appreciable increase in the stress), ultimate strength ( $\sigma_u$ ) (the maximum stress a material can withstand), ultimate strain ( $\epsilon_u$ ) and toughness ( $u_f$ ) are outlined in Table 6.6.

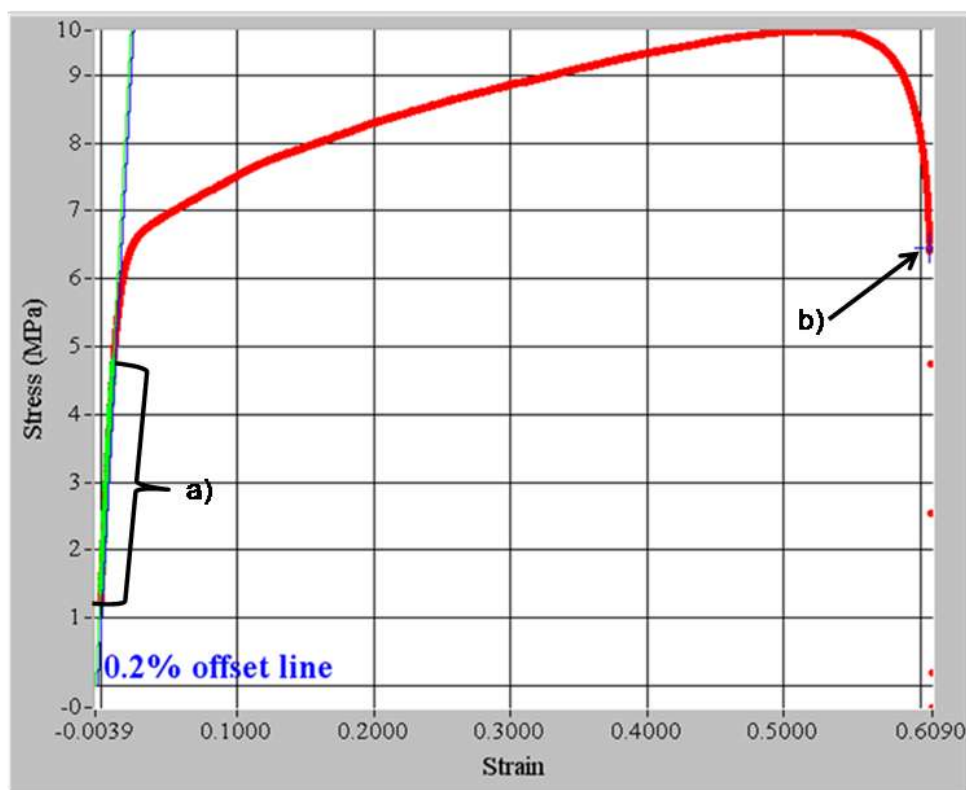


**Figure 6.14:** Typical stress-strain nanotensile profile where a) is the linear portion of the slope from which Young's Modulus is determined; and b) depicts the fracture point of the sample.

**Table 6.6:** Experimental values obtained from nanotensile analysis of the crosslinked and non-crosslinked fibres.

| Formulation | E (MPa) | $\sigma_y$ (MPa) | $\sigma_u$ (MPa) | $\epsilon_u$ | $u_f$ (J/cm <sup>3</sup> ) |
|-------------|---------|------------------|------------------|--------------|----------------------------|
| 1           | 401.295 | 8.555            | 10.78            | 0.399        | 3.89                       |
| 2           | 91.330  | 3.960            | 4.860            | 0.4455       | 1.465                      |
| 3           | 254.755 | 8.375            | 9.845            | 0.2595       | 0.81                       |
| 4           | 253.155 | 6.220            | 8.710            | 0.4370       | 2.970                      |
| 5           | 283.440 | 6.465            | 9.245            | 0.5605       | 4.320                      |
| 6           | 111.545 | 2.31             | 3.745            | 0.609        | 1.63                       |
| 7           | 37.695  | 1.495            | 3.755            | 1.3130       | 3.990                      |
| 8           | 267.865 | 3.965            | 4.535            | 0.0400       | 3.965                      |
| 9           | 284.98  | 2.575            | 7.90             | 0.206        | 0.88                       |
| 10          | 189.760 | 4.750            | 6.335            | 0.6280       | 3.545                      |

As illustrated in Figure 6.15, addition of drug caused a drastic decrease in the Young's Modulus of the PVA nanofibres, which is related to an increase in the elasticity of the nanofibrous membranes. The elasticity increase may be due to the plasticizing effect the drugs have on the nanofibres.

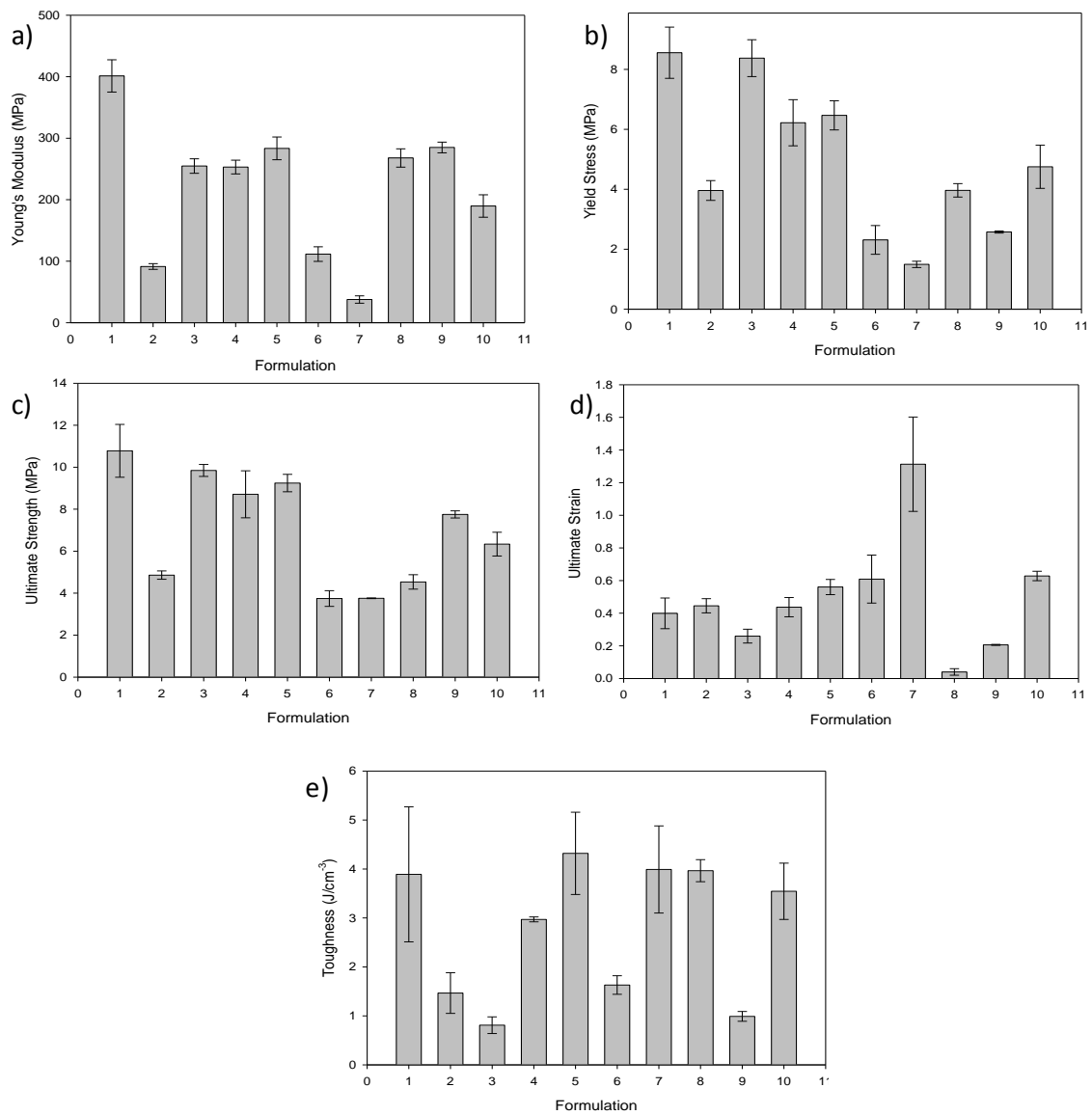


**Figure 6.15:** Vertical bar chart each outlining variations between the 10 formulations of a) Young's Modulus ( $E$ ; MPa); b) Yield Stress ( $\sigma_y$ ; MPa); c) Ultimate Strength ( $\sigma_u$ ; MPa); d) Ultimate Strain ( $\epsilon_u$ ); e) Toughness ( $u_f$ ; J/cm<sup>3</sup>) of Formulations 1-10.

Non-crosslinked drug-loaded nanofibres demonstrated high variation in the elastic properties when differing concentrations of PVA were electrospun. A Young's Modulus of  $91.330 \pm 4.67$  MPa and  $37.695 \pm 6.02$  MPa were obtained for fibres electrospun from PVA solutions of concentrations  $10\% w/v$  and  $8\% w/v$  respectively. This variation in elasticity can be attributed to the differing fibre diameters illustrated in Figure 6.6b and Figure 6.7b. Non-crosslinked drug loaded nanofibres demonstrated higher elasticity properties than crosslinked drug loaded nanofibres. This can be attributed to the nanofibres slipping past one another, and aligning along the tensile pull axis. Crosslinking showed a distinct decrease in the elasticity of the nanofibres, which can be attributed to nanofibres being unable to slip past each other due to crosslinks formed between individual fibres, thus increasing the stiffness of the nanofibres.

Addition of INH caused a substantial decrease in the ultimate strength of the nanofibres from  $10.78 \pm 1.26$  MPas to  $4.86 \pm 0.20$  MPas, whereas addition of RIF showed an insignificant change in the ultimate strength of the material, the findings which are discussed in further detail in *Section 6.3.9.3*. Crosslinking improved the strength of the drug-loaded nanofibres from  $3.755 \pm 0.015$  MPas to ultimate strengths ranging from  $4.535 \pm 0.345$  MPas to  $7.92 \pm 0.02$  MPas for RIF-loaded nanofibres and  $4.86 \pm 0.2$  MPas to ultimate strengths ranging from  $8.71 \pm 1.12$  MPas to  $9.245 \pm 0.415$  MPas for INH-loaded nanofibres. Although, crosslinking improved the ultimate strength and stiffness of drug-loaded samples, crosslinking of RIF-loaded nanofibrous membranes produced very brittle membranes, as they failed in tension at relatively low values of strain.

### 6.3.9 Molecular Mechanics Assisted Model Building and Energy Refinements

A molecular mechanics conformational searching procedure was employed to acquire the data employed in the statistical mechanics analysis, and to obtain differential binding energies of a Polak–Ribiere algorithm and to potentially permit application to polymer composite assemblies. MM+ is a HyperChem™ modification and extension of Norman Allinger's Molecular Mechanics program MM2 (Warhurst *et al.*, 2003) whereas AMBER, is a package of computer programs for applying molecular mechanics, normal mode analysis, molecular dynamics and free energy calculations to simulate the structural and energetic properties of molecules (Pearlman *et al.*, 1995).

#### 6.3.9.1 MMER analysis

Molecular mechanics energy relationship (MMER), a method for analytico-mathematical representation of potential energy surfaces, was used to provide information about the contributions of valence terms, noncovalent Coulombic terms, and noncovalent Van der Waals interactions in tensile properties and drug release kinetics. The MMER model for potential energy factor in various molecular complexes can be written as:

$$E_{\text{molecule/complex}} = V_{\Sigma} = V_b + V_{\theta} + V_{\varphi} + V_{ij} + V_{hb} + V_{el}$$

Equation 6.1

where,  $V_{\Sigma}$  is related to total steric energy for an optimized structure,  $V_b$  corresponds to bond stretching contributions (reference values were assigned to all of a structure's bond lengths),  $V_{\theta}$  denotes bond angle contributions (reference values were assigned to all of a structure's bond angles),  $V_{\varphi}$  represents torsional contribution arising from deviations from optimum dihedral angles,  $V_{ij}$  incorporates Van der Waals interactions due to non-bonded interatomic distances,  $V_{hb}$  symbolizes hydrogen-bond energy function and  $V_{el}$  stands for electrostatic energy (Choonara *et al.*, 2011).

In the present MM study, the global energy relationships for the various complexes derived after assisted model building and energy refinements are as follows:

$$E_{PVA} = 18.517 V_{\Sigma} = 1.067 V_b + 5.969 V_{\theta} + 9.212 V_{\varphi} + 4.086 V_{ij} - 1.818 V_{hb}$$

Equation 6.2

$$E_{PVA-PVA} = 26.483 V_{\Sigma} = 2.187 V_b + 17.167 V_{\theta} + 12.1 V_{\varphi} - 1.254 V_{ij} - 3.717 V_{hb}$$

Equation 6.3

$$E_{INH} = 6.445 V_{\Sigma} = 0.422 V_b + 0.691 V_{\theta} + 7.482 V_{\varphi} + 5.499 V_{ij} - 0.168 V_{hb}$$

Equation 6.4

$$E_{PVA2-INH} = 15.761 V_{\Sigma} = 2.349 V_b + 14.804 V_{\theta} + 12.726 V_{\varphi} - 9.021 V_{ij} - 5.096 V_{hb}$$

Equation 6.5

$$E_{RIF} = 70.743 V_{\Sigma} = 4.040 V_b + 28.166 V_{\theta} + 32.796 V_{\varphi} + 6.737 V_{ij} - 0.998 V_{hb}$$

Equation 6.6

$$E_{PVA2-RIF} = 76.781 V_{\Sigma} = 6.170 V_b + 44.409 V_{\theta} + 43.893 V_{\varphi} - 11.463 V_{ij} - 6.228 V_{hb}$$

Equation 6.7

$$E_{GA} = 1.425 V_{\Sigma} = 0.0291 V_b + 0.0622 V_{\theta} + 0.804 V_{\varphi} + 0.529 V_{ij}$$

Equation 6.8

$$E_{PVA2-GA3} = 15.176 V_{\Sigma} = 2.540 V_b + 18.135 V_{\theta} + 17.081 V_{\varphi} - 18.088 V_{ij} - 4.492 V_{hb}$$

Equation 6.9

### 6.3.9.2 Formulation of drug-loaded PVA fibres

The first part of the present study involved the elucidation of the effect of addition of drugs on the nanotensile properties of PVA nanofibres, drugs viz. INH and RIF were sandwiched between two PVA polymeric rings as shown in Figure 6.16. The addition of individual drugs significantly affected the tensile properties of nanofibres with a substantial decline in Young's Modulus.

The drug incorporation results presented in this study are in line with the previously reported work by Wu and McGinity, 1999, where chlorpheniramine maleate and ibuprofen were used to influence the mechanical properties of polymeric films and termed the drugs as "non-traditional plasticizers" causing a reduction in Young's Modulus. Interestingly, all the energy values viz., bonding and non-bonding energies underwent stabilization with all

$\Delta E$  values in negative (Table 6.7) confirming the conformational stability and compatibility as well as thermodynamic and steric rationality of the three molecules in conjugation with each other.

### 6.3.9.3 Tensile analysis of drug-loaded PVA nano fibres

For the prediction of the effect of addition of drugs on the tensile properties of PVA fibres, there have not been many fully atomistic simulations of drug-loaded polymers in which tensile properties have been calculated as a function of energy values of the complexed molecular structure. To explain the mechanism underlying the performance of drug-loaded nanofibrous matrix, we hereby propose that the mechanical properties of the nanofibres may be predominantly dependent on the available volume and cohesive energy density (CED) of/between the polymer fragments based on the various intra- and inter-molecular interactions both in terms of bonded and non-bonded energy terms. A typical relation between Young's Modulus (E) and molar volume can be derived based on bulk Modulus/Young's Modulus equations derived by Roberts *et al.*, 1991 as follows:

$$K = x \cdot \frac{E_{coh}}{V}$$

Equation 6.10

$$K = \frac{E}{3(1 - 2\nu)}$$

Equation 6.11

where,  $K$  is bulk modulus,  $E_{coh}$  is energy of vaporization ( $J.mol^{-1}$ ),  $V$  is the molar volume ( $cm^3.mol^{-1}$ ),  $\nu$  is Poisson's ratio and  $x$  is a constant related to the cubic lattice of the molecule under investigation.

Equating Equation 6.10 and Equation 6.11,

$$E \propto \frac{1}{V}$$

Equation 6.12

Also,

$$CED \propto \frac{1}{V}$$

Equation 6.13

From Equation 6.12 and Equation 6.13, it is clear that molar volume defines the elastic as well cohesive properties of a polymeric architecture.



**Table 6.7:** Calculated energy parameters (kcal/mol) of polymer-crosslinker and drug loaded crosslinked-polymer assemblies.

| Name   | $\Delta$ Energies <sup>a</sup> |                            |                             |                                |                           |                              |
|--|--------------------------------|----------------------------|-----------------------------|--------------------------------|---------------------------|------------------------------|
|  | $\Delta$ Total <sup>b</sup>    | $\Delta$ Bond <sup>c</sup> | $\Delta$ Angle <sup>d</sup> | $\Delta$ Dihedral <sup>e</sup> | $\Delta$ Vdw <sup>f</sup> | $\Delta$ H-bond <sup>g</sup> |
| PVA <sub>2</sub> <sup>h</sup>                  | -10.551                        | 0.153                      | 5.229                       | -6.324                         | -9.426                    | -0.081                       |
| PVA <sub>2</sub> -GA <sub>3</sub> <sup>i</sup> | -15.582                        | 0.1657                     | 0.7814                      | 2.569                          | -18.421                   | -0.775                       |
| PVA <sub>2</sub> -INH <sup>j</sup>             | -17.167                        | -0.36                      | -3.054                      | -6.856                         | -13.266                   | -1.211                       |
| PVA <sub>2</sub> -RIF <sup>k</sup>             | -20.445                        | -0.157                     | -0.924                      | -1.003                         | -16.946                   | -1.513                       |

<sup>a</sup>  $\Delta E_{binding} = E(Host.Guest) - E(Host) - E(Guest)$ ; <sup>b</sup> Total steric energy for an optimized structure  
<sup>c</sup> Bond stretching contributions; <sup>d</sup> Bond angle contributions; <sup>e</sup> Torsional contribution; <sup>f</sup> Van der Waals interactions; <sup>g</sup> Hydrogen-bond energy function; <sup>h</sup> Two PVA molecules in conjugation; <sup>i</sup> Three GA molecules in conjugation with two PVA molecules; <sup>j</sup> An INH molecule in conjugation with two PVA molecules; <sup>k</sup> An RIF molecule in conjugation with two PVA molecules

Conceptually, the addition of a plasticizer may lead to lowering of rigidity of the polymer matrix thereby lowering of elastic modulus and ultimate strength as is evident from the experimental results and is in line with previous studies (Gil *et al.*, 2006). The complexation of PVA molecules with the drug molecules lead to a decrease in vdWf by ~13kcal/mol and ~17kcal/mol for INH and RIF, respectively, (Table 6.7) which in turn may lead to a decrease in CED thereby decreasing the Young's Modulus (Equation 6.10-Equation 6.13). This reduction in cohesion may help the adjacent polymer chains to stretch/slide over each other thereby increasing the elongation of the fibres. Apart from this, the drugs may impart different volumes fraction to the polymeric matrix dependent of the molecular size of the drug molecule.

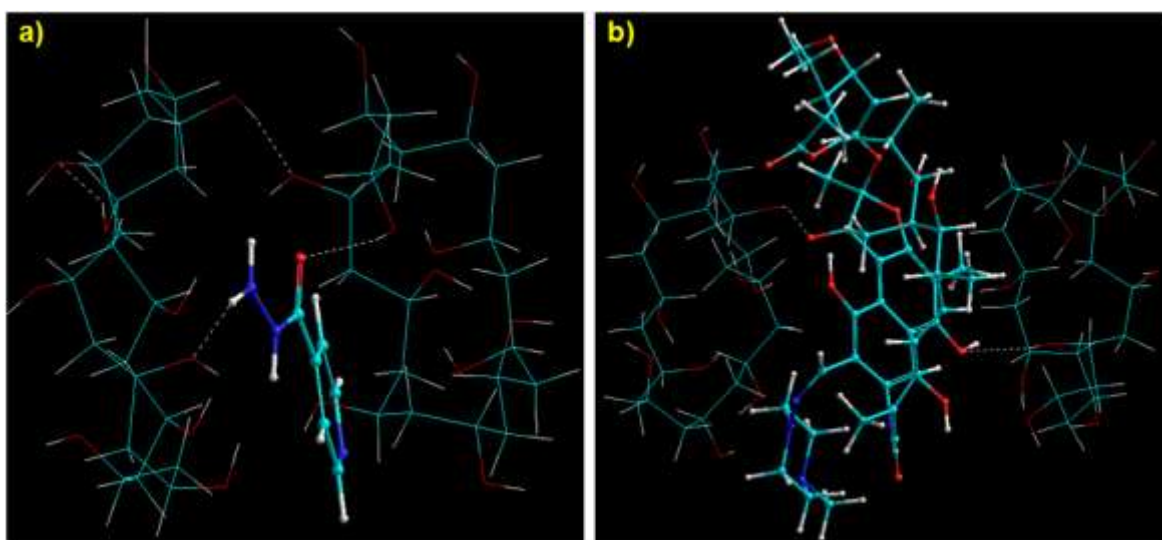


**Figure 6.16:** Visualization of energy minimized geometrical preferences of two PVA molecules in conjugation with a) an isoniazid molecule; and b) a rifampicin molecule showcasing the intra- and inter-molecular interactions after molecular simulations in vacuum. Color codes for elements: C (cyan), O (red), N (blue) and H (white).

In the case of INH, acting as a soluble plasticizer, it showed a high affinity to diffuse into and interact with the polymer molecules (as shown in Figure 6.16a; Equation 6.2 and Equation 6.3) by forming non-bonding interactions in terms of hydrogen bonding contribution (because of the presence of amine groups) and vdWf (the  $\Delta E$  of all these energies is negative; Table 6.7) and hence lead to an increasing in polymer's mobility. In this way, the brittle character of the polymer may decrease with an increase in plasticizer's concentration (Gutierrez-Rocca and McGinity, 1994).

On the other hand, the effect of RIF incorporation on nanotensile properties was not significant as compared to drug free fibres. Although the energy of stabilization was highest in this case (Equation 6.2, Equation 6.3, Equation 6.6 and Equation 6.7;  $\Delta E = -20.445\text{kcal/mol}$ ), the plasticizer effect was not as pronounced as in the case of INH. The below mentioned three reasons may be responsible for the ultimate strength regain in case of RIF thereby retaining the tensile properties of the initially optimized fibres:

1. Firstly, because of poor aqueous solubility of RIF, the drug particles may cause filling up of pores leading to a decrease in porosity of the polymer matrix. According to Spriggs' equation (Spriggs, 1961):

$$E = E_0 \exp(-bP)$$

Equation 6.14

where,  $E$  is the Young's Modulus,  $E_0$  is the Young's Modulus at zero porosity,  $P$  is the porosity and  $b$  is a constant in Spriggs' equation.

It is clear from the above exponential relationship that a decrease in porosity will lead to a comparative increase in Young's Modulus as observed in the experimental results.

2. Secondly, the drug crystals (superfluous) may cause filling of the existing cracks, notches, voids or crazing in the polymeric fibre being tested leading to a increase in rigidity and decrease in movability of the adjacent PVA chains finally leading to a increase in Young's Modulus (Gutierrez-Rocca and McGinity, 1994).
3. Thirdly, the large molecular size of RIF than INH may reduce the volume between two polymer chains leading to an increase in Young's Modulus as compared to INH loaded fibres (Equation 6.10-Equation 6.13).

4. As depicted in Figure 6.16b, the RIF molecule is forming a complex with PVA molecules in form of a crosslinker connecting two molecules together further decreasing the volume and hence increasing the young's Modulus.

The experimental rheological results can also be substantiated based on the above mentioned points. The poor solubility and large molecular size of RIF molecule as compared to better solubility and smaller molecular size seems to be responsible for the more viscosity imparted by RIF to the PVA solution. It can be visualized from Figure 6.16a that INH being soluble acted as “highly penetrable” molecule resulting in homogeneous increase of concentration. However, poorly soluble RIF particles acted as a partially penetrable particles resulting in an increased concentration located in the inter-particles shared zone making the viscosity dissipation less predominant in that area (Figure 6.16b) (Omari *et al.*, 2006). Additionally, RIF being a mild crosslinker (see point 4 above), decreased the “elastic-to-viscous force ratio” as a function of crosslink density causing a more viscous solution with higher Young's Modulus than the drug free polymer solution further necessitating the use of an 8%<sup>w/v</sup> PVA solution for electrospinning.

Hence, we can say that the drugs influenced the nanotensile characteristics by acting as “non-traditional biomedical tensile modifiers of polymeric nanofibres”.

#### **6.3.9.4 Performance of crosslinked PVA electrospun fibres**

In the next part of the molecular static study, the fabrication of PVA based electrospun nanofibrous system and the post-fabrication crosslinking of formed nanofibrous matrix with glutaraldehyde vapours was simulated. The energy changes brought about by crosslinking of the polymeric system are given in Equation 6.2, Equation 6.3, Equation 6.8 and Equation 6.9 and the resulting energy and geometrical minimizations are depicted in Table 6.7 and Figure 6.17, respectively. As the tensile analysis was conducted on both non-crosslinked and crosslinked nanofibres, we elucidated the conformational effect addition of individual components in form of two PVA chains in conjugation with each other and three glutaraldehyde molecules in conjugation with the two PVA chains, respectively, during the initial stage of static simulations.

PVA is known to exhibit interactions with dialdehydes such as glutaraldehyde (with an acid solution which catalyzes acetalization reaction) where it display concentration-dependent intra- and inter-molecular crosslinking and complexation of the polymer matrix (Peng *et al.*, 2011). It is evident from Table 6.7, PVA<sub>2</sub> was energetically stabilized by 10.551kcal/mol (Equation 6.2 and Equation 6.3) in terms of London-dispersion forces due

to presence of vinyl groups ( $\Delta E = -9.426$ ) and torsional stabilization ( $\Delta E = -6.324\text{kcal/mol}$ ) leading to the formation of a network structure - with smaller intermolecular H-bonds measuring  $2.168\text{\AA}$  creating space ( $\sim$ volume) between two chains to slide over each other. Once the polymer network was geometrically optimized and energetically minimized, we disposed three glutaraldehyde molecules in close proximity of two PVA chains ( $\text{PVA}_2\text{-GA}_3$ ) in such a way that the crosslinker molecules sandwiched the polymer chains (Figure 6.17).

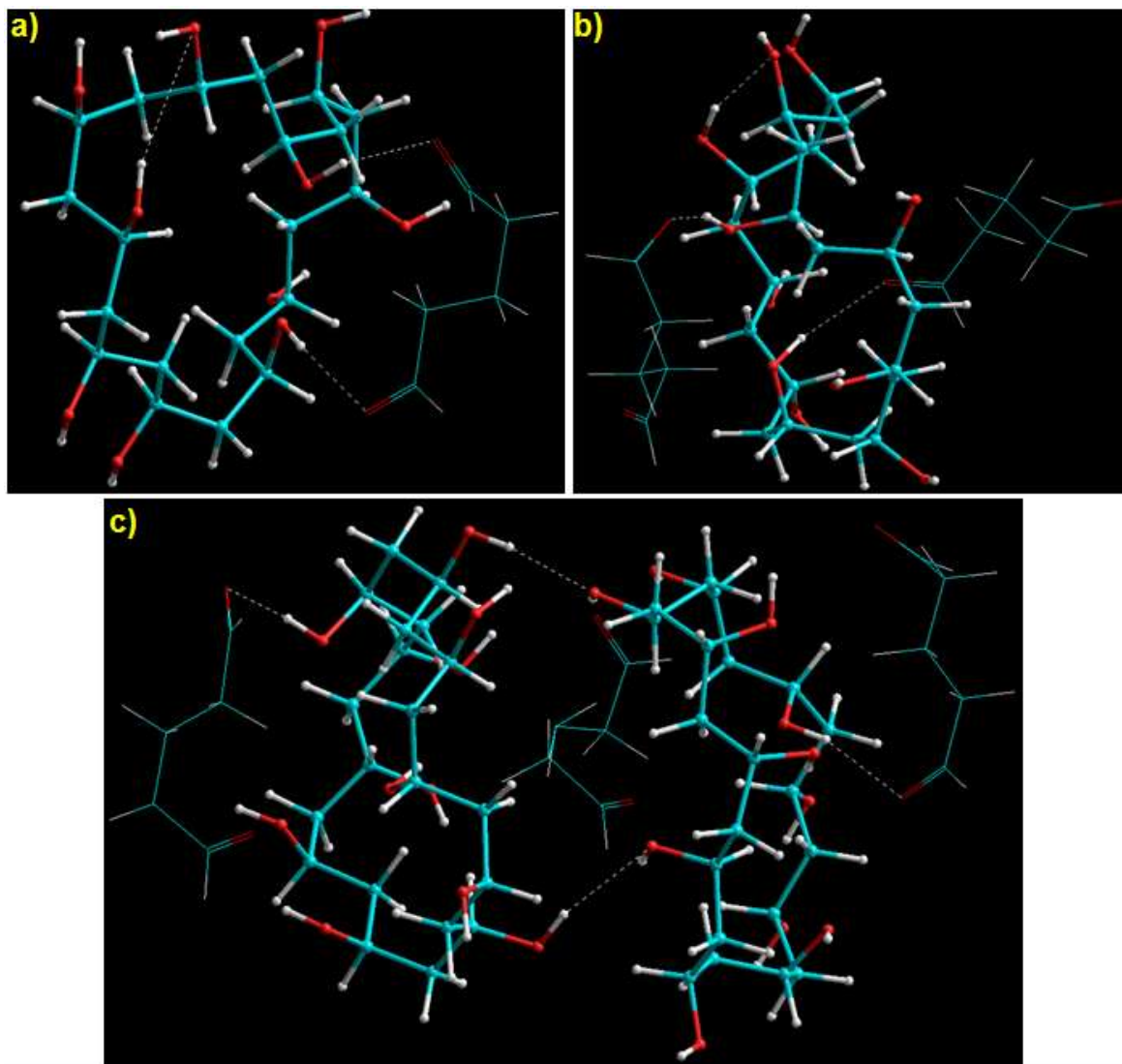


**Figure 6.17:** Visualization of energy minimized geometrical preferences of a) PVA-glutaraldehyde showing the double linking; b) PVA in conjugation with two glutaraldehyde molecules showcasing the intra- and inter- molecular interactions; and c) Two PVA molecules in conjugation with three glutaraldehyde molecules showcasing the intra- and inter- molecular interactions after molecular simulations in vacuum. Color codes for elements: C (cyan), O (red) and H (white).

After energy minimization,  $\text{PVA}_2\text{-GA}_3$  was stabilized by  $15.582\text{kcal/mol}$  as compared to PVA/GA summation because of non-bonding interactions in terms of strong Van der

Waals forces (vdWf;  $\Delta E = -18.421\text{kcal/mol}$ ) along with intra- and inter-molecular H-bonding energy ( $\Delta E = -0.775\text{kcal/mol}$ ). Although the total steric energy was  $-ve$  in magnitude, the interesting feature of PVA<sub>2</sub>-GA<sub>3</sub> energy minimization was an increase in all the three bonding interaction energies, viz. bond stretching, bond angle and torsional contributions, causing the formation of a strained network structure - with smaller intramolecular H-bonds averaging  $1.9855\text{\AA}$ . This crosslinking may further bring two PVA chains closer leading to formation of some more inter-polymeric H-bonds, as shown in Figure 6.17, further forming a dense polymer network. These results are in line with the earlier reported studies where the glutaraldehyde crosslinked PVA membranes displayed better strength and the stereospecificity in presence of glutaraldehyde molecules (Peng *et al.*, 2011).

The complexation of two 10-monomer units' PVA chains with three glutaraldehyde molecules lead to an increase in torsional strain causing a decrease in volume available for movement of polymer chains w.r.t. each other. This decrease in volume may have caused a substantial increase in Young's Modulus and ultimate strength of Formulations 3 and 8 as compared to Formulations 2 and 7, respectively. This seems obvious as an increase in cohesion will restrain the adjacent polymer chains to stretch/slide over each other thereby decreasing the elongation of the fibres. Apart from this, the water soluble crosslinker-glutaraldehyde, used in this investigation showed a high affinity to diffuse into and interact with the polymer molecules (as shown in Figure 6.17a-b) by forming non-bonding interactions in terms of hydrogen bonding contributions and vdWf and hence lead to a decreased polymer's mobility. In this way, the crystalline character of the polymer may decrease with an increase in crosslinker concentration (Peng *et al.*, 2011). Regarding the effect of crosslinker concentration on the tensile properties, Griebel *et al.*, 2005, reported a logarithmic dependency of the Young's Modulus on the amount of cross-links and deduced the following relationship:

$$P(r) = E_0 + \alpha \ln(r)$$

Equation 6.15

where,  $P$  was a estimator to predict Young's Modulus,  $\alpha$  a constant and  $E_0$  a parameter with units of GPa.

Furthermore, in accordance with the Lennard-Jones energy potential, the elastic modulus is a measure of the rigidity of materials and is directly related to the energy of interaction between molecules and their distance of separation (Roberts *et al.*, 1991). Our simulation results showed that increased chemical cross-links may cause disturbance at high

crosslink densities resulting in distortion of bond lengths, angles, and torsions from their equilibrium values eventually causing strained and rigid-framework (Figure 6.17c). Additionally, the build-up of increased cohesion between adjacent polymer chains (intermolecular crosslinking) may initiate a significant axial stress providing a reasonable explanation for the experimentally observed reinforcement and rigidification of the formulations with increased crosslinker concentrations.

These results are coherent with earlier reported results where the inclusion of chemical and physical cross-links, increases the Young's Modulus of a crosslinked composite as fitted in the experimental results (Griebel *et al.*, 2011).

#### **6.4 Concluding Remarks**

In the recent decade, tremendous efforts have been placed on investigating PVA nanofibres for biomedical applications. Electrospinning proved to be a versatile technique in fabricating drug-loaded PVA nanofibres, ideal for prolonged drug delivery. Modification through crosslinking using GA vapours may produce relatively less-toxic PVA nanofibres possessing properties which are ideal for prolonged drug delivery. The PVA nanofibres demonstrated good-drug loading capabilities, and drug release kinetics which are important factors in drug delivery, and showed an improvement in the overall strength of the nanofibrous membranes.

Formulation 3 was identified as the most suited formulation for INH release, by demonstrating the most control of INH release over a period of 12 hours, while Formulation 9 was selected as the ideal formulation most suited for RIF release, by demonstrating the most control of RIF release over a period of 12 hours. These formulations were thus selected for further *in vivo* analysis in a pig model. The addition of drugs had a significant effect on the Young's Modulus values effecting both the plastic and elastic deformation of the fibres by acting as non-traditional biomedical tensile modifiers of polymeric nanofibres. Finally, molecular mechanistic studies as well as image processing analysis corroborated well with the experimental findings and the influence of formulation variables as well as that of drugs on the performance of vapour crosslinked PVA nanofibres was determined on the basis of energy transformations and voxel intensities, respectively.

## CHAPTER 7

### ***IN VITRO AND IN VIVO ANALYSIS OF THE MULTI-COMPONENT MEMBRANOUS DRUG DELIVERY SYSTEM IN RELATION TO A MARKETED GOLD STANDARD FORMULATION***

---

#### **7.1 Introduction**

Achieving a predictable and reproducible therapeutic response to a drug that is included in a formulation is the primary objective of dosage form design (Aulton, 2002). The application of new technologies has enabled the resurrection of older molecules and the term 'new drugs from old' was coined. As previously discussed in *Chapter 1*, 'old' or established drugs are reformulated through a variety of means to ensure enhanced safety and efficacy, thus 'resurrecting' older drugs. Novel modes of drug delivery are employed to develop an ideal drug delivery system which provides the correct quantity of drug to the appropriate part of the body, at the right time and for the required period. Formulation strategies to attain such objectives include delivering the same drug by a different route, prolonging the therapeutic effect (with the use of prolonged release systems), providing unique dosage regimens (i.e. once daily administration) or plasma profiles, or by improving patient compliance (easing complicated therapeutic regimens) (Crowley and Martini, 2004). The proposed MMDDS boasts such resurrection of rifampicin and isoniazid by delivering both drugs in a single dosage form, providing enhanced bioavailability through targeted drug delivery and ensuring consistent drug release over a prolonged period of time.

The preceding chapters of the present dissertation described the formulation, development and *in vitro* behavior of the individual components comprising the MMDDS, however, the *in vitro* drug release behavior of the MMDDS in its entirety is yet to be determined. The current chapter therefore focuses on the behavior of the MMDDS in its entirety. A marketed gold standard formulation containing rifampicin and isoniazid was selected and investigated for both *in vitro* and *in vivo* drug release behaviour and subsequently compared to the efficacy of the proposed MMDDS.

##### **7.1.1 Overview of MMDDS formulation components**

The purpose of this study was the development of a "smart" multi-layered membranous system intended to deliver multiple drugs to their respective sites of absorption within the GIT. The preceding chapters of the present dissertation identified the various formulation

variables to be employed in the fabrication of the drug delivery system and are summarised in Figure 7.1. The membranous system is composed of two components, intended for drug delivery at the upper gastric or intestinal region of the GIT respectively. CHT and PEC were selected as the pH-responsive polymers as CHT is pH-responsive to low ( $\pm$ pH1.2) pH ranges while PEC is pH-responsive to higher ( $\pm$ pH6.8) pH ranges. The water insoluble backing layer is further discussed in the present chapter and was formulated employing the hydrophobic polymer, ethylcellulose.

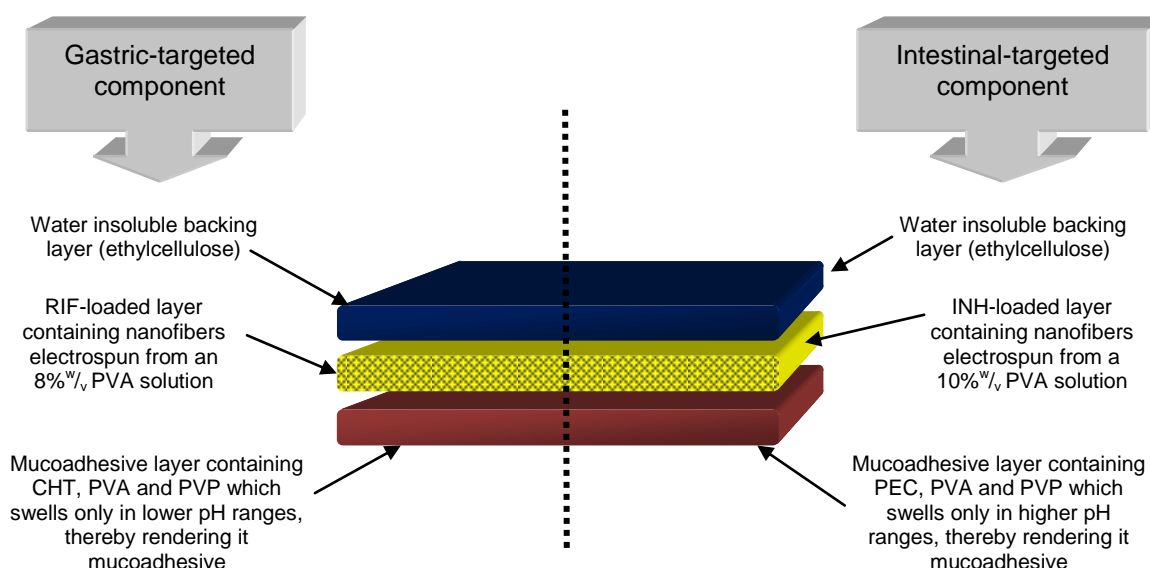


**Figure 7.1:** Schematic overview of the componential architecture of the MMDDS.

### 7.1.2 Selection of an appropriate animal model for *in vivo* analysis

*“The use of animal models in science, and in particular, biomedical research, is accepted by the majority of lay people and scientists alike as being necessary to the advancement of useful knowledge that brings about relief from suffering.”*

The above statement by Chow and co-authors (2008) adequately summarizes the importance of the use of animal models in research and development. Animal model use will remain a necessity in the research and development of countless drugs and newer therapies for the relief of human suffering, until science is able to develop alternative models and systems that are equally reliable and robust. Prior to being accepted and utilized in common medical practice as safe and effective therapies, there are legislative requirements that require that all new drug delivery devices and therapies undergo rigorous clinical trials, which determine the safety and efficacy of the new product. Such



regulations are required since basic *in vitro* analysis of therapies is non-physiological and pose significant limitations. Although information obtained from *in vitro* analysis is especially important in establishing mechanisms and behavior of a drug or delivery system, *in vivo* analysis can identify how the mechanisms and behaviour are affected under clinical conditions, and animal models are therefore important for “proof of principle” research. This form of research, and the information obtained from it, is especially important when assessing the safety and efficacy of both the drug and the delivery system (Chow *et al.*, 2008).

Animal models, specifically in biomedical research, can be defined as “a living organism with an inherited, naturally acquired or induced pathological process that in one way or another closely resembles the same phenomenon in man” (Wessler, 1976). When experimenting with animals, it is a fundamental requirement to ensure the aptness of an animal model that would allow human-related validation of the important data and information gathered from them (Nunoya *et al.*, 2007). The use of the swine model in biomedical research has become increasingly common as an alternative to the dog or primate species, based not only on the regulatory and ethical pressure questioning the use of other models, but also due to their comparative anatomy and physiology in relation to humans (Swindle and Smith, 2000; Nunoya *et al.*, 2007). It should be noted that even though animal models are unable to perfectly mimic the human condition, the pig has been identified as a suitable non-primate animal model for preclinical evaluation due to its much closer resemblance to humans (Patterson *et al.*, 2008).

Therefore, *in vivo* analysis of the biocompatibility and drug release behaviour of the MMDDS was conducted employing a swine model, based on the premise that the swine model demonstrates the closest similarity to gastro-intestinal human anatomy and physiology (Nunoya *et al.*, 2007). Appropriate ethics approval was obtained from the relevant ethical committee (Appendix C) prior to commencing the study. Ultra Performance Liquid Chromatography (UPLC) was employed to analyze the drug content in the blood samples obtained during animal studies.

## **7.2 Materials and Methods**

### **7.2.1 Materials**

The materials described in *Section 4.2.1* and *Section 4.4.1* were employed in the fabrication of the gastric- and intestinal-targeted mucoadhesive layers respectively, while the RIF- and INH-loaded nanofibrous matrices were fabricated employing the materials

described in *Section 6.2.1*. Polymers ethylcellulose (Ph Eur viscosity 9m.Pa.s) purchased from Fluka® (Sigma Aldrich (Pty) Ltd., St Louis, MO, USA) and Eudragit® RS PO obtained from Evonik Industries (Evonik Röhm GmbH, Pharma Polymers, Kirschenallee, P-64 293, Darmstadt, Germany) were utilized to assemble the MMDDS. The solvents 2,2,2-Trifluoroethanol (purity  $\geq 99,0\%$  GC grade); isopropanol and acetone were purchased from Sigma (Sigma Aldrich Chemie GmbH, Steinheim, Germany). All other reagents employed were of analytical grade and used as purchased without further purification. Double-deionised water was obtained from a Milli-Q Water Purification System (Millipore, Bedford MA, USA).

UPLC-grade solvents, employed for UPLC measurements included Acetonitrile (ACN) 200 (ROMIL-SpS™ Super Purity Solvent (CH<sub>3</sub>CN), Assay >99.9%) and Methanol 215 (ROMIL-SpS™ Super Purity Solvent (MeOH) Assay >99.9%) which were purchased from Romil Pure Chemistry (Waterbeach, Cambridge, England) and double de-ionized water which was obtained from a Milli-Q water purification system (Milli-Q, Millipore, Billerica, MA, USA). Oases HLB cartridges, for solid phase extraction, were provided by Waters (Milford, MA, USA). Isoniazid (INH) (Sigma Aldrich (Pty) Ltd., St. Louis, Missouri, USA), rifampicin (RIF) and the internal standards including methylparaben (MP) employed for *in vitro* analysis and furosemide (FUR) employed for *in vivo* analysis were obtained from Sigma (Sigma Aldrich (Pty) Ltd., St. Louis, Missouri, USA) and were of analytical grade and employed without further purification. A total of 5 female white pigs were employed in the study, each healthy and with an average weight of 35kg. Fresh blank plasma was routinely drawn and supplied from the catheterized pigs. Rifinah®, a marketed gold standard formulation was obtained from Sanofi-Aventis (Sanofi-Aventis (Pty) Ltd., Midrand, South Africa). The Acquity UPLC® BEH RP18 1.7 $\mu$ m column (2.1x100mm) was utilized to separate analytes, while Sep-Pak® Vac ICC (100mg) CN Cartridges were obtained from Waters Corporation (Milford, MA, USA). The sample vials employed was 2mL ANSI48 vials which were LCMS certified and clear, pre-slit PTFE silicone screw-top vials.

## **7.2.2 Fabrication of the MMDDS**

### **7.2.2.1 Mucoadhesive layer**

Membranes were fabricated as described in *Section 4.2.3* and *Section 4.4.3* for the optimized gastric- and intestinal-targeted mucoadhesive layers respectively. Briefly, the polymers were combined in the ratios defined via optimization studies and included: 1.001%<sup>w/v</sup> of CHT, 4.750%<sup>w/v</sup> PVA and 4.004%<sup>w/v</sup> of PVP for the gastric-targeted mucoadhesive layer and 2%<sup>w/v</sup> of PEC, 3.375%<sup>w/v</sup> of PVA and 6%<sup>w/v</sup> of PVP for the

intestinal-targeted mucoadhesive layer. Film-cast membranes were cut into dimensions of 20x30mm and thereafter stored with desiccants in airtight containers until further processing was completed.

#### **7.2.2.2 Drug-loaded layer**

Drug-loaded nanofibrous matrices were electrospun employing the solution and processing parameters described in *Section 6.2.2*. Briefly, the solution parameters included an 8%<sup>w/v</sup> solution of PVA containing 2%<sup>w/v</sup> RIF and 5%<sup>w/v</sup> Tween<sup>®</sup> 80 for the gastric-targeted component, and 10%<sup>w/v</sup> PVA containing 2%<sup>w/v</sup> RIF and 0.1%<sup>w/v</sup> silicone for the intestinal-targeted component. The electrospinning setup, as illustrated in Figure 5.2, involved applying 20kV, supplied by a Glassman High Voltage, INC (High Bridge, NJ, USA) to the drug-polymer solutions. The resultant electrospun fibres were collected on an aluminium sheet connected to a grounded counter electrode. Electrospinning was carried out at ambient room conditions for periods ranging between 5-8 hours, cut into 20x30mm dimensions and stored with a desiccant until further processing was conducted. The nanofibrous matrices were thereafter modified via a post-treatment involving glutaraldehyde (GA) vapour induced crosslinking. Crosslinking was conducted employing the method described in *Section 6.2.3*. RIF-loaded nanofibres were crosslinked for a period of 12 hours in the presence of 30:10mL of GA:HCl while INH-loaded nanofibres were crosslinked for a period of 24 hours in 15:5mL GA: HCl. *In vitro* drug release studies indicated that these crosslinking parameters demonstrated the most control over the release of the entrapped drugs, an ideal characteristic in the development of the MMDDS.

#### **7.2.2.3 Assembling the MMDDS**

The individual layers of the MMDDS were assembled as follows (Figure 7.2): the drug-loaded nanofibrous matrix was attached to the respective mucoadhesive layer by employing a 60%<sup>w/v</sup> solution of Eudragit<sup>®</sup> RS PO (i.e. the RIF-loaded nanofibrous matrix was attached to the gastric-targeted mucoadhesive layer for the gastric delivery of RIF, while the INH-loaded nanofibrous matrix was attached to the intestinal-targeted mucoadhesive layer for the intestinal delivery of INH). Thereafter, a 30%<sup>w/v</sup> solution of ethylcellulose (prepared in a 1:1 solution of isopropanol: acetone) was then film-cast over the existing layers to form the water-insoluble backing layer or coating which would protect the entrapped drug from the harsh gastrointestinal environment. The coating was thereafter allowed to dry for a period of 24 hours and the MMDDS was thereafter stored in an airtight container with a desiccant until further analysis was conducted.

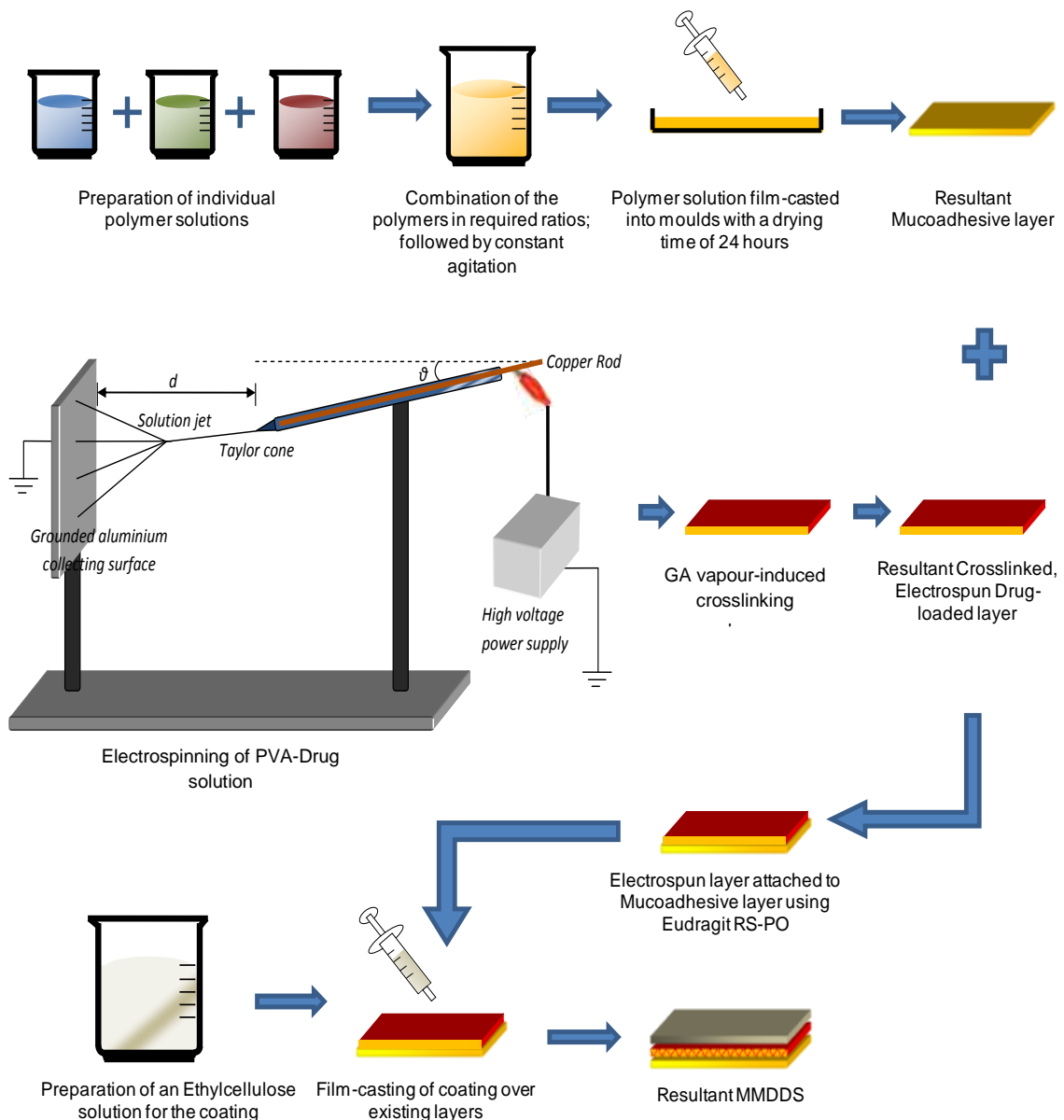


**Figure 7.2:** Schematic illustration of the fabrication of the MMDDS in its entirety. The gastric- and intestinal-targeted components differed with regard to the polymer type and quantity, and crosslinking procedure.

### 7.2.3 Comparative analysis of the *in vitro* drug release behaviour of the MMDDS in relation to a marketed gold standard formulation

#### 7.2.3.1 *In vitro* dissolution

*In vitro* drug release studies were conducted using a six-station USP apparatus II (Erweka DT 700 GmbH Germany), in which an MMDDS containing 150mg of RIF and 75mg of INH was placed within the vessel under a stainless steel ring mesh assembly. This prevented the paddle from inflicting physical/mechanical damage to the drug delivery system which can potentially alter the drug release characteristics, in addition to preventing any erratic fluctuation due to unstable hydrodynamics (Pillay and Fassihi, 2000). Each vessel contained 900mL of PBS, which was heated to a temperature of 37°C prior to the addition

of the MMDDS and the stainless steel ring mesh assembly. The apparatus was calibrated for a 12 hour run, and the rotating paddle method was selected with a rotational speed of 50rpm. Sampling occurred at hourly intervals and involved the drawing of 5mL of now drug incorporated solution from the dissolution vessel. An equal quantity of the removed buffer was replaced with fresh buffer to maintain sink conditions. Samples were then subject to UV spectrophotometry and drug quantity was determined using a standard calibration curve.

To determine whether the MMDDS prevents INH release in upper gastric conditions, complete MMDDS was subject to *in vitro* conditions typical of the upper gastric region for 3 hours (900mL of PBS, 1.2 pH; 37°C), corresponding to the duration that the MMDDS would be present in the gastric region. Thereafter, only the intestinal-targeted component was transferred to a corresponding vessel for 12 hours which simulated the intestinal region of the GIT (900mL of PBS, 6.8 pH; 37°C), while the gastric-targeted component was maintained in conditions typical of the upper gastric region of the GIT for the remainder of the study. The above method was identified to closely resemble the conditions the MMDDS would be exposed to. Based on the architectural design of the MMDDS, the gastric-targeted component is maintained in the upper gastric region for a prolonged period of time through mucoadhesion, and was therefore maintained in simulated gastric conditions for the entire duration of the study. In contrast, the intestinal-targeted component was subject to 3 hours of simulated gastric conditions (simulating the duration required for the intestinal-targeted component to pass through the upper gastric region), and thereafter transferred to a fresh dissolution vessel which subjected the intestinal-targeted component to conditions which simulate the intestinal region of the GIT. The samples were thereafter analyzed via the UPLC method depicted in *Section 7.2.3.2*. The test was performed in triplicate (n=3).

For comparative purposes, a marketed gold standard formulation, Rifinah<sup>®</sup>, containing 150mg of RIF and 75mg of INH was also subject to the *in vitro* dissolution test. Rifinah<sup>®</sup> tablets disintegrated within the first three hours of the study, and were thus exposed only to conditions simulating the upper gastric region of the GIT (900mL of PBS, 1.2 pH; 37°C). Samples were thereafter analysed employing Ultra Performance Liquid Chromatography (UPLC) analysis.

#### **7.2.3.2 UPLC analysis of *in vitro* dissolution samples**

A Waters Acquity™ Ultra Performance Liquid Chromatography (UPLC) system employing Empower Pro Software (Waters<sup>®</sup>, Milford, MA, USA) coupled with a PDA detector was

utilized to determine the quantity of the individual drugs present in the dissolution samples. UPLC is useful in the simultaneous quantification of multiple drugs (analytes) present in a single sample. UPLC typically requires a mobile and stationary phase for separation of multiple analytes, which in turn is detected by a photodiode-array (PDA) detector. A sample, which contains the analyte is dissolved in the mobile phase and thereafter pumped through the stationary phase (a chromatographic column packed with the stationary phase). Depending on the degree of interactions between the stationary phase and the analytes, the retention time of the various analytes or drugs will vary, and thus allow for identification, quantification and separation of multiple drugs in one sample (Chey, 2011).

#### *7.2.3.2.1 Priming solvents employed in the washing protocol*

Prior to analysis of samples, the UPLC system was primed by a 'washing protocol' of two cycles of 10 minutes each. The solvents employed in the priming of the UPLC pumps included a weak needle wash solution containing 10%<sup>v/v</sup> acetonitrile and 90%<sup>v/v</sup> double de-ionized water, and a strong needle wash solution of 90%<sup>v/v</sup> acetonitrile and 10%<sup>v/v</sup> double de-ionized water. These solutions were also used to equilibrate the system after sample analysis, removing any analytes which may have lodged in the column during the analysis of the previous sample.

#### *7.2.3.2.2 Mobile phases employed for sample analysis*

The binary mobile phase employed for sample analysis included pure acetonitrile (ACN) and 0.1% formic water (FW) at differing ratios (gradient method). The formic water was prepared by dissolving 1mL of formic acid in 999mL of double de-ionized water.

In all instances, only double de-ionized water obtained from a Milli-Q filtration system (Millipore, Johannesburg) with a resistivity of 18.2MΩcm<sup>-1</sup> was used to prepare the UPLC solvents employed in both UPLC priming and sample analysis. Furthermore, all mobile phases, needle washes (both strong and weak), and any solvents employed in sample preparation were filtered using a 0.22µm pore size Cameo Acetate membrane filter (Millipore Co., Bedford, MA, USA).

#### *7.2.3.2.3 UPLC-PDA analysis for drug content quantification*

UPLC separation was achieved on an Acquity UPLC<sup>®</sup> BEH RP18 1.7µm column (2.1 x 100mm) set at a temperature of 25°C. The column was initially primed following a washing protocol which included a strong needle wash and a weak needle wash. The binary mobile phase consisted of formic water (0.1% formic acid) and acetonitrile (ACN)

following the gradient analysis run time as indicated in Table 7.1. A flow rate of 0.40mL/min was selected with an injection volume of 2µL. The run time was three minutes and the system was allowed to equilibrate for 5 minutes prior to analyzing the next sample, thus removing any late eluting interferences. The photodiode-array (PDA) detector was set to detect and quantify drug content at a wavelength of 263nm. Methylparaben was employed as the internal standard to compensate for sample preparation losses and drug content was quantified by determining the ratio of the Area Under the Curve of the drug to be quantified vs. the Area Under the Curve of the internal standard ( $AUC_D / AUC_{IS}$ ).

**Table 7.1:** UPLC Gradient method parameters for the simultaneous quantification of isoniazid and rifampicin.

| <b>Time (minutes)</b> | <b>Flow Rate (mL/min)</b> | <b>%A</b> | <b>%B</b> |
|-----------------------|---------------------------|-----------|-----------|
| 0                     | 0.40                      | 100       | 0         |
| 0.63                  | 0.40                      | 95        | 5         |
| 1.5                   | 0.40                      | 20        | 80        |
| 1.6                   | 0.40                      | 0         | 100       |
| 1.94                  | 0.40                      | 60        | 40        |
| 2.8                   | 0.40                      | 100       | 0         |

*%A= 0.1%<sub>v</sub> formic water and %B= pure acetonitrile*

### 7.2.3.3 Construction of calibration curves employing a known series of analytical standards

Stock solutions of INH (0.083mg/mL); RIF (0.1668mg/mL) and MP (1.0mg/mL) were prepared in PBS (RIF – pH 1.2; INH – pH 1.2 and 6.8). Working standard solutions were prepared by a series of dilutions (5 dilutions each) of INH and RIF with known concentrations for analytical evaluation in the preparation of the calibration curve. 1.5mL of each dilution was combined with 0.5mL of the internal standard solution and passed through a 0.22µm Cameo Acetate membrane filter (Millipore Co., Bedford, MA, USA) into 2mL ANSI48 vials, which were then subject to analysis. The content of RIF and INH was analyzed at wavelengths of 263nm. A linear curve was generated on SigmaPlot® V10.0 software, with the observed AUC ratio (ratio of the Area Under the Curve (AUC) of the drug peak ( $AUC_D$ ) vs. the internal standard peak ( $AUC_{IS}$ ) plotted on the y-axis against the corresponding concentrations (mg/mL) plotted on the x-axis. With the intercept set at 0, the  $R^2$  values were determined to be 0.9983 of RIF and 0.9980 of INH.

## **7.2.4 Comparative analysis of the *in vivo* drug release behaviour of the MMDDS in relation to a marketed gold standard formulation employing a swine model**

Prior to commencement of the *in vivo* studies, clearance was obtained from the Animal Ethics Clearance Committee (Appendix C1), University of the Witwatersrand.

### **7.2.4.1 Surgical implantation of the jugular vein catheter**

Upon arrival at the Central Animal Services lab, pigs were habituated to ensure efficient and accurate blood sampling. Pigs were anesthetized with ketamine (11mg/kg I.M.) and midazolam, (0.3mg/kg I.M.) prior to the surgery. Buprenorphine (0.05mg/kg I.M.) and carprofen (4mg/kg I.M.) were administered for both analgesia and inflammation. The surgical area (the left neck and shoulder area) of the pigs were thereafter prepared for surgery by shaving the area, followed by sterilization. Once intubated, the anaesthesia was maintained with 2% isoflurane in 100% oxygen. In an aseptic environment, the jugular vein was exposed by an incision made dorsal to the jugular groove on the left lateral aspect of the neck. To prevent the jugular vein from collapsing during the surgery, the catheter (a 7 French gauge double lumen 35cm catheter (CS-28702) obtained from Arrow Deutschland GmdH, Erding, Germany) was first tunnelled subcutaneously to the exit point, located on the cranial aspect of the scapular. The externalised injection ports of the catheter were sutured to the skin of the pig so as to limit excessive movement and bending. Thereafter, the catheter was surgically inserted approximately 10cm into the left jugular vein as depicted in Figure 7.3 via blunt dissection. The lumen of the catheter was fastened to the wall of the vein using a purse suture technique. Both the incision and exit points were sutured. In order to assess the functioning of the catheter, blood was removed via the catheter and the catheter was thereafter flushed with heparinised saline (1000i.u. of heparin in 1L of 0.9% saline). Throughout the entire duration of the surgery, the pigs' vital signs (i.e. heart rate, blood pressure, respiratory rate and body temperature) were kept under constant observation. Following the surgical procedure, the pigs were allowed 8-10 days to recover. During this time, the habituation procedure continued to facilitate the process of blood sampling. Throughout the study, the catheter was flushed with heparinised saline three times a day, while the entry and exit points were continuously monitored for any sign of infection, which was treated appropriately.



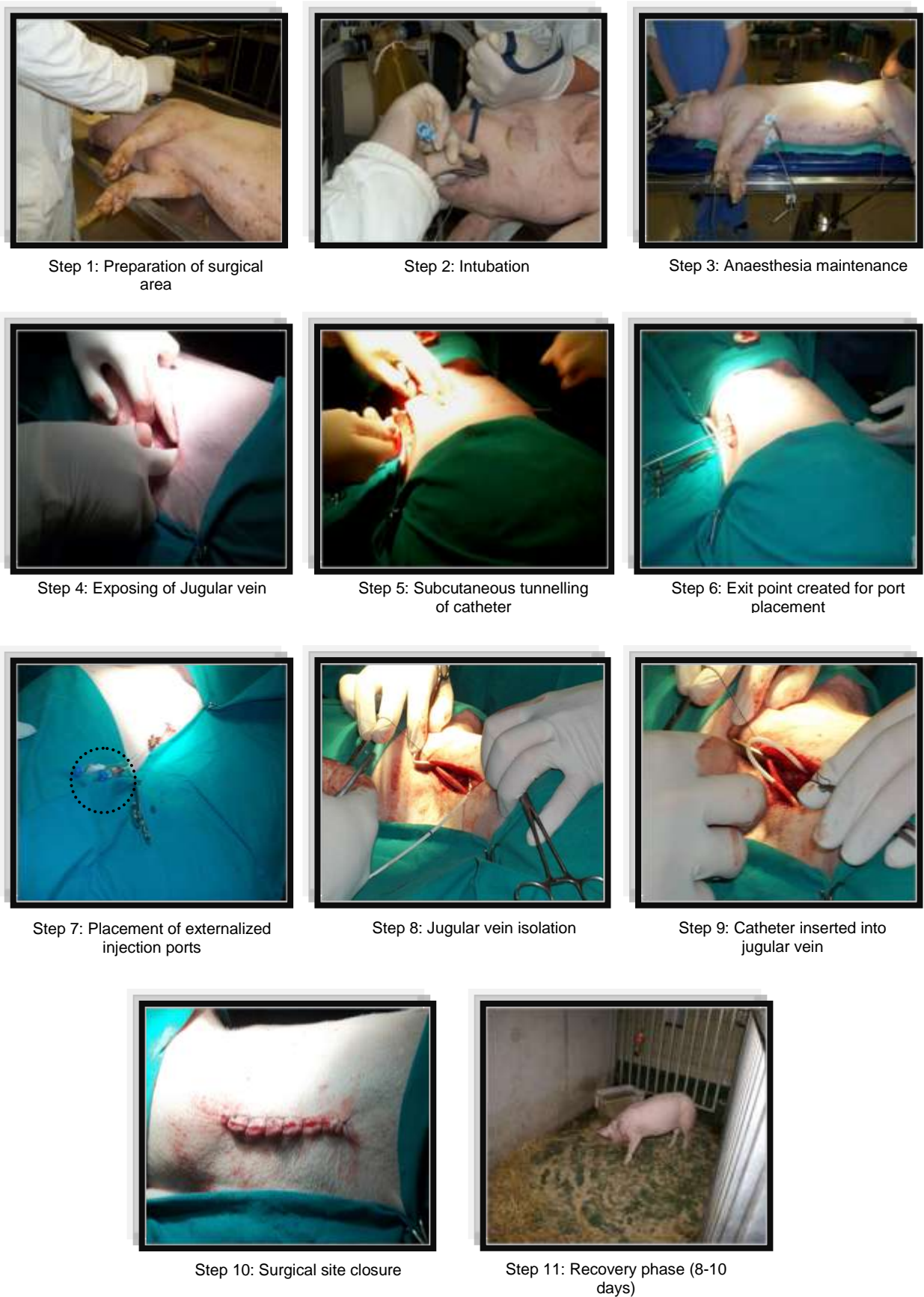


**Figure 7.3:** Sequential digital images depicting the surgical procedure for the implantation of the chronic jugular vein catheter.

#### 7.2.4.2 Administration of the MMDDS or marketed gold standard formulation

To facilitate dosage administration, pigs were sedated in order to insert an intra-gastric tube. A total of 5 pigs (n=5) were orally dosed with either the MMDDS or marketed gold standard formulation via an intra-gastric tube as illustrated in Figure 7.4. This avoided physical alteration of the system which may occur through mastication by the pigs. Dormicum® and Anaket® were injected directly into the jugular vein catheter. When sedated, anaesthesia was maintained with 2% isoflurane in 100% oxygen and the pigs' vital signs were constantly monitored. The intra-gastric tube was then inserted into the stomach of the pig while the pig was held upright. To ensure that the drug delivery system was not still lodged in the intra-gastric tube, 50mL of water was poured down the tube prior to removal of the tube. While under sedation, all surgical sites were inspected for infection and (if required) sutures were repaired. The pig was returned to its pen to recover under observation.



Step 1: Dormicum® and Anaket® administration



Step 2: Anaesthesia maintenance



Step 3: Intra-gastric tubing and dosage administration



Step 4: Inspection of surgical sites and injection ports for infection, and re-suturing of damaged sutures

**Figure 7.4:** Sequential digital images depicting the process of dosage administration.

### **7.2.4.3 Blood sampling protocol**

Blood sampling occurred at predetermined time points over a 24 hour period (0, 2, 4, 6, 8, 10, 12, 16, 20 and 24 hours) after the pigs were orally dosed with either the marketed gold standard formulation (Rifinah<sup>®</sup>) or the MMDDS. The pigs were distracted with food which eased the blood sampling procedure. The chronic jugular vein catheter was disinfected and an aseptic technique was utilised to draw blood from the externalized injection ports. This prevented the introduction of any foreign organisms, thus abating infection. Prior to removal of blood from the ports, the catheter was flushed with heparinised saline to clear any clots and remove old blood, ensuring an efficient sampling procedure. 10mL blood samples were then drawn and placed in a lithium heparin Vacutainer<sup>®</sup>. The catheters were once again flushed with heparinised saline, clearing the catheters and ports of any blood present, thus preventing future blocking of the ports from occurring. Blood samples were centrifuged at 5000rpm for 15 minutes, removing the red blood cells. The plasma supernatant was then removed and frozen at -72°C until required.

### **7.2.4.4 Plasma extraction of drug**

In order to minimize the quantity of blood obtained from the pigs, a single method was developed to extract both RIF and INH from a single plasma sample. Briefly, the method involved a process of protein precipitation (deproteination), freeze-liquid and solid-phase extraction (SPE) for the successful extraction of both drugs as depicted in Figure 7.5. Plasma samples (obtained from blood sampling) were thawed at room temperature. 0.5mL of the thawed plasma was added to 10mL centrifuge tubes. The sample was subject to deproteination and freeze-liquid extraction of RIF by adding 3mL of ACN. The plasma-ACN mixture was then vigorously vortexed (Vortex genie 2, Bohemia, NY, USA) for 60 seconds, facilitating deproteination. Centrifugation at 3000rpm for 15 minutes (Optima<sup>®</sup> LE-80K, Beckman, USA) caused both protein precipitation and the “movement” of RIF from the aqueous phase (where it is poorly soluble) to the ACN phase (where RIF is relatively more soluble). Freezing at -72°C produced three immiscible layers – the lower protein precipitate, the middle aqueous phase (now containing only INH) and the upper ACN layer (containing RIF). Upon removal from the -72°C freezer, the upper ACN layer thawed faster than the aqueous layer, and was then decanted into a 10mL glass test tube and stored until UPLC analysis was conducted. The remaining contents of the centrifuge tube, consisting primarily of the aqueous phase (which contains INH), was then subject SPE as follows: Sep-Pak<sup>®</sup> Vac ICC CN Cartridges obtained from Waters (Water Corporation, Milford, MA, USA) were conditioned 1mL methanol and 1mL deionized water. Thereafter, the aqueous phase of the plasma sample was then loaded onto the cartridges post-conditioning. A 2mL quantity of 30%<sup>v/v</sup> methanol was determined to be the

most efficacious elutant that achieved the most desirable recovery of the drug from the plasma. The entire SPE procedure (conditioning to elution) was facilitated with the use of a Visiprep Vacuum Manifold and Standard Lid (Water Corporation, Milford, MA, USA). Once eluted, the INH containing methanol was added to the RIF containing ACN (obtained from freeze-liquid extraction) and the sample was spiked with 40 $\mu$ L furosemide (FUR) (employed as the internal standard at a concentration of 0.01mg/mL). The spiked sample was then passed through a 0.22 $\mu$ m Cameo Acetate membrane filter (Millipore Co., Bedford, MA, USA) into 2mL ANSI 48 vials and subjected UPLC analysis as depicted in *Section 7.2.4.6*.

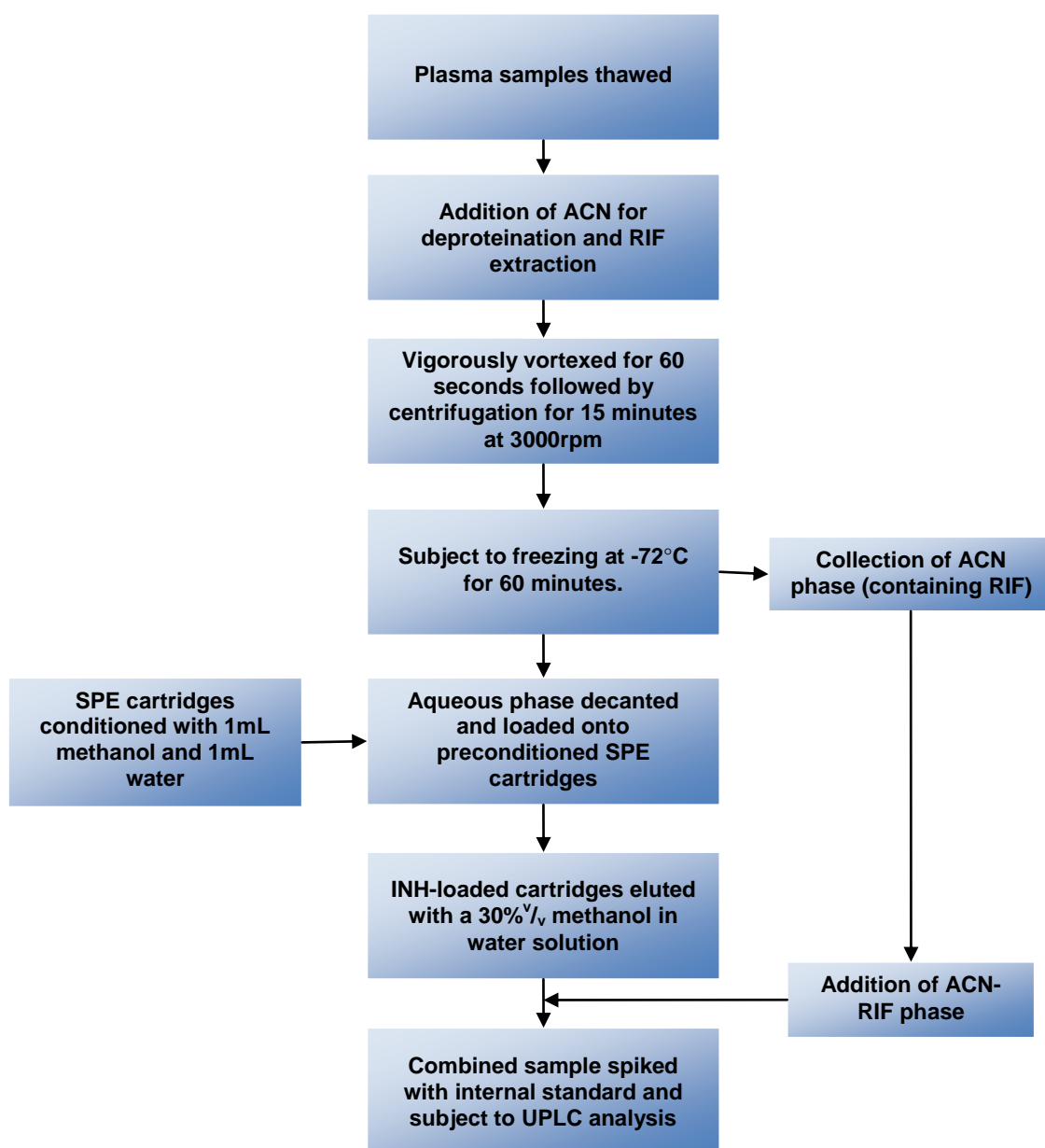


**Figure 7.5:** Schematic depicting the simultaneous plasma extraction method of RIF and INH.

#### **7.2.4.5 Determination of plasma extraction efficiency**

Three concentrations of RIF and INH were utilized to spike blank plasma for the preparation of the extracted samples. An equal concentration of the respective drug was prepared in a mixture of 30%<sub>v/v</sub> methanol and ACN mixture (2:3<sub>v/v</sub>) solution as the unextracted samples. The recoveries of RIF and INH from plasma were determined by comparing the peak area ratios of the extracted standards vs. those of unextracted standards at different concentration levels over the relevant concentration range. FUR was employed as the internal standard to compensate for sample preparation losses, and drug content was quantified by determining the ratio of the Area Under the Curve of the drug to be quantified vs. the Area Under the Curve of the internal standard ( $AUC_D / AUC_{IS}$ ).

#### **7.2.4.6 UPLC-PDA analysis for drug content quantification**

UPLC separation was achieved on an Acquity UPLC<sup>®</sup> BEH RP18 1.7 $\mu$ m column (2.1 x 100mm) set at a temperature of 30°C. The column was initially primed following a washing protocol which included a strong and weak needle wash. The binary mobile phase consisted of formic water (0.1%<sub>v/v</sub> formic acid) and acetonitrile (ACN) following the gradient method indicated in Table 7.1, *Section 7.2.3.2*. A flow rate of 0.40mL/min was selected with an injection volume of 10 $\mu$ l. The run time was 2.3 minutes and the system was thereafter allowed to equilibrate for 5 minutes prior to analyzing the subsequent sample. The photodiode array (PDA) detector was set to detect and quantify drug content at a wavelength of 272nm. Furosemide was employed as the internal standard and drug content was quantified by determining the ratio of the Area Under the Curve of the drug ( $AUC_D$ ) to be quantified vs. the Area Under the Curve of the internal standard ( $AUC_{IS}$ ).

#### **7.2.4.7 Preparation of analytical standards for the construction of the calibration curves**

Stock solutions of INH (0.25mg/mL in water); RIF (0.25mg/mL in a 10% ACN solution) and FUR (0.01mg/mL in a 10% ACN solution) were prepared and respectively. Working standard solutions of RIF and INH were prepared by a series of dilutions (5 each), obtaining concentrations ranging from 5 to 30 $\mu$ g/mL, for analytical evaluation of the calibration curve. The calibration curves were constructed by spiking 0.5mL of blank plasma with 125 $\mu$ l of the respective drug solution. The samples were then subject to plasma extraction as detailed in *Section 7.2.4.4* and thereafter subject to UPLC analysis as depicted in *Section 7.2.4.6*. A linear curve was generated on SigmaPlot<sup>®</sup> V10.0 software, with the observed ratio (ratio of the Area Under the Curve of the drug peak ( $AUC_D$ ) vs. the Area Under the Curve of the internal standard peak ( $AUC_{IS}$ )) plotted on the

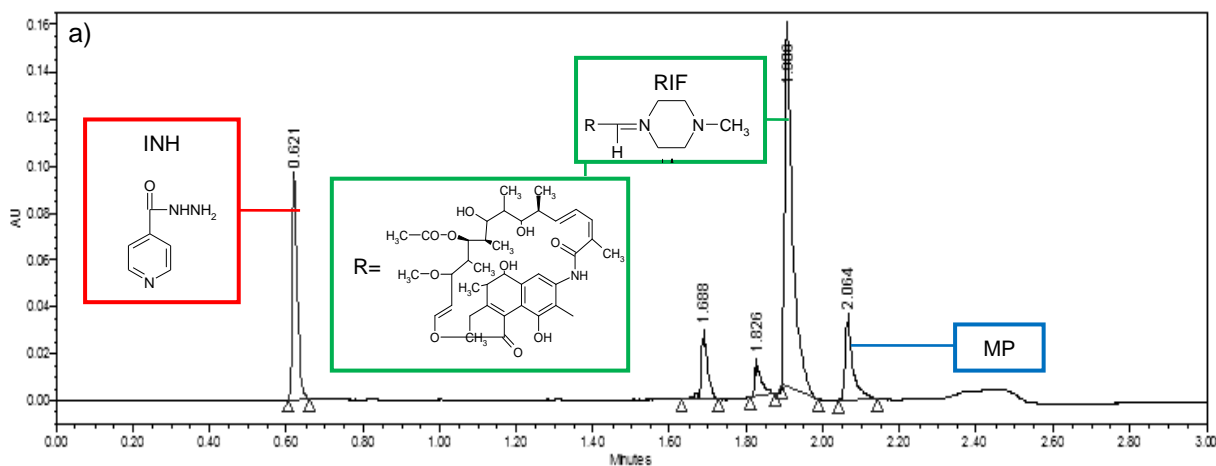
y-axis against the corresponding concentrations ( $\mu\text{g/mL}$ ) plotted on the x-axis. With the intercept set at 0, the  $R^2$  values were determined to be 0.9958 and 0.996 for RIF and INH respectively.

### 7.3 Results and Discussion

#### 7.3.1 *In vitro* comparison of marketed formulations

##### 7.3.1.1 Chromatograms obtained through UPLC analysis

Figure 7.6 demonstrates the resultant chromatograms obtained from UPLC analysis of the *in vitro* dissolution samples. The UPLC method described enabled rapid simultaneous measurement of RIF and INH for the *in vitro* dissolution samples. As illustrated in Figure 7.6, use of the gradient method described resulted in sharp and symmetrical peaks. Furthermore, good peak resolution and separation was achieved, substantiating the appropriateness of the UPLC method for the simultaneous quantification of both drugs and complete elution is achieved in less than three minutes under the chromatographic conditions described. RIF, INH and methylparaben (MP) obtained retention times at 0.621, 1.903 and 2.064 respectively. INH, which is highly soluble in water, elutes when the constitution of the mobile phase is primarily formic water. RIF and MP, which are readily soluble in the organic phase (ACN), thus elutes when the mobile consists of a substantially larger fraction of ACN.



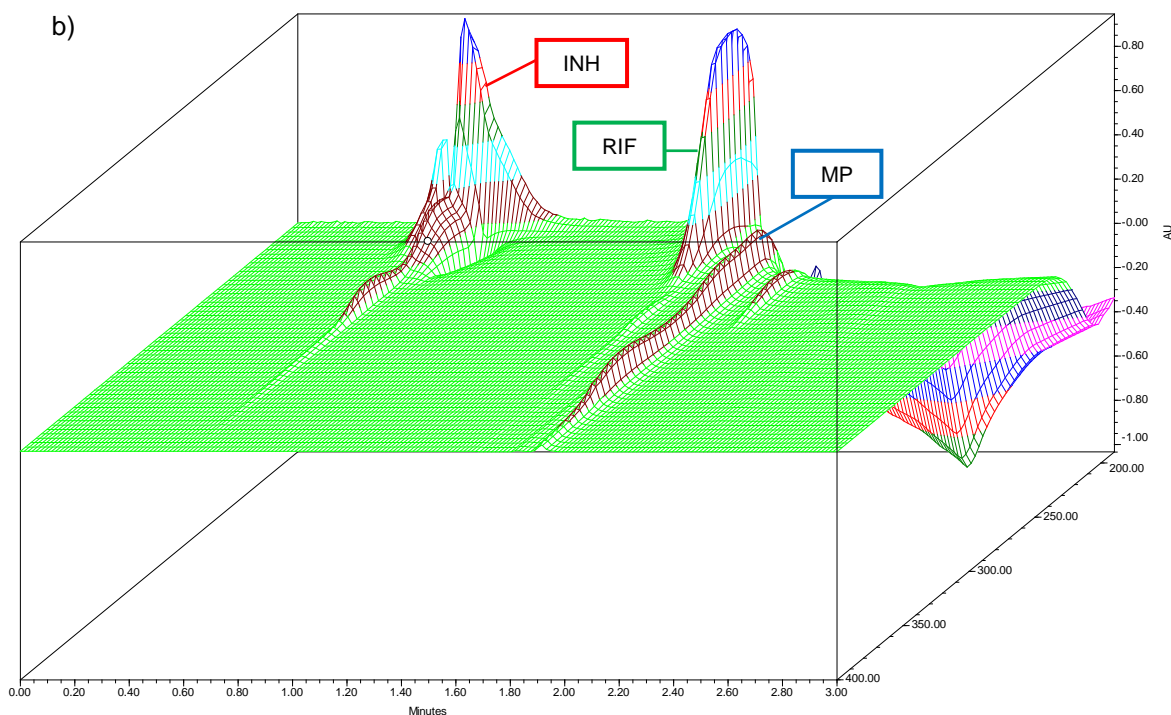


**Figure 7.6:** A typical a) two-dimensional chromatogram and b) three-dimensional chromatogram obtained from the UPLC analysis of *in vitro* dissolution samples at a wavelength of 263nm depicting the distinct separation of INH ( $R_t=0.621$ ), RIF ( $R_t=1.903$ ) and MP ( $R_t=2.064$ ).

### 7.3.1.2 Calibration Curves

Figure 7.7a displays the calibration curve obtained for RIF in PBS (pH 1.2; 37°C); and Figure 7.7b displays the calibration curve obtained for INH in PBS (pH 6.8; 37°C), with an  $R^2$  value of 0.9983 and 0.9980 respectively. The regression equations were determined to be  $y=24.397x$  and  $y=35.252x$  for the RIF and INH calibration curves respectively, and the  $R^2$  values demonstrate good linearity.

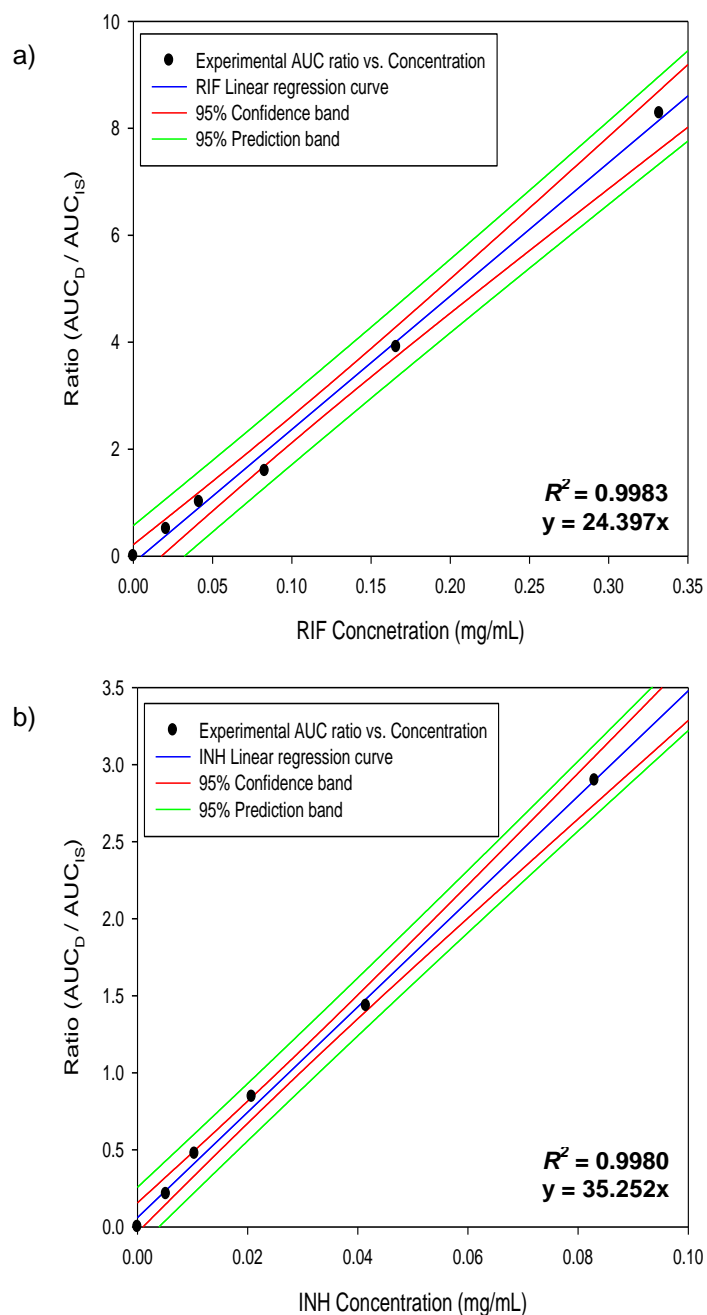


**Figure 7.7:** Constructed calibration curves of a) RIF in PBS (pH1.2; 37°C) at a wavelength of 263nm and b) INH in PBS at a wavelength of 263nm (pH 6.8; 37°C).

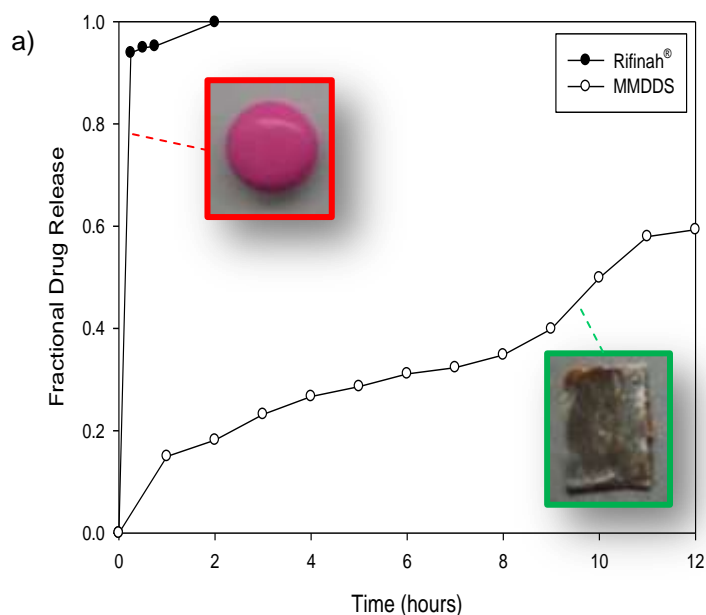
### 7.3.1.3 *In vitro* drug release

The MMDDS demonstrated near zero-order release of both incorporated drugs, as illustrated in Figure 7.8. *In vitro* dissolution studies revealed that  $59.31 \pm 0.0257\%$  of RIF was released in a controlled manner over the 12 hour study duration while  $81.11 \pm 0.0235\%$  of INH was release in a controlled manner after 12 hours in a simulated intestinal environment. Furthermore, Figure 7.8b clearly demonstrates minimal release of INH from the MMDDS (<5% of the total drug incorporated), while the MMDDS was exposed to conditions simulating the gastric region of the GIT. INH release was only



initiated when the intestinal-targeted component was exposed to conditions typical of the intestinal region of the GIT. As such, it can be concluded that the MMDDS successfully segregated the delivery of RIF and INH, thereby mitigating any deleterious drug interactions. These results substantiate that site-specific drug delivery was successfully achieved with the MMDDS. In contrast, the marketed gold standard formulation demonstrated extensive dose dumping tendencies (>70% drug released within the first 15 minutes), demonstrating extremely poor control over drug release. Furthermore, there is no segregation of the drugs in terms of release, hence promoting the deleterious drug interaction known to occur between RIF and INH in an acidic environment, detrimentally affecting the oral bioavailability of RIF from the Rifinah<sup>®</sup> tablets.

The prolongation and control of drug release obtained from the MMDDS can be primarily attributed to crosslinking of the PVA nanofibres employing glutaraldehyde vapours. Furthermore, site-specificity was achieved by employing pH-responsive polymers. Incorporation of PEC to the intestinal targeted layer not only ensured prolonged mucoadhesion of the intestinal targeted component, but also ensured minimal release of INH from the MMDDS when exposed to simulated gastric conditions. CHT, on the other hand, promotes mucoadhesion of the gastric-targeted component, and thus ensuring prolonged release of RIF in the gastric region of the GIT.



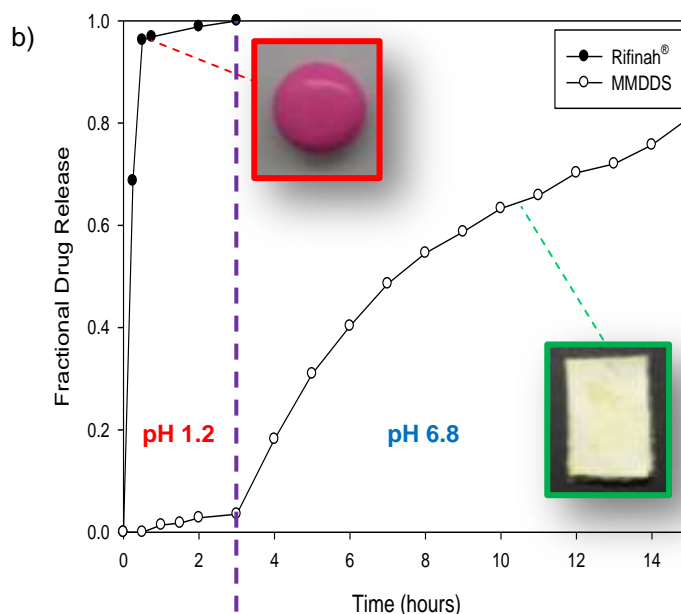


**Figure 7.8:** Comparative *in vitro* dissolution profiles of a) rifampicin and b) isoniazid from the Rifinah<sup>®</sup> (with the digital image highlighted in red) and MMDDS (with the digital image highlighted in green) (SD < 0.0336 for all MMDDS cases; and SD < 0.155 for all Rifinah<sup>®</sup> cases).

### 7.3.2 *In vivo* analysis

#### 7.3.2.1 Chromatograms obtained through UPLC analysis

Figure 7.9 demonstrates the resultant chromatograms obtained from UPLC analysis of plasma samples. The UPLC assay method described enabled rapid simultaneous measurement of RIF and INH for the *in vivo* obtained plasma samples. As illustrated in Figure 7.9, sharp and symmetrical peaks were obtained. Furthermore, the chromatogram demonstrated that sharp peaks with good separation was achieved, substantiating the appropriateness of the UPLC assay method for the simultaneous quantification of both drugs after extraction from a single plasma sample. The chromatogram also displayed a level chromatographic baseline. RIF, INH and FUR obtained retention times of 0.674, 1.962 and 2.134 minutes respectively. INH, which is highly soluble in water, elutes when the constitution of the mobile phase is primarily formic water. RIF and FUR, which are readily soluble in the organic phase (ACN), thus elutes when the mobile consists of a substantially larger fraction of ACN.

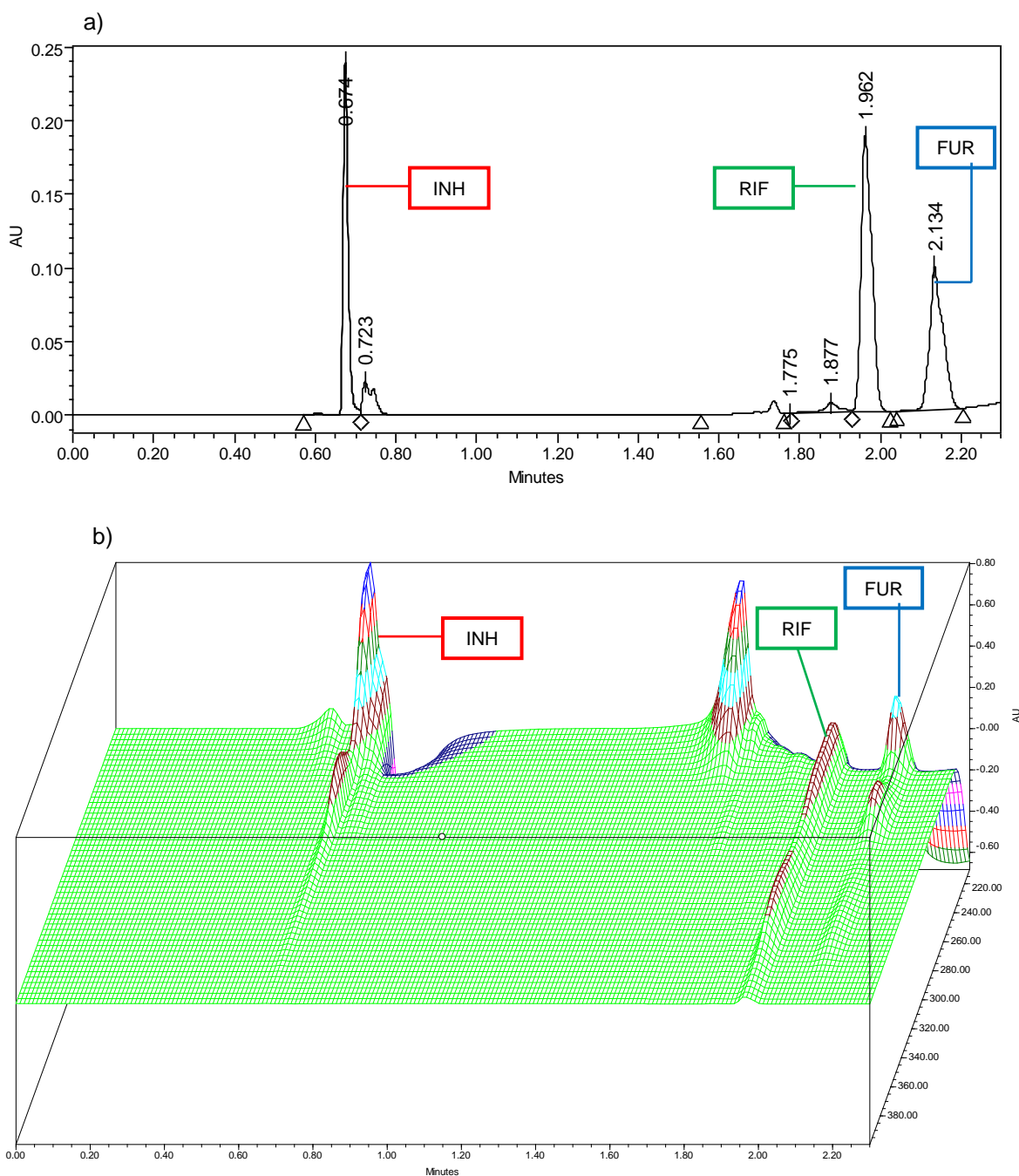


**Figure 7.9:** A typical a) two-dimensional chromatogram and b) three-dimensional chromatogram obtained from UPLC analysis, depicting the distinct separation of INH ( $R_t=0.674$ ), RIF ( $R_t=1.962$ ) and FUR ( $R_t=2.134$ ) at 272nm obtained from porcine plasma samples.

### 7.3.2.2 Recovery efficiency

Recovery was determined to be  $84.175 \pm 1.095\%$  and  $77.93 \pm 0.87\%$  for RIF and INH respectively. The remaining drug may have been still trapped in the plasma, or did not elute during SPE (i.e. was still trapped within the SPE cartridge). Therefore it can be deduced that good recovery was obtained when employing the described method for the simultaneous extraction of both RIF and INH from a single plasma sample, minimizing time, costs and use of materials.

### 7.3.2.3 Calibration curves

Figure 7.10a displays the calibration curve obtained for RIF when extracted from plasma in PBS (pH 1.2; 37°C); and Figure 7.10b displays the calibration curve obtained for INH when extracted from plasma in PBS (pH 6.8; 37°C), with an  $R^2$  value of 0.9958 and 0.9960 respectively. The regression equations were determined to be  $y=0.0684x$  and  $y=0.0319x$  for the RIF and INH calibration curves respectively, and the  $R^2$  values demonstrate good linearity.

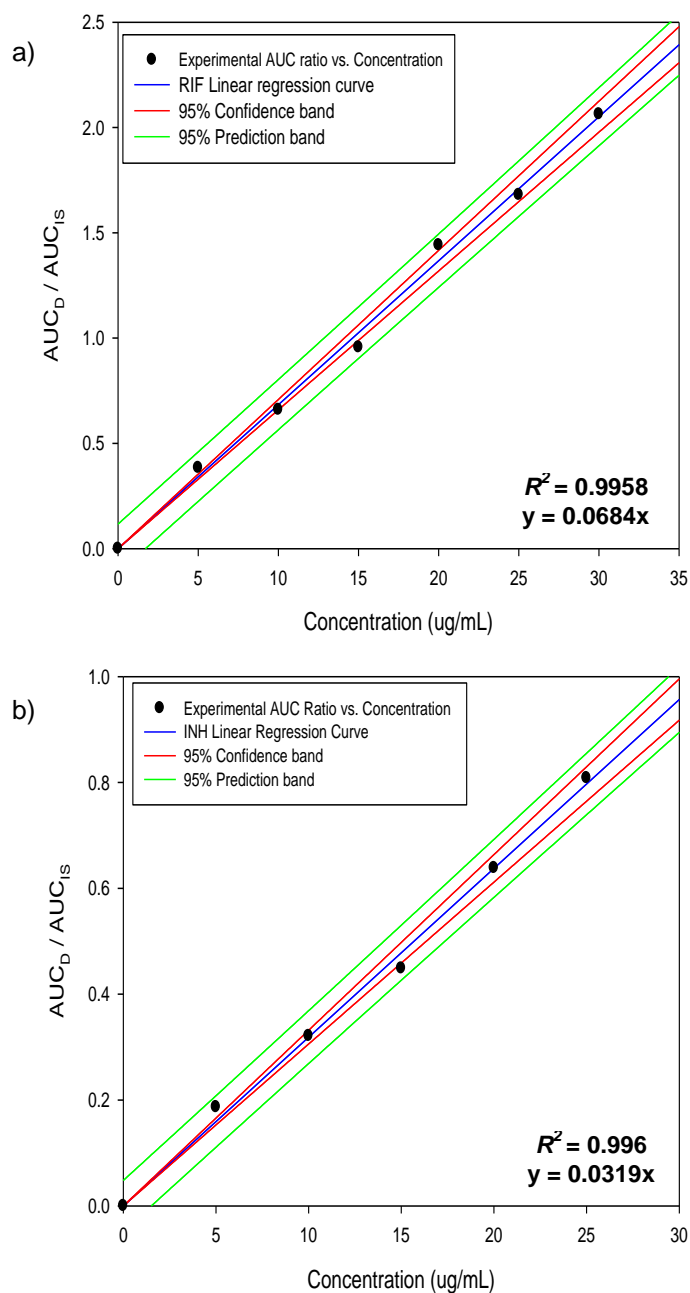


**Figure 7.10:** Constructed calibration curves of a) RIF and b) INH when extracted from plasma at a wavelength of 272nm.

#### 7.3.2.4 Comparative *in vivo* plasma concentration profiles

The comparative plasma concentration profiles of RIF and INH reveal marked differences when administered as the MMDDS or as Rifinah<sup>®</sup> tablets as illustrated in Figure 7.11. Although Rifinah<sup>®</sup> tablets achieved a higher maximum plasma concentration ( $C_{max}$ ) of RIF ( $C_{max}=1.589\pm 0.389\mu\text{g/mL}$ ) as opposed to the MMDDS, where a  $C_{max}$  of  $0.478\pm 0.01005\mu\text{g/mL}$  was achieved, only the MMDDS was able to achieve consistent or steady state plasma concentrations throughout the duration of the study (Figure 7.11a). As a result, side effects experienced due to high drug concentrations can be avoided, ultimately improving patient compliance. To achieve steady state concentrations, Rifinah<sup>®</sup> tablets are typically administered more often throughout the day, resulting in complicated treatment regimens. The MMDDS is able to overcome the requirement of multiple doses, thus easing complex treatment regimens. Furthermore, the variability in the quantity of drug released from the Rifinah<sup>®</sup> tablets was extremely high as opposed to the MMDDS.

The *in vivo* plasma concentration profiles of the MMDDS and Rifinah<sup>®</sup> shown in Figure 7.11b reveals that for the first 2 hours post-dosing, minimal INH is released from the MMDDS ( $0.369\pm 0.027\mu\text{g/mL}$ ), whereas a concentration of  $2.45\pm 0.325\mu\text{g/mL}$  is achieved from Rifinah<sup>®</sup> within the same time frame. These results obtained within the first two hours subsequent to oral dosing provide the fundamental evidence of the efficiency of the MMDDS in terms of site-specific drug delivery. Due to enhanced site-specific drug delivery, a greater quantity of INH is released in the intestine where a larger degree of absorption is acquired. This can be seen from a comparison of the 2 hour blood sample where the plasma concentration of INH was considerably lower ( $0.369\pm 0.027\mu\text{g/mL}$ ) from the MMDDS, corresponding to the time when the drug delivery system is yet to pass through the gastric region of the GIT, as opposed to the 4 hour blood sample ( $1.7744\pm 0.0473\mu\text{g/mL}$ ), corresponding to when the drug delivery system has entered the intestine. Furthermore, the reduced quantity of INH release in the gastric region decreased the occurrence of the deleterious drug interaction between RIF and INH from occurring, hence improving the bioavailability of RIF. As illustrated in Figure 7.11b, the MMDDS achieved consistent plasma levels of INH throughout the duration of the study as opposed to Rifinah<sup>®</sup> tablets, where very erratic plasma concentration of INH were observed, demonstrating desirable release behaviour of the MMDDS in the swine model.

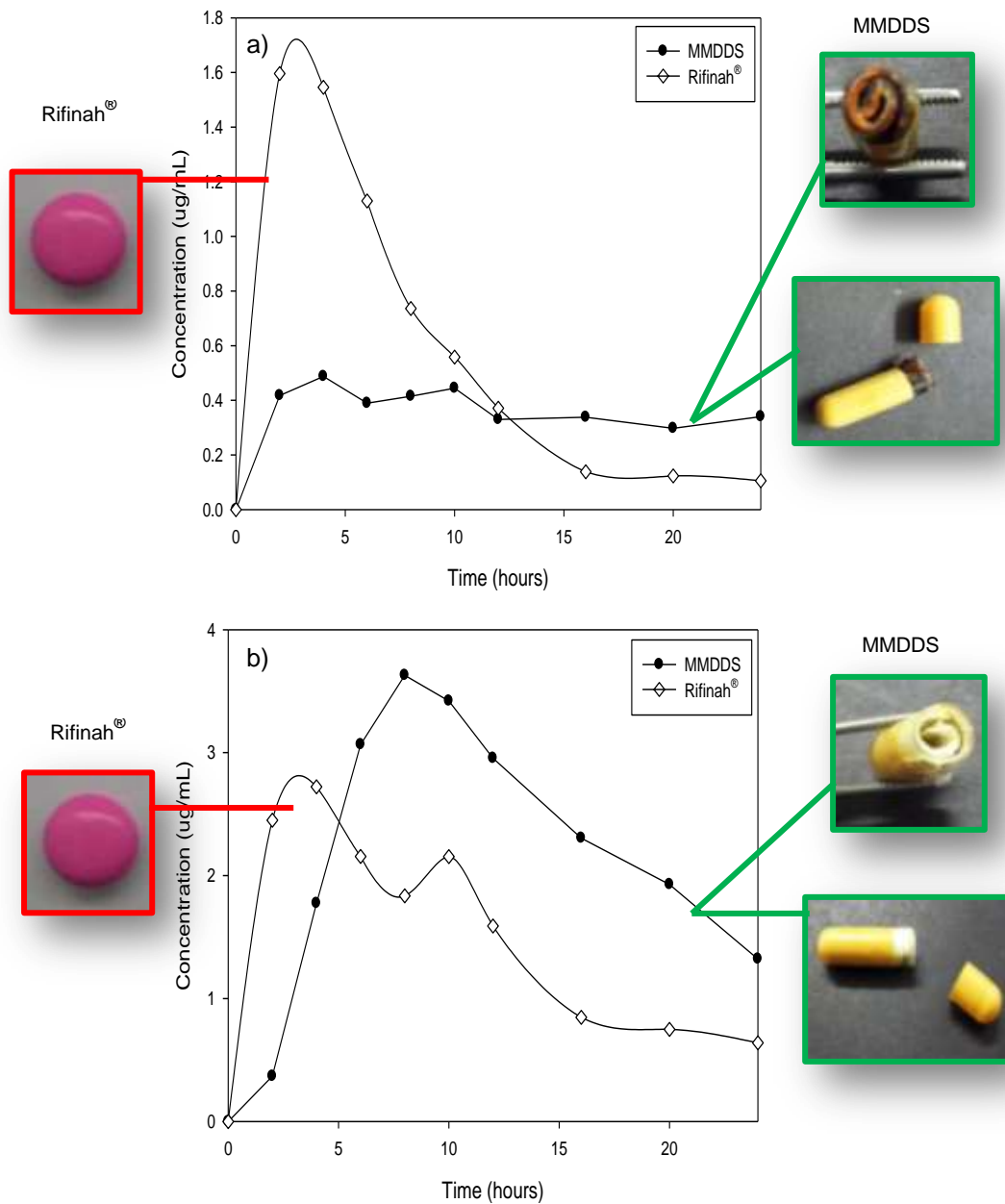


**Figure 7.11:** Comparative plasma concentration profiles of a) RIF and b) INH with corresponding digital images of the MMDDS and Rifinah® formulations which were orally administered to a swine model (SD < 0.0473 for all MMDDS cases; SD < 0.389 for all Rifinah® cases).

#### 7.4 Concluding Remarks

The primary goal of the present chapter was to determine whether the MMDDS was able to achieve improved drug release characteristics of RIF and INH as opposed to a marketed gold standard formulation, Rifinah®. Both *in vitro* and *in vivo* analysis clearly identified the MMDDS as a superior formulation in terms of both the rate of drug delivery and ensuring segregated drug delivery of the drugs incorporated. *In vitro* analysis demonstrated that greater control over drug release was achieved with the MMDDS as

opposed to Rifinah<sup>®</sup> where extreme dose dumping was observed. Furthermore, *in vitro* studies highlighted the ability of the MMDDS in segregating drug delivery, which was further corroborated with data presented with *in vitro* analysis. In addition to providing targeted and segregated delivery of the respective drugs, the MMDDS further benefited the therapeutic efficacy of the respective drugs by providing release behaviour that was more reproducible and consistent with minimal fluctuations. It should be noted that the *in vivo* analysis of the MMDDS in pigs caused no notable side-effects or other detrimental circumstances in the pigs acquired (See Appendix C2).

## CHAPTER 8

### CONCLUSIONS AND RECOMMENDATIONS

---

#### 8.1 Conclusions

The dynamic and rapidly advancing field of drug delivery has led to numerous innovations, all improving the safety and efficacy of modern day drug therapies. Many new modes of drug administration have been identified and improved throughout the years. However, of the global drug delivery market share, a hefty fraction deals with improving the bioavailability of orally administered drugs. Apart from the benefits associated with oral drug delivery in terms of patient compliance, the limitations which affect oral bioavailability can be easily overcome. Furthermore, the physiology of the human gastro-intestinal system can be exploited for targeted and site-specific drug delivery, by employing smart polymers which respond to changes in the surrounding environment.

Patient compliance has been identified as a major success-limiting factor in the eradication of many diseases (e.g. TB, HIV). In addition, poor patient compliance has been identified as a leading cause for many drug-resistant strains of many infectious diseases such as TB. The fundamental basis for poor patient compliance can largely be attributed to the complex dosing regimens imposed on them as part of a standard therapeutic intervention. Multiple doses taken several times a day generally makes standard treatment regimens “a difficult pill to swallow” for many patients, ultimately threatening compliance, and ultimately the patients therapeutic outcome.

The present dissertation therefore aimed to develop a novel multi-component membranous drug delivery system (MMDDS), which is able to overcome the limitations of oral drug delivery and improve patient compliance by ensuring site-specific and segregated delivery of multiple drugs, in a controlled manner, while protecting the drug delivery system from the harsh gastric environment. The MMDDS comprised of two components, a gastric- and intestinal-targeted membrane system, each comprising of a pH-responsive mucoadhesive layer, a drug containing layer, and a water insoluble coat. rifampicin and isoniazid were identified as the model drugs, to investigate the efficacy of the formulation. The MMDDS was developed in a logical step-wise manner (i.e. each layer at a time), and each component was developed and optimized separately after



exhaustive preliminary studies identified the appropriate method, polymer combinations and quantities required to impart the desired properties.

Extensive *in vitro* analysis led to the identification of formulation variables for the respective gastric- and intestinal-targeted mucoadhesive layers which comprise the MMDDS. A Central Composite Design generated 13 formulations for each component, which were analyzed and the respective mucoadhesive layers were subsequently optimized for prolonged mucoadhesion in their respective regions within the GIT. The optimized formulations underwent further *in vitro* analysis to determine the behaviour of the system under conditions which simulate the human gastro-intestinal environment, and to determine the effect of simulated human gastro-intestinal conditions on the MMDDS.

The second layer of each component, containing the model drugs, was developed through modification of polymeric nanofibres, synthesized via a horizontal electrospinning setup. Drug entrapment efficiency and uniformity of nanofibres produced via the electrospinning of poly(vinyl alcohol) solutions closely met the desirable criteria, and was therefore employed for further modification via vapour-induced crosslinking. Crosslinking caused provided the qualities necessary for the controlling drug release in a prolonged release fashion. The formulation closely meeting the desired criteria was identified and subject to further *in vitro* characterization and modelling, providing useful information in predicting the behaviour of the MMDDS *in vivo*.

Each component was then assembled to form the MMDDS, while a water insoluble coat was employed to protect the incorporated drugs from the harsh gastric environment. Subsequent to *in vitro* analysis, which proved both efficacy of the system in terms of both site-specific and prolonged drug delivery, the MMDDS was subject to *in vivo* analysis in a swine model. For comparative purposes, a marketed gold standard formulation, Rifinah<sup>®</sup>, was also subject to the same *in vitro* and *in vivo* studies. Results indicated that MMDDS was able to segregate the delivery of the incorporated drugs, rifampicin and isoniazid, while ensuring relatively consistent plasma levels of the incorporated drugs in the swine model. In conclusion, the marketed formulation demonstrated inferior properties in terms of control over drug release as compared to the developed MMDDS.

The fact that drugs with completely different properties were successfully incorporated within the system with minor adjustments to the processing parameters, and still achieving the desired properties of prolonged release, demonstrates the versatility of the system.

Overall, the MMDDS was able to overcome many of the limitations associated with oral drug delivery, with the potential of site-specific delivery of multiple drugs incorporated in one system.

## **8.2 Recommendations**

Subsequent to the success of the developed MMDDS in both *in vitro* and *in vivo* investigations described in the present dissertation, it is recommended that further analysis is conducted to determine the efficacy of the drug delivery system in human subjects. It is further recommended that the exact location of mucoadhesion of each component is established and the exact site of drug release be identified employing techniques such as gamma-scintigraphic technology. For comparative purposes, marketed formulations should also be analyzed employing the same techniques, allowing identification of which product is superior in terms of drug release and improved bioavailability.

Furthermore, the system developed by the present dissertation may be successfully applied to any number of bioactives, particularly those that are acid-sensitive, have narrow therapeutic absorption windows, bioactives which cause local irritation of the gastric mucosa (e.g. NSAIDs), bioactives which are absorbed only within specific regions of the GIT, such as the gastric region (e.g. rifampicin), intestinal region (e.g. isoniazid) or the colon (5-aminosalicylic acid, prodrugs of mesalazine and sulfasalazine), and bioactives which accelerate the degradation of others in acidic media (e.g. isoniazid and pyrazinamide cause the degradation of rifampicin).

For scale-up purposes, it is recommended that the preparatory process of the MMDDS be simplified. Film-casting can be easily scaled-up; however, an industrial scale electrospinner needs to be developed. In this manner, individual membranes need not be fabricated, but rather large “sheets” of the MMDDS be fabricated and trimmed to the required sizes upon completion of membrane fabrication and assembly.

## REFERENCES

---

Abu-Huwajj, R., Assaf, S., Salem, M., Sallam, A., (2007). Mucoadhesive dosage form of lidocaine hydrochloride: I. mucoadhesive and physicochemical characterization. *Drug Development and Industrial Pharmacy*, **33**, 855-864.

Agoram, B., Woltosz, W.S., Bolger, M.B., (2001). Predicting the impact of physiological and biochemical processes on oral drug bioavailability. *Advanced Drug Delivery Reviews*, **50**, S41–S67.

Ahmed, F., Pakunlu, R.I., Brannan, A., Bates, F., Minko, T., Discher, D.E., (2006). Biodegradable polymersomes loaded with both paclitaxel and doxorubicin permeate and shrink tumors, inducing apoptosis in proportion to accumulated drug. *Journal of Controlled Release*, **116**, 150-158.

Ahrabi, S.F., Madsen, G., Dyrstad, K., Sande, S.A., Graffner, C., (1997). Development of pectin matrix tablets for colonic delivery of model drug ropivacaine, *In: 12<sup>th</sup> Annual Meeting of the AAPS*, Boston, MA, USA.

Åkerman, S., Viinikka, P., Svarfvar, B., Putkonen, K., Järvinen, K., Kontturi, K., Näsman, J., Urtti, A., Paronen, P., (1998). Drug permeation through a temperature-sensitive poly(*N*-isopropylacrylamide) grafted poly(vinylidene fluoride) membrane. *International Journal of Pharmaceutics*, **164**, 29-36.

Albin, G., Horbett, T.A., Ratner, B.S., (1985). Glucose sensitive membranes for controlled delivery of insulin: Insulin transport studies. *Journal of Controlled Release*, **2**, 153-164.

Albin, G.W., Horbett, T.A., Miller, S.R., Ricker, N.L., (1987). Theoretical and experimental studies of glucose-sensitive membranes. *Journal of Controlled Release*, **6**, 267-291.

Alema, H., Duwez, A.-S., Lussis, P., Lipnik, P., Jonas, A.M., Demoustier-Champagne, S., (2008). Microstructure and thermo-responsive behavior of poly(*N*-isopropylacrylamide) brushes grafted in nanopores of track-etched membranes. *Journal of Membrane Science*, **308**, 75-86.

Allcock, H.R., Ambrosio, AM., (1996). Synthesis and characterization of pH-sensitive poly (organophosphazene) hydrogels, *Biomaterials*, **17(23)**, 2295-2302.

Alsarra, I.A., Hamed. A.Y., Alanazi, F.K., Neau, S.H., (2011). Rheological and Mucoadhesive Characterization of Poly(vinylpyrrolidone) Hydrogels Designed for Nasal Mucosal Drug Delivery. *Archives of Pharmaceutical Research*, **34(4)**, 573-582.

Altinkaya, S.A., Yenal, H., Ozbas, B., (2005). Membrane formation by dry-cast process, Model validation through morphological studies. *Journal of Membrane Science*, **249**, 163-172.

Ameye, D., Mus, D., Foreman, P., Remon, J.P., (2005). Spray-dried Amioca (R) starch/Carbopol® 974P mixtures as buccal bioadhesive carriers. *International Journal of Pharmaceutics*, **301**, 170-180.

Andrews, G.P., Lavery, T.P., Jones, D.S., (2009). Mucoadhesive polymeric platforms for controlled drug delivery. *European Journal of Pharmaceutics and Biopharmaceutics*, **71(3)**, 505-518.

Ankareddi, I., Brazel, C.S., (2007). Synthesis and characterization of grafted thermo-sensitive hydrogels for heating activated controlled release. *International Journal of Pharmaceutics*, **336**, 241-247.

Anseth, K.S., Metters, A.T., Bryant, S.J., Martens, P.J., Elisseeff, J.H., Bowman, C.N., (2002). In situ forming degradable networks and their application in tissue engineering and drug delivery. *Journal of Controlled Release*, **78**, 199-209.

Attia, M.A., El-Gibaly, I., Shaltout, S.E., Fetih, G.N., (2004). Transbuccal permeation, anti-inflammatory activity and clinical efficacy of piroxicam formulated in different gels. *International Journal of Pharmaceutics*, **276**, 11-28.

Atyabi, F., Khodaverdi, E., Dinarvand, R., (2007). Temperature modulated drug permeation through liquid crystal embedded cellulose membranes. *International Journal of Pharmaceutics*, **339**, 213-221.

Aulton, M.E., (2002). *Pharmaceutics: The Science of Dosage Form Design*, Second Edition. Churchill Livingstone, Edinburgh, UK.

Awad, G.A.S., Charrueau, C.A.A., Allain, P., Chaumeil, J.C., (2002). Formulation and evaluation of bioadhesive pellets containing different carbomers made by extrusion-spheronization. *STP Pharma Sciences*, **12**, 157-162.

Baker, R.W., (2004). *Membrane Technology and Applications*, Second Edition. John Wiley & Sons, Ltd, Chichester, UK.

Baji, A., Mai, Y.-W., Wong, S.-C., Abtahi, M., Chen, P., (2010). Electrospinning of polymer nanofibers: Effects on oriented morphology, structures and tensile properties. *Composites Science and Technology*, **70**, 703-718.

Baldi, F., Malfertheiner, P., (2003). Lansoprazole fast disintegrating tablet: A new formulation for an established proton pump inhibitor. *Digestion*, **67**, 1-5.

Barrett, A., (1999). "Crunch time in pill land. Behind all the frantic drug mergers" *Business Week* **Nov 22**, 52-54.

Batchelor, H.K., Banning, D., Dettmar, P.W., Hampson, F.C., Jolliffe, I.G., Craig, D.Q.M., (2002). An in vitro mucosal model for prediction of the bioadhesion of alginate solutions to the oesophagus. *International Journal of Pharmaceutics*, **238**, 123-132.

Batchelor, H.K., Tang, M., Dettmar, P.W., Hampson, F.C., Jolliffe, I.G., Craig, D.Q.M., (2004). Feasibility of a bioadhesive drug delivery system targeted to oesophageal tissue. *European Journal of Pharmaceutics and Biopharmaceutics*, **57**, 295-298.

Baumgarten, P.K., (1971). Electrostatic spinning of acrylic microfibers. *Journal of Colloid and Interface Science*, **36**, 71-79.

Baumgartner, S., Smid-Korbar, J., Vrečer, F., Kristl, J., (1998). Physical and technological parameters influencing floating properties of matrix tablets based on cellulose ethers. *STP Pharma Sciences*, **8**, 285-290.

Bernkop-Schnurch, A., König, V., Leitner, V.M., Krauland, A.H., Brodnik, I., (2004). Preparation and characterisation of thiolated poly(methacrylic acid)-starch compositions. *European Journal of Pharmaceutics and Biopharmaceutics*, **57**, 219-224.

Bernkop-Schnürch, A., (2005). Mucoadhesive systems in oral drug delivery. *Drug Discovery Today: Technologies*, **2(1)**, 83-87

Bhardwaj, N., Kundu, S.C., (2010). Electrospinning: A fascinating fiber fabrication technique, *Biotechnology Advances*, **28**, 325–347.

Blanco, J.F., Sublet, J., Nguyen, Q.T., Schaetzel, P., (2006). Formation and morphology studies of different polysulfones-based membranes made by wet phase inversion process. *Journal of Membrane Science*, **283**, 27-37.

Bolto, B., Tran, T., Hoang, M., Xie, Z., (2009). Crosslinked poly(vinyl alcohol) membranes. *Progress in Polymer Science*, **34**, 969-981.

Brahim, S., Narinesingh, D., Guiseppi-Elie, A., (2003). Release Characteristics of Novel pH-Sensitive p(HEMA-DMAEMA) Hydrogels Containing 3-(Trimethoxy-silyl) Propyl Methacrylate. *Biomacromolecules*, **4**, 1224-1231.

Cai, Z.-X., Mo, X.-M., Zhang, K.-H., Fan, L.-P., Yin, A.-L., He, C.-L., Wang, H.-S., (2010). Fabrication of Chitosan/Silk Fibroin Composite Nanofibers for Wound-dressing Applications. *International Journal of Molecular Sciences*, **11**, 3529-3539.

Cartier, S., Horbett, T.A., Ratner, B.D., (1995). Glucose-sensitive membrane coated porous filters for control of hydraulic permeability and insulin delivery from a pressurized reservoir. *Journal Membrane Science*, **106**, 17-24.

Carelli, V., di Colo, G., Nannipieri, E., Poli, B., Serafini, M.F., (2000). Polyoxyethylenepoly(methacrylic acid-co-methyl methacrylate) compounds for site-specific peroral delivery. *International Journal of Pharmaceutics*, **202**, 103-112.

Casper, C.L., Stephens, J.S., Tassi, N.G., Chase, D.B., Rabolt, J.F., (2004). Controlling surface morphology of electrospun polystyrene fibers: effect of humidity and molecular weight in the electrospinning process. *Macromolecules*, **37**, 573-578.

Casper, C.L., Yamaguchi, N., Kiick, K.L., Rabolt, J.F., (2005). Functionalizing electrospun fibers with biologically relevant macromolecules. *Biomacromolecules*, **6**, 1998-2007.

Chanda, R., Roy, A., Bahadur, S., Saha, S., Das, S., Choudhury, A., (2010). Floating drug delivery: A potential alternative to conventional therapy. *International Journal of PharmTech Research*, **2(1)**, 49-59.

Chao, G.T., Qian, Z.Y., Huang, M.J., Kan, B., Gu, Y.C., Gong, C.Y., Yang, J.L., Wang, K., Dai, M., Li, X.Y., Gou, M.L., Tu, M.J., Wei, Y.Q., (2007). Synthesis, characterization, and hydrolytic degradation behavior of a novel biodegradable pH-sensitive hydrogel based on polycaprolactone, methacrylic acid, and poly (ethylene glycol), *Published online in Wiley InterScience (www.interscience.wiley.com)*. DOI: 10.1002/jbm.a.31362

Chen, G., Hoffman, A.S., (1995). Graft copolymers that exhibit temperature-induced phase transitions over a wide range of pH. *Nature*, **373**, 49-52.

Chen, J.P., Sun, Y.M., Chu, D.H., (1998). Immobilization of alpha-amylase to a composite temperature-sensitive membrane for starch hydrolysis. *Biotechnology Progress*, **14**, 473-478.

Chen, J., Park, K., (2000). Synthesis and characterization of superporous hydrogel composites. *Journal of Controlled Release*, **65**, 73-82.

Chen, S., Pieper, R., Webster, D.C., Singh, J., (2005). Triblock copolymers: synthesis, characterization, and delivery of a model protein. *International Journal of Pharmaceutics*, **288**, 207-218.

Chen, S., Singh, J., (2005a). *In vitro* release of levonorgestrel from phase sensitive and thermo-sensitive smart polymer delivery systems. *Pharmaceutical Development and Technology*, **10**, 319-325.

Chen, S., Singh, J., (2005b). Controlled delivery of testosterone from smart polymer solution based systems: In vitro evaluation. *International Journal of Pharmaceutics*, **295**, 183-190.

Cheng, L.H., Abd, Karim. A., Seow, C.C., (2008). Characterisation of composite films made of konjac glucomannan (KGM), carboxymethyl cellulose (CMC) and lipid. *Food Chemistry*, **107**, 411-418.

Chew, S.Y., Wen, J., Yim, E.K., Leong, K.W., (2005). Sustained release of proteins from electrospun biodegradable fibres. *Biomacromolecules*, **6(4)**, 2017-2024.

Chey L., (2011). High Performance Liquid Chromatography explained. Available at: <http://www.articlesbase.com/electronics-articles/high-performance-liquid-chromatography-explained-4848714.html>. Accessed on: March 13, 2012.

Choi, J.S., Leong, K.W., Yoo, H.S., (2008). In vivo wound healing of diabetic ulcers using electrospun nanofibers immobilized with human epidermal growth factor (EGF). *Biomaterials*, **29**, 587-596.

Choonara, Y.E., Pillay, V., Ndesendo, V.M.K., du Toit, L.C., Kumar, P., Khan, R.A., Murphy, C.S., Jarvis, D.-L., (2011). Polymeric emulsion and crosslink-mediated synthesis of super-stable nanoparticles as sustained-release anti-tuberculosis drug carriers. *Colloids and Surfaces B Biointerfaces*, **87**, 243-254.

Chourasia, M.K., Jain, S.K., (2003). Pharmaceutical approaches to colon targeted drug delivery systems. *Journal of Pharmacy & Pharmaceutical Sciences*, **6**, 33-66.

Chourasia, M.K., Jain, S.K., (2004). Polysaccharides for colon targeted drug delivery. *Drug Delivery*, **11**, 129-148.

Chow, P.K.H., Ng R.T.H., Ogden, B.E., (2008). Using Animal Models in Biomedical Research: A Primer for the Investigator. World Scientific Publishing Co. Pte. Ltd., Singapore.

Chowdary, K.P.R., Srinivasa-Rao, Y., (2004). Mucoadhesive Microspheres for Controlled Drug Delivery. *Biological & Pharmaceutical Bulletin*, **27(11)**, 1717-1724.

Chu, L.-Y., Park, S.-H., Yamaguchi, T., Nakao, S.-I., (2001). Preparation of thermo-responsive core-shell microcapsules with a porous membrane and poly (N-isopropylacrylamide) gates. *Journal of Membrane Science*, **192(1)**, 27-39.

Chu, L.-Y., Li, Y., Zhu, J.-H., Wang, H.-D., Liang, Y.-J., (2004a). Control of pore size and permeability of a glucose-responsive gating membrane for insulin delivery. *Journal of Controlled Release*, **97**, 43-53.



- Chu, L.-Y., Liang, Y.-J., Chen, W.-M., Ju, X.-J., Wang, H.-D., (2004b). Preparation of glucose-sensitive microcapsules with a porous membrane and functional gates. *Colloids and Surfaces B: Biointerfaces*, **37**, 9-14.
- Chun, S.W., Kim, J.D., (1996). A novel hydrogel-dispersed composite membrane of poly (N-isopropylacrylamide) in a gelatin matrix and its thermally actuated permeation of 4-acetamidophen. *Journal of Controlled Release*, **38**, 39-47.
- Chunder, A., Sarkar, S., Yu, Y., Zhai, L., (2007). Fabrication of ultrathin polyelectrolyte fibers and their controlled release properties. *Colloids and Surfaces B: Biointerfaces*, **58**, 172-179.
- Chung, H.J., Lee, Y., Park, T.G., (2008). Thermo-sensitive and biodegradable hydrogels based on stereocomplexed Pluronic multi-block copolymers for controlled protein delivery. *Journal of Controlled Release*, **127**, 22-30.
- Cohn, D., Sosnik, A., Levy, A., (2003). Improved reverse thermo-responsive polymeric systems. *Biomaterials*, **24**, 3707-3714.
- Cohn, D., Sosnik, A., Garty, S., (2005). Smart hydrogels for in situ generated implants, *Biomacromolecules*, **6**, 1168-1175.
- Collaud, S., Warloe, T., Jordan, O., Gurny, R., Lange, N., (2007). Clinical evaluation of bioadhesive hydrogels for topical delivery of hexylaminolevulinate to Barrett's esophagus. *Journal of Controlled Release*, **123**, 203-210.
- Crowley, P.J., Martini, L.G., (2004). Formulation design: new drugs from old. *Drug Discovery Today: Therapeutic Strategies*, **1(4)**, 537-542.
- Csetneki, I., Filipcsei, G., Zrinyi, M., (2006). Smart nanocomposite polymer membranes with on/off switching control. *Macromolecules*, **39**, 1939-1942.
- Csóka, G., Gelencsér, A., Makó, A., Marton, S., Zelkó, R., Klebovich, I., Antal, I., (2007). Potential application of Metolose<sup>®</sup> in a thermo-responsive transdermal therapeutic system. *International Journal of Pharmaceutics*, **338**, 15-20.

D'Emanuele, A., Jevprasesphant, R., Penny, J., Attwood, D., (2004). The use of a dendrimer-propranolol prodrug to bypass efflux transporters and enhance oral bioavailability. *Journal of Controlled Release*, **95(3)**, 447-453.

Danckwerts, M.P., (2000). Optimization and Development of a Core-in-Cup Tablet for Modulated Release of Theophylline in Simulated Gastrointestinal Fluids. *Drug Development and Industrial Pharmacy*, **26(7)**, 767-772.

Danckwerts, M.P., Ebrahim, S., Pillay, V., (2003). Pharmaceutical formulation of a fixed-dose anti-tuberculosis combination. *The International Journal of Tuberculosis and Lung Disease*, **7(3)**, 289-297.

Daniliuc, L., De Kesel, C., David, C., (1992). Intermolecular interactions in blends of poly(vinyl alcohol) with poly(acrylic acid)-1. FTIR and DSC studies. *European Polymer Journal*, **28(11)**, 1365-1371.

Daniliuc, L., David, C., (1996). Intermolecular interactions in blends of poly(vinyl alcohol) with poly(acrylic acid): 2. Correlation between the states of sorbed water and the interactions in homopolymers and their blends. *Polymer*, **37(23)**, 5219-5227.

Davis, S.S., (2005). Formulation studies for absorption windows. *Drug delivery technology*, **10(4)**, 249-257.

Deitzel, J.M., Kleinmeyer, D., Harris, N., Beck Tan, N.C., (2001). The effect of processing variables on the morphology of electrospun nanofibers and textiles. *Polymer*, **42**, 261-272.

Desai, S., Bolton, S., (1993). A floating controlled-release drug-delivery system—in-vitro in-vivo evaluation. *Pharmaceutical Research*, **10**, 1321-1325.

Desai, J., Alexander, K., Riga, A., (2006). Characterization of polymeric dispersions of dimenhydrinate in ethyl cellulose for controlled release. *International Journal of Pharmaceutics*, **308**, 115-123.

Deschepper, E., Thas, O., Ottoy, J.P., (2006). Regional residual plots for assessing the fit of linear regression models. *Computational Statistics and Data Analysis*, **50**, 1995-2013.

Deshpande, A.A., Shah, N.H., Rhodes, C.T., Malick, W., (1997). Development of a novel controlled-release system for gastric retention. *Pharmaceutical Research*, **14**, 815-819.

Dhaliwal, S., Jain, S., Singh, H.P., Tiwary, A.K., (2008). Mucoadhesive microspheres for gastroretentive delivery of acyclovir: In vitro and in vivo evaluation. *The AAPS Journal*, **10**, 322-330.

Dinarvand, R., Ansari, M., (2003). Temperature modulated permeation of hydroxyl urea through thermotropic liquid crystals embedded in poly-HEMA. *Journal of Membrane of Science*, **223**, 217-226.

Discher, D.E., Ahmed, F., (2006). Polymersomes. *Annual Review of Biomedical Engineering*, **8**, 323-341.

Dispenza, A., (2009). Radiation process of polymers. Available at: [www.pa.ibf.cnr.it/nabla/T03.html](http://www.pa.ibf.cnr.it/nabla/T03.html). Accessed on: March 29, 2009.

Dodou, D., Breedveld, P., Wieringa, P.A., (2005). Mucoadhesives in the gastrointestinal tract: revisiting the literature for novel applications. *European Journal of Pharmaceutics and Biopharmaceutics*, **60**, 1-16.

Don, T.-M., Huang, M.-L., Chiu, A.-C., Kuo, K.-H., Chiu, W.-Y., Chiu, L.-H., (2008). Preparation of thermo-responsive acrylic hydrogels useful for the application in transdermal drug delivery systems. *Materials Chemistry and Physics*, **107**, 266-273.

Dong, L.Y., Yan, Q., Hoffman, A.S., (1992). Controlled release of amylase from a thermal and pH-sensitive, macroporous hydrogel. *Journal of Controlled Release*, **19**, 171-178.

Doshi, J., Reneker, D.H., (1995). Electrospinning process and applications of electrospun fibers. *Journal of Electrostatics*, **35**, 151-160.

Dufresne, M.-H., Leroux, J.-C., (2004). Study of the Micellization Behavior of Different Order Amino Block Copolymers with Heparin. *Pharmaceutical Research*, **21(1)**, 160-169.

du Toit, L.C., Pillay, V., Danckwerts, M.P., Penn, C., (2008). Formulation and statistical optimization of a novel crosslinked polymeric anti-tuberculosis drug delivery system. *Journal of Pharmaceutical Sciences*, **97(6)**, 2176-2207.

Dupeyrón, D., González, M., Sáez, V., Ramón, J., Rieumont, J., (2005). Nano-encapsulation of protein using an enteric polymer as carrier. *Institution of Electrical Engineers Proceedings-Nanobiotechnology*, **152(50)**, 165-168.

Eaimtrakarn, S., Itoh, Y., Kishimoto, J., Yoshikawa, Y., Shibata, N., Murakami, M., Takada K., (2002). Gastrointestinal mucoadhesive patch system (GI-MAPS) for oral administration of G-CSF, a model protein. *Biomaterials*, **23**, 145-152.

Eaimtrakarn, S., Prasad, Y.V.R., Puthli, S.P., Yoshikawa, Y., Shibata, N., Takada, K., (2003). Possibility of a patch system as a new oral delivery system. *International Journal of Pharmaceutics*, **250**, 111-117.

Fedorak, R.N., Bistriz, L., (2005). Targeted delivery, safety, and efficacy of oral enteric coated formulations of budesonide. *Advanced Drug Delivery Reviews*, **57**, 303-316.

Ferreira, L., Vidal, M.M., Gil, M.H., (2000). Evaluation of poly (2-hydroxyethyl methacrylate) gels as drug delivery systems at different pH values. *International Journal of Pharmaceutics*, **194**, 169-180.

Frenot, A., Chronakis, I., (2003). Polymer nanofibers assembled by electrospinning, *Current Opinion in Colloid and Interface Science*, **8**, 64-75.

Furth, M.E., Atala, A., Van Dyke, M.E., (2007). Smart biomaterials design for tissue engineering and regenerative medicine. *Biomaterials*, **28**, 5068-5073.

Garg, S., Kumar, G., (2007). Development and evaluation of a buccal bioadhesive system for smoking cessation therapy. *Die Pharmazie*, **62**, 266-272.

GBI Research Report, (November, 2010). Oral Drug Delivery Market - Controlled and Sustained Release to be Major Revenue Generators. Available at: <http://www.prlog.org/11109603-gbi-oral-drug-delivery-market-controlled-and-sustained-release-to-be-major-revenue-generators.html>. Accessed on: June 14, 2011.

George, M., Abraham, T.E., (2007). pH sensitive alginate-guar gum hydrogel for the controlled delivery of protein drugs. *International Journal of Pharmaceutics*, **335**, 123-129.

Gibbon, J.C. (Ed), (2005). South African Medicines Formulary, 7<sup>th</sup> Edition. Division of Clinical Pharmacology, University of Cape Town, Health and Medical Publishing Group, SAMA, Cape Town, South Africa.

Gil, E.S., Hudson, S.M., (2004). Stimuli-responsive polymers and their bioconjugates. *Progress in Polymer Science*, **29**, 1173-1222.

Gil, N., Saska, M., Negulescu, I., (2006). Evaluation of the effects of biobased plasticizers on the thermal and mechanical properties of poly(vinyl chloride). *Journal of Applied Polymer Science*, **102(2)**, 1366-1373.

Giunchedi, P., Juliano, C., Gavini, E., Cossu, M., Sorrenti, M., (2002). Formulation and in vivo evaluation of chlorhexidine buccal tablets prepared using drug-loaded chitosan microspheres. *European Journal of Pharmaceutics and Biopharmaceutics*, **53**, 233-239.

Goddard, E.D., Hannan, R.B., (1976). Cationic polymer/anionic surfactant interactions. *Journal of Colloid Interface Science*, **55(1)**, 73-79.

Gohel, M.C., Sarvaiya, K.G., (2007). A Novel Solid Dosage Form of Rifampicin and Isoniazid With Improved Functionality. *AAPS PharmSciTech*, **8(3)**, Article 68.

González Canga, A., Fernández Martínez, N., Sahagún Prieto, A.M., García Vieitez, J.J., Díez Liébana, M.J., Díez Láiz, R., Sierra Vega, M., (2010). Dietary fiber and its interaction with drugs. *Nutrición Hospitalaria*, **25(5)**, 535-539.

Goodman, K., Hodges, L.A., Band, J., Stevens, H.N.E., Weitschies, W., Wilson, C.G., (2010). Assessing gastrointestinal motility and disintegration profiles of magnetic tablets by a novel magnetic imaging device and gamma scintigraphy. *European Journal of Pharmaceutics and Biopharmaceutics*, **74**, 84-92.

Goswami, T., Jasti, B., Li, X.L., (2008). Sublingual drug delivery. *Critical Reviews in Therapeutic Drug Carrier Systems*, **25**, 449-484.

Goto, T., Morishita, M., Kavimandan, N.J., Takayama, K., Peppas, N.A., (2006). Gastrointestinal transit and mucoadhesive characteristics of complexation hydrogels in rats. *Journal of Pharmaceutical Sciences*, **95**, 462-469.

Gottschalk, C.W., Fellner, S.K., (1997). History of the science of dialysis. *American Journal of Nephrology*, **17** (3-4), 289-298.

Grabovac, V., Guggi, D., Bernkop-Schnürch, A., (2005) Comparison of the mucoadhesive properties of various polymers. *Advanced Drug Delivery Reviews*, **57**, 1713-1723.

Grabovac, V., Föger, F., Bernkop-Schnürch, A., (2008). Design and *in vivo* evaluation of a patch delivery system for insulin based on thiolated polymers. *International Journal of Pharmaceutics*, **348**, 169-174.

Griebel, M., Hamaekers, J., Wildenhues, R., (2005). Molecular dynamics simulations of the influence of chemical cross-links on the elastic moduli of polymer-carbon nanotube composites. Available at: [www.ins.uni-bonn.de](http://www.ins.uni-bonn.de). Accessed on: June 23, 2011.

Gudeman, L.F., Peppas, N.A., (1995). pH-sensitive membranes from poly(vinyl alcohol)/poly(acrylic acid) interpenetrating networks. *Journal of Membrane Science*, **107**, 239-248.

Guggi, D., Kraulanda, A.H., Bernkop-Schnürch A., (2002). Systemic peptide delivery via the stomach: *in vivo* evaluation of an oral dosage form for salmon calcitonin. *Journal of Controlled Release*, **92**, 125-135.

Gupta, P., Elkins, C., Long, T.E., Wilkes, G.L., (2005). Electrospinning of linear homopolymers of poly(methyl methacrylate): exploring relationships between fiber formation, viscosity, molecular weight and concentration in a good solvent. *Polymer*, **46**, 4799-4810.

Gutierrez-Rocca, J.C., McGinity, J.W., (1994). Influence of water soluble and insoluble plasticizers on the physical and mechanical properties of acrylic resin copolymers. *International Journal of Pharmaceutics*, **103**, 293-301.

Gutowska, A., Bark, J.S., Kwon, I.K., Bae, Y.H., Cha, Y., Kim, S.W., (1997). Squeezing hydrogels for controlled oral drug delivery. *Journal of Controlled Release*, **48**, 141-148.

Guo, B.L., Gao, Q.Y., (2007). Preparation and properties of a pH/temperature-responsive carboxymethyl chitosan/poly (N-isopropylacrylamide) semi-IPN hydrogel for oral delivery of drugs. *Carbohydrate Research*, **342**, 2416-2422.

Hanks, P.L., Lloyd, D.R., (2007). Deterministic model for matrix solidification in liquid-liquid thermally induced phase separation. *Journal of Membrane Science*, **306**, 125-133.

Harding, S.E., Davis, S.S., Deacon, M.P., Fiebrig, I., (1999). Biopolymer mucoadhesives, *Biotechnology & Genetic Engineering Reviews*, **16**, 41-86.

Harris, D., Fell, J.T., Sharma, H.L., Taylor, D.C., (1990). GI transit of potential bioadhesive formulations in man: a scintigraphic study. *Journal of Controlled Release*, **12**, 45-53.

Harsulkar, A.A., Sreenivas, S.A., Mandade, R.J., Wakada, R.B., (2011). Polymers in mucoadhesive drug delivery system- A Review. *International Journal of Drug Formulation and Research*, **2(3)**, 61-67.

He, G., Xuan, G., Ruan, H., Chen, Q., Xu, Y., (2005). Optimization of angiotensin I-converting enzyme (ACE) inhibition by rice dregs hydrolysates using response surface methodology. *Journal of Zhejiang University SCIENCE B*, **6B**, 508–513.

He, C.-L., Huang, Z.-M., Han, X.-J., Liu, L., Zhang, H.-S., Chen, L.-S., (2006). Coaxial electrospun poly(L-lactic acid) ultrafine fibers for sustained drug delivery. *Journal of Macromolecular Science, Part B: Physics*, **45**, 515-524.

Heimbach, T., Oh, D.-M., Li, L.Y., Forsberg M., Savolainen, J., Leppänen, J., Matsunaga, Y., Flynn, G., Fleisher, D., (2003). Absorption Rate Limit Considerations for Oral Phosphate Prodrugs. *Pharmaceutical Research*, **20(6)**, 848-856.

Helliwell, M., (1993). The use of bioadhesives in targeted delivery within the gastrointestinal tract, *Advanced Drug Delivery Reviews*, **11**, 221-251.

Hester, J.F., Olugebefola, S.C., Mayes, A.M., (2002). Preparation of pH-responsive polymer membranes by self-organization. *Journal of Membrane Science*, **208**, 375-388.

Hennink, W.E., van Nostrum, C.F., (2002). Novel crosslinking methods to design Hydrogels. *Advanced Drug Delivery Reviews*, **54**, 13-36.

Hinrichs, W.L.J., Schuurmans-Nieuwenbroek, N.M.E., van de Wetering, P., Hennink, W.E., (1999). Thermo-sensitive polymers as carriers for DNA delivery. *Journal of Controlled Release*, **60**, 249-259.

Ho, M.-H., Kuo, P.-Y., Hsieh, H.-J., Hsien, T.-Y., Hou, L.-T., Lai, J.-Y., Wang, D.-M., (2004). Preparation of porous scaffolds by using freeze-extraction and freeze-gelation methods. *Biomaterials*, **25**, 129-138.

Hodges, L.A., Connolly, S.M., Band, J., O'Mahony, B., Ugurlu, T., Turkoglu, M., Wilson, C.G., Stevens, H.N.E., (2009). Scintigraphic evaluation of colon targeting pectin-HPMC tablets in healthy volunteers. *International Journal of Pharmaceutics*, **370**, 144-150.

Hogerstrom, H., Edsman, K., Strwmme, M., (2003). Low-frequency dielectric spectroscopy as a tool for studying the compatibility between pharmaceutical gels and mucus tissue. *Journal of Pharmaceutical Sciences*, **92**, 1869-1881.

Hohman, M.M., Shin, M., Rutledge, G., Brenner, M.P., (2001). Electrospinning and electrically forced jets. II. Applications. *Physics of Fluids*, **13**, 2221-2236.

Hu, Z., Shimokawa, T., Ohno, T., Kimura, G., Mawatari, S.S., Kamitsuna, M., Yoshikawa, Y., Masuda, S., Takada, K., (1999). Characterization of norfloxacin release from tablet coated with a new pH-sensitive polymer, P-4135F. *Journal of Drug Targeting*, **7(3)**, 223-232.

Hu, K., Dickson, J.M., (2008). Modelling of the pore structure variation with pH for pore-filled pH-sensitive poly (vinylidene fluoride)-poly (acrylic acid) membranes. *Journal of Membrane Science*, **321**, 162-171.

Huang, J., Wang, X.L., Qi, W.S., Yu, X.H., (2002). Temperature sensitivity and electrokinetic behavior of a *N*-isopropylacrylamide grafted microporous polyethylene membrane. *Desalination*, **146**, 345-351.

Huang, Z.-M., Zhang, Y.-Z., Kotakic, M., Ramakrishna, S., (2003). A review on polymer nanofibers by electrospinning and their applications in nanocomposites. *Composites Science and Technology*, **63**, 2223-2253.

Huang, Z.-M., He, C.-L., Yang, A., Zhang, Y., Han, X.-J., Yin, J., Wu, Q., (2006). Encapsulating drugs in biodegradable ultrafine fibers through co-axial electrospinning. *Journal of Biomedical Materials Research Part A*, **77A**, 169-179.



Huang, H.Y., Shaw, J., Yip, Y., Wu, X.Y., (2008). Microdomain pH Gradient and Kinetics inside Composite Polymeric Membranes of pH and Glucose Sensitivity. *Pharmaceutical Research*, **25**, 1150-1157.

Ichikawa, H., Fukumori, Y., (2000). A novel positively thermo-sensitive controlled-release microcapsule with membrane of nano-sized poly (*N*-isopropylacrylamide) gel dispersed in ethylcellulose matrix. *Journal of Controlled Release*, **63**, 107-119.

Iemma, F., Spizzirri, U.G., Puoci, F., Muzzalupo, R., Trombino, S., Cassano, R., Leta, S., Picci, N., (2006). pH-Sensitive hydrogels based on bovine serum albumin for oral drug delivery. *International Journal of Pharmaceutics*, **312**, 151-157.

Ignatova, M., Manolova, N., Markova, N., Rashkov, I., (2009). Electrospun Non-Woven Nanofibrous Hybrid Mats Based on Chitosan and PLA for Wound-Dressing Applications, *Macromolecular Bioscience*, **9**, 102-111.

Jackson, S.J., Perkins, A.C., (2001). In vitro assessment of the mucoadhesion of cholestyramine to porcine human gastric mucosa. *European Journal of Pharmaceutics and Biopharmaceutics*, **52**, 121-127.

Jacobsen, J., Bjerregaard, S., Pedersen, M., (1999). Cyclodextrin inclusion complexes of antimycotics intended to act in the oral cavity - drug supersaturation, toxicity on TR146 cells and release from a delivery system. *European Journal of Pharmaceutics and Biopharmaceutics*, **48**, 217-224.

Jeong, B.M., Lee, D.S., Bae, Y.H., Kim, S.W., (2000). In situ gelation of PEG-PLGA-PEG triblock copolymer aqueous solutions and degradation thereof. *Journal of Biomedical Materials Research*, **50**, 171-177.

Jeong, Y.-I., Prasad Yvmacr, R., Ohno, T., Yoshikawa, Y., Shibata, N., Kato, S., Takeuchi, K., Takada, K., (2001). Application of Eudragit P-4135F for the delivery of ellagic acid to the rat lower small intestine. *Journal of Pharmacy and Pharmacology*, **53(8)**, 1079-1085.

Jeong, B., Kim, S.W., Bae, Y.H., (2002). Thermo-sensitive sol-gel reversible hydrogels, *Advanced Drug Delivery Reviews*, **54**, 37-51.

Jia, J., Duan, Y.Y., Wang, S.H., Zhang, S.F., Wang, Z.Y., (2007). Preparation and characterization of antibacterial silver-containing nanofibers for wound dressing applications. *Journal of US-China Medical Science*, **4**, 52–54.

Jiang, H., Hu, Y., Li, Y., Zhao, P., Zhu, K., Chen, W., (2005). A facile technique to prepare biodegradable coaxial electrospun nanofibers for controlled release of bioactive agents. *Journal of Controlled Release*, **28(108)**, 237-243.

Jiang, H., Hu, Y., Zhao, P., Li, Y., Zhu, K., (2006). Modulation of protein release from biodegradable core-shell structured fibres prepared by coaxial electrospinning. *Journal Biomedical Material Research Part B Applied Biomaterials*, **79**, 50-57.

Jin, S., Liu, M., Zhang, F., Chen, S., Niu, A., (2006). Synthesis and characterization of pH-sensitivity semi-IPN hydrogel based on hydrogen bond between poly(N-vinylpyrrolidone) and poly(acrylic acid), *Polymer*, **47**, 1526-1532.

Jung, Y.H., Kim, H.Y., Lee, D.R., Park, S.Y., Khil, M.S., (2005). Characterization of PVOH nonwoven mats prepared from surfactant-polymer system via electrospinning. *Macromolecular Research*, **13(5)**, 385-390.

Kai, G., Min, Y., (2001). AAc photografted porous polycarbonate films and its controlled release system. *Journal of Controlled Release*, **71**, 221-225.

Kang, G.D., Cheon, S.H., Song, S.C., (2006a). Controlled release of doxorubicin from thermo-sensitive poly (organophosphazene) hydrogels. *International Journal of Pharmaceutics*, **319**, 29-36.

Kang, G.D., Cheon, S.H., Khang, G., Song, S.C., (2006b). Thermo-sensitive poly(organophosphazene) hydrogels for a controlled drug delivery. *European Journal of Pharmaceutics and Biopharmaceutics*, **63**, 340-346.

Kao, S.T., Teng, M.Y., Li, C.L., Kuo, C.Y., Hsieh, C.Y., Tsai, H.A., Wang, D.M., Lee, K.R., Lai, J.Y., (2008). Fabricating PC/PAN composite membranes by vapor-induced phase separation. *Desalination*, **233**, 96-103.

Kararli, T.T., (1995). Comparison of the gastrointestinal anatomy, physiology, and biochemistry of humans and commonly used laboratory animals. *Biopharmaceutics and Drug Disposition*, **16**, 351-380.

Katono, H., Sanui, K., Ogata, N., Okano, T., Sakurai, Y., (1991). Drug release off behavior and deswelling kinetics of thermo-responsive IPNs composed of poly(acrylamide-co-butyl methacrylate) and poly(acrylic acid). *Polymer Journal*, **23**, 1179-1189.

Kawashima, Y., Niwa, T., Takeuchi, H., Hino, T., Itoh, Y., (1992). Hollow microspheres for use as a floating controlled drug delivery system in the stomach. *Journal of Pharmaceutical Sciences*, **81**, 135-140.

Khan, M.Z., Prebeg, Ž., Kurjakovi, N., (1999). A pH-dependent colon targeted oral drug delivery system using methacrylic acid copolymers. I. Manipulation of drug release using Eudragit L100-55 and Eudragit S100 combinations. *Journal of Controlled Release*, **58**, 215-222.

Khan, M.Z., Stedul, H.P., Kurjaković, N., (2000). A pH-dependent colon-targeted oral drug delivery system using methacrylic acid copolymers. II. Manipulation of drug release using Eudragit L100 and Eudragit S100 combinations. *Drug Development and Industrial Pharmacy*, **26(5)**, 549-554.

Khare, A.R., Peppas, N.A., (1993). Release behavior of bioactive agents from pH-sensitive hydrogels. *Journal of Biomaterials Science, Polymer Edition*, **4(3)**, 275-289.

Khutoryanskiy, V.V., (2011). Advances in Mucoadhesion and Mucoadhesive Polymers. *Macromolecular Bioscience*, **11(6)**, 748-764.

Kim, C.-J., Lee, P.I., (1992). Hydrophobic Anionic Gel Beads for Swelling-Controlled Drug Delivery. *Pharmaceutical Research*, **9(2)**, 195-199.

Kim, Y.H., Bae, Y.H., Kim, S.W., (1994). pH/temperature-sensitive polymers for macromolecular drug loading and release. *Journal of Controlled Release*, **28**, 143-152.

Kim, S.Y., Cho, S.M., Lee, Y.M., Kim, S.J., (2000). Thermo- and pH-Responsive Behaviors of Graft Copolymer and Blend Based on Chitosan and N-Isopropylacrylamide. *Journal of Applied Polymer Science*, **78**, 1381-1391.

Kim, K., Luu, Y.K., Chang, C., Fang, D., Hsiao, B.S., Chu, B., Hadjiargyrou, M., (2004). Incorporation and controlled release of a hydrophilic antibiotic using poly(lactide-co-glycolide)-based electrospun nanofibrous scaffolds. *Journal of Controlled Release*, **98**, 47-56.

Kim, I.S., Oh, I.J., (2005a). Drug release from the enzyme-degradable and pH-sensitive hydrogel composed of glycidyl methacrylate dextran and poly (acrylic acid). *Archives of Pharmacal Research*, **28(8)**, 983-987.

Kim, M.H., Kim, J.-C., Lee, H.Y., Kim, J.D., Yang, J.H., (2005b). Release property of temperature-sensitive alginate beads containing poly (*N*-isopropylacrylamide). *Colloids and Surfaces B: Biointerfaces*, **46**, 57-61.

Kim, T.G., Lee, D.S., Park, T.G., (2007). Controlled protein release from electrospun biodegradable fiber mesh composed of poly (caprolactone) and poly (ethylene oxide). *International Journal of Pharmaceutics*, **338**, 276-283.

Kim, G.-M., Asran, A.S., Michler, G.H., Simon, P., Kim, J.-S., (2008). Electrospun PVA/Hap nanocomposite nanofibers: biomimetics of mineralized hard tissues at a lower level of complexity. *Bioinspiration and Biomimetics* 3 046003 (12pp).

Kitano, S., Koyama, Y., Kataoka, K., Okano, T., Sakurai, Y., (1992). A novel drug delivery system utilizing a glucose responsive polymer complex between poly(vinyl alcohol) and poly(*N* vinyl-2-pyrrolidone) with a phenylboronic acid moiety. *Journal of Controlled Release*, **19**, 162-170.

Kolff, W.J., Scribner, B.H., (2002). The artificial kidney and its effect on the development of other artificial organs, The development of renal haemodialysis, Lasker Clinical Medical Research Award. *Nature Medicine*, **8(10)**, 1063-1065.

Kommuru, T.R., Gurley, B., Khan, M.A., Reddy, I.K., (2001). Self-emulsifying drug delivery systems (SEDDS) of coenzyme Q10: formulation development and bioavailability assessment. *International Journal of Pharmaceutics*, **212**, 233-246.

Kontturi, K., Mafé, S., Manzanares, J.A., Svarfvar, B.L., Viinikka, P., (1996). Modelling of the Salt and pH Effects on the Permeability of Grafted Porous Membranes. *Macromolecules*, **29**, 5740-5746.

Koo, C.M., Ham, H.T., Choi, M.H., Kim, S.O., Chung, I.J., (2003). Characteristics of polyvinylpyrrolidone-layered silicate nanocomposites prepared by attrition ball milling. *Polymer*, **44**, 681-689.

Koski, A., Yim, K., Shivkumar, S., (2004). Effect of molecular weight on fibrous PVA produced by electrospinning. *Materials Letters*, **58**, 493-497.

Kou, J.K., Amidon, G.L., Lee, P.I., (1988). pH-Dependent Swelling and Solute Diffusion Characteristics of Poly(Hydroxyethyl Methacrylate-CO-Methacrylic Acid) Hydrogels. *Pharmaceutical Research*, **5(9)**, 592-597.

Krause, B., Van der Vegt, N.F.A., Wessling, M., (2002). New ways to produce porous polymeric membranes by carbon dioxide foaming. *Desalination*, **144**, 5-7.

Kriegel, C., Kit, K.M., McClements, D.J., Weiss, J., (2009). Electrospinning of chitosan-poly(ethylene oxide) blend nanofibers in the presence of micellar surfactant solutions. *Polymer*, **50**, 189-200.

Krogel, I., Bodmeier, R., (1999). Floating or pulsatile drug delivery systems based on coated effervescent cores. *Journal of Pharmaceutical Sciences*, **187**, 175-184.

Kruk, M.E., Schwalbe, N., (2006). The Relation between Intermittent Dosing and Adherence: Preliminary Insights. *Clinical Therapeutics*, **28(12)**, 1989-1995.

Kulkarni, R.D., Goddard, E.D., Kanner, B., (1977), Mechanism of Antifoaming Action, *Journal of Colloid and Interface Science*, **59(3)**, 468-476.

Kulkarni, A., Rao, M., (2007). Biochemical characterization of an aspartic protease from *Vigna radiata*: Kinetic interactions with the classical inhibitor pepstatin implicating a tight binding mechanism. *Biochimica et Biophysica Acta*, **1774**, 619-627.

Kumar, A., Srivastava, A., Galaev, I.Y., Mattiasson, B., (2007). Smart polymers: Physical forms and bioengineering applications. *Progress in Polymer Science*, **32**, 1205-1237.

Kumar, A., (2009). Smart polymeric materials: where chemistry and biology can merge. Available at: [www.iitk.ac.in/directions/dirnet7/PP~ASHOK~FFF.pdf](http://www.iitk.ac.in/directions/dirnet7/PP~ASHOK~FFF.pdf). Accessed on: March 29, 2009.

Kumar, K.V., Sivakumar, T., Tamizhmani, T., (2011a). Colon targeting drug delivery system: A review on recent approaches. *International Journal of Pharmaceutical and Biomedical Research*, **2(1)**, 11-19.

Kumar, P., Pillay, V., Choonara, Y.E., Modi, G., Naidoo, D., du Toit, L.C., (2011b). *In Silico* Theoretical Molecular Modeling for Alzheimer's Disease: The Nicotine-Curcumin Paradigm in Neuroprotection and Neurotherapy. *International Journal of Molecular Sciences*, **12**, 694-724.

Kwon, Y.M., Kim, S.W., (2004). Biodegradable Triblock Copolymer Microspheres Based On Thermo-sensitive Sol-Gel Transition, *Pharmaceutical Research*, **21(2)**, 339-343.

Lai, P.-L., Shieh, M.-J., Pai, C.-L., Wang, C.-Y., Young, T.-Y., (2006). A pH-sensitive EVAL membrane by blending with PAA. *Journal of Membrane Science*, **275**, 89-96.

Lally, S., Mackenzie, P., LeMaitre, C.L., Freemont, T.J., Saunders, B.R., (2007). Microgel particles containing methacrylic acid: pH-triggered swelling behavior and potential for biomaterial application. *Journal of Colloid and Interface Science*, **316**, 367-375.

Larsen, W.A., McCleary, S.J., (1972). The Use of Partial Residual Plots in Regression Analysis. *Technometrics*, **14**, 781-790.

Lee, Y.M., Shim, J.K., (1997). Preparation of pH/temperature responsive polymer membrane by plasma polymerization and its riboflavin permeation. *Polymer*, **38(5)**, 1227-1232.

Lee, S.J., Yoo, J.J., Lim, G.J., Atala, A., Stitzel, J., (2007). In vitro evaluation of electrospun nanofiber scaffolds for vascular graft application. *Journal of Biomedical Materials Research Part A*, **83A(4)**, 999-1008.

Lehr, C.M., Bouwstra, J.A., Schacht, E.H., Junginger, H.E., (1992). In vitro evaluation of mucoadhesive properties of chitosan and some other natural polymers. *International Journal of Pharmaceutics*, **78**, 43-48.

Leung, S.H.S., Robinson, J.R., (1990). Polymer structure features contributing to mucoadhesion. II. *Journal of Controlled Release*, **12**, 187-194.

Leung, V., Ko, F., (2011). Biomedical applications of nanofibers. *Polymers for Advanced Technologies*, **22**, 350–365.

Li, S.K., D'Emanuele, A., (2001). On-off transport through a thermo-responsive hydrogel composite membrane. *Journal of Controlled Release*, **75**, 55-67.

Li, D., Xia, Y., (2004). Electrospinning of nanofibers: Reinventing the wheel? *Advanced Materials*, **16**, 1151-1170.

Li, D., Krantz, W.B., Greenberg, A.R., Sani, R.L., (2006a). Membrane formation via thermally induced phase separation (TIPS): Model development and validation. *Journal of Membrane Science*, **279**, 50-60.

Li, Y., Huang, Z., Lü, Y., (2006b). Electrospinning of nylon-6,66,1010 terpolymer. *European Polymer Journal*, **42**, 1696-1704.

Liang, L., Feng, X., Peurrung, L., Viswanathan, V., (1999). Temperature-sensitive membranes prepared by UV photopolymerization of *N*-isopropylacrylamide on a surface of porous hydrophilic polypropylene membranes. *Journal of Membrane Science*, **162**, 235-246.

Liang, A.C., Chen, L.I.H., (2001). Fast-dissolving intraoral drug delivery systems. *Expert Opinion on Therapeutic Patents*, **11**, 981-986.

Liang, D., Hsiao, B.S., Chu, B., (2007). Functional electrospun nanofibrous scaffolds for biomedical applications. *Advanced Drug Delivery Reviews*, **59**, 1392-1412.

Lin, D.J., Chang, H.H., Chen, T.C., Lee, Y.C., Cheng, L.P., (2006). Formation of porous poly (vinylidene fluoride) membranes with symmetric or asymmetric morphology by immersion precipitation in the water/TEP/PVDF system. *European Polymer Journal*, **42**, 1581-1594.

Lin, H.L., Wang, S.H., Chiu, C.K., Yu, T.L., Chen, L.-C., Huang, C.C., Cheng, T.H., Lin, J.M., (2010). Preparation of Nafion/poly(vinyl alcohol) electro-spun fiber composite membranes for direct methanol fuel cells. *Journal of Membrane Science*, **365**, 114-122.

Liu, Y., Li, K., (2005). Preparation of SrCe<sub>0.95</sub>Yb<sub>0.05</sub>O<sub>3-α</sub> hollow fibre membranes: Study on sintering processes. *Journal of Membrane Science*, **259**, 47-54.

Liu, S.Q., Tong, Y.W., Yang, Y.Y., (2005a). Incorporation and in vitro release of doxorubicin in thermally sensitive micelles made from poly (N-isopropylacrylamide-co-N,N-dimethylacrylamide)-b-poly (D,L-lactide-co-glycolide) with varying compositions. *Biomaterials*, **26(24)**, 5064-5074.

Liu, S.Q., Tong, Y.W., Yang, Y.Y., (2005b). Thermally sensitive micelles self-assembled from poly (N-isopropylacrylamide-co-N,N-dimethylacrylamide)-b-poly(D,L-lactide-co-glycolide) for controlled delivery of paclitaxel. *Molecular Biosystems*, **1(2)**, 158-165.

Liu, S.Q., Wiradharma, N., Gao, S.J., Tong, Y.W., Yang, Y.Y., (2007a). Bio-functional micelles self-assembled from a folate-conjugated block copolymer for targeted intracellular delivery of anticancer drugs. *Biomaterials*, **28**, 1423-1433.

Liu, Y., Meng, L., Lu, X., Zhang, L., He, Y., (2007b). Thermo and pH sensitive fluorescent polymer sensor for metal cations in aqueous solution. *Polymers for Advanced Technologies*, **19(2)**, 137-143.

Liu, Y., He, J.-H., Yu, J.-Y., Zeng, H.-M., (2008). Controlling numbers and sizes of beads in electrospun nanofibers. *Polymer International*, **57**, 632-636.

Liu, Y., Bolger, B., Cahill, P.A., McGuinness, G.B., (2009). Water resistance of photocrosslinked polyvinyl alcohol based fibers. *Materials Letters*, **63**, 419-421.

Liu, W., Yang X.-L., Winston Ho, W.S., (2010). Preparation of Uniform-Sized Multiple Emulsions and Micro/Nano Particulates for Drug Delivery by Membrane Emulsification, *Journal of Pharmaceutical Sciences*, **100**, 75-93.

Loh, X.J., Sung, K.B.C., Li, J., (2008). Synthesis and water-swelling of thermo-responsive poly(ester urethane)s containing poly(3-caprolactone), poly(ethylene glycol) and poly(propylene glycol). *Biomaterials*, **29**, 3185-3194.



Lonsdale, H., (1982). The growth of membrane technology. *Journal of Membrane Science*, **10**, 81-181.

Lowman, A.M., Peppas, N.A., (1999). Solute transport analysis in pH-responsive, complexing hydrogels of poly (methacrylic acid-g-ethylene glycol). *Journal of Biomaterials Science, Polymer Edition*, **10**, 999-1009.

Lu, P., Ding, B., (2008). Applications of Electrospun Fibres, *Recent Patents on Nanotechnology*, **2**, 169-182

Lue, S.J., Hsu, J.-J., Chen, C.-H., Chen, B.-C., (2007). Thermally on-off switching membranes of poly (*N*-isopropylacrylamide) immobilized in track-etched polycarbonate films. *Journal of Membrane Science*, **301**, 142-150.

Lue, S.J., Hsu, J., Wei, T., (2008). Drug permeation modeling through the thermo-sensitive membranes of poly(*N*-isopropylacrylamide) brushes grafted onto micro-porous films. *Journal of Membrane Science*, **321(2)**, 146-154.

Luo, X., Berlin, D.L., Betz, J., Payne, G.F., Bentley, W.E., Rubloff, G.W., (2010). In situ generation of pH gradients in microfluidic devices for biofabrication of freestanding, semi-permeable chitosan membranes. *Lab on a Chip*, **10**, 59-65.

Luong-Van, E., Grøndal, L., Chua, K.N., Leong, K.W., Nurcombe, V., Cool, S.M., (2006). Controlled release of heparin from poly( $\epsilon$ -caprolactone) electrospun fibres. *Biomaterials*, **27**, 2042-2050.

Luu, Y.K., Kim, K., Hsiao, B.S., Chu, B., Hadjiargyrou, M., (2003). Development of a nanostructured DNA delivery scaffold via electrospinning of PLGA and PLA-PEG block copolymers. *Journal of Controlled Release*, **89**, 341-353.

Madhav, N.V.S., Shakya, A.K., Shakya, P., Singh, K., (2009). Orotransmucosal drug delivery systems: A review. *Journal of Controlled Release*, **140**, 2-11.

Maffei, P., Borgia, S.L., Sforzini, A., Yasin, A., Ronchi, C., Ceschel, G.C., (2004). Design and in vitro–in vivo evaluation of a bi-layered tablet containing benzocaine for local buccal administration. *Journal of Drug Delivery Science and Technology*, **14**, 363-372.

Maggi, L., Segale, L., Conti, S., Machiste, E.O., Salini, A., Conte, U., (2005). Preparation and evaluation of release characteristics of 3TabGum, a novel chewing device. *European Journal of Pharmaceutical Sciences*, **24**, 487-493.

Mahkam, M., (2005). Using pH-Sensitive Hydrogels Containing Cubane as a Crosslinking Agent for Oral Delivery of Insulin, *Published online 15 July 2005 in Wiley InterScience (www.interscience.wiley.com)*. DOI: 10.1002/jbm.b.30279

Majerik, V., Charbit, G., Badens, E., Horv'ath, G., Szokonya, L., Bosc, N., Teillaud, E., (2007). Bioavailability enhancement of an active substance by supercritical antisolvent precipitation. *Journal of Supercritical Fluids*, **40**, 101-110.

Makai, M., Csanyi, E., Nemeth, Z., Palinkas, J., Eros, I., (2003). Structure and drug release of lamellar liquid crystals containing glycerol. *International Journal of Pharmaceutics*, **256**, 95-107.

Mania-Pramanik, J., Kerkar, S.C., Mehta, P.B., Potdar, S., Salvi, V.S., (2008). Use of vaginal pH in diagnosis of infections and its association with reproductive manifestations. *Journal of Clinical Laboratory Analysis*, **22(5)**, 375-379.

Manglik, R.M., Wasekar, V.M., Zhang, J., (2001), Dynamic and equilibrium surface tension of aqueous surfactant and polymeric solutions. *Experimental Thermal and Fluid Science*, **25(1-2)**, 55-64.

Maretschek, S., Greiner, A., Kissel, T., (2008). Electrospun biodegradable nanofiber nonwovens for controlled release of proteins. *Journal of Controlled Release*, **127**, 180-187.

Mariappan, T.T., Singh, S., (2003). Regional gastrointestinal permeability of rifampicin and isoniazid (alone and their combination) in the rat. *The International Journal of Tuberculosis and Lung Disease*, **7(8)**, 797-03.

Mariappan, T.T., Jindal, K.C., Singh, S., (2004). Overestimation of rifampicin during colorimetric analysis of anti-tuberculosis products containing isoniazid due to formation of isonicotinyl hydrazone. *Journal of Pharmaceutical and Biomedical Analysis*, **36(4)**, 905-908.

Mason, P., (2010). Conference on 'Malnutrition matters', Symposium 8: Drugs and nutrition, Important drug-nutrient interactions. *Proceedings of the Nutrition Society*, **69**, 551-557.

Mathematica™ Image Processing and Analysis Guide, Wolfram Mathematica Documentation Center, Wolfram Research, Inc. Available at: <http://reference.wolfram.com/mathematica/guide/ImageProcessing.html>. Accessed on: June 12, 2011.

Matsuyama, H., Teramoto, M., Nakatani, R., Maki, T., (1999). Membrane Formation via Phase Separation Induced by Penetration of Nonsolvent from Vapor Phase. II: Membrane Morphology. *Journal of Applied Polymer Science*, **74**, 171-178.

Matsuyama, H., Iwatani, T., Kitamura, Y., Teramoto, M., Sugoh, N., (2001a). Formation of Porous Poly(ethylene-co-vinyl alcohol) Membrane via Thermally Induced Phase Separation. *Journal of Applied Polymer Science*, **79**, 2449-2455.

Matsuyama, H., Yano, H., Maki, T., Teramoto, M., Mishima, K., Matsuyama, K., (2001b). Formation of porous flat membrane by phase separation with supercritical CO<sub>2</sub>. *Journal of Membrane Science*, **194**, 157-163.

Matsuyama, H., Yamamoto, A., Yano, H., Maki, T., Teramoto, M., Mishima, K., Matsuyama, K., (2002). Effect of organic solvents on membrane formation by phase separation with supercritical CO<sub>2</sub>. *Journal of Membrane Science*, **204**, 81-87.

Matsuyama, H., Okafuji, H., Maki, T., Teramoto, M., Kubota N., (2003). Preparation of polyethylene hollow fiber membrane via thermally induced phase separation. *Journal of Membrane Science*, **223**, 119-126.

McConnell, E.L., Fadda, H.M., Basit, A.W., (2008). Gut instincts: Explorations in intestinal physiology and drug delivery. *International Journal of Pharmaceutics*, **364**, 213-226.

Meka, I., Kesavan, B., Kalamata, V.N., Eaga, C.M., Bandari, S., Vobalaboina, V., Yamsani, M.R., (2009). Design and evaluation of polymeric coated minitabets as multiple unit gastroretentive floating drug delivery systems for furosemide. *Journal of Pharmaceutical Sciences*, **98**, 2122-2132.

Merkle, H.P., Anders, R., Wermerskirchen, A., (1990). Mucoadhesive buccal patches for peptide delivery, In: *Bioadhesive Drug Delivery Systems*, Lenaerts, V., Gurny, R., (Eds). CRC Press, Boca Raton FL, USA.

Messina, J., Darwish, M., Fine, P.G., (2008). Fentanyl buccal tablet. *Drugs Today*, **44**, 41-54.

Meyer, M.C., Straughn, A.B., Mhatre, R.M., Hussain, A., Shah, V.P., Bottom, C.B., Cole, E.T., Lesko, L.L., Mallinowski, H., Williams, R.L., (2000). The Effect of Gelatin Cross-Linking on the Bioequivalence of Hard and Soft Gelatin Acetaminophen Capsules. *Pharmaceutical Research*, **17**, 962-966.

Mi, F.-L., Liang, H.-F., Wu, Y.-C., Lin, Y.-S., Yang, T.-F., Sung, H.-W., (2005). pH-sensitive behavior of two-component hydrogels composed of N,O-carboxymethyl chitosan and alginate. *Journal of Biomaterials Science, Polymer Edition*, **16(11)**, 1333-1345.

Mika, A.M., Childsa, R.F., Dickson, J.M., (1999). Chemical valves based on poly (4-vinylpyridine)-filled microporous membranes. *Journal of Membrane Science*, **153**, 45-56.

Milhem, O.M., Myles, C., McKeown, M.B., Attwood, D., D'Emanuele, A., (2000). Polyamidoamine Starburst<sup>®</sup> dendrimers as solubility enhancers. *International Journal of Pharmaceutics*, **197**, 239-241.

Mit-Uppatham, C., Nithitanakul, M., Supaphol, P., (2004). Ultrafine electrospun polyamide-6 fibers: effect of solution conditions on morphology and average fiber diameter. *Macromolecular Chemistry and Physics*, **205**, 2327-2338.

Miyata, T., Uragami, T., Nakamae, K., (2002). Biomolecule-sensitive hydrogels. *Advanced Drug Delivery Reviews*, **54**, 79-98.

Mizutani, A., Kikuchi, A., Yamato, M., Kanazawa, H., Okano, T., (2008). Preparation of thermo-responsive polymer brush surfaces and their interaction with cells. *Biomaterials*, **29**, 2073-2081.

Mohan, B., Sharda, N., Singh, S., (2003). Evaluation of the recently reported USP gradient HPLC method for analysis of anti-tuberculosis drugs for its ability to resolve

degradation products of rifampicin. *Journal of Pharmaceutical and Biomedical Analysis*, **31(3)**, 607-612.

Mouly, S., Paine, M.F., (2003). P-glycoprotein increases from proximal to distal regions of human small intestine. *Pharmaceutical Research*, **20**, 11595-11599.

Murphy, C., Pillay, V., Choonara, Y.E., du Toit, L.C., Ndesendo, V.M.K., Chirwa, N., Kumar, P., (2011). Optimization of a Dual Mechanism Gastrofloatable and Gastroadhesive Delivery System for Narrow Absorption Window Drugs. *AAPS PharmSciTech*, Published online 3 November 2011, DOI: 10.1208/s12249-011-9711-1

Mythri, G., Kavitha, K., Kumar, M.R., Sd. Singh, J., (2011). Novel Mucoadhesive Polymers –A Review. *Journal of Applied Pharmaceutical Science*, **1(8)**, 37-42.

Na, K., Lee, K.L., Lee, D.H., Bae, Y.H., (2006). Biodegradable thermo-sensitive nanoparticles from poly (L-lactic acid)/poly (ethylene glycol) alternating multi-block copolymer for potential anti-cancer drug carrier. *European Journal of Pharmaceutical Sciences*, **27**, 115-122.

Nagahama, H., Nwe, N., Jayakumar, R., Koiwa, S., Furuike, T., Tamura, H., (2008). Novel biodegradable chitin membranes for tissue engineering applications. *Carbohydrate Polymers*, **73**, 295-302.

Nakamura, K., Nara, E., Akiyama, Y., (2006). Development of an oral sustained release drug delivery system utilizing pH-dependant swelling of carboxyvinyl polymer. *Journal of Controlled Release*, **111**, 309-315.

Nakayama, H., Kaetsu, I., Uchida, K., Sakata, S., Tougou, K., Hara, T., Matsubara, Y., (2002). Radiation curing of intelligent coating for controlled release and permeation. *Radiation Physics and Chemistry*, **63**, 521-523.

Natu, M.V., de Sousa, H.C., Gil, M.H., (2010). Effects of drug solubility, state and loading on controlled release in bicomponent electrospun fibres. *International Journal of Pharmaceutics*, **397**, 50–58

Ndesendo, V.M.K., Pillay, V., Choonara, Y.E., Buchmann, E., Bayever, D.N., Meyer, L.C.R., (2008). Current intravaginal drug delivery approaches employed for the

prophylaxis of HIV/AIDS and prevention of sexually transmitted infections. *AAPS PharmSciTech*, **9(2)**, 505-520.

Ndesendo, V.M.K., Pillay, V., Choonara, Y.E., Khan, R.A., Meyer, L., Buchmann, E., Rosin, E., (2009). *In vitro* and *ex vivo* bioadhesivity analysis of polymeric intravaginal caplets using physicomechanics and computational structural modelling. *International Journal of Pharmaceutics*, **370**, 151-159.

Ng, C.C., Cheng, Y.-L., Saville, B.A., (2001). Thermo-responsive polymer membrane for the local delivery of drugs. *Journal of Sexual and Reproductive Medicine*, **1**, 21-27.

Niimi, Y., Ueyama, K., Yamaji, K., Yamane, S., Tayama, E., Sueoka, A., Kuwana, K., Tahara, K., Nose, Y., (1997). Effects of ultrathin silicone coating of porous membrane on gas transfer and hemolytic performance. *Artificial Organs*, **21(10)**, 1082-1086.

Nunoya, T., Shibuya, K., Saitoh, T., Yazawa, H., Nakamura, K., Baba, Y., Hirai., T., (2007). Use of miniature pig for biomedical research, with reference to toxicologic studies. *Journal of Toxicological Pathology*, **20**, 125-132.

Obaidat, A.A., Park, K., (1997). Characterization of protein release through glucose-sensitive hydrogel membranes. *Biomaterials*, **18**, 801-806.

Ohya, S., Sonoda, H., Nakayama, Y., Matsuda, T., (2005). The potential of poly (N-isopropylacrylamide) (PNIPAM)-grafted hyaluronan and PNIPAM-grafted gelatin in the control of post-surgical tissue adhesions. *Biomaterials*, **26**, 655-659.

Okahata, Y., Noguchi, H., Seki, T., (1986). Thermo-selective permeation from a polymer-grafted capsule membrane. *Macromolecules*, **19**, 493-494.

Omari, A., Tabary, R., Rousseau, D., Leal Calderon, F., Monteil, J., Chauveteau, G., (2006). Soft water-soluble microgel dispersions: Structure and rheology. *Journal of Colloid Science*, **302(2)**, 537-546.

Owens, T.S., Dansereau, R.J., Sakr, A., (2005). Development and evaluation of extended release bioadhesive sodium fluoride tablets. *International Journal of Pharmaceutics*, **288**, 109-122.

Packhaeuser, C.B., Schnieders, J., Oster, C.G., Kissel, T., (2004). In situ forming parenteral drug delivery systems: an overview. *European Journal of Pharmaceutics and Biopharmaceutics*, **58**, 445-455.

Pakravan, M., Heuzey, M.C., Ajjia, A., (2011). A fundamental study of chitosan/PEO electrospinning. *Polymer*, **52**, 4813-4824.

Pape, P.G., (1983). Silicons: Unique Chemicals for Petroleum Processing, *Journal of Petroleum Technology*, **35(7)**, 1197-1204.

Park, H., Robinson, J.R., (1987). Mechanisms of mucoadhesion of poly(acrylic acid) hydrogels. *Pharmaceutical Research*, **4**, 457-464.

Park, Y.S., Ito, Y., Imanishi, Y., (1998). Permeation control through porous membranes immobilized with thermo-sensitive polymer. *Langmuir*, **14**, 910-914.

Park, S.-B., You, J.-O., Park, H.-Y., Haam, S.J., Kim, W.-S., (2001). A novel pH-sensitive membrane from chitosan TEOS IPN; preparation and its drug permeation characteristics. *Biomaterials*, **22**, 323-330.

Park, K.H., Song, S.C., (2006). Morphology of spheroidal hepatocytes within injectable, biodegradable and thermo-sensitive poly(organophosphazene) hydrogel as cell delivery vehicle. *Journal of Bioscience and Bioengineering*, **101**, 238-242.

Patel, J.K., Patel, M.M., (2007). Stomach Specific Anti-Helicobacter Pylori Therapy: Preparation and Evaluation of Amoxicillin-Loaded Chitosan Mucoadhesive Microspheres. *Current Drug Delivery*, **4**, 41-50.

Patterson, J.K., Lei, X.G., Miller, D.D., (2008). The Pig as an Experimental Model for Elucidating the Mechanisms Governing Dietary Influence on Mineral Absorption. *Experimental Biology and Medicine*, **233**, 651-664.

Pawlak, A., Mucha, M., (2003). Thermogravimetric and FTIR studies of chitosan blends, *Thermochimica Acta*, **396**, 153-166.

Pearlman, D.A., Case, D.A., Caldwell, J.W., Ross, W.S., Cheatham, T.E., De-Bolt, S., Ferguson, D., Seibel, G., Kollman, P., (1995). AMBER, a package of computer programs

for applying molecular mechanics, normal mode analysis, molecular dynamics and free energy calculations to simulate the structural and energetic properties of molecules. *Computer Physics Communications*, **91**, 1-41.

Peng, F., Jiang, Z., Hoek, E.M.V., (2011). Tuning the molecular structure, separation performance and interfacial properties of poly(vinyl alcohol)–polysulfone interfacial composite membranes. *Journal of Membrane Science*, **368(1–2)**, 26–33.

Peppas, N.A., Sahlin, J.J., (1996). Hydrogels as mucoadhesive and bioadhesive materials: a review. *Biomaterials*, **17**, 1553-1561.

Pereira, C.C., Nobrega, R., Borges, C.P., (2000). Spinning process variables and polymer solution effects in the die-swell phenomenon during hollow fiber membrane formation. *Brazilian Journal of Chemical Engineering*, **17**, 4-7.

Pillay, V., Fassihi, R., (2000). A novel approach for constant rate delivery of highly soluble bioactives from a simple monolithic system, *Journal of Controlled Release*, **67**, 67-78.

Pham, Q.P., Sharma, U., Mikos, A.G., (2006). Electrospinning of Polymeric Nanofibers for Tissue Engineering Applications: A Review. *Tissue Engineering*, **12(5)**, 1197-1211.

Podual, K., Doyle III, F.J., Peppas, N.A., (2000). Glucose-sensitivity of glucose oxidase-containing cationic copolymer hydrogels having poly (ethylene glycol) grafts, *Journal of Controlled Release*, **67**, 9-17.

Prabakaran, D., Singh, P., Jaganathan, K.S., Vyas, S.P., (2004). Osmotically regulated asymmetric capsular systems for simultaneous sustained delivery of anti-tubercular drugs. *Journal of Controlled Release*, **95(2)**, 239-248.

Prabhu, S., Ortega, M., Ma, C., (2005). Novel lipid-based formulations enhancing the in vitro dissolution and permeability characteristics of a poorly water-soluble model drug, piroxicam. *International Journal of Pharmaceutics*, **301**, 209-216.

Pund, S., Joshi, A., Vasu, K., Nivsarkar, M., Shishoo, C., (2010). Multivariate optimization of formulation and process variables influencing physico-mechanical characteristics of site-specific release isoniazid pellets. *International Journal of Pharmaceutics*, **388(1-2)**, 64-72.



Pund, S., Joshi, A., Vasu, K., Nivsarkar, M., Shishoo, C., (2011). Gastroretentive delivery of rifampicin: In vitro mucoadhesion and in vivo gamma scintigraphy. *International Journal of Pharmaceutics*, **411**, 106-112.

Qi, H., Hu, P., Xu, J., Wang, A., (2006). Encapsulation of drug reservoirs in fibers by emulsion electrospinning: morphology characterization and preliminary release assessment. *Biomacromolecules*, **7**, 2327-2330.

Qiu, M., Feng, Jun., Fan, Y., Xu, N., (2009). Pore evolution model of ceramic membrane during constrained sintering. *Journal of Material Sciences*, **44**, 689-699.

Raissi, S. and Eslami Farsani R., (2009). Statistical Process Optimization Through Multi-Response Surface Methodology. *World Academy of Science, Engineering and Technology*, **51**, 267-271.

Ramires, P.A., and Milella, E., (2002). Biocompatibility of poly(vinyl alcohol)-hyaluronic acid and poly(vinyl alcohol)-gellan membranes crosslinked by glutaraldehyde vapours. *Journal of Materials Science: Materials in Medicine*, **13**, 119-123.

Ranade, V.V., (1991). Drug Delivery Systems 5A. Oral Drug Delivery. *Journal of Clinical Pharmacology*, **31**, 2-16.

Rastogi, R., Sultana, Y., Aqil, M., Ali, A., Kumar, S., Chuttani, K., Mishra, A.K., (2007). Alginate microspheres of isoniazid for oral sustained drug delivery. *International Journal of Pharmaceutics*, **334**, 71-77.

Rathbone, M.J., Drummond, B.K., Tucker, I.G., (1994). The oral cavity as a site for systemic drug delivery. *Advanced Drug Delivery Reviews*, **13(1-2)**, 1-22.

Rathi, R.C., Kopečková, P., Říhová, B., Kopeček, J., (1991). N-(2-Hydroxypropyl)methacrylamide copolymers containing pendent saccharide moieties. Synthesis and bioadhesive properties. *Journal of Polymer Science Part A: Polymer Chemistry*, **(29)**, 1895-1991.

Reneker, D.H., Chun, I., (1996). Nanometre diameter fibres of polymer, produced by electrospinning. *Nanotechnology*, **7**, 216-223.

Reneker, D.H., Yarin, A.L., (2008). Electrospinning jets and polymer nanofibers. *Polymer*, **49**, 2387-2425.

Rezwan, K., Chen, Q.Z., Blaker, J.J., Boccaccini, A.R., (2006). Biodegradable and bioactive porous polymer/inorganic composite scaffolds for bone tissue engineering. *Biomaterials*, **27**, 3413-3431.

Roberts, R.J., Rowe, R.C., York, P., (1991). The relationship between Young's modulus of elasticity of organic solids and their molecular structure. *Powder Technology*, **65**, 139-146.

Rouge, N., Buri, P., Doelker, E., (1996). Drug absorption sites in the gastrointestinal tract and dosage forms for site-specific delivery. *International Journal of Pharmaceutics*, **136**, 117-139.

Rowe, R.C., Sheskey, P.J., Quinn, M.E., (Eds), (2009). Handbook of Pharmaceutical Excipients, 6<sup>th</sup> Edition. The Pharmaceutical Press and American Pharmacist Association, London, UK.

Roy, S., Pal, K., Anis, A., Pramanik, K., Prabhakar, B., (2009). Polymers in Mucoadhesive Drug Delivery System: A Brief Note. *Designed Monomers and Polymers*, **12**, 483-495.

RoyChowdhury, P., Kumar, V., (2006). Fabrication and evaluation of porous 2,3-dialdehydecellulose membrane as a potential biodegradable tissue engineering scaffold. *Journal of Biomedical Materials Research Part A*, **76A(2)**, 300-309.

Sa-nguanrukksa, J., Rujiravanit, R., Supaphol, P., Tokura, S., (2004). Porous polyethylene membranes by template-leaching technique: preparation and characterization. *Polymer Testing*, **23**, 91-99.

Sáez-Martínez, V., Pérez-Álvarez, L., Merrero, M.T., Hernáez, E., Katime, I., (2008). pH-Sensitive microgels functionalized with folic acid. *European Polymer Journal*, **44(5)**, 1309-1322.

Salamat-Miller, N., Chittchang, M., Johnston, T.P., (2005). The use of mucoadhesive polymers in buccal drug delivery. *Advanced Drug Delivery Reviews*, **57**, 1666-1691.

Sant, V.P., Smith, D., Leroux, J.-C., (2004). Novel pH-sensitive supramolecular assemblies for oral delivery of poorly water soluble drugs: preparation and characterization. *Journal of Controlled Release*, **97**, 301-312.

Sant, V.P., Smith, D., Leroux, J.-C., (2005). Enhancement of oral bioavailability of poorly water-soluble drugs by poly (ethylene glycol)-block-poly (alkyl acrylate-co-methacrylic acid) self-assemblies. *Journal of Controlled Release*, **104**, 289-300.

Santus, G., Baker, R.W., (1995). Osmotic drug delivery: a review of the patent literature. *Journal of Controlled Release*, **35**, 1-21.

Sastry, S.V., Nyshadham, J.R. and Fix, J.A., (2000). Recent technological advances in oral drug delivery - a review. *Pharmaceutical Science and Technology Today*, **3(4)**, 138-145.

Satoh, K., Takayama, K., Machida, Y., Suzuki, Y., Nakagaki, M., Nagai, T., (1989). Factors affecting the bioadhesive property of tablets consisting of hydroxypropyl cellulose and carboxyvinyl polymer. *Chemical & Pharmaceutical Bulletin*, **37(5)**, 1366-1368.

Satturwar, P., Eddine, M.N., Ravenelle, F., Leroux, J.-C., (2007). pH-responsive polymeric micelles of poly (ethylene glycol)-b-poly (alkyl(meth) acrylate-co-methacrylic acid): Influence of the copolymer composition on self-assembling properties and release of candesartan cilexetil. *European Journal of Pharmaceutics and Biopharmaceutics*, **65**, 379-387.

Sawicka, K.M., Gouma, P., (2006). Electrospun composite nanofibers for functional applications. *Journal of Nanoparticle Research*, **8**, 769-781.

Schellekens, R.C.A., Stellaard, F., Mitrovic, D., Stuurman, F.E., Kosterink, J.G.W., Frijlink, H.W., (2008). Pulsatile drug delivery to ileo-colonic segments by structured incorporation of disintegrants in pH-responsive polymer coatings. *Journal of Controlled Release*, **132**, 91-98.

Schiller, C., Frohlich, C.P., Giessmann, T., Siegmund, W., Mönnikes, H., Hosten, N., Weitschies, W., (2005). Intestinal fluid volumes and transit of dosage forms as assessed by magnetic resonance imaging. *Alimentary Pharmacology & Therapeutics*, **22**, 971-979.

Schmaljohann, D., (2006). Thermo- and pH-responsive polymers in drug delivery. *Advanced Drug Delivery Reviews*, **58**, 1655-1670.

Schmitz, T., Leitner, V.M., Bernkop-Schnürch, A., (2005). Oral Heparin Delivery: Design and In Vivo Evaluation of a Stomach-Targeted Mucoadhesive Delivery System. *Journal of Pharmaceutical Sciences*, **94(5)**, 966-973.

Scrivener, C.A., Schantz, C.W., (1947). Penicillin: New methods for its use in dentistry. *Journal of the American Dental Association*, **35**, 644-647.

Seeley, R.R., Stepheds, T.D., Tate, P, (1995). *Anatomy and Physiology*, 3<sup>rd</sup> Edition, Mosby-Year Book, Inc., St. Louis, Missouri, USA.

Segale, L., Maggi, L., Machiste, E.O., Conti, S., Conte, U., Grenier, A., Besse, C., (2007). Formulation design and development to produce orodispersible tablets by direct compression. *Journal of Drug Delivery Science and Technology*, **17**, 199-203.

Sekel, K., (1999). "Pharmaceutical price controls could do more harm than good" *Scientific Computing & Instrumentation*, July, 6.

Shen, Z., Mitragotri, S., (2002). Intestinal Patches for Oral Drug Delivery. *Pharmaceutical Research*, **19(4)**, 391-395.

Sher, P., Ingavle, G., Ponrathnam, S., Benson, J.R., Li, N.-H., Pawar, A.P., (2009). Novel/Conceptual Floating Pulsatile System Using High Internal Phase Emulsion Based Porous Material Intended for Chronotherapy. *AAPS PharmSciTech*, **10(4)**, 1368-1380.

Shieh, M.J., Lai, P.S., Young, T.H., (2002). 5-Aminosalicylic acid permeability enhancement by a pH -sensitive EVAL membrane. *Journal of Membrane Science*, **204**, 237-246.

Shim, W.S., Kim, J.-H., Park, H., Kim, K., Kwon, I.C., Lee, D.S., (2006). Biodegradability and biocompatibility of a pH- and thermo-sensitive hydrogel formed from a sulphonamide-modified poly (ε-caprolactone-co-lactide)-poly (ethylene glycol)-poly (ε-caprolactone-co-lactide) block copolymer. *Biomaterials*, **27**, 5178-5185.

Shin, H.S., Kim, S.Y., Lee, Y.M., (1997). Indomethacin Release Behaviors from pH and Thermo-responsive Poly( vinyl alcohol) and Poly(acrylic acid) IPN Hydrogels for Site-Specific Drug Delivery. *Journal of Applied Polymer Science*, **65**, 685-693.

Shishoo, C.J., Shah, S.A., Rathod, I.S., Savale, S.S., Vora, M.J., (2001). Impaired bioavailability of rifampicin in presence of isoniazid from fixed dose combination (FDC) formulation. *International Journal of Pharmaceutics*, **228**, 53-67.

Shojaei, A.H., (1998). Buccal Mucosa As A Route For Systemic Drug Delivery: A Review. *Journal of Pharmacy and Pharmaceutical Sciences*, **1(1)**, 15-30.

Shtanko, N.I., Kabanov, V.Y., Apel, P.Y., Yoshida, M., Vilenskii, A.I., (2000). Preparation of permeability-controlled track membranes on the basis of 'smart' polymers. *Journal of Membrane Science*, **179**, 155-161.

Sill, T.J. and Von Recum, H.A., (2008). Electrospinning: Applications in drug delivery and tissue engineering. *Biomaterials*, **29**, 1989-2006.

Singh, D.K., and Ray, A.R., (1999). Controlled release of glucose through modified chitosan membranes. *Journal of Membrane Science*, **155**, 107-112.

Singh, S., Mariappan, T.T., Sharda, N., Chakraborti, A.K., (2000a). The reason for an increase in decomposition of rifampicin in the presence of isoniazid under acid conditions. *Pharmacy and Pharmacology Communications*, **6(11)**, 405-410.

Singh, S., Mariappan, T.T., Sharda, N., Singh, B., (2000b). Degradation of rifampicin, isoniazid and pyrazinamide from prepared mixtures and marketed single and combination products under acid conditions. *Pharmacy and Pharmacology Communications*, **6(11)**, 491-494.

Singh, S., Mariappan, T.T., Sankar, R., Sarda, N., Singh, B., (2001). A critical review of the probable reasons for the poor/variable bioavailability of rifampicin from anti-tubercular fixed-dose combination (FDC) products, and the likely solutions to the problem. *International Journal of Pharmaceutics*, **228**, 5-17.

Singh, B., Kumar, R., Ahuja, N., (2004). Optimizing drug delivery systems using systematic "Design of Experiments." Part I: Fundamental aspects. *Critical Reviews<sup>TM</sup> in Therapeutic Drug Carrier Systems*, **22**, 27-105.

Singh, B., Sharma, N., Chauhan, N., (2007). Synthesis, characterization and swelling studies of pH responsive psyllium and methacrylamide based hydrogels for the use in colon specific drug delivery. *Carbohydrate Polymers*, **69**, 631-643.

Singla, A.K. and Chawla, M., (2001). Chitosan: some pharmaceutical and biological aspects – an update. *Journal of Pharmacy and Pharmacology*, **53**, 1047-1067.

Smart, J.D., (2005). The basics and underlying mechanisms of mucoadhesion. *Advanced Drug Delivery Reviews*, **57**, 1556-1568.

Soga, O., van Nostrum, C.F., Fens, M., Rijcken, C.J.F., Schiffelers, R.M., Storm, G., Hennink, W.E., (2005). Thermo-sensitive and biodegradable polymeric micelles for paclitaxel delivery. *Journal of Controlled Release*, **103**, 341-353.

Sogias, I.A., Williams, A.C., Khutoryanskiy, V.V., (2008). Why is Chitosan Mucoadhesive? *Biomacromolecules*, **9**, 1837-1842.

Soppimath, K.S., Kulkarni, A.R., Aminabhavi, T.M., (2001). Chemically modified polyacrylamide-g-guar gum-based crosslinked anionic microgels as pH-sensitive drug delivery systems: preparation and characterization. *Journal of Controlled Release*, **75**, 331-345.

Sosnik, A. and Cohn, D., (2004). Ethoxysilane-capped PEO-PPO-PEO triblocks: a new family of reverse thermo-responsive polymers. *Biomaterials*, **25**, 2851-2858.

Speers, M., (1999), Economic aspects of controlled drug delivery. In: E. Mathowitz, Editor, *Encyclopaedia of Controlled Drug Delivery*, **1**, John Wiley and Sons, New York 341-347.

Spoehr, R., Reber, N., Wolf, A., Alder, G.M., Ang, V., Bashford, C.L., Pasternak, C.A., Omichi, H., Yoshida, M., (1998). Thermal control of drug release by a responsive ion track membrane observed by radio tracer flow dialysis. *Journal of Controlled Release*, **50**, 1-11.

Spriggs, R.M., (1961). Expression for Effect of Porosity on Elastic Modulus of Polycrystalline Refractory Materials. Particularly Aluminum Oxide. *Journal of the American Ceramic Society*, **44**, 628-629.

Sriamornsak, P., (2003). Chemistry of pectin and its pharmaceutical uses: a review. *Silpakorn University International Journal*, **3(1-2)**, 206-228.

Sriamornsak, P., Thirawong, N., Weerapol, Y., Nunthanid, J., Sungthongjeen, S., (2007). Swelling and erosion of pectin matrix tablets and their impact on drug release behavior. *European Journal of Pharmaceutics and Biopharmaceutics*, **67(1)**, 211-219.

Stamatialis, D.F., Papenburg, B.J., Giron´es, M., Saiful, S., Bettahalli, S.N.M., Schmitmeier, S., Wessling, M., (2008). Medical applications of membranes: Drug delivery, artificial organs and tissue engineering. *Journal of Membrane Science*, **308**, 1-34.

Stayton, P.S., El-Sayed, M.E.H., Murthy, N., Bulmus, V., Lackey, C., Cheung, C., Hoffman, A.S., (2005). Smart delivery systems for biomolecular therapeutics. *Orthodontics & Craniofacial Research*, **8**, 219-225.

Streubel, A., Siepmann, J., Bodmeier, R., (2003). Floating matrix tablets based on low density foam powder: effects of formulation and processing parameters on drug release, *European Journal of Pharmaceutical Sciences*, **18**, 37-45.

Sudhakar, Y., Kuotsu, K., Bandyopadhyay, A.K., (2006). Buccal bioadhesive drug delivery - A promising option for orally less efficient drugs. *Journal of Controlled Release*, **114**, 15-40.

Suma, K., Tsuji, T., Takeuchi, Y., (1981). Clinical performance of microporous polypropylene hollow-fiber oxygenator. *Annals of Thoracic Surgery*, **32(6)**, 558-562.

Sun, Y.-M., Hsu, S.-C., Lai, J.-Y., (2001). Transport Properties of Ionic Drugs in the Ammonio Methacrylate Copolymer Membranes. *Pharmaceutical Research*, **18(3)**, 304-310.

Sun, H., Liu, S., Ge, B., Xing, L., Chen, H., (2007a). Cellulose nitrate membrane formation via phase separation induced by penetration of nonsolvent from vapour phase. *Journal of Membrane Science*, **295**, 2-10.

Sun, G., Zhang, X.-Z., Chu, C.-C., (2007b). Formulation and characterization of chitosan-based hydrogel films having both temperature and pH sensitivity. *Journal of Material Science: Mater Med*, **18**, 1563-1577.

Surana, A.S., Kotecha, R.K., (2010). An overview on various approaches to oral controlled drug delivery system via gastroretention. *International Journal of Pharmaceutical Sciences Review and Research*, **2(2)**, 68-72.

Swindle, M.M., Smith A.C., (2000). Informational resources on swine in biomedical research. In: Smith C editors. *AWIC Resource Series*, **No. 11**. Bethesda: USDA: Agricultural Research Service.

Swisher, D.A., Sendelbeck, S.L., Fara, J.W., (1984). Adherence of various oral dosage forms to the esophagus. *International Journal of Pharmaceutics*, **22(2-3)**, 219-228.

Taepaiboon, P., Rungsardthong, U., Supaphol, P., (2006). Drug-loaded electrospun mats of poly(vinyl alcohol) fibres and their release characteristics of four model drugs. *Nanotechnology*, **17**, 2317-2329.

Taepaiboon, P., Rungsardthong, U., Supaphol, P., (2007). Vitamin-loaded electrospun cellulose acetate nanofiber mats as transdermal and dermal therapeutic agents of vitamin A acid and vitamin E. *European Journal of Pharmaceutics and Biopharmaceutics*, **67**, 387-397.

Tan, J.P.K., Goh, C.H., Tam, K.C., (2007). Comparative drug release studies of two cationic drugs from pH-responsive nanogels. *European Journal of Pharmaceutical Sciences*, **32**, 340-348.

Tanaka, N., Imai, K., Okimoto, K., Ueda, S., Tokonaga, Y., Ibuki, R., Higaki, K., Kimura, T., (2006). Development of novel sustained-release system, disintegration-controlled matrix tablet (DCMT) with solid dispersion granules of nilvadipine (II): In vivo evaluation. *Journal of Controlled Release*, **112**, 51-56.

Tang, M., Zhang, R., Bowyer, A., Eisenthal, R., Hubble, J., (2003). A Reversible Hydrogel Membrane for Controlling the Delivery of Macromolecules. *Biotechnology and Bioengineering*, **82(1)**, 47-53.



Tang, C., Saquing, C.D., Harding, J.R., Khan, S.A., (2010). In Situ Cross-Linking of Electrospun Poly(vinyl alcohol) Nanofibers. *Macromolecules*, **43**, 630-637.

Tangri, P. and Madav, N.V.S., (2011). Oral Mucoadhesive Drug Delivery Systems: A Review. *International Journal of Biopharmaceutics*, **2(1)**, 36-46.

Tanno, F.K., Sakuma, S., Masaoka, Y., Kataoka, M., Kozaki, T., Kamaguchi, R., Ikeda, Y., Kokubo, H., Yamashita, S., (2008). Site-Specific Drug Delivery to the Middle-to-Lower Region of the Small Intestine Reduces Food-Drug Interactions that Are Responsible for Low Drug Absorption in the Fed State. *Journal of Pharmaceutical Sciences*, **97(12)**, 5341-5353.

Tao, J. and Shivkumar, S., (2007). Molecular weight dependent structural regimes during the electrospinning of PVA. *Materials Letters*, **61**, 2325-2328.

Thanou, M., Florea, I., Langemeyër, M.W.E., Verhoef, J.C., Junginger, H.E., (2000). N-Trimethylated Chitosan Chloride (TMC) Improves the Intestinal Permeation of the Peptide Drug Buserelin *In Vitro* (Caco-2 Cells) and *In Vivo* (Rats). *Pharmaceutical Research*, **17(1)**, 27-31.

Thirawong, N., Nunthanid, J., Puttipipatkachorn, S., Sriamornsak, P., (2007). Mucoadhesive properties of various pectins on gastrointestinal mucosa: An *in vitro* evaluation using texture analyzer. *European Journal of Pharmaceutics and Biopharmaceutics*, **67(1)**, 132-140.

Thomas, J.A., (1995). Drug-Nutrient Interactions. *Nutrition Reviews*, **53(10)**, 271-282.

Thomas, J.B., Tingsanchali, J.H., Rosales, A.M., Creecy, C.M., McGinity, J.W., Pappas, N.A., (2007). Dynamics of poly (ethylene glycol)-tethered, pH responsive networks. *Polymer*, **48**, 5042-5048.

Tian, D., Dubois, P.H., Jerome, R., (1999). Biodegradable and biocompatible inorganic-organic hybrid materials: 4. Effect of acid content and water content on the incorporation of aliphatic polyesters into silica by the sol-gel process. *Polymer*, **40**, 951-957.

Tomlinson, E., (1987). Theory and practice of site-specific drug delivery. *Advanced Drug Delivery Reviews*, **1**, 87-198.

Tritely, T., Cohen, Y., Cost, J., (2000). Characterization of glucose-sensitive insulin release systems in simulated in vivo conditions. *Biomaterials*, **21**, 1679-1687.

Tutuian, R., Castell, D.O., (2006). Gastroesophageal reflux monitoring: pH and impedance. *GI Motility online*, doi:10.1038/gimo31 Available at: <http://www.nature.com/gimo/contents/pt1/full/gimo31.html>

Vandamme, T.F., Lenourry, A., Charrueau, C., Chaumeil, J., (2002). The use of polysaccharides to target drugs to the colon. *Carbohydrate Polymers*, **48**, 219-231.

Varshosaz, J., and Falamarzian, M., (2001). Drug diffusion mechanism through pH-sensitive hydrophobic/polyelectrolyte hydrogel membranes. *European Journal of Pharmaceutics and Biopharmaceutics*, **51**, 235-240.

Varshosaz, J., and Hajian, M., (2004). Characterization of drug release and diffusion mechanism through hydroxyethylmethacrylate/methacrylic acid pH sensitive hydrogel. *Drug Delivery*, **11(1)**, 53-58.

Varum, F.J.O., Merchant, H.A., Basit, A.W., (2010). Oral modified-release formulations in motion: The relationship between gastrointestinal transit and drug absorption. *International Journal of Pharmaceutics*, **395**, 26-36.

Venugopal, J., Zhang, Y.Z., Ramakrishna, S., (2005). Electrospun nanofibres: biomedical applications. *Proceedings of the Institution of Mechanical Engineers 218 Part N: Journal of Nanoengineering and Nanosystems*, 35-45.

Wang, X., Fang, D., Yoon, K., Hsiao, B.S., Chu, B., (2006). High performance ultrafiltration composite membranes based on poly(vinyl alcohol) hydrogel coating on crosslinked nanofibrous poly(vinyl alcohol) scaffold. *Journal of Membrane Science*, **278**, 261-268.

Warhurst, D.C., Craig, J.C., Adagu, I.S., Meyer, D.J., Lee, S.Y., (2003). The relationship of physico-chemical properties and structure to the differential antiplasmodial activity of the cinchona alkaloids. *Malaria Journal*, **2**: 26.

Weber, S.A., Opheim, K.E., Smith, A.L., Wong, K., (1983). High-Pressure Liquid Chromatographic Quantitation of Rifampin and Its Two Major Metabolites in Urine and Serum. *Reviews of Infectious Diseases*, **5**, S433-S439.

Wei, J.S., Zeng, H.B., Liu, S.Q., Wang, X.G., Tay, E.H., Yang, Y.Y., (2005). Temperature- and pH-sensitive core-shell nanoparticles self-assembled from poly(n-isopropylacrylamide-co-acrylic acid-co-cholesteryl acrylate) for intracellular delivery of anticancer drugs. *Frontiers in Bioscience: a journal and virtual library*, **10**, 3058-3067.

Weitschies, W., Blume, H., Mönnikes, H., (2010). Magnetic marker monitoring: High resolution real time tracking of oral solid dosage forms in the gastrointestinal tract. *European Journal of Pharmaceutics and Biopharmaceutics*, **74**, 93-101.

Wessler, S. (1976). Introduction: What is a model? Pp. xi-xvi in *Animal Models of Thrombosis and Hemorrhagic Diseases*. Proceedings of the Workshop on Animal Models of Thrombosis and Hemorrhagic Diseases, which was organized by the Institute of Laboratory Animal Resources and held March 12-13, 1975, in Washington, D.C. Washington, D.C.: U.S. Department of Health, Education, and Welfare.

Whitehead, K., Karr, N., Mitragotri, M., (2008). Discovery of synergistic permeation enhancers for oral drug delivery. *Journal of Controlled Release*, **128(2)**, 128-133.

van de Witte, P., Dijkstra, P.J., van den Berg, J.W.A., Feijen, J., (1996). Phase separation processes in polymer solutions in relation to membrane formation. *Journal of Membrane Science*, **117**, 1-31.

Wu, C., McGinity, J.W., (1999). Non-traditional plasticization of polymeric films. *International Journal of Pharmaceutic*, **177**, 15–27.

Wu, L., Yuan, X., Sheng, J. (2005). Immobilization of cellulase in nanofibrous PVA membranes by electrospinning. *Journal of Membrane Science*, **250**, 167-173.

Xie, J., Wang, C.H., (2006). Electrospun micro- and nanofibers for sustained delivery of paclitaxel to treat C6 glioma *in vitro*. *Pharmaceutical Research*, **23(8)**, 1817-1826.

Xu, X., Yang, L., Xu, X., Wang, X., Chen, X., Liang, Q., Zeng, J., Jing, X., (2005). Ultrafine medicated fibers electrospun from W/O emulsions. *Journal of Controlled Release*, **108**, 33-42.

Xu, X., Chen, X., Xu, X., Lu, T., Wang, X., Yang, L., Xing, X., (2006). BCNU-loaded PEG-PLLA ultrafine fibres and their in vitro antitumor activity against Glioma C6 cells. *Journal of Controlled Release*, **12(114)**, 307-316.

Yadav, V.K., Gupta, A.B., Kumar, R., Yadav, J.S., Kumar, B., (2010). Mucoadhesive Polymers: Means of Improving the Mucoadhesive Properties of Drug Delivery System. *Journal of Chemistry and Pharmaceutical Research*, **2**, 418-32.

Yamagata, T., Morishita, M., Kavimandan, N.J., Nakamura, K., Fukuoka, Y., Takayama, K., Peppas, N.A., (2006). Characterization of insulin protection properties of complexation hydrogels in gastric and intestinal enzyme fluids. *Journal of Controlled Release*, **112**, 343-349.

Yang, L.B., Chu, J.S., Fix, J.A., (2002). Colon-specific drug delivery: new approaches and in vitro/in vivo evaluation. *International Journal of Pharmaceutics*, **235**, 1-15.

Yang, B., Yang, W., (2003). Thermo-sensitive switching membranes regulated by pore covering polymer brushes. *Journal of Membrane Science*, **218**, 247-255.

Yang, W.-C., Xie, R., Pang, X.-Q., Ju, X.-J., Chu, L.-Y., (2008). Preparation and characterization of dual stimuli-responsive microcapsules with a superparamagnetic porous membrane and thermo-responsive gates. *Journal of Membrane Science*, **321**, 324-330.

Yao, L., Haas, T.W., Guiseppi-Elie, A., Bowlin, G.L., Simpson, D.G., Wnek, G.E., (2003). Electrospinning and Stabilization of Fully Hydrolyzed Poly(Vinyl Alcohol) Fibres. *Chemistry of Materials*, **15**, 1860-1864.

Ying, L., Kang, E.T., Neoh, K.G., Kato, K., Iwata, H., (2004). Drug permeation through temperature-sensitive membranes prepared from poly(vinylidene fluoride) with grafted poly(*N*-isopropylacrylamide) chains. *Journal of Membrane Science*, **243**, 253-262.

Yoon, J.-Y., Park, K.-H., Song, S.-C., (2007). A thermo-sensitive poly (organophosphazene) hydrogel for injectable tissue-engineering applications. *Journal of Biomaterials Science, Polymer Edition*, **18**, 1181-1193.

Youn, Y.S., Jung, J.Y., Oh, S.H., Yoo, S.D., Lee, K.C., (2006). Improved intestinal delivery of salmon calcitonin by Lys18-amine specific PEGylation: Stability, permeability, pharmacokinetic behavior and in vivo hypocalcemic efficacy. *Journal of Controlled Release*, **114**, 334-342.

Yu, D.-G., Shen, X.-X., Branford-White, C., White, K., Zhu, L.-M., Annie Bligh, S.W., (2009a) Oral fast-dissolving drug delivery membranes prepared from electrospun polyvinylpyrrolidone ultrafine fibres. *Nanotechnology*, **20**, 1–9.

Yu, D.-G., Zhu, L.-M., White, K., Branford-White, C., (2009b). Electrospun nanofiber-based drug delivery systems. *Health*, **1**, 67-75.

Yuen, K.H., (2010). The transit of dosage forms through the small intestine. *International Journal of Pharmaceutics*, **395**, 9-16.

Zeleny, J., (1935). The role of surface instability in electrical discharges from drops of alcohol and water in air at atmospheric pressure. *Journal of the Franklin Institute*, **219**, 659-675.

Zeng, J., Xu, X., Chen, X., Liang, Q., Bian, X., Yang, L., Jing, X., (2003). Biodegradable electrospun fibers for drug delivery. *Journal of Controlled Release*, **92**, 227-231.

Zeng, J., Aigner, A., Czubyko, F., Kissel, T., Wendorff, J.H., Greiner, A., (2005a). Poly(vinyl alcohol) nanofibers by electrospinning as a protein delivery system and the retardation of enzyme release by additional polymer coatings. *Biomacromolecules*, **6**, 1484-1488.

Zeng, J., Yang, L., Liang, Q., Zhang, X., Guan, H., Xu, X., Chen, X., Jin, X., (2005b). Influence of the drug compatibility with polymer solution on the release kinetics of electrospun fiber formulation. *Journal of Controlled Release*, **105**, 43-51.

Zhao, Y., Kang, J., Tan, T., (2006). Salt, pH- and temperature-responsive semi-interpenetrating polymer network hydrogel based on poly(aspartic acid) and poly(acrylic acid). *Polymer*, **47**, 7702-7710.

Zhang, K. and Wu, X.Y., (2002). Modulated insulin permeation across a glucose-sensitive polymeric composite membrane. *Journal of Controlled Release*, **80**, 169-178.

Zhang, K. and Wu, X.Y., (2004). Temperature and pH-responsive polymeric composite membranes for controlled delivery of proteins and peptides. *Biomaterials*, **25**, 5281-5291.

Zhang, L., Xu, T., Lin, Z., (2006a). Controlled release of ionic drug through the positively charged temperature-responsive membranes. *Journal of Membrane Science*, **281**, 491-499.

Zhang, Y.Z., Wang, X., Feng, Y., Li, J., Lim, C.T., (2006b). Ramakrishna S. Coaxial electrospinning of (fluorescein isothiocyanate-conjugated bovine serum albumin)-encapsulated poly(epsilon-caprolactone) nanofibers for sustained release. *Biomacromolecules*, **7**, 1049-1057.

Zhang, L., Yu, P., Luo, Y., (2006c). Separation of caprolactam–water system by pervaporation through crosslinked PVA membranes. *Separation and Purification Technology*, **52**, 77–83.

Zhang, J. and Misra, R.D.K., (2007). Magnetic drug-targeting carrier encapsulated with thermo-sensitive smart polymer: Core-shell nanoparticle carrier and drug release response. *Acta Biomaterialia*, **3**, 838-850.

Zhang, H., Nie, H., Li, S., White, C.J.B., Zhu, L., (2009). Crosslinking of electrospun polyacrylonitrile/hydroxyethyl cellulose composite nanofibers. *Material Letters*, **63**, 1199-1202.

Zhong, S.P., Teo, W.E., Zhu, X., Beuerman, R., Ramakrishna, S., Yung, L.Y.L., (2007). Development of a novel collagen–GAG nanofibrous scaffold via electrospinning. *Materials Science and Engineering C*, **27**, 262–266.

Zhou, Y., Yan, D., Dong, W., Tian, Y., (2007). Temperature-Responsive Phase Transition of Polymer Vesicles: Real-Time Morphology Observation and Molecular Mechanism. *The Journal of Physical Chemistry B*, **111**, 1262-1270.

Zou, H., Jiang, X.T., Kong, L.S., Gao, S., (2008). Design and evaluation of a dry coated drug delivery system with floating-pulsatile release. *Journal of Pharmaceutical Sciences*, **97**, 263-273.

Zvonar, A., Berginc, K., Kristl, A., Gašperlin, M., (2010). Microencapsulation of self-microemulsifying system: Improving solubility and permeability of furosemide. *International Journal of Pharmaceutics*, **388**, 151-158.

---

# APPENDICES

---



## APPENDIX A

---

### Abstracts of Conference Proceedings

## APPENDIX A1

---

### Membranous drug delivery devices for oral administration

Rubina P. Shaikh, Tasneem Kader, Prof. Viness Pillay, Yahya E. Choonara, Lisa C. du Toit  
University of the Witwatersrand, Department of Pharmacy and Pharmacology, 7 York Road,  
Parktown, 2193, Johannesburg, South Africa

\*Correspondence: [viness.pillay@wits.ac.za](mailto:viness.pillay@wits.ac.za)

**Purpose:** The objective of this study is to compare polymers, polymer concentrations and the methods of fabrication of membranous drug delivery systems and their effects on drug release. As the oral route of drug administration poses to be one of the most favourable and extensively employed routes of administration, these membranous systems will be employed in the oral delivery of drugs.

**Methods:** For comparative reasons, two methods i.e. Immersion Precipitation (IP) and Film-casting (FC) and two polymers, namely poly(vinyl alcohol) (PVA) and cellulose acetate phthalate (CAP) were investigated in the preparation of the membranous systems. PVA membranes were prepared using 2.5%, 5%, and 10%w/v concentrations of polymer solutions with water as a solvent and CAP membranes were prepared using 10%, 15% and 20%w/v concentrations of polymer solutions with acetone as a solvent. Moulds used in the preparation of the membranes were 4 cm in diameter with a depth of 0.5 cm. Moulds were lubricated with liquid paraffin to facilitate ease of removal. Diphenhydramine HCl was incorporated as a model drug at a concentration of 50µg/ml (200µg/membrane).

**FC:** 4 mls of the polymer solutions were then pipetted into moulds and allowed to dry for a period of 24 hours. The resultant membranes were stored with desiccants prior to undergoing a dissolution test.

**IP:** 4 mls of the polymer solutions were pipetted into moulds and allowed to dry for a period of 30 minutes. The moulds were then placed in a coagulation bath containing nonsolvents (Hexane for PVA and Water for CAP) and left for a period of 24 hours. These membranes were then allowed to dry at ambient conditions for a period of 24 hours. Resultant membranes were stored with desiccants prior to undergoing a dissolution test.

**Results:** Dissolution studies were performed in duplicate at 37±0.5°C in simulated gastric fluid (SGF), at pH 1.2, for 2 hours. Samples were analyzed at time intervals of 15 minutes, 30 minutes, 1 hour, 1.5 hours and 2 hours.

**PVA membranes:** Drug encapsulation in PVA membranes were excellent (approx. 200µg/membrane). PVA membranes prepared using FC showed better control over drug release those prepared using IP. The best control was shown with 10% PVA using FC where 45% of drug was released in the first 15 minutes and 70% was released in 2 hours. The poorest control was shown with 2.5% PVA using IP where 70% of drug was released over the first 15 minutes and 100% over 2 hours.

**CAP membranes:** Drug encapsulation in CAP membranes prepared using IP was much poorer than all other membranes produced. This can be attributed to drug being released from the CAP membranes into the nonsolvent water when immersed in the coagulation bath during fabrication. Drug release from the CAP membranes was very controlled as the CAP membranes do not dissolve in pH 1.2. Total drug released ranged from 30-60% over 2 hours with the different membranes produced. 10% CAP membranes prepared using IP showed the most controlled release with an average of 6% being released in the first 15 minutes, and a total of 30% released over 2 hours, while CAP membranes prepared using FC showed the poorest control over drug release with 30% being released over the first 15 minutes and 65% 2 hours.

**Conclusions:** This study demonstrates that CAP membranes show the best control over drug release in a pH of 1.2 as compared to PVA membranes. Higher polymer concentrations also controlled drug release more effectively than lower concentrations. As drug encapsulation in CAP membranes was poor as compared to PVA membranes using IP, FC illustrates a more promising method of fabrication in the preparation of CAP membranes.

## APPENDIX A2

---

### Evaluation of Electrospun Polymeric Membranes for Potential Rate-Modulated Drug Delivery

Rubina P. Shaikh, Viness Pillay\*, Yahya E. Choonara and Lisa C. du Toit  
University of the Witwatersrand, Department of Pharmacy and Pharmacology, 7 York Road,  
Parktown, 2193, Johannesburg, South Africa

\*Correspondence: [viness.pillay@wits.ac.za](mailto:viness.pillay@wits.ac.za)

#### Purpose

This study evaluated the process of electrospinning for the development of a micro-fibrous polymeric membrane system and the potential for rate-modulated drug delivery.

#### Methods

*Electrospinning:* Polymers including polyvinyl alcohol (PVA) and poly(ethylene oxide) (PEO) were investigated for electrospun membrane formation. Solutions of PVA and PEO (10-30%<sup>w/v</sup>) were prepared. A plasticizer was incorporated, as well as varying concentrations of polymer solvents such as water and a water: propan-2-ol solvent system, were investigated. Drug-loading was attempted by dissolving model drug, diphenhydramine HCl (DPH) in the polymeric solution prior to electrospinning. Polymer solutions were subjected to a predetermined voltage and allowed to electrospin for a time period sufficient to produce acceptable membranes. *Microscopic evaluation:* Electrospun fibres underwent microscopic evaluation to assess fibre morphology, size and consistency. *Fourier Transform Infrared Spectroscopy (FTIR):* FTIR spectroscopy was performed in order to assess any constituent interactions in the formulation due to electrospinning. *Drug Entrapment Efficacy (DEE):* DEE studies were conducted on the fibres and quantified using a standard curve generated for DPH.

#### Results and Discussion

Plasticizer addition resulted in a higher elasticity and strength of membranes. Of the polymers selected for electrospinning, fibres spun from PEO resulted in poorly formed membranes compared to PVA. The physicochemical properties of membranes prepared using different solvents differed vastly. With water as the solvent, resilient membranes were prepared with relatively smaller fibre sizes, whereas the fibre sizes of water: propan-2-ol membranes were inconsistent and were prone to rupture. Fibres produced were micrometer in size. Parallel, nonwoven and uniform fibre membranes were formed from PVA while PEO solutions formed woven membranes with inconsistent fibre sizes. An ideal voltage applied to the polymer solution during electrospinning promoted adequate elongation of the fibres resulting in smaller fibre diameters as seen with the PVA membranes. Electrospinning produced no significant changes on the polymer as demonstrated by the FTIR spectra generated, where the polymer backbone remained intact upon exposure to the voltage associated with electrospinning. Studies indicated that the DEE value was significantly higher with PVA as compared to PEO (93.5% vs. 54% for PVA and PEO respectively), thus indicating that PVA possessed a greater potential for entrapping DPH due to its hydrophilic nature.

#### Conclusions

Electrospinning produced no significant physicochemical changes to the properties of the polymers selected. Furthermore, electrospun membranes showed relatively superior drug entrapment and fibres were found to have an adequate size range for modulated drug delivery.

## APPENDIX A3

---

### Development of a pH-responsive, Mucoadhesive Membrane Intended for Prolonged Oral Drug Delivery

Rubina Shaikh, Viness Pillay\*, Yahya E. Choonara and Lisa C. du Toit, Valence M.K. Ndesendo and Pradeep Kumar

University of the Witwatersrand, Department of Pharmacy and Pharmacology, 7 York Road, Parktown, 2193, Johannesburg, South Africa.

\*Correspondence: [viness.pillay@wits.ac.za](mailto:viness.pillay@wits.ac.za)

**Purpose:** Chitosan (CHT) (0.5-3%w/v), which swells only in lower pH ranges, was investigated for the development of gastric-responsive mucoadhesive membrane intended for prolonged oral drug delivery.

**Methods:** In addition to CHT, Poly(vinyl alcohol) (1-5%w/v), which improved the membrane's physicochemical properties and Poly(vinylpyrrolidone) (2-10%w/v) which improved mucoadhesive properties were included in the formulation. A 2-Factor Central Composite Design (13 formulations) was used to determine the optimal formulation. The polymeric solutions were film-cast and dried at ambient conditions to produce mucoadhesive membranes (MM). *pH-responsive mucoadhesion* was determined by exposing the MM to Simulated Human Gastric Fluid (pH 1.2) and Simulated Human Intestinal Fluid (pH 6.8) for 12 hours, and tested at 2 hour intervals using a textural analyzer. *Surface morphology*, which affects mucoadhesive properties, was assessed using SEM analysis. Molecular Mechanics Computations were employed to elucidate the intermolecular interactions, responsible for mucoadhesion, involved between the polymers and mucosa.

**Results:** There was a substantial difference in the mucoadhesive properties of the MM when exposed to the different pH ranges. The MM's were highly mucoadhesive at lower pH ranges as compared to higher ranges. Membranes were irregular in surface morphology, thus promoting mucoadhesion through stronger mechanical interactions. Furthermore, the spatial disposition and energetic profile of the sterically constrained and geometrically optimized multi-polymeric complex corroborated the experimental results in terms of drug release and mucoadhesive strength of the fabricated MM.

**Conclusions:** The pH-responsive nature of the MM can potentially produce prolonged site-specific drug release in the gastric region of the gastrointestinal tract for multiple drug regimens or single drug formulations.

## APPENDIX A4

### Synthesis of Multilayered Mucoadhesive Membranes for Prolonged and Site-Specific Oral Drug Delivery

Rubina P. Shaikh, Viness Pillay\*, Yahya E. Choonara and Lisa C. du Toit.

Department of Pharmacy and Pharmacology, University of the Witwatersrand, 7 York Road, Parktown, 2193 Johannesburg, South Africa

\*Corresponding author: [viness.pillay@wits.ac.za](mailto:viness.pillay@wits.ac.za)

#### Purpose:

The purpose of this study was to formulate and evaluate a novel polymeric drug delivery system comprising an upper gastric and intestinal targeted multilayered membrane system, for site-specific oral delivery of model drugs rifampicin and isoniazid respectively.

#### Methods:

*Mucoadhesive Membrane Fabrication:* Solutions of chitosan (1.0-2.0%<sup>w/v</sup>) for the gastric targeted component and pectin (1.3-2.7%<sup>w/v</sup>) for the intestinal targeted component, added to a solution containing polyvinylpyrrolidone (4.0-8.0%<sup>w/v</sup>) and Poly(vinyl alcohol) (PVA) (2.00-4.75%<sup>w/v</sup>) before film-casting and dried at room temperature for membrane formation.

*Preparation of Electrospun Drug-loaded nanofibrous membranes:* Solutions (10%<sup>w/v</sup> PVA with 2%<sup>w/v</sup> INH and 8%<sup>w/v</sup> PVA with 2%<sup>w/v</sup> RIF) were electrospun on a horizontal electrospinning rig with an optimised collector to capillary tip distance of 24cm or 28cm for INH and RIF nanofibrous membranes respectively with an applied voltage of 20kV.

*Modification by Vapour-Induced Crosslinking:* Crosslinking was performed in the presence of GA vapours in a closed environment. INH- and RIF-loaded PVA nanofibrous membranes were suspended over 15-60mL of the GA solution and allowed to crosslink for 6-24 hours.

*Drug Entrapment Efficiency (DEE) Determination:* Accurately weighed samples of drug-loaded nanofibrous membranes were dissolved in 100mL of PBS (INH: pH 6.8; RIF: pH 1.2). The drug content was analyzed by UV spectrophotometry and computed from a standard linear curve of the drug in PBS.

*In-Vitro Drug Release Study:* *In vitro* drug release studies were performed using a USP 33 apparatus II rotating paddle method, set at 50rpm, in which a single nanofibrous membrane of known mass was placed in 900mL of PBS (INH: pH 6.8; RIF: pH 1.2) at 37°C. Sampling occurred at hourly intervals for 12 hours and with analysis by UV spectroscopy.

*pH-responsive Mucoadhesivity Analysis:* Mucoadhesive membranes were exposed to test parameters as described in drug release studies and tested for mucoadhesion at 2 hour intervals over 12 hours using a textural analyzer.

*Scanning Electron Microscopy Studies:* Surface morphology of the nanofibrous membranes was analyzed by SEM to qualitatively elucidate nanofiber diameter and network density.

*Elucidation of Tensile properties:* Physicomechanical properties of the crosslinked and non-crosslinked nanofibrous membranes were determined using a nanoTensile<sup>®</sup> tester.

#### Results and Conclusions:

DEE tests demonstrated a high entrapment of 98.77±1.384% and 95.07±1.988% of INH and RIF respectively. Drug release results showed that the crosslinking time and quantity of GA had a profound effect on prolonging the release characteristics of the nanofibrous membranes. SEM analysis revealed uniform, cylindrical fibers with diameters of 372.5±28.61nm and 631±57.78nm for INH and RIF respectively. Crosslinking produced denser packing of nanofibers within the membrane which facilitated prolonged drug release characteristics. Crosslinking notably decreased the elasticity and increased the ultimate strength and yield stress of the nanofibrous membrane. Mucoadhesion, determined by measuring the Work of Adhesion from a typical force: distance obtained from textural analysis was 7.5e<sup>-3</sup>±2.96e<sup>-3</sup>J and 2.03e<sup>-2</sup>±5.43e<sup>-3</sup>J for optimised gastric targeted membranes and intestinal targeted membranes respectively. Membranes maintained their mucoadhesive properties over 12 hours only showing a decrease in mucoadhesion of 20-40% after 8 hours.

**Note:** Ethics approval for *in vivo* studies obtained from Wits Animal Ethics Screening Committee, AESC No: 2009/01/05.

## APPENDIX B

---

### Abstracts of Papers Published/Submitted

## APPENDIX B1

---

*AAPS PharmSciTech*, Vol. 11, No. 1, March 2010 (© 2010)  
DOI: 10.1208/s12249-010-9403-2

---

### *Review Article*

---

## **A Review of Multi-Responsive Membranous Systems for Rate-Modulated Drug Delivery**

**Rubina P. Shaikh,<sup>1</sup> Viness Pillay,<sup>1,2</sup> Yahya E. Choonara,<sup>1</sup> Lisa C. du Toit,<sup>1</sup> Valence M. K. Ndesendo,<sup>1</sup> Priya Bawa,<sup>1</sup> and Shivaan Cooppan<sup>1</sup>**

*Received 28 September 2009; accepted 19 February 2010; published online 19 March 2010*

**Abstract.** Membrane technology is broadly applied in the medical field. The ability of membranous systems to effectively control the movement of chemical entities is pivotal to their significant potential for use in both drug delivery and surgical/medical applications. An alteration in the physical properties of a polymer in response to a change in environmental conditions is a behavior that can be utilized to prepare 'smart' drug delivery systems. Stimuli-responsive or 'smart' polymers are polymers that upon exposure to small changes in the environment undergo rapid changes in their microstructure. A stimulus, such as a change in pH or temperature, thus serves as a trigger for the release of drug from membranous drug delivery systems that are formulated from stimuli-responsive polymers. This article has sought to review the use of stimuli-responsive polymers that have found application in membranous drug delivery systems. Polymers responsive to pH and temperature have been extensively addressed in this review since they are considered the most important stimuli that may be exploited for use in drug delivery, and biomedical applications such as in tissue engineering. In addition, dual-responsive and glucose-responsive membranes have been also addressed as membranes responsive to diverse stimuli.

**KEY WORDS:** Dual-responsive membranes; Glucose-responsive membranes; Membranous drug delivery systems; "On-off" gating mechanisms; pH; Stimuli-responsive polymers; Temperature.

## APPENDIX B2



### The application of a crosslinked pectin-based wafer matrix for gradual buccal drug delivery

Rubina P. Shaikh,<sup>1</sup> Viness Pillay,<sup>1</sup> Yahya E. Choonara,<sup>1</sup> Lisa C. Du Toit,<sup>1</sup> Valence M. K. Ndesendo,<sup>1</sup> Pradeep Kumar,<sup>1</sup> Riaz A. Khan<sup>2</sup>

<sup>1</sup>Faculty of Health Sciences, Department of Pharmacy and Pharmacology, University of the Witwatersrand, Parktown, Johannesburg 2193, South Africa

<sup>2</sup>Department of Medicinal Chemistry, College of Pharmacy, Qassim University, Qassim 51452, Kingdom of Saudi Arabia

Received 26 May 2011; revised 20 October 2011; accepted 13 November 2011

Published online in Wiley Online Library (wileyonlinelibrary.com). DOI: 10.1002/jbm.b.32668

**Abstract:** The purpose of this study was to develop cross-linked wafer matrices and establish the influence of the crosslinker type and processing sequence on achieving gradual buccal drug delivery. Three sets of drug-loaded cross-linked pectin wafers were produced employing the model water-soluble antihistamine, diphenhydramine and were compared with noncrosslinked wafers. The formulations were crosslinked with CaCl<sub>2</sub>, BaCl<sub>2</sub>, or ZnSO<sub>4</sub> pre- or postlyophilization (sets 1 and 2) as well as pre- and postlyophilization (set 3), respectively. The surface morphology, porosimetry, molecular vibrational transitions, textural attributes, thermal and *in vitro* drug release were characterized and supported by *in silico* molecular mechanics simulations. Results revealed that crosslinked wafers produced smaller pore sizes (107.63 Å) compared with noncrosslinked matrices (180.53 Å) due to molecular crosslinks formed between pectin chains. Drug release performance was de-

pendent on the wafer crosslinking production sequence. Non-crosslinked wafers displayed burst-release with 82% drug released at  $t_{30\text{min}}$  compared with first-order kinetic profiles obtained for prelyophilized crosslinked matrices (50% released at  $t_{30\text{min}}$  followed by steady release). Wafers cross-linked postlyophilization displayed superior control of drug release (40% at  $t_{30\text{min}}$ ). Molecular mechanics simulations corroborated with the experimental data and established that Ba<sup>++</sup>, having the largest atomic radii (1.35 Å) formed a number of ionic bridges producing wafers of higher porosity (0.048 cm<sup>2</sup>/g) and had more influence on drug release. © 2012 Wiley Periodicals, Inc. *J Biomed Mater Res Part B: Appl Biomater* 00B:000–000, 2012.

**Key Words:** buccal drug delivery, wafer matrix, crosslinked mucoadhesive polymers, lyophilization, porosimetry, molecular mechanics simulations

**How to cite this article:** Shaikh RP, Pillay V, Choonara YE, du Toit LC, Ndesendo VMK, Kumar P, Khan RA. 2012. The application of a crosslinked pectin-based wafer matrix for gradual buccal drug delivery. *J Biomed Mater Res Part B* 2012;00B:000–000.



# Crosslinked electrospun PVA nanofibrous membranes: elucidation of their physicochemical, physicomechanical and molecular disposition

Rubina P Shaikh, Pradeep Kumar, Yahya E Choonara, Lisa C du Toit and Viness Pillay<sup>1</sup>

Department of Pharmacy and Pharmacology, Faculty of Health Sciences, University of the Witwatersrand, 7 York Road, Parktown, 2193, Johannesburg, South Africa

E-mail: [viness.pillay@wits.ac.za](mailto:viness.pillay@wits.ac.za)

Received 9 September 2011

Accepted for publication 20 February 2012

Published 19 March 2012

Online at [stacks.iop.org/BF/4/025002](http://stacks.iop.org/BF/4/025002)

## Abstract

The effects of modifying electrospun poly(vinyl alcohol) (PVA) nanofibers through crosslinking using glutaraldehyde (GA) are explored in this paper. Various concentrations of PVA solutions containing model drugs rifampicin (RIF) and isoniazid (INH) were electrospun and thereafter crosslinked using GA vapors. PVA nanofibers demonstrated high drug entrapment efficiency of  $98.77\% \pm 1.384\%$  and  $95.07\% \pm 1.988\%$  for the INH- and RIF-loaded PVA nanofibers, respectively. The surface morphology, molecular vibrational transitions, tensile attributes and *in vitro* drug release were characterized and supported by *in silico* molecular mechanics simulations. Results indicated that crosslinking caused a significant reduction in the rate of drug release where  $81.11\% \pm 2.35\%$  of INH and  $59.31\% \pm 2.57\%$  of RIF were released after 12 h. Tensile properties such as the ultimate strength and Young's modulus increased after crosslinking, caused by crosslinks forming between PVA nanofibers as was revealed through scanning electron microscopy analysis. Fourier Transform infrared analysis was conducted to further support the mode of crosslinking. Additionally, image processing analysis was carried out to quantify the effect of formulation variables on the morphology of nanofibers. Furthermore, the effect of GA-induced crosslinking and addition of drugs on the performance of electrospun fibers was further elucidated and conceptualized using a molecular mechanics assisted model building and energy refinement approach via molecular mechanics energy relationships by exploring the spatial disposition of energy-minimized molecular structures of the polymer, crosslinker and the drugs.

(Some figures may appear in colour only in the online journal)

## **APPENDIX C**

---

### **Animal Ethics Clearance**

# APPENDIX C1

## Animal Ethics Clearance Certificate

UNIVERSITY OF THE WITWATERSRAND, JOHANNESBURG

STRICTLY CONFIDENTIAL

ANIMAL ETHICS SCREENING COMMITTEE (AESC)

CLEARANCE CERTIFICATE NO. 2009/01/05

APPLICANT: Prof V Pillay

SCHOOL: Pharmacy and Pharmacology

DEPARTMENT:

LOCATION:

PROJECT TITLE: In vivo assessment of novel biocompatible polymeric drug delivery systems in pigs

### Number and Species


40 pigs

Approval was given for the use of animals for the project described above at an AESC meeting held on 27.01.2009. This approval remains valid until 27.01.2011

The use of these animals is subject to AESC guidelines for the use and care of animals, is limited to the procedures described in the application form and to the following additional conditions:

- a) Clinical monitoring of the animals for the first 24 hours after drug dosing to ensure that no unwanted side-effects occur. This monitoring should be performed by the investigators as guided by the CAS veterinarian.
- b) A written report should be submitted to the AESC on the clinical safety of the drug combinations observed in one animal per drug combination before proceeding to further animals in each drug combination group.
- c) A letter addressed to the chairperson of AESC should be provided to indicate the exact pharmacological combinations being studied and the route of delivery of these combinations. Obviously this should be provided when the appropriate combinations are known.
- d) The protocol should be revised with the inclusion of a detailed description of the procedure that will be employed for intraduodenal infusion and the person qualified to do this.
- e) The protocol should be revised with a justification and rationale for the use of 2 calcium channel blockers employed together as implied by the present protocol.
- f) Discussion should occur with the CAS veterinarian regarding the precise procedures required for the collection of blood and CSF samples.


Signed: \_\_\_\_\_

  
(Chairperson, AESC)

Date: \_\_\_\_\_

06/02/2009

I am satisfied that the persons listed in this application are competent to perform the procedures therein, in terms of Section 23 (1) (c) of the Veterinary and Para-Veterinary Professions Act (19 of 1982)

Signed:   
(Registered Veterinarian)

Date: 09/02/09

cc: Supervisor:  
Director: CAS  
Works 2000\ain0015\AESCcert.wps

## APPENDIX C2

### Animal Ethics Research Outcome Report

#### Central Animal Service

Medical School, 7 York Road, Parktown 2193, South Africa • Tel: +27 11 717-1301 • Fax: +27 11 643-4318



#### RESEARCH OUTCOME REPORT

**Clearance Certificate No:** 2009/01/05

**Applicant:** Professor Viness Pillay

**Department:** Pharmacy and Pharmacology

**Title:** *In vivo* assessment of novel biocompatible polymeric drug delivery systems in pigs.

#### Dear Animal Users

It is with great satisfaction that we can relay the positive outcome of the research entitled "The *in vivo* assessment of a novel biocompatible polymeric drug delivery system in pigs" with clearance certificate number: 2009/01/05. Central Animal Service acquired a batch of 40 pigs for *in vivo* research with the Department of Pharmacy and Pharmacology, for the determination of the biocompatibility of novel polymeric drug delivery systems.

The afore mentioned applicant, Professor Viness Pillay, and his research group, including Ms. Rubina Shaikh, ensured that an ongoing surveillance program continued on a daily basis to assess the health and well being of the pigs during and post study. Furthermore, the CAS team ensured that the animals were assessed for their health status both before and after the study to determine whether the researchers or research material caused any effects which detrimentally affected the pigs' health and well-being. We are confident to say that no unforeseen or fatal circumstance due to the researcher or research material were observed as the pigs maintained an acceptable health status both during the study, and after completion of the study.

Kind Regards,

A blue ink signature of Dr Leith Meyer.

Dr Leith Meyer  
Director of the Central Animal Services  
University of the Witwatersrand

17/4/2012  
Date